



INTERNATIONAL CONFERENCE
ON HYBRID IMAGING

IPET 2024



7–11 October 2024
IAEA Headquarters
Vienna, Austria
#IPET2024

International Conference on Hybrid Imaging

(IPET-2024)

7 – 11 October 2024

IAEA Headquarters, Vienna, Austria

Organized by the IAEA

In Cooperation with:



Latin American Association of Societies of Biology and Nuclear Medicine



ANZSNM
The Society For All
Nuclear Medicine Professionals

Australian and New Zealand Society of Nuclear Medicine



Asia Oceania Federation of Nuclear Medicine and Biology



Arab Society of Nuclear Medicine



European Association of Nuclear Medicine



European Society of Radiology



International Centers for Precision Oncology Foundation



International Society of Radiolabeled Blood Elements



International Society of Radiology



Radiological Society of North America



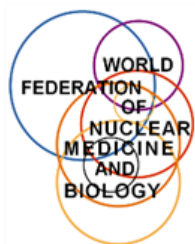
Society of Nuclear Medicine and Molecular Imaging



European Union of Medical Specialists



World Association of Radiopharmaceutical and Molecular Therapy



World Federation of Nuclear Medicine and Biology

BOOK OF ABSTRACTS

IAEA-CN-326

The material in this book has been supplied by the authors and has not been edited. The views expressed remain the responsibility of the named authors and do not necessarily reflect those of the government of the designating Member State(s). The IAEA cannot be held responsible for any material reproduced in the book.

Contents

IAEA-CN-326/8.....	1
IAEA-CN-326/9.....	2
IAEA-CN-326/10	4
IAEA-CN-326/11	5
IAEA-CN-326/12	6
IAEA-CN-326/13	7
IAEA-CN-326/14	9
IAEA-CN-326/15	11
IAEA-CN-326/16	13
IAEA-CN-326/17	15
IAEA-CN-326/19	16
IAEA-CN-326/20	20
IAEA-CN-326/21	22
IAEA-CN-326/23	24
IAEA-CN-326/24	25
IAEA-CN-326/27	26
IAEA-CN-326/30	27
IAEA-CN-326/32	28
IAEA-CN-326/34	30
IAEA-CN-326/35	31
IAEA-CN-326/36	32
IAEA-CN-326/39	34
IAEA-CN-326/40	35
IAEA-CN-326/42	37
IAEA-CN-326/43	38
IAEA-CN-326/44	39
IAEA-CN-326/45	41
IAEA-CN-326/46	42
IAEA-CN-326/47	43
IAEA-CN-326/48	45
IAEA-CN-326/51	47
IAEA-CN-326/52	48
IAEA-CN-326/54	50
IAEA-CN-326/55	52
IAEA-CN-326/57	54
IAEA-CN-326/59	56
IAEA-CN-326/62	59

IAEA-CN-326/64	61
IAEA-CN-326/65	63
IAEA-CN-326/66	66
IAEA-CN-326/68	68
IAEA-CN-326/69	70
IAEA-CN-326/70	72
IAEA-CN-326/71	73
IAEA-CN-326/72	75
IAEA-CN-326/73	77
IAEA-CN-326/74	80
IAEA-CN-326/76	81
IAEA-CN-326/77	82
IAEA-CN-326/80	85
IAEA-CN-326/81	86
IAEA-CN-326/82	88
IAEA-CN-326/84	89
IAEA-CN-326/85	92
IAEA-CN-326/86	94
IAEA-CN-326/87	95
IAEA-CN-326/88	96
IAEA-CN-326/89	97
IAEA-CN-326/91	98
IAEA-CN-326/92	100
IAEA-CN-326/93	101
IAEA-CN-326/95	103
IAEA-CN-326/96	105
IAEA-CN-326/97	107
IAEA-CN-326/98	108
IAEA-CN-326/99	110
IAEA-CN-326/100	112
IAEA-CN-326/101	113
IAEA-CN-326/102	115
IAEA-CN-326/103	117
IAEA-CN-326/104	119
IAEA-CN-326/105	121
IAEA-CN-326/106	123
IAEA-CN-326/107	125

IAEA-CN-326/111	129
IAEA-CN-326/112	131
IAEA-CN-326/113	132
IAEA-CN-326/114	133
IAEA-CN-326/115	134
IAEA-CN-326/116	135
IAEA-CN-326/118	137
IAEA-CN-326/119	138
IAEA-CN-326/120	140
IAEA-CN-326/122	142
IAEA-CN-326/123	143
IAEA-CN-326/124	145
IAEA-CN-326/125	147
IAEA-CN-326/126	149
IAEA-CN-326/127	151
IAEA-CN-326/129	152
IAEA-CN-326/130	154
IAEA-CN-326/131	157
IAEA-CN-326/132	159
IAEA-CN-326/134	160
IAEA-CN-326/135	162
IAEA-CN-326/138	166
IAEA-CN-326/139	168
IAEA-CN-326/140	169
IAEA-CN-326/141	171
IAEA-CN-326/142	173
IAEA-CN-326/143	175
IAEA-CN-326/144	176
IAEA-CN-326/145	177
IAEA-CN-326/146	178
IAEA-CN-326/147	179
IAEA-CN-326/148	181
IAEA-CN-326/149	182
IAEA-CN-326/151	185
IAEA-CN-326/152	188
IAEA-CN-326/153	192
IAEA-CN-326/154	194

IAEA-CN-326/155	196
IAEA-CN-326/156	197
IAEA-CN-326/157	199
IAEA-CN-326/158	201
IAEA-CN-326/159	204
IAEA-CN-326/160	207
IAEA-CN-326/161	209
IAEA-CN-326/162	211
IAEA-CN-326/163	213
IAEA-CN-326/164	215
IAEA-CN-326/165	217
IAEA-CN-326/166	218
IAEA-CN-326/167	220
IAEA-CN-326/168	221
IAEA-CN-326/169	222
IAEA-CN-326/170	223
IAEA-CN-326/171	225
IAEA-CN-326/172	226
IAEA-CN-326/173	227
IAEA-CN-326/174	229
IAEA-CN-326/175	230
IAEA-CN-326/176	232
IAEA-CN-326/177	234
IAEA-CN-326/178	235
IAEA-CN-326/179	237
IAEA-CN-326/180	239
IAEA-CN-326/182	241
IAEA-CN-326/185	243
IAEA-CN-326/186	244
IAEA-CN-326/187	246
IAEA-CN-326/188	248
IAEA-CN-326/189	249
IAEA-CN-326/191	251
IAEA-CN-326/192	252
IAEA-CN-326/193	254
IAEA-CN-326/195	255
IAEA-CN-326/196	256

IAEA-CN-326/197	258
IAEA-CN-326/198	260
IAEA-CN-326/199	262
IAEA-CN-326/200	264
IAEA-CN-326/202	265
IAEA-CN-326/203	267
IAEA-CN-326/204	269
IAEA-CN-326/205	271
IAEA-CN-326/206	273
IAEA-CN-326/207	274
IAEA-CN-326/208	275
IAEA-CN-326/210	277
IAEA-CN-326/211	278
IAEA-CN-326/212	280
IAEA-CN-326/213	282
IAEA-CN-326/214	284
IAEA-CN-326/215	286
IAEA-CN-326/217	288
IAEA-CN-326/219	290
IAEA-CN-326/220	292
IAEA-CN-326/221	294
IAEA-CN-326/222	297
IAEA-CN-326/223	298
IAEA-CN-326/224	300
IAEA-CN-326/225	302
IAEA-CN-326/227	304
IAEA-CN-326/229	306
IAEA-CN-326/230	308
IAEA-CN-326/232	309
IAEA-CN-326/233	311
IAEA-CN-326/236	315
IAEA-CN-326/237	316
IAEA-CN-326/240	318
IAEA-CN-326/241	320
IAEA-CN-326/243	322
IAEA-CN-326/244	324
IAEA-CN-326/245	325

IAEA-CN-326/246	327
IAEA-CN-326/247	329
IAEA-CN-326/248	330
IAEA-CN-326/249	332
IAEA-CN-326/251	334
IAEA-CN-326/252	335
IAEA-CN-326/253	336
IAEA-CN-326/254	337
IAEA-CN-326/255	339
IAEA-CN-326/256	340
IAEA-CN-326/257	342
IAEA-CN-326/259	344
IAEA-CN-326/262	345
IAEA-CN-326/263	347
IAEA-CN-326/265	351
IAEA-CN-326/266	353
IAEA-CN-326/267	355
IAEA-CN-326/268	356
IAEA-CN-326/270	362
IAEA-CN-326/271	364
IAEA-CN-326/272	366
IAEA-CN-326/273	368
IAEA-CN-326/274	370
IAEA-CN-326/275	372
IAEA-CN-326/277	375
IAEA-CN-326/278	376
IAEA-CN-326/279	378
IAEA-CN-326/280	380
IAEA-CN-326/282	383
IAEA-CN-326/283	385
IAEA-CN-326/284	387
IAEA-CN-326/286	391
IAEA-CN-326/287	393
IAEA-CN-326/288	395
IAEA-CN-326/289	398
IAEA-CN-326/291	400
IAEA-CN-326/292	402

IAEA-CN-326/293	404
IAEA-CN-326/294	406
IAEA-CN-326/296	408
IAEA-CN-326/297	409
IAEA-CN-326/299	411
IAEA-CN-326/300	415
IAEA-CN-326/301	420
IAEA-CN-326/302	422
IAEA-CN-326/303	425
IAEA-CN-326/304	428
IAEA-CN-326/305	430
IAEA-CN-326/307	432
IAEA-CN-326/308	434
IAEA-CN-326/310	435
IAEA-CN-326/312	436
IAEA-CN-326/314	438
IAEA-CN-326/317	439
IAEA-CN-326/318	442
IAEA-CN-326/319	444
IAEA-CN-326/320	446
IAEA-CN-326/321	448
IAEA-CN-326/322	449
IAEA-CN-326/324	451
IAEA-CN-326/325	453
IAEA-CN-326/326	455
IAEA-CN-326/327	457
IAEA-CN-326/328	459
IAEA-CN-326/329	461
IAEA-CN-326/332	462
IAEA-CN-326/333	463
IAEA-CN-326/336	464
IAEA-CN-326/338	466
IAEA-CN-326/339	468
IAEA-CN-326/340	470
IAEA-CN-326/342	472
IAEA-CN-326/344	473
IAEA-CN-326/345	475

IAEA-CN-326/346	477
IAEA-CN-326/347	478
IAEA-CN-326/348	479
IAEA-CN-326/349	481
IAEA-CN-326/350	483
IAEA-CN-326/351	484
IAEA-CN-326/353	486
IAEA-CN-326/355	488
IAEA-CN-326/356	490
IAEA-CN-326/361	492
IAEA-CN-326/362	495
IAEA-CN-326/363	496
IAEA-CN-326/364	497
IAEA-CN-326/365	499
IAEA-CN-326/366	502
IAEA-CN-326/367	504
IAEA-CN-326/368	508
IAEA-CN-326/369	509
IAEA-CN-326/370	511
IAEA-CN-326/371	513
IAEA-CN-326/372	516
IAEA-CN-326/373	517
IAEA-CN-326/374	519
IAEA-CN-326/375	520
IAEA-CN-326/376	521
IAEA-CN-326/378	522
IAEA-CN-326/379	523
IAEA-CN-326/380	526
IAEA-CN-326/384	532
IAEA-CN-326/386	536
IAEA-CN-326/387	538
IAEA-CN-326/388	539
IAEA-CN-326/389	541
IAEA-CN-326/391	544
IAEA-CN-326/392	546
IAEA-CN-326/393	548
IAEA-CN-326/394	550

IAEA-CN-326/395	552
IAEA-CN-326/396	553
IAEA-CN-326/397	555
IAEA-CN-326/398	557
IAEA-CN-326/399	559
IAEA-CN-326/400	561
IAEA-CN-326/401	563
IAEA-CN-326/402	565
IAEA-CN-326/405	567
IAEA-CN-326/406	569
IAEA-CN-326/407	571
IAEA-CN-326/408	572
IAEA-CN-326/409	573
IAEA-CN-326/410	574
IAEA-CN-326/413	576
IAEA-CN-326/414	578
IAEA-CN-326/415	579
IAEA-CN-326/417	581
IAEA-CN-326/418	583
IAEA-CN-326/419	585
IAEA-CN-326/421	587
IAEA-CN-326/422	588
IAEA-CN-326/423	592
IAEA-CN-326/424	594
IAEA-CN-326/425	596
IAEA-CN-326/428	598
IAEA-CN-326/430	600
IAEA-CN-326/432	602
IAEA-CN-326/433	603
IAEA-CN-326/434	605
IAEA-CN-326/437	608
IAEA-CN-326/438	610
IAEA-CN-326/439	612
IAEA-CN-326/440	614
IAEA-CN-326/441	616
IAEA-CN-326/442	617
IAEA-CN-326/443	619

IAEA-CN-326/444	621
IAEA-CN-326/446	623
IAEA-CN-326/447	625
IAEA-CN-326/448	627
IAEA-CN-326/451	628
IAEA-CN-326/452	630
IAEA-CN-326/454	632
IAEA-CN-326/456	634
IAEA-CN-326/458	635
IAEA-CN-326/463	635
IAEA-CN-326/464	638
IAEA-CN-326/466	640
IAEA-CN-326/467	642
IAEA-CN-326/469	644
IAEA-CN-326/470	647
IAEA-CN-326/471	651
IAEA-CN-326/477	654
IAEA-CN-326/478	656
IAEA-CN-326/482	657
IAEA-CN-326/483	659
IAEA-CN-326/484	660
IAEA-CN-326/485	661
IAEA-CN-326/486	663
Glossary of Terms.....	665

Challenges in the production of [¹⁸F]Florbetapir radiopharmaceuticals using CFN-MPS200 synthesizers at Siriraj Cyclotron

T. Siriprapa, T. Thientunyakit

Nuclear Medicine, Siriraj Hospital, Mahidol University, Thailand

Background

In the field of Nuclear medicine, numerous radiopharmaceuticals serve in the diagnosis of Alzheimer's disease (AD). [¹⁸F]Florbetapir stands among the approved radiopharmaceuticals for clinical applications, particularly in detecting Amyloid-β (Aβ) deposition in brain tissues through Positron Emission Tomography (PET) scans. Since 2015, Siriraj Cyclotron Center, Division of Nuclear Medicine, Department of Radiology, Faculty of Medicine, Siriraj Hospital has been the sole center in Thailand dedicated to developing [¹⁸F]Florbetapir for clinical research applications.

Methodology

This article succinctly outlines the challenges faced by the PET radiopharmaceuticals production team at Siriraj Cyclotron Center, with a specific focus on the hurdles encountered in [¹⁸F]Florbetapir radiosynthesis using CFN-MPS200 synthesizers covering aspects such as adopting the CFN-MPS200 software, temperature optimization, reduction of residual impurities, and improvement of synthesis yield.

Results

We successfully adopted CFN-MPS200 software for [¹⁸F]Florbetapir synthesis and purification. The temperature was optimized for the chemical reaction and our system. Residual solvents, such as ethanol, acetonitrile, and dimethyl sulfoxide were within acceptable limits, and the overall yield, specific activity, and radiochemical purity of [¹⁸F]Florbetapir were 21.4±0.2% (not decay corrected), 5.24±2.25 TBq/mmol and 96.1±3.2%, respectively.

Conclusions

[¹⁸F]Florbetapir can be manufactured according to GMP-compliant conditions and is readily available for routine clinical research applications at the Division of Nuclear Medicine, Siriraj Hospital.

Peptide Receptor Radionuclide Therapy (PRRT) for Neuroendocrine Tumours: Real-World Outcomes and Safety Profile Across Diverse Sites in Brazil

C. T. Mesquita¹, M. F. Rezende², I. C. Palazzo³, G. V. Gomes⁴, J. M. Correia⁵

¹Hospital Universitário Antônio Pedro – UFF, Brazil

²Hospital Vitória / Hospital Samaritano Barra, Brazil

³Hospital Pro-Cardíaco, Brazil

⁴Clínica Núcleos, Brazil

⁵Instituto do Câncer do Ceará, Brazil

Background

Peptide receptor radionuclide therapy (PRRT) has established itself as a pivotal treatment option for gastroenteropancreatic neuroendocrine tumours (GEP-NETs). Despite its FDA approval 2018 based on the NETTER-1 trial focusing on midgut neuroendocrine tumours, the clinical application extends to various NET types. This study presents real-world outcomes and implementation data from four tertiary treatment centres in Brazil, highlighting the safety profile of PRRT across different NET sites.

Methodology

A retrospective analysis encompassing January 2007 to January 2021 was conducted across four Brazilian hospitals, involving 160 histologically confirmed NET patients treated with [¹⁷⁷Lu]Lu-DOTA-TATE PRRT. Clinician-evaluated data encompassed demographics, efficacy, and toxicity.

Results

Of the 160 patients (83 female), the median [¹⁷⁷Lu]Lu-DOTA-TATE treatments were four (range 1-8). Tumour localization included midgut (28%), pancreas (27.5%), foregut (17.5%), neuroendocrine CUP (11%), hindgut (7%), lung (3%), and other sites (6%). Median progression-free survival (PFS) was 11.9 months, with a 31% mortality rate. Notably, only four patients experienced significant renal toxicity, and haematological toxicity occurred in 12 patients.

Conclusion

While observing a higher utilization rate in non-midgut sites, such as the pancreas and foregut, the median PFS was lower than NETTER-1 trial outcomes, aligning with the inclusion of higher-risk tumours. Despite this, PRRT exhibited a notably low incidence of treatment-related toxicity in our cohort, establishing its safety with minimal haematological and renal effects.

Clinical Relevance/Application

In the context of a developing country like Brazil, our study not only underscores the diverse applicability of Peptide Receptor Radionuclide Therapy (PRRT) across various neuroendocrine tumour (NET) sites but also highlights its notable safety profile. The higher utilization of PRRT in non-midgut sites, such as the pancreas and foregut, reveals a growing acceptance and integration of this treatment modality into clinical practice. Despite the challenges associated with higher-risk tumours, as reflected in a lower median progression-free survival compared to established trials, the strikingly low incidence of treatment-related toxicity in our cohort

reinforces the safety and tolerability of PRRT in a resource-constrained setting. Particularly noteworthy is the minimal occurrence of significant renal and haematological toxicities, suggesting that PRRT can be administered with confidence even in environments with limited healthcare resources.

Clinical indications for performing bone scintigraphy in patients under 25 years of age

P. Korol

Shupyk National Healthcare University of Ukraine, Kiev, Ukraine

Aim

Determine the clinical indications for performing planar bone scintigraphy (PBS) and hybrid imaging (SPECT/CT) in patients under 25 years of age.

Methodology

In the Department of Nuclear Medicine of our University, a retrospective evaluation of clinical indications for bone scanning was carried out over a period of 3 years. PBS and then SPECT/CT on the area of interest were performed 2.5 hours after intravenous administration of ^{99m}Tc -MDP in dose calculated by age.

Results

We evaluated 77 patients (30 men and 47 women), average - 17.21 ± 5.12 years. The most common indication for bone scan was the metabolic activity of a primary bone lesion (BL) of non-malignant aetiology (44/77, 57.16%). The non-malignant aetiology was predominantly due to primary benign bone tumours (27/44, 61.36%), including osteoid osteoma - 11, then enchondroma - 7, aneurysmal bone cyst - 5, osteochondroma - 3, exostosis - 1. In 15 (19.49%) patients, the indication was to identify bone metastases due to non-skeletal malignancies (Hodgkin's lymphoma, melanoma, medulloblastoma, neuroblastoma, nephroblastoma). Primary malignant BL was diagnosed in 14 out of 77 patients (18.17%). Other rare indications were fibrous dysplasia, sacroiliitis, trauma (4/77, 5.18%). In 65% of cases, patients complained of bone pain. In 63/77 (81.81%) patients, BL was present mainly in the inferior extremities. PBS was performed in all patients, except for 5 cases with a malignant neoplasm extraosseous aetiology. Of the 72 patients, PBS was positive in 26 (36.11%) cases, while negative in the pool phase and positive only in the late phase - in 17 (22.07%). Positive both PBS and SPECT/CT were detected in 47 (65.27%) patients, and in 5 patients had negative planar and positive SPECT/CT (melanoma - 2, nephroblastoma - 1, fibrous dysplasia - 1, medulloblastoma - 1).

Conclusion

PBS and SPECT/CT are still an informative nuclear method, an important addition to other diagnostic methods. In young patients, the main clinical indication for a bone scan is the assessment of primary BL of benign aetiology. With high sensitivity, these imaging modalities can detect the metabolic activity of BL of various aetiologies (non-malignant, malignant, inflammatory).

**An Audit of High Risk Areas for Radioactive Contamination in Nuclear Medicine
Department at Ocean Road Cancer Institute**

F. S. Sabaya

Ocean Road Cancer Institute, United Republic of Tanzania

Background

The 'Wipe test' is an effective quality control test to determine radioactive contamination in Nuclear Medicine departments and it is recommended that it should be performed routinely on a weekly or monthly basis. The objective of the study was to conduct an audit of the work areas routinely used by the Nuclear Medicine technologists (NMTs) for possible risks due to radioactive contamination.

Methodology

A survey for radioactive contamination was done of high-risk areas using the wipe test method. Entrances to the camera rooms, the floor surfaces around the imaging beds of the three camera rooms, the injection areas and the dispensing areas where radiopharmaceuticals are prepared were wiped for removable surface contamination of Technetium-99m isotope. The wipe samples were subsequently assayed using an automatic gamma well counter to determine the radioactive counts of each area. Count rate above twice the background level was considered as failing the wipe test.

Results

A total of 16 surfaces broadly classified under 4 areas were wiped for a period of 4 weeks. Each surface was wiped 12 times during that period making a total of 48 wipe samples per week and 192 in total for all the areas for the 4 weeks. A pass total of 47% (n=91) of the total surfaces wiped over the 4 weeks period were recorded and 53% (n=101) having exceeded the recommended acceptable limit thus failing the wipe test. The surfaces with the most contamination were in the radiopharmacy and the injection areas.

Conclusion

Radioactive contamination in the department resulted mostly from spillages during preparations and injections of radiopharmaceuticals. Radioactive counts from surface contamination following wipe test should be within the recommended acceptable limit for removable radioactive contamination which is less than twice the background counts, above which is considered as failing the test.

Keywords: surface contamination, radioactivity, wipe test, gamma counter

SPECT and SPECT/CT Somatostatin Receptor Scintigraphy in the Detection of Residual and Recurrent Medullary Thyroid Carcinoma

V. Artiko, M. Veljkovic, J. Petrovic, M. Stojiljkovic, I. G. Milojevic, S. Odalovic, D. S. Saranovic

Center for Nuclear Medicine with PET, University Clinical Center of Serbia, Faculty of Medicine University of Belgrade, Serbia

Background

Medullary thyroid carcinoma (MTC) is an aggressive neuroendocrine tumour originated from calcitonin-producing parafollicular C cells of thyroid gland, representing around 3%-10% of all thyroid cancers. Elevated serum calcitonin can be used both as a helpful parameter in initial MTC diagnosis and as a follow-up after surgery. There has not yet been established a single sensitive diagnostic tool that can reveal all MTC metastases, so adequate staging of the disease can be difficult. The aim of our research was to evaluate the usefulness of somatostatin receptor scintigraphy (SRS) with SPECT and SPECT/CT in detecting of residual/recurrent disease of surgically threatened MTC patients with elevated serum calcitonin levels.

Methodology

In the period from May of 2021 to March of 2023, 28 patients, mean age 59.7 ± 7.8 years, were referred to our center for SRS with calcitonin serum levels still being elevated 3 months after surgery. The study was performed 2h after application of radiopharmaceutical, using SPECT/CT. SPECT is being performed with two detectors, rotating around the patient 360 degrees, 180 degrees each in step and shoot mode, at the angle of 5 degrees per position, total duration 15 min. After SPECT acquisition, follows low dose CT region of interest, used for MPR reconstruction. CT is used also for attenuation correction. SPECT matrix is 128x128. Foci of increased [^{99m}Tc]Tc-HYNIC TOC uptake on both SPECT and SPECT/CT images were interpreted visually by two nuclear medicine specialists and interpreted according to Krenning score system.

Results

From 28 MTC patients with elevated serum calcitonin, 12 (42.9%) were interpreted with positive SPECT/CT findings, later confirmed to be MTC metastases. Of those 12 patients, 6 patients had very low Krenning score (grade 1 or 2) while remaining 6 patients had high Krenning score (grade 3 or 4). Based on SPECT images alone, only those patients with high Krenning scores were interpreted as positive, accounting for only 6/28 (21.4%) patients.

Conclusion

Based on the limited number of patients with elevated serum calcitonin levels, [^{99m}Tc]Tc-HYNIC TOC scintigraphy can reveal residual/recurrent MTC in above 40% of the cases. When comparing SPECT and SPECT/CT, the latter was found to be superior in correctly identifying MTC metastases, especially in patients with low Krenning score.

Impact of data-driven respiratory gating algorithm on small lesions in PET/CT imaging

S. Bugingo

King Faisal Hospital Rwanda, Kigali, Rwanda

Background

Respiratory motion induces artifacts in PET/CT imaging that may introduce significant image distortion, and an important cause of diagnostic uncertainty, particularly for lesions located in the lung/diaphragm interface.

Our primary objective was to assess the effects of a data-driven respiratory gating (DDG) algorithm on lesion maximum standardized uptake value (SUV_{max}) and volume for small lesions with low and moderately low target-to-background ratios.

Methodology

We used the QUASARTM Programmable Respiratory Motion Phantom, which is designed to move cylindrical inserts in the superior-inferior direction within a torso shaped acrylic oval varying both speed and amplitudes.

We have built an insert compatible with Quasar phantom motion platform that allows the simulation of the background. The insert was filled with water to simulate the liver density (~ 1.07 g/cm³) and with water and polystyrene beads to mimic lung density (~ 0.3 g/cm³). We placed inside the insert a glass sphere with 13 mm inner diameter to represent a small tumour. Both insert and sphere were filled with [¹⁸F]FDG solutions of different concentrations to attain different target-to-background ratios.

For the acquisitions, we used the Whole Body PET/CT protocol that includes the Q.Static acquisition mode, in which an automated motion correction technique is integrated. DDG-PET data were derived from a portion of the total PET data ($\sim 50\%$) in the end-expiration (EE) phase at 30% offset from the end-inspiration (EI) phase of each respiratory cycle. We investigated effects of data-driven respiratory gating algorithm on lesion maximum standardized uptake value (SUV_{max}) and volume by comparing DDG-PET images and non-gated PET images, both reconstructed with two available algorithms: VUE Point FX (VP) and Q.Clear (QC).

Results

For the 3:1 target-to-background ratio (TBR), the motion correction with DDG PET increased the lesion SUV_{max} by the average of $25 \pm 13\%$ for VP and $26 \pm 17\%$ for QC. The lesion volume decreased by $35 \pm 15\%$ for VP and $31 \pm 36\%$ for QC. For 3:1 TBR lung case, the motion correction with DDG PET increased the lesion SUV_{max} by the average of $26 \pm 10\%$ for VP and $27 \pm 17\%$ for QC. The lesion volume decreased by $31 \pm 40\%$ for VP and $27 \pm 32\%$ for QC. In these cases, the average was done over 4, 6, 8 and 10 mm motion amplitudes.

For the 4:1 TBR, the motion correction with DDG-PET increased the lesion SUV_{max} by the average of $28 \pm 12\%$ for VP and $33 \pm 12\%$ for QC. The lesion volume decreased by $39 \pm 13\%$ for VP and $39 \pm 10\%$ for QC. In this case the average was done over 4, 6, 8, 10, 12 and 15 mm motion amplitudes.

Conclusion

Application of DDG was found to significantly increase the lesion SUVmax and decrease its volume with respect to non-gated images, by mitigating the blurring effects of respiratory motion, and to give more accurate representations of uptake as well.

Keywords: PET/CT, respiratory motion, small lesion, DDG, SUVmax and volume

The Usual, Searching for the Unusual in Ga-68-Dotatate Images

V. Soroa, E. Pegüino, M. del Carmen Alak, K. Quinteros

INTECNUS, MAT, CNEA, Argentina

Objective

Our patients were evaluated for the overexpression of the Somatostatin receptors (SSTR) 2 with Ga-68 DOTATE PET/CT (Ga-DOTA), taking in account the biodistribution findings in the neuroendocrine tumours (NETs).

Methodology

The images were acquired with a PET/CT GE Discovery IQ model with CT for attenuation correction and anatomical localization.

Patients were orally hydrated and discontinued Somatostatin medication. An I.V. injection of 0.04mCi/Kg, with a minimum dose of 4mCi (1.400 MBq)/patient of labelled Ga-DOTA was administered. Whole body images were acquired 45/60 minutes after the injection.

During this study 23 baseline scans and 2 follow-up Ga-DOTA scans were recorded, 15 females, 8 men, with ages between 21-74 years old.

Suspected diagnoses with either biochemical evidence or symptoms: 1 paraganglioma/pheochromocytoma, 1 paraneoplastic syndrome with oncogenic osteomalacia in search of the primary, 4 lung NETs, 1 insulinoma and 15 gastroenteropancreatic NETS; with uncertain conventional images to identify pathology, progression or new lesions.

Results

Normal Ga-DOTA uptake was seen in organs expressing the SSTR receptors including the; hypophysis, salivary glands, thyroid gland, residual thymic tissue, liver, spleen (including accessory splenic tissue), adrenal glands, kidneys, breast, uterus and pancreatic activity which could be diffuse or focal. Renal excretion of tracer was noted in the urinary tract. Low grade physiological uptake was seen in areas of inflammation including lymph nodes after COVID-19 vaccination, recent surgical scars and adenomatoid thyroid. Pathological uptake was seen a known meningioma. One adrenal metastasis was identified on a follow-up scan on which this lesion had an increase of SUV_{max} by 20%. This lesion was confirmed histologically.

The paraganglioma/pheochromocytoma patient with abdominal surgery had multiple bone metastases and recurrence in cervical lymph node.

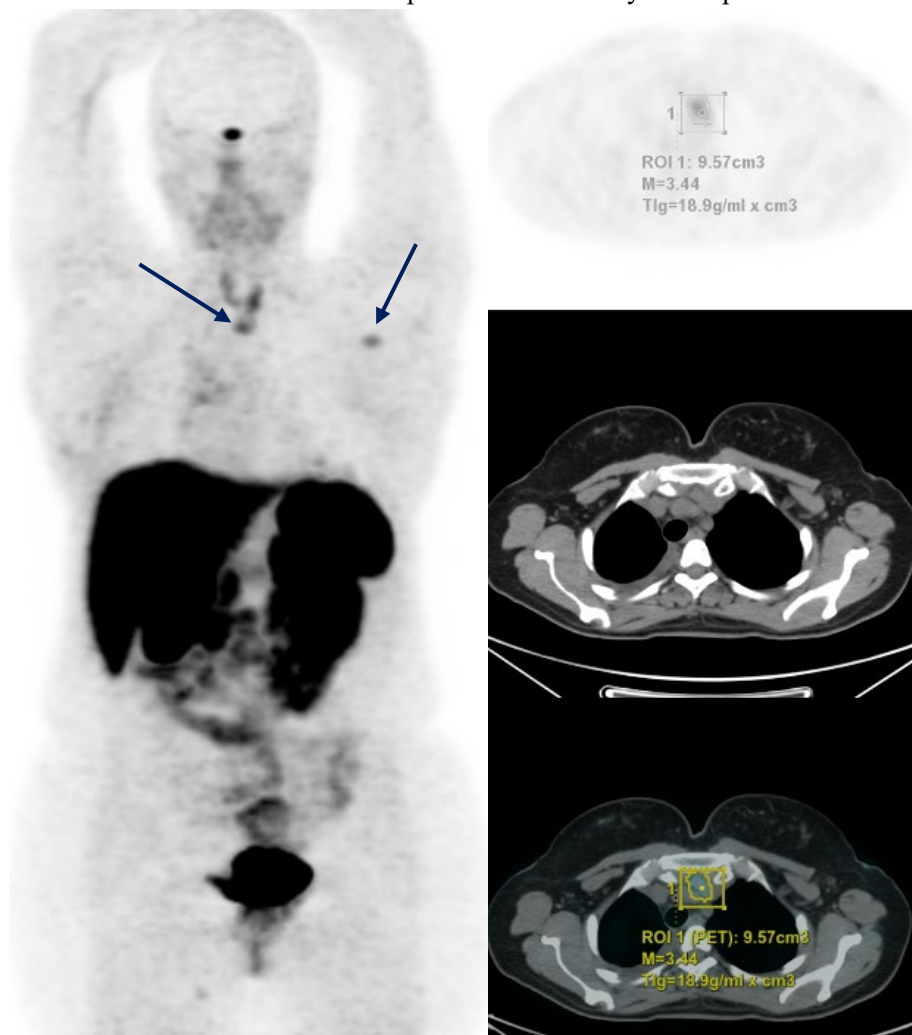
The Ga-DOTA scan was unable to detect the primary lesion in the patient with paraneoplastic osteomalacia however, the scan detected multiple bone metastases initially which was not detected on the follow-up scan.

In the four patients with lung NETs, two had stable disease, one developed mediastinal and bone metastases and one developed hepatic metastasis.

The Ga-DOTA scan was negative for the insulinoma patient.

The 15 patients with gastroenteropancreatic NETS had varying imaging findings. One patient had abnormal pancreatic activity and two liver metastases. Three patients known with pancreatic NETs progressed with liver metastases. Four patients had colon tumours they presented with abnormal uptake

in liver lesions, retroperitoneal, para-uterine and mediastinal lymph nodes. One of the two patients with rectal disease had stable disease the other had a partial response to treatment with a decrease in the SUVmax. Abnormal Ga-DOTA uptake localised only to the prostate was seen in several cases.



Normal receptor activity in Hypophysis, Thymus, Thyroid and Covid adenopathy

Conclusion

Knowledge of physiological biodistribution of SSTRs in body tissues facilitated the final diagnoses.

Diagnostic performance of [⁶⁸Ga]Ga-FAPI in signet ring cell carcinoma stomach in comparison to FDG: An initial experience

M. Gupta, U. Batra, P. S. Choudhury, S. Goel, V. Goel, S. Goyal, G. Gupta, S. Singh, S. Swamy M S, V. Talwar

Department of Nuclear Medicine, Rajiv Gandhi Cancer Institute and Research Centre, Delhi, India

Background

Signet ring cell carcinoma (SRCa) imaging is challenging due to the known limitations of FDG PET/CT. Hence, identifying new targets with better diagnostic capabilities is an unmet patient need. Fibroblast activating protein (FAP) expressing cancer-associated fibroblasts (CAFs) makes a significant component of most epithelial tumours. In recent times, FAP inhibitors (FAPI) have been found to be promising for theranostics in many cancers. Here, we present our initial experience of [⁶⁸Ga]Ga-FAPI-46 PET/CT in SRCa stomach compared to FDG PET/CT.

Methodology

This is an initial experience of an ongoing prospective open-label single institutional study (RES/SCM/59/2023/54). This data set includes 21 histologically proven stomach SRCa (13 stagings and 8 recurrences) with both FAPI and FDG PET/CT available. The single voxel maximum standard uptake value (SUV_{max}) of the primary, lymph node, metastasis, and the right lobe of the liver (as background) were recorded. Histopathological correlation was done for metastasis (M stage) and recurrence accuracy. Wilcoxon's signed-rank test was used to compare SUV_{max} and target-to-background ratio (TBR), while McNemar's test was used to compare the diagnostic performance of two modalities. ROC curve was generated for FAPI to find out the best SUV_{max} cutoff for recurrence prediction.

Results

Out of 13 staging SRCs patients, FDG showed peritoneal metastasis in 3/7 patients with diagnostic sensitivity, specificity, PPV, NPV and accuracy of 42.8%, 100%, 100%, 60%, and 69.2%. Meanwhile, FAPI detected all 7/7 peritoneal metastases with 100% diagnostic accuracy. Mean±SD TBR of primary (1.53±0.53 Vs 7.2±4.65) and node (0.69±0.37 Vs 3.31±3.21) for FDG Vs FAPI showed significant difference (P value <0.05). For recurrence, FDG detected 3/5 while FAPI detected 5/5 cases with diagnostic sensitivity, specificity, PPV, NPV and accuracy of 60%, 33.3%, 60%, 33.3%, 50% and 100%, 66.6%, 83.3%, 100%, 87.5% for FDG and FAPI respectively. Mean ± SD TBR of the recurrent site (1.44±0.79 Vs 7.61±4.18) for FDG Vs FAPI showed a significant difference (P value 0.028). ROC curve analysis showed the best cutoff of >4.3 SUV_{max} for FAPI with sensitivity 100% and specificity 66.6% (AUC 0.933, P value <0.001) for recurrence.

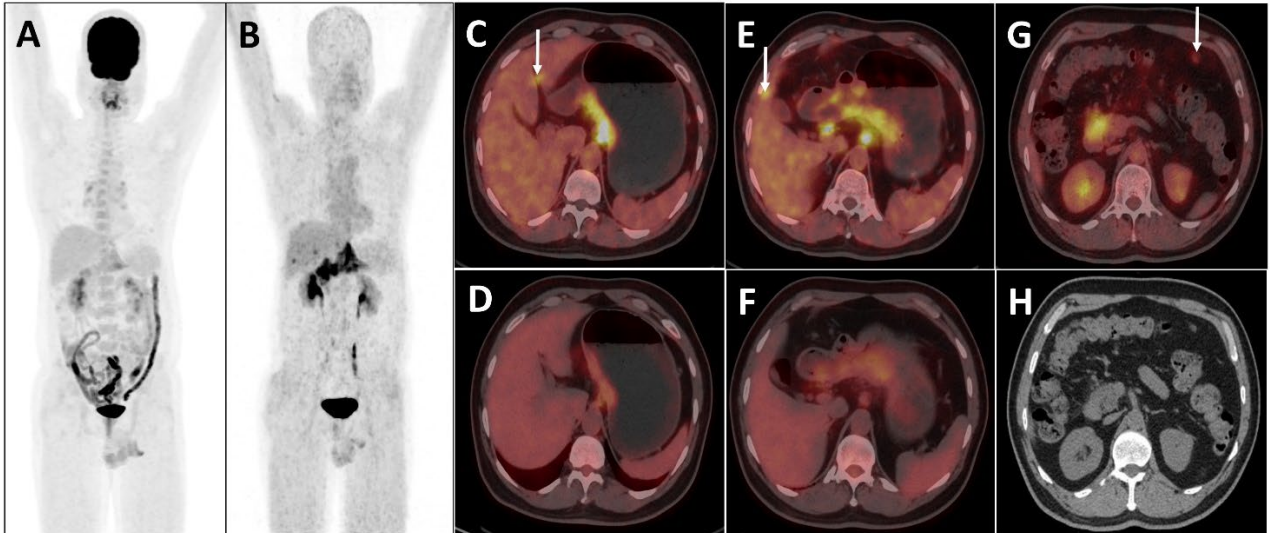


Figure 1. [^{18}F]FDG and [^{68}Ga]Ga-FAPI PET/CT maximum intensity projection (image A and B), fused axial (image C, D, E, F and G) and CECT axial image (image H).

A 47-year-old male with signet ring cell carcinoma stomach, whole body FDG PET/CT with CECT abdomen for staging showed mildly avid advanced stomach lesion with regional lymph nodes (image A, D, F). [^{68}Ga]Ga-FAPI PET/CT revealed strongly avid advanced stomach lesion with regional lymph nodes, and peritoneal deposits in peri-hepatic, falciform ligament and omentum (image B, C, E, G, H). A diagnostic laparoscopy was positive for peritoneal metastasis.

Learning points: FAPI PET/CT showed peritoneal disease and had better target to back-ground ratio.

Conclusions

FAPI PET/CT was found to have significantly better diagnostic performance for M staging and recurrence for SRCa of the stomach. Our initial experience showed a promising impact of FAPI PET/CT in tailoring the diagnostic laparoscopy and management of SRCa patients.

[⁶⁸Ga]Ga-FAPI PET/CT in the Evaluation of Gastric Cancer: Comparison with [¹⁸F]FDG PET/CT

I. Kostadinova, P. Bochev, G. Mateva, N. Novoselska, M. Garcheva-Tsacheva

Clinic of Nuclear Medicine, University Hospital Acibadem City Clinic Mladost, Bulgaria

Background

Gastric cancer (GC) is the fifth most common malignant tumour and the third most common cause of cancer death in the world. Therefore, accurate diagnosis, staging and restaging are crucial for planning of appropriate therapy strategy. [¹⁸F]FDG PET/CT is often used for staging and preoperative evaluation of GC but it has been reported to have a low detection rate especially in some histological types, such as signet-ring cell, mucinous and poorly differentiated adenocarcinoma and moreover specificity is relatively low, because of physiologic uptake within gastric wall and false positive result in gastritis. Therefore other more sensitive radiopharmaceuticals are needed in the evaluation of GC. Recently radiolabeled inhibitors of fibroblast activation protein, such as [⁶⁸Ga]Ga-FAPI were used to visualize FAP-expressing tumours, including not only their primary sites but their metastases, as well. The role of [⁶⁸Ga]Ga-FAPI PET/CT in patients with GC is now under evaluation in few reports. The aim of the study was to evaluate the role of [⁶⁸Ga]Ga-FAPI PET/CT in GS for staging and restaging and to compare the results with [¹⁸F]FDG PET/CT.

Methodology

Twenty-eight patients-Pts (18 men and 10 women, aged 38-71, in the stages between T3-4 N1-3 and M0-1) with histologically proven gastric cancer, were recruited for the investigation within the period 2021-2023. They underwent [⁶⁸Ga]Ga-FAPI PET/CT (2MBq/kg) for staging- in 9 of them and for restaging in 19 with as a whole 50 investigations. In 16/28 of the patients [¹⁸F]FDG PET/CT (2MBq/kg) was also performed with as a whole of 21 investigations.

Results

Normal result, without evidence of metastases was registered in 10 of the patients after surgery/chemotherapy/immunotherapy and in 18 Pts- metastases were found in regional and/ or distant lymph nodes, liver, peritoneum or lung (Fig.1). In 7/18 of the Pts (37.5% of the cases) investigated with both radiopharmaceuticals, more lesions were found with [⁶⁸Ga]Ga-FAPI PET/CT, mostly in peritoneum and abdominal lymph nodes, as in 5 of them histological type of the tumours was mucinous or signet ring cell. There was a better contrast with [⁶⁸Ga]Ga-FAPI, with SUV_{max} of the primary tumour of 13.5 and 7.9 of the metastases, compared with SUV_{max} of 2.8 of the metastases with [¹⁸F]FDG / without focal activity of the primary tumour.

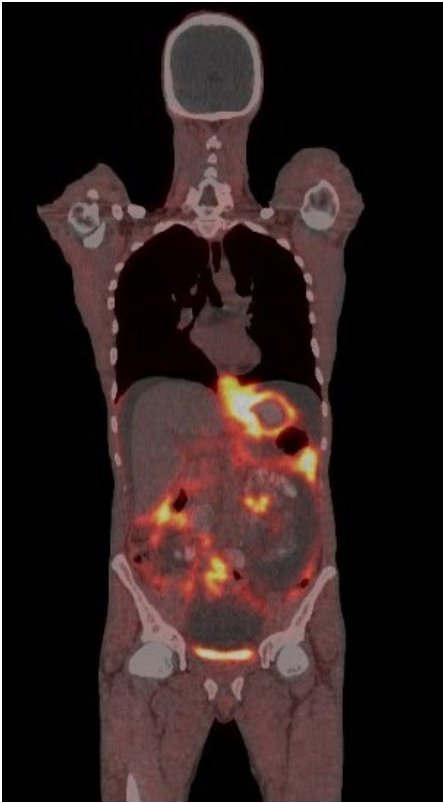


Figure 1. [^{68}Ga]Ga-FAPI-46 PET/CT in a patient with a gastric cancer, peritoneal carcinomatosis and ascites, T4N2M1

Conclusion

According to our preliminary data, we consider that [^{68}Ga]Ga-FAPI PET/CT is a very promising tool for evaluation of patients with advance GC, more sensitive than [^{18}F]FDG PET/CT and could be recommended as a method of choice for staging and restaging in order to plan the most appropriate therapy.

The Role of SPECT and SPECT/CT Somatostatin Receptor Scintigraphy in the Management of Gastric Neuroendocrine Neoplasms

J. Petrovic, M. Veljkovic, S. Odalovic, I. G. Milojevic, M. Stojiljkovic, M. Petrovic, D. S. Saranovic, V. Artiko

Center for Nuclear Medicine, University Clinical Center of Serbia, Faculty of Medicine
University of Belgrade, Serbia

Aim

The aim of the investigation is assessment of the role of somatostatin receptor scintigraphy (SRS) in the management of gastric neuroendocrine neoplasms (NENs). Indications for investigation were diagnosis of primary tumours, follow-up after the therapy and for the assessment of the appropriate choice of treatment.

Methodology

From 39 investigated patients, 8 had confirmed enterochromaffin-like (ECL) cells tumour, one serotoninoma, two gastrinomas and 28 had confirmed NENs. Tumours were classified as grade (G) NENs G1 (n=9), NENs G2 (n=21) and NECs G3 (n=9). Somatostatin receptor scintigraphy (SRS) with SPECT (n=24) and SPECT/CT (n=15) was performed 2h and 24h after i.v. administration of 740 MBq [^{99m}Tc]EDDA/HYNIC TOC. SPECT was performed during 15 min with two detectors, rotating around the patient 180 degrees each, in step and shoot mode, at the angle of 5 degrees per position. In 15 patients SPECT acquisition was followed by CT of the region of interest, with MPR reconstruction and attenuation correction. SPECT matrix was 128x128.

Results

From the total of 39 patients, 16 had true positive (TP), 14 true negative (TN), 5 false positive (FP) and 4 false negative (FN) findings. FP findings were caused by recent surgery (n=3) or local inflammation (n=2), while 2 FN findings were caused by the small size of the lesion (less than 1 cm) and 2 by poorly differentiated tumours. Sensitivity was 80,00%, specificity 73.68%, positive predictive value (PPV) was 76.19%, negative predictive value (NPV) was 77.78% and accuracy 76.92%. SPECT/CT contributed in 7/15 patients, in 5 confirming the positive finding (Krenning score 2) and in 2 excluding it in comparison to SPECT. In 8 patients Krenning score was 4, in 6 patients it was 3 and in 2 it was 2. There was significantly ($p < 0.05$) higher number of increased CgA values in TP than in TN patients. Mean Ki 67 value in TP patients was $9.11 \pm 6.89\%$, while in TN patients it was 4.14 ± 1.83 , which is not significantly different at $p < 0.05$ (the t-value is 1.48318, the p-value is 0.080094). In 17 patients (43.6%) SRS changed the management of the patients (in 10 surgery was repeated, in 5 somatostatin analogue therapy was introduced and in 2 peptide receptor radionuclide therapy).

Conclusion

In conclusion, our results confirmed the value of SRS in the diagnosis and follow-up of the patients with gastric NENs after surgery, if recurrences or metastases are suspected, as well as for appropriate choice of the therapy.

Utility of PET/CT in staging colorectal cancer, a comparison with CT

D. Z. H. Oliver

INCan, Mexico

Objective

Determine the usefulness of PET/CT with [18F]FDG versus Computed Tomography of three regions (thorax, abdomen and pelvis), in the initial staging of patients diagnosed with colorectal cancer.

Methodology

A retrospective and analytical study was carried out; in which all cases of patients with colorectal cancer who underwent staging PET/CT and CT were included, with a difference between studies of less than three weeks, within a private hospital in Mexico.

It was determined from these cases through the file:

- Gender
- Age at diagnosis
- Primary tumour site and histological type.
- Date of PET/CT and CT for staging.

These cases were also evaluated using the dedicated PET/CT workstation and Carestream Health:

- Primary lesion (whether identified or not, size and SUVmax).
- Secondary lesions (whether identified or not, location, number, size and SUVmax).

Results

A higher prevalence of the disease was found in males (60%), with a median age at diagnosis of 64 years. 73.3% of the tumours developed in the left colon (including the rectum) and 100% were epithelial tumours of the adenocarcinoma type. PET/CT identified 73.3% of primary lesions (vs. 53.3% by CT) and 66.7% of regional lymph nodes (vs. 33.3% by CT). It also managed to identify 9 cases with distant metastatic disease (vs. 5 by CT). Therefore, PET/CT changed the N staging of 8 patients (5 increased their staging and 3 decreased) and the M staging of 4 patients (all with an increased staging).

When evaluating the N staging by PET/CT and CT, the number of affected nodes was taken into account, according to the TNM classification, taking as positive in the case of PET/CT, those that were avid for the FDG and quantitatively a higher SUVmax than the vascular pool; while for CT, those with a short axis diameter greater than 10 mm were considered positive. Derived from this analysis and comparison, the change in the staging of 8 patients results; In those patients who had a decrease in their staging (3), no FDG avidity was observed in the nodes that were referred to as positive by CT, and/or the SUVmax was lower than the vascular pool.

In the semiquantitative analysis, the average SUVmax of the primary lesions identified was 8.39; finding a significant correlation between this value and the laterality of the primary tumour; where right colon tumours, which are associated with molecular characteristics with a worse prognosis, presented higher SUVmax values; without finding a significant correlation with the staging of the patients.

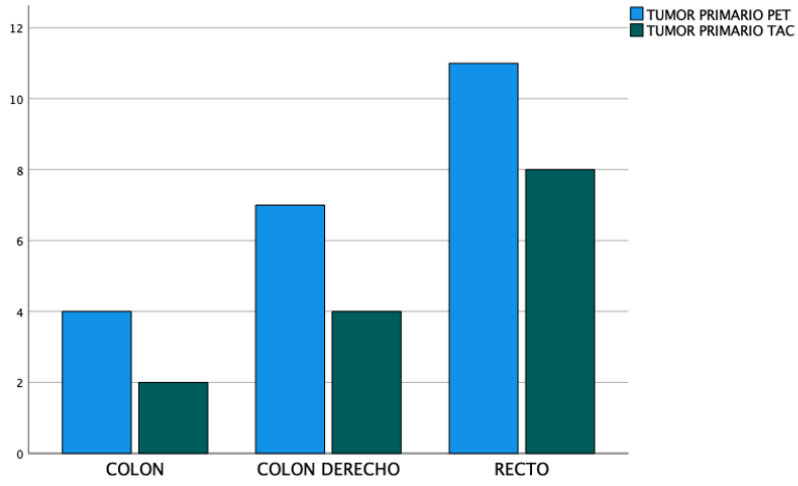


Figure 1

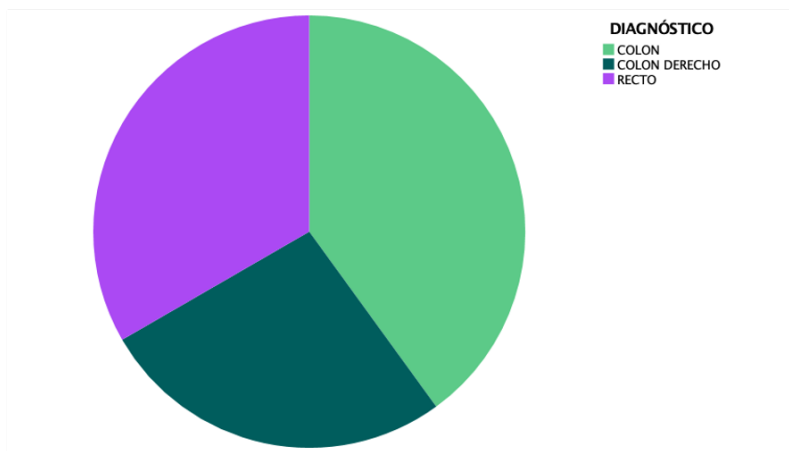


Figure 2

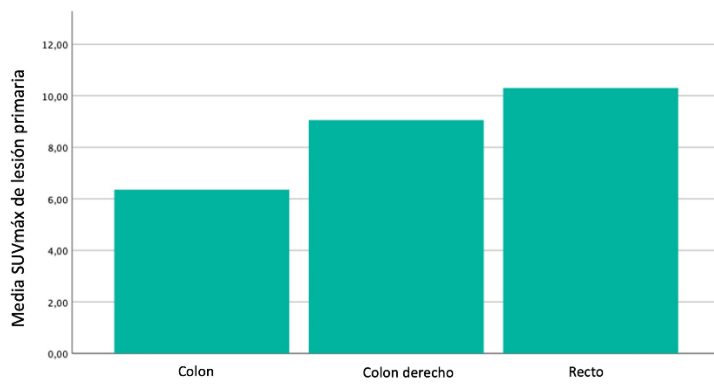


Figure 2

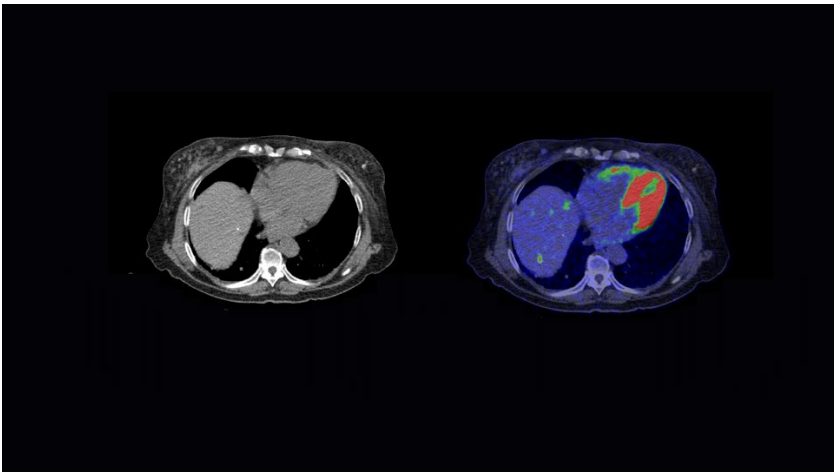


Figure 3

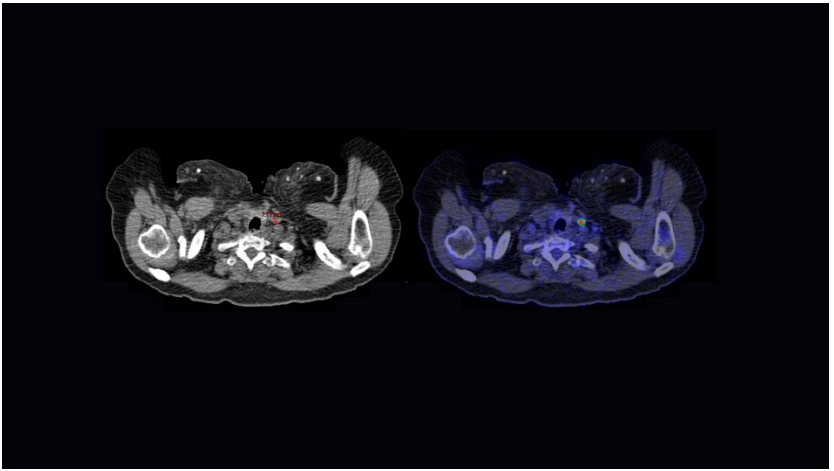


Figure 4

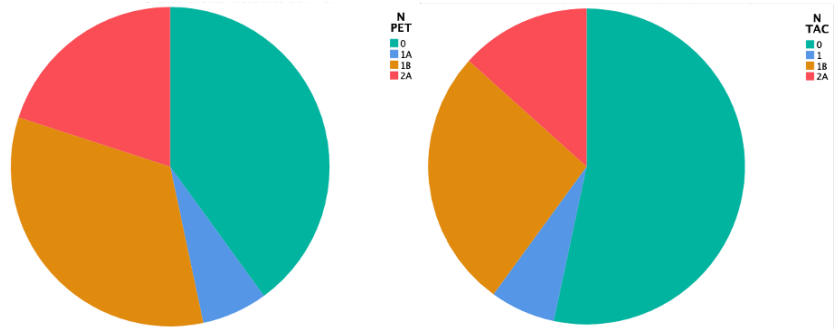


Figure 5

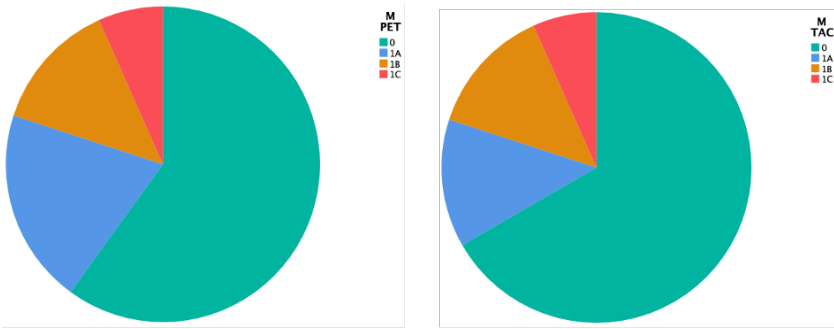


Figure 6

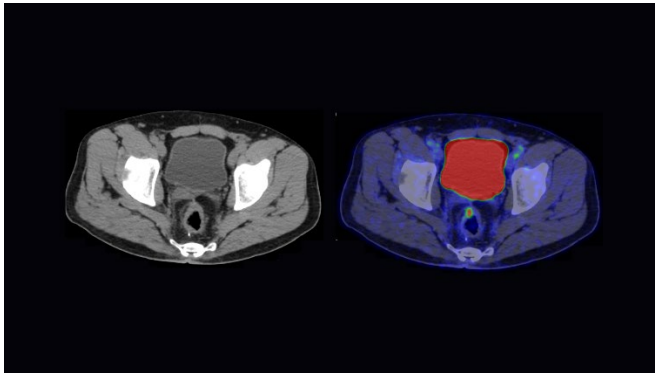


Figure 9

Conclusion

In the staging of patients with colorectal cancer, PET/CT proved to be more efficient in detecting primary and secondary lesions versus three-region CT. Additionally, the lymph node and metastatic staging changed in 8 and 4 patients respectively, which has been shown to have a direct prediction on patient survival and mortality.

Quality Management of SPECT Equipment for Nuclear Medicine Practice

H. Ndagire, E. Okello

Uganda Heart Institute, Mulago Hospital, Uganda

Two and three dimensional(2D) images can be obtained using common imaging equipment called single-photon emission computed tomography (SPECT).

The nuclear medicine department's quality control division is crucial since it makes sure that there is as little radiation exposure as possible throughout imaging procedures. Image quality is directly impacted by the fundamental functionality of nuclear medicine equipment, which helps to shape high-quality diagnostic images. the methods for ensuring the quality of nuclear medicine, which include the use of imaging and non-imaging devices to precisely measure and identify radiation.

The aim of this study is explain and summaries the standard nuclear medicine quality control (QC) procedure to achieve consistent and high standard diagnostic image quality and describe the routine quality control procedures for the gamma camera to obtain high-quality diagnostic images

The GC acquires 3D images by rotating around the patient at various angles, known as projection from zero to 360 degrees. These features help to see more details to overcome any uncertainty presented by 2D images. In SPECT-CT, computed tomography (CT) components improve the attenuation correction to enhance image resolution and anatomical localization. It is critical that all aspects of the QC procedure, including 2D and 3D, will be performed frequently on various frequencies to upkeep the consistent reproducibility of acquired images.

Daily checks for energy peaking, background radiation, and crystal uniformity with a collimator are recommended (extrinsic uniformity). Flood field source made of Cobalt-57 (Co-57), which has a half-life of 272 days and gamma energy of 122 keV is used for daily uniformity checks of crystal (extrinsic uniformity).

Co-57 based flood field source is recommended as its gamma energy is near Tc-99m (140 keV). Any issue with uniformity will be rectified as it can deteriorate the overall diagnostic quality of images. CT warm-up is performed daily to ensure that the x-ray tube is working correctly. The SPECT-CT mechanical and software center is evaluated weekly by checking the Center of Rotation (COR). Intrinsic uniformity is checked once a week to ensure that the crystal performs appropriately. The integral uniformity(IU) at the center field of view(CFOV) and valuable field of view(UFOV) is calculated using the following formula:

$$\%IU = \frac{\text{Maximum counts of pixel} - \text{Minimum counts of pixel}}{\text{maximum counts of pixel} + \text{minimum counts of pixel}} \times 100$$

GC spatial resolution is checked annually with the help bar phantom and Jaszczak phantom. SPECT-CT registration is checked with the help of a gadolinium-153 radioactive source.

Quality control is a collaborative endeavour involving all members of a department, rather than an individual duty. Given the possibility of radiation exposure in an NM department, it becomes much more crucial. Any small defect in quality control can have a detrimental effect on the overall diagnostic quality of pictures, increasing the radiation exposure of patients. Radiologist, nuclear medicine technologist, radiology manager, nurses, service engineers, medical physicists, and administrative personnel are among the team members who will

actively engage in the QA plan. Maintaining standard services and lowering the risk of QC failure can be accomplished through regular meetings and an evidence-based strategy.

Sentinel lymph node effectiveness in patients with endometrial carcinoma treated at the Gynecological Oncology Service of the "Dr. Alejandro Dávila Bolaños" Military School Hospital and Nora Astorga National Center for Radiotherapy January to December 2023

V. E. Rosales Obregón^{1,2}, O. Marin², C. Corea²

¹ National Radiotherapy Center, Nora Astorga Hospital, Nicaragua

² Dr. Alejandro Davila Bolaños Military School Hospital, Nicaragua

Background

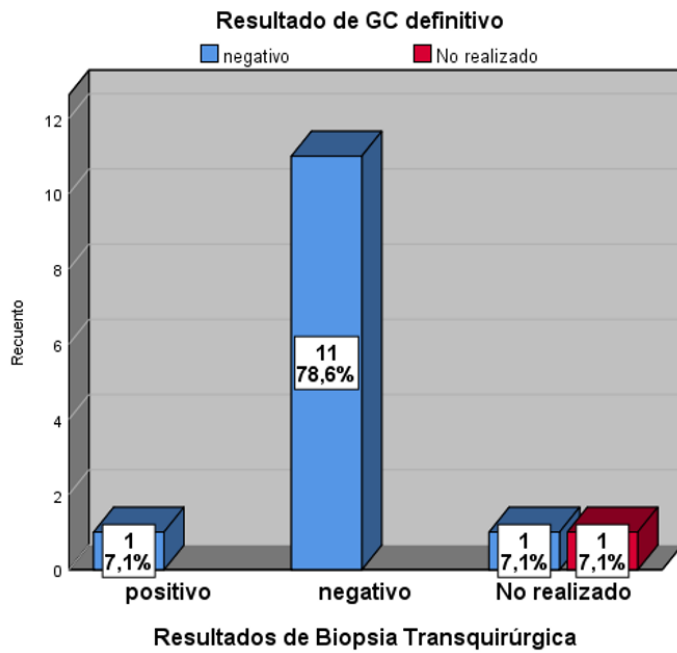
A case series study was carried out in the Department of Gynaecological Oncology of the Military School Hospital “Dr. Alejandro Dávila Bolaños” during the period from January to December 2023 whose objective was to evaluate the effectiveness of sentinel lymph node detection in patients with endometrial carcinoma in early stages, whose usefulness is being evaluated through multiple publications in the world and in our country constitutes the first experience of application of Such a technique in pathologies other than breast cancer or melanoma where its use is widely validated.

Methodology

An observational, descriptive, prospective, cross-sectional, and analytical design was applied. A total of 14 patients with endometrial carcinoma who met the inclusion and exclusion criteria were included, and a lesion analysis of a sample of 50 lymph nodes was performed. The data obtained were processed in the SPSS v25 program, presented in descriptive and contingency statistics tables for the analysis of diagnostic tests.

Results

A mean age of 55.70 ± 9.286 years was presented. Urban areas predominated, with university and high school education, professional and housewife, married. Clinical characteristics were described: obese, with abnormal uterine bleeding, late menopause, nulliparity, presence of diabetes mellitus, and arterial hypertension. The detection of sentinel lymph node in sentinel lymph node imprint biopsy with double detection technique using methylene blue and ^{99m}Tc lymphofast had a sensitivity of 81%, specificity 100.0%, PPV (+) 100.0%, PPV (-) 90.0%. An association was established between the result of sentinel lymph node imprint biopsy and the result of the definitive biopsy $p=0.040$ with statistical significance. Only 4 cases with pelvic lymphadenectomy.



	GC Biopsia impronta*	GC Biopsia impronta * Linfadenectomía
Sensibilidad	0,0%	81,0%
Especificidad	91,6%	100,0%
VPP (+)	0.0%	100,0%
VPP (-)	100,0%	90,0%
Verdadero positivo (VP)	0	1
Falso positivo (FP)	1	0
Verdadero negativo (VN)	11	10
Falso negativo (FN)	0	1

Conclusion

A significant impact on the effectiveness of sentinel lymph node detection in patients with endometrial carcinoma in early stages treated at the Gynaecological Oncology Service of the "Dr. Alejandro Dávila Bolaños" Military School Hospital (HMEADB) during the period from January to December 2023 was evidenced with the dual application with methylene blue and Technetium 99.

Clinical uses of 99m Tc Tektrotyd somatostatin receptor SPECT/CT

M. Garcheva-Tsacheva, G. Mateva, I. Kostadinova, P. Bochev

Clinic of Nuclear Medicine, University Hospital Acibadem City Clinic Mladost, Bulgaria

Background

Somatostatin-receptor imaging is an important part of the diagnosis, treatment planning and follow-up of patients with neuroendocrine tumours (NET.) There are multiple radiopharmaceuticals available for accessing somatostatin receptor overexpression (especially SSTR2 subtype). We aimed to summarize our experience with [^{99m}Tc]Tektrotyd, since it has not been so widely used, especially for controlled studies, in comparison with ¹¹¹In-Octerotide and [⁶⁸Ga]DOTA, and the information regarding indications and clinical performance is scarce.

Methodology

We retrospectively reviewed all the studies performed with [^{99m}Tc]Tektrotyd in our department during 2023. The examinations were carried out 2-4 hours post i.v. administration of 555 MBq 99m TcEDDA/HYNIC-TOC (Tektrotyd, Polatom). All the patients had whole body planar scintigraphy, followed by SPECT/CT of the neck and chest and/or abdomen and pelvis, depending on the diagnosis and the findings from the scintigraphy. 22 patients were examined in total (11 men and 11 women, aged 36-80). We identified 3 groups of patients according to the indication for the study, In group 1 patients (n=5) were referred for NET screening because of clinical symptoms - suspicion for tumour induced osteomalacia, high chromogranin level or suspicion for adrenal tumours (Cushing syndrome, hypertensive crisis). In group 2 patients(n=9) the examination was combined with [¹⁸F]FDG PET/CT in one month period, because of intermediate level of differentiation - Ki 67 >5% or disseminated disease (sometimes in presence of secondary tumour), for accessing receptor status and disease heterogeneity. The rest of patients (n=8), group 3, were with known and treated NET and 99m Tc Tektrotyd SPECT/CT was done as a follow-up study.

Results

In the group referred for NET screening all of the 99m Tc Tektrotyd SPECT/CT studies were negative and provided no additional clinical information. In group 2 we visualized in 2 out of 9 patients both: somatostatin-receptor positivity and FDG-avidity. This patients were with Ki 67-2% but disseminated disease and the positive FDG PET was useful for their treatment adjustment and determined their worse prognosis. In all of the patients who were proved to have only FDG-avid disease (n=7, all with Ki 67 > 10%) and no somatostatin-receptor expression, the [^{99m}Tc]Tektrotyd was excluded from the follow-up, as well as Somatostatin analogues from therapy. In the follow-up group all of the patients had stable disease – either no progression of metastatic disease or no evidence of recurrence after radical treatment.

Conclusion

99m Tc Tektrotyd SPECT/CT is useful examination for visualization of somatostatin- receptor expression, especially having in mind cost effectiveness, availability and radiation burden. It is important for therapy, as well as for follow-up selection. The combination with [¹⁸F]FDG PET/CT gives additional information about disease heterogeneity, prognosis and treatment approach.

Assessment of Knowledge and Attitudes of Radiographers Towards Radiation Protection Awareness and Dose Reduction in Tanzania

J. Ndumbaro¹, L. Haule², E. Mmanyi³

¹ Department of Radiology & Imaging, EMMH, Dar es Salaam, United Republic of Tanzania

² Mbeya Regional Referral Hospital, United Republic of Tanzania

³ Charles Kulwa Memorial Hospital, United Republic of Tanzania

Background

The use of ionizing radiation is associated with a risk inducing malignant disease and causing eye damage to the patient and the personnel. Radiation protection awareness, knowledge and attitudes is essential for medical personnel in ensuring that possible risk do not outweigh the benefits of medical diagnostic imaging. This study aimed to assess the knowledge and attitude of radiographers towards radiation protection awareness in Tanzania.

Objectives

The objective of this study was to assess the current knowledge and attitudes of radiographers towards radiation protection awareness and dose reduction in Tanzania.

Methodology

A cross-sectional study was carried out among practicing radiographers in five selected hospitals in Tanzania. The study was carried out from February to October 2023. The survey comprised of 25 questions involving socio-demographic information and general information related to radiation protection and dose reduction. Data were analysed statistically using the statistical Package For Social Sciences (SPSS).

Results

A total of 120 radiographers participated in the study (25% females and 75% males). Most of the participants (95%) were aware of radiation protection and dose reduction. The analysis based on participant characteristics in relation to overall knowledge and attitudes of radiographers towards radiation protection awareness and dose reduction.

Conclusion

The results demonstrate that radiographers have an overall good knowledge and understanding the effect of radiation with academic education having a significant influence on their daily activities performance.

Keywords: Knowledge, Attitudes, Radiation Protection, Awareness Dose reduction

PET Imaging: Comprehensive Simulation Software and Iterative Algebraic Reconstruction Advancements

M. Taube, S. J. Sciutto

CIT Santa Cruz CONICET / Facultad de Cs. Exactas, Universidad Nacional de La Plata,
Argentina

Background

In recent years, studies using PET/CT scanners have proven to be a valuable tool for enhancing medical diagnostics. Data acquisition procedures and reconstruction algorithms are key factors in improving the diagnostic capability of these studies.

The aim of this work is to develop comprehensive simulation software covering all stages of the image generation process. To simulate the interaction processes between radiation and matter, utilizing custom-developed routines for a chosen phantom. In this case, we have worked with a NEMA phantom. In this case, simulations have been performed on an ideal PET/CT system, neglecting effects such as spurious events, noise, etc., with the purpose of providing an advantageous environment to clearly highlight the characteristics of the reconstruction algorithm.

The simulation-reconstruction chain can be divided into smaller steps where simulation data is collected in maps of activity. Once the activity map is simulated, a reconstruction algorithm is applied to the activity map, such as the iterative algebraic method Maximum Likelihood Expectation Maximization (MLEM).

Results

The result of the reconstruction process is a three-dimensional map of reconstructed activity. It is important to remind that having data generated at all stages of image reconstruction allows for useful comparisons to assess the quality of the reconstruction process. This work discusses the current state of development of the mentioned software and presents some initial results, with the primary goal of improving the diagnostic capability of PET/CT studies and serving as a valuable tool for nuclear medicine.

FDG PET/CT in melanoma

I. G. Milojevic, S. Odalovic, M. Stojiljkovic, J. Petrovic, M. Veljkovic, D. Sobic-Saranovic, V. Artiko

Clinical Center of Serbia, University of Belgrade, Serbia

Objective

To evaluate the usefulness of [¹⁸F]FDG PET/CT in patients with advanced melanoma.

Methodology

This study included 230 consecutive melanoma patients who were sent for the [¹⁸F]FDG PET/CT. The inclusion criteria were: histopathologically verified melanoma stage III or IV; absence of other malignancy / infection; glycemia ≤ 11 mmol/l. The final study population consisted of 200 patients. After the first [¹⁸F]FDG PET/CT, the follow-up was performed after 8 ± 12 months, for therapy response evaluation.

Results

Pathological findings were present in 140 patients. Sensitivity of [¹⁸F]FDG PET/CT was estimated as 99%, specificity as 47%. Comparing to previous MDCT, [¹⁸F]FDG PET/CT upstaged 44% patients, especially these with widespread disease. Majority of patients had lower extremities as primary localization of disease. SUV max and inguinal disease localization (local recurrence) were independent predictors of progression free survival (HR 1.02, CI 1.00-1.11, $p < 0.05$), (HR 11.06, CI 1.11-126.00, $p < 0.05$), respectively.

Sixty patients came to the follow-up. Follow up [¹⁸F]FDG PET/CT revealed stable disease in 40%, partial remission in 7%, progression of disease in 38% and complete remission in 15% patients. Perhaps the higher number of relapses was caused by later responses to immunotherapy and short-term responses to target therapy. Therapy type (immunotherapy or target therapy) did not correlate significantly with the [¹⁸F]FDG PET/CT follow up result ($p = 0.752$, $\rho = -0.346$).

Conclusion

[¹⁸F]FDG PET/CT has good sensitivity in evaluation of advanced melanoma. Small lesions and brain localization reduce the specificity of the examination. SUV max and locally advanced disease can be predictors of PFS. Follow up [¹⁸F]FDG PET/CT should be done at least on 6 months period, only if there is suspicion of presence of active disease.

Keywords: advanced melanoma, [¹⁸F]FDG PET/CT

Importance of the hybrid SPECT/CT imaging in the differential diagnosis of cardiac amyloidosis

D. S. Saranovic, V. Artiko, I. G. Milojevic, S. Odalovic, J. Petrovic, M. Stojiljkovic, M. Veljkovic, N. Vujosevic

Faculty of Medicine University of Belgrade, Center for Nuclear Medicine with PET, University Clinical Center of Serbia, Serbia

Background

Differential diagnosis between transthyretin (ATTR) and light chain (LC) cardiac amyloidosis is important, because of different treatment options.

Aim: To evaluate the accuracy of bone seeking SPECT/CT method in the diagnosis and differential diagnosis of cardiac ATTR and LC amyloidosis in our Centre.

Methodology

From August 2017 to January 2024, one-hundred-fifteen patients (mean age 64 ± 14 range 19-90 years, 61 males) with heart failure with preserved ejection fraction (HFpEF) and echocardiography findings suspected for CA were included in the study. In 89 subjects whole-body scintigraphy (WBS) and SPECT/CT were performed 3 hours after i.v. application of 555MBq of [^{99m}Tc]Tc-DPD, while in 26 patients 1 and 3 hours planar chest and heart scans and 3 hours SPECT/CT were performed after i.v. application of 740MBq of [^{99m}Tc]Tc-PYP. Perugini grading scale was used for semi-quantitative assessment of the accumulation of radiopharmaceuticals in the extracellular space of the heart muscle on WBS. In 26 patients with [^{99m}Tc]Tc-PYP scintigraphy heart to contra lateral lung ratio (H/CL) was calculated. SPECT/CT was used to confirm or exclude the accumulation of radiopharmaceuticals in the extracellular space of the heart muscle. Myocardial biopsy and or laboratory findings and clinical follow-up were used as the gold standard for evaluation of the accuracy of the method.

Results

Findings of SPECT/CT in 115 patients were as follows: without accumulation of [^{99m}Tc]Tc-PYP or [^{99m}Tc]Tc-DPD (grade 0) in extracellular space of the heart muscle in 89 patients (77%), faint uptake (grade 1) in 6 patients (5%), moderate uptake similar to surrounding bone (grade 2) in 8 patients (7%) and high uptake (grade 3) in 13 patients (11%). 21 out of 115 patients (18%) had moderate to high uptake, and in 19 ATTRh or ATTRw was confirmed (90%). In two patients with moderate uptake, AL amyloidosis was confirmed, as well as in 5 patients with uptake on SPECT/CT. In comparison to WBS and planar chest and heart scintigraphy, SPECT/CT had added value in 3 patients with faint uptake, 2 patients with moderate uptake, and 11 patients with high blood pool uptake without accumulation in the extracellular space of the heart muscle. Overall sensitivity of SPECT/CT was 91%, specificity 94%, and accuracy 90%.

Conclusion

Our results indicate that SPECT/CT with bone-seeking radiopharmaceuticals has added value over planar and whole-body methods in 14% of patients and is more accurate for the evaluation of CA.

Acknowledgement

Funded by the European Union. Views and opinions expressed are however those of the author(s) only and do not necessarily reflect those of the European Union or the European Education and Culture Executive Agency (EACEA). Neither the European Union nor the granting authority can be held responsible for them. (EDUQUAN) ERASMUS-JMO-2021-HEI-TCH-RSCH
15 patients from this study are part of IAEA CRP ITAC (E13055).

Clinical Utility of Metabolic Tumour Volume (MTV) and Total Lesion Glycolysis (TLG) in Lymphoma using Artificial Intelligence (AI) in [¹⁸F]FDG PET/CT: an Initial Experience at Tertiary Care Hospital of Pakistan

H. Dilawar

Department of Nuclear Medicine and Molecular Imaging, Karachi Institute of Radiotherapy and Nuclear Medicine, Pakistan

Background

Metabolic Tumour Volume (MTV) and Total Lesion Glycolysis (TLG) are SUV based derived functional parameters which measure metabolic activity in an entire tumour mass to reflect tumour burden. Aims and Objectives: To calculate the MTV and TLG using artificial intelligence by automated Multi-Foci Segmentation Software (MFS), to compare baseline and post chemotherapy MTV and TLG in patient of Hodgkin's and Non-Hodgkin's Lymphoma

Methodology

We prospectively included 29 patients (mean age 49 ± 15.5 years, 21 males and 8 females) who underwent the baseline and post chemotherapy [¹⁸F]FDG PET/CT scan. Median difference of MTV and TLG at baseline and post-chemotherapy were explored using Wilcoxon sign rank test. Mann-Whitney U test was applied to find out the median difference of MTV and TLG among patients who reported Complete Metabolic Response (CMR) versus those who reported Partial Metabolic Response (PMR). Chi-square/Fisher Exact test was also applied to see the relationship of responses with baseline characteristics. The p-value of <0.05 was considered as significant.

Results

Of 29 patients, majority of the patients presented with Non-Hodgkin lymphoma 20 (69%) whereas 9 (31%) presented with Hodgkin lymphoma, 20 (69%) out of 29 patients showed CMR while 9 (31%) patients showed PMR. The median MTV at baseline and post-chemotherapy was significantly higher among patients who reported PMR as compared to those who reported CMR (p-value <0.05). Similarly, the median TLG at baseline and post chemotherapy was significantly higher among patients who reported PMR as compared to the patients who reported CMR (p-value <0.05).

Conclusion

The significantly high MTV and TLG values were noted at baseline and post chemotherapy in patients who reported PMR as compared to CMR.

Keywords: Metabolic Tumour Volume, Total Lesion Glycolysis, Multifoci Automated Segmentation, artificial intelligence, lymphoma, [¹⁸F]FDG PET/CT

Navigating Prostate Cancer Detection: A Comparative Analysis of Biparametric and Multiparametric MRI in Biopsy-Naive Patients

S. Ab Hamid, A. Awang, K. A. Mohd Ghani

Universiti Putra Malaysia, Malaysia

Background

Biparametric magnetic resonance imaging (bpMRI), consisting of T2-weighted imaging (T2WI) and diffusion-weighted imaging (DWI), has emerged as a promising alternative to multiparametric MRI (mpMRI), which includes dynamic contrast imaging (DCE), for identifying and guiding targeted biopsies in patients suspected of having prostate cancer (PCa). It is noteworthy that bpMRI lacks the capability to upgrade peripheral zone PI-RADS 3 to PI-RADS 4 without DCE.

Objective

This study aims to evaluate the efficacy of bpMRI compared to mpMRI in biopsy-naive patients with elevated prostate-specific antigen (PSA) levels and abnormal digital rectal examination results, scheduled for transperineal MRI/transrectal ultrasound fusion prostate biopsy (TFB).

Methodology

We conducted a retrospective single-center study involving 298 biopsy-naive patients who underwent PI-RADSv2.1-compliant mpMRI prior to TFB. Clinically significant prostate cancer (csPCa) was defined as ISUP grade ≥ 2 in any core. Two experienced radiologists independently assessed images based on PI-RADSv2.1 criteria, with separate evaluations for bpMRI and mpMRI sequences spaced three months apart. The reference standard was histopathology results from TFB.

Results

PI-RADS 3, 4, and 5 were scored in 32.2%, 38.6%, and 29.2% of cases, respectively. In the mpMRI/bpMRI test comparison, the detection rates of PCa and csPCa by bpMRI and mpMRI were comparable (51.3% vs. 57.9%, 44.0% vs. 48.0%, both $P > 0.05$), with no statistical significance. Twenty cases without cancer were upgraded to PI-RADS 4 on mpMRI, and four PI-RADS 3 cases with csPCa were not upgraded (bpMRI).

Conclusion

Both bpMRI and mpMRI exhibited comparable diagnostic efficacies in patients with clinical suspicion of prostate cancer, potentially addressing constraints related to time and contrast agent usage.

Overcoming Challenges in Establishing Nuclear Medicine Diagnostic Capabilities: A Case Study of Implementing PET/CT Services on a Remote Island like Mauritius without a Cyclotron

H. Sonea¹, M. Allarakha²

¹Jawaharlal Nehru Hospital Nuclear Medicine Dept Rose Belle Mauritius

²Ministry of Health and Wellness, Mauritius

Background

This case study explores the challenges encountered and successfully overcome in establishing nuclear medicine diagnostic capabilities, specifically the implementation of PET/CT services on the remote island of Mauritius. Despite the absence of a cyclotron facility on the island, the ambition to introduce PET/CT services was addressed through a strategic collaboration with CYROI (Cyclotron Réunion Océan Indien) in Reunion Island, located a mere 30-minute flight away. A memorandum of understanding is in the pipeline to facilitate the importation of [¹⁸F]FDG, the required radionuclide, leveraging the frequent and convenient flight connections.

Overcoming the hurdle of staff training was made possible through the support of the International Atomic Energy Agency (IAEA), which sponsored comprehensive training programs for various professionals, including doctors, technologists, physicists, and radiopharmacists. During the last IAEA coordinators meeting held in Mauritius, discussions ensued regarding the modality of training, highlighting the necessity for tailored programs suited to Mauritius' unique circumstances. It was agreed upon to utilize the IAEA's online Human Health Campus (DATOL) to implement comprehensive training for new recruits of nuclear medicine technologists. This approach was deemed essential as there are currently no institutions in Mauritius offering such specialized training. The Ministry of Health and wellness has been approached to provide local resource persons and identify a suitable institution to oversee and accredit this course. Attention was also turned to the challenges faced during the construction of the facility to house the PET/CT services.

The construction process revealed some shortcomings in designing a building conducive to efficient patient flow and lacked adequate space for essential infrastructure such as the UPS room. The multidisciplinary team, consisting of physicists, doctors, and technologists, collaborated to devise creative solutions, ensuring a seamless and functional environment for both staff and patients. Particularly, the team worked diligently to provide a comprehensive safety assessment report in line with the requirements of the Radiation Safety and Nuclear Security Authority. This ensured that the facility not only met diagnostic needs but also adhered to stringent safety standards, guaranteeing the well-being of both patients and staff. To validate the feasibility of importing [¹⁸F]FDG from Reunion, a dummy delivery was executed, simulating the transportation of radiopharmaceuticals over the short flight distance. The results demonstrated the practicality of such deliveries, taking into account the radioactive decay of the substance. This trial affirmed the viability of sustaining a consistent supply of [¹⁸F]FDG for the PET/CT services. The supply of radiopharmaceuticals from a local private hospital having a baby cyclotron as a support is also under consideration.

Conclusion

In conclusion, the establishment of PET/CT services on a remote island faced numerous challenges, from logistical issues to facility design constraints. However, the collaborative

efforts of the interdisciplinary team, coupled with strategic partnerships and innovative problem-solving, have triumphed over these obstacles. The case study underscores the proverbial wisdom that "where there is a will, there is a way," emphasizing the importance of determination and resourcefulness in overcoming challenges and realizing ambitious goals in the field of nuclear medicine.

Challenge of hybrid PET/CT technology in low- and middle-income countries. Impact of the PET/CT in Cuba and the advantage of its own cyclotron

L. R. Paleo¹, M. G. Cancio²

¹Hermanos Ameijeiras Hospital, Cuba

²Centro Especializado de Diagnóstico y Terapia (CEDT), Cuba

Background

The implementation of positron emission tomography combined with computed tomography (PET/CT) in low- and middle-income countries faces significant challenges, but also presents crucial opportunities for improving healthcare. The limited availability of financial resources hinders the acquisition and maintenance of PET/CT equipment.

Objective

Show the results of the implementation of PET/CT technology in Cuba with support from the IAEA and compare the studies before and after the implementation of the cyclotron.

Results

In Cuba, 2535 PET/CT studies have been carried out since the launch of the PET/CT equipment in a period of 7 years, of these 72% were carried out with [¹⁸F]FDG produced in the Cuban cyclotron in a period of 2 years. More than 90 percent of the studies were performed on patients with oncologic disease for staging. In 11 percent of patients, the course of action or staging changed when comparing the PET/CT result with other diagnostic studies.

Conclusion

The implementation of PET/CT technology in low- and middle-income countries poses challenges, but also offers opportunities to make a leap in the quality of medical care. Overcoming financial barriers and promoting global collaborations are essential to ensure that cutting-edge technologies are accessible to everyone, regardless of their economic location. The support of the IAEA was essential to assimilate the new technology through the training of human resources in experience centers. The learning curve had a rapid ascent as we were able to count on IAEA experts for advice on each of the key points to implement PET/CT hybrid technology. The technology was well received by healthcare physicians, mainly in haematology and oncology.

Migrated (OMENTAL) IUCD: A case report

H. M. Mohammed¹, U. A. Gwaram²

¹Department of Radiology, BAZE University Hospital Abuja, Nigeria

²Department of Surgery, BAZE University Hospital Abuja, Nigeria

Background

Contraception is an essential component of sexual and reproductive health issues used worldwide especially in Nigeria, which has a high fertility rate. The intrauterine contraceptive device (IUCD) is one of the most frequently used safe, effective, economical and reversible contraceptive method for most women regardless of their health status. However, many complications associated with the IUCD have also been described like migration to adjacent organs. Incidence of migration is about 0.5 to 1/1000 only 1. In this report, we present a complication of the IUCD in which the device perforated the uterus and migrated to the omentum.

Case Report

Mrs ZS, a 24-year-old housewife with one child who was referred from a peripheral hospital to the radiology department of BAZE University Hospital for Ultrasound and pelvic CT with a 3 day history of mild RIF abdominal pain with no other additional symptom. She had spontaneous vaginal delivery 7 weeks prior to presentation with IUD insertion a week ago. She experienced pain and bleeding during the IUCD insertion but was told it was normal. The pain continued which led to her referral. On presentation, she was calm, not pale, anicteric and not dehydrated. Pulse rate was 88bpm while her blood pressure was 120/80mmHg. Her abdomen was generally tender, but the tenderness was more marked at the right iliac fossa. Vaginal speculum examination was normal.

Ultrasound examination (FIG I) revealed an echogenic structure seen in-between the bowel loops which were thickened with no IUCD in the endometrial cavity. The CT Scanogram (fig II) showed the IUCD high up in the abdomen and axial images with coronal and sagittal reconstruction (fig III) showed the migrated IUCD entwined in omentum surrounded by bowel loops.

She was planned for exploratory laparotomy with IUCD removal which was successful (fig IV). She did not receive any blood transfusion. She received antibiotics, intravenous fluids and analgesics. She commenced oral intake and was discharged the next day in a stable condition.

Figure 1. USS Images

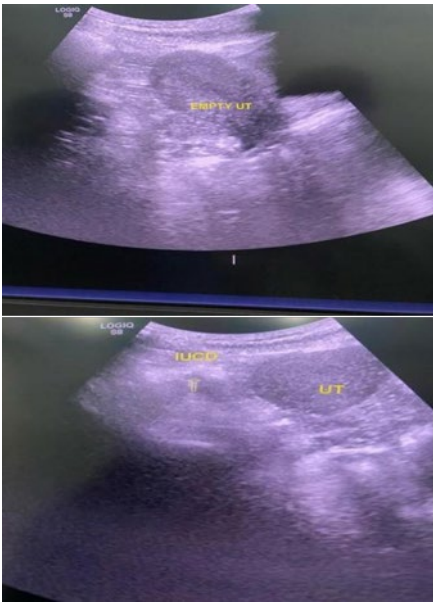


Figure 2. Scanogram

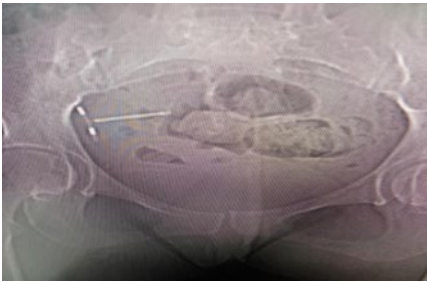


Figure 3. Coronal Reformatted CT



Figure 4. After Surgery



Keywords: Contraception, laparotomy, intra uterine contraceptive device

Radiation Safety in Radionuclide Therapy

S. Somanesan

Singapore General Hospital, Singapore

Background

Radionuclide therapy in a growing arm of Nuclear Medicine that has had a resurgence in the last few decades due in part to the number of newer therapeutic radiopharmaceutical agents available for radionuclide therapies. The radiation safety program in the delivery of radionuclide therapy service is significant as the radioactivity involved is generally high with the need to ensure radiation safety procedures for staff, patient, general public and the environment. Typically, a large mean infused radioactivity (e.g.: 5000 MBq/patient) is utilised, with possible contamination of staff and environment, close proximity of staff to patient and/or source and frequent treatments for these cancer patients.

Methodology

The radiation exposure to both radiopharmacy, medical physicist, nursing and clinical staff and others as a result of these newer radionuclide treatment involving alpha (α) and beta (β) radionuclides were assessed due to the highly energizing α and β particles. The availability of commercially available local shields, barriers were assessed as well as a detailed literature review concerning radiation safety aspects in the preparation and administration of the new alpha and beta emitting radionuclides was undertaken. Another key component of radionuclide therapy service delivery is the presence of internationally available harmonised and sustained radiation safety training not just for the staff of the department of Nuclear Medicine and Molecular Imaging but also to the other non-radiation hospital staff such as inpatient ward nurses. The overseeing of this training and supervision of personnel, in radiation safety aspects such as decontamination techniques in the event of a radioactive spill were compared across institutions as well.

Results

A comprehensive set of best practice guidelines for clinical radiation safety during therapy has been developed based on the collective operational experience radiation safety professionals over the years while providing radionuclide therapy service at SGH. Significant findings in lutetium-177 and actinium-225 radionuclide therapy administered in an unshielded room is presented.

Conclusion

The guidance contained in this presentation will assist radiation safety professionals in the implementation of safe, practical, reproducible and effective radionuclide therapy programs, even at small sites with limited to no experience in radionuclide therapies.

Radium Dichloride Micellar Solution: Overcoming Limitations

R. Santos-Oliveira

Brazilian Nuclear Energy Commission- Nuclear Engineering Institute, Laboratory of Nanoradiopharmacy, Rio de Janeiro, Brazil

Background

Radium-223, known for its alpha-emitting properties, was previously utilized in treating bone metastases in castration-resistant prostate cancer, but it led to short-term adverse effects such as diarrhoea and vomiting due to its elimination via the gastrointestinal tract.

Aim

This study aimed to address these drawbacks by employing a nanosized micellar form of [²²³Ra]RaCl₂.

Methodology

The creation of this micellar form involved mixing [²²³Ra]RaCl₂ aqueous solution with a Pluronic F127 micellar dispersion, resulting in an average particle size of about 149 nm, as determined through dynamic light scattering.

Results

Investigations conducted on healthy mice revealed that this micellar version exhibited strong bone-targeting abilities and was primarily expelled through renal pathways, in contrast to the gastrointestinal route observed with the non-micellar form. The pharmacokinetic assessment showed a reduced distribution volume and an extended elimination half-life. Furthermore, biochemical evaluations demonstrated that this micellar form did not significantly alter various enzymatic activities in the treated mice. When applied in the treatment of osteosarcoma, the micellar version led to tumour regression characterized by extensive necrotic areas in the treated specimens. This study underscores the efficacy of micellar suspensions as nanocarriers in enhancing drug delivery, mitigating side effects, and increasing the therapeutic index in cancer treatments. The micellar solution's path of renal excretion potentially lessens gastrointestinal side effects while preserving its bone-targeting capabilities.

Conclusion

The findings confirm the effectiveness and safety of the micellar [²²³Ra]RaCl₂ in reducing gastrointestinal elimination, facilitating renal excretion, and successfully diminishing osteosarcoma. Nevertheless, the authors advocate for additional research to evaluate the therapy's efficacy and for clinical application, including investigations into dose-response relationships and organ/tissue dosimetry. This article thoroughly explores the advantages of using a nanomicellar formulation of [²²³Ra]RaCl₂ in oncology, particularly in treating osteosarcoma, emphasizing its enhanced safety and precise targeting features.

Report of the first PET/MRI imaging using [68Ga] Ga@GO@Fe3O4-cys-CdTe nanocomposite in Iran

S. Y. F. Hosseini-zhad¹, A. Amiri², H. Zare², M. E. Kalantari², S. F. Zenjanab¹

¹ Radiation Application Research School, Nuclear Science and Technology Research Institute, Iran

² Department of Physics, Yazd University, Iran

Background

The development of unified positron emission tomography and magnetic resonance imaging (PET/MRI) agents flourished a new scenario for cancer diagnosis, treatment, and follow-up. Multimodal imaging integrates morphological and functional details from different modalities, which cannot provide a comprehensive pathophysiological outline, individually. In-vivo radioisotope delivery has been the main focus of research on radiolabeled graphene oxide (GO) nanosheets.

Methodology

In this context, we present the functionalization of the surface of GO nanosheets with Fe₃O₄ magnetic nanoparticles, cysteine amino acid as an interface ligand, and cadmium telluride quantum dots. GO@Fe₃O₄-Cys-CdTe was characterized by photoluminescence (PL), Transmission electron microscopy (TEM), Fourier transform infrared spectroscopy (FTIR), X-ray powder diffraction (XRD), Scanning electron microscopy (SEM), and vibrating sample magnetometers (VSM) analytical methods. To enable In-vivo PET imaging, the GO@Fe₃O₄-cys-CdTe QDs were labeled with ⁶⁸Ga to yield [68Ga] Ga@GO@Fe₃O₄-cys-CdTe QDs. Furthermore, serum stability tests were performed and the biological behaviour of the nanocomposite was evaluated in rats bearing fibrosarcoma tumour.

Results

Taking into account that in radioimmunoscinigraphy, the accepted ratio of tumour to other organs uptake is 1.5–2, and here the tumour to blood uptake ratios of [68Ga] Ga-Go@ Fe₃O₄-Cys-CdTe were 0.78, 1.33 and 3.60 at 60, 90 and 120 min post injection respectively, These results suggested remarkable tumour uptake. Tumour uptake of the [68Ga] Ga-Go@ Fe₃O₄-Cys-CdTe at three evaluated times (60, 90 and 120 min) are 1.53%, 1.75% and 2.41% suggesting "2 h" after injection as the best time for imaging. MR images were taken 1 h post injection of NPs (Figure 1.)

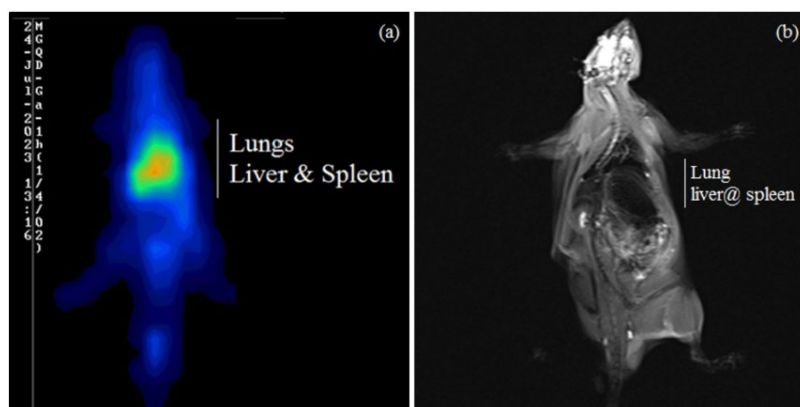


Figure 1. PET image of [^{68}Ga] Ga-Go@ Fe $_3\text{O}_4$ -Cys-CdTe radio nanocomposite in normal rat (a), T_2 -weighted MRI images of GO@Fe $_3\text{O}_4$ -CysCdTe at Fe concentrations of 0.4 (mM) at 3.0 T (b)

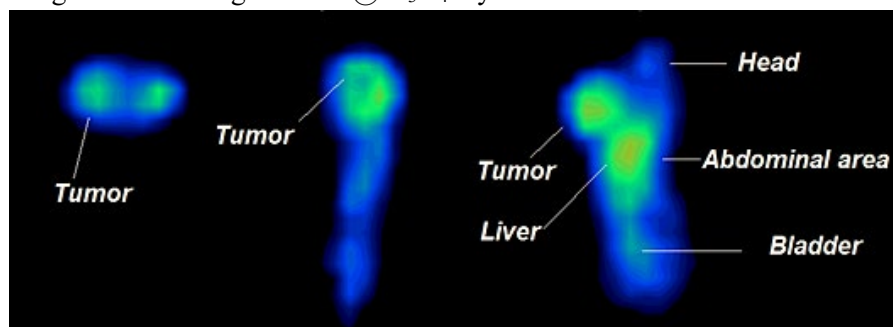


Figure 2. Coincidence imaging of the [^{68}Ga] Ga-Go@ Fe $_3\text{O}_4$ -Cys-CdTe in rats bearing fibrosarcoma tumour at 60 min post injection.

Conclusion

Positron-emitting radionuclide along with a magnetic (Fe $_3\text{O}_4$) component will help to design a bimodal imaging probe (PET/MRI) which will offer the advantages of combined imaging techniques and further possible used in localized hyperthermia/radionuclide therapy for treatment of cancer (Figure. 2).

Overall, [^{68}Ga] Ga@GO@Fe $_3\text{O}_4$ -cys-CdTe QDs nanocomposite shows great promise as a radiolabeled imaging agent owing to high accumulation in tumour region.

Zirconium-89 labeled-quantum dots as a potential in vivo dual-modality PET/OI cancer imaging agent

S. F. Zenjanab, S. Y. F. Hosseininezhad

Nuclear Science and Technology Research Institute, AEO, Iran

Aim

The present study focuses on the synthesis and biodistribution of cadmium telluride quantum dots labeled with zirconium-89, as a bimodal nano composite containing a fluorescent component (QDs) and a positron emitting element to make a PET/FLI bimodal imaging agent.

Methodology

Synthesis and characterization of cadmium telluride quantum dots (size and fluorescent properties), radiolabeling and quality control, and then animal studies including investigating biodistribution, tumour accumulation, mechanism of excretion of radiolabeled compound from the body and PET images have been studied.

The in vivo behaviour of [⁸⁹Zr]Zr-CdTe QDs was evaluated and compared with [⁸⁹Zr]Zr-Chloride using PET imaging.

Results

The results indicated the rapid and targeted accumulation of radio labeled nanoparticles in the tumour.

Conclusion

Due to the superior properties of the zirconium-89 radioisotope and appropriate biodistribution, these labeled nanoparticles were introduced as potential PET/FLI bimodal imaging agent.

Significance of the Perugini G1 score on scintigraphy with bisphosphonates in the diagnosis of cardiac amyloidosis

C. Stan^{1,2}, C. Chirion¹, D. Stanescu¹, R. Adam^{2,3}, G. Neculae^{2,3}, S. Badelita⁴, A. Jercan^{2,4}, D. Coriu^{2,4}, M. Draghici⁵, C. Dobrea⁶, S. Onciul⁷, R. Jurcut^{2,3}

¹ Department of Nuclear Medicine and Ultrasonography, Fundeni Clinical Institute, Bucharest, Romania

² Carol Davila University of Medicine and Pharmacy, 020021 Bucharest, Romania.

³ Department of Cardiology, Expert Center for Rare Genetic Cardiovascular Diseases, “Prof. Dr. C.C. Iliescu” Emergency Institute for Cardiovascular Diseases, Bucharest, Romania

⁴ Department of Hematology, Fundeni Clinical Institute, Bucharest, Romania

⁵ Department of Neurology, Fundeni Clinical Institute, Bucharest, Romania

⁶ Department of Pathological Anatomy, Fundeni Clinical Institute, Bucharest, Romania

⁷ Department of Cardiology Floreasca Emergency Clinical Hospital, Emerald Medical Center, Bucharest, Romania

Background

Amyloidosis is a heterogeneous group of diseases caused by extracellular deposition of insoluble fibrils in multiple organs. Several types of amyloid can infiltrate the heart resulting in a restrictive cardiomyopathy, heart failure, and arrhythmias. The most clinically relevant cardiac involvement occurs in primary light-chain (AL) amyloidosis, hereditary or variant transthyretin amyloidosis (ATTRv), and wild-type transthyretin (ATTRwt) amyloidosis. In recent years, the sensitivity of bisphosphonate scintigraphy (BS) has been validated for the non-invasive diagnosis of cardiac amyloidosis. The semi quantitative visual grading score (Perugini) G2/G3 is pathognomonic for amyloid cardiomyopathy with ATTR. BS together with cardiac imaging (US or MRI) can diagnose ATTR amyloidosis, only if AL amyloidosis is excluded, by measuring free light chains (kappa, lambda and K/L ratio) in serum and urine with immunofixation. Subcostal radiotracer intensity uptake at the level of the left ventricle (G1 score) is often challenging and compliance with the acquisition, including SPECT, and interpretation protocols, decrease false positive or negative results.

Objective: In this paper, we intend to present some cases with equivocal uptake score and low sensitivity of BS in the diagnosis of cardiac amyloidosis.

Results

In the period 01.2017 - 01.2023, we studied all the 244 referred patients, for the screening or confirmation of cardiac amyloidosis. G1 score was found in 7 patients: 1 ATTRile127Val, 4 AL amyloidosis, and 2 were negative for ATTRv or AL amyloidosis. The prevalence of the G1 score in the nuclear medicine department of the Fundeni Clinical Institute and Affidea Bucharest was 2.8%. Equivocal semi-quantitative score (G1) can be present in AL amyloidosis in some genetic variants, or at the onset of ATTR amyloidosis.

Conclusion

The G1 visual score in BS must trigger a diagnostic chain to exclude AL amyloidosis or to confirm an ATTR amyloidosis at the onset or with a genetic variant less sensitive to BS.

Gall Bladder Visualization Following [¹⁷⁷Lu]Lu-DOTA-TATE Therapy Not Observed in Prior Diagnostic or Therapeutic Scans

G. Mundaca, T. Massardo, A. Rojas, J. Donoso, F. Gómez

Nuclear Medicine Section, Hospital Clínico Universidad de Chile (HCUCH), Chile

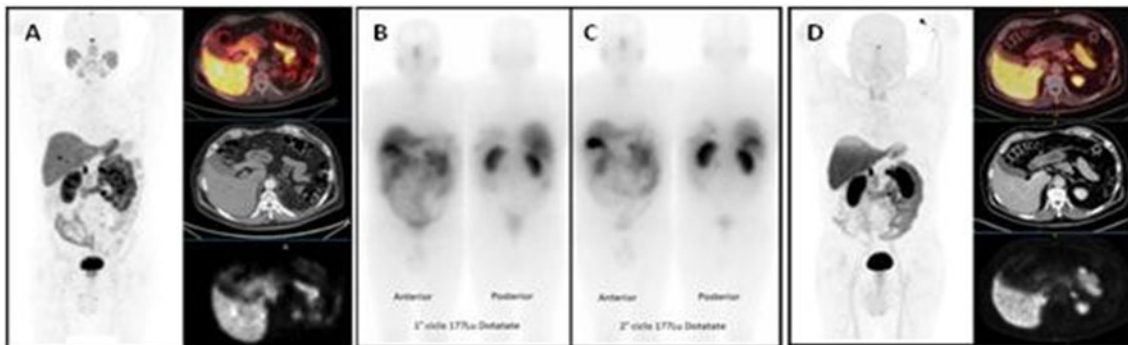
Background

Neuroendocrine tumours (NETs) represent only 0.5% of all malignant neoplasms. The incidence varies from 2.5 to 8.3 per 100,000 populations and has seen an exponential increase over the last decades. Therapy with beta-emitter radiolabelled somatostatin peptide analogues with Yttrium-90 or Lutetium-177 is indicated for patients with functioning NETs with overexpression of somatostatin receptors on their surface.

In our center, 24 patients have been admitted for treatment since 2006 to date, with 94 cycles of therapy in total, mostly with Lutetium-177; since 2019 we follow the NETTER trial. All administrations have a whole body biodistribution scan 24 hours post therapy; in none of them we have observed biliary excretion of the radiopharmaceutical similarly to observed with Gallium-68 DOTAS or Fluorine-18 AIF-NOTA-Octreotide (FAN) for diagnostic PETs.

Clinical Case

61-year-old male with pancreatic neuroendocrine tumour diagnosed and resected in 2022. While being treated with Sandostatin®, he presented local recurrence with a small liver lesion in the right lobule and a vertebral lesion suggestive of secondary involvement, evidenced in PET/CT with [⁶⁸Ga]DOTA in 2023, so the multidisciplinary committee indicated [¹⁷⁷Lu]Lu-DOTA therapy. Our patient has already received 3/4 cycles (7.4 GBq/each). See Figures A-D.



A. ⁶⁸Ga-DOTA PET/CT scan showing increased uptake in the pancreatic remnant lesion, liver lesion and left para-aortic lymph node.

B. Biodistribution scan performed with planar gamma camera after the first cycle of ¹⁷⁷Lu-DOTA with moderate and irregular uptake in the liver (gallbladder projection) interpreted as a possible new liver lesion.

C. Biodistribution scan after the second cycle of ¹⁷⁷Lu-DOTA, 3 months later shows uptake in the liver (gallbladder projection) now of greater intensity and better definition; a PET was requested to rule out further tumor involvement.

D. PET/CT ¹⁸F-FAN showing lesion in pancreatic remnant, disappearance of the hepatic lesion and persistence of left paraaortic adenopathy. Gallbladder without morphological or uptake abnormalities.

Discussion

Currently, only two similar cases have been published in the literature, however, both were in their first dose of [¹⁷⁷Lu]Lu-DOTA. Subsequent to planar imaging, one patient underwent SPECT/CT in the same instance and another was studied with magnetic resonance (MRI) ruling out secondary hepatic involvement. In our case, we performed PET/CT with FAN. On the other hand, physiological uptake in the gallbladder has been described as an incidental finding in ¹¹¹In-octreotide scintigraphy, as well as in [⁶⁸Ga]DOTANOC PET as a rare finding.

Among all NETs, the prevalence of gallbladder involvement is 0.5%, representing approximately 2.1% of all gallbladder tumours. Epidemiological data on metastatic gallbladder involvement of a primary NET have not been reported. In contrast, the liver is a frequent site of metastasis, independent of the location of the primary; patients presenting with metastatic lesions approximately 80% will have liver involvement.

NETs are a growing neoplasm. The liver is a frequent site of metastasis, but not the gall bladder. Due to the increased survival of patients with metastatic NETs with radiolabelled peptide therapy; it is frequently indicated for the management of well differentiated cases. Although, until now, the visualisation of the gallbladder in scans after [¹⁷⁷Lu]Lu-DOTA-TATE administration has been physiological, it is necessary to rule out previously undocumented liver metastases, especially when there is a change in shape and/or intensity of uptake at this level in scans of the same patient.

This false positive should be recognized and could have been avoided with the use of SPECT CT not available in our center; however, the CT from the PET System we have could be employed if there is a new clinical doubt in case of possible intratherapy progression considering the high cost of this theranostics cases. Another option are PET/CT with [⁶⁸Ga]DOTA or FAN, depending on availability or morphological imaging such as MRI.

Role of a Careful Quality Control of the acquisition and interpretation in multigated ventriculography in a cardio-oncology patient

G. M. Soto, A. R. Flores, O. Barajas, E. Chaigneau, J. Dupouy, F. Gomez, T. M. Vega, A. Matamala

Hospital Clinico Universidad de Chile, Chile

Background

47yo female with arterial hypertension under enalapril and amlodipine, BMI 34.9 kg/cm², with right breast cancer cT4bN2M0; biopsies: infiltrating ductal carcinoma poorly differentiated; ER(+)^{90%}; PR(+)^{90%}; HER2(+); FISH(+); Ki67:70%;luminal B.

She received 6 cycles of neoadjuvant chemotherapy (Carboplatin, Docetaxel and Trastuzumab) with good tolerance and tumour size decrease; in May 22 total mastectomy and axillar dissection was performed with residual disease (pT1c and pTN0) which new anti-HER-2 treatment indicated for 14 cycles every 21 days plus adjuvant radiotherapy. Periodic clinical and lab controls as well as cardiac evaluation were performed. Multigated ventriculography with Tc99m-labelled red blood cells (MUGA) in July 2022 showed good biventricular systolic function, narrow RR duration histogram and adequate intra and interventricular synchrony and preserved left ventricular volume.

She continued her protocol without incidents, asymptomatic; in her 8th cycle, MUGA presented a slightly altered triggering and some shorter beats with left ventricular ejection fraction (LVEF) within normal limits. The EKG showed sinus rhythm, non-specific abnormal repolarization and prolonged QT. After the 11th cycle a new MUGA (**Figure A**) showed a marked abnormality of the heart rate histogram and a decrease in manual and automatic LVEF and also in the right ventricular ejection fraction (RVEF); the report suggested to evaluate for arrhythmias. A prior thorax CT, showed opacities compatible with residual actinic damage (**Figure B**). A new EKG, demonstrated a baseline sinus rhythm, bigeminy, ventricular extrasystoles with incomplete LBBB, plus anteroseptal non-specific ventricular repolarisation disorders (**Figure C**).

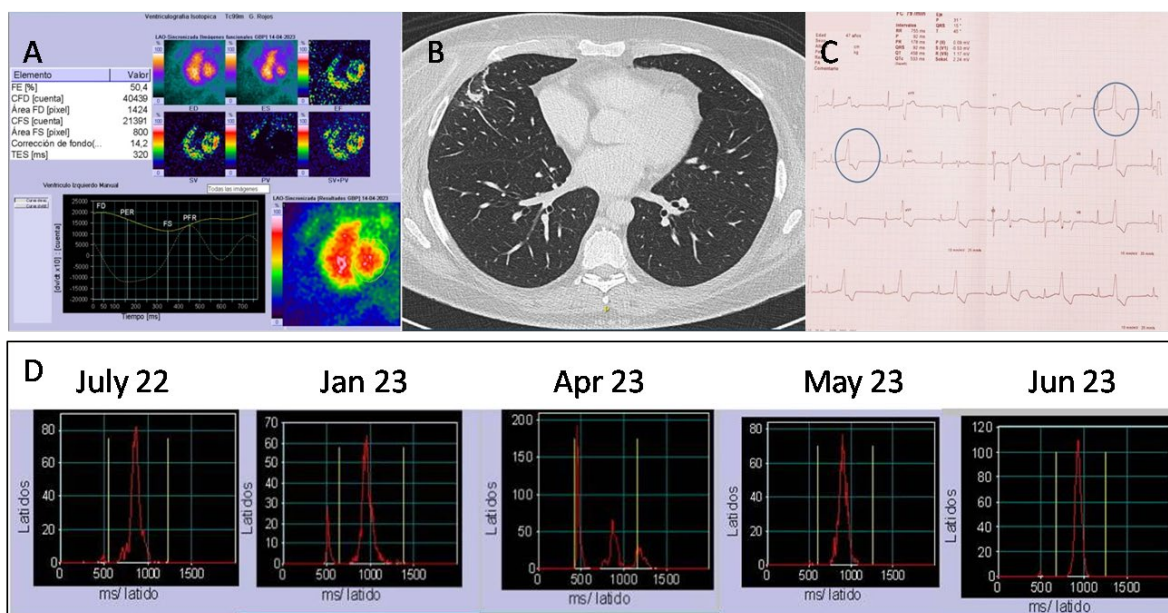
She reported greater fatigue, no dyspnea, or angina and occasional palpitations; specific cancer treatment was temporarily suspended. Cardiologists evaluated the patient: normal Pro BNP; arrhythmia Holter: frequent ventricular extrasystoles in pairs. Heart failure was ruled out and treatment was authorized to continue, completing the 14 cycles, without incidents or cardiac disease evidence. MUGA was repeated biventricular function recovery. Subsequently, MUGA, found preserved left function with significant LVEF increase. Right ventricular function was decreased, persisting mildly abnormal.

The **Table** shows biventricular systolic function values and the histograms of consecutive beats (**Figure D**). The diastolic function analysis also showed an important worsening in time to peak filling rate (TTPFR) that improved in the last controls; peak filling rate/stroke volume expressed in %/sec was also abnormal and then recovered.

Final diagnosis: Cardiotoxicity due to monoclonal antibodies in a hypertensive patient with breast cancer already undergoing chemo and radiotherapy.

Several oncologic agents currently used in some tumours can cause mainly dilated cardiomyopathy and heart failure with myocardial damage, occasionally irreversible. Both short and long-term cardiotoxicity, with or without thorax radiation-induced toxicity may be present. Its degree is also dependent on factors such as gender, age and other traditional cardiovascular risk factors. Periodic rest MUGA allows to follow-up biventricular function in these patients. The technique even allows to evaluate diastolic early dysfunction. Careful attention of the EKG gating may detect rhythm abnormalities.

2022 ESC Guidelines on cardiooncology do not include MUGA as first line imaging method due to radiation exposure, however it could be used in cases where the high reproducibility of the technique is needed.



Planar Technique		July 22	Jan 23	Apr 23	May 23	June 23
LVEF (%)	manual	63.4	58.7	50.4	56.0	65.4
	automatic	58.8	51.6	46.9	54.5	61.5
RVEF (%)	manual	60.1	53.0	45.3	50.7	41.5

Effect of Correction Methods on Image Resolution of Myocardial Perfusion Imaging using SPECT Combined with CT Hybrid Systems

N. L. Helal¹, H. M. Tantawy², Y. G. Abdelhafez³, I. E. Saad²

¹Nuclear & Radiological Safety Research Center, Egyptian Atomic Energy Authority, Egypt

²Department of Clinical Oncology and Nuclear Medicine, Faculty of Medicine, Cairo University, Egypt

³Nuclear Medicine Unit, South Egypt Cancer Institute, Assiut University, Egypt

Background

It is very important to obtain a reliable diagnostic image to provide a better evaluation of heart conditions. This can be done by increasing the image resolution of myocardial perfusion imaging (MPI) using SPECT/CT hybrid system.

Aim

The purpose of this study is to evaluate the image resolution of MPI by different correction methods such as Attenuation correction (AC), Scatter correction (SC), both attenuation and scatter correction together (ACSC) and compare them with that of no-correction (NC).

Methodology

A total of 114 patients, 43 females and 71 males, Patient's raw data were processed and analysed using the program provided with the processing computer for calculations. The short axis (coronal) slices resulted from the raw data reconstruction was chosen to draw the curve profile to identify the line spread function on the image to create the FWHM curve. Profile statistics were calculated to obtain the value of FWHM. Statistical analysis was made for the calculated FWHM values for AC, SC, ACSC, and NC to determine the best image resolution. It turns out that applying the scatter correction method alone yields better FWHM value for myocardial perfusion images than when using attenuation correction, and both attenuation and scatter correction.

Conclusion

Image Resolution has been significantly improved by using scatter correction, attenuation correction, and both methods together when compared with the non-corrected image resolution during the reconstruction of SPECT/CT myocardial perfusion images.

Keywords: SPECT/CT; attenuation correction; scatter correction; image resolution; FWHM

Medullary Thyroid Carcinoma Plus Multiple Metastases Detected By [¹⁸F]FDG/PET/CT

J. H. A. Cordova

Instituto Nacional de Enfermedades Neoplásicas, Peru

Background

Medullary thyroid carcinoma (MTC) constitutes 5-10% of all thyroid cancers. It does not originate in thyroid cells, but in calcitonin producing C cells, is an aggressive form of thyroid cancer and can present regional or distant metastases, mainly in lung, liver and bone. At the time of diagnosis serum calcitonin (CT) and carcinoembryonic antigen (CEA) are the most important markers. The detection of the lesion and metastases by imaging techniques is very important for the treatment of the disease. Conventional imaging is the most commonly used, however, these may be limited when lesions are small or undetectable, currently metabolic imaging such as PET/CT with [¹⁸F]FDG has proven useful in patients with very high CT and CEA values with short doubling time.

Case Report

This is a case report of a 27-year-old male patient with a history of Cushing's disease and calcitonin (05.02.2020): 19618, had FNA compatible with medullary cancer BETESDA VI, for which he underwent total thyroidectomy + bilateral cervical dissection in another institution (03.10.20), whose pathology was: MEDULAR THYROID CARCINOMA of 3 cm, N 34/42, MX. Subsequently, he was admitted to our institution (15.10.20) where he had controls and CEA was found (28.11.2020): 3.53. In 2021 Sanger sequencing of the RET gene was performed, variant c.2410>A (p.Val804Met) was detected, which confers moderate risk, markers: CT (19.01.2021):1312 and CEA (17.02.2021): 4.51, continues in controls with CT: (27.08.2022):4185 and CT: (10.2022): 4639, GGO was performed (19.09.22): Increased uptake left coxofemoral joint, MRI (16.01.23): bilateral avascular necrosis femoral head predominantly left. CT:(14.04.2023): 6818, due to elevated CT levels, it was decided to do PET/CT with [¹⁸F]FDG (21.04.23): hypermetabolic hypodense lesion, hepatic segment III, hypodense tissue adjacent to prevascular mediastinum and some pulmonary nodules not associated with metabolism. CT:(08. 07.07.2023): 7092 and CT: (30.09.2023): 7666, with these results liver nodule resection was performed (01.09.23): compatible with metastasis of medullary thyroid carcinoma of 1.8x1.5cm. The patient has CT scans (11.2023): round nodes, contrast hyperenhancers 8 mm in right IA/B group, fractures due to insufficiency of the T8 and T11 vertebral bodies, no signs of recurrence in the abdomen. CT (01.12.2023): 6221, neck ultrasound (16.12.23): IA oval lymph node, 2.9 mm, fusiform, heterogeneous, hypoechogenic images, up to 11 x 4.8 mm in group IV right, suggestive of adenopathy. Impressed adenopathy up to 6.2 x 4.8 mm in group VII. A PET/CT study was performed with [¹⁸F]FDG (02.02.2024): new hypermetabolic lesions of metastatic appearance in cervical and mediastinal nodes, as well as an increase of prevascular mediastinal lesions, pulmonary nodules and lytic bone lesions. For these reasons the patient is tributary to therapy with multikinase inhibitor (cabozantinib): he will receive his first dose.

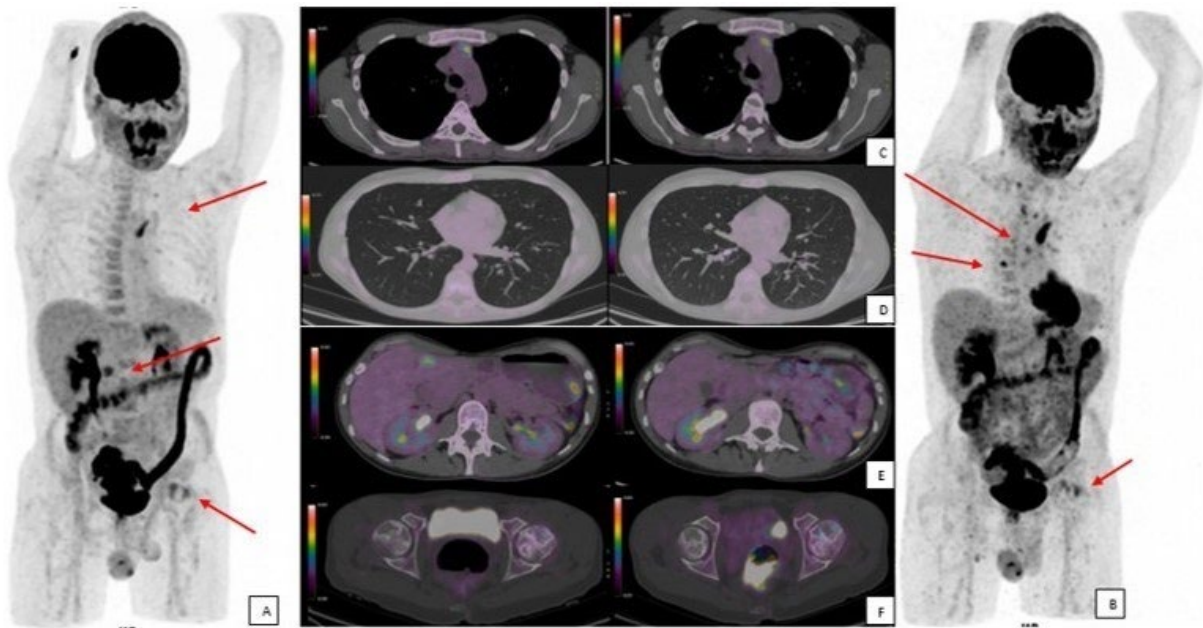


Fig.1 PET-CT with 18F-FDG of a 27-year-old male patient with medullary thyroid cancer plus multiple metastases. (A) Baseline MIP showing evidence of liver metastasis (B) Re-staging MIP showing disease progression at the nodal, pulmonary and bone level, as well as good response at the hepatic level. (C, D and E) PET-CT in axial slices at the level of the mediastinum, pulmonary, liver and left femur, showing morphological and metabolic progression.

Conclusion

Medullary thyroid cancer can be aggressive and present with RET gene mutations, as well as increased calcitonin and CEA values, associated with short doubling time, and it is here where PET/CT with [¹⁸F]FDG can be useful to demonstrate progression.

Novel Radiopharmaceutical ⁶⁸Ga-DOTA-D-Alanine-BoroPro Expands the Scope of Fibroblast Activation Protein Imaging Across Malignant and Non-Malignant Pathologies

C. L. S. Cuevas¹, E. Azorin-Vega¹, G. Ferro-Flores¹, N. P. J. Mancilla¹, M. L. Gutiérrez¹, B. E. Ocampo-García¹, J. V. Ahumada², P. Vallejo-Armenta²

¹ Instituto Nacional de Investigaciones Nucleares, Mexico

² Instituto Nacional de Cancerología, Mexico

Background

A novel radiopharmaceutical inhibitor tailored for SPECT imaging of the tumour microenvironment, specifically aimed at fibroblast activation protein (FAP), has been developed based on the ^{99m}Tc-HYNIC-D-Alanine-BoroPro (^{99m}Tc-HYNIC-iFAP). This study focuses on the development of a new radiotracer, ⁶⁸Ga-DOTA-D-Alanine-BoroPro (⁶⁸Ga-iFAP), for PET imaging and evaluate its efficacy in identifying FAP expression in both malignant and non-malignant tissues.

Methodology

The synthesis process involved a coupling reaction between p SCN-benzene-DOTA and HYNIC-iFAP for the ⁶⁸Ga labeling process, and radiochemical purity verification was made using the radio-HPLC method. To evaluate specificity, ⁶⁸Ga-iFAP was tested in HCT116 cells, where FAP expression was confirmed through immunofluorescence and Western blot analysis. Furthermore, biodistribution and biokinetic studies were performed in murine models. The uptake of ⁶⁸Ga-iFAP at the myocardial level in mice subjected to induced infarction was assessed.

This study also included three healthy volunteers and three patients. Among the patients, two were diagnosed with high-grade glioblastoma and breast cancer, while the other one had recently experienced a myocardial infarction. For each patient, PET/CT imaging was conducted after the intravenous administration of ⁶⁸Ga-iFAP, and subsequently, initial images of ⁶⁸Ga-iFAP were captured for both healthy individuals and the aforementioned patients.

Results

The ligand DOTA-D-Alanine-BoroPro, employed in the synthesis, underwent comprehensive characterization using UV-Vis, FT-IR, and UPLC mass spectroscopy, confirming its chemical purity at 98%. The resulting ⁶⁸Ga-iFAP displayed a radiochemical purity surpassing 95%. Additionally, in vitro and in vivo studies showcased the targeted binding of ⁶⁸Ga-iFAP to FAP, its swift renal elimination, and its effective visualization of locations associated with diverse cancers, such as glioblastoma, breast tumours, prostate cancer, and myocardial infarction.

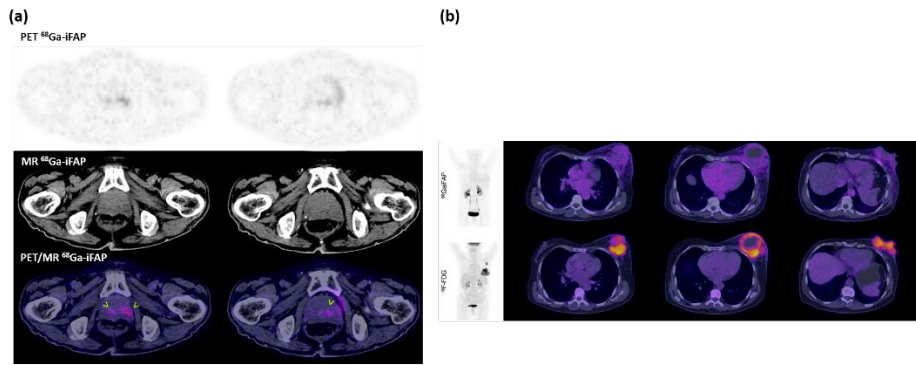


Figure 1. (a) Patient diagnosed with high-grade glioblastoma exhibiting radiopharmaceutical ⁶⁸Ga-iFAP uptake in lesion associated with prostate cancer. (b) Comparative imaging of radiopharmaceuticals ⁶⁸Ga-iFAP and ¹⁸F-FDG uptake in a patient with triple-negative breast cancer.

Conclusion

The PET imaging radiotracer ⁶⁸Ga-DOTA-D-Alanine-BoroPro (⁶⁸Ga-iFAP) exhibits promising attributes as a novel radiotracer for detecting fibroblast activation protein (FAP) in both malignant and non-malignant tissues. Analytical results affirm its resilient stability in human serum, its in vitro and in vivo specificity for FAP, and swift rapid renal clearance through the kidneys. The findings of this study emphasize the importance of conducting additional research, including dosimetric and clinical studies, to validate the sensitivity and specificity of ⁶⁸Ga-iFAP PET imaging in detecting FAP expression.

A retrospective study on the concordance of the OSEM and Q. Clear reconstruction algorithms in [¹⁸F]FDG PET/CT imaging of female patients with breast cancer

T. J. Lam, S. I. Gacula

Cardinal Santos Medical Center, Philippines

Background

As of 2020, female breast cancer has surpassed lung cancer as the leading cause of cancer incidence worldwide. The management of breast cancer involves a multidisciplinary approach with nuclear medicine and molecular imaging techniques, particularly positron emission tomography-computed tomography (PET/CT) using fluorine-18 fluorodeoxyglucose ([¹⁸F]FDG), playing an important role. The current standard for PET/CT imaging reconstruction is the use of the ordered subset expectation maximization (OSEM), an iterative statistical algorithm. Innovatively, a relatively new Bayesian penalized-likelihood (BPL) iterative PET reconstruction algorithm developed by GE Healthcare, called Q.Clear, has been introduced into GE PET/CT scanners. This study examined the concordance of the Q.Clear algorithm with the standard OSEM algorithm in the interpretation of PET/CT imaging in female breast cancer patients at different stages of management.

Methodology

This is a retrospective cohort study of PET/CT scans of female patients with biopsy-proven breast cancer, categorized into three groups according to clinical indication. A total of 4,460 [¹⁸F]FDG PET/CT scans were performed between March 2017 to May 2021. Out of 639 PET/CT scans of adult, female patients with histopathologically proven invasive mammary carcinoma, 105 eligible scans were included in this study. Scans were categorized to one of three groups according to clinical indication: staging prior to initiation of treatment (S-PET), evaluation of response to interim or completed treatment (T-PET), and surveillance for the detection disease recurrence (R-PET). The Shapiro-Wilk test was performed to verify normal distributions. Paired T-test was used to determine the mean difference of SUV and SUL parameters between the Q.Clear and OSEM reconstruction algorithms, for reference regions in the liver and MBP and identifiable target lesions across the entire cohort. The p-value generated from the statistical calculator determined the significance level of each group. A p-value of less than 0.05 was considered statistically significant. Cohen's kappa (k) was used to calculate the intraclass correlation coefficient between the two algorithms for the three groups.

Results

PET/CT scans of 105 female breast cancer patients, aged 24-89 years, with mean BMI of 24.9 ± 4.5 , referred for staging (34%), treatment evaluation (22%), and recurrence detection (44%) were included. Intraclass correlation coefficients demonstrated perfect agreement ($k=1.0$) for all groups. Metabolic responses per lesion had moderate agreement ($k=0.593$) with more favorable responses seen in Q.Clear for discordant lesions. Significantly higher average SNR for liver and target lesions ($p<0.0001$ and $p=0.0008$, respectively) and average SUV_{max} and SUL_{max} for target lesions ($p=0.0254$ and $p=0.0267$, respectively) were calculated in Q.Clear. Differences for SUV and SUL parameters of reference regions were not statistically significant.

Conclusion

Q.Clear and OSEM algorithms were concordant for staging, treatment evaluation, and recurrence detection in PET/CT scans of female breast cancer patients. Q.Clear may be used preferably for its higher SNR. However, we recommend using the same PET/CT reconstruction algorithm for treatment evaluation due to significant differences in SUV_{max} and SUL_{max} for target lesions between the two algorithms.

Trends in the Utilization of Hybrid-Imaging Facilities in Africa and their Impacts in Managing Cancer and Other Non-Oncologic Clinical Disorders

Y. J. Lagebo

School of Medicine, College of Health Sciences, AAU, Addis Ababa, Ethiopia

Background

The well termed radiation related Medical Hybrid Imaging Facilities at common contemporary use for clinical applications are SPECT/CT, PET/CT and PET/MRI. These facilities are mainly employed in Nuclear Medicine & Molecular Imaging (NMMI) practices. Cancer has been one of the enormously daunting phenomena to the public health of the Global Community both in the developed and developing nations. The crucial roles being played currently by these imaging facilities to accurately diagnose cancer and other fatal non-communicable diseases (NCDs) are unequivocally apparent.

Methodology

The survey-based study embracing the combination of qualitative and quantitative approach of the prevailing data observations, collection and their critical analysis was conducted via extensive literature review including the most recently published articles on hybrid-imaging. In addition, special-survey-focus was also paid to observe the African scenario regarding these facilities via pertinent literature explorations including the IAEA references, one to one interview administered to few experienced professionals through personal communications as well as the complimentary critical observations & analysis of the author.

Results

This survey-based study has proved that the prevailing total number of hybrid imaging facilities (SPECT/CT, PET/CT & PET/MRI) in Africa has been observed to be extremely low compared to that in the other developed regions of the world which in turn has adversely impacted the effective management of cancer & other fatal NCDs in Africa. For example, in 2022 the total number of PET/CT cameras in Africa was 63 most of which were installed only in seven African countries among 54 & currently there is only one advanced version functional PET/MRI in Africa. However, many countries in Africa currently are on the move towards initiating NMMI Programs which makes the future optimistic & promising to the continent concerning the accessibility of hybrid imaging facilities. The study has also indicated that significant technical progresses on Hybrid-Imaging-Facilities specially within this decade (3-5 years) along with the associated continuing developments in novel radiopharmaceuticals & contrast agents have been playing pivotal roles in rendering them to be incrementally conducive to more accurately diagnose a variety of cancers & NCDs which are currently the major causes of morbidities & mortalities to the global communities.

Conclusion

Some of the technological drawbacks that have been observed earlier with the hybrid imaging facilities which in turn have hampered their broader clinical roles at present are continuing to be resolved significantly and their diversified/broader clinical applications are being enhanced contemporarily. The practical applications of such facilities along with their corresponding novel radiopharmaceuticals and contrast agents for the effective management of Cancer & other NCDs have been meaningfully

actualized in most countries within the affluent Global Regions unlike that in Africa. Consequently, the prevailing management of Cancer & Other fatal NCDs in most African countries is unacceptably low & highly compromised due to the absence/inadequate availability of these facilities.

A Comparative Study of Low kVp Protocols for Paediatric Cardiac CT

E. M. Attalla¹, M. S. Aboul Hamad², M. A. Donya²

¹National Cancer Institute, Cairo University, Cairo, Egypt

²Radiology Department, ALNAS Hospital, Cairo, Egypt

Purpose

To investigate the feasibility and effectiveness of utilizing lower potential voltage (kVp) as a dose reduction strategy in paediatric cardiac imaging while maintaining clinically acceptable image quality, we aim to develop evidence-based protocols for safe and effective paediatric cardiac imaging, promoting best practices in the field.

Background

Congenital heart disease (CHD), the most prevalent birth anomaly, poses a significant life-threatening risk to infants. Infant cardiac computed tomography angiography (CTA) has become a pivotal tool for evaluating complex CHD cases. Optimizing CT radiation doses necessitates techniques to reduce exposure while preserving diagnostic image clarity. Modern CT systems incorporate dose modulation and customized protocols to achieve this balance, particularly in paediatric imaging, where children are more susceptible to radiation's effects.

Methodology

All ECG-gated cardiac CT examinations were performed on a third-generation dual-source CT system (SOMATOM DRIVE; Siemens Healthineers, Germany), mean age (9.57 ± 6.67 months) and mean weight (6.9 ± 2.29 Kg). 200 children were examined using the 70-kVp protocol, whereas 200 children received the 100-kVp protocol. Radiation metrics ($CTDI_{vol}$, DLP) were compared between the two acquisition techniques using SPSS V.22.0 software where a nonparametric test, the independent sample Mann Whitney U test, was used to compare the two paediatric groups based on KVp (70 & 100). A diagnostic radiologist and a paediatric cardiologist visually evaluated all CTA images.

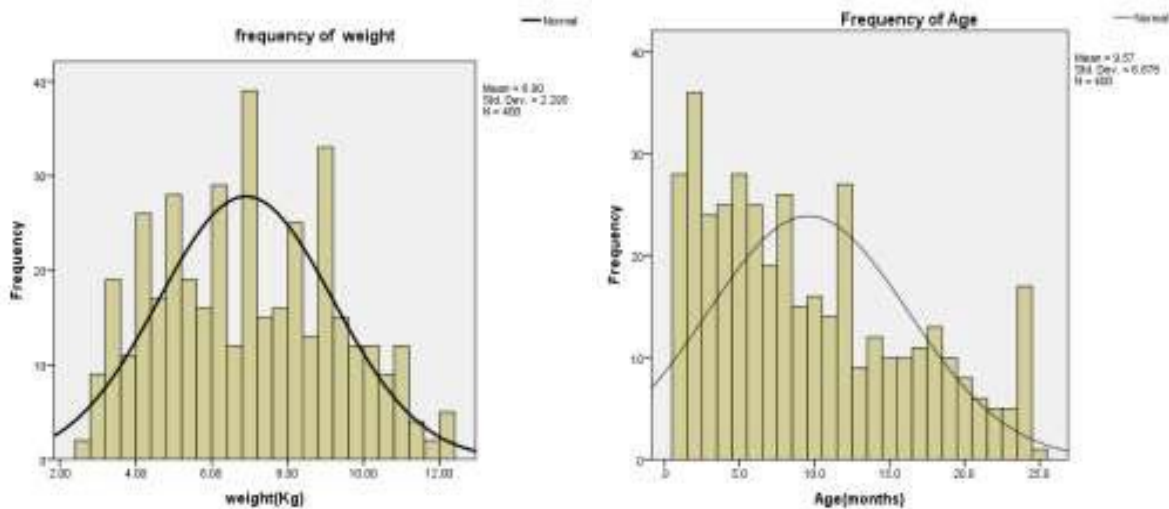


Figure 1. Weight and age distribution of patients who had ECG-gated cardiac computed tomography.

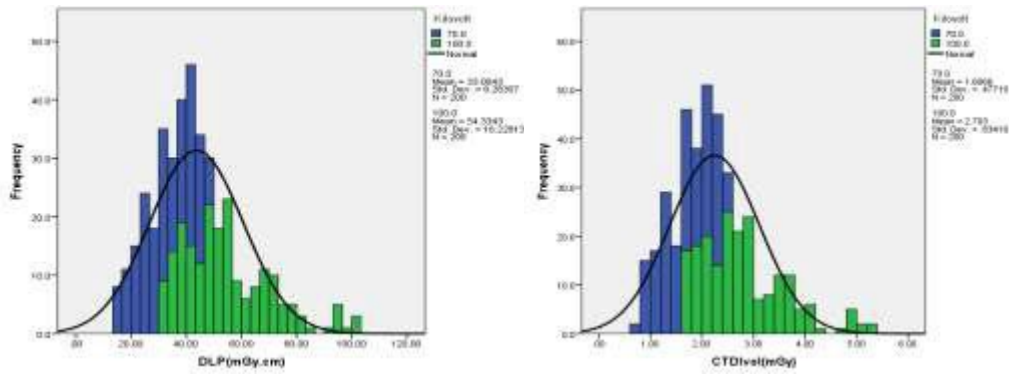


Figure 2. Comparison between distribution of dose length product (DLP) and volumetric computed tomography dose index (CTDI_{vol}) based on applied tube voltage.

Results

Applied Voltage	No. of patients	CTDI _{vol} (mGy)	DLP (mGy.cm)	Age (months)	Weight (Kg)
		Mean ±SD (min – max)	Mean ±SD (min – max)	Mean ±SD (min – max)	Mean ±SD (min – max)
(70kVp)	200	1.69 ±0.47 (0.75 – 2.49)	33 ±9.28 (14.59 – 48.44)	10 ±6.6 (1 – 25)	7.2 ±2.1 (2.72 – 12)
(100kVp)	200	2.79 ±0.83 (1.6 – 5.31)	54.33 ±16.22 (31.13 – 103.3)	8.9 ±6.6 (1 – 24)	6.5 ±2.4 (2.6 – 12)

Table 1: Age (months), Weight (Kg) and Radiation metrics (CTDI_{vol} & DLP) of paediatric cardiac CT examinations for two different protocols based on applied tube voltage (70&100 kVp)

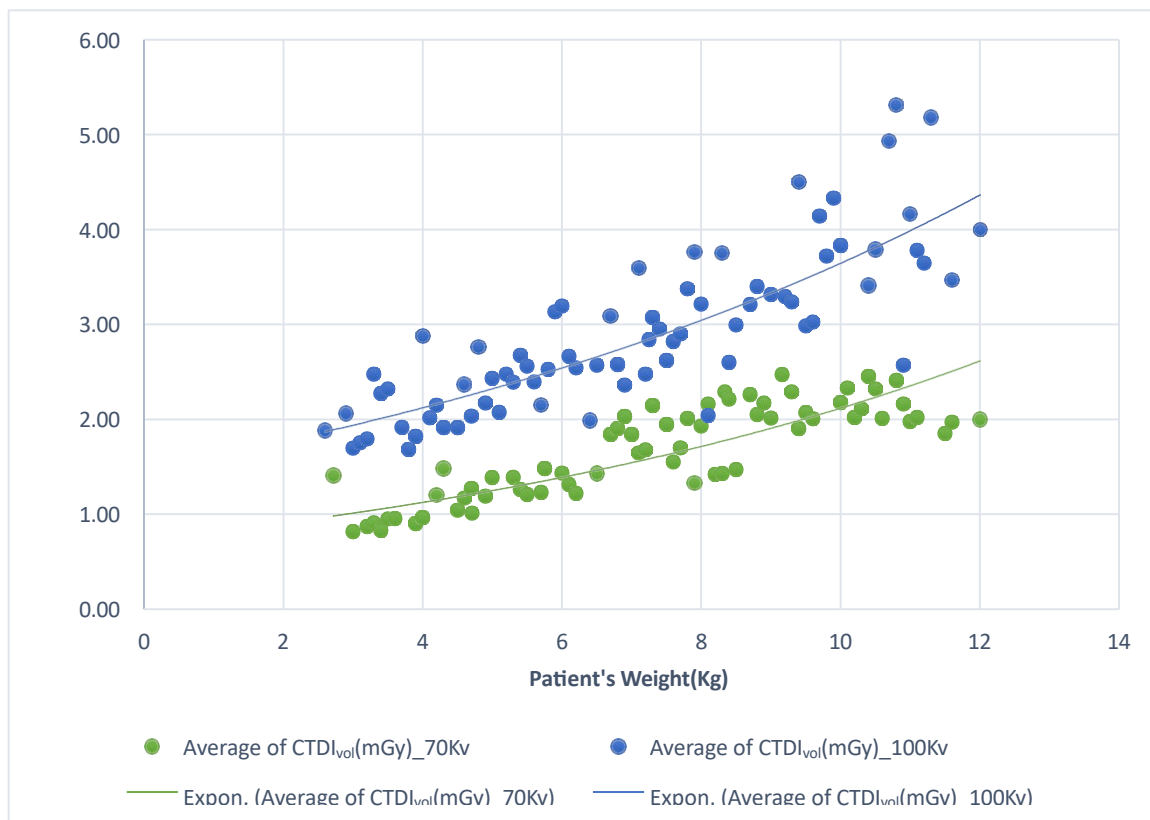


Figure 3. Comparison between the average volumetric computed tomography dose index (CTDI_{vol}) as a function of patient's weight based on applied tube voltage (70&100) kV.



Figure 4. Comparison between the average dose length product (DLP) as a function of patient's weight based on applied tube voltage (70&100) kV.

Median (IQR)

Radiation metrics	Group(A)_70 kVp (N=200)	Group(B)_100 kVp (N=200)	P - value
CTDI _{vol} (mGy)	1.68 (0.83)	2.67 (1.2)	0.000
DLP (mGy.cm)	32.77 (16.15)	51.94(23.39)	0.000

Table 2: Independent Samples Mann-Whitney U Test between Group (A) _70kVp and Group (B) _100kVp

According to Mann-Whitney U Test, Volume CT dose index and Dose length product were significantly lower in the 70-kVp group compared with the 100-kVp group

The mean CTDI_{vol} and the mean dose-length product were 1.69 mGy and 33 mGy-cm for 70- and 2.79 mGy and 54.33 mGy-cm for 100-kVp scans, respectively (P < .001). The mean CTDI_{vol} was 39% lower at 70 kVp than at 100 kVp.

Conclusion

Paediatric ECG-gated cardiac CT scans performed at 70 kVp significantly reduce radiation exposure compared to traditional high peak kilovoltage (100 kVp) scans, without compromising diagnostic image quality. Therefore, 70 kVp has emerged as the preferred approach for contrast- enhanced, ECG-gated cardiac CT examinations in children.

Tertiary Hyperparathyroidism Detected by MIBI SPECT-CT: An interesting Case Report at NINMAS

S. Reza

National Institute of Nuclear Medicine & Allied Sciences, Bangladesh

Background

Tertiary hyperparathyroidism is a life-threatening condition in patients with chronic kidney disease (CKD). It occurs as a sequel of long-standing secondary hyperparathyroidism which results from hypocalcaemia in CKD patients. In hypocalcaemia, parathyroid glands are stimulated to produce parathormone (PTH) to combat hypocalcaemia. In long standing hypocalcaemia, parathyroid glands start functioning autonomously, produce excess of PTH which results in high serum calcium level despite of withdrawal of calcium and vitamin D supplementation and the condition of high serum creatinine, high PTH, high serum calcium, and low serum phosphorus is known as tertiary hyperparathyroidism (THPT). Its definite treatment is surgery. Dual head SPECT with combined CT scan plays an excellent role in the localization of parathyroid adenoma/hyperplasia in CKD patients.

Case Report

A 48 years old diabetic, hypertensive female presented with generalized weakness and pain in both lower limbs for last two months. She was a patient of chronic kidney for a long time and had H/O repeated episodes of nephrocalcinosis which were treated accordingly. Biochemically she had very high level of PTH- 1069 pg/ml (normal range 9 – 80 pg/ml), Serum calcium level 11.2 mg/dl (normal range 8.6 -10.3mg/dl) and serum phosphate level was 2.02 mmol/l (normal 2.05 to 4.50 mmol/L). At present, her serum creatinine was 4.72 mg/dl (normal range 0.6 – 1.2 mg/dl). The patient was referred to NINMAS for detection and localization of parathyroid adenoma/hyperplasia. Ultrasonography of neck showed multinodular goitre with two hypoechoic soft tissue masses near upper pole of left lobe.

Patient underwent ^{99m}Tc Sestamibi SPECT/CT parathyroid scintigraphy at scintigraphy division of NINMAS which showed two focal activities near upper and mid region of left lobe of thyroid gland, at level C5-6.

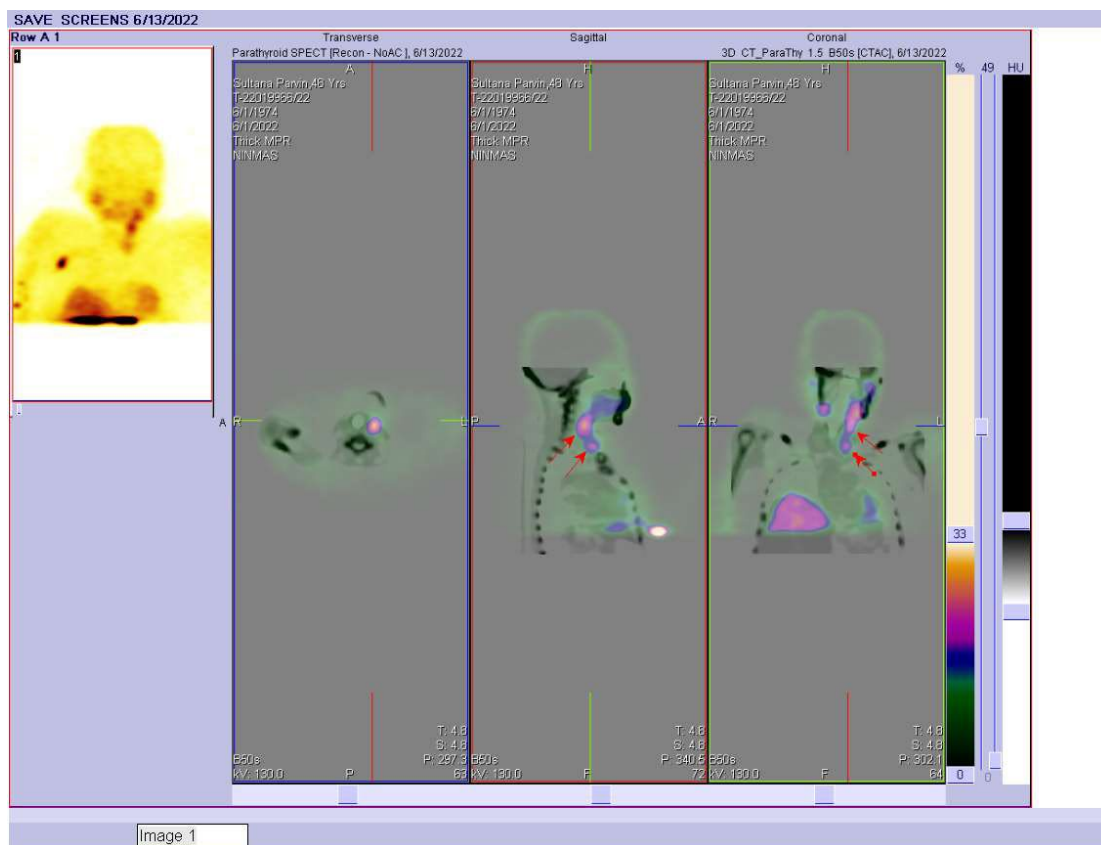


Figure 1. A 48years old female positive for parathyroid Adenoma in Hybrid SPECT/CT Tc-99m Sestamibi Scan

Conclusion

Untreated tertiary hyperparathyroidism is associated with similar risks to those of primary hyperparathyroidism. SPECT - CT fusion is a great imaging technique that provides a three-dimensional functional image with advanced contrast resolution to improve preoperative localization of parathyroid adenoma/hyperplasia.

Efficacy of 18F-Fluorodeoxyglucose PET/CT in Pyrexia Of Unknown Origin : A South Indian experience

B. Jois, R V Parameswaran, T. Syriac

Manipal Hospitals, India

Background

Pyrexia of unknown origin (PUO) refers to a condition in which the non-immunocompromised patient has body temperature that rises above 38.3°C on multiple occasions / persisting fever for at least 3 weeks or multiple febrile episodes in at least 3 weeks for which no explanation can be found. The differential diagnosis of PUO is grouped into 4 major categories: infections, non-infectious inflammatory disorders, malignancies, and miscellaneous. Conclusive diagnosis cannot be attained in most cases in spite of aggressive workup with advanced diagnostic procedures. As early phase of the disease seldom shows substantial anatomic changes, conventional radiologic techniques are less helpful. [18F]FDG PET/CT scan, if used at an early stage helps establish an early diagnosis and treatment by avoiding repetition of unnecessary tests.

Objective

To analyze the efficacy of 18F-Fluorodeoxyglucose PET/CT in Pyrexia Of Unknown Origin

Methodology

This was a cross-sectional study conducted at a quaternary care center in South India from January 2022 to December 2023. Data of 100 patients who met the PUO criteria and had [18F]FDG PET/CT were analysed. Whole body [18F]FDG PET/CT images were obtained from vertex to feet using a dedicated 16-slice PET/CT scanner.

Results

Out of the 100 patients studied, 73 were males, 27 females; predominantly in the age groups of 31-40 years and 61-70 years.

Spectrum of final diagnosis of the patients is detailed in Table 1. Forty two percent of the patients were detected with lymphadenopathy; histopathology of the nodes in 32% of these patients had either infective/malignancy/inflammatory causes (tuberculosis, non-caseating granuloma, lymphoma, Kikuchi's disease), reactive nodes in 6% of patients and was inconclusive in 4%.

Out of 100 cases analysed, majority of the cases were detected with infective pathology (63%), 14% malignancy and 12% inflammatory disorders. A total of 78 patients, scan had positive correlation (78%), out of which 11 were true negative in which no abnormal findings were detected either in PET/CT or in gold standard tests, which in these cases were culture and serology. 49 from total of 63 infective cases (78%), 10 from total of 14 malignancy (71%), and 8 from total 12 inflammatory cases (67%) showed positive correlation with respect to the corresponding findings on PET/CT corroborating with final diagnosis confirmed by histopathology/culture and serology.

Fifteen patients showed negative correlation and 7 patients were inconclusive. The overall sensitivity was 89% with a specificity of 61%.

Table 1. Spectrum of cases analysed

CASES	Total(n)	Positive	Negative	Inconclusive	True-negative
Abscess(splenic/liver/intramuscular)	5	5			
Autoimmune disease	3	2	1		
Cholangitis	1	1			
Colitis	1	1			
Enteric fever	4	1	3		
Hansen's disease	1		1		
Infective endocarditis	1	1			
Lung infection	11	10		1	
Lymphadenopathy(Granuloma, lymphoma)	42	32	6	4	
Myelodysplastic syndrome	1		1		
Meningitis	2	1	1		
Myeloproliferative disorder	1	1			
Plasma cell dyscrasias	2		1	1	
Prostatitis	1	1			
Pyelonephritis	7	7			
Sinusitis	2	1	1		
Spondylodiscitis	1	1			
Thyroiditis	1	1			
Vasculitis	2	1		1	
Total	100	67	15	7	11

Conclusion

[18F]FDG PET/CT, with its high sensitivity, assists in early detection thereby initiating prompt treatment and improving prognosis, when done as an initial investigation. The added ability to image multiple organs and pathologies associated in a single procedure, establishes superiority of PET/CT in detection of PUO over other imaging modalities.

AI-Enhanced CT Imaging for Precise Early Detection of Lung Cancer: A Comprehensive Approach Leveraging Deep Learning

A. Ayadi^{1,2}, N. Ahmed², I. Hammami^{1,2}

¹ Tunisian Center for Nuclear Sciences and Technology, Tunisia

² Research Laboratory on Energy and Matter for Nuclear Science Development (LR16CNSTN02), National Center for Nuclear Science and Technology, Tunisia

Background

Lung cancer stands out as a significant global health challenge, imposing a considerable burden on healthcare systems. The timely detection of this disease plays a pivotal role in enhancing patient prognosis and treatment outcomes. Embracing the potential of artificial intelligence (AI) in medical imaging processes has emerged as a promising strategy to boost diagnostic accuracy and efficiency in lung cancer screening.

Objectives

This study aims to introduce a robust diagnostic aid system for the early detection of lung cancer from CT images, leveraging shape and texture attributes to achieve effective lung nodule classification. Given the critical importance of early detection in lung cancer, the integration of AI tools enhances the potential for precise and timely diagnoses.

Methodology

The proposed methodology encompasses three pivotal steps. Firstly, a semantic segmentation step is implemented, utilizing the U-Net convolutional neural network. Following this, a feature extraction and selection step occurs, with the chosen features applied in the subsequent classification step using a convolutional neural network (CNN). This comprehensive approach ensures an effective and nuanced lung nodule detection process.

Results

The outcomes showcase a high level of accuracy in both the segmentation and classification of pulmonary nodules through deep learning (DL). The U-Net algorithm achieves an impressive accuracy of 99.16% and a Dice Coefficient (DSC) of 88.44% in segmentation. The classification results, distinguishing between nodules and non-nodules, reach an accuracy of 90.36%. Further classifications accurately discern subsolid nodules (solid or non-solid) with 91.89% accuracy and assess the malignancy of nodules with an accuracy of 91.54%.

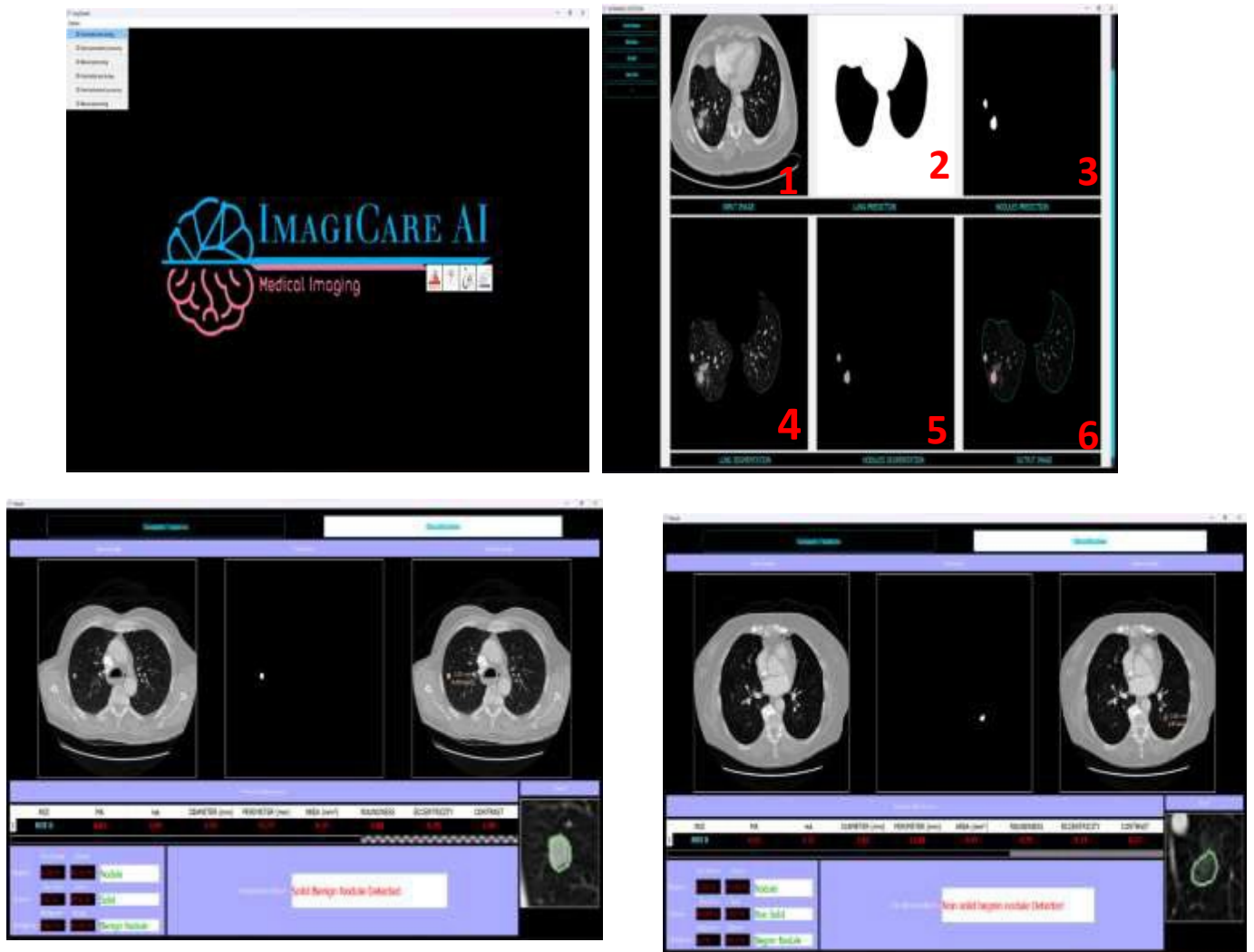
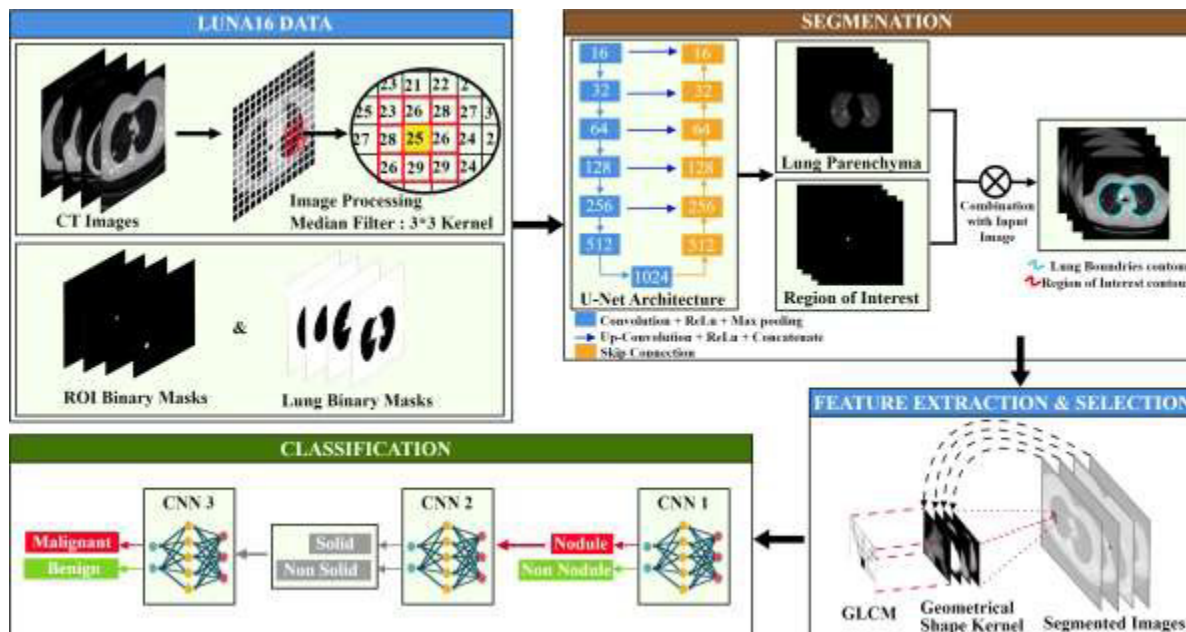


Figure 1. (a) IMAGICARE INTERFACE; (b) Segmentation Window with Labels: (1) Input Image, (2) Studied Organ Prediction, (3) Nodule Prediction (ROI), (4) Studied Organ Segmentation - Lungs, (5) Nodule Segmentation, (6) Segmented Image; (c) (d) Classification Window.

Conclusion

In summary, this study presents a robust diagnostic aid system demonstrating high accuracy in the early detection of lung cancer from CT images. The integration of AI, particularly utilizing deep learning techniques, proves instrumental in achieving enhanced precision in lung nodule classification. These results underscore the potential of the proposed system as a valuable tool for clinicians and healthcare professionals, contributing to improved healthcare outcomes. Future endeavors will explore applying this developed method in CT/PET imaging.

Graphical Abstract



Highlights

- The integration of AI in medical imaging holds tremendous promise for revolutionizing lung cancer screening, offering a more precise and efficient approach.
- Our deep learning-powered lung nodule detection system showcased remarkable segmentation accuracy (99.16%) through the implementation of the U-Net algorithm.
- The proposed methodology seamlessly combines semantic segmentation using the U-Net algorithm with attribute-based classification employing a CNN.
- Noteworthy achievements include high accuracy in distinguishing nodules from non-nodules (90.36%), accurately classifying subsolid nodules (91.89%), and determining the malignancy of nodules (91.54%).
- These results underscore the potential for significant advancements in early lung cancer detection and diagnosis.
- The study highlights the invaluable contribution of AI tools in reshaping lung tumour screening, offering promising prospects for substantial improvements in patient outcomes.

Initial Implementation of PSMA-Directed Theranostics for Prostate Cancer in Lebanon: An Early Clinical Appraisal

M. Haidar¹, N. Saliba¹, N. E. Ghawi¹, N. Omran¹, Y. Ghosn¹, Y. Jabbour¹, M. E. Jebai¹, E. A. Chawareb², A. A. Ghanem¹, A. El-Hajj²

¹ Department of Diagnostic Radiology, American University of Beirut Medical Center, Beirut, Lebanon

² Department of Surgery, Division of Urology, American University of Beirut Medical Center, Beirut, Lebanon

Background

PSMA-based theranostics represent an emerging frontier in advanced prostate cancer treatment. This study aims to assess the safety and efficacy of PSMA-based theranostics in managing metastatic castration-resistant prostate cancer (PCa) among Lebanese patients.

Methodology

This retrospective study includes 28 male patients diagnosed with advanced PCa and treated with PSMA-based theranostics between January 2016 and December 2022. The inclusion criteria was the following: male patient with PCa who had undergone radical therapy, hormonal therapy, or chemotherapy and showed rising PSA levels and disease progression on Ga-PSMA PET/CT. To be included in the study, some patients underwent FDG PET/CT to rule out mismatch avid lesions. This study focuses on the changes in Ga-PSMA uptake on follow-up imaging, bone pain improvement, disease outcome, and adverse effects.

Results

The mean age of patients was 75 years. Patients received two to five doses of Lu-PSMA and faced treatment interruption due to financial difficulties. Three of these patients were switched to Ac-PSMA due to disease progression.

Initially, all patients received either radical prostatectomy (8/28) or radical radiotherapy (20/28).

Moreover, prior to starting Lu-PSMA treatment, patients had received first line hormonal therapy (22/28) and chemotherapy (23/28). In addition to that, at the time of the first Lu-PSMA cycle, all patients had metastasis, with bone and lymph node metastasis being the most common.

The results came as following: Ga-PSMA uptake on imaging was reduced in 43% (12/28) of patients, while 39% (11/28) reported relief from bony pain. All three patients (100%) who received Ac-PSMA had improvement in bony pain and decreased Ga-PSMA uptake on subsequent imaging. All patients reported significant improvement in quality of life. Furthermore, 14% (4/28) of patients achieved complete remission and 43% (12/28) had either a partial response to treatment or stable disease.

However, disease progression occurred in 21% (6/28) of cases, and 21% (6/28) of patients died due to the following reasons: 7% (2/28) due cardiovascular disease, 7 % (2/28) due to sepsis, 4% (1/28) due to COVID infection, and 4% (1/28) progression of metastatic of PCa (Figure 1). Adverse effects were also reported, 4% (1/28) experienced salivary gland toxicity and 32% (9/28) experienced bone marrow suppression.

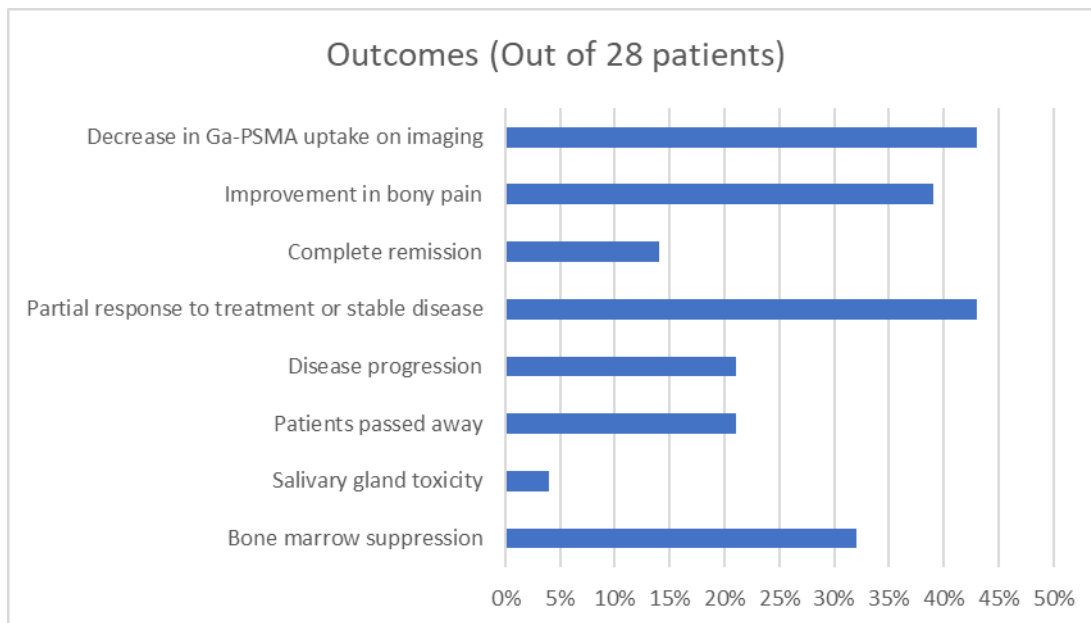


Figure 1. Various outcomes of PSMA PET/CT

Conclusion

PSMA-based theranostics can safely improve quality of life and increase overall survival rate in patients with advanced PCa. PSMA PET/CT has a significant impact on patient management and leads to significant pain reduction, decrease in PSA levels, and improved survival rates when compared to conventional approaches. PSMA PET/CT emerges as an available and effective therapeutic option with transformative implications on patient outcomes, particularly in the context of metastatic castrate-resistant prostate cancer (MCRP). Further studies are needed to evaluate the long-term efficacy and safety of PSMA-based theranostics in a larger cohort of patients.

Quantifying Radiation Exposure: Biokinetic Analysis and Dosimetry of [¹⁸F]F-PSMA-1007 in Prostate Cancer Patients Using PET/CT Imaging

M. A. Said

Institut Kanser Negara, Malaysia

Background

Positron Emission Tomography-Computed Tomography (PET/CT) utilizing prostate-specific membrane antigen (PSMA) ligands is pivotal in diagnosing prostate cancer. The novel tracer, [¹⁸F]F-PSMA-1007, offers enhanced production and biokinetic advantages over the standard [⁶⁸Ga]Ga-PSMA-11. However, limited dosimetry data exists for [¹⁸F]F-PSMA-1007, particularly in prostate cancer patients. Our study addresses this gap, focusing on 4 patients to comprehensively investigate the biokinetics and dosimetry dynamics of [¹⁸F]F-PSMA-1007, aiming to optimize imaging protocols, ensure patient safety, and refine treatment strategies in the context of prostate cancer diagnosis and management.

Methodology

Imaging procedures were conducted on a GE HealthCare MI DR system, utilizing a 3-D mode PET acquisition protocol. Emission data underwent corrections for randoms, scatter, and decay, followed by reconstruction using an ordered subset expectation maximization (OSEM) algorithm. The reconstruction parameters included 2 iterations with 21 subsets and Gauss filtering for a transaxial resolution of 5 mm at full width at half-maximum (FWHM). Attenuation correction was performed using unenhanced low-dose CT data, reconstructed with a slice thickness of 3.75 mm.

Patients

To assess initial dosimetry, four healthy volunteers underwent [¹⁸F]F-PSMA-1007 PET/CT scans at multiple time points up to 180-minutes post-injection. Written informed consent was obtained from all patients (n=5) with newly diagnosed high-risk prostate cancer. Imaging was performed 20-, 60-, and 180-minutes post-injection, and data were retrospectively analysed following local ethics committee approval.

Radiation Dosimetry

Dosimetry analysis utilized by using MIM Software Version 7.4.5. Automatic rigid co-registration and manual correction were applied to PET and CT datasets. Organs, including kidneys, liver, spleen, whole heart, upper and lower large intestine, parotid glands, submandibular glands, and urinary bladder, were segmented into volumes of interest (VOI) by using Contour Protégé AI+'s features. Time activity curves (TACs) were generated for all organs, with curve fitting applied according to the software. Cumulative activities (Å) were calculated between time points using various methods, and residence times for source organs were determined. Absorbed and effective dose calculations were performed using the MRT SurePlan™ package.

Results

The average absorbed dose for all patients was determined to be 0.02 mGy/MBq, with the kidneys registering the highest absorbed dose (AD) at 0.11, followed by the liver and spleen at 0.10. Subsequently, the submandibular, parotid, and adrenal glands recorded a dose of 0.09, the gallbladder

0.5, the brain 0.3, and the thyroid, rectum, prostate, and urinary bladder each exhibited absorbed dose of 0.2 mGy/MBq.

Conclusion

In conclusion, our study emphasizes the prospective role of [¹⁸F]F-PSMA-1007 in PET/CT imaging for prostate cancer diagnosis, particularly noting the kidneys as a critical organ at risk. These findings provide essential insights for enhancing patient safety and fine-tuning treatment strategies, especially in cases of high-risk prostate cancer.

Comparison of LVEF estimations from planar and gated SPECT radionuclide blood pool studies between conventional NaI versus ZnCd SPECT/CT machines

T. Thientunyakit¹, S. Chirakarnjanakorn², K. Korphaisarn², C. Sethanandha¹, T. Thongpraparn¹, P. Mali¹

¹Department of Radiology, Faculty of Medicine Siriraj Hospital, Mahidol University, Thailand

²Department of Medicine, Faculty of Medicine Siriraj Hospital, Mahidol University, Thailand

Background

Monitoring of LVEF has been used to detect anthracycline cardiotoxicity. LVEF was monitored with equilibrium radionuclide angiocardiology (ERNA) because of its low interobserver variability, high accuracy, and reproducibility. Echocardiography and Gated Blood Pool SPECT (GBPS) were subsequently developed to evaluate LVEF with the advantage of non-ionizing radiation and a 3-dimensional technique. Recently, Cadmium Zinc Telluride (CZT) detectors were claimed to outperform conventional Sodium Iodide (NaI) detectors concerning image resolution and count sensitivity. However, the effect of quantitative differences on LVEF results between two detectors is limited. This study compared individual LVEF estimations between ERNA and GBPS using the conventional NaI and CZT SPECT/CT scanners and echocardiography.

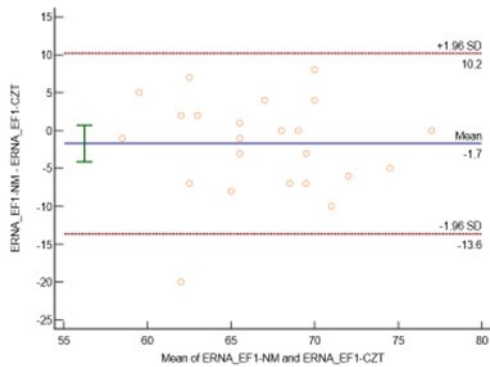
Methodology

This single-center study is a part of an international, multicentre, prospective, observational study called the International Imaging in Cardio-Oncology Study (ICOS). We included 30 female patients at least 18 years of age who were newly diagnosed with breast cancer and scheduled for anthracycline-based chemotherapy. Those with prior chemotherapy, pre-existing cardiac dysfunction, and prior significant cardiovascular or other medical conditions were excluded. All patients underwent baseline ERNA, GBPS, and echocardiography on the same day with clinical assessment. The ERNA and GBPS were performed using approximately 740 MBq (20 mCi) of in-vivo labeled technetium-99m red blood cells and scanned with NaI SPECT/CT (NM), followed by CZT SPECT/CT. Image acquisition and reconstruction followed the ICOS's protocol. LVEF estimation from ERNA (EF analysis software), GBPS (BGS software), and echocardiography (modified Simpson's) were analysed and compared using paired t-test and Bland-Altman plot. P-value < 0.05 was considered as statistical significance.

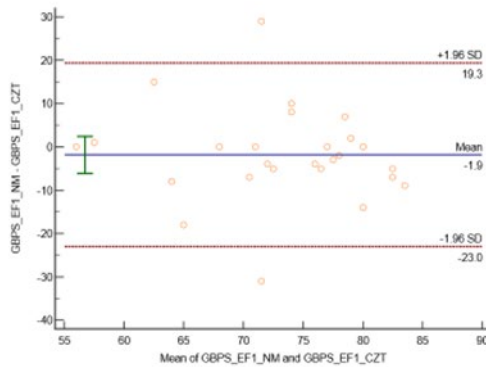
Results

Twenty-seven of thirty female patients with breast cancer, aged 55.23±10.09 years, BMI 23.55±3.49 kg/m² underwent all three imaging studies. No patient demonstrated cardiac symptoms or abnormal LVEF (<50%). The average LVEF was 66.17±5.34% (NM) versus 67.44±5.49% (CZT) using ERNA, 71.37±8.93% (NM) and 73.96±9.50% (CZT) using GBPS, and 70.55±4.41% using echocardiography. Significant differences were found when comparing ERNA with GBPS and ERNA with echocardiography, regardless of the detector types (P-value <0.001 – 0.003). However, there were no significant differences between LVEF results using the same technique from different machines or between GBPS versus echocardiography. The overall trend of LVEF results was higher in GBPS > Echo > ERNA in both NM and CZT SPECT/CT machines. The Bland-Altman plots demonstrated that the average difference of individual LVEF was largest between ERNA vs. GBPS (5.2 to 6.5 EF units lower), followed by ERNA vs. echocardiography (3.6 to 4.4 EF units lower) and GBPS vs.

echocardiography (0.8 to 2.9 EF units higher), respectively. The CZT showed an average of 1.7 (ERNA) to 1.9 (GBPS) EF units higher LVEF than using NM.



ERNA NM vs. CZT



GBPS NM vs. CZT

Conclusion

The differences in individual LVEF estimations between techniques (ERNA vs GBPS) are more significant than between machines or detector types. The average LVEF estimated by echocardiography significantly differed with ERNAs but not GBPSs. Generally, higher LVEFs were estimated by GBPS, followed by echocardiography and ERNA, respectively. LVEF estimation using CZT SPECT/CT is also higher than conventional NaI SPECT/CT. However, the differences are minimal when the same technique is used.

Synthesis and evaluation of radioiodinated Alpha Mangostin for targeting estrogen receptor α in breast cancer

W. Nurhidayah¹, K. Kannaka², H. Suzuki², T. Subroto¹, T. Uehara², M. Muchtaridi^{3,4}

¹ Department of Chemistry, Faculty of Mathematics and Natural Sciences, Universitas Padjadjaran, Indonesia

² Graduate School of Pharmaceutical Sciences, Chiba University, Japan

³ Department of Pharmaceutical Analysis and Medicinal Chemistry, Faculty of Pharmacy, Universitas Padjadjaran, Indonesia

⁴ Research Collaboration Centre for Radiopharmaceuticals Theranostic, Indonesia

Background

Alpha mangostin (AM), the most representative xanthone derivative isolated from Mangosteen rind, has been reported pharmacologically to be associated with breast cancer in vitro and in vivo. Although the pharmacological effects of AM would be involved in estrogen receptor α (ER α), there are no reports of AM binding to ER α .

Methodology

In this study, we prepared iodine-125 (125I)-labeled MA ([125I]I-AM) and investigated the binding of [125I]I-AM to ER α using breast cancer cell line MCF-7. To investigate the applicability of radioiodine-labeled AM as a radiopharmaceutical for breast cancer, [125I]I-AM was injected into nude mice bearing MCF-7.

Results

The uptake of [125I]I-AM into MCF-7 cells was inhibited by AM and tamoxifen, suggesting that the uptake of [125I]I-AM was partially mediated by ER α . In addition, biodistribution studies using MCF-7 bearing nude mice showed that [125I]I-AM accumulated in tumour tissues, although the deiodination occurred. Therefore, further studies such as preventing deiodination without AM properties are required.

(a) The uptake of [125I]I-AM in MCF-7 cells from 0.5 h to 3 h was measured. (b) The uptake of [125I]I-AM was measured in the presence or absence of 1 mM AM, 1 mM Estradiol, and 1 mM Tamoxifen. *: $p < 0.05$

Conclusion

these studies indicated that the cellular uptake of [125I]I-AM was partly mediated by ER α . In addition, [125I]I-AM showed tumour accumulation in vivo, although the deiodination occurred. Therefore, further studies such as preventing deiodination without AM properties are required. These results suggested that AM would be a useful platform for the development of new radiopharmaceutical for breast cancer targeting ER α .

Keywords: Alpha mangostin; estrogen receptor; breast cancer; Radioiodinated; 125-Iodine

[18F]FDG/PET/CT in determining disease activity in patients of Spinal Tuberculosis and guiding Anti-Tubercular therapy (ATT)

P. Verma^{1,2}, B. Hadole³, T. Rathod³, S. Basu^{1,2}

¹ Radiation Medicine Centre, Bhabha Atomic Research Centre, India

² Homi Bhabha National Institute, India

³ Department of Orthopaedics, Seth GSMC and King Edward Memorial Hospital, India

Background

Inadequate duration of anti-tubercular therapy (ATT) leads to increasing prevalence of multidrug-resistant tuberculosis (MDR-TB). Therefore, appropriate evaluation of disease activity is mandatory to determine treatment duration. Recent literature shows higher sensitivity of FDG/PET/CT in detecting spinal TB activity compared to CT/MRI.

Aim

To evaluate the metabolic disease activity and its resolution with ATT in patients of spinal tuberculosis with help of functional non-invasive objective imaging in form of [¹⁸F]FDG/PET/CT.

Methodology

This was a longitudinal study of 50 patients of spinal tuberculosis on ATT evaluated clinically and radiologically. Enrolled patients underwent baseline and sequential FDG/PET/CT scans at 6, 12 and 18 months, with calculation of the SUVmax and thereby assessing disease activity. ATT was stopped on absence of FDG uptake (metabolic activity) in the lesion and patients were followed up regularly. Statistical analysis was done using SPSS software to reach statistically significant results.

Results

Out of 50 patients, 25% were MDR-TB and 16% required surgery. 44% required ATT for 0-6 months, 34% for 6-12 months, 24% for 12-18 months and 18% for >18 months. The mean SUVmax per vertebral body lesion was 5.20. Nine patients had metabolic activity on PET/CT even after 18 months of ATT. Serial scans showing decreasing SUVmax trend were termed responding lesions. Unlike pulmonary tuberculosis absence of acid-fast bacilli in the sputum is not applicable for paucibacillary deep-seated lesions like spinal tuberculosis. The patients with non-FDG avid healed lesions were followed up for 6 months after being declared cured and none showed recurrence in 6-months follow-up.

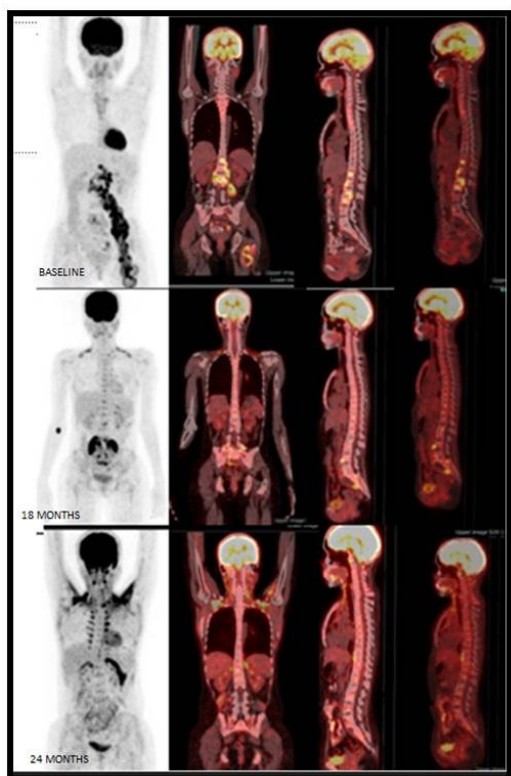


Figure 1. Baseline [^{18}F]FDG/PET/CT [MIP, fused coronal, sagittal, and sagittal bone window] images of 28-year-old lady with recently diagnosed spinal tuberculosis revealed hypermetabolic lytic sclerotic thoracic and lumbosacral lesions and left paravertebral soft tissue (abscess). 18-month images demonstrate FDG uptake in the vertebral lesions and the left paravertebral soft tissue-residual active disease. 24-month images showed no significant FDG concentration in the above mentioned lesions-healed status.

Conclusion

In our study, there was decrease in disease activity with increasing duration of ATT while the duration at which the patients achieved healed status was variable. Although literature advocates administration of ATT for up to 18 months, we found 9 patients having residual disease activity on FDG/PET/CT and required ATT beyond 18 months. Therefore, ATT should be tailor-made as per patient and not administered for fixed duration as a policy. Inordinate long duration of ATT can lead to toxicity and non-compliance. While inadequate short duration breeds resistance, so it is important to administer ATT for the appropriate duration of the disease. Hence, the need for objective monitoring of disease activity by imaging and thereby healing is important before discontinuing ATT. FDG/PET/CT as a functional imaging can be useful for objective evaluation of real-time disease activity and ascertaining healed status in spinal TB. The changes in the SUVmax following ATT can be employed as a reliable marker for ascertaining the disease activity.

Utilization of [¹⁸F]FDG PET/CT in evaluating disease activity in Takayasu Arteritis

I. J. Isip¹, I. Bandong², A. D. Sevilla¹

¹St. Luke's Medical Center Quezon City, Philippines

²Philippine Society of Nuclear Medicine, Philippines

Background

Takayasu arteritis (TAK) is an inflammatory condition of the large vessels and its branches, commonly affecting females in the second to third decade of life with an annual incidence rate of 0.4–3.4 per million people. This case report will discuss the role of PET/CT scan in the evaluating disease activity and treatment response in TAK.

Case Report

Presenting a 29-year-old Filipina with abdominal pain, left carotid bruit and blood pressure difference in all extremities. Her CT angiography showed fusiform dilatation and wall thickening of the aorta; carotid/vertebral duplex scan revealed multiple stenotic lesions with elevated inflammatory biomarkers. She was diagnosed with TAK and was managed with Methotrexate. Post-therapy PET/CT scan revealed hypermetabolism in the thoracic aorta and vertebral arteries (Figure 1A) accompanied by normal inflammatory biomarkers.

Follow-up imaging showed regression of stenotic lesions and stable wall thickening of the aorta, and normal inflammatory biomarkers. PET/CT scan showed metabolic progression in multiple small- and large-sized arteries (Figure 1B and D). After Methotrexate dose titration, she remained asymptomatic for 2 years until she experienced severe abdominal pain with elevated inflammatory biomarkers. CT angiography showed morphologically stable findings while her PET/CT scan revealed new hypermetabolic foci in the proximal descending aorta and metabolic progression in the vertebral arteries (Figure 1C and E). She was diagnosed with refractory TAK and started on Tocilizumab.

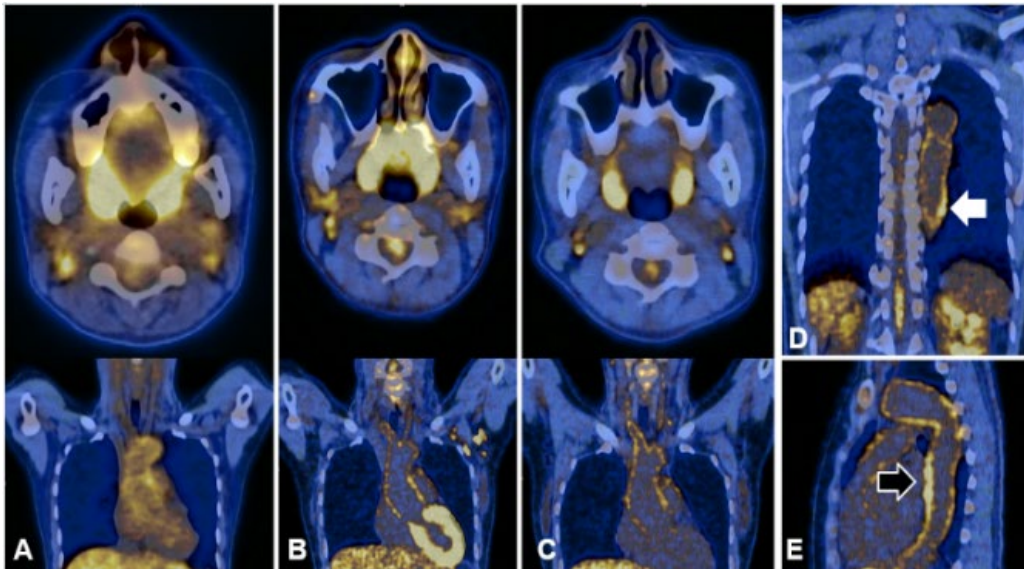


Figure 2. Comparative PET-CT images from 2019 to 2023. The baseline images (A) show mild hypermetabolism in the ascending aorta, aortic arch and bilateral vertebral arteries (PETVAS 2-3). Follow-up scan (B) showed metabolic progression with new hypermetabolic foci in the proximal descending aorta (PETVAS 2-3), new hypermetabolic activity in the wall of the proximal descending aorta (PETVAS 2-3; D, white arrow). The latest PET scan (C) showed metabolic progression with new hypermetabolic foci in the walls of the proximal descending aorta (PETVAS 3; E, black arrow).

Discussion

TAK is an auto-immune disease of the large vessels presenting with non-specific symptoms. Early diagnosis and monitoring are crucial to prevent early cardio/cerebrovascular disease.

Scoring systems are used to diagnose and evaluate TAK which includes clinical features, imaging modalities, and inflammatory biomarkers however the latter have low sensitivity, specificity, and accuracy. In addition, immunosuppressive medications can resolve clinical symptoms and suppress inflammatory biomarkers making monitoring disease/treatment response more challenging.

CT angiography can identify stenoses and vascular wall thickening however, contrast agent allergy and nephrotoxicity limits its use. [^{18}F]FDG PET/CT can provide early assessment of inflammatory arterial wall lesions and evaluation of treatment response after therapy.

In 2018, the European Medical Association, Society of Nuclear Medicine and Medicine and the PET Group recommends the use of PETVAS scoring system in interpreting large vessel vasculitis using [^{18}F]FDG PET/CT. It has a sensitivity of 70-90% and correlates with disease activity, wherein decreased vascular FDG uptake correlates with clinical remission. Immunosuppressive treatments can cause resolution of symptoms and regression of inflammatory biomarkers; but increased vascular uptake on PET/CT suggests that the lesion persists but with a lower level of activity. Studies suggests that clinical, laboratory markers and angiography are inadequate in assessment of disease activity and recommends [^{18}F]FDG PET/CT imaging to improve patient outcomes.

Conclusion

We have presented a diagnosed case of TAK showing persistent and progressive hypermetabolism in both small- and large-sized blood vessels in contrast to the stable morphologic findings on conventional imaging. We highlight the significance of [^{18}F]FDG PET/CT in the early assessment of disease activity and evaluating treatment response.

Amyloid light chain amyloidosis with extracardiac uptake on Technetium-99m pyrophosphate cardiac scan

I. J. Isip¹, I. Bandong²

¹ St. Luke's Medical Center Quezon City, Philippines

² Philippine Society of Nuclear Medicine, Philippines

Background

Amyloidosis is a protein misfolding disorder causing organ dysfunction. It commonly occurs in elderly males and worldwide incidence of 5 to 13 cases per million per year. Unchanged median survival of 5 months from diagnosis suggests continued delays in diagnosis. The case will describe the role of technetium-99m pyrophosphate cardiac scintigraphy (PYP scan) in the diagnosis of primary systemic amyloidosis.

Case Report

The patient presented with a 6-month history of intermittent bipedal oedema and non-specific systemic symptoms with elevated creatinine and proteinuria. She was diagnosed and managed as a case of glomerulonephritis however, persistently increasing serum creatinine and proteinuria prompted renal biopsy which revealed renal amyloidosis. Series of laboratory and imaging tests were ordered based on the diagnostic algorithm for suspected systemic amyloidosis which suggested cardiac involvement.

A PYP scan (Figure 2) was done which showed grade 1 myocardial uptake with a heart-to-contralateral ratio of 1.33. Diffuse PYP uptake in the liver and spleen suggested other organ involvement, hence the liver biopsy. Unfortunately, the patient expired due to fatal arrhythmia. The liver and partial autopsy reports, as well as mass spectroscopy confirmed the light-chain amyloidosis involving the kidneys, liver and heart.

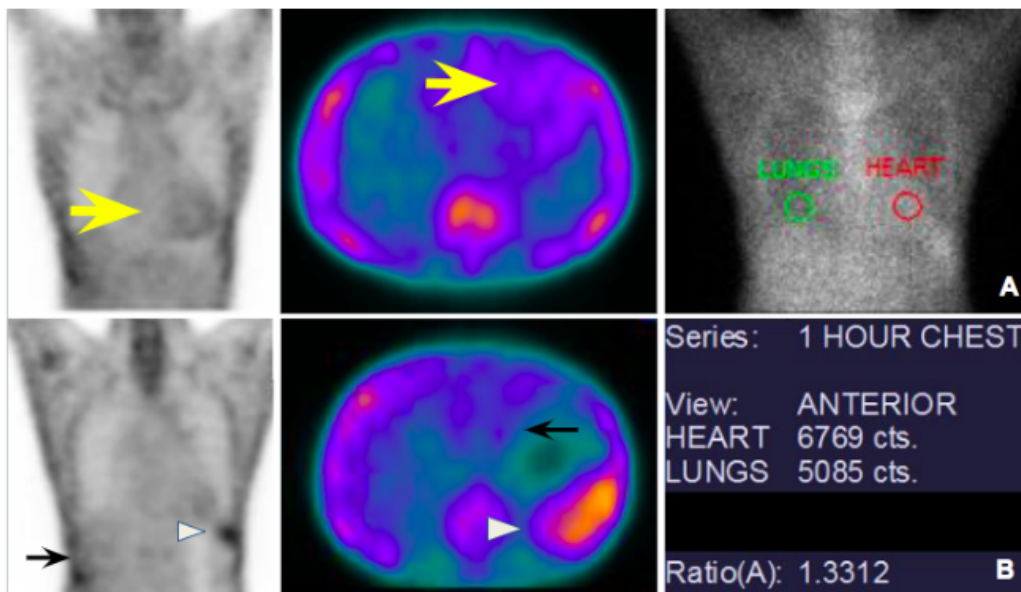


Figure 2. Technetium-99m pyrophosphate cardiac scan. Planar and SPECT imaging were obtained 1 hour and 3 hours after intravenous administration of Tc-99m pyrophosphate. Semi-quantitative SPECT images show grade 1 myocardial uptake (yellow arrows) with extracardiac findings of mild diffuse uptake in the liver (black arrows) and intense uptake in the spleen (white arrowheads). Quantitative analysis was performed by drawing regions of interest over the planar images of the heart and contralateral lung (A). The calculated heart-to-contralateral lung ratio is 1.33 (B). A ratio of >1.5 at one hour is classified as ATTR positive.

Discussion

Amyloidosis is caused by the deposition of amyloid fibrils that cause organ dysfunction. The prognosis depends on the type and amount of fibril deposition on the affected organ upon diagnosis. Early diagnosis and reduction of circulating amyloid fibrils is the goal of management.

Amyloidosis can either be localized or systemic. Primary systemic amyloidosis is usually of the light-chain type (AL type) with 76% of patients have cardiac involvement, with renal (53%), liver (18%), and nerve (24%) involvement, with cardiac involvement being the best predictor of mortality and morbidity compared to other organs. Diagnostic work-up includes confirmation of multi-organ involvement. Some cases show negative or equivocal laboratory results which necessitates tissue biopsy of the suspected organ involved. PYP scan offers a non-invasive approach to diagnosing ATTR amyloidosis without endomyocardial biopsy. A case of ATTR amyloidosis reported persistently increased PYP uptake in the heart and abdominal walls which identified an alternative possible biopsy site to confirm the diagnosis. Similarly, extracardiac technetium-99m PYP uptake suggested multiple organ involvement and provided an alternative biopsy site.

Bisphosphonate radiotracers such as technetium-99m 3,3-diphosphono-1,2-propanodicarboxylic acid (DPD) and technetium-99m hydroxymethylene diphosphonate (HMDP) are used in ATTR cardiac scintigraphy. Hepatic and splenic HMDP uptake is exclusively seen in the AL type of amyloidosis while DPD liver uptake is noted in both ATTR and AL amyloidosis. Extracardiac HMDP/DPD uptake suggests amyloid burden in other organs and determines disease extent. A similar study concluded increased cardiac uptake with extra-cardiac findings are diagnostic and prognostic in amyloidosis cases.

Conclusion

Early detection remains the key to a better prognosis in amyloidosis however tissue biopsy remains the gold standard in confirming the diagnosis. The case underscores the diagnostic role of PYP scan in detecting any extracardiac amyloid burden and suggests possible biopsy sites in AL amyloidosis.

Experience in establishing a PET/CT unit in one nuclear medicine department: Main constraints encountered!

L. B. Omrane¹, I. Slim², A. Mhiri²

¹ Centre National de Radioprotection, Hôpital d'Enfants Bab Sâadoun, Tunis, Tunisia

² Nuclear Medicine Department, Salah Azaiez Institute, Tunis, Tunisia

Background

PET today appears to be an essential technique in oncology. Its association with another imaging modality will allow precise assessments to characterize the progress of cancer or possible recurrences. It therefore has a role both in diagnostic and also therapeutic strategies.

But, given investment and operating costs, the implementation of such equipment must be analysed in order to know medical benefits which would justify such an investment.

This new medical imaging technology was implemented in Nuclear Medicine department at the oncologic Salah AZAIEZ Institute in Tunis in 2019. For this, the department which opened its doors since 1970 saw a remodelling to find the necessary space for installation of a PET/CT unit as well as the implementation of compliance rules for such equipment.

During installation of the PET/CT unit, various modifications took place: Reorganization of the hot lab area in order to accommodate PET/CT, creation of specific injection boxes, creation of an extension in order to accommodate room for images interpretation and offices and thus free up space for the new unit.

The installation of such equipment generated many constraints. These were of different orders: radiation protection, environment, layout of the future unit...

Through this work, we have attempted to list the main constraints encountered in the installation of our PET/CT

Optimization Methylene Diphosphonate Radiopharmaceutical to enhance Affordability and Accessibility in Resource-Limited Settings

J. Zulu^{1,2}, , B. Mudenda Hang'ombe⁴

¹ Department of Nuclear Medicine, University Teaching Hospital, Lusaka Zambia

² Department of Pharmacy, Levy Mwanawasa Medical University, Lusaka, Zambia

⁴ University of Zambia, School of the Veterinary Medicine, Lusaka, Zambia

Aim

The primary objective of this research was to assess the stability and quality of Methylene Diphosphonate (MDP) aliquots when stored at ambient conditions over a defined period. By delving into the intricacies of ambient storage, we sought to not only expand our understanding of MDP stability but also uncover potential cost-effective solutions that may enhance the accessibility of this critical diagnostic substance. A comparative analysis between ambient-stored MDP aliquots and those stored in refrigerated and frozen conditions formed a core component of this study. This research also aimed to explore additives that may further enhance the stability of ambient-stored MDP aliquots.

Methodology

An experimental design was applied, and data collected from observing results from the controlled laboratory. The research was conducted at the University Teaching Adult Hospital Nuclear Hot Laboratory in Zambia. In all, 40 MDP aliquots kept at ambient conditions and labeled with Technetium-99m (^{99m}Tc) were tested. The data was analysed using Stata 14.

Results

Results showed that ambient stored MDP aliquots had RCPs between 98% and 99%, far greater than the 90% minimal need. The RCP varied between 99% and 100% for those stored in cold and freezing environments.

Conclusion

Potentially useful for low-resource nations, the results highlighted the fact that cold chain storage may be difficult to sustain throughout periods of power outages.

Keywords: Technetium, Methylene di phosphate, Radiochemical purity, Radiopharmaceutical, ambient conditions

Lymph Node or Secondary Tuberculosis

M. R. Montecinos

Nuclear Medicine, Bolivia

Background

Tuberculosis (TB) still represents a public health problem in developing countries like Bolivia. PET/CT with [18F]FDG plays an important role in the study of lymphadenopathy of secondary origin; However, its sensitivity and specificity are reduced when an infectious disease such as TB is suspected at the same time as the oncological disease. This work aims to study the findings of PET/CT with [18F]FDG in patients with hypermetabolic lymphadenopathy with an underlying neoplastic disease, but also with images suggestive of pulmonary TB.

Methodology

A retrospective analysis of PET/CT studies of 23 patients with various neoplasms (lymphoma, lung cancer and breast cancer) and radiological signs of pulmonary TB was performed. Of this number, 17 patients were included who also presented hypermetabolic hiliomediastinal lymphadenopathy with a differential diagnosis of infectious origin due to TB or secondary origin. The average age of the patients was 56 years (range 22-81 years). The radiological characteristics of the lung lesions were also studied and the maximum standardized uptake value (SUVmax) of the lymph nodes considered pathological was analysed.

Results

Of the patients included in the study, 36% had been referred for lymphoma; 19% for lung cancer, 13% for breast cancer and the remainder for other neoplasms (rectal, ovarian, thyroid cancer, tumour of unknown origin and head and neck cancer). 29% were referred for restaging, 29% for initial staging, and 24% for control of response to treatment. The study showed the presence of hiliomediastinal hypermetabolic lymphadenopathy in all patients included with an average SUV_{máx} of 5.7. In these patients, the existence of centrilobular micronodules was confirmed in 31% of the cases, peripheral micronodules with little or moderate metabolism in the other 31%, or the coexistence of both lesions in 69%. 44% of those studied confirmed TB using specific laboratory techniques. Of the remaining percentage, 56% ruled out the disease using the same techniques and the other 44% did not perform any control study.

Conclusion

PET/CT with [18F]FDG allows evaluating the presence of malignancy at the lymph node level in multiple neoplasms. The sensitivity of the technique is reduced given that the radiotracer is not specific to the oncological area, so it can concentrate on sites of infection/inflammation, a fact that leads to secondary false positives. In a country with high rates of infectious diseases, the coexistence of cancer and TB is not an isolated event; However, the correct characterization of the lesions and a laboratory study could modify the treatment and management of patients, although it must be taken into account that the negativity of the laboratory results does not necessarily mean that the patient is free of TB, given the varied sensitivity of the tests (65-98%). In our study, patients diagnosed with TB received timely treatment and continued their oncological therapy.

Role of Pet/Ct with 18F-FDG as a Tool in Restaging, Treatment Response Control, Prognosis and Planning of Stereotactic Body Radiotherapy (Sbrt) in Cervical Cancer, a Series of Cases

M. R. Montecinos

Nuclear Medicine, Bolivia

Background

Cervical cancer is a pathology with high mortality rates among Bolivian women. The latest guidelines suggest the use of PET/CT with 18F-FDG for restaging and control of response to treatment by identifying lymphadenopathy and secondary lesions, in addition to their metabolic behaviour, it can be used to delineate the specific volume to be treated with stereotactic body radiation therapy (SBRT). Five patients with cervical cancer in whom the technique was applied to control response to treatment and SBRT planning are presented.

Case Studies

Case 1 : 57-year-old patient with no previous treatment, complains of heavy menstrual bleeding. She presents with a lesion that extends from the cervix to the lower third of the vagina, generating pyeloureteral ectasia and left hydronephrosis. PET/CT showed a lesion in the cervix with a Standard Uptake Lean body mass (SUL) of 4.6. After SBRT, control PET/CT shows absence of tumour activity consistent with a complete metabolic response.

Case 2: 48-year-old patient receiving chemotherapy (CT) and radiotherapy (RT). PET/CT was performed and reported a lesion in the vaginal vault with SUL of 12.7. Ten months later, the study showed no lesions suggestive of neoproliferative activity thus a complete metabolic response.

Case 3: 38-year-old patient, treated with CT and brachytherapy (BT), with signs of recurrence. PET/CT is performed for restaging and SBRT planning. A lesion SUL of 6.1 is reported in the rectovesical space. After treatment, the new study shows a decrease in SUL by 2, which according to PERCIST 1.0 corresponds to a partial metabolic response.

Case 4: 31-year-old patient, with previous hysterectomy, with CT and RT. PET/CT was performed for suspected recurrence. A lesion in the vaginal vault with SUL of 3.6 is reported. After SBRT a reduction in the size and metabolic activity of the tumour is observed with a residual SUL of 1.4, classified as a partial metabolic response.

Case 5: 43-year-old patient treated with RT and BT for exophytic lesion with vaginal infiltration and parametrial involvement. PET/CT was requested for restaging and SBRT planning, which described a cervical lesion of 40x18x71mm (APxTxCC) and SUL of 14.60. After therapy, a control CT scan was performed, which shows progression of the disease. The patient died due to disease related complications.

Conclusion

Studies suggest that PET/CT with 18F-FDG is useful when evaluating the response to treatment, the SUL and the metabolic response would allow us to access the prognosis. Those patients with a complete response would have better survival. Patients with partial metabolic response and stable disease could be affected by disease recurrence in the future. High SUL or SUVmax values are related to higher mortality. On the other hand, low SUL values could be related to a better response to treatment. PET/CT is also important in SBRT since metabolism allows the target volume to be treated to be more precisely delineated and thus damage the normal surrounding tissue is limited.

IPET / Hybrid Imaging

K. Banza

Hôpital Général De Références Mère Et Enfant De Ngaba, Republic of the Congo

Background

PET (positron emission tomography or PET scan) is the standard medical imaging test in oncology. It provides a hybrid scintigraphic image used in nuclear medicine and improves the preoperative identification of sentinel lymph nodes in breast cancer patients.

About PET/CT In DR Congo

The DR Congo does not yet have a hybrid imaging IPET device, but the incidence of cancer of mixed forms remains relevant.

This study aims to draw the attention of the authorities and donors to the possibility of PET scanning in the diagnosis, treatment (efficacy) and post-treatment monitoring of cancers.

With a population estimated at 102,300,000 inhabitants (2023) spread over 26 provinces and 145 territories, it would be desirable to have an installation in each provincial capital. However, priority is given to Greater Katanga, because it is a mining area, and to Kinshasa, the capital of the DRC.

The only nuclear medicine service with a GAMMA Camera CT, which is used for scintigraphy in university clinics in Kinshasa, dates from 1970. Its service has a licence to supply a pharmaceutical product (technetium-99 metastable) through the CGEA from a company in South Africa; the same will be true for other radioisotopes such as [¹⁸F]FDG, fluoro-CHOLINE and fluoro-DOPA for PET/CT.

However, the creation of a cyclotron installation is necessary for the operation of PET/CT equipment; for the early detection of cancer in medical imaging would be of great importance and must be installed next to the PET/CT (in the same building).

Current installations available: Radiography, MRI, CT, Mammography, Dental Panoramic, Radiotherapy, Gamma Camera CT, Osteodensitometry.

Once the PET/CT project is implemented, staff training will be essential as they will not have sufficient information. Considering the cost of maintenance/cost of consumables and personal requirements, are expensive; the project falls to the Congolese government through the Ministry of Health and the regulatory authority of ionizing radiation. There are no limits if the principles are clearly defined. Upstream, it is necessary to train staff and ensure the supply of consumables to avoid stock shortages; downstream, it is necessary to ensure the maintenance of installed equipment.

Methodology

Hybrid imaging IPET is a little-known modality in current practice in our country, we carried out a documentary study noting the indications and methods of execution as well as the interest of this examination in the management of cancers.

Conclusion

PET scanning is an opportunity for DR Congo in the early and comprehensive treatment of cancer. It should not be left behind in the acquisition of new technologies if it is to hope to achieve universal health coverage for its population.

This conference is useful for us to exchange and acquire new knowledge.

Exaltation of the anticancer activity of newly synthesized pyranopyridine derivative as a theranostic nanoconjugate: radio-synthesis and iv-vitro/in-vivo studies

T. M. Sakr, H. A. Shamsel-Din, M. M. Swidan, A. B. Ibrahim, M. A. Motaleb

Hot Labs Center, Egyptian Atomic Energy Authority, Egypt

Background

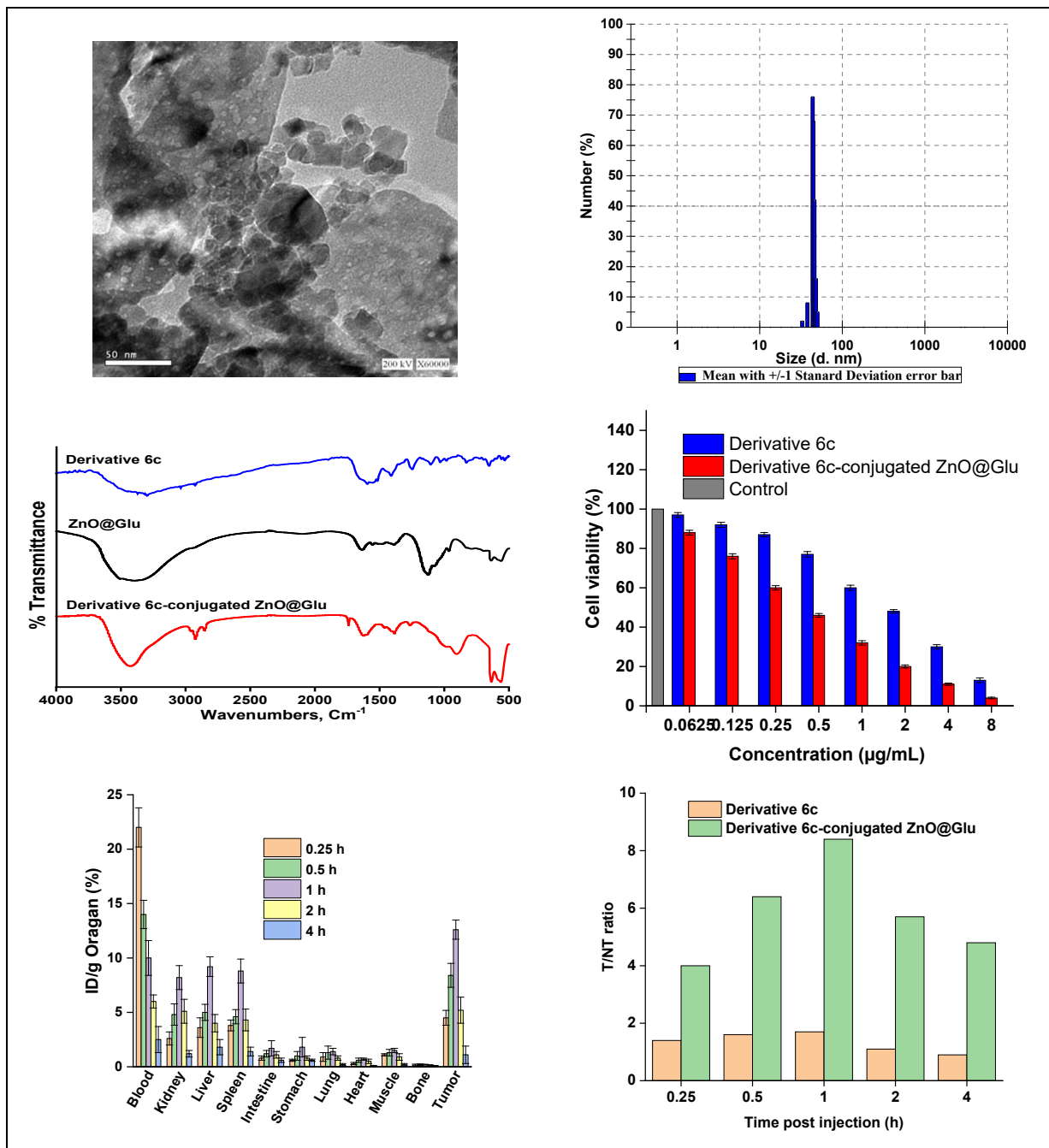
Nano-theranostic is gaining prominence for simultaneous diagnostics and therapy of certain cancers owing to its full potential for target-ability accompanied with low adverse effects. Pyranopyridine-based scaffolds have become a hot target for cancer research because of their intriguing biological properties. Herein, the study aimed to synthesis a novel anticancer agent based pyranopyridine derivative and augment its anti-proliferative potential as a theranostic nano-conjugate.

Methodology

Three novel pyranopyridine derivatives were synthesized using one pot technique compromising multicomponent cyclocondensation of resorcinol, malononitrile, aromatic aldehydes and cyclohexanone in the presence of catalyst under controlled microwave irradiation. The synthesized compounds (6a-6c) were investigated by different elemental techniques (FTIR, ¹H-NMR, ¹³C-NMR and mass spectroscopy) and assessed for their cytotoxicity and in-vitro anticancer potential against human breast carcinoma cell line (MCF-7). The most potent synthesized compound (6c) was covalently conjugated to the in-situ prepared glutamic acid capped zinc oxide nanoparticles (ZnO@Glu). The prepared nano-conjugate (derivative 6c-conjugated ZnO@Glu) was fully characterized, in-vitro biologically screened against MCF-7 and evaluated in-vivo in both normal and tumour-bearing Albino mice after being optimally radiolabeled with iodine-131 radionuclide [¹³¹I].

Results

Every synthetic molecule demonstrated cytotoxicity against MCF-7, with derivative 6c demonstrating the strongest anti-proliferative impact with an IC₅₀ of 1.9 µg/ml, while derivatives 6a and 6b showed IC₅₀ of 3.3 and 2.5 µg/ml, respectively. Furtherly, derivative 6c-conjugated ZnO@Glu was probably prepared and demonstrated 34 ± 3.8 nm in diameter and 45 ± 4.19 nm in hydrodynamic size with -18mV zeta potential. Its growth suppressive impact against MCF-7 was clearly potential as it boasted ~ 4.2 times lower IC₅₀ than derivative 6c, indicating significant anti-proliferative impact (0.45 and 1.9 µg/ml, respectively). When radioiodinated [¹³¹I]I-derivative 6c was evaluated in-vivo in tumour-bearing mice, the maximal tumour accumulation was 4.9 % ID/g at 1 h after intravenous injection, with a target/non-target ratio of 1.75. On the other hand, the in-vivo assessment of radioiodinated [¹³¹I]I-derivative 6c-conjugated ZnO@Glu revealed a maximal tumour accumulation of 12.6 %ID/g at 1 h after IV, with a target/non-target ratio of 8.4.



Conclusion

[¹³¹I]-derivative 6c-conjugated ZnO@Glu could be utilized for concomitant diagnosis and therapy of cancer with the use of I-131, which has maximal beta and gamma energies of 606.3 and 364.5 keV, respectively.

Can PET CT predict the future response of chemotherapy after one cycle?, a retrospective study

E. Ahmed

Health Radiation Research Department, Egyptian Atomic Energy Authority Cairo, Egypt

Background

In Egypt as well as in the whole world, breast cancer is increasing in number and aggressiveness, effective treatments have increased survival as well as quality of life. Monitoring the effect of treatment as early as possible is crucial to ensure that the chosen treatment is the most effective and will lead to desired result, and if not, to allow a rapid change in treatment. Aim of the study is to find out if [¹⁸F]FDG PET/CT (2-deoxy-2- [fluorine-18] fluoro- D-glucose integrated with computed tomography) can predict remission rate of breast cancer after one cycle of chemotherapy.

Methodology

This study involved 30 cases of breast cancer (in a private centre) (mean age, 47.44; age range, 32-71 years) who were under chemotherapy and underwent FDG PET/CT at least before and after the first cycle and after completion of the whole treatment. We Reviewed the last scan and divided the patients into responders and non-responders according to the results of the last scan (according if the patient totally cured or not). After that we measured SUV max of the first scan SUV max 0 and the SUV max of the next scan SUV max1. The metabolic response was calculated using the following formula: SUV change rate (Δ SUVmax%) = [(PET/CT SUVmax 0 - PET/CT SUVmax 1)/PET/CT 0 SUVmax] x100.

Results

Comparison between responders and non responders. The group of metabolic responders shows that The Δ SUVmax % was more than 30%. The group of non-metabolic responders, Δ SUVmax % was below 20%.

Conclusion

We can use PET/CT results to predict the effect of chemotherapy to save time, effort, and expenses and to achieve better results in shorter time.

Role of Interim PET/CT After 2 Cycles of ABVD Chemotherapy in Patients with Hodgkin Lymphoma in Vietnam

Nguyen Quang Toan^{1,2}, Pham Van Thai², Le Thanh Dung²

1 National Cancer Hospital, Vietnam

2 Hanoi Medical, Vietnam

Background

Hodgkin lymphoma (HL) is a highly curable disease, with > 90% of patients becoming long-term survivors. The combination of doxorubicin, bleomycin, vinblastine and dacarbazine (ABVD), as first-line treatment, induces a durable remission in 75%-88% of the HL cases. Interim PET/CT (iPET) has been included in the treatment guidelines for stages of HL after 2 cycles of ABVD chemotherapy by the NCCN and ESMO to determine appropriate treatment regimens reduces side effects and toxicity of chemicals compared to other treatment regimen. We assessed the role of iPET in response assessment and selection of treatment regimen value of iPET interpreted using the Deauville criteria in HL patients treated with 2 cycles of ABVD chemotherapy, follow-up two group iPET (-) and iPET (+) event-free and overall survival (PFS and OS) in Vietnam.

Methodology

The study was carried out Retrospective and prospective descriptive study on 100 patients at K Hospital from March 2020 to March 2024. Patients were examined clinically, subclinically, had a CT scan or PET/CT film pre-treatment, then received ABVD chemotherapy after 2 cycles of being taken and evaluated iPET to assess early response according to Deauville score (DS) scale and choose the next chemotherapy to continued treatment based on the guideline of NCCN and follow-up.

Results

In a total of 100 patients, 15-45 common age, male/female: 1/1,2, mean age 32±13.8 (youngest age 9 years old, oldest age 73 years old). Total 66 patients (66%) had CT scan and 34 patients (34%) had base PET/CT scan pre-treatment. Lymph nodes above the diaphragm (70%) and lymph nodes both above and below the diaphragm (26,7%), 90 patients had lymph nodes short-axis average diameter of lymph nodes 27.10±8.3 mm. Bulky tumour in 10 patients (10%) and extra lymphatic lesions in 15 patients. Patients with early stage I-II accounted for 72%, advanced stage III-IV accounted for 28%. After 2 cycles of ABVD chemotherapy, the response rate on PET/CT was iPET(-) 78% (of which DS- 1 point 88,5%) and iPET (+) 22% (of which DS- 4 point 72,7%). The prognostic index of IPS low-risk group (0-2) complete response was 73,1%. In the high-risk group IPS (4-7) partial metabolic response and no metabolic response was 50 % according to Lugano classification. The 3 years disease-free survival (PFS) rate of the iPET (-) was 93,6% and iPET (+) was 40.9% (p<0,0001). The Se, Sp, NPV and PPV of iPET for predicting treatment outcome were 0.723, 0.89, 0.936, 0.59, respectively. In univariable and multivariable analyses, iPET retained an independent prognostic factor of PFS (p<0,05,respectively).

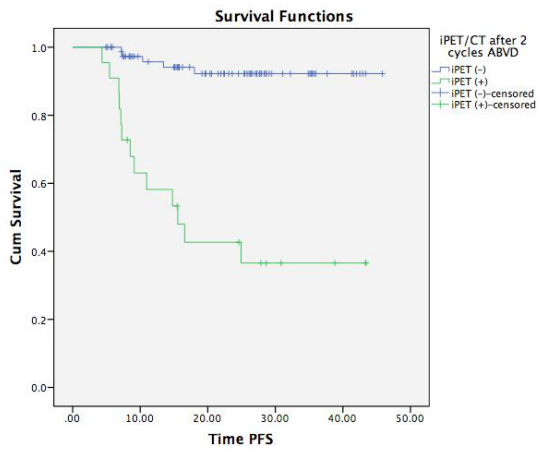


Figure 1. Box shows EFS follow-up of two group iPET (-) and iPET (+) in Vietnam.

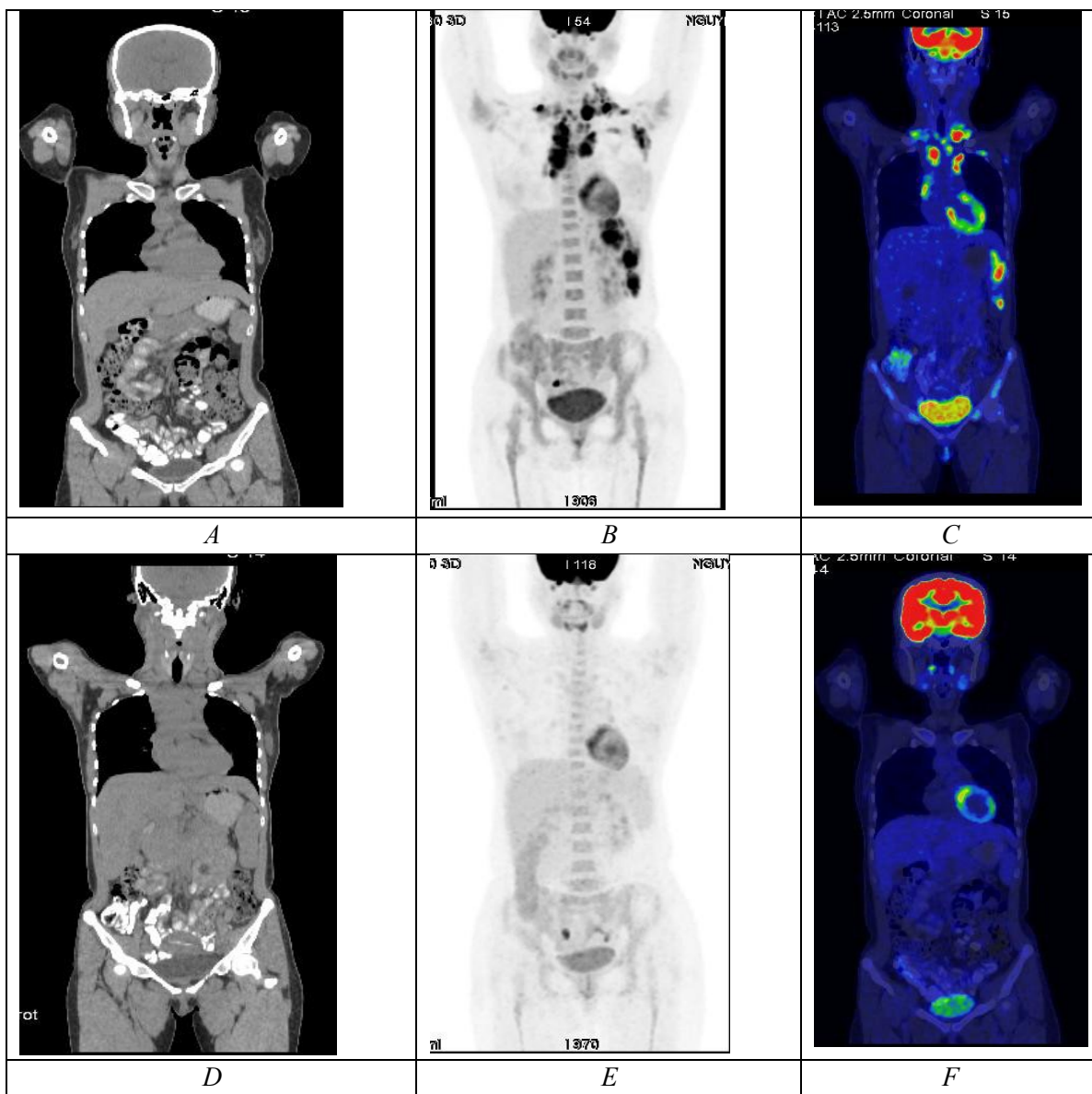


Figure 2. Coronal image show a lot of cervical and mediastinal lymph node lesions, after 2 cycles ABVD chemical, iPET scans: No longer lesion or abnormally increased metabolism of lymph nodes and spleen parenchyma - CMR- DS - 1 point (picture D-F).

Conclusion

Interim PET/CT has an important role in providing prognostic information in the treatment of ABVD chemotherapy in HL patients, reducing the toxicity of chemotherapy and orienting the next treatment modality.

Development of evaluation and quality control protocols for mammography

C. Yegros¹, E. Quintana², L. Recalde²

¹ National University of Asunción, Paraguay

² Polytechnic School, National University of Asunción, Paraguay

Background

Mammography is a medical diagnostic study performed by taking a radiographic image directly on the breasts, at low doses of radiation, with specialized ionizing radiation-emitting equipment called a Mammogram. It's the main one for the early detection of diseases of breast origin, which is why it's essential to guarantee the operability and correct functioning of the equipment that performs this study; particularly in low-income countries, such as Paraguay, where at the state level there is 1 mammographer for every 50,000 women, which implies low-quality control of radiation emissions, low access to this health system, and in special to preventive medical check-ups.

Aim

To guarantee this safety in the mammographic area, it's necessary to establish verification programs and quality controls.

Methodology

To carry it out, this project evaluates its operation and the quality of its ray emission, through controls of physical parameters in its radiation generators, through the measurement of its main parameters and the elaboration of a checklist based on the technical standards established by the local regulatory authority and international standard (IAEA); and the implementation of these techniques and quality protocols for mammographers, in different imaging services, in order to evaluate the control program and the meters to guarantee radiological safety and dose levels for operators, technical service personnel, and patients. The project is based on the experimental study, through the development, verification and testing with equipment that measures physical parameters (dose, dose rate, KVP, HVL) for mammographers, through the adaptation and implementation of the international standard IAEA -TECDOC- 1517, for mammography quality control and advice from the local Radiological Regulatory Authority (ARRN). The measurement equipment used was the black RTI PIRANHA® and an own design for measurement of pressure, height and position. for the benefit of users of this equipment in public health

Results

Verifications and controls were carried out on 8 mammographers with the instruments acquired and designed, in public and private institutions in Asunción and the Central Department. 62.5% of them have their parameters within the tolerance ranges. 37.5% worked, but with values above expectations. Its calibration was suggested.

Conclusion

It was demonstrated that it is possible to obtain information on the situational status of the mammographs, verify the quality of the image, the dose rate to determine the level of radiation emitted by the equipment and guarantee the radiological protection of technical personnel and users, as well as the scopes of dose adjustments and dose rate, if necessary. With these data it's possible to foresee

solutions to avoid unnecessary stops of operation, all with the aim of guaranteeing radiological safety and facilitating decision-makers with the tasks of planning, justifying the renewal or maintenance of mammographs, in a country with scarce and deficient infrastructure and biomedical equipment.

Over View of the First Hybrid Imaging System Tunkey Project In The Country- Tanzania's Experience

S. O. Yusuph¹, J. Mwaiselage², W. Ngoye³

¹ Medical Physicist Section, Ocean Road Cancer Institute, Dar es Salaam, Tanzania

² Ocean Road Cancer Institute, Dar es Salaam, Tanzania

³ Tanzania Atomic Energy Commission, Dodoma, Tanzania

Background

Tanzania is one of the low-resourced countries where more than 60% of cancer patients are hospitalised with late-stage cancer with treatment intentions beyond palliation. It is also one of the African countries that spend a lot of money to send patients abroad who intentionally need hybrid imaging . It is estimated that Tanzania spends more than 2 million USD every year on PET/CT scans alone outside the country. In order to diagnose cancer earlier and conserve the country's scarce resources, the government of the United Republic of Tanzania decided to set up a PET/CT scanner and provided USD 8 million in the 2021/2023 financial year for the construction, procurement of the PET/CT scanner and cyclotron, commissioning and training of staff. The project was turnkey and included the construction of the building for the hybrid imaging system, procurement of equipment, installation and commissioning, training of staff and training of the hybrid imaging system. Training was provided by the supplier prior to installation by sending hospital experts abroad. The International Atomic Energy Agency (IAEA) was also involved in the project. The IAEA trained our staff, including nuclear physicians, technologists and medical physicists. The IAEA will also send an expert to develop standard operating procedures (SOP) and finalize the acceptance test, which was conducted according to the National Electrical Manufacturers Association (NEMA) protocol.

To date the commissioning of the PET/CT scan with Ge-68 has been completed and patients have registered so that the first scan can be performed in the third week of March 2024. The Siemens with 64 slice was introduced in the country to save more than 200 Tanzanian's who are referred abroad for PET/CT abroad every year. It will also save clients from neighbouring countries including Zambia, Malawi, Democratic republic of Congo and Comoro.

The aim of this paper is to give the first experiences in the country of the commissioning test necessary for a successful clinical implementation of the PET/CT hybrid imaging system. Implementation of the project will help the country not only to reduce the funds for sending patients abroad, but also to diagnose tumour at very early stages.

Determination of Changes in the Density and Biodistribution of [¹⁸F]FDG in Bone Marrow Secondary to Stimulation by Colony Stimulating Factor Using PET/CT in Paediatric Patients with Lymphoma

A. Z. Pardo

Medico Radiologo Pediatra, Mexico

Background

Lymphoma frequently affects the bone marrow, in a multifocal or diffuse manner. Biopsy and bone marrow aspiration are used to determine infiltration, so iliac crest biopsy may not detect it. The usefulness of [¹⁸F]FDG PET/CT for staging, restaging, and specifying the bone marrow aspiration site is known.

Objectives

Demonstrate changes in bone marrow uptake and density in 8 paediatric patients with lymphoma.

Methodology

Radiopharmaceutical uptake values in SUV_{max}, and density in HU, in the skull, humerus, sternum, L1 vertebral body, right iliac and femur, in [¹⁸F]FDG PET/CT, before, during and after, are described. of the treatment. The values were compared with the result of the bone marrow aspirate.

Results

8 patients were included, 6 with Hodgkin lymphoma and 2 with non-Hodgkin lymphoma, with an average age of 12.5 years. All cases presented a decrease in bone density more evidently during treatment. An increase in SUV_{max} was observed in the sternum and vertebral bodies in the baseline study, which decreased at the end of treatment. Two patients with negative bone marrow aspirate showed focal hyperuptake in the baseline study: 1 in the right humerus, with a pathological fracture and another with a diffuse form, confirmed by bone marrow aspirate. All patients demonstrated decreased bone marrow density at all sites evaluated.

Discussion

Currently, [¹⁸F]FDG PET/CT is considered the staging method of choice for patients with lymphoma, with accuracy for detecting bone marrow infiltration of 96.7 to 99.3%. In this review, more sites of disease were detected with [¹⁸F]FDG PET/CT that bone marrow aspirate could not identify, especially in case of multifocal disease. All patients showed generalized decrease in bone density on tomography.

Conclusion

The [¹⁸F]FDG PET/CT study allows defining the infiltration site(s) in multiple locations of the bone marrow, unlike the bone marrow aspirate which is limited to a single study area.

Detection of Intracardiac Metastases of Osteosarcoma Using Hybrid Imagenology

A. Z. Pardo

Medico Radiologo Pediatra, Mexico

Background

Osteosarcoma is the most common primary bone tumour in children and adolescents. The most frequent sites of metastasis are lung and bone. Imaging findings of cardiac involvement are rarely reported and may be difficult to recognize. Echocardiography is the most used test for the study of cardiac lesions and pericardial disease, due to its accessibility and low cost. Magnetic resonance imaging provides information on infiltration of cardiac and mediastinal structures, vascularization, and secondary functional alterations. Bone scintigraphy detects blast lesions, as well as mineralized metastatic lesions in soft tissues. PET/CT identifies lesions by determining glycolytic activity using [¹⁸F]FDG or cell proliferative activity using [¹⁸F]FLT. Tomography and conventional radiology have a limited role in the detection of intracardiac metastases from osteosarcoma.

Case

14-year-old female diagnosed with osteoblastic osteosarcoma of the proximal humerus and metastatic to the lung. Prior to induction chemotherapy, he presented with pulmonary thromboembolism. Echocardiography demonstrates occupying lesions in the right cavities, which are observed with contrast-enhanced magnetic resonance imaging of the heart and confirmed during surgery. The histopathological report concludes intracardiac lesions, consistent with metastasis of high-grade osteosarcoma. The primary tumour shows a notable increase in volume postoperatively. Staging studies are repeated, and tumour progression is concluded at the local level. Radical surgery with amputation is performed. After chemotherapy and surgical resection, the patient developed an increase in retropectoral volume. Restaging is advanced. Bone scintigraphy with SPECT reveals a focal blast zone at the left ventricular base and an indeterminate lesion in the L4 vertebral body. [¹⁸F]FLT PET/CT was requested, identified increased tumour proliferative activity in the left retropectoral region, cardiac lesion and in lytic bone lesions located in the L4 vertebral body and left pubic ramus.

Discussion

The fusion of tomography and resonance images with PET/CT and Scintigraphy in patients with osteosarcoma allowed us to identify intracardiac metastases early, with greater precision than conventional radiographic studies. Whole-body PET/CT imaging allows distant lesions to be identified with greater sensitivity and specificity.

Conclusion

The coregistration of anatomofunctional images in patients with osteosarcoma presents greater sensitivity and specificity to detect cardiac metastases from osteosarcoma.

Pheochromocytoma and Paraganglioma Detection with Ga-68-DOTATATE PET/CT

N. C.M. Gülaldi, B. Cagdas

University of Health Sciences, Ankara Bilkent City Hospital, Department of Nuclear Medicine, Ankara, Türkiye

Background

Pheochromocytomas and paragangliomas are rare neuroendocrine tumours that arise from chromaffin cells of the adrenal medulla and peripheral neural crest cells, respectively. Expression of the somatostatin receptor is often found in this type of tumour. In this study, the Ga-68-DOTATE PET/CT imaging of patients referred for diagnosis of primary or metastatic lesions of pheochromocytoma and for paraganglioma diagnosis were retrospectively analysed.

Methodology

The study included 17 pheochromocytoma patients, 11 paraganglioma patients, and 1 glomus tumour patient. Levels of nor-metanephrine and metanephrine were measured in urine and plasma over 24 hours. Following 45–60 minutes of radiopharmaceutical injection, Ga-68-DOTATE PET/CT scans were conducted. To potentially screen for metastases, images of the patients were assessed for both the main lesion areas and whole-body segments. Even though all patients with paraganglioma and glomus tumours as well as 11 patients with pheochromocytoma had histopathologic evidence, only six pheochromocytoma patients were diagnosed based on MRI imaging, clinical symptoms, and blood and urine metanephrine values. SUVmax values of positive lesions and plasma and urine levels of nor-metanephrine and metanephrine were calculated using paired sample t-tests to determine the mean values for each group. Any prediction about urine and plasma biochemical levels with lesion detection was estimated using linear regression analyses.

Results

Ga68-DOTATE PET/CT scan was used to find lesions that were confirmed by histopathology as well as in any symptomatic patients. The mean SUVmax values for the pheochromocytoma group and the paraganglioma-glomus tumour group were 28.79 ± 20.6 , 16.94 ± 12.1 respectively. Each group's mean values did not fall into a homogeneous distribution. The Wilcoxon signed-rank test revealed a significant difference in mean values between the pheochromocytoma and paraganglioma groups ($p < 0.05$). Linear regression analyses did not reveal any significant prediction model for the urine and plasma biochemical levels and SUVMax values ($p > 0.05$).

Conclusion

The high sensitivity of Ga68-DOTATATE somatostatin receptor PET/CT allows for the detection of pheochondroma and paraganglioma-gliomus tumours as well as their metastases. The study only included cases that were histopathologically proven, so more clarification is required regarding the scan's specificity. In this investigation, there was no correlation found between SUVMax values and the levels of nor-metanephrine and metanephrine in the blood and urine, nor between the prediction model and activity levels. A test that can be safely used in cases of suspected pheochromocytoma, paraganglioma, and glomus tumour, as well as for metastasis screening, is Ga 68-DOTATATE PET/CT imaging.

The Utilization of [¹⁸F]FDG PET/CT in the Management of Lymphoma, Our Practice in Royal Hospital

N. K. Al-Bulushi¹, Z. A. Bimani¹, S. A. Ghaithi², K. A. Nabhani¹, F. A. Sawafi¹, A. A. Obaidani¹, K. A. Beriki², M. A. Tarshi¹

¹The Royal Hospital, Oman

²Oman Medical Speciality Board, Oman

Background

[¹⁸F]FDG is with no doubt the modality of choice in the management of lymphoma. Whereas the incidence of Hodgkins' Lymphoma (HL) is about 2.4 per 100,000 per year, 5% of all newly diagnosed malignancies are due to Non-Hodgkins' Lymphoma (NHL). Given this burden, the improper utilization of PET/CT if present, should be checked. This retrospective analysis aims to assess the current practices at the Royal Hospital compared to the international best practice; EANM/SNMMI and NCCN guidelines.

Methodology

The digital records of all adult patients with lymphoma from January 2016 to December 2020, were included in this retrospective study. The history was reviewed from the time of their diagnosis to the completion of treatment and follow-up [¹⁸F]FDG PET/CT scans.

Results

Out of 474 patients who had [¹⁸F]FDG PET/CT for Lymphoma, 19 were excluded as they were still in the paediatric age group, 5 had unconfirmed histopathology and 2 had a second malignancy. Hence, the total number included in this analysis is 405 (270 NHL & 135 HL), 221 males and 184 females with an age range of 18-86 years.

Discussion

The departments requested ¹⁸F-PET/CT for lymphoma are adult oncology (AO), Haemato-oncology (HO), and radiotherapy (RT). 85% of the first scans were baseline staging, 75% interim-PET, and 85% end of therapy, which agrees with the international guidelines. However, the deviation from the guidelines was noted after the end of therapy. In this cohort the Deauville scores for the end-of-therapy scan were complete remission in 65% and 90% and partial response or progression in 35% and 10% in NHL and HL, respectively. 95 patients with NHL and 42 with HL had annual surveillance with, 50% being referred from RT, 35% from AO, and 15% from HO. The number of follow-up scans was variable in each patient, for those with NHL, 77 patients had 1-3 scans and 18 had 4-6 scans. For the HL patients, 31 patients had 1-3 scans and 11 had 4-7 scans. The outcome of those scans was 88 % stable and 12% relapsed disease in NHL and 90% stable and 10% relapsed disease in HL (P=0.585).

Conclusion

Given that treatment of lymphoma is long-term, with relatively less aggressive neoplasms, the benefit of accurately staging and response to treatment may cut costs in the long run. We found that most referring departments follow the international guidelines in utilizing [¹⁸F]FDG PET/CT at the time of staging till the end of therapy. There was an unusual amount of follow-up studies with no significant change in the

outcome, as the estimated expenditure of those scans (800 OMR /PET/CT scans) was approximately 97,600 OMR (244,000 EU). Not to mention the unjustified exposure to radiation. Therefore, we recommend a revision of current practices in the management of Lymphoma at the Royal Hospital.

Rationale and development of linear tetra-aspartic acid peptide for Gallium-68 chelation

S. Shiratori¹, W. Jiradilok², B. Tuesuwan²

¹ Division of Nuclear Medicine, Department of Radiology, Faculty of Medicine Siriraj Hospital, Mahidol University, Thailand

² Department of Food and Pharmaceutical Chemistry, Faculty of Pharmaceutical Sciences, Chulalongkorn University, Thailand

Background

Gallium-68 (Ga-68) chelation plays a crucial role in the development of PET imaging. With the availability of Germanium-68/Gallium-68 generator, the trivalent of Ga-68 cation can form a stable complex with various macrocyclic and acyclic bifunctional chelating agents such as NOTA, DOTA, HBED-CC. Recently, we succeeded to develop a linear peptide bifunctional chelating agent by mimic chemical structure of NOTA. In this research, we aim to synthesize a new linear tetra-aspartic acid (TAA) peptide using the same approach that develop trajectory similar to previous research by mimic chemical structure of DOTA.

Methodology

Linear tetra-aspartic acid peptide was prepared using automate solid phase peptide synthesis (SPPS) and purified by preparative TLC. Subsequently, [⁶⁸Ga]GaCl₃ 2.0 mL 2.27-2.65 mCi was added to solution of TAA 50 microlitre (10.56 nmol) with acetate buffer 1.0 mL and heated at 100°C for 15 min. Sep-Pak C18 cartridge was used in purification.

Results

The crude product of TAA was purified using preparative TLC to give 3.12% total yield. With ESI-MS analysis, TAA was found $m/z = 479.1 [M+H]^+$, which corresponding to its molecular weight. The radioactivity of [⁶⁸Ga]Ga-TAA was found to be 937-997 microCi, radiochemical yield was 75-83%. In addition, pH of radiolabelled product was in range of 4.5–5.0. TAA was designed to contain four N-dentate and five O-dentate, which can form N₄O₂ hexadentate at ambient temperature in the similar manner to DOTA.

Conclusion

The rationale design of TAA was to mimic chemical structure of DOTA. TAA was successfully synthesized by SPPS. This research demonstrated the possibility of Ga-68 chelation to TAA. Future work includes its potential to conjugate to anti-cancers, other biologically active molecules as a new small peptide chelator for Ga-68 labelling.

Exploring PET-PSMA Efficacy in the Initial Staging of Prostate Carcinoma: Insights from King Hussein Cancer Center

A. Abdulkadir, A. Al-Ibraheem

King Hussein Cancer Center (KHCC), Jordan

Background

The aim of this study was to investigate the effectiveness of positron emission tomography (PET) and prostate specific membrane antigen (PSMA) imaging in comparison to computed tomography (CT), magnetic resonance imaging (MRI), and skeletal scintigraphy for the initial staging of patients recently diagnosed with intermediate- and high-risk local prostate carcinoma.

Methodology

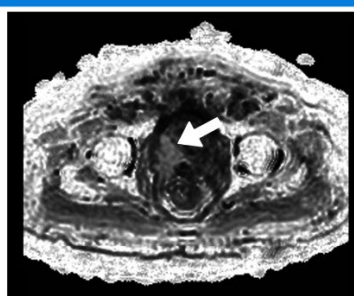
In this study, 202 patients recently diagnosed with prostate carcinoma were initially evaluated using a multimodality approach. This approach involves initial assessment through the utilization of [⁶⁸Ga]Ga-PSMA PET/CT, MRI, CT, and skeletal scintigraphy. Patients were exclusively enrolled if they were categorized as high- or intermediate-risk. A comparison of the sensitivity and specificity of these modalities was conducted, with established histology post-prostatectomy serving as the reference standard.

Results

A total of 202 patients with intermediate- and high-risk prostate carcinoma were enrolled. [⁶⁸Ga]Ga-PSMA PET/CT exhibited superior performance over other modalities, demonstrating statistical significance ($p < 0.05$, each). [⁶⁸Ga]Ga-PSMA PET/CT had comparable accuracy to MRI in primary disease detection but a higher accuracy for nodal disease (97.1% vs. 82%, $p = 0.03$). It also outperformed CT scans in nodal detection (97.1% vs. 73.8%), extra-pelvic lymph nodes (100% vs. 69%), and bone lesions via skeletal scintigraphy (100% vs. 60%). Furthermore, the reliance on the staging results retrieved from [⁶⁸Ga]Ga-PSMA PET/CT changed the management scheme for 97 patients (48%).



Pelvic PET/CT



Pelvic MRI



Conclusion

[⁶⁸Ga]Ga-PSMA PET/CT is an invaluable imaging tool for patients with intermediate- and high-risk prostate carcinoma. This novel imaging approach outperformed all other imaging modalities in the

assessment of local, locoregional, and distant disease spread, with a significant impact on the management plan.

Radiolabeled Drug Encapsulated Liposomes for Imaging and Treatment of Osteomyelitis

M. S. Günay¹, A. Taş¹, S. Çalamak², Ş. Nigiz³, D. Kart³, A. Ç. İnkaya⁴

¹ Hacettepe University Faculty of Pharmacy, Department of Radiopharmacy, Türkiye

² Lokman Hekim University Faculty of Pharmacy, Department of Basic Pharmaceutical Science, Türkiye

³ Hacettepe University Faculty of Pharmacy, Department of Pharmaceutical Microbiology, Türkiye

⁴ Hacettepe University Faculty of Medicine, Department of Infectious Diseases and Clinical Microbiology, Türkiye

Background

Osteomyelitis is the swelling and inflammation of bone tissue caused by infection, traumatic injuries, surgical procedures, prostheses, etc. accompanied by bone destruction. It was aimed to formulate levofloxacin (LEV) encapsulated, nanosized, PEGylated, radiolabeled liposomes.

Methodology

In this study, LEV encapsulated, PEGylated, nanosized formulations were prepared by film method (6) and size reduction was performed by extrusion method and following characterized (measurement of mean particle size and distribution, zeta potential, percentage of entrapment efficiency). In vitro drug release analyses and in vitro antimicrobial activity analysis studies were performed for both two different bacterial strains. Liposomes were labeled with Ga-68 by a chelator according to the method of Helbok et al. and labeling efficiency was calculated by detecting the radioactivity with a gamma counter.

Results

LEV-encapsulated, PEGylated liposomes were formulated with 237±3,7 nm mean particle size and narrow size distribution and about 9% encapsulation efficiency. Liposomes obtained by the film method were observed under a polarized light microscope (Figure 1).

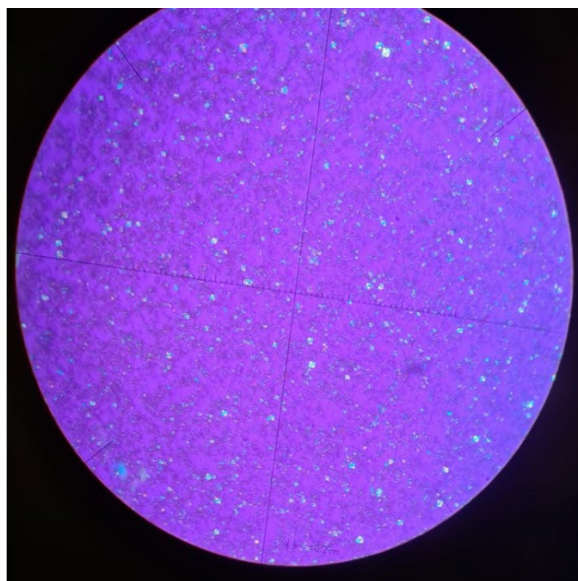


Figure 1. Polarized light microscope image of the LEV encapsulated formulation (x40).

For the formulation of LEV-encapsulated liposomes, in vitro release was analysed and it was found that approximately 80% of LEV was released at the end of the 8th hour (9, 10). MIC ($\text{ng}\times\text{mL}^{-1}$) values were calculated for LEV-encapsulated liposomes as a result of in vitro antibacterial analysis. Accordingly, while $1.22 \pm 0.4 \text{ ng}\times\text{mL}^{-1}$ was found for *E. coli*, the MIC value for *S. aureus* was $9.76 \pm 2.8 \text{ ng}\times\text{mL}^{-1}$. Liposomes were labeled by chelator. The labeling efficiency of liposomes with Ga-68 will be completed very soon.

Conclusion

LEV-containing, radiolabeled liposomes were successfully formulated and characterized for the diagnosis and treatment of osteomyelitis. In vitro antibacterial activity of liposomes was evaluated as significantly high which could be potential for further studies.

Diagnostic Test Accuracy of PET/MRI in Head and Neck Squamous Cell Carcinoma: A Systematic Review and Meta-Analysis

A. Al-Ibraheem¹, A. Abdlkadir¹, K. Herrmann², J. Bomanji³, H. Jadvar⁴, H. Shi⁵, A. Mansour¹, D. Paez⁶, A. Chiti⁷, A. Scott⁸

¹ King Hussein Cancer Center, Jordan

² University Hospital Essen, Germany

³ University College London, England

⁴ University of Southern California, USA

⁵ Zhongshan Hospital Fudan University, China

⁶ International Atomic Energy Agency, Austria

⁷ IRCCS Ospedale San Raffaele, Italy

⁸ Austin Health, Australia

Background

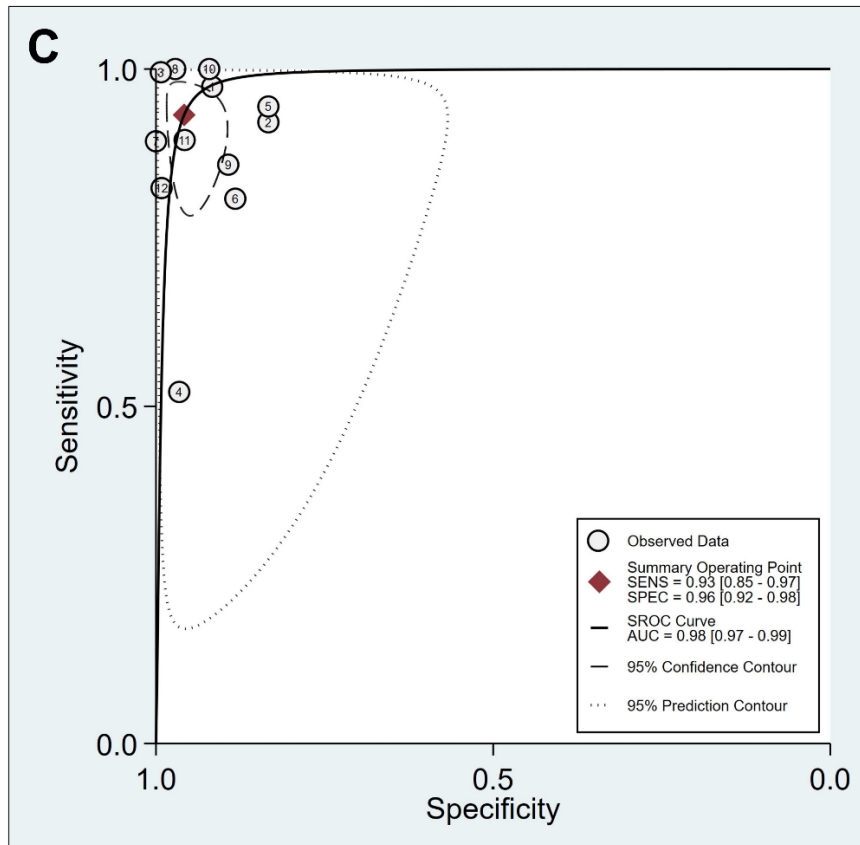
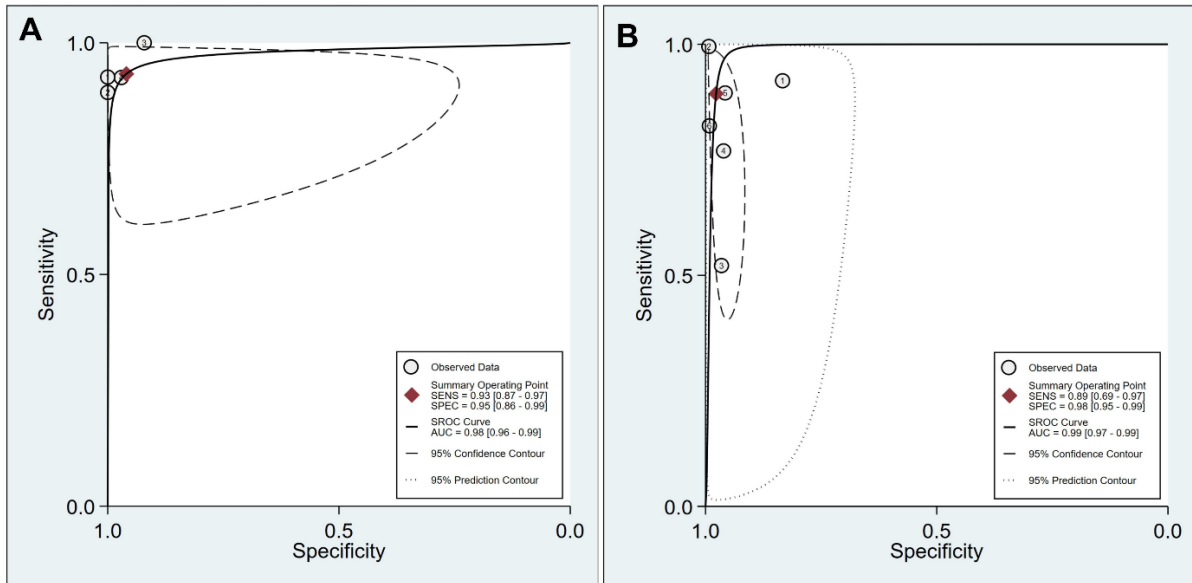
The increased availability of the novel hybrid positron emission tomography/magnetic resonance imaging (PET/MRI) has made it possible to examine its growing potential in various oncological contexts. This systematic review and meta-analysis aims to examine the diagnostic utility of PET/MRI for primary, locoregional, and nodal disease detection in patients with head and neck squamous cell carcinoma (HNSCC).

Methodology

A comprehensive literature search was employed to extract relevant research from PubMed, and Scopus databases. The terms used were “FDG”; “fluorodeoxyglucose”; “head and neck cancer”; “HNSCC”; “PET/MRI”; “PET-MRI”; “positron emission tomography/magnetic resonance imaging”; “sensitivity”; “specificity”; “accuracy”; “diagnosis”; and “detection.” The process of extracting pertinent information and obtaining the complete text was carried out. Any reports that did not involve hybrid PET/MRI or had a sample size of less than ten patients were excluded.

Results

A total of 15 studies was found addressing diagnostic test accuracy for PET/MRI within the chosen subject domain. Only 12 studies were deemed suitable for inclusion in the subsequent meta-analysis. For primary disease evaluation, the aggregated sensitivity and specificity values were determined to be 93% and 95% per patient, respectively. Whereas the aggregated sensitivity and specificity for locoregional evaluation were 93% and 96%, respectively. Furthermore, the pooled sensitivity, and specificity for the detection of nodal disease were established at 89% and 98% per-lesion, respectively.



Conclusion

PET/MRI has excellent potential for identifying primary, locoregional and nodal HNSCC. Therefore, in instances where it is accessible, PET/MRI can be advocated as the preferred approach for the thorough assessment of HNSCC.

Exploring the In Vivo biodistribution of ambient-stored Technetium-99m Labeled Methylene Diphosphate (99mTc-MDP) Radiopharmaceutical aliquots in Infected Rat Models

J. Zulu¹, R. Sakala²

¹ Levy Mwanawasa Medical University, Department of Pharmacy Lusaka, Zambia

² University Teaching Hospitals - Adult, Department of Nuclear Medicine, Zambia

Background

Antimicrobial resistance (AMR) is posing a serious global problem. Accurate diagnostic procedures are crucial to the effectiveness of the treatment of infectious diseases. The use of radiopharmaceuticals like Technetium-99m Methylene Diphosphonate (99mTc-MDP) is considered a reliable diagnostic method; however, availability and affordability matter. While the literature has revealed that MDP aliquots kept at frozen and refrigerated conditions remain of good quality, this research explored the viability of MDP aliquots kept at ambient conditions.

Methodology

A laboratory-based experimental study was conducted at the University Teaching Adult Hospital in Lusaka, Zambia, and data was collected by observing results from the controlled laboratory and biodistribution tests in infected rat models. In all, 80 MDP aliquots kept at ambient conditions and labelled with technetium-99m were tested, and biodistribution studies were done on a total of twelve infected rat models.

Results

Stata 14 was used to analyze the data; the radiochemical purity of the 72 MDP aliquots stored at ambient conditions out of the 80 ranged from 98% to 99%, which is much higher than the required minimum of 90%. For the 8 that were kept in frozen and refrigerated conditions, the radiochemical purity ranged from 99% to 100%.

Conclusion

The MDP samples maintained at ambient temperature exhibited exceptional radiochemical purity and demonstrated favourable biodistribution patterns by effectively localizing to the specific regions of interest in rat models with infections. In spells of difficulties in maintaining a cold chain, the findings show potential for low-resource countries, who may have challenges maintaining cold chain storage throughout due to power outages.

Keywords: radiopharmaceutical, technetium-99m, methylene diphosphate, ambient conditions, radiochemical purity, biodistribution

Imaging spectrum of hepatic sarcoidosis: Series of 3 cases

A. Jain

Vijaya Diagnostic Center Ltd, India

Background

Hepatic involvement by sarcoidosis is reported in 50 to 80% patients in biopsy / autopsy series, but less than 5% may suffer from symptomatic disease. On regular imaging including USG and CECT abdomen hepatic sarcoidosis might remain occult or might mimic malignant neoplastic disease. Purpose of this case series is to illustrate the spectrum of hepatic sarcoidosis imaging findings and to establish that FDG PET/CT scan is a superior modality for evaluation of hepatic sarcoid involvement than CECT alone.

Case Details

Presenting three cases in whom hepatic involvement by sarcoidosis was detected by increased FDG uptake, while CT appearance was different in all 3 cases and probably represented different stages of hepatic sarcoid involvement.

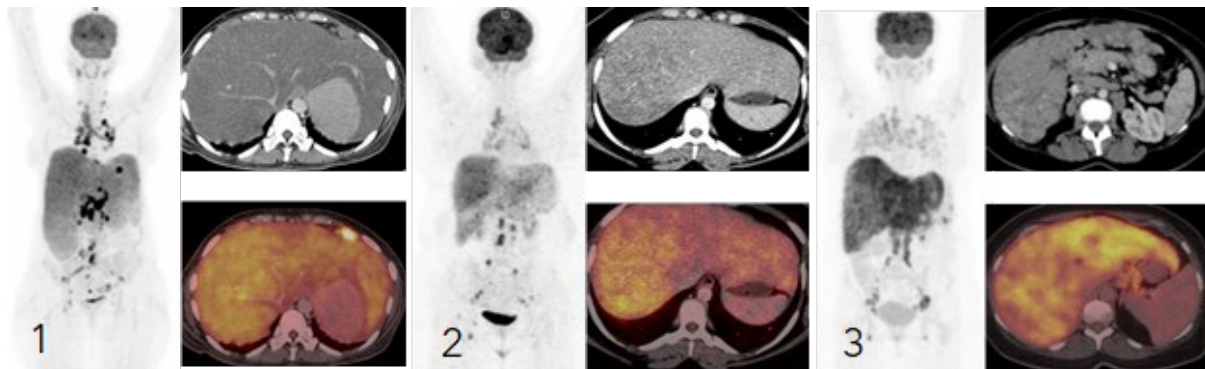


Image 1: MIP image shows FDG uptake in liver lesions, mediastinal and abdominal lymph nodes and cross-sectional images showing diffuse hepatomegaly with low attenuation and increased FDG uptake.
Image 2: MIP image shows FDG uptake in liver lesions, mediastinal and abdominal lymph nodes and cross-sectional images showing infiltrative hepatic lesion with increased FDG uptake.
Image 3: MIP image shows FDG uptake in bilateral lung lesions, liver lesions, mediastinal and abdominal lymph nodes; and cross-sectional images showing cirrhotic appearing liver with increased FDG uptake.

The first case was 40-year-old female, had presented with weight loss, loss of appetite and weakness since few months. Her Routine blood investigations were within normal limits. USG and CT abdomen showed hepatomegaly with diffuse fatty infiltration and splenomegaly. Along with diffuse hepatomegaly with low attenuation on CT images, FDG PET/CT scan (Image 1) showed diffusely increased FDG uptake in liver parenchyma along with generalized lymphadenopathy with typical distribution of paratracheal and hilar lymph nodes.

Second case was an otherwise asymptomatic, 30-year-old female. She found to have mediastinal lymphadenopathy on a routine health check-up. FDG PET/CT scan (Image 2) showed geographical areas of increased FDG uptake in liver parenchyma with corresponding CECT images showed subtle infiltrative pattern of enhancement and no mass effect. Other findings include lung parenchymal involvement in form of subpleural/perifissural nodules with typical paratracheal & bilateral hilar lymph nodes.

Third case was 38-year-old female who had presented with loss of appetite and fatigue since few months. She had been diagnosed with liver cirrhosis and pulmonary Koch's on initial evaluation and was put on anti-tubercular treatment. Since there was no improvement in her clinical condition, a FDG PET scan was requested. Apart from nodular liver surface and diffuse nodular enhancement of liver parenchyma, FDG PET/CT scan (Image 3) showed diffusely increased FDG uptake in liver parenchyma generalized lymphadenopathy and typical lung parenchymal involvement in form of tiny peribronchovascular nodules. It also showed bilateral parotid involvement.

Discussion

Hepatomegaly is the most common liver abnormality seen on CT in sarcoidosis, which is anyway quite non-specific, moreover may not be present in every cases. Other CT findings include multiple small focal hepatic lesions, representing granulomas, which may become more confluent with increasing size and appear as geographical hypo enhancing areas. Rarely, these changes can progress to portal hypertension and cirrhotic changes, because of chronic inflammation and fibrosis in the portal triads.

In significant number of cases CT might not reveal any abnormality or it might be difficult to attribute the findings to sarcoidosis such as hepatomegaly and cirrhotic changes. Increased FDG uptake not only makes it easy to pick up focal hepatic sarcoid lesion but also establishes sarcoid involvement in non-specific findings such as hepatomegaly and cirrhotic changes. Apart from this, being a whole body scan it can also provide important clues to pinpoint diagnosis of sarcoidosis.

Conclusion

FDG PET/CT scan is a sensitive technique for hepatic sarcoidosis. Moreover, being a whole body scan it not only provides specific clues to pinpoint diagnosis of sarcoidosis, but also gives a comprehensive overview of the disease burden.

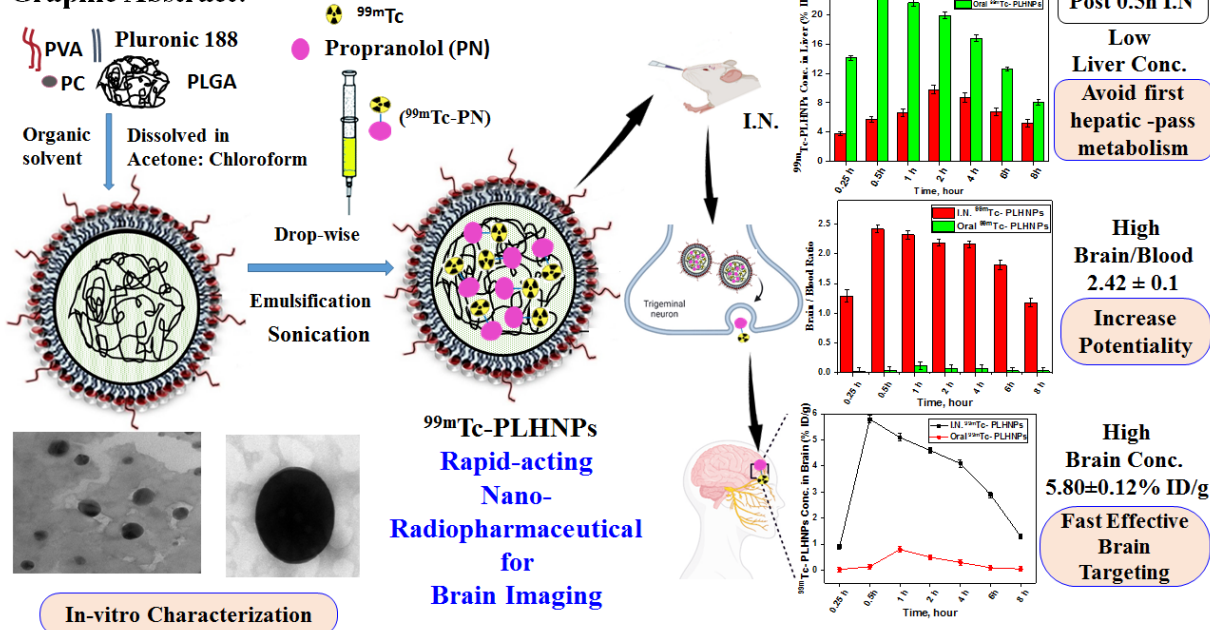
Amelioration of brain targeting for intranasal propranolol hydrochloride loaded PLGA-lipid hybrid nanoparticles and its biodistribution study by radiobiological evaluation

R. Albash¹, A. M. Fahmy¹, H. A. Shamsel-Din², A. B. Ibrahim²

¹ Faculty of Pharmacy, Cairo University, Egypt

² Labeled Compounds, Hot Labs Center, Egyptian Atomic Energy Authority, Egypt

Graphic Abstract:



Background

The brain imaging in Nuclear medicine play very important role to image the changes in brain uptakes that reflect changes in the blood brain barrier. Therefore, imaging these changes at an early stage has potential for improved diagnosis and can inform management decision making. The aim of this study is to formulate intranasal Nano-Radiopharmaceutical with rapid brain targeting for use in brain imaging due to the fast potentiality of penetration through the blood brain barrier for management of brain imaging by intranasal administration especially in emergency cases.

Methodology

The ^{99m}Tc-propranolol hydrochloride (^{99m}Tc-PN) was prepared by direct labeling method and factors affecting on the radiolabeling yield (RLY) were studied. The Nano-Radiopharmaceutical (^{99m}Tc-PLHNPs) was prepared by double emulsification method. Briefly, PLGA, PC, SAA (50 mg) was dissolved in 2 mL of acetone: chloroform mixture. ^{99m}Tc-PN was added drop-wise to the organic phase and stirred at 37°C for 1 hour to remove any trace from the organic solvent. Finally, the fabricated dispersion was sonicated for 5 min. the in-vitro characterization was studied and optimized. The in-vivo biodistribution and efficacy for brain targeting of ^{99m}Tc-PLHNPs were evaluated after oral or intranasal administration (I.N.) in mice (25-30g/mice) up to 8h. The percentage of ^{99m}Tc-PLHNPs per gram of

brain and blood (%ID/g), brain/blood ratio and pharmacokinetics parameters were calculated for efficacy evaluation.

Results

The ^{99m}Tc -PN was prepared in maximum RLY $93\pm 2.5\%$ using 4 mg of PN and 2 mg of sodium dithionite as a reducing agent at pH 5 for 15 min as a reaction time at room temperature (25°C). The optimum ^{99m}Tc -PLHNPs had entrapment efficiency percent (EE%) of $78.00\pm 0.71\%$, particle size (PS) of $104.50\pm 2.04\text{nm}$, polydispersity index (PDI) of 0.429 ± 0.038 , and zeta potential (ZP) of $24.80\pm 1.26\text{mV}$. It also showed a spherical shape under a transmission electron microscope. ^{99m}Tc -PLHNPs showed $91.40\pm 1.85\%$ of RLY with in-vitro stability up to 24 h that suitable for assessment of brain targeting and *in-vivo* biodistribution. ^{99m}Tc -PLHNPs presented low liver concentration at all-time intervals post I.N. due to avoid the first hepatic pass metabolism. ^{99m}Tc -PLHNPs showed higher and faster brain targeting with $5.80\pm 0.12\% \text{ID/g}$ and a high brain-to-blood ratio 2.42 ± 0.14 at 0.5h after intranasal administration in addition to controlled blood levels and sustained release up to 8h that confirm the fast efficacy for brain targeting of ^{99m}Tc -PLHNPs and possibility to be used in brain imaging especially in emergency cases.

Conclusion

The ^{99m}Tc -PLHNPs was fabricated as spherical with narrow size and high EE%. The *in vivo* biodistribution study for intranasal administration of ^{99m}Tc -PLHNPs confirmed the fast potentiality and efficacy for brain targeting of ^{99m}Tc -PLHNPs with high brain concentration ($5.80\pm 0.12\% \text{ID/g}$) and high brain-to-blood ratio of 2.42 ± 0.14 at 0.5 h after intranasal administration. The ^{99m}Tc -PLHNPs could be used an innovative intranasal rapid-acting Nano-Radiopharmaceuticals for brain imaging.

Diagnostic value of ⁶⁸Gallium DOTA TATE PET/CT in unsuspected dural venous sinus relapse in resected meningiomas. Comparison with MRI.

Yamila Blumenkrantz, Gabriel Bruno, Paola Corona, Sonia Traverso, Christian Gonzalez, Alejandra Aguilera

Fundación Centro Diagnóstico Nuclear, Argentina

Background

After surgery, meningioma relapse is a relevant finding, with a rate up to 40% within ten years. MRI is the established imaging modality as a first step during the follow up of intracranial meningioma surgeries. However, structural imaging modalities have their limitations, especially in lesions located at the skull base, compromising bone structures or nearby the falx cerebri, being hard to differentiate scar tissue from active tumour. Meningiomas overexpress type 2 somatostatin (SST) receptors and therefore show high affinity to ⁶⁸Gallium DOTATATE, a SST analog. If the diagnosis of recurrence is unclear after morphologic studies, a ⁶⁸Gallium DOTATATE PET/CT, as a second step, is considered the standard of care. Nevertheless, diagnosis of tumour relapse can be challenging. MRI could not detect tumour relapse in specific locations that would be essential in patient follow-up and the diagnosis of relapse could be incomplete without another exam. Parasagittal meningiomas can invade dural venous sinuses due to its proximity to superior sagittal sinus. It is important to be aware of dural involvement to define treatment strategy. Thus, the aim of our study was to assess dural sinus relapse (DSR) with MRI and ⁶⁸Gallium DOTATATE PET/CT in meningioma post-surgical patients.

Methodology

We included between August 2018 and May 2023, 30 patients who underwent intracranial meningioma surgery and performed ⁶⁸Gallium DOTA TATE PET/CT in the first year after surgery, using a GE Discovery 710 PET/CT. We conducted an observational and retrospective analysis in order to assess DSR. All patients included had a contrast-enhancing MRI performed during follow up, before PET/CT assessment.

Results

The cohort had a mean of 55 y/o (30-77) and 21 (70%) were female. Twenty (20, 67%) patients showed non-specific post-surgical changes and 10 (33%) had compatible images with tumour relapse in MRI. Only one (10%) patient had dural sinus involvement reported in MRI. Fifteen (50%) had compatible findings with tumour recurrence in ⁶⁸Gallium DOTA TATE PET/CT, of whom 8 (53%) showed DSR with SUVmax mean of 10.8 (6.2-21.4). In all the cases, the superior sagittal sinus was involved, in 3 patients (38%) 2 or more dural venous sinuses were involved. In 4 (26%) patients, DSR was the only positive finding in ⁶⁸Gallium DOTA TATE PET/CT, a significant difference with DSR depicted by MRI.

Conclusion

Dural sinus relapse after meningioma intracranial surgery is a frequent finding. ⁶⁸Gallium DOTA TATE PET/CT seems to be superior to MRI for its evaluation. MRI could underestimate dural venous sinus involvement in tumour recurrence, a significant proportion of patients with meningioma relapse would not be detected by MRI. Further studies will be necessary to determine clinical impact of this finding.

A tumour-sensitive theranostics scaffold based on a nanoscale metal organic framework (^{99m}Tc -DOX loaded $\text{Fe}_3\text{O}_4@^{\text{III}}\text{Fe}$ -Tannic acid) for pH controlled doxorubicin delivery and enhanced chemo/chemodynamic therapy

M. M. Swidan¹, N. S. Wahba², T. M. Sakr³

¹ Labeled Compounds Department, Hot Labs Center, Egyptian Atomic Energy Authority, Egypt

² Department of Pharmacology and Toxicology, Faculty of Pharmacy, Zagazig University, Egypt

³ Radioactive Isotopes and Generators Department, Hot Labs Center, Egyptian Atomic Energy Authority, Egypt

Background

Radionuclides-based cancer theranostics were confronted with obstacles such limited real-time visualization and inadequate therapeutic impact due to non-specific *in-vivo* distribution. Recently, chemodynamic theranostic (CDT) have been in the spotlight of current advances for personalized cancer management. However, chemodynamic effectiveness is hampered by poor acidic tumour microenvironment (TME) the tumour's glutathione (GSH) antioxidant effect and inadequate endogenous H_2O_2 . Herein, we designed a new in-situ activatable theranostic (^{99m}Tc -DOX loaded AA- $\text{Fe}_3\text{O}_4@^{\text{III}}\text{Fe}$ -TA) to specifically recognize and eradicate cancer cells with H_2O_2 -catalyzed hydroxyl radical ($\bullet\text{OH}$) burst cascade in addition to the chemotherapeutic effect of DOX combined with radionuclide-based concurrent diagnosis.

Methodology

The theranostic-platform (^{99m}Tc -DOX loaded AA- $\text{Fe}_3\text{O}_4@^{\text{III}}\text{Fe}$ -TA) was constructed in a core-shell metal organic framework (MOF) structure where an acid-responsive cross-linked matrix of TA- Fe^{3+} was immobilized on the surface of ascorbic acid-decorated iron-oxide nanoparticles (AA- Fe_3O_4 NPs), followed by loading of technetium-99m labeled doxorubicin (^{99m}Tc -DOX). Also, the *in-vitro* as well as *in-vivo* biological evaluation was assessed.

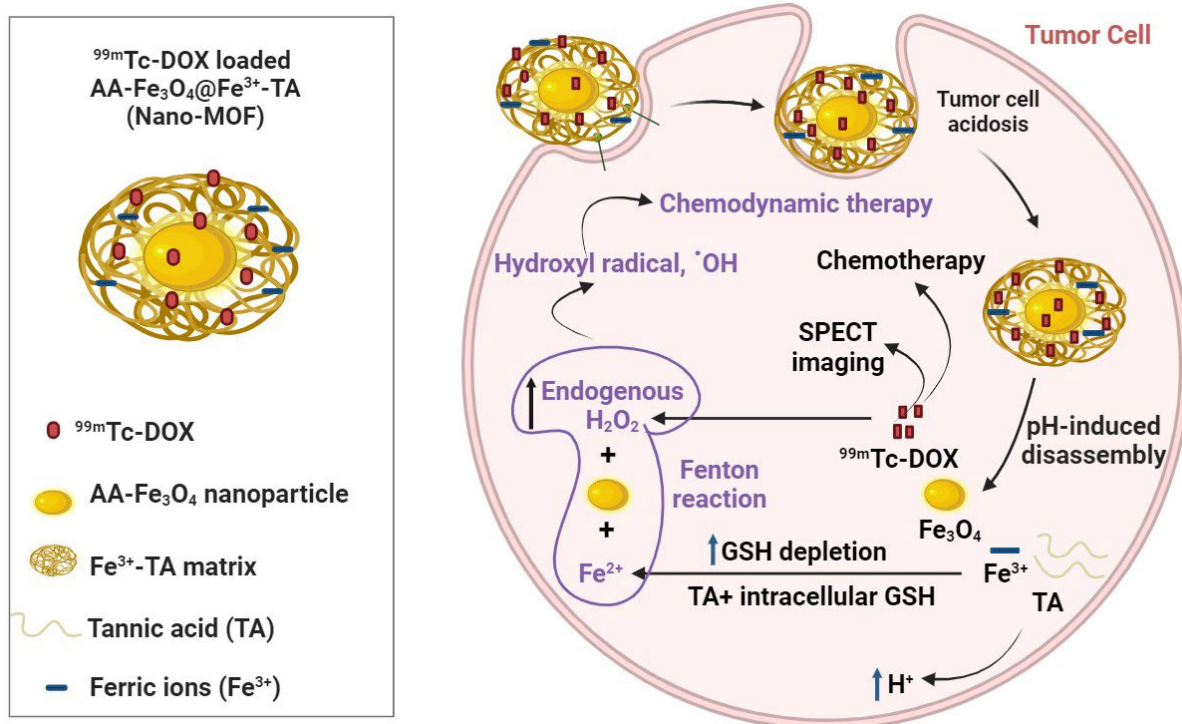
Results

The theranostic-platform demonstrated appropriate physicochemical characteristics with 62 ± 3.8 nm particle size, 82 ± 5.2 nm hydrodynamic size, - 18 mV zeta potential, efficient crosslinking of Fe^{3+} -TA shell onto AA- Fe_3O_4 NPs and 94 ± 0.8 % ^{99m}Tc -DOX loading efficiency. The *in-vitro* release studies revealed that ^{99m}Tc -DOX loaded AA- $\text{Fe}_3\text{O}_4@^{\text{III}}\text{Fe}$ -TA demonstrated pH-dependent spatiotemporal release where only 10 % ^{99m}Tc -DOX was released at the physiological (pH 7.4) while 94 % was released at pH 5 (simulating tumour's pH). This means that the biocompatible and biodegradable platform had the ability to accumulate passively inside tumours with little payload leakage in the systemic circulation. Once the platform enters tumour cells, the MOF shell might degrade due to the acidic nature of the tumour microenvironment (TME), releasing free Fe^{3+} , TA, and a sustained release of ^{99m}Tc -DOX. The released ^{99m}Tc -DOX could be employed as SPECT imaging tracer for concurrent tumour diagnosis in addition to its chemotherapeutic effect as well as the ability to increase the intracellular H_2O_2 concentration. Moreover, the released TA might be able to increase the acidification level of cancer cells overcoming the tumour's modest acidity. Both of the released Fe^{3+} , TA and the endogenous GSH could engage in a redox reaction that depletes GSH and reduces Fe^{3+} to Fe^{2+} ions which subsequently catalyze

the elevated concentration of H_2O_2 to reactive $\bullet OH$ via Fenton-like reaction, increasing the effectiveness of chemodynamic therapy. Furthermore, the *in-vivo* evaluation in tumour-bearing mice showed significant radioactivity accumulation in the tumour lesion (14.6 ± 0.5 % ID/g at 1 h post-injection.) which demonstrate an advancement over the naked ^{99m}Tc -DOX that exhibited a maximum of 1.5 % ID/g only.

Conclusion

The biodegradable ^{99m}Tc -DOX loaded AA- $Fe_3O_4@Fe^{III}$ -TA could be designed as a tumour-selective SPECT tracer with high therapeutic effect for precis chemodynamic theranostic.



Role of [⁶⁸Ga]PSMA PET/CT in initial disease assessment and follow-up of prostate cancer

Nguyen Xuan Canh¹, Ngo Van Tan¹, Cao Van Khanh², Le Nho Quoc¹, Nguyen Hoang Ai Ly¹, Tran Bao Huy¹, Tran Thanh Tam¹

¹ Department of Nuclear Medicine, Choray Hospital, Vietnam

² Department of Nuclear Medicine, Military Hospital 175, Vietnam

Background

Many imaging modalities have been used in diagnosis and follow-up of prostate cancer and PET/CT with [⁶⁸Ga]PSMA has emerged as a superior technique compared to conventional imaging. We aimed to investigate the effectiveness of PSMA PET/CT in initial disease assessment and follow-up of prostate cancer.

Methodology

This retrospective study included prostate cancer patients undergoing PSMA PET/CT imaging during 3 months from November 2023 to January 2024 at Cho Ray hospital. The results of PSMA PET/CT were descriptively analysed and compared with MRI and bone scan to determine the role of PSMA PET/CT in initial disease assessment and follow-up of prostate cancer.

Results

A total of 35 prostate cancer patients with mean age of 73.9 ± 6.9 years were in the study. The number and proportion of patients with pathological Gleason score 6, 7, 8, 9, 10 were 2 (5.7%), 13 (37.1%), 2 (5.7%), 13 (37.1%) and 1 (2.9 %), respectively. Four patients (11.4 %) were not collected a Gleason score.

Among 11 (31.4 %) prostate cancer patients who have not received specific treatment, 7 have Gleason 9, 1 Gleason 8, 2 Gleason 7 and 1 Gleason 6. The mean PSA concentration is 118.7 ng/ml (14.7-392). PSMA PET/CT presented malignant prostate lesions with intense uptake in 8 patients (72.7 %) and prostate indeterminate lesions with equivocal uptake in 3 patients (27.3 %). Six patients (54.5 %) had seminal vesicle invasion and 5 (45.5 %) had both regional lymph node and bone metastases. PSA concentration in the group with regional lymph nodes and bone metastases was 203.8 ng/ml, higher than the non-metastatic group with PSA 47.7 ng/ml (p value = 0.21). In 10 patients undergoing prostate MRI, which detected 9/10 (90 %) prostate cancer lesions (PI-RADS 4-5), while PSMA PET/CT detected 7 /10 (70 %) prostate cancer lesions (PSMA-RADS 4-5). Of 4 patients with negative [^{99m}Tc]MDP bone scan, 2 had bone metastases detected by PSMA PET/CT.

Among 24 (68.6 %) patients received treatment with one or a combination of surgery, radiotherapy, androgen deprivation therapy (ADT) and chemotherapy, PSMA PET/CT showed that 14 (58.3 %) patients had regional lymph node metastases, 11 (45.8 %) had bone metastases and 2 (8.3 %) had liver metastases during follow-up. Of 9 patients developing biochemical recurrence with mean PSA concentration of 7.6 ng/ml (0.35-29.3) after radical prostatectomy (including 2 using adjuvant ADT), 4 (44.4 %) patients had locally recurrent lesions identified on PSMA PET/CT and 2 of these received negative MRI findings for local recurrence. To compare with bone scan in 11 patients, PSMA PET/CT detected bone metastases in 6 (54.5 %) patients, while bone scan did those in 5 (45.5 %) patients, along with 1 false positive and 1 false negative case. Bone metastatic lesions were presented more numerous and higher tracer avid on PSMA PET/CT than bone scan images.

Conclusion

PSMA PET/CT was effective in detecting local recurrence after radical prostatectomy, regional lymph node and bone metastasis in prostate cancer. The role of PSMA PET/CT in detecting primary lesions needs to be further evaluated.

Keywords: Positron Emission Tomography / Computed Tomography (PET/CT), [⁶⁸Ga]PSMA, prostate cancer.

Development of a Dual-Drug Loaded Polymeric Nanoparticle System for Theragnostic Purposes

B. Güngör, S. Teksoz, A. İçhedef

Institute of Nuclear Sciences, Ege University, Türkiye

Background

During the last centuries one of the deadliest diseases that is becoming increasingly widespread day by day is cancer and it is involved in most research for diagnosis and treatment purposes. This disease, which varies among individuals, can also be found in highly heterogeneous forms within a single tumour structure. Many studies have focused on systems involving combinations of two active substances in cases of cancer resistance to treatment. Selectivity and overcoming multi-drug resistance play a significant role in the stronger effect of systems containing dual active substances. In this study, the combination of doxorubicin (DOX) and thymoquinone (TQ) was loaded into polymeric nanoparticles, which are drug carrier systems targeting specific molecules, and then folate conjugation was performed to enable active targeting of the system to the tumour. Finally, the system was radiolabeled with technetium-99m which is an ideal imaging radionuclide.

Methodology

In this study, polyethylene glycol-b-poly-epsilon-caprolactone (PEG-b-PCL) copolymer was synthesized via metal-free cationic ring-opening polymerization to achieve controlled micelle concentration. To ensure efficient radiolabeling, a pyrazole diamine chelating agent was synthesized and conjugated to the micelles. Structural analysis of all synthesis steps was conducted via Nuclear Magnetic Resonance (NMR). Furthermore, the characterization of polymeric micelles was performed using Dynamic Light Scattering (DLS) and Scanning Electron Microscopy (SEM). Doxorubicin and thymoquinone were loaded into the micelles at specific ratios, and the amount of drug entrapped in the synthesized micelles was detected using the high-performance liquid chromatography (HPLC) method. Finally, folate-conjugated polymeric micelles were radiolabeled with technetium-99m and in vitro cell culture studies were conducted.

Results

It was determined from DLS results that the polymeric micelles were synthesized in the range of 100-150 nm. Additionally, from SEM images, it can be observed that the micelles are spherical in shape. The drug loading efficiency into the drug carrier system was found to be 66% for DOX and 40% for TQ, as determined by HPLC analysis. The radiolabeling efficiency with technetium-99m was found to be above 85%. In vitro uptake and toxicity experiments of the radiolabeled system were conducted.

Conclusion

It is believed that the drug carrier system obtained in this study will provide significant benefits to the literature in terms of simultaneous therapy and imaging.

Acknowledgement: This study was conducted with funding support from the Ege University Scientific Research project numbered FDK-2021-22255, as well as through support from The Scientific and

Technological Research Council of Turkey (TUBITAK) via the Research Fellowship Programme (BIDEB-2211C) for PhD Students.

Development and Evaluation of a Radiolabeled Drug Delivery System for Multimodal Cancer Imaging

O. Çetin^{1,2}, Ç. İçhedef¹, E. Betancourt Fernandez², J. R Herance Camacho², S. Teksöz¹

¹ Institute of Nuclear Sciences, Ege University, Türkiye

² Vall d'Hebron Research Institute, Spain

Background

The main objective of this study is to design and evaluate a radiolabeled drug delivery system as a multimodal imaging agent. In present study, a radiolabeled drug loaded biotin-mediated polymeric magnetic nanoparticle system was developed. The superparamagnetic iron oxide nanoparticles loaded into doxorubicin (DOX) and biotin conjugated polymeric nanoparticles as a drug delivery system that will function both in cancer treatment and diagnosis. For this aim, DOX loaded biotin receptor-targeted magnetic polymeric nanoparticles were radiolabeled with Zirconium-89. This innovative combination serves as a dual-function drug delivery system for cancer treatment and diagnosis.

Methodology

To begin with, iron oxide (IO) nanoparticles were prepared by co-precipitating ferric and ferrous chloride salts with a molar ratio of Fe (III)/Fe(II) 2:1. Subsequently, the biotin-PEI conjugate was obtained, followed by the preparation of the DOX and iron oxide-loaded polymeric nanoparticle system using the double emulsion method. Furthermore, the characterization PLGA/PEI/lipid-IO nanoparticles were performed by Dynamic Light Scattering (DLS), Fourier Transform Infrared Spectroscopy (FTIR), Scanning Electron microscopy (SEM) and Transmission Electron Microscopy (TEM). The high-performance liquid chromatography (HPLC) method was used to detect the amount of drug entrapped in the synthesized PLGA/PEI/lipid-IO nanoparticles.

In conclusion, the cheating system(p-SCN-Bn-deferoxamine) was conjugated to DOX-loaded polymeric nanoparticles for radiolabeling study. Then radiolabeling with Zirconium-89 was performed and biological studies were performed.

Results

The hydrodynamic average size of the nanoparticles was determined as $189.48 \text{ nm} \pm 18.08$ (n=8) using DLS. FTIR analysis confirmed the presence of functional groups on the surface of magnetic nanoparticles, with absorption peaks at 552 and 413 cm^{-1} indicating the Fe-O bond. The formation of the PEI-biotin conjugate was confirmed by ¹H-NMR spectroscopy. TEM images depicted spherical DOX-loaded PLGA/PEI/lipid-IO-BIO nanoparticles, with a particle size distribution of $17.91 \pm 3.04 \text{ nm}$ (n=10) determined using ImageJ. HPLC analysis revealed a drug loading capacity of $56.71 \pm 3.209\%$. According to the results of FTIR analysis the DFO was conjugated PLGA/PEI/lipid-IO-BIO nanoparticles. Radiolabeling efficiency of PLGA/PEI/lipid-IO-BIO-DOX-DFO nanoparticles with Zirconium-89 was found to be higher than 70%, confirmed by nanodrop analysis. The radiolabeled system was further evaluated through biological research.

Conclusion

Nuclear medicine and molecular imaging have provided a multidisciplinary collaboration, making it a stimulating and hugely varied area in which to make a career in chemistry. Systems formed by drug,

polymer and radionuclide combination offer the most promising opportunities in the diagnosis and treatment of many diseases.

Acknowledgement

This study was conducted with funding support from the Ege University Scientific Research project numbered FDK-2021-22867, as well as through support from The Scientific and Technological Research Council of Turkey (TUBITAK) via the Research Fellowship Programme (BIDEB-2214A and BIDEB-2211C) for PhD Students.

Complementary Role of Tc-99m HMPAO and ECD Brain SPECT with MRI co-registration in Multimodality Presurgical Imaging of Epilepsy- A Low Resourced Single Center Experience

A. Pallewatte¹, L. S. Selvanayagam²

¹ National Hospital of Sri Lanka, Sri Lanka

² Post Graduate Institute of Medicine, University of Colombo, Sri Lanka

Background

Best management option for refractory or medically resistant Epilepsy in young patients is surgery. However, it is performed on a small percentage of patients in our institution. Prerequisite for effectiveness depends on accurate delineation of ictal focus. Our institution's main tools in investigating epilepsy patients include EEG and imaging modalities MRI, SPECT and PET/CT. These modalities detect perfusion abnormalities associated with seizures in ictal and interictal phases. Even-though PET/CT better reflects brain glucose metabolism as function compared to SPECT we mainly rely on inter-ictal SPECT due to lower cost and other logistics. This study analyses imaging findings, localisation of ictal focus, surgical and non-surgical management and final outcome in a cohort of patients along with demographic data. Our institution caters to patients above 14 years and clinicians first perform EEG and MRI. Because of high cost, only patients having equivocal findings on these two modalities or those planned for surgery were referred to Neuro SPECT/PET/CT as decided at initial multidisciplinary meeting (MDT). Some patients undergo both ictal and interictal imaging while majority undergo only inter-ictal imaging.

Methodology

Data from all patients with positive MRI findings, referred to Nuclear Imaging Unit of National Hospital for epilepsy SPECT-imaging from 01-02-2019 to 31-01-2020 were analysed as a retrospective observational study. Patients' clinical data, EEG findings, sex, age was obtained. Tc-99m ECD/HMPAO were used in perfusion imaging depending on availability. MRIs were performed with Siemens-Skyra-3T scanner and SPECT with Siemens-Symbia-S dual-head gamma camera having Neuroanalysis software package- "Scenium"-(Siemens-Healthineers-Germany). MDT interpretations on patient images manually co-registered with MRI were analysed. Only patients' inter-ictal SPECT findings (i.e. hypoperfusion) were used for study and those with incomplete data were excluded. Institutional Ethical approval was obtained.

Results

There were 16 patients (10 male and 6 female) referred by multidisciplinary team during study period with mean age of 18.4 years (range 14-26 years).

MRI and MRI/EEG findings were hippocampal atrophy in 5 patients, cortical dysplasia-3, gliosis/encephalomalacia-5 and non specific T2 signal or suspicious of tumour-3.

As per MDT decisions, there were positive findings (hypoperfusion) in inter-ictal SPECT in 13 patients (81%). MRI and SPECT location with diagnostic agreement was seen 9/13(69%). EEG, MRI and SPECT localization agreement seen in 7/13(54%) while diagnoses were inconclusive in 4/13(31%). Out of 9 patients with MRI and SPECT agreement, SPECT after co-registration, showed larger lesions

and/or additional areas of hypo-perfusion in 5 patients compared to MRI. Out of the remaining 4, only 2 were decided to have localized lesions suitable for surgery.

Conclusion

Our institutional protocol was to reserve SPECT only for essential cases due to low resources. Limited access to PET/CT/SPECT and inconsistent supply of radiopharmaceuticals-ECD/HMPAO further hampered this. However as per results above, inter-ictal SPECT with manual MRI co-registration and final interpretation at MDT is useful in deciding and filtering patients suitable for surgery (69% MRI-interictal SPECT diagnostic agreement). Diagnostic uncertainties also could be resolved using inter-ictal SPECT (in spite of its well-known low sensitivity) in our set-up thereby optimising use of neuro-nuclear imaging facilities, reducing surgical morbidity, further improving clinical management of epilepsy patients.

The Role of PET/CT in Infection and Inflammation, Al Busaídi Khalid

K. Al Busaidi

Royal Hospital, Oman

Background

Evaluation of infection and inflammation is clinically very important and needs good investigations; and this requires using sensitive and reliable imaging modalities for both diagnosis and follow-up. The PET/CT scan is one of the imaging modalities that are increasingly being used for the purpose of detecting and following up infectious and inflammatory process.

Methodology

The [¹⁸F]FDG is the PET tracer that is widely used around the world for cases of infection and inflammation in different parts of the body. It has been found that the white blood cells (activated by either an infectious pathogen or as a consequence of inflammatory process) show high energy consumption and avidity for [¹⁸F]FDG tracer; and therefore, the process of infection/inflammation leads to high FDG uptake. The detection of such process by FDG tracer is far earlier before the appearance of morphological changes (which are usually detected in other conventional anatomical imaging modalities); and this gives an advantage of early detection and diagnosis of disease and results in early treatment. In addition, this evolving modality provides technical imaging advantages, for example, allowing short duration of imaging with high spatial resolution as well as being non-invasive and offering the ability of fusing the data with other anatomical images.

Results

Reviewing the literature in this topic showed that PET/CT scan is being used in different types of infection and inflammation. For instance, pyrexia of unknown origin (PUO) is a serious indication nowadays for PET/CT scan, which provides the technique to scan the whole body in order to detect the source of infection. Moreover, in the diagnosis of cardiovascular infections (e.g. infective endocarditis, electronic device infection, prosthetic valve infection and vascular graft infection) and inflammatory cardiovascular diseases (e.g. Giant cell arteritis and Takayasu arteritis), the PET/CT scan is considered a reliable and non-invasive imaging modality that shows a good sensitivity. In addition, in the evaluation of infection and inflammation of the bones and joints, the PET/CT has a great value for confirming the diagnosis and assessing the activity of the disease. Rheumatoid arthritis is a very good example for inflammatory joint diseases in which PET/CT has a big role during the course of treatment. Evaluating prosthetic joints and assessing the diabetic foot to rule out osteomyelitis are other indications for PET/CT scan. Many other inflammatory and infectious diseases might also be evaluated by PET/CT (such as tuberculosis, sarcoidosis, HIV-related diseases and inflammatory bowel diseases).

Conclusion

The use of [¹⁸F]FDG PET/CT scan has an important role in the diagnosis of inflammatory and infectious process in the body and more importantly to detect the source of infection in some cases (especially in cases of PUO) and to evaluate the activity of the inflammatory disease, which consequently helps the treating physicians in their treatment plans. The era of PET/CT scan needs to be explored and more

researches to be done as it provides (with evolving new tracers) a reliable non-invasive and sensitive method for diagnosis and follow-up of different types of diseases.

Utility of molecular breast imaging in the detection of mucinous breast cancer: A case report

I. S. Bandong¹, M. T. Buenaflor², R. A. Conlu

¹Diagnostic Breast Imaging Society of the Philippines and Philippine Society of Nuclear Medicine, Philippines

²Philippine College of Radiology, Philippines

Background

Mucinous breast cancer (MBC), also known as colloid carcinoma, occurs in women older than 55 years and is generally considered to have a favourable prognosis (Bitencourt, et al 2016). The 10-year survival rate is about 90.4% (Marrazon et al, 2020).

Molecular breast imaging (MBI) is a physiologic approach to breast cancer detection. MBI using a gamma camera is performed with [^{99m}Tc]sestamibi. MBI detects additional foci of occult breast cancer in 9.0% of women with newly diagnosed breast cancer, has a high sensitivity for detecting high-risk lesions, and detects 98% of invasive breast cancer and 91.0% of ductal carcinoma in situ (Muzahri 2020).

The objective of this case report is to describe the utility of MBI in detecting mucinous breast cancer.

Case Report

A 51-year-old asymptomatic Filipino female with family history of breast cancer. She had digital breast tomosynthesis (Figure 1) showed group of dense masses in the anterior third of the mid inner left breast. On breast ultrasound (Figure 2), these masses correspond to cluster of irregular hypoechoic solid masses. Molecular breast imaging (Figure 3) was done and demonstrated two sestamibi avid foci at the mid inner left breast with T/B ratio of 1.3, corresponding to the masses seen on mammogram and breast ultrasound. Biopsy was done and it revealed invasive carcinoma with mucinous features.

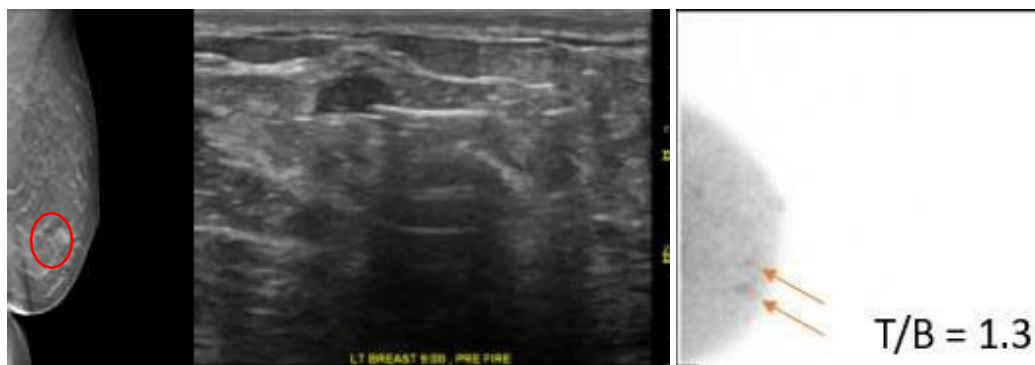


Figure 1

Figure 2

Figure 3

Discussion

MBC is a well-differentiated type of adenocarcinoma that typically contains abundant extracellular mucin secreted by tumour cells. It is an uncommon histologic type that accounts for about 2% of all invasive breast carcinomas (Bitencourt, et al 2016). MBC occurs predominantly in patients who postmenopausal or elderly. MC has a favorable prognosis with the 5-year disease-free survival rates range from 81% to 94% (Garcia et al, 2018)

The most common mammographic appearance is low-density, round, or oval masses with circumscribed margins. Microlobulated margins have been associated with highermucin content. Sonographically, these are isoechogenic echotexture relative to subcutaneous fat echo and a good sound transmission (Bitencourt, et al 2016).

Molecular breast imaging (MBI) is a new nuclear medicine technique that utilizes small semiconductor-based γ -cameras in a mammographic configuration to provide high-resolution functional images of the breast (O'Connor et al, 2009)

Tumours present high expression of cellular proliferation factors, high mitotic rates, intense angiogenesis and high mitochondrial activity and density. These factors are the main determinants for the concentration of [^{99m}Tc]sestamibi in the lesion. Papilliferous and mucinous carcinomas, with lesser cellularity and slow growth, frequently do not show significant concentrations of the radiotracer (Moriguchi et al 2010)

Conclusion

MBI plays an important complementary role for both breast cancer screening and evaluation of breast cancer especially in indeterminate or inconclusive mammography or sonographic findings.

Keywords: Mucinous breast cancer, Molecular breast imaging, Technetium-99m sestamibi

[¹⁸F]FDG PET/CT and MRI mutual relationship in cervical cancer response assessment after combined radiotherapy treatment

S. Lucic, D. Stojanovic, J. Licina, M. Spirovski, O. Ivanov

Medical Faculty University of Novi Sad, Oncology Institute of Vojvodina, Serbia

Background

Combined chemoradiotherapy (CRT) is the standard treatment option for locally advanced cervical cancer. An adequate assessment of response and timely detection of tumour recurrence after CRT treatment is of great importance. Even though there is no consensus about the needed time interval until the first diagnostic examination after CRT, preferred and considered as a reliable diagnostic tool MRI is usually performed in first 3 months after the end of treatment. Aim of this study was to determine whether the implementation of [¹⁸F]FDG PET/CT in diagnostic algorithm could improve cervical cancer post treatment response evaluation.

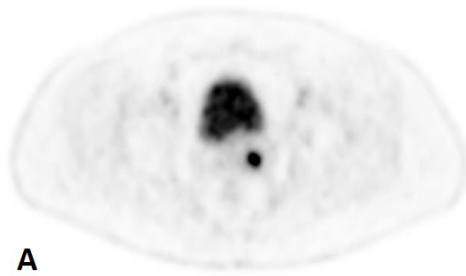
Methodology

Study included 41 female patients (mean age 53.39±11.85; range 31-77, median 56) with locally advanced cervical cancer FIGO stage IB2-IVA treated with combined chemotherapy and external beam radiation therapy (EBRT) with concomitant intracavitary brachytherapy were included in the study. Pelvic and abdominal MRI exam were performed 2-4 months after treatment, followed by [¹⁸F]FDG PET/CT in order to estimate early therapy effects. Diagnostic studies results were positive, negative and equivocal for rest/recurrent tumour presence, and they were compared to control MRI exam done at least six months after CRT completion. Progression free (PFS) and overall survival (OS) was calculated. Data sets were statistically analysed with two-tailed Chi squared and Cohen kappa test, Kaplan-Meier survival curves and Log rank test for progression free and overall survival. With the level of confidence determined at p<0.05. Sensitivity, specificity, and diagnostic accuracy of both techniques were calculated.

Results

Cohen kappa test indicated good agreement between [¹⁸F]FDG PET/CT and follow up study with κ coefficient of 0.64 (95%CI 0.456/0.832), and only fair agreement between MRI and follow up of κ 0.36 (95%CI 0.342-0.548).

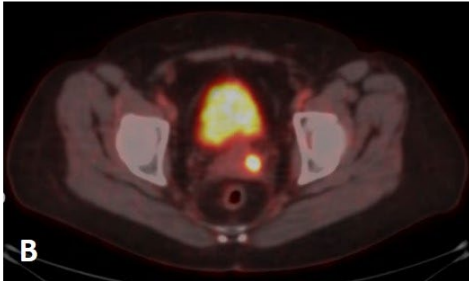
Sensitivity, specificity, and diagnostic accuracy of MRI were determined at 88.23%, 54.16%, and 68.29%, respectively, while for PET/CT the values were 70.83%, 70.83%, and 82.92%, respectively. With Kaplan-Meier survival analysis both diagnostic modalities showed statistical significant for PFS and OS survival with Log-rank, p <0.001. Mean PFS was 22.45+1.94 (95%CI 18.64/26.25), and median was 18 (95%CI 12.19/23.81). OS mean 28.34+1.39 (95%CI 26.22-31.65) median 30 (24.56-35.43). Example of concordant diagnostic imaging results is shown in picture.



A



C



B

Concordant posttreatment ^{18}F -FDG PET/CT and MRI findings indicated the presence of posttherapy metabolically active cervical cancer residual tumor in A. PET, B. fused PET/CT and C. MRI axial plane.

Conclusion

Diagnostic accuracy of both MRI and ^{18}F FDG PET/CT in therapy response evaluation after CRT was in concordance with most of the reported in the literature. ^{18}F FDG PET/CT showed good concordance with follow up results, better than MRI, and with an impact on progression free and overall survival study resulted are allowing us to conclude that, aligned to MRI, ^{18}F FDG PET/CT can be helpful diagnostic tool in post-RT cervical carcinoma evaluation.

Local Experience on Radioguided Occult Lesion Localization (ROLL) for Non-Palpable Breast Lesions: A Single-Center Case Series

R. A. Inting¹, N. Bustos², C. A. Carbonell¹

¹The Medical City Ortigas Nuclear Medicine and PET/CT Center, Philippines

²The Medical City Ortigas Breast Center, Philippines

Background

Breast cancer is the leading malignancy among women and the second leading cause of cancer-related deaths following lung cancer. Early diagnosis and prompt treatment are vital and still convey the best patient outcomes. Lesions that cannot be detected by physical examination but display asymmetry, microcalcification, and distortion on scanning methods such as mammography and US are defined as non-palpable breast lesions (NPBLs).

To perform breast conserving surgery in these patients, the tumour needs to be localized correctly before excision. Wire-guided localization (WGL) has long been regarded as the standard. In practice however, it has its disadvantages.

Radioguided occult lesion localization (ROLL) is a newer method that takes advantage of the tumour localizing capacity of a small amount of a nuclear radiotracer to identify the culprit lesion. A gamma probe is then used intraoperatively to detect the radioactive primary tumour site to excise the non-palpable lesion.

Multiple studies comparing both suggest that ROLL is as effective as WGL for the excision of non-palpable breast lesions on top of improved patient outcomes by reducing localization and operation time, preventing healthy tissue excision and achieving clearer margins. Global literature may produce substantial accounts, but information regarding its use in the Philippines has been insufficient.

Cases

Case 1: A 46-year-old female with a solitary focus of tracer activity in the left breast, at the 1 o'clock position relative to the nipple marker.

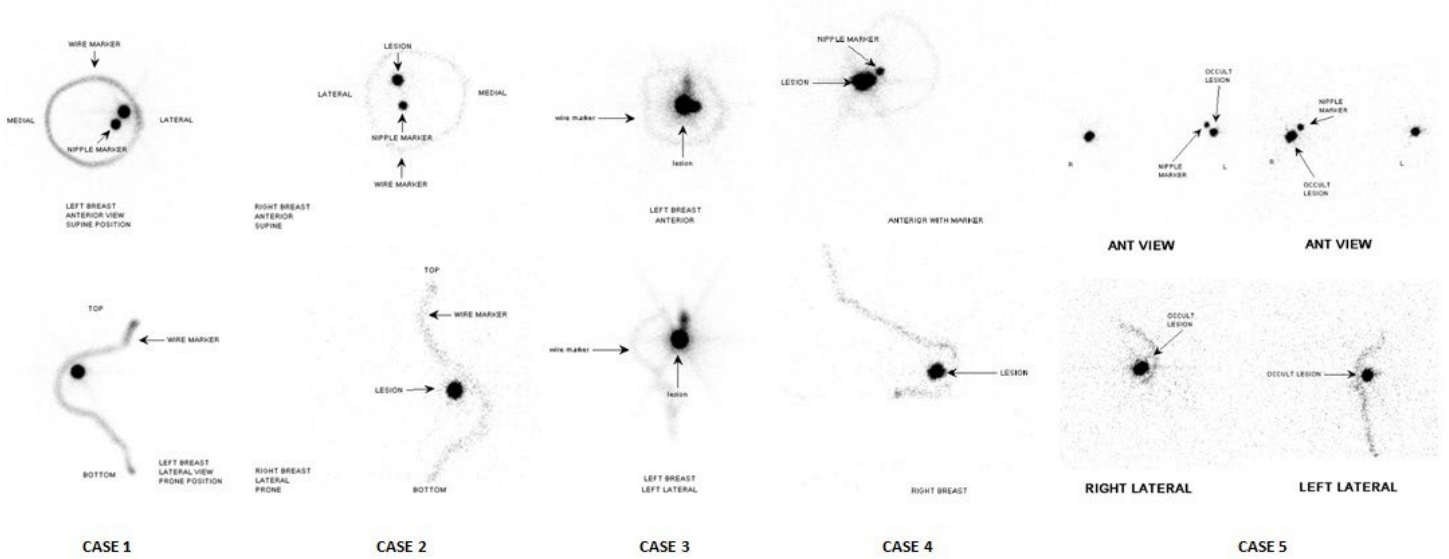
Case 2: A 54-year-old female with a solitary focus of tracer activity in the right breast, at the 11 o'clock relative to the nipple marker.

Case 3: A 45-year-old female with a solitary focus of tracer activity in the left breast, at the 1 o'clock position relative to the nipple marker.

Case 4: A 49-year-old female with a solitary focus of tracer activity in the right breast, at the 8 o'clock position relative to the nipple marker.

Case 5: A 46-year-old female presenting with two (2) foci of tracer activities in both breasts, at the 4 o'clock and at the 7 – 8 o'clock positions, in the left and right breasts, respectively.

All five (5) patients underwent successful surgical excision and all had benign histologic findings.



Conclusion

This case series highlights rare documented cases on the utilization of ROLL in the detection of NPBLs in the Philippines, which still currently uses WGL as the standard. With various multinational studies already documenting its efficiency, non-inferiority and relative advantages over WGL, ROLL holds great potential as a promising and viable alternative, serving as an impetus for its widespread use in the local setting.

Variability of physiological cardiac uptake in explorations by positron emission tomography with 18 fluoro-2-deoxyglucose

D. B. Padrón, L. M. Pérez

Hospital Hermanos Ameijeiras, Cuba

Background

¹⁸F-fluoro-2-deoxyglucose positron emission tomography has become one of the preferred imaging modalities for the diagnosis and prognosis of different types of cancer. Variations in myocardial ¹⁸F-fluoro-2-deoxyglucose uptake have been observed in routine positron emission tomography oncology studies, and it is sometimes difficult to assess in clinical practice whether myocardial uptake is physiological or not.

Methodology

35 patients with a diagnosis of Lymphoma were retrospectively analysed with the aim of evaluating the variability of physiological cardiac uptake in ¹⁸F-fluoro-2-deoxyglucose positron emission tomography scans. These patients had undergone two examinations carried out in the department of Nuclear Medicine and Radiotherapy of the Hermanos Ameijeiras Surgical Clinical Hospital. The patients were divided into two groups according to the presence of variation of myocardial uptake in relation to the maximum SUV between the two scans.

Results

The mean age was 44.83, with a predominance of obesity and hypertension as main risk factors (17.14% and 14.3% respectively). The majority of patients received chemotherapy, the presence of some cardiac uptake pattern was observed in 13 patients (37.14%) and 11 patients (31.42%) presented a change in the uptake pattern between the studies performed. In the initial studies, the focal pattern was observed more frequently (14.29%) while in the later studies the focal over diffuse pattern predominated (11.43%). No significant differences were observed between the parameters of the examinations. In relation to the presence of variation in myocardial uptake, no associations were found between clinical and examination parameters.

Conclusion

Cardiac uptake of ¹⁸F-fluoro-2-deoxyglucose is frequent in patients with Lymphoma and variations in the intensity of uptake and a change in the uptake pattern between patients and in different studies of the same patient can be observed. Cardiovascular risk factors and parameters of explorations such as aid are not related to the variation in cardiac uptake.

Keywords: Cancer/imaging diagnosis, Positron Emission Tomography, Cardiac Disease Risk Factors.

Computerized Tomography Findings of Oesophageal Cancer in Patients Scanned at Tikur Anbessa Specialized Hospital and Associated Risk Factors from April 2018 to August 2020

A. A. Umer

Tikur Anbessa Specialized Hospital, Ethiopia

Background

Computerized tomography is a diagnostic imaging used for staging of oesophageal cancer and help in guiding type of treatment. The purpose of this study is to determine CT stage of oesophageal cancer in all patients sent to radiology department of TASH for two years and three months.

Methodology

After ethical clearance hospital based prospective cross-sectional study were conducted on CT scan images of 276 patients in the department of radio diagnosis, Tikur Anbessa Specialized Hospital [TASH]. These patients were oesophageal cancer patients sent to department of radiology for CT scan staging. All 276 patients have endoscopic biopsy results in study period from April 2018 to August 2020. After obtaining consent, from 276 patients, patients address, age, gender, duration, dietary habit and presentation were extracted directly from patient interview. All 276 biopsy results copies were obtained directly from patients themselves. All 276 CT images were evaluated. Finding like the site of involvement, degree and length of wall thickening, and lymph nodal and distant metastases were looked for and finally the finding staged using revised oesophageal staging 7th edition manual (2009). Site of involvement correlated with endoscopic biopsy. Descriptive statistics was performed.

Results

The study showed majority of patient (80%) came to TASH with advanced disease. 171 (61.9%) patients came from Oromia and the rest 108 (38%) came from other part of the country. Arsi region alone took share of 89 patients which is (31%) of total. 143 (51.8%) patients are male and the rest 133 (48.2%) are female. Dietary hot food habit consumption seen in majority of patient which contribute to 231 (83.7%) and the remaining consume warm food. Concerning the site of involvement 168 (60.9%) patient have lesion in distal oesophagus followed by middle oesophagus 70 (25%). Majority of patients 204(73.9%) had squamous cell carcinoma and the rest had adenocarcinoma.

Conclusion

Most of patient had advanced disease for which surgery has no role in patient treatment and almost all of these patients came from Oromia regional state with Arsi region took high percentage with almost all of them have dietary risk factor of consuming very hot food.

Deep-Learned Estimation of Glomerular Filtration Rate of Kidneys from a Low-Dose Single Time-Point Renal SPECT/CT Scan

H. Mahani, M. Askari

Radiation Applications Research School, Nuclear Science and Technology Research Institute, Iran

Background

Glomerular filtration rate (GFR) is a measure indicating the functional performance of kidneys ranging from zero to 120 mL/min/1.73 m². Estimated GFR (eGFR) is highly dependent on age, gender, body mass index (BMI), diet, and lifestyle. It is well known that low eGFRs are associated with chronic kidney diseases and an increase in kidney cancer risk. In this work, we aim to predict the eGFR from a single time-point renal SPECT/CT scan using a deep-learned regression neural network.

Methodology

To do so, 315 low-dose static renal [^{99m}Tc]Tc-DTPA SPECT/CT scans were paired and labeled with the corresponding blood test-extracted eGFR as ground truth. The patients were selected in a way their eGFRs cover a reasonably wide range. Partitioning of the dataset into training, validation, and test sets was 5:1:1. The SPECT/CT scans were also pre-processed to further suppress the image noise and resampling. Data augmentation was also employed to enrich the dataset. A dual-channel (SPECT and CT images) deep neural network (DNN) was exploited. Root mean square error (RMSE) and R² score were then calculated to evaluate the performance of the proposed network.

Results

The evaluation metrics prove the promising performance of the proposed regression DNN in such a task. The deep regression model gives rise to an RMSE of 0.11 and an R² score of 0.93 both indicating an accurate prediction of eGFR from a low-dose single time-point renal SPECT scan. The incorporation of CT anatomical data leads to a superior performance of the regression DNN compared with a single-channel (SPECT-only) architecture in terms of accuracy. The results show that there is a correlation between low eGFRs (< 60 mL/min per 1.73 m²) and a modestly higher risk of kidney cancer.

Conclusion

The findings demonstrate that deep learning accurately predicts eGFR using a single-shot SPECT scan without performing dynamic imaging. Therefore, static SPECT/CT-derived eGFR using deep learning enables the prediction of kidney failure and hence estimation of kidney cancer risk.

Keywords: Kidney; Renal SPECT/CT; Static imaging; GFR; Deep learning

Hybrid imaging technologies integration into practical and scientific work of the Interventional Radiology Department of the «N.N. Blokhin National Medical Research Center of Oncology» of the Ministry of Health of the Russian Federation

Dmitry Frantsev

Interventional Radiology, Russian Federation

The Interventional Radiology Department of the «N.N. Blokhin National Medical Research Center of Oncology» of the Ministry of Health of the Russian Federation includes a clinical department of radiosurgical methods of diagnostics and treatment, consisting of 17 rooms with 30 beds, and a radiology unit consisting of 4 operating rooms equipped with angiographic complexes with the possibility of flat-detector computed tomography (FDCT), expert-class ultrasound diagnostic devices, video endoscopic equipment, including the possibility of endobiliary fluorescence diagnostics. The Interventional Radiology Department is the largest in the Russian Federation in terms of the number and range of diagnostic and therapeutic radiosurgical procedures performed on patients suffering from cancer. Since 2021, hybrid imaging technologies, namely FDCT, video endoscopy (including cholangioscopy) with the possibility of endobiliary video fluorescence diagnostics have been actively introduced into the practical and scientific work of the department.

In 2023, more than 4,000 diagnostic and therapeutic interventional radiologic procedures were performed, among them using hybrid imaging technologies:

- 192 transarterial chemoembolizations under combined control of digital subtraction angiography and flat-detector computed tomography for primary and secondary liver tumours;
- 39 cryoablations for liver and kidney tumours under combined control of ultrasound navigation, digital subtraction angiography and flat-detector computed tomography;
- 7 endobiliary biopsies and 10 procedures of endobiliary photodynamic therapy under combined control of video endoscopy (spy glass) and fluoroscopy in malignant tumours of bile ducts;
- 13 blockades of the parietal plexus ganglion in chronic pain syndrome under combined control of fluoroscopy and flat-detector computed tomography;
- 8 ureteral stenting using Rendezvous technology under combined video endoscopic and fluoroscopic control in iatrogenic injuries.

The aim of this work is to demonstrate the possibilities of hybrid imaging technologies in the treatment of cancer patients in the largest interventional radiology department in the Russian Federation.

Logistics and associated problems in establishing a theranostic center with special reference to developing countries

Ajai Kumar Shukla, Satyawati Deswal, Manisha Pradhan

Department of Nuclear Medicine, Dr. Ram Manohar Lohia Institute of Medical Sciences, India

Background

The specialty of nuclear medicine is fast expanding by virtue of its capability to provide functional as well as morphological information. However, in developing countries the growth is not as rapid as is seen in developed countries though developing countries have large proportion of global population. In Indian scenario the number of Nuclear Medicine facilities have grown at a moderate pace and as of now there are 520 centers in a population of 1.4 billion.

Methodology

The attributable reasons for relatively lesser number of nuclear medicine facilities can be described as:

1. Space constraints and rigorous compliance of regulatory requirement prevents growth as many centers have inadequate infrastructure.
2. Inadequate funding available in creation of a functioning nuclear medicine facility. Infrastructure requires large magnitudes of funding as initial investments and thereafter continuous and sustained functioning of department is a major challenge for many centers.
3. The limited availability of trained and qualified (in accordance with AERB guidelines) manpower for functioning of a nuclear medicine facility. In India government/private sectors together provide annual intake of more than 50 medical postgraduates and about 250 technologists apart from some institutions having intake for PhD programs as well. With new AIIMS being opened, this intake is likely to increase and may contribute to faster growth of nuclear medicine facilities.
4. Availability and access of commonly used radionuclides such as I-123, Tl-201, and many therapeutic radiopharmaceuticals like Y-90, $^{68}\text{Ge}/^{68}\text{Ga}$ generators and alpha emitters are not produced in India and are therefore imported. It may not be out of place to mention that BRIT, Mumbai although economical in terms of cost but has been not been able to largely meet the requirements of ^{99}Mo - $^{99\text{m}}\text{Tc}$ generator and I-131 for the existing nuclear medicine facilities.

Results

Although a significant and visible improvement has already been done, the initiatives by agencies are worth mentioning and it is expected that in near future, the growth and expansion would register the quantum jump to cater to large cross section of population both in terms of horizontal and vertical growth:

- Various bodies such as DAE (Department of Atomic Energy), the Union Health Ministry and states should work in coherence to uplift the growth of nuclear medicine.

- Public-private partnership (PPP) mode can be explored as one of solutions to tide over the crisis particularly in Government sectors.
- To encourage private sectors for taking initiatives to establish more NM centers to inch towards the required number to benefit population at large.
- Price capping for all diagnostic and therapeutic procedures can be made mandatory as per AYUSHMAN or CGHS prices.
- Encourage inclusion of all diagnostic and therapeutic procedures of NM in most of the health insurance schemes being offered.

Conclusion

Indigenous initiatives taken both at government and non-government levels are likely to overcome the logistic problems including availability and access of theranostic radionuclides and hence, help enhancing the current pool of nuclear medicine facilities in the country.

PET/CT with [¹⁸F]PSMA for Prostate Cancer Patients: Initial Experience in Ukraine

Y. Kmetyuk¹, I. Burina¹, A. Ashykhmin², O. Solodyannikova²

¹ Clinical Hospital "Feofaniya", Ukraine

² National Cancer Institute, Ukraine

Background

Prostate cancer is one of the leading causes of cancer-related mortality in Ukraine. According to the National Cancer Registry of Ukraine, over 10,000 new cases of prostate cancer are registered annually. Prior to the implementation of [¹⁸F]PSMA-1007, patients were imaged using conventional methods such as computed tomography (CT), magnetic resonance imaging (MRI), and bone scintigraphy. We began producing [¹⁸F]PSMA-1007 in our production department in March 2023 and started imaging patients using this method since then.

Methodology

The standard dose of [¹⁸F]PSMA-1007 was 3.5 MBq/kg. We used a Siemens Biograph64 PET/CT scanner. The imaging protocol included the administration of the radiopharmaceutical followed by scanning at 120 minutes post-injection. The scans were interpreted by two independent specialists, and the results were compared with previous staging methods. We also assessed the risk stratification of patients prior to scanning.

Results

A total of 150 patients were imaged. Pre-scan risk stratification included Gleason score and PSA level. The images of these patients were compared with the results of conventional staging methods. In 45% of cases, the disease stage was altered following [¹⁸F]PSMA-1007 imaging. The main limitations were cases with false-positive uptake, particularly in inflammatory processes.

Conclusion

The introduction of [¹⁸F]PSMA-1007 in our center has significantly improved patient management, allowing for more accurate disease staging and adjustment of therapeutic approaches.

Radiation Protection for personnel in PET/CT imaging: Strategies to lower occupational exposure

E. Rotich

Kenyatta University Teaching Referral and Research Hospital, Kenya

Background

The use of hybrid imaging, especially PET/CT requires a multidisciplinary team that is involved in every step of the process. Given the energy (511keV) of the fluorine-18, it is hard to use the conventional lead gowns for effective shielding. This creates a unique case when it comes to radiation protection. There is also monitoring of extremities which may receive high levels of radiation since the inverse square law cannot apply here because of the proximity. Therefore, proper shielding is required for protection and working for a shorter time will significantly reduce the dose received by the worker. This is only possible with experience as the newer members of staff take longer to master the workflow but after some time even their doses are much lower.

Area classification, that is controlled and uncontrolled areas, must be properly demarcated to ensure that process flow and patient flow is seamlessly executed. Shielding during design is also crucial for radiation protection since it is the main factor that will determine optimization.

Staff Exposure is mainly from handling of syringes, vials, waste, or patients injected with radiopharmaceuticals (preparing the patient on the couch). These are the main radiation protection concerns. Another concern is contamination which needs to be checked after getting out of the PET preparation lab.

Methodology

Data will be collected by checking the usage of protective equipment that is provided for radiation protection. Optimization of protection will also be checked to see how the use of distance, time and shielding will help to lower the occupational doses. Work and process flow will also be used to see how it can help to lower occupational dose when the process is seamless. Digital dosimeters will be used to assess the dose received by the occupational worker and survey meters will be used to check the radiation levels in the room.

Results

Occupational workers at a nuclear medicine facility benefit by using tools such as syringe shields, lead blocks, Tabletop shield used during dispensing, shielded syringe carrier, lead pots holding the vial, lead lined waste containers, dose calibrator shields among others. Using semi-automated dispenser will lower the dose significantly than when dispensing manually. The technologist gets a higher dose when injecting patients than when they use automatic injectors.

Conclusion

Occupational workers using PET/CT imaging modality are exposed to higher doses compared to other diagnostic modalities. It is therefore very important that protective measures are put in place to ensure that their doses are kept as low as reasonably achievable. The protective equipment for radiation

protection should also be working well and it should be used well to ensure maximum protection of the worker. The Kenya Nuclear Regulatory Authority has set the limits of exposure to workers and our hospital ensures that the workers are continually monitored so that no workers exceed their limits.

Assessing the clinical utility of Gallium68 Citrate PET/CT imaging in the identification of active from inactive disease and in the evaluation of therapy response in Spinal Tuberculosis

J. Hephzibah

Christian Medical College Vellore, India

Proposed Objectives

The objective of this study was to evaluate Gallium 68 Citrate PET/CT imaging in Spinal Tuberculosis (TB). The study had three specific aims. Firstly, to see if Gallium 68 Citrate PET/CT imaging could discriminate between active and inactive disease. Secondly, to evaluate Gallium 68 Citrate PET/CT imaging for assessing treatment response. The third aim was to assess the clinical utility of Gallium 68 Citrate PET/CT in comparison to other imaging studies used in the routine management of spinal TB.

Methodology

Thirty-five patients known with TB spine were included. All patients had a baseline Gallium 68 Citrate PET/CT. Fifteen patients had a follow-up Gallium 68 Citrate PET/CT after 9-12 months of anti-tubercular therapy (ATT).

Results

On baseline study 25 patients had avid spinal lesions with corresponding CT features of infective spondylodiscitis. Ten had non-avid spine lesions but, the corresponding CT images showed infective spondylodiscitis. Among the 10 patients with non-avid spine lesions four had avid extraosseous lesions, two had avid lung nodules and mediastinal nodes and two had foci of muscle uptake (iliacus and psoas). Fifteen patients had a follow-up Gallium 68 Citrate PET/CT after 9-12 months of ATT. These included six patients who had no abnormal uptake on baseline, they also did not have any abnormal uptake on the follow-up study. Of the seven patients who had avid spine lesions on the baseline study all had a good clinical response rate, with six patients having no abnormal uptake and one showing less uptake on follow-up imaging. Two patients with avid lung and muscle lesions on baseline showed resolution of uptake on follow-up imaging.

Conclusion

Only 71.4% (25/35) showed avidity of the tracer in the spinal disease at baseline in the presence of definite clinical, microbiological and radiological (X-ray/ CT/ MRI) features of infective spondylodiscitis. Hence Gallium 68 Citrate PET/CT may not fare as a good diagnostic tool with relatively lower sensitivity in detecting active TB.

The possible reasons for absence of uptake in the remaining 28.5% cases (10/35 patients) included the presence of significant lysis and erosions of the vertebral bodies on CT. In addition, on correlation with MRI spine, all these patients had abscesses (either intra-osseous/ epidural/ soft tissue/ paravertebral) leading to decrease in cellular content and bacterial localization.

On follow up, absence of uptake in those with baseline avid lesions correlated well with the good clinical improvement at the end of ATT treatment. This also had a good correlation with presence of sclerosis or bone fusion on X-ray and CT, decrease in abscesses, edema, discitis and hyper-intensity on

T1W weighted images. Hence Gallium 68 Citrate PET/CT may be a robust marker of therapeutic response and can be used as a guide for clinicians in deciding the cessation or continuation of ATT in dubious cases.

Normal organ dosimetry resulting from [¹⁷⁷Lu]PSMA therapy in patients with metastatic castration-resistant prostate cancer (mCRPC)

B. Khiewvan¹, O. Pattanawong², K. Chuamsaamarkkee^{2,3}, P. Charoenphun^{2,3}, T. Thongpraparn¹, N. Poon-iad¹

¹ Division of Nuclear Medicine, Department of Radiology, Faculty of Medicine Siriraj Hospital, Mahidol University, Bangkok, Thailand

² Master of Science Program in Medical Physics, Faculty of Medicine Ramathibodi Hospital, Mahidol University, Bangkok, Thailand

³ Division of Nuclear Medicine, Department of Diagnostic and Therapeutic Radiology, Faculty of Medicine Ramathibodi Hospital, Mahidol University, Bangkok, Thailand

Background

Lu-177 prostate-specific membrane antigen (PSMA) therapy is a novel treatment for patients with metastatic castration-resistant prostate cancer (mCRPC) who experience tumour progression after surgery, RT, ADT, and CMT. Post-treatment dosimetry is performed to evaluate the absorbed dose in normal organs, aiming to avoid possible toxicity. The objective of this study is to assess dosimetry in normal organs among prostate cancer patients who have undergone [¹⁷⁷Lu]PSMA treatment.

Methodology

The dosimetry for salivary glands, liver, kidneys, red marrow, and the whole body was evaluated from post-treatment whole-body planar scans at three times (1 hour, 1 day, and 7 days) after the administration of [¹⁷⁷Lu]PSMA treatment. The dosimetry was performed using the Medical Internal Radiation Dosimetry (MIRD) schema from OLINDA/EXM v.2.2 in Hermes dosimetry software. The dosimetry results were reported for mean, standard deviation (SD), median, and range.

Results

The retrospective study was conducted on prostate cancer patients treated with [¹⁷⁷Lu]PSMA between July 2019 and January 2023 at the Division of Nuclear Medicine, Department of Radiology, Faculty of Medicine, Siriraj Hospital, Bangkok, Thailand. The study included 32 patients with a total of 59 PSMA cycles. Among them, 13 patients received [¹⁷⁷Lu]PSMA treatment for 1 cycle, 13 for 2 cycles, 4 for 3 cycles, and 2 for 4 cycles. The patients' ages ranged from 47 to 84 years old, with a median age of 68 years and a mean age of 68.63 years, with a standard deviation (SD) of 8.59 years. The injected activities ranged between 5.00 and 7.24 GBq. The median dose administered was 5.79 GBq, with a mean and SD of 5.78 ± 0.32 GBq. The absorbed doses in normal organs were as follows: Red marrow: 0.006-0.141 mGy/MBq (mean \pm SD = 0.030 ± 0.027 mGy/MBq), Total body: 0.013-0.176 mGy/MBq (mean \pm SD = 0.039 ± 0.032 mGy/MBq), Liver: 0.018-2.62 mGy/MBq (mean \pm SD = 0.128 ± 0.336 mGy/MBq), Salivary glands: 0.082-2.96 mGy/MBq (mean \pm SD = 0.644 ± 0.435 mGy/MBq), Kidneys: 0.236-1.86 mGy/MBq (mean \pm SD = 0.775 ± 0.33 mGy/MBq).

Conclusion

The absorbed dose to normal organs from Lu-177 PSMA treatment was within the accepted range and did not exceed tolerated limits.

Advancing Colorectal Cancer Diagnosis through Hybrid Imaging and Drug-Designed Radiolabeled Peptides Targeting UNC5 Receptors

T. Dallegi

National Center for Nuclear Sciences and Technologies, Tunisia

Background

For over thirty years, nuclear imaging has become an indispensable technique in modern medicine, radiating across various medical specialties such as cardiology, neurology, and hepatogastroenterology. One of the most interesting applications of nuclear imaging is scintigraphy using radiopharmaceuticals that bind to specific targets for early cancer diagnosis. In this context, UNC5A, UNC5B, UNC5C, and UNC5D dependence receptors are part of the UNC5 dependence receptor family, transmembrane proteins that all bind to the same ligand, Netrin 1. These receptors have been implicated in several cellular processes such as migration, survival, and cellular differentiation. They have garnered particular interest as it has been suggested that they play a role in controlling colorectal tumourigenesis.

Methodology

The aim is to design radiotracers targeting UNC5 receptors to provide accurate diagnosis or specific and effective treatment against colorectal cancer by targeting tumour cells while minimizing side effects on healthy cells. This work is summarized here in three sections: The first section briefly summarizes the context and generalities associated with cancer, dependence receptors, and nuclear imaging. The second section presents the bioinformatics tools used, specifying the objectives to be achieved as well as molecular docking techniques and modelling. The third section presents the results of docking of the various variants of the UNC5 receptor, molecular modelling, and the study of ligand-receptor complexes. In recent years, studies have highlighted the involvement of certain molecules in the development and progression of colorectal cancer. Among these, Netrin 1 and its UNC5 receptors have garnered increasing interest due to their potential role in this disease. Our objective is to identify *in silico* peptides that can selectively bind to UNC5 receptors and label them with technetium-99m, Ga-68 and Cu to develop a new diagnostic approach consisting of designing new radiopharmaceuticals targeting UNC5 receptors, which have a role in detecting the presence and activity of this receptor in colorectal cancer tissues. This report describes an innovative diagnostic approach against colorectal cancer using the design of radiolabeled peptides specific to UNC5 receptors. Our *in silico* study includes modelling, validation, docking, and the design of peptides specific to UNC5 receptors. Furthermore, we performed energy minimization of both the ligand and receptors, contributing to protein stabilization by bringing them to their minimum energy state. Secondly, molecular docking of the proteins revealed the region of Netrin 1 that interacts with UNC5A, UNC5B, UNC5C, and UNC5D receptors. Finally, we successfully designed the selected peptides with DOTA and different radionuclides. Using these radiolabeled peptides, we performed a second molecular docking to assess their affinity and binding potential with the target receptors.

Results

Through this additional selection step, we identified the best peptide, which demonstrated the strongest affinity and the best binding capacity to the receptors. our aims to open new perspectives in the field of

colorectal cancer diagnosis by exploiting the specific properties of radiolabeled peptides targeting UNC5 receptors.

Conclusion

The results obtained through these different stages provide a solid foundation for future studies aiming to optimize diagnostic and therapeutic approaches in the fight against colorectal cancer.

The Current Scenario of Nuclear Medicine Education and Human Resource in India - A Bird's Eye View

M. Bhardwaj, S. Deswal, A. K. Shukla

Department of Nuclear Medicine, Dr. Ram Manohar Lohia Institute of Medical Sciences, India

Background

The expansion of NM in India is getting impetus for diagnostic and therapeutic facilities. Today 24 of 28 States (85.7%) and 4 of 8 Union Territories (50%) in India have NM facility. Developing countries like India have 1 PET/ 0-2.5 SPECT system per million people. Contrary, developed countries have more than 3 PET and 10 SPECT systems per million people. India has 0.1-0.5 NM physicians as compared to 10 NM physicians in developed countries per million of population. Not more than 40 centers are added per year (as per 5 years average) except for year 2022-23 in which about 80 facilities were added. Currently there are 520 AERB approved operational NM facilities including 18 university-based NM institutions, 24 medical cyclotrons and 150 high dose therapy facilities in India. Asian continent has about 828 NM centers contributing to 58 % of total 1427 NM institutions existing worldwide. In other areas, Asia's contribution is 62.5% (NM physicians), 40.6 % (medical physicists), 59.1% (technologists). Non-clinical NM courses across India include B.Sc., M.Sc., DMRIT, PG Diploma, Ph.D. programs. The first MD program in NM started in 1990 and now more than 70 NM PGs (MD/DNB) are produced every year in India out of 65,335 MD seats available for all specialties.

Methodology

This cross-sectional study attracted 63 responses from 11-17 February 2024 through a structured questionnaire comprising of 19 questions developed using Google forms which was circulated among non-clinical NM stakeholders electronically. A qualitative data was collected on curriculum, training, academic and professional growth, infrastructure, decision to pursue career in NM, interest in further research, and job security. We determined decision-making factors and gathered opinions if current course curriculum is beneficial to in-training NM stakeholders to work in healthcare industry. A comprehensive analysis of data was undertaken using Microsoft Excel and IBM SPSS software.

Results

Respondents comprised 64.5% (40) males and 36.5% (23) females with predominant age group of 24-30 years. 79% (49) of respondents showed interest in going for higher studies and 90.5% (57) expressed their desire to qualify RSO certification. 41.3% (26) reported existing NM course curriculum, infrastructure, and clinical practice to be excellent. However, 50.8 % (30) respondents suggested for uniform course contents, infrastructure, and standardisation of regulations for entry and higher NM studies across India. Respondents also indicated that NM courses were opted by choice hinting that there is a growing interest amongst aspirants for speciality of NM. Many respondents expressed their willingness to take up the job of medical physicist in healthcare industry as well.

Conclusion

The comprehensive coverage of NM pan India can only be ensured by bridging vertical and horizontal gap. Also, increasing number of NM facilities and human resources/million of population will help to bridge existing gap between available and required facilities (i.e. supply and demand). International and

national bodies should take the lead to remove disparity in nomenclature of courses offered in NM globally. Uniformities in terms of course contents/duration, training programmes and infrastructure must be monitored and ensured by professional and regulatory bodies of respective countries and their alignment with global standards.

Enhancing Ovarian Cancer Diagnosis with AI-Generated Pseudo-CT Images from PET Data

A. H. Farshchitabrizi^{1,2}, M. H. Sadeghi³, S. Sina^{1,3}, F. Giammarile⁴

¹ Radiation Research Center, Shiraz University, Iran

² Namazi Hospital, Shiraz University of Medical Sciences, Iran

³ School of Mechanical Engineering, Shiraz University, Iran

⁴ Nuclear Medicine and Diagnostic Imaging Section, Division of Human Health, International Atomic Energy Agency, Austria

Background

In the realm of oncological imaging, the synthesis of Pseudo-CT images from PET scans represents a groundbreaking advancement. This innovation stems from the necessity to perform attenuation correction in PET imaging, a process traditionally dependent on the integration with CT scans, which inadvertently escalates the patient's exposure to ionizing radiation. The application of artificial intelligence (AI), particularly deep learning techniques, promises a novel solution to this issue by enabling the generation of pseudo-CT images directly from PET data, thereby circumventing the need for additional CT imaging.

Methodology

Leveraging the capabilities of advanced AI architectures, this study employed Generative Adversarial Networks (GANs)—specifically Conditional GAN, Wasserstein GAN, and Cycle GAN—to generate pseudo-CT images from uncorrected PET scans. The research utilized a dataset of 55 PET/CT scans from patients with ovarian cancer, segmenting the data into 45 scans for training the models and 10 for test. The models were meticulously optimized to accurately replicate the anatomical information typically provided by CT scans, thus enabling the effective attenuation correction of PET images based on the generated pseudo-CT images. The optimization process focused on adjusting learning rates, input batch sizes, and the generator-to-discriminator ratio, aiming to maximize the fidelity of the pseudo-CT images.

Results

The Cycle GAN architecture emerged as the most effective in producing pseudo-CT images that closely mimic the anatomical detail and density distribution of real CT scans. Statistical analyses, including Mean Absolute Error (MAE) and Mean Squared Error (MSE), validated the accuracy of the pseudo-CT images, suggesting a viable pathway to achieving PET attenuation correction without the inherent risks of additional radiation exposure. For CT reconstruction, the errors for the entire patient cohort were calculated as 4.17 ± 0.96 and 5.66 ± 1.01 , indicating an error margin of about 2%. However, challenges remain in achieving the level of detail and contrast resolution necessary for clinical evaluation, highlighting areas for further improvement in AI model development.

Conclusion

The generation of pseudo-CT images from PET scans using AI technology marks a pivotal step forward in oncological imaging. This approach not only mitigates the radiation risk associated with traditional attenuation correction methods but also holds the potential to streamline and enhance the diagnostic

process for cancer patients. As AI models continue to evolve, the feasibility of integrating pseudo-CT generation into clinical workflows becomes increasingly promising, potentially revolutionizing cancer diagnosis by offering a safer, more efficient alternative to conventional imaging techniques. Future endeavours should focus on refining these models to improve image quality and validate their clinical applicability, paving the way for a new era in non-invasive cancer diagnosis.

A comparative study on different GAN architecture in generating Attenuation-Corrected PET Images

A. H. Farshchitabrizi^{1,2}, M. H. Sadeghi³, S. Sina^{1,3}, F. Giammarile⁴, M. Karimipourfard³

¹ Radiation Research Center, Shiraz University, Iran

² Namazi Hospital, Shiraz University of Medical Sciences, Iran

³ School of Mechanical Engineering, Shiraz University, Iran

⁴ Nuclear Medicine and Diagnostic Imaging Section, Division of Human Health, International Atomic Energy Agency, Austria

Background

The utility of Positron Emission Tomography (PET) in diagnosing and managing malignancies is unparalleled, especially given its ability to provide metabolic insights at the cellular level. However, the accuracy of PET imaging is hindered by attenuation artifacts, a phenomenon where the signal is reduced due to the absorption of photons by the body's tissues. Traditionally, this challenge is addressed through attenuation correction methods that often require the use of additional anatomical imaging techniques, such as CT scans, raising concerns over increased radiation exposure for patients. The advent of artificial intelligence (AI) offers a novel pathway to overcoming these limitations, presenting an opportunity to generate attenuation-corrected PET images without the need for concurrent anatomical imaging.

Methodology

This study explores the potential of deep learning, specifically Convolutional Neural Networks (CNNs) and Generative Adversarial Networks (GANs), to perform attenuation correction on PET images. The approach involved training various GAN architectures, including Conditional GAN, Wasserstein GAN, and Cycle GAN, using a dataset of 55 PET/CT scans from patients diagnosed with ovarian cancer. The objective was to refine these models to accurately generate attenuation-corrected PET images from uncorrected scans, thus bypassing the need for CT-based correction. The networks were trained using a split of 45 scans for training and 10 for test, optimizing for learning rates, batch sizes, and the balance between generator and discriminator functions to achieve high fidelity in image reconstruction.

Results

Among the tested architectures, Cycle GAN demonstrated the highest efficacy in generating attenuation-corrected PET images, with an error margin of 1%, indicating high accuracy and precision. Statistical evaluation, including Mean Absolute Error (MAE) and Mean Squared Error (MSE), confirmed the reliability of the generated images compared to their CT-corrected counterparts. This was statistically substantiated by a MAE and MSE of 2.15 ± 0.34 and 3.14 ± 0.56 , respectively. This breakthrough underscores the potential of AI in enhancing PET imaging's diagnostic capabilities while mitigating the associated risks of radiation exposure from additional CT scans.

Conclusion

The successful generation of attenuation-corrected PET images through AI represents a significant advancement in medical imaging. By eliminating the need for CT scans for attenuation correction, this approach not only reduces radiation exposure but also streamlines the diagnostic process for

malignancies, particularly ovarian cancer. Future research should focus on further refining AI models for broader applications and exploring the integration of this technology into clinical practice, potentially transforming the landscape of cancer diagnosis and treatment.

Clinical Management and Therapeutic Challenges in a Case of Erdheim-Chester Disease through PET/CT scan: Rare Study Case and Literature Review

M. S. Ahmad

Department of Nuclear medicine, Al-Ahli Hospital, Palestine

Background

Erdheim-Chester disease (ECD) is a rare form of non-Langerhans histiocytosis characterized by the infiltration of tissues by foamy histiocytes and lipid-laden macrophages. This article presents a rare study case of ECD and provides a comprehensive literature review on the clinical management and therapeutic challenges associated with the disease.

Case Summary

A 54-year-old was diagnosed with a disease. After her PET exam, she was prescribed Vemurafenib for five sessions. A second PET scan showed that the patient and treatment were incompatible. A decision was made. The patient will receive five Cladribine treatments. The treatment caused electrolyte imbalances, abdominal pain, mild left ventricle relaxation during diastole with a small amount of fluid around the heart, a mass in the right atrium indicating potential cardiac involvement, kidney soft tissue thickening, and femur and tibia bone marrow hardening.

Results

Vemurafenib had a progressive response rate of 39.16% after 5 cycles, but Cladribine showed a partial response rate of 2.5% after 1 cycle. However, after 5 cycles, Cladribine demonstrated a better therapeutic response rate of 25.8%. The treatment responses showed significant differences between Vemurafenib and 1 cycle Cladribine, and Vemurafenib and 5 cycles Cladribine with p-values 0.023 and 0.011, respectively. These studies demonstrate the effectiveness of Vemurafenib and Cladribine in treating ECD at different anatomical locations.

Conclusion

While Vemurafenib remains an important therapeutic option in select cases of ECD, Cladribine appears to offer a more comprehensive and reliable treatment approach, particularly in patients with refractory or progressive disease.

Incidentally detected malignant tumours on F-18 PSMA-1007 PET/CT beyond prostate cancer: (Our center experience)

S. Moustafa

Assiut University, Egypt

Abstract

18F-PSMA PET/CT plays an important role in the assessment of prostate cancer patients. However, PSMA is a misnomer, and it is expressed in non-prostatic malignancies.

Extrapolating this principle, the present study aimed to describe 18 F-PSMA avidity in different malignancies that incidentally have co-existed in patients with prostate cancer who underwent 18 F-PSMA PET/CT in our patient population. Our study explored PSMA-avid intra-hepatic cholangiocarcinoma which is noticed before the patient was symptomatic. The point here is the early diagnosis and potential therapeutic purpose of PSMA avidity especially in one of aggressive cancers with subsequent early accurate patient management and better outcome.

Background

Prostate-specific membrane antigen (PSMA) is a type II transmembrane glycoprotein highly overexpressed on prostate cancer epithelial cells; for that, PSMA has potential diagnostic imaging and therapeutic purposes for prostate cancer in a variety of clinical scenarios.

PSMA is also expressed, to varying degrees, in different kinds of solid cancers and lymphoproliferative disorders.

Moreover this overexpression, subsequently helps the possibility of PSMA theranostic applications outside prostate cancer, especially in the case of limited lines of treatment in some cancers.

Cholangiocarcinoma is the second most common primary hepatic malignant tumour; it is an aggressive tumour with a 5-year survival rate of less than 5 %. In our study, we reported PSMA-avid different types of cancers, one case of intra-hepatic cholangiocarcinoma that was detected early on 18 F-PSMA PET/CT conducted as a part of follow-up for prostate cancer and confirmed by biopsy.

Methodology

Enrolment of 120 18-F PSMA PET/CT study for patients with prostate cancer, any incidental neoplastic PSMA non-prostatic uptakes on PSMA PET/CT were included in our study then followed up until the final diagnosis was reached.

Results

We detected five different solid cancers that expressed PSMA activity, including one patient each with pancreatic cancer, rectal cancer, bladder cancer, hepatocellular carcinoma, and intra-hepatic cholangiocarcinoma.

Recently, its avidity to hepatocellular carcinoma (HCC) has also been reported and to a lesser extent, 68Ga-PSMA accumulation in cholangiocarcinoma with skeletal metastasis has been reported. We identified PSMA-avid intra-hepatic cholangiocarcinoma earlier with no definite symptoms or signs that seemed to be related to cholangiocarcinoma in a patient with treated prostate cancer and undetectable PSA level; who underwent PSMA PET/CT follow-up; yet unfortunately only intense PSMA-avid hepatic uptake is identified on the scan with no clear underlying CT changes noticed; further imaging

correlation didn't conclude definite diagnosis. On follow-up 3 months later; the patient started to complain of right hypochondrial pain; PSMA PET/CT was done that showed persistent intense PSMA-avid hepatic focal lesion with hypodense CT changes; for that biopsy was taken that confirmed intra-hepatic cholangiocarcinoma (Fig.1).

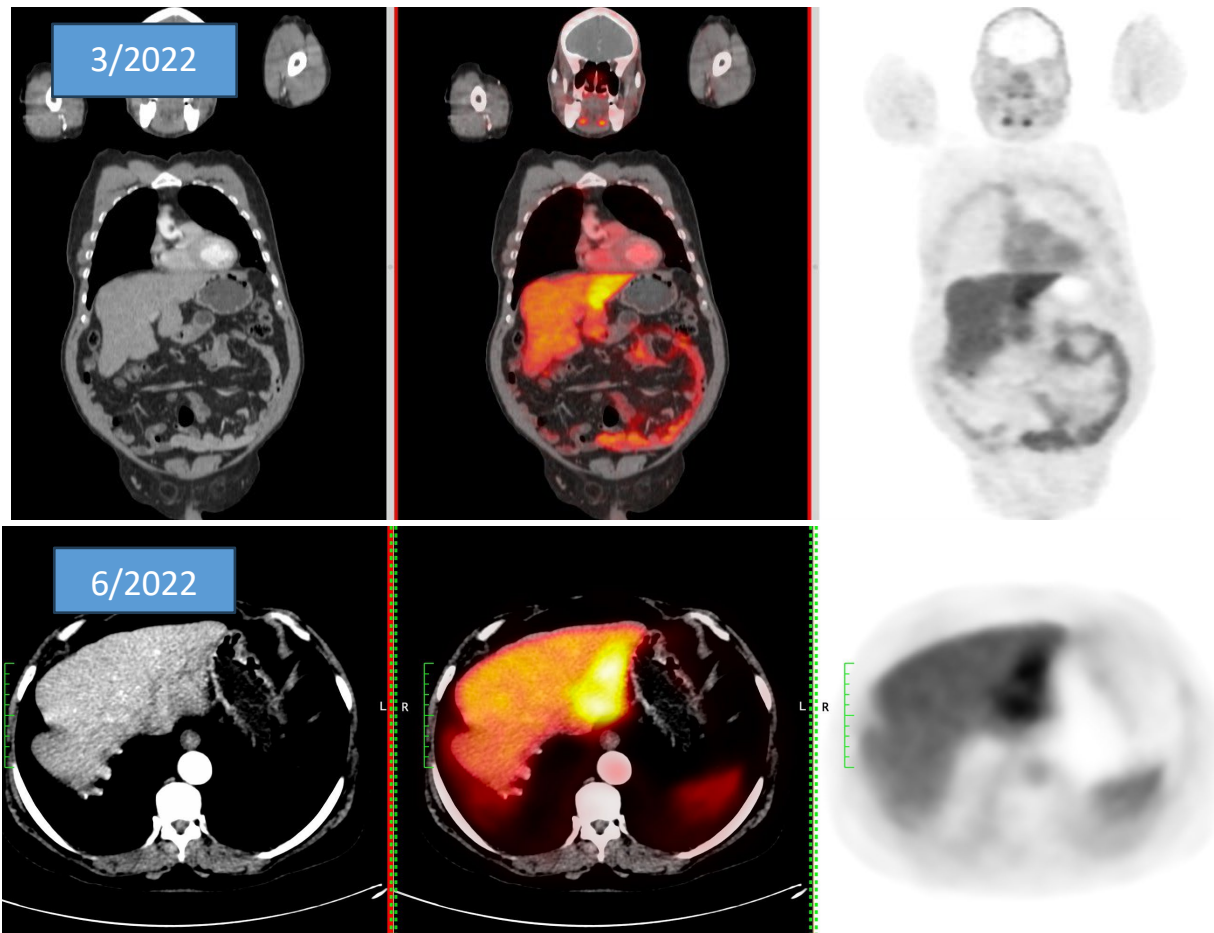


Figure 1.

Conclusion

It is important to be aware of neoplastic PSMA uptake beyond prostatic malignancies to optimize image interpretation and accurate implementation of patient management with potential widening of therapeutic aims especially in aggressive cancers with limited available lines of treatment.

Harmonization of [¹⁸F]FDG brain PET/CT images using only a cylindrical phantom**A. C. Fischer da Silveira Fischer, L. da Silva de Souza, J. Bueno Salazar, F. Ramos de Oliveira, C. M. Moriguchi Jeckel, A. M. Marques da Silva**¹ Pontifical Catholic University of Rio Grande do Sul (PUCRS), Brazil² Hospital de Clínicas de Porto Alegre (HCPA), Brazil³ University of São Paulo, Faculty of Medicine, Clinical Hospital FMUSP (HCFMUSP), Brazil**Background**

Harmonizing [¹⁸F]FDG brain PET/CT quantification aims to reduce variations across equipment, reconstruction algorithms, and protocols, ensuring consistent and reliable results. It is crucial for establishing PET as a robust biomarker for clinical decision-making and research since cross-population and center comparisons contribute to better understanding and treating neurodegenerative diseases. Harmonization strategies for quantitative PET have been validated clinically for various tumours. However, harmonizing PET/CT for neurodegenerative diseases still represents a challenge because some strategies require expensive phantoms and complex analysis. This study aims to evaluate whether a simple method using only a cylindrical phantom, originally developed for oncologic PET, can be applied to PET brain harmonization.

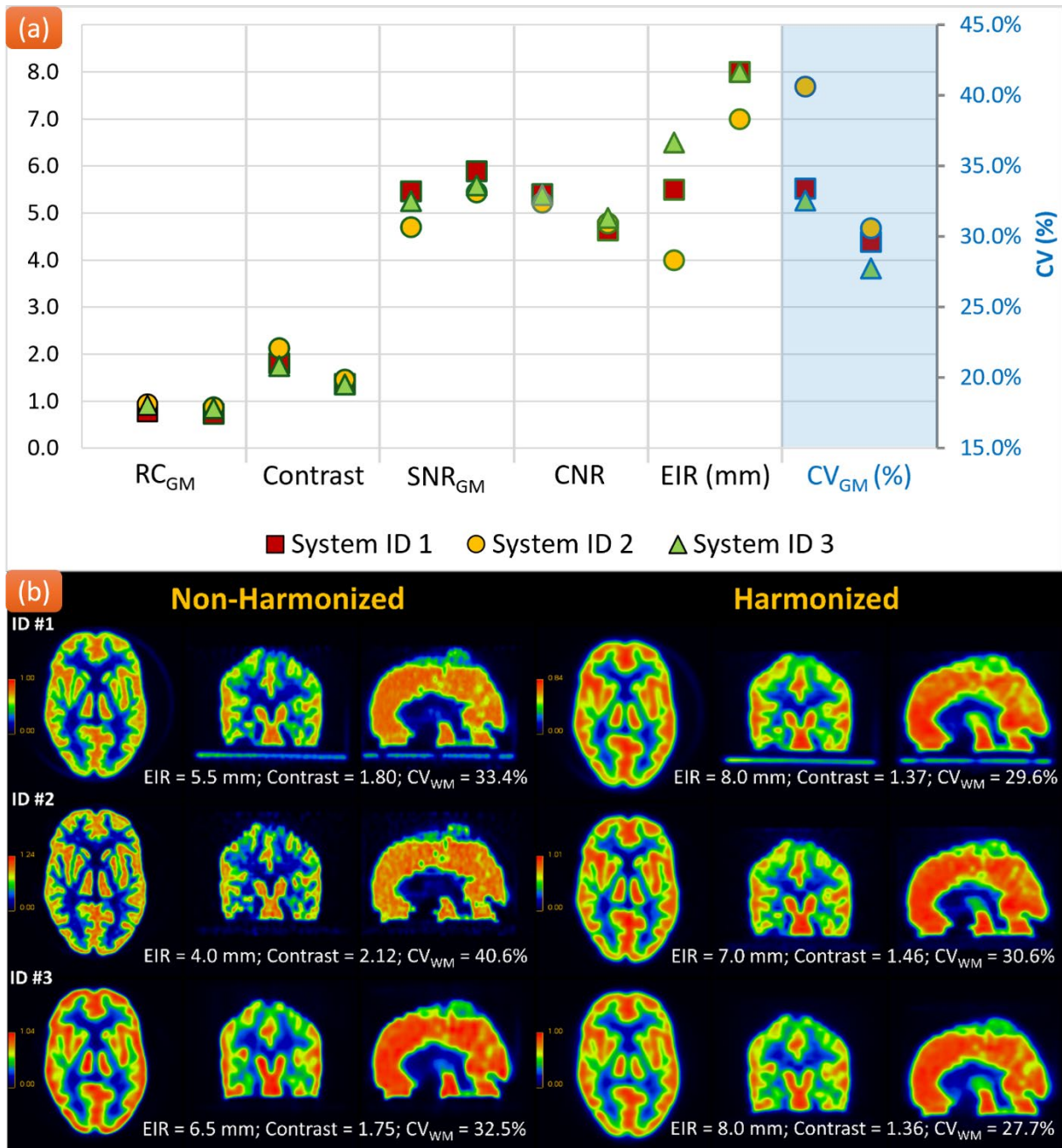
Methodology

We evaluated the strategy published by Namías et al. (2018), which uses resolution and noise measurements from a cylindrical phantom to simulate NEMA IQ phantom spheres and determine the optimal smoothing filters that best harmonize the PET scanner performance according to the EARL accreditation program. PET/CT scans of a cylindrical phantom containing ~70MBq of [¹⁸F]FDG were acquired for 20min/bed in three PET/CT systems (System ID #1: Discovery 600; #2: Discovery 710; #3: Discovery IQ; GE Healthcare, USA). The raw data were reconstructed using each site's clinical protocol (CP) without post-filtering. The PET Harmonization Toolbox was used to find the post-filtering that complied with EARL fluorine-18 standards 1. To evaluate the strategy performance in the neurological context, a Hoffman 3D brain phantom filled with an [¹⁸F]FDG solution of ~33kBq/mL, was scanned for 30min in the three PET/CT systems and the raw data was reconstructed using each site CP and the filtering identified by the toolbox. Image quality (IQ) metrics were extracted from the Hoffman PET images, before and after harmonization: gray matter (GM) recovery coefficient (RC), GM RC; contrast between the GM and white matter (WM); signal and contrast to noise ratio (SNR and CNR); coefficient of variation in the WM (CV_{wm}), to evaluate image uniformity; and effective spatial image resolution (EIR). The Maximum Differences (MD) between the CP and the harmonized values were calculated.

Results

The optimal post-filters were 7.5mm, 5.9mm, and 5.4mm for systems ID #1, #2 and #3, respectively. The strategy was succeeded on reduce the variability between different PET/CT systems in terms of EIR (MD of 2.5mm to 1mm after harmonization) and CV_{wm} (MD of 8.10% to 2.84%), without significant loss of contrast, SNR and CNR (values shown on Figure 1 (a)). The harmonized images were also more uniform and noiseless (lower CV_{wm}), apparent on Figure 1 (b)). Moreover, the obtained EIR are near the recommended for harmonization in the literature – 8mm (Shekari et al., 2013; Joshi A, Koeppe RA & Fessler JA, 2009).

Figure 1. (a) Image quality metrics and (b) Visual comparison of phantom PET images before (left) and after (right) harmonization.



In (a) the symbols on the left of each image quality metric represents the values obtained from images reconstructed with the clinical protocol of each site and, in the right, from harmonized images.

Conclusion

We concluded that the strategy published by Namías et al. (2018) can be employed in the harmonization of [^{18}F]FDG brain PET/CT images. The method only needs a cylindrical phantom scan, making harmonization workflow more accessible, especially in small departments.

Acknowledgment

This study was financed in part by the Coordenação de Aperfeiçoamento de Pessoal de Nível Superior – Brasil (CAPES) – Finance Code 001.

Prognostic potential of SPECT/CT MIBI parameters in the staging of osteosarcomas

F. L. Ramírez^{1,2}, M. C. H. Hernández^{1,2}, I. Acero³, D. Arguelles⁴, D. H. Oliver⁴

¹ Hospital Angeles Universidad, Mexico

² Instituto Nacional de Rehabilitación “Luis Guillermo Ibarra Ibarra”, Mexico

³ IMSS-Bienestar, Mexico

⁴ Instituto Nacional de Cancerología Mexico, Mexico

Background

Osteosarcomas are rare and aggressive neoplasms that most frequently originate in long bones. They often occur in the second and third decade of life with another peak in frequency in older adults. Its origin is multifactorial, from mechanobiological signals, genetic mutations to a favourable microenvironment. In recent decades, overall survival and event-free survival rates have not improved, which is why in the era of personalized medicine the development of better predictive models is necessary. In nuclear medicine, [18F]FDG PET/CT parameters have been used to assess its role as a predictive model. In 2023, Pedersen et al. highlighted the prognostic value of Metabolic Tumour Volume (MTV) as a good prognostic marker.

Aim

Determine the prognostic value of SPECT/CT MIBI parameters to evaluate the molecular activity of osteosarcoma at the time of diagnosis.

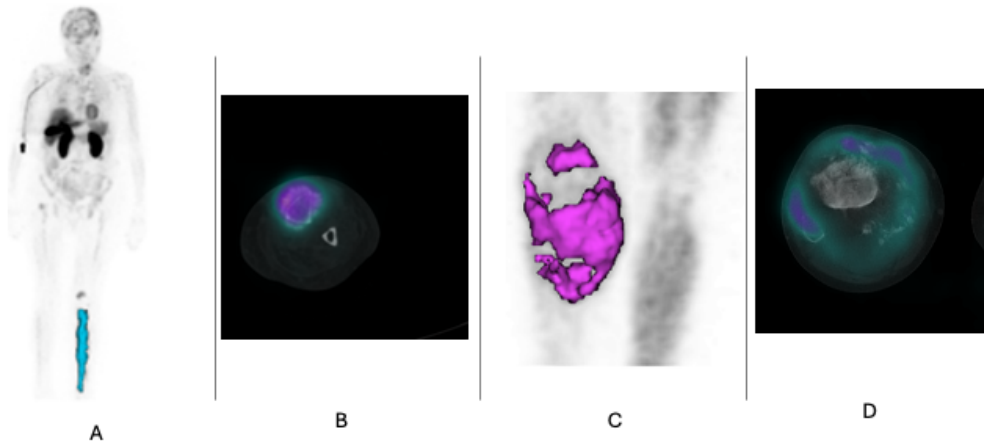
Methodology

This was a retrospective study in which a total of 22 patients were evaluated from January 2022 to October 2023 who underwent SPECT/CT MIBI for staging by histopathological diagnosis of osteosarcoma. The SPECT/CT MIBI parameters of the primary tumour were subsequently evaluated using the MM Oncology license from Syngo Siemens (image 1). The distribution of the data was evaluated using the Shapiro-Wilk normality test, based on a significance level of $p < 0.05$, the distribution of the data was identified as non-parametric, the relationship between the quantitative variables was examined using the Spearman correlation coefficient.

Results

Of a total of 22 patients, 11 (50%) were men and 11 (50%) were women. The average age of 30.14 years (30 years 2 months) with a median of 20.5 years (20 years 6 months), in an age range of 8 to 75 years. Presence of metastasis was observed in 12/22 patients (54.5%). High-grade tumours were identified in half of the patients analysed (11/22) and low-grade tumours in the other half. In the correlation between Tumour Volume MIBI (TVMIBI) and Total Activity, a correlation coefficient $R=0.636$ and significance (bilateral) $P<0.0001$ was found. In the correlation between Max and Peak, $R=0.989$ and $P < 0.0001$ were found.

Image 1



A and B, 75-year-old female patient diagnosed with osteosarcoma. C and D, 16-year-old female patient with a diagnosis of chondroblastic osteosarcoma.

Conclusion

There is a moderate positive correlation between TVMIBI and Total Activity, indicating that higher TVMIBI is associated with higher levels of tumour activity. A very strong, positive correlation between Max and Peak per size of 1 cm³, suggesting that regions of maximum MIBI uptake tend to also have the highest activity values when normalized by size. We can identify that they are useful as a biomarker in staging to predict high tumour activity and could suggest an unfavourable prognosis. It is necessary to follow up on this study to be able to evaluate the usefulness of these parameters in the prediction of response to treatment, overall survival, and event-free survival in the future.

Correlation of mammography and ultrasound in detecting breast lesions

F. Ahmed

Breast Imaging Radiology, Ethiopia

Background

Breast cancer, the most prevalent malignancy among women, has become a leading cause of death. Early detection through screening has significantly improved outcomes, yet there remains a lack of comparative data between mammography and ultrasonography in breast cancer detection.

Objective

The study was aimed to assess comparative analysis of mammography and ultrasound among women who underwent breast mammography and ultrasonography at Tikur Anbessa Specialized Hospital, Addis Ababa University.

Methodology

Institutional based retrospective cross-sectional study was conducted. The sample size for the study was 173 patient records who underwent breast mammography and ultrasonography. A structured data extraction sheet from Picture Archive Communication System was used. The collected data was coded and entered into EpiData Entry version 3.1 and exported to SPSS Statistics version 24.00 for analysis. Descriptive analyses were done by computing proportions and summary statistics. The information was presented by using table and figures.

Results

This study reveals that sonography correlates better with pathology diagnoses for breast lesions compared to mammography, especially for malignant cases. Sonography demonstrates higher sensitivity in detecting malignancies, particularly in dense breasts and younger age groups, while mammography shows greater specificity. These findings align with international studies and suggest the complementary roles of sonography and mammography in breast cancer detection.

Conclusion

Ultrasound is more sensitive (84.85%) than mammography in detecting breast pathology, while mammography is more specific (92.31%) in identifying specific breast lesions. More studies are needed to improve breast screening, focusing on early initiation and increasing awareness. Encouraging residents to conduct research on breast pathology and integrating breast imaging into specialized rotations can enhance proficiency. Establishing women-friendly clinics offering comprehensive screenings for breast, cervical, and ovarian cancers would improve accessibility and patient care.

Synthesis and Potential Application of a Novel ⁶⁴⁺⁶⁷Cu-Labeled Pyrazolone Complex in Cancer Theranostics

H. A. Shamsel-Din¹, M. A. Gizawy¹, M. M. Abdou²

¹ Labeled Compounds Department, Hot Labs Center, Egyptian Atomic Energy Authority, Egypt

² Egyptian Petroleum Research Institute, Egypt

Background

Cancer theranostics, which combines diagnostic and therapeutic techniques, holds great promise for personalized medicine. The utilization of copper radioisotopes, namely positron-emitting copper-64 (⁶⁴Cu, with a half-life of 12.7 hours) and beta particle-emitting copper-67 (⁶⁷Cu, with a half-life of 61.8 hours), is pivotal. This allows for both low-dose imaging before therapy and higher-dose treatment in the same patient, facilitating accurate dosimetric calculations and therapy quantification. Dual labeling with Cu-64 and Cu-67 enables both positron emission tomography (PET) imaging and targeted radiation therapy. Pyrazolone derivatives have demonstrated significant anticancer activity in vitro and in vivo through various mechanisms such as apoptosis induction, autophagy regulation, and cell cycle disruption. This study presents a newly synthesized pyrazolone complex labeled with copper isotopes (Cu-64 and Cu-67) as a potential candidate for cancer theranostics.

Methodology

Greener and environmentally benign methodology for pyrazolone derivative using maltose as biodegradable catalyst under solvent-free. The synthesis of the pyrazolone complex involved multi-step organic synthesis techniques, including coordination of the ligand with copper ions and subsequent radiolabeling with Cu-64 and Cu-67 isotopes. The labeling parameters such as pyrazolone ligand amount, pH of the medium and reaction time were optimized. Characterization techniques such as nuclear magnetic resonance (NMR) spectroscopy, mass spectrometry, and elemental analysis were employed to confirm the structure and purity of the complex.

Results

3H-pyrazol-3-one derivative was synthesized in excellent yield about 97.5 %. The newly synthesized pyrazolone complex exhibited high purity and stability, as evidenced by spectroscopic and analytical data. Radiolabeling with Cu-64 and Cu-67 isotopes was achieved with high efficiency and specific activity. High radiochemical yield of $95.10 \pm 0.41\%$ and in-vitro stability in serum up to 12h have been obtained. In vitro studies demonstrated selective binding of the complex to cancer cells with high target to non-target ratio (T/NT) equals 6.24 ± 0.09 in tumour bearing mice at 30 min post injection, indicating its potential for tumour targeted imaging and therapy.

Discussion

The successful synthesis and radiolabeling of the pyrazolone complex highlight its potential as a versatile agent for cancer theranostics. The dual labeling with Cu-64 and Cu-67 isotopes enables both diagnostic imaging using positron emission tomography (PET) and therapeutic applications through targeted radiation therapy. Further preclinical studies are warranted to evaluate the efficacy and safety of this novel complex in cancer models.

Conclusion

In summary, the synthesis of a novel $^{64+67}\text{Cu}$ -labeled pyrazolone complex represents a significant advancement in the development of multifunctional agents for cancer theranostics. This study lays the foundation for further research aimed at harnessing the potential of this complex for personalized cancer management.

Deep Learning: A Supportive Tool for Bone Scintigraphy Analysis

P. Kanchanapiboon, A. Teyateeti

Division of Nuclear Medicine, Department of Radiology, Faculty of Medicine Siriraj Hospital, Mahidol University, Thailand

Background

Bone scintigraphy plays a crucial role in detecting conditions like osteoblastic metastases, which are common in prostate cancer. With recent advancements, deep learning (DL) has been increasingly applied to support diagnostic processes, especially in binary classification to distinguish between 'positive' and 'negative' cases. DL excels at identifying critical differences in medical images, given it has been trained on a sufficient volume of expert-annotated data. Despite challenges posed by limited data availability, our research demonstrates that DL can achieve dependable diagnostic results through the use of three specific techniques: data augmentation, dropout, and label smoothing.

Methodology

This study analysed 302 whole-body images using the ResNet-50 and ResNet-101 models to train and test the Artificial Intelligence (AI) algorithms. Data augmentation techniques were primarily applied to significantly increase the diversity of training images. Alternatively, dropout and label smoothing were implemented to reduce the models' reliance on specific features and ensure more balanced confidence in predictions, respectively. Additionally, Gradient-weighted Class Activation Mapping (GradCam) was used to visually highlight critical regions in the images, enhancing clinical trust in AI-driven diagnostics. The models were trained using the MMClassification toolbox, an open-source image classification toolbox based on PyTorch.

Results

Starting with baseline accuracies of 83.5% for ResNet-50 and 84.1% for ResNet-101, we applied data augmentation techniques, resulting in increased accuracy: ResNet-50 to 85.7% and ResNet-101 to 95.1%. This enhancement particularly demonstrates ResNet-101's superior ability to leverage augmented data. The introduction of dropout led to better generalization and increased ResNet-50's accuracy to 89.0%, highlighting the importance of a varied focus in models to achieve consistent diagnostic accuracy across clinical settings. The unchanged performance of ResNet-101 suggests its inherent resistance to overfitting. Further, combining data augmentation with label smoothing slightly adjusted ResNet-50's accuracy to 89.6% and reduced ResNet-101's to 94.5%, indicating a complexity threshold beyond which additional modifications no longer improve results. The study also revealed that using all three regularization techniques together did not enhance classification performance further, suggesting an optimal complexity level for these techniques. The synergy between GradCam and the model's prediction confidence emphasizes its utility and the critical role of these methodologies as supporting in disease detection.

Conclusion

This study underscores deep learning's critical role in enhancing bone scintigraphy analysis for detecting conditions like osteoblastic metastases. Through the careful application of data augmentation, dropout, and label smoothing, we achieved notable improvements in the diagnostic accuracy of the ResNet-50

and ResNet-101 models. Particularly, the ResNet-50 model demonstrated significant enhancements, while the more complex ResNet-101 model peaked in performance with data augmentation alone. Furthermore, the integration of GradCam has made the AI decision-making process transparent to clinicians, boosting trust. This study not only improves AI's reliability in detecting bone diseases with limited data but also advances its broader use in diagnostics, potentially enhancing patient care.

A Machine Learning Approach based on Rest Myocardial Perfusion Image Radiomics to Detect the Presence of Hibernating Myocardium: A Proof-of-Concept Study

B. Khangembam, C. Patel, J. Jaleel, A. Roy, P. Gupta

Department of Nuclear Medicine, All India Institute of Medical Sciences, India

Aim

To assess the feasibility of a machine learning (ML) approach using radiomics features of perfusion defects on rest myocardial perfusion imaging (MPI) to detect the presence of hibernating myocardium.

Methodology

Data of patients who underwent ^{99m}Tc -sestamibi MPI and ^{18}F -FDG cardiac PET/CT for myocardial viability assessment were retrieved. Rest MPI data were processed on ECToolbox and polar maps were saved using NFile PMap tool. The reference standard for defining hibernating myocardium was the presence of mismatched perfusion-metabolism defect with impaired myocardial contractility at rest. Perfusion defects on the polar maps were delineated with regions of interest (ROIs) after spatial resampling and intensity discretization. Replicable random sampling allocated 80% (257) of the perfusion defects of the patients from January 2017 to September 2022 to the training set and the remaining 20% (64) to the validation set. An independent dataset of perfusion defects from 29 consecutive patients from October 2022 to January 2023 was used as the testing set for model evaluation. 110 first and second-order texture features were extracted for each ROI. After feature normalization and imputation, 14 best-ranked features were selected using a multistep feature selection process including Logistic Regression and Fast Correlation Based Correlation Filter. 13 supervised ML algorithms were trained with stratified 5-fold cross-validation on the training set and validated on the validation set. The ML algorithms with a Log Loss of <0.688 and <0.672 in the cross-validation and validation steps were evaluated on the testing set. Performance matrices of the algorithms assessed included area under the curve (AUC), classification accuracy (CA), F1 score, precision, recall, and specificity. To provide transparency and interpretability, SHAP (SHapley Additive exPlanations) values were assessed and depicted as beeswarm plots.

Results

239 patients (214 males; mean age 56 ± 11 years) were enrolled in the study. There were 371 perfusion defects (321 in the training and validation sets; 50 in the testing set). Based on the reference standard, 168 perfusion defects had hibernating myocardium (139 in the training and validation sets; 29 in the testing set). On cross-validation, six ML algorithms with Log Loss <0.688 had AUC >0.800 . On validation, 10 ML algorithms had a Log Loss value <0.672 , among which six had AUC >0.800 . On model evaluation of the selected models on the unseen testing set, nine ML models had AUC >0.800 with Gradient Boosting Random Forest (xgboost) [GB RF (xgboost)] achieving the highest AUC of 0.860 and could detect the presence of hibernating myocardium in 21/29 (72.4%) perfusion defects with a precision of 87.5% (21/24), specificity 85.7% (18/21), CA 78.0% (39/50) and F1 Score 0.792. Four models depicted a clear pattern of model interpretability based on the beeswarm SHAP plots. These were GB RF (xgboost), GB (scikit-learn), GB (xgboost), and Random Forest.

Conclusion

Machine learning using radiomics features of perfusion defects on rest myocardial perfusion images can detect the presence of hibernating myocardium.

Radiosynthesis of $^{64+67}\text{Cu}$ -oxadiazole dianiline derivative as a promising agent for simultaneous tumour PET imaging and radiotherapy

M. A. Gizawy¹, M. S. Ayoup², A. S. Kodous^{3,4}, M.A. Motaleb¹

¹Labeled compound Department, Hot Laboratories Center, Egyptian Atomic Energy Authority, P.O. Box 13759, Cairo, Egypt

²Chemistry Department, Faculty of Science, Alexandria University, P.O. Box 426, Ibrahimia, Alexandria, Egypt

³Radiation Biology Department, National Center for Radiation Research and Technology (NCRRT), Egyptian Atomic Energy Authority (EAEA), P.O. Box 13759, Cairo, Egypt

⁴Department of Molecular Oncology, Cancer Institute (WIA), Adyar, Chennai, Tamil Nadu 600038, India

Background

Triple-negative breast cancer (TNBC), which accounts for 15–20% of all breast cancers, is a therapeutic challenge because of the absence of druggable targets including the estrogen receptor, progesterone receptor, and HER2. However, TNBC tumours often overexpress the human epidermal growth factor receptor (EGFR), which helps predict anti-EGFR targeted therapy. EGFR expression in breast cancer is linked to aggressiveness, proliferation, and genomic instability. 1,2,4-oxadiazoles have been reported to have intriguing antibacterial, anti-inflammatory, anti-rhinoviral, and anticancer properties. Many commercially available medications with the 1,2,4-oxadiazole ring were introduced to the market. This study aimed to provide an easy method for the synthesis of the $^{64+67}\text{Cu}$ -oxadiazole dianiline complex ($^{64+67}\text{Cu}$ -ODDA).

Methodology

The synthesis of 2,2'-(1,2,4-oxadiazole-3,5-diyl) dianiline was performed and characterized by different spectral data. Then, the newly synthesized oxadiazole dianiline derivative was radiolabeled with ^{64}Cu and ^{67}Cu theranostic pair. Thereafter, in-vitro bioevaluation of the $^{64+67}\text{Cu}$ -oxadiazole dianiline complex against the breast cancer cell line (MCF-7) was done. Docking computations were performed using the Auto Dock 4.2 module toward the angiogenesis receptor protein, EGFR. In-vivo biodistribution on normal and solid tumour-bearing rats was carried out. The PET/CT scans were performed using a preclinical NanoPET/CT scanner.

Results

A novel oxadiazole dianiline derivative was successfully prepared in a good yield. The derivative was labeled efficiently with ^{64}Cu and ^{67}Cu theranostic pair and the results showed that the radiochemical purity of the $^{64+67}\text{Cu}$ -oxadiazole dianiline complex was 97% at 30 μg ODDA and pH 4, and its stability was up to 24 h. The stability of the complex in human plasma was found to be high. Biodistribution studies revealed that the uptake of $^{64+67}\text{Cu}$ -oxadiazole dianiline in the tumour-bearing mice was $7.8 \pm 0.4\%$ ID/organ in the solid tumour at 0.5 h which increased with time till reached the maximum value of 18 ± 0.3 ID/organ% at 2 h. Rapid and efficient tumour targeting, together with fast renal excretion, highlights the tumour-targeting potential of the radiotracer. Furthermore, PET imaging provided sufficient visualization of tumours in rats. Our findings suggest that $^{64+67}\text{Cu}$ -oxadiazole dianiline can be useful for the theranostic application of breast carcinomas.

Conclusion

This study introduces a new $^{64+67}\text{Cu}$ -oxadiazole dianiline which can pave theranostics approach in personalized targeted radiotherapy to compensate different cancer types, particularly these types which exhibit overexpression of EGFR. Additionally, this radioconjugate may be useful probe for the PET/CT evaluation of triple negative breast cancer.

Role of Metabolic PET/ CT Parameters in Correlation to Various Clinico-Pathologic Features of NSLC Moustafa, H. 1 Fadl, N.2, Elantably, I.2 , Elahmadawy, M.2

H. M. Moustafa¹, M. Elahmadawy², I. Elantably², N. Fadl²

¹ Nuclear Medicine, Kasr El-Aini School of Medicine, Cairo University, Egypt

² National Cancer Institute, Cairo University, Egypt

Background

Predicting prognosis of NSLC included not only some traditional histologic features such, but also some potential pathological indicators as degree of desmoplasia, tumour necrosis%, tumour budding, tumour nuclear grade, cytological differentiation, tumour infiltrating lymphocytes% and risk stratification pathological scoring. Metabolic PET/ CT avidity is studied to elucidate its relation to tumour invasiveness, aggressiveness and in determining prognosis of cancer patients. The aim of this study was to examine the predictive value of metabolic PET\CT parameters in correlation to various clinico-pathologic features in non-small cell lung cancer (NSCLC) patient and to elucidate its relation to the extent of tumour aggressiveness.

Methodology

This is a prospective study that carried on fifty one of enrolled patients histologically proven as NSCLC lung cancer were evaluated by initial PET\CT scan for primary lung tumour , lymph nodes and distant metastases status and its correlation to potential pathologic indicators.

Results

Our findings are quite concordant with other studies regarding the significant association between the maximal SUV of lung tumour and primary tumour subtypes with statistically significant difference ((P=0.023). Regarding MTV and TLG, which positively and significantly correlate with primary tumour diameter with (P=0.003) and (P=0.003) respectively. Also, our findings regarding correlation of the cytological differentiation score and SUV mean proved significant correlation with P=0.023. There is possible utility of the peak SUV and mean SUV of lung tumour as a surrogate marker for tumour aggressiveness. Also the radiological consolidation to tumour ratio proved to positively and significantly correlates with tumour subtype, tumour nuclear grade score, tumour necrosis % score and risk stratifying pathological score (P = 0.006), (P = 0.001), (P = 0.020) and (P = 0.009) respectively. Also, there was significant correlation was found with 1 years PFS and the tumour budding with P=0.043.

Conclusion

In this study, multivariate analysis disclosed that consolidation/ tumour ratio had significant correlation as the only independent parameter with impact on PFS.

PET/CT NEMA body phantom image reconstruction study using small voxel size for improved lesion detection

K. Senica, L. Lezaic, S. Rep

Department for Nuclear Medicine, University Medical Centre Ljubljana, Slovenia

Background

Positron emission tomography combined with computed tomography (PET/CT) is an integral part of patient management in oncology and provides both metabolic and anatomic information. In majority of PET/CT scanners image reconstruction is traditionally performed using the $4 \times 4 \times 4 \text{ mm}^3$ voxel size, resulting in relatively low spatial resolution which consequently introduces the partial-volume effect (PVE) that negatively affects images both visually and quantitatively. The goal of our study was to explore the effect of different voxel size ($2 \times 2 \times 2 \text{ mm}^3$ vs. $4 \times 4 \times 4 \text{ mm}^3$ voxel size) on the image quality systematically at a set of different low-to-high target to background ratios to simulate the conditions of routine clinical application, where the accumulation of [^{18}F]fluorodeoxyglucose (^{18}F]FDG) in patient whole body imaging is differently intense.

Methodology

We used the NEMA body phantom with six fillable spheres of different diameters. The spheres and background were filled with a solution of [^{18}F]FDG, in ratio spheres vs background 2:1, 3:1, 4:1 and 8:1. In all images reconstructed with $2 \times 2 \times 2 \text{ mm}^3$ and $4 \times 4 \times 4 \text{ mm}^3$ voxel size the contrast recovery coefficient (CRC), contrast to noise ratio (CNR) in standardized uptake value (SUV) were evaluated. We analysed CRC, CNR and SUV values independently in three ways: for spheres with diameters ≤ 13 mm, for spheres with diameters ≥ 17 mm, and for all spheres together, respectively.

Results

For phantom spheres ≤ 13 mm, we found significantly higher CRC, SUV and CNR using small-voxel reconstructions. CRC and SUV did not differ for large spheres (≥ 17 mm) using $2 \times 2 \times 2 \text{ mm}^3$ and $4 \times 4 \times 4 \text{ mm}^3$ voxel size size. On the other hand, CNR for large spheres (≥ 17 mm) was significantly lower in $2 \times 2 \times 2 \text{ mm}^3$ compared to the $4 \times 4 \times 4 \text{ mm}^3$ voxel size images. The results are graphically presented in Figure 1.

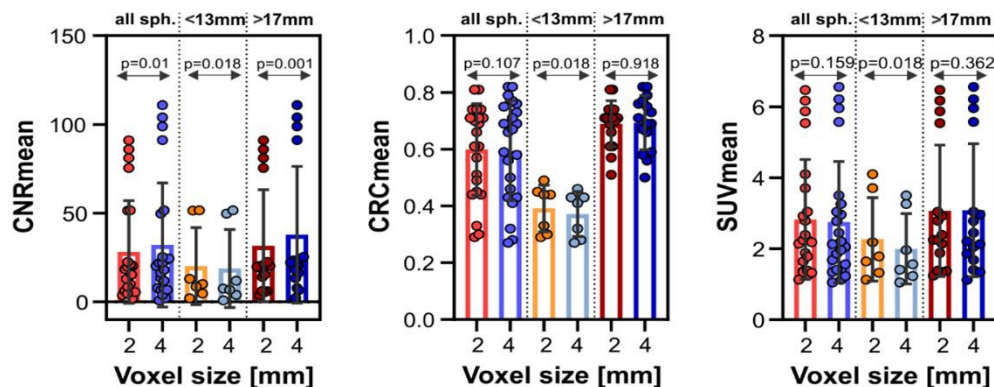


Figure 1. Graphically presented CRC_{mean} , CNR_{mean} and SUV_{mean} between the $2 \times 2 \times 2 \text{ mm}^3$ and $4 \times 4 \times 4 \text{ mm}^3$ voxel size.

Conclusion

Our results confirmed the previously published findings and further proved that the use of small ($2 \times 2 \times 2 \text{ mm}^3$) voxel size improves localization of smaller volumes with various radioactivity concentrations in PET which can be beneficial in diagnostic assessment of small lesions improving precise lesion localization and contrast.

Detection rate of bone metastasis on whole body bone scan of prostate cancer patients with rising serum prostate-specific antigen following radical prostatectomy

A. Teyateeti¹, C. Poenateetai¹, A. Teyateeti², P. Kanchanapiboon¹, P. Pusuwan¹

¹ Division of Nuclear Medicine, Department of Radiology, Faculty of Medicine Siriraj Hospital, Mahidol University

² Division of Radiation Oncology, Department of Radiology, Faculty of Medicine Siriraj Hospital, Mahidol University

Background

Positron emission tomography/computed tomography (PET/CT) with prostate cancer-specific tracers is currently the recommended imaging for prostate cancer patients with rising serum prostate-specific antigen (PSA) following radical prostatectomy (RP). However, whole body bone scan (BS) might be an optimal imaging for detection of bone metastasis in particular patients. Objective of this study is to determine the detection rate of bone metastasis on BS and the predictive factors for BS positivity. Ultimate goal is to identify where BS remains applicable.

Methodology

This is a retrospective study performed in 200 prostate patients with rising serum PSA after RP who underwent BS between January 2018 and April 2022. The data collected were pre-operative clinical parameters, pathological findings, treatments, serial PSA levels including a PSA level that prompted clinician to request a BS (trigger PSA), follow-up data, and radiographic results. BS were reviewed by consensus of 3 nuclear medicine physicians and results were classified as positive or negative studies in conjunction with supporting evidence, i.e., follow-up imaging, clinical data or treatments. Data analysis was performed using descriptive statistics. Analysis of predictive factors associated with bone scan positivity was conducted using logistic regression model and reported as odds ratio (OR) and 95% confidence interval (95% CI).

Results

The median trigger PSA level was 0.3 ng/ml (0.009-157) with PSA level < 0.5 ng/ml in 136 patients (68%). Majority of patients were at the first episode of PSA rising (71%) and did not receive androgen-deprivation therapy at time of BS (79%). Of the total 200 patients, only 15 patients (7.5%) had positive BS. Remarkably, all positive BS showed metastatic lesions ≤ 5 lesions. Patients with positive BS had significantly higher trigger PSA levels compared to those with negative BS (1.68 vs 0.29 ng/mL; $p < 0.0001$). Analysis of PSA kinetics revealed that short PSA doubling times (PSADT) and high PSA velocities were significantly associated with positive BS (4.42 vs 12.21 months; $p = 0.001$ and 0.12 vs 0.01 ng/mL/month; $p < 0.0001$, respectively). Logistic regression model showed that Gleason scores (8-10 vs 6-7; OR 3.139, 95% CI 1.031-9.557, $P = 0.044$), trigger PSA (> 1 vs ≤ 1 ng/mL; OR 9.173, 95% CI 3.014-27.921, $P < 0.0001$), and PSADT (< 6 vs ≥ 6 months; OR 9.714, 95% CI 1.618-58.311, $P = 0.013$) were associated with BS positivity.

Conclusion

Detection rate of bone metastasis on BS of post-RP prostate cancer patients with median serum PSA level of 0.3 mg/ml is only 7.5%. However, probability of positive BS is much higher in patients with

Gleason score 8-10, PSADT < 6 months and trigger PSA > 1 ng/mL. BS is probably applicable for detection of bone metastasis among these patients.

Possible predictive factors for positive bone scan

Factors	OR (95%CI)	P
GS: 6-7 vs 8-10	3.139 (1.031-9.557)	0.044
PSA nadir after RP: < 0.1 vs ≥ 0.1 ng/mL	2.569 (0.884-7.468)	0.083
Trigger PSA at 1 st bone scan: ≤ 1.0 vs > 1.0 ng/mL	9.173 (3.014-27.921)	< 0.0001
Time from RP to trigger PSA: < 48 vs ≥ 48 months	1.436 (0.5-4.123)	0.520
PSADT: ≥ 6 vs < 6 months	9.714 (1.618-58.311)	0.013
ADT at time of bone scan: no vs yes	2.0 (0.645-6.206)	0.230
Episode of PSA rising: 1 st vs 2 nd or more	1.705 (0.578-5.029)	0.334

GS = Gleason score, PSA = prostate-specific antigen, RP = radical prostatectomy, PSADT = PSA doubling times, ADT = androgen-deprivation therapy, OR = odd ratio

Super-Resolution of FDG PET/CT Images Based on Generative Adversarial Networks and Adversarial Optimization

H. K. Mahmoud

Engineering Department, Nuclear Research Center, Egyptian Atomic Energy Authority, Egypt

Background

Computed-Tomography (CT) scan shows some organs and tissues details inside the body, while Positron Emission Tomography (PET) scan shows some abnormal activity. Fusion of CT and PET scan (PET/CT) show more details and information, but it is limited resolution and for resolution enhancement it requires a relatively long scanning time and therefore leads to a high radiation dose. The objective of this work is obtaining super-resolution images from PET/CT scan with minimum scanning time to optimize the highest image quality with the minimum radiation dose.

Methodology

In this work, GANs (Generative Adversarial Networks) are utilized for image resolution increasing, allowing the generation of high-quality images from low-resolution inputs. GANs generate high-quality realistic images through training 2 neural networks simultaneously called generator and discriminator. The generator network takes a low-resolution image as input and generates the visually high-resolution image using the sampling layers that increase the image resolution. The discriminator network distinguishes between the output images from the generator and the ground truth images. These images used for improving the visual quality of images, enhancing details of PET/CT images after that Adversarial optimization technique is used to optimize image enhancement process by simultaneously training a generator to improve image quality and a discriminator to distinguish between enhanced and original images.

Results

18F-Fluorodeoxyglucose (18-F-FDG) PET/CT scans dataset was collected with different scanning time (24, 18, 12, 6 minutes) divided into four groups: full duration scan, quarter, half and three quarters duration scan. the image quality merits were calculated for the different scanning time (that affected the radiation dose) to trade off between the image quality and the radiation dose. The results are evaluated quantitatively using four merits: PSNR (Peak-Signal-to-Noise-Ratio), MAPE (Mean-Absolute-Percentage-Error), SSIM (Structural-Similarity), and CRC (Contrast-Recovery-Coefficient) as shown in the table.

Scanning time	Normal images				Super Resolution images			
	PSNR	MAPE	SSIM	CRC	PSNR	MAPE	SSIM	CRC
Full Scan	50	0	1	1	50	0	1	1
Three Quarters	43.4	0.08	0.930	0.893	50	0	0.999	0.978
Half Scan	36.5	0.21	0.814	0.705	49.5	0.01	0.992	0.912
Quarter Scan	31.9	0.26	0.746	0.639	48.7	0.07	0.984	0.884

The results show; the image quality merits of the normal images are high affected with scanning time while the image quality of super resolution images is less affected and mostly the same information can be obtained using shorter scanning time.

Conclusion

GANs and adversarial optimization techniques are powerful tools for image resolution increasing, as they can learn to generate high-quality images. And hence super-resolution images could be obtained from FDG PET/CT scan with the shorter scanning time and minimum radiation dose.

Quantum Audit in a Highly Complex Nuclear Medicine Service: Experience at the National Cancer Institute Bogota Colombia March 2023

M. C. Martinez Becerra, L. S. Castillo, A. M. Londoño Tobon, B. E. Quiroz Revelo

National Cancer Institute, Colombia

Background

The International Atomic Energy Agency (IAEA) developed an audit program for quality management in the practice of Nuclear Medicine (QUANUM) aimed at the culture of analysis, review of systematic internal processes, patient safety, and radiological protection, among others. This paper shares the experience, challenges, and opportunities in the implementation of a comprehensive quality system for the nuclear medicine group of the National Cancer Institute (INC), based on the QUANUM audit visit carried out by international experts, allowing the evaluation and compliance with international standards aimed at efficiency, Quality, safety and reliability in the provision of clinical services in nuclear medicine.

Methodology

A self-evaluation of the quality standards of practice in nuclear medicine (diagnosis, therapy) and highly complex radiopharmacy of the National Cancer Institute was carried out based on the review and verification of the evaluation criteria provided by the QUANUM tool, based on this, work tables composed of medical physicists were carried out. Radiation protection officers, technologists, nuclear physicians, pharmaceutical chemists, and administrators; An update and construction of formats, documents, and instructions, as well as, a standardization of the standard operating procedures (SOPs) of the service were accomplished. Internal and external audits were executed with national experts in the evaluation of QUANUM requirements.

Results

In March 2023, the IAEA expert group was made up of two nuclear medicine doctors, a medical physicist, a nuclear medicine technician, and a radiopharmaceutical chemist was carried out in March 2023. They were in charge of evaluating compliance and adherence to the proposed requirements. As a result of the CUNUMUM evaluation visit, a compliance score of 98.5% was obtained for the year 2023, showing a growth of 15.3% compared to the result of the previous visit carried out in 2013 (83.2%), which showed an improvement in the processes raising the quality of the service offered to the patient.

Conclusion

In Colombia, some entities regulate the safe practice in the use of radiation sources and equipment, the authorization of health services, and good manufacturing practices. The implementation of a comprehensive system for quality management in nuclear medicine (QUANUM) allowed us to evaluate the regulatory criteria at the institutional level, complying with international standards focused mainly on guaranteeing and improving medical practice based on patient safety and optimization in radiological protection of the service. The results obtained position the INC as a national and international benchmark.

Keywords: Nuclear Medicine, QUANUM, Quality Management

Delaying Initial Radioiodine Therapy Does Affect Response in Intermediate Risk Differentiated Thyroid Cancer

S. S. Medina-Ornelas

Nuclear Medicine and Molecular Imaging Department, Hospital Angeles Lindavista, Mexico

Background

The optimal time of initiating radioactive iodine (RAI) therapy for differentiated thyroid cancer (DTC) patients is controversial. We investigate the relationship between the timing of initiating RAI and the clinical response based on dynamic stratification risk in intermediate-risk DTC patients in Mexican population.

Methodology

We evaluated 132 patients with intermediate-risk DTC who received a dose of RAI to 100-150 mCi and were retrospectively reviewed. The patients were divided into 2 groups agreeable initial therapy (between total thyroidectomy and initial RAI), called time interval therapy (TIT): Group A: TIT < 6 months (n=69), and Group B: TI ≥ 6 months (n=63). Six and twelve months after RAI and recently, we followed up these patients and evaluated the therapy response with neck ultrasound, whole-body scan and SPECT/CT and measures of thyroglobulin and antibodies antithyroglobulin. According to the therapy stratification system, the therapy responses to RAI were assessed as either as excellent response (ER), biochemical incomplete response (BIR), indeterminate response (IR) and structural incomplete response (SIR) at every follow-up. We conducted a univariate and multivariate analyses to determine different factors associated with difference responses. A $p < 0.05$ was considered to be statistically significant. Statistical analyses were conducted with software SPSS (version 22).

Results

Group A had significantly lower BIR rates (14.2 vs 38.2 and 4.7 vs 39.5, all $P < 0.05$, respectively) and higher ER rates (72.8 vs 34.1 and 86.2 vs 44.2, all $P < 0.05$, respectively) than group B during dynamic follow-ups. By univariate and multivariate analyses, prolonged TIT (HR: 5.66, 95%CI: 1.811-22.018, $P = 0.003$), histology aggressive (HR: 7.98, 95%CI: 3.022-21.567, $P = 0.002$), nodal extension (HR: 5.66, 95%CI: 1.199-14.257, $P = 0.005$) were manifested to be independent risk factors for IR, SIR and BIR. Doses of 150 mCi was statically significant in patients with more than two risk factors to higher rates of ER ($p = 0.0045$)

Conclusion

Early treatment with RAI is associated with greater biochemical response, and ER. Delayed initial RAI (≥6 months after thyroidectomy) is associated with poor response and poor outcome. Doses of 150 mCi had better response in patients with more than two risk factors.

Delaying Initial Radioiodine Therapy Does Affect Response in Intermediate Risk Differentiated Thyroid Cancer

S. S. Medina-Ornelas

Nuclear Medicine and Molecular Imaging Department, Hospital Angeles Lindavista, Mexico

Background

The optimal time of initiating radioactive iodine (RAI) therapy for differentiated thyroid cancer (DTC) patients is controversial. We investigate the relationship between the timing of initiating RAI and the clinical response based on dynamic stratification risk in intermediate-risk DTC patients in Mexican population.

Methodology

We evaluated 132 patients with intermediate-risk DTC who received a dose of RAI to 100-150 mCi and were retrospectively reviewed. The patients were divided into 2 groups agreeable initial therapy (between total thyroidectomy and initial RAI), called time interval therapy (TIT): Group A: TIT < 6 months (n=69), and Group B: TI ≥ 6 months (n=63). Six and twelve months after RAI and recently, we followed up these patients and evaluated the therapy response with neck ultrasound, whole-body scan and SPECT/CT and measures of thyroglobulin and antibodies anti-thyroglobulin. According to the therapy stratification system, the therapy responses to RAI were assessed as either as excellent response (ER), biochemical incomplete response (BIR), indeterminate response (IR) and structural incomplete response (SIR) at every follow-up. We conducted a univariate and multivariate analyses to determine different factors associated with difference responses. A $p < 0.05$ was considered to be statistically significant. Statistical analyses were conducted with software SPSS (version 22).

Results

Group A had significantly lower BIR rates (14.2 vs 38.2 and 4.7 vs 39.5, all $P < 0.05$, respectively) and higher ER rates (72.8 vs 34.1 and 86.2 vs 44.2, all $P < 0.05$, respectively) than group B during dynamic follow-ups. By univariate and multivariate analyses, prolonged TIT (HR: 5.66, 95%CI: 1.811-22.018, $P = 0.003$), histology aggressive (HR: 7.98, 95%CI: 3.022-21.567, $P = 0.002$), nodal extension (HR: 5.66, 95%CI: 1.199-14.257, $P = 0.005$) were manifested to be independent risk factors for IR, SIR and BIR. Doses of 150 mCi was statically significant in patients with more than two risk factors to higher rates of ER ($p = 0.0045$).

Conclusion

Early treatment with RAI is associated with greater biochemical response, and ER. Delayed initial RAI (≥6 months after thyroidectomy) is associated with poor response and poor outcome. Doses of 150 mCi had better response in patients with more than two risk factors.

[¹⁸F]PSMA PET/CT in the evaluation of prostate cancer patients with biochemical recurrence after radical therapy and correlation with clinicopathological features

S. S. Medina-Ornelas

Nuclear Medicine and Molecular Imaging Department, Hospital Angeles Lindavista, Mexico

Objective

Evaluate the diagnostic performance of [¹⁸F]PSMA PET/CT in the evaluation of prostate cancer (PCa) patients with biochemical recurrence (BCR) following radical prostatectomy (RP) or radiotherapy (RT) and valuation of clinicopathological features.

Methodology

A retrospective analysis was performed on 96 consecutively patients from November 2019 to February 2024, with BCR PCa. We included patients with PCa with initial Gleason Score (GS) ranging from 6 to 10, initially treated with either RP (50 patients) or RT (46 patients). Association between clinicopathologic characteristics (prostate-specific antigen, PSA, and Gleason Score, GS) and PET/CT indexes were analysed. Descriptive statistics was used to display patient data as median, mean, standard deviation range, or percentages, where applicable. Correlation among PET/CT indexes (SUV_{max} and MTV) and variables were evaluated with Spearman's rank correlation coefficient. Wilcoxon Mann-Whitney U test was used to test the subgroups (PSA > 10 ng/mL vs PSA ≤ 10 ng/mL; Gleason Score ≥ 8 vs Gleason Score < 8) PET indexes differences.

Results

[¹⁸F]PSMA PET/CT was positive in 75 patients (78%), indeterminate in 5 patients (5%), and negative in 16 patients (17%). Particular findings were the following: local uptake (prostate bed or prostate gland) was observed in 44 patients (45%); 18 of these patients also showed nodal disease and in 7 patients bone uptake co-existed. Only nodal uptake was observed in regional sites in 20 patients (21%), non-regional nodal in 10 patients (10%); and bone metastatic disease in 13 patients (13%). A multivariate analysis showed that for PSA values 0.2 – 2 ng/mL [¹⁸F]PSMA PET/CT was positive in 43 patients (44%); a univariate analysis showed for [¹⁸F]PSMA PET/CT was positive for PSA values less than 0.2 ng/mL in 9 patients; 0.2 – 1 ng/mL in 11 patients; 1.1 – 2 ng/mL in 23 patients; 2.1 - 4 ng/mL in 17 patients and 4.1 – 10 ng/mL in 14 patients. In addition, we found a significant relationship between SUV_{max} values and GS, patients with Gleason Score ≥ 8 had higher SUV_{max} levels at recurrence sites (p = 0,005). Patients with MTV higher levels had PSA > 10 ng/mL (p = 0.005)

Conclusion

We concluded that [¹⁸F]PSMA PET/CT is a highly sensitive and accurate tool in PCa patients with BCR even with low levels of PSA regardless of the initial radical treatment. With these findings we confirm the excellent potential of [¹⁸F]PSMA PET/CT granting earlier detection of BCR, improving patient care and better prognosis.

Influence of bone uptake in initial evaluation of prostate cancer patients with [¹⁸F]PSMA and its relationship with modified D'Amico risk classification

S. S. Medina-Ornelas

Nuclear Medicine and Molecular Imaging Department, Hospital Angeles Lindavista, Mexico

Background

One of the most common indications of [¹⁸F]PSMA PET/CT is in patients with biochemical recurrence following curative treatment for prostate cancer (PCa), whereas data with [¹⁸F]PSMA on outcomes of primary staging at the time of initial diagnosis is limited.

Aim

We investigate, the association between the serum prostate-specific antigen (PSA) levels and the findings on [¹⁸F]PSMA PET/CT for primary staging, regarding the proportion and site of prostate cancer metastases focus on bone uptake, and the association with modified D'Amico risk classification.

Methodology

81 patients with newly diagnosed PCa, in whom a PSMA PET/CT was performed for primary staging between November 2019 to February 2024, were retrospectively studied. Patients were divided into risk groups as low, intermediate, or high risk, according to a modification in the D'Amico classification system as ISUP grade 3 tumours were included in the high-risk group. [¹⁸F]PSMA PET/CT findings were compared among risk groups as well as PSA levels, clinical T stages, and ISUP grades. Additionally, the study aimed to investigate the proportion of PSMA-positive lesions in different anatomical locations (miN1, miM1a-c). A logistic regression analysis was performed to investigate the association between PSA levels and the findings on [¹⁸F]PSMA PET/CT. Finally, we analysed an SUV_{max} threshold to identify bone metastases using ROC curve analysis with a cut-off value of 10.

Results

81 patients were included with a median PSA of 16.5 ng/mL (5.4-218.3 ng/mL) and a median Gleason score was 8 (range: 6–10). Of these, 17 (21 %), 41 (51 %), and 30 (28 %) were in the low-, intermediate-, and high-risk groups, respectively. Of these, 61 (75 %) were found to have metastatic disease (miN1, and/or miM1a-c) on [¹⁸F]PSMA PET/CT. The proportion of patients with metastatic disease increased with rising PSA levels. In 47 (58 %) patients we found abnormal uptake in at least one bone. Of these, 16 (34%) patients are at low risk, 15 (32 %) patients are at intermediate risk, and 16 (34 %) in high risk. The frequency of bone uptake was not associated with PSA, Gleason score, or D'Amico risk classification (p=0.24). 21 (44 %) patients had definite prostate cancer bone metastases, whereby an SUV_{max} threshold of ≥ 10 . The PSA level was a significant predictor for the presence of nodal metastases on PSMA PET/CT (p<0.05).

Conclusion

Metastatic disease was found in 61 (75 %) of patients at primary staging. The initial PSA level and D'Amico classification were a significant predictor of the presence of metastases on [¹⁸F]PSMA PET/CT. These findings support the use of PSMA PET/CT in the initial staging of

PCa. The cut-off value of ≥ 10 had true bone metastases. The current results might have important implications for the counseling and treatment of patients with PCa.

Biodistribution of Single Vial Ethambutol Kit for Tuberculosis Infection: Preliminary Study

A. Aries¹, Karyadi¹, S. Aguswarini¹, E. Lestari¹, W. Lestari¹, A. Ariyanto¹, Widyastuti Widjaksana¹

¹ Research Center for Radioisotope, Radiopharmaceutical and Biodosimetry Technology, National Research and Innovation Agency, Indonesia

Background

Tuberculosis (TB), caused by *Mycobacterium tuberculosis*, is the world's infectious disease leading cause of death. Early detection of TB is very important due to the increased risk of transmitting TB to healthy person at late TB detection. We have developed single vial ethambutol kit preparation for TB detection after labelled with Technetium-99m (^{99m}Tc). The aim of this study is to carry out the biodistribution of ethambutol labelled technetium-99m in healthy mice. Single vial Ethambutol kit preparation was then labelled by using technetium-99m Pertechnetate solution. Radiochemical purity of [^{99m}Tc]Tc-Ethambutol was the determined by using thin layer chromatography. The biodistribution was performed at 1, 3 and 24 h time point (n=3) in healthy BALB/c male mice. The result shows that the highest uptake of [^{99m}Tc]Tc-Ethambutol was found in kidney followed by blood and bladder, which decreased with time. Thus, this biodistribution study provides an initial overview of the [^{99m}Tc]Tc-Ethambutol distribution in vivo that will be useful for further research such as [^{99m}Tc]Tc-Ethambutol biodistribution in TB infected mice.

Keywords: Tuberculosis, Technetium-99m, Ethambutol, Kit, Radiopharmaceutical

Machine Learning Performance Analysis on the Influence of BMI on PET/CT Dosimetry

M. K. A. Karim, H. Murat, L. Bashiru

Department of Physics, Universiti Putra Malaysia, Malaysia

Background

Accurate measurement of radiopharmaceutical doses, particularly F-18 fluorodeoxyglucose (FDG), is paramount for obtaining precise diagnostic insights in positron emission tomography and computed tomography (PET/CT) scans. Recognizing the Body Mass Index (BMI) as a significant determinant that influences FDG dosimetry—owing to its association with metabolic rates and the distribution of compounds throughout the body—this study embarks on elucidating the effect of BMI on FDG dosimetry in PET/CT imaging. To achieve this, we propose a novel approach by integrating machine learning techniques to conduct a comprehensive retrospective analysis of patient data. This methodological innovation aims to harness the predictive power of machine learning to offer a nuanced understanding of how BMI variations modulate FDG dose absorption and distribution, thereby enhancing the accuracy of PET/CT diagnostic procedures.

Methodology

In the study, a cohort of 1000 patients (484 males and 516 females) who had undergone PET/CT examinations at a cancer center in Klang Valley, Malaysia, during the period of 2022 to 2023, was included retrospectively. BMI measurements and corresponding FDG doses administered were documented for each patient. Statistical analyses, including correlation and regression models, considering potential confounding factors such as patient demographics and clinical characteristics, were conducted to evaluate the association between BMI and FDG dosimetry. Data on $^{18\text{F}}\text{FDG}$ activity and patient demographics (weight, height, gender, age, BMI) were recorded and analysed. Analysis of variance (ANOVA) was conducted to assess the statistical significance between groups, with a significance level set at $p < 0.05$. Several supervised learning algorithms (SVM, Random Forest and kNN) were utilized to construct 4 types of classification models with different input datasets which were named as Model 1, Model 2, and Model 3. The supervised classification performance was evaluated in terms of heatmap confusion matrix, recall (sensitivity), precision (PPV), F1-score, accuracy, receiver operating characteristic (ROC) and area under the curve (AUC).

Results and Discussion

Table 1 tabulate the demography of patients-based gender. BMI was classified into 4 types, Underweight (UW), Standard (SW), Overweight (OW) and Obese (OB). The total mean injected dose and effective dose value of $^{18\text{F}}\text{FDG}$ and CTDI_{vol} for PET/CT were 9.65 ± 1.43 MBq; 0.31 ± 0.09 mSv; and 9.20 ± 33.61 mGy respectively. The injected and effective doses for PET varied between 0.85 and 15.08 MBq and 0.01 and 0.39 mSv, respectively. The CTDI_{vol} values ranged from 1.36 to 16.92 mGy, with corresponding effective doses ranging from 0.01 to 32.41 mSv. The study found that the injected and effective doses of PET were significantly lower compared to those of CTDI_{vol} . The mean effective dose of CT exceeded the approximate effective radiation dose allowed for hybrid PET/CT examination of (22.7 mSv), highlighting the need to optimize PET/CT protocol doses to keep doses as low as reasonably achievable.

Table 1: Subject's demography

Parameters	Male	Female	All Patients
Number of Patients	484	516	1000
Weight (kg)	64.75 ± 16.20 (19.4-140)	60.02 ± 14.60 (19.9 - 112.4)	64.74 ± 16.16 (19.4 - 140)
Height (cm)	161.10 ± 9.22 (103-186)	155.36 ± 5.96 (126 - 173)	161.05 ± 9.921 (103 - 186)
BMI (kgm ⁻²)	24.88 ± 5.20 (12.48 - 47.32)	24.81 ± 5.73 (12.53 - 41.42)	24.84 ± 5.48 (12.48 - 47.32)

Values are presented as mean ± SD

BMI - Body Mass Index

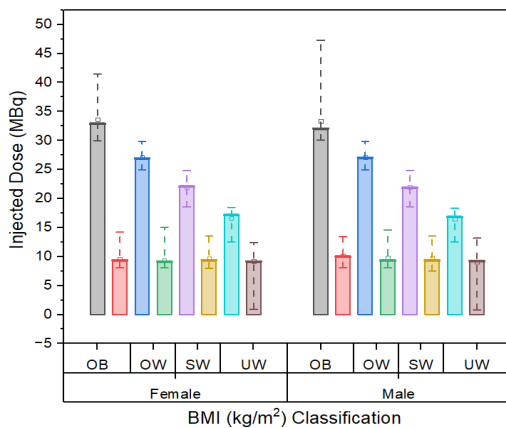


Figure 1. Shows bar graph of BMI categories to administered activity.

We indicate Model 1 had the best overall performance with the highest accuracy of 79%, as well as the highest weighted average of precision, recall, and F1-score at 0.79 respectively as compared to other models (Figure 2). Notably, we also observed the superiority of model in classifying the BMI and their corresponding doses.

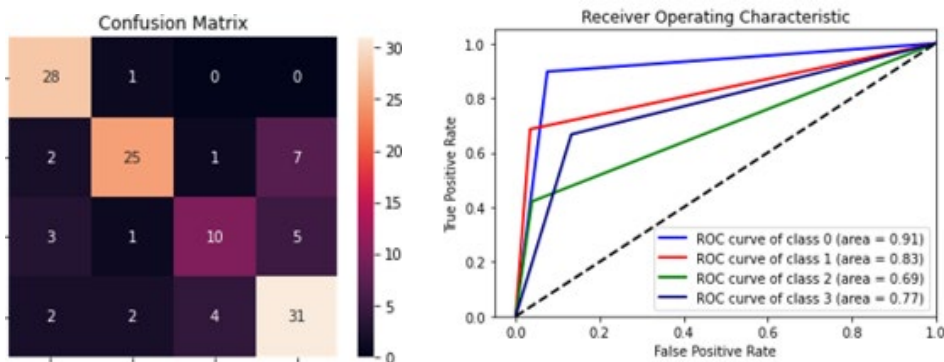


Figure 2. The scattered plot graph of effective dose against administered activity.

Conclusion

In conclusion, the analysis of radiation dose in PET/CT examinations demonstrated a significant correlation between activity levels and goodness of fit. The machine learning proposed in this study facilitates efficient and accurate estimation of radiation dose linked to BMI. This research lays the

groundwork for constructing models to refine PET/CT acquisition protocols, predict radiation dose, and evaluate the impact of BMI on dose administration.

^{99m}Tc Radiolabeling of Palm Shell Charcoal: A Potential Radiotracing Agent for Lung SPECT-CT Scan

M. Munir¹, I. Saptiama¹, K. S. S. Putri², M Marlina¹, M Subechi¹, A M. Forentin¹, A. Nurmanjaya¹, M Maiyesni¹, T Ariyanto³, G Suhariyono⁴, I. Prasetyo³

¹ Research Center for Radioisotope, Radiopharmaceutical, and Biodosimetry Technology, National Research and Innovation Agency (BRIN), Indonesia

² Laboratory of Pharmaceutics and Pharmaceutical Technology, Faculty of Pharmacy, Universitas Indonesia, Indonesia,

³ Department of Chemical Engineering, Faculty of Engineering, Universitas Gadjah Mada, Indonesia

⁴ Research Center for Radiation Safety Technology and Metrology, National Research and Innovation Agency (BRIN), Indonesia

Background

Recent studies reveal the important role of lung scintigraphy in lung cancer staging and radiotherapy planning for its patients, which requires lung perfusion and ventilation methods to achieve optimal imaging results. The perfusion method can be performed using radiopharmaceutical kits, while the latter one typically utilizes Technegas® with limited availability and is expensive. Therefore, alternative ventilation imaging agents should be developed to support lung diagnosis practice.

Methodology

The inhalable carbon powder was prepared from palm shell-based activated charcoal through high-energy milling, and characterized. The ^{99m}Tc-labeling of carbon powder was optimized in terms of SnCl₂ concentration, powder amount, incubation time, and pH. ^{99m}Tc-carbon was washed using water and then analysed for radiochemical purity using methanol 85% and Whatman no.1 paper as mobile and stationary phase, respectively. Subsequently, the radiolabeled carbon was assessed for cellular uptake in A549 and TIG-1 cells as lung cancer and normal lung cells, respectively.

Results

Table 1 and 2 shows that 3 h high energy milling with powder:ball ratio of 1:5 was the optimal parameter to produce carbon powder with a high surface area (626 m²/g) and particle size within the inhalable powder range (>5 μm).

Table 1. Carbon powder porosity

No.	Carbon Preparation		Surface Area (m ² /g)	Pore diameter (nm)	Pore volume (mL/g)
	Milling Time	Powder:Ball Ratio			
1	1 h	1:5	625	3.83	0.115
2	2 h	1:5	627	3.82	0.153
3	3 h	1:5	626	3.40	0.178
4	6 h	1:5	568	3.82	0.182
5	12 h	1:5	426	3.83	0.127
6	1 h	1:10	610	3.80	0.147
7	1 h	1:20	600	3.38	0.204

Table 2. The particle size distribution of carbon powder

No.	Carbon Preparation		Dx (10) (μm)	Dx (50) (μm)	Dx (90) (μm)	Span
	Milling Time	Powder:Ball Ratio				
1	1 h	1:5	0.916	4.01	10.20	2.31
2	2 h	1:5	0.652	2.30	5.85	2.26
3	3 h	1:5	0.522	1.71	4.14	2.11
4	6 h	1:5	1.00	7.76	47.30	5.97
5	12 h	1:5	0.969	4.46	13.60	2.84
6	1 h	1:10	0.601	2.02	5.91	2.63
7	1 h	1:20	0.682	2.62	18.10	6.65

The optimization of the radiolabeling parameter is shown in Figure 1. It is shown that the yield increases with the increase of SnCl₂ and carbon weight. The yield also increased with a longer incubation time of up to 30 min, followed by a stagnant yield. The increase of pH gradually reduced the radiochemical yield since higher pH tends to produce ^{99m}TcO(OH)₃⁻ which makes it difficult to radiolabel the carbon. Although the obtained radiochemical yield was around 80% (Figure 1) carbon washing using water can increase radiochemical purity to 99.99% (Figure 2).

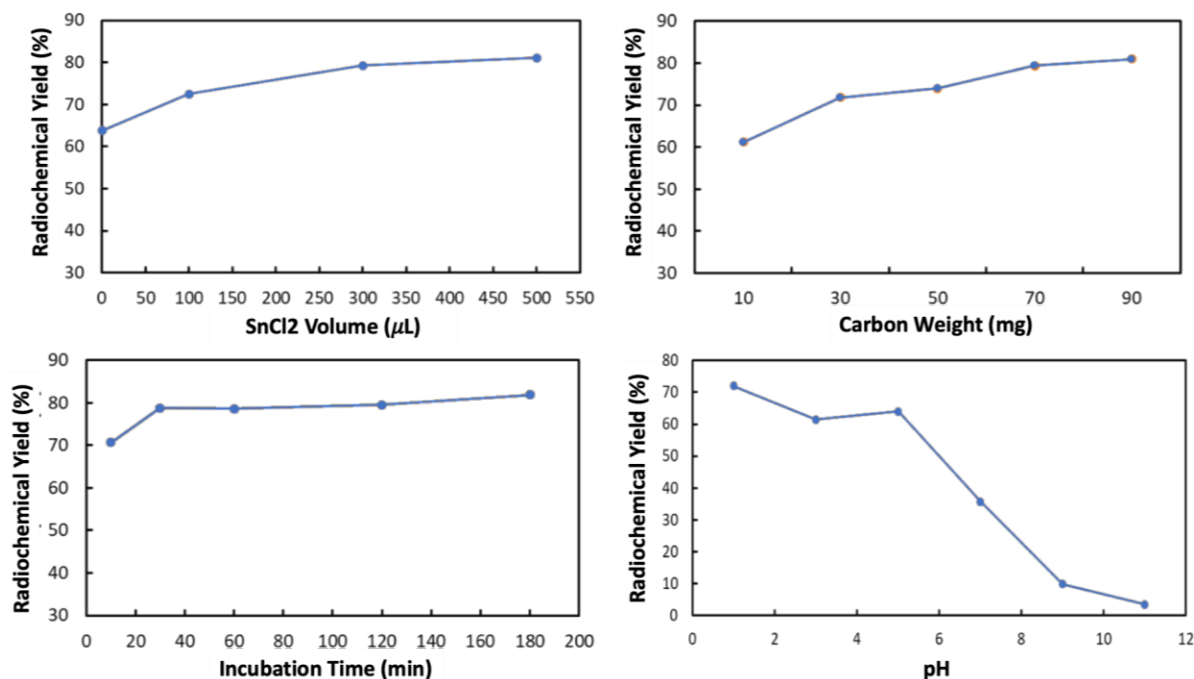


Figure 1. ^{99m}Tc-labeling of carbon powder with optimization parameter of SnCl₂ concentration, powder amount, incubation time, and pH

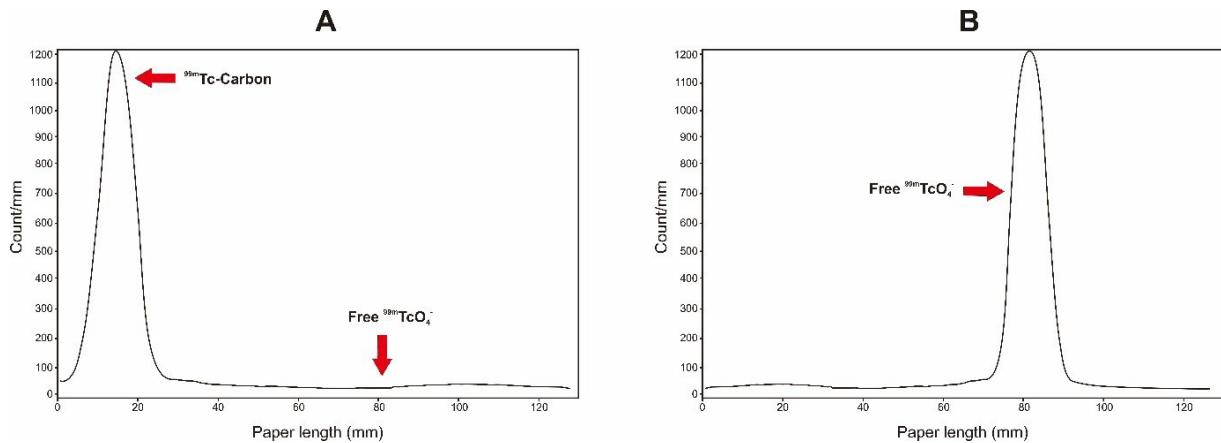


Figure 2. Radiochromatogram of ^{99m}Tc -labeled carbon (left) and ^{99m}Tc pertechnetate as a standard (right)

Figure 3 shows that the cellular uptake of ^{99m}Tc -carbon in A549 (28-30%) dan TIG-1 (40-48%) is higher than that of ^{99m}Tc pertechnetate (<1%). Figure 2 reveals that cellular uptake in cancer cells was higher than that in normal cells due to the higher lipid content in the cellular membrane of tumour that attract hydrophobic carbon. This finding might be beneficial for cancer diagnosis due to selectivity to cancer cells. Nevertheless, further investigation is required to explain this finding.

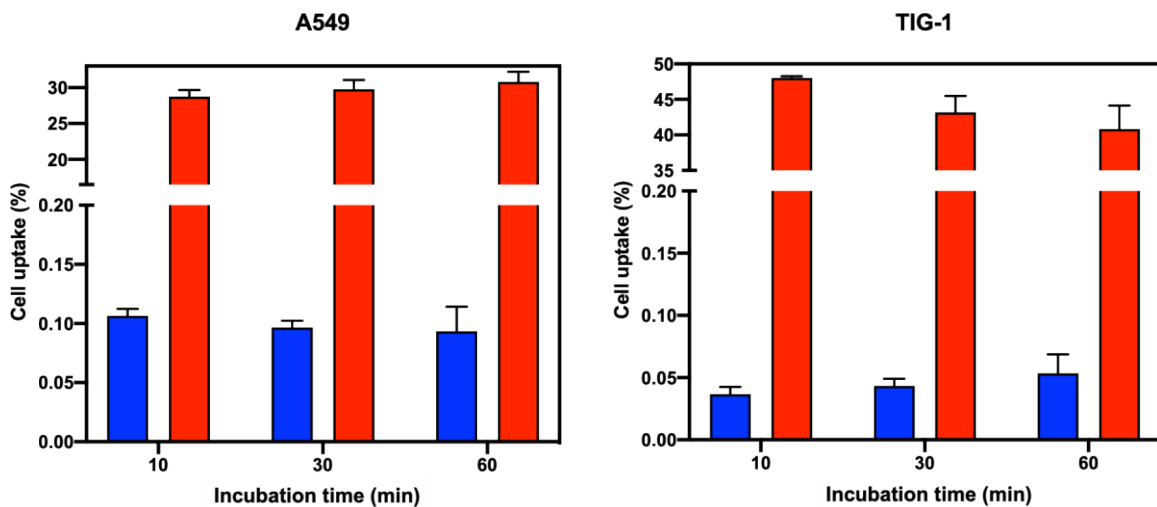


Figure 3. Cellular uptake of ^{99m}Tc and ^{99m}Tc -carbon in A549 dan TIG-1 cells.

Conclusion

In this study, ^{99m}Tc -radiolabeled inhalable carbon powder was successfully prepared as potential lung ventilation scintigraphy agent. Nevertheless, further study should be performed prior to clinical stage development, including toxicity assessment, aerosol performance test, and in vivo study to evaluate the actual lung deposition and image quality, which are scheduled in 2024.

Hybrid Au-198[Au]/Gd-153[Gd] nanoparticles as potential multipurpose theragnostic agent for Photothermal/SPECT/CT/MRI

H. Setiawan¹, A. Nurmanjaya¹, A. Pujiyanto¹, M. Muflikhah², A. Fikri¹, S. Juliyanto¹, F. Rindiyantono¹, R. Ritawidya¹

¹Research Center for Radioisotope Radiopharmaceuticals and Biodosimetry Technology, National Research and Innovation Agency, Indonesia

²Research Center for Nuclear Beam Analysis Technology, National Research and Innovation Agency, Indonesia

Background

Gold nanoparticles (AuNPs) as a multifunctional material are widely used in various applications due to their physicochemical characteristics. The high X-ray absorption and biocompatibility of AuNPs make them one of the most promising contrast agents for computed tomography (CT). Combining AuNPs with gadolinium makes it possible for the material to also be detected using magnetic resonance imaging (MRI). The addition of radioactive Gd-153 or Au-198 to Gd-Au nanomaterials makes them compatible with SPECT/CT/MRI contrast as well. Further modification in the form of AuNPs and the use of Gd-157 allow these hybrid nanoparticles to be superior for therapeutic photothermal therapy and candidate for GdNCT(Gd-Neutron Capture Therapy) agents.

Methodology

The fabrication of hybrid nanoparticles is done in stages by making one of the elements the core of the nanohybrid material. If Au nanoparticles are made as the core, Au-nanosphere, nanorod or nanostar are first made and then conjugated with chelators that will bind gadolinium. Meanwhile, if Gd nanoparticles are to be made as the core, Gd nanoparticles are made which are then wrapped by Au as the outer shell (Au-nanoshell) as illustrated in Figure 1.

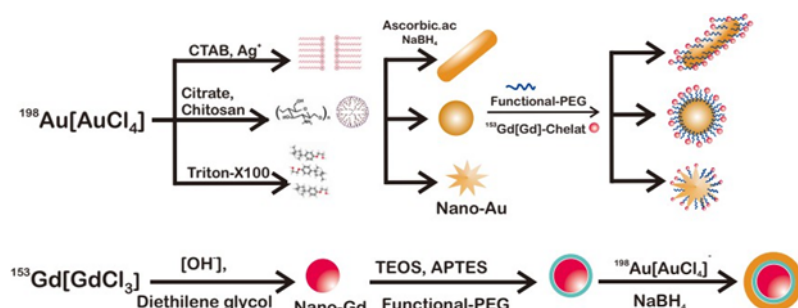


Figure 1. Schematic of the preparation of Gd-Au hybrid nanoparticles using Gd-153 and Au-198 Radiotracers

The key components for making AuNPs are irradiated Au-foil, which is used to make Au-198 radiotracer in HCl, and Chloroauric acid. The stabilizers used as synthesis templates are chitosan, sodium citrate, and CTAB. While the reduction process uses ascorbic acid and Sodium borohydrate. The purification process of Au core nanoparticles was carried out by a high-speed centrifugation. While, preparation of Gd nanoparticle core (GdNP) prepared using Gadolinium chloride with surfactant-based stabilizer.

The manufacture of Gd-153 and Au-198 radiotracers was carried out at the G.A Siwabessy research reactor facility, which were then target dissolved at the Radioisotope and Radiopharmaceutical Technology Installation as illustrated in Figure (2). Radiotracer was added to the process of making Au-198[AuCl₄] and Gd-153[GdCl₃] solutions as raw materials for making Au-198[Au]-NP and Gd-153[Gd]-NP core materials. Characterization was performed using UV-Vis, PSA, TEM, Gamma Spectrometer, Gamma well counter, and Radioactive TLC-scanner.

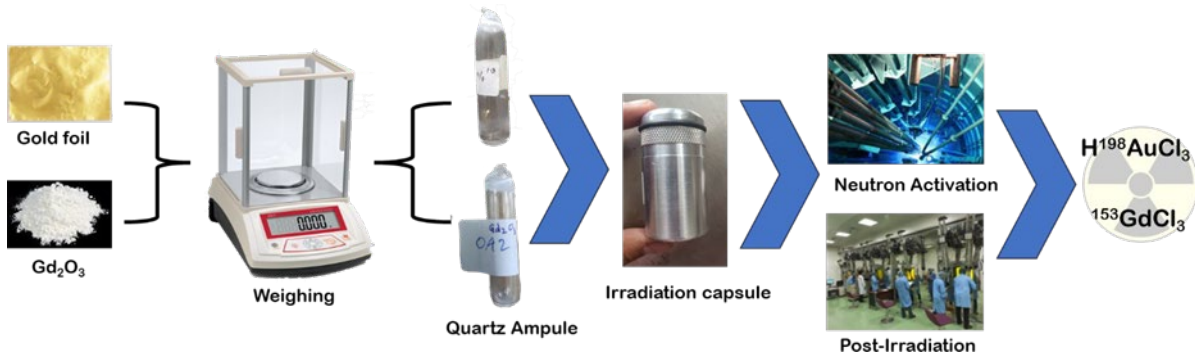


Figure 2. Illustration of the preparation the H¹⁹⁸Au-198[AuCl₄] and Gd-153[GdCl₃] solutions

Results

The preparation of radioactive solutions of Au-198[AuCl₄⁻] and Gd-153[GdCl₃] as radiotracer raw materials showed excellent radiochemical purity >98% as shown in Figure 3. While the purity of radionuclides Au-198 and Gd-153 showed appropriate gamma energy Figure 4. Gold nanoparticles as a core can be synthesized in various shapes and sizes according to requirements (Figure 5.a-c). While the Gadolinium nanoparticle core prepared by the polyol method produced <5 nm particles (Figure 5.d).

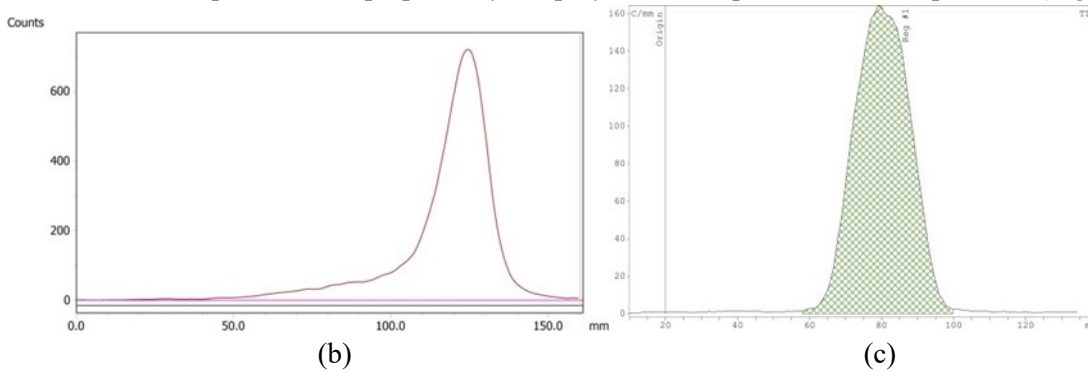


Figure 3. TLC chromatograms of (a) H¹⁹⁸Au-198[AuCl₄] and (b) Gd-153[GdCl₃] showing the radiochemical purity of the radioactive forms Au³⁺ and Gd³⁺, respectively.

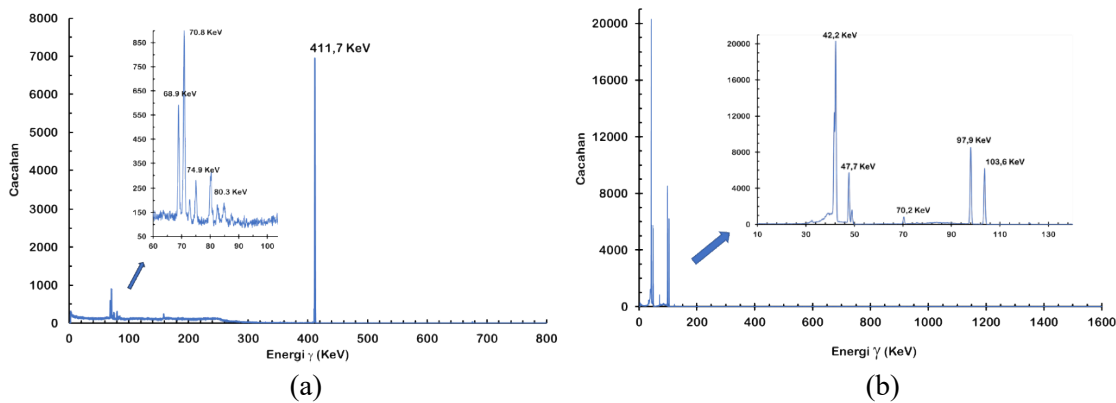


Figure 4. Radionuclide purity of

(a) $H^{198}AuCl_4$ [^{198}Au : 411 KeV; X-ray: 70.8 (K α 1), 68.8 (K α 2), 80.3 (K β 1), 82.4(K β 1)] and
 (b) $H^{153}GdCl_3$ [^{153}Gd : 97.4, 103.1, 69.6 KeV; X-ray: 41.5 (K α 1), 40.9 (K α 2), 47.3 (K β 1), 48.2 (K β 2)]

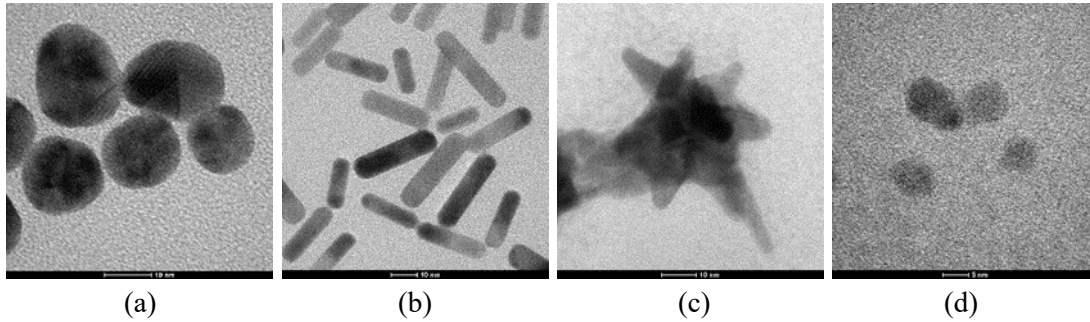


Figure 5. TEM images Gold nanoparticles in the shape of (a) spheres, (b) rods, (c) stars and (d) clusters of Gd₂O₃ nanoparticles

In gold Nanorods as core and Gd bound to PAMAM-DOTA on the outside, showing almost the same relativity value as commercial contrast MRI (Gadovist). Furthermore, by utilizing the photothermal ability of gold nanorods and adding antibodies as a guide, targeted nanohybrid theragnostic is more promising (Setiawan et al., 2021). The preparation of Gd₂O₃ nanoparticles as the core of nanohybrid was carried out by polyol method, the observation of cold nano-Gd₂O₃ using 3T MRI was carried out in the Radiology facility of the Hospital (Figure 6), while the observation of nano Gd-153[Gd₂O₃] was carried out using a solo-mobile gamma camera (Figure 7). The process of encapsulating the core gadolinium nanoparticles using gold nanoshells is done by adding Au-198[AuCl₄] so that the Gadolinium core is covered by Au. Nanohybrid separation was done by centrifugation, and the gamma energy of the nanohybrid was observed using the gamma well counter (Figure 8).

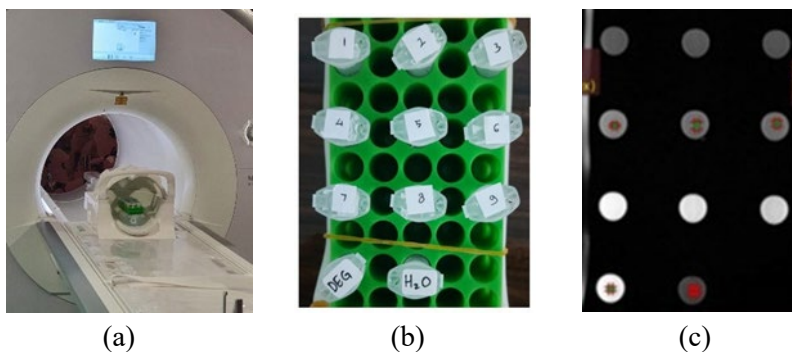


Figure 6. (a) positioning settings on the MRI 3T (b) GdNP solution and the solvent in the microtube (c) Imaging results of GdNP using MRI 3T

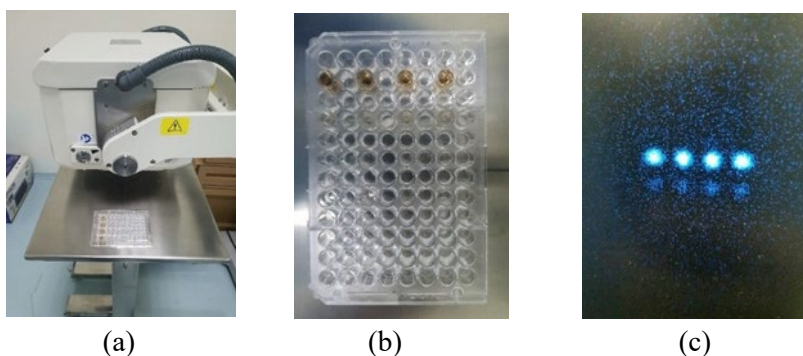


Figure 7. (a) Positioning settings on the gamma camera (b) Gd-153[GdNP] solution in a 96-well plate (c) Imaging results using Gamma camera

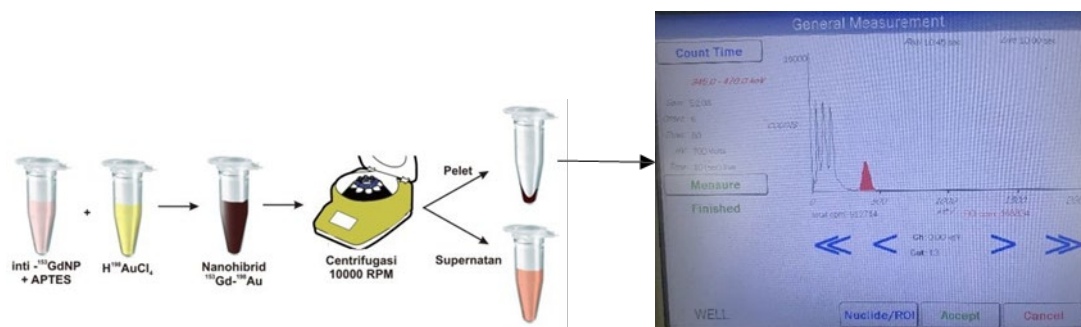


Figure 8. Schematic of hybrid Au-Gd nanoparticle formation. Gamma energy Gd-Au of hybrid nanoparticles (centrifuged pellets) showed two energy patterns for Gd-153 and Au-198

Conclusion

Au-Gd-based nanoparticles are very promising to be one of the Hybrid Imaging for SPECT/CT/MRI because of the advantages of each component. The modification process needs to be developed for the most effective structure and targeted properties, especially for possible therapeutic applications such as photothermal or GdNCT.

Microcalcifications at Mammography and Molecular Breast Imaging in a young adult Filipina: A case report

I. S. Bandong^{1,2,3}, M. T. Buenaflor², R. A. Conlu^{1,2}

¹ Philippine Society of Nuclear Medicine, Philippines

² Philippine College of Radiology, Philippines

³ Diagnostic Breast Imaging Society of the Philippines, Philippines

Background

Microcalcifications (MCs) are associated with premalignant and proliferative breast disease, and their identification facilitates the prevention of invasive disease. MCs may play a prognostic role in invasive carcinomas. Carcinomas with MCs appear to have worse outcomes compared with those without MCs (Logullo et al 2022).

Molecular breast imaging (MBI) is a physiologic approach to breast cancer detection. MBI using a gamma camera is performed with ^{99m}Tc-sestamibi. MBI detects additional foci of occult breast cancer in 9.0% of women with newly diagnosed breast cancer, has a high sensitivity for detecting high-risk lesions, and detects 98% of invasive breast cancer and 91.0% of ductal carcinoma in situ (Muzahri 2020).

The objective of this case report is to describe the usefulness of MBI in detecting malignancy in young adult Filipina with microcalcifications in mammogram.

Case Report

A 33-year-old Filipino female with palpable left breast mass. She had digital breast tomosynthesis (Figure 1) showed partially obscured hyperdense mass in the posterior third of the lower inner quadrant of the left breast. Magnification view ((Figure 2) demonstrates a cluster of pleomorphic microcalcifications in the anterior third of the upper outer quadrant of the right breast. Molecular breast imaging (Figure 3) sestamibi avid foci in the upper outer quadrant of the right breast and lower inner quadrant of the left breast. PET CT scan (Figure 4) confirms the FDG avid lesion in the left breast and left axillary lymph node.

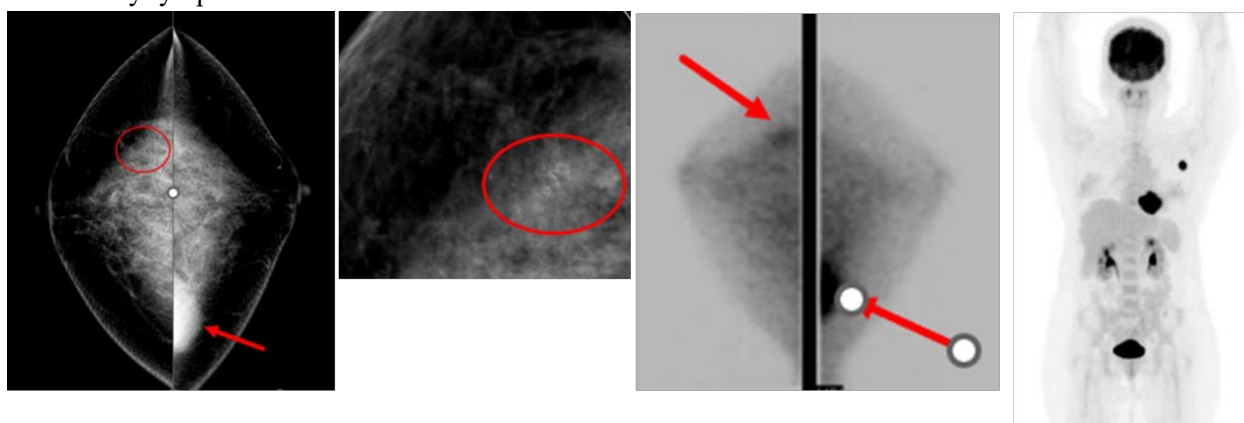


Figure 1

Figure 2

Figure 3

Figure 3

Figure 1: Mammogram shows pleomorphic calcifications (red circle) in the upper outer quadrant of the right breast and partially obscured hyperdense mass (red arrow) in the lower inner quadrant of the left

breast. Figure 2: Magnification view shows cluster of pleomorphic calcifications (red circle). Figure 3: MBI shows sestamibi avid foci in the upper outer quadrant of the right breast (red circle) and lower inner quadrant of the left breast (red arrow). Figure 4. PET CT confirms the FDG avid lesion in the left breast and left axillary lymph node

Biopsy was done and showed ductal carcinoma in situ on the right breast lesion and Her2 positive invasive breast carcinoma in the left breast

Discussion

Ductal carcinoma in situ (DCIS) DCIS is a segmental disease arising from a terminal duct lobular unit with the potential to progress within the duct system up to the lactiferous ducts and nipple. Most DCIS lesions are diagnosed mammographically (70–90%), being rarely detected clinically.

Microcalcifications alone are likely the most reliable mammographic indicators of DCIS in women younger than 50 years (Salvatorelli et al, 2020).

MBI is a physiologic approach to breast cancer detection. MBI detects additional foci of occult breast cancer in 9.0% of women with newly diagnosed breast cancer, has a high sensitivity for detecting high-risk lesions, and detects 98% of invasive breast cancer and 91.0% of DCIS (Huppe et al, 2018)

Conclusion

MBI is important supplement imaging for both breast cancer screening and evaluation of breast cancer especially in indeterminate or inconclusive mammography findings.

Keywords: microcalcifications, DCIS, Molecular breast imaging, Tc-99m sestamibi

Experience of using 18 FDG PET/CT in planning and evaluating the effectiveness of treatment in the ablation of liver metastases

A. Ashykhmin¹, O. Solodyannikova¹, Y. Kmetiyuk², S. Hrabovetskyi²

¹National Cancer Institute, Kyiv, Ukraine

²Clinical Hospital "Feofaniya", Kyiv, Ukraine

Background

Thermal ablation is used in our institution to ablate liver metastases from colorectal cancer. Thermal ablation has the advantage of causing localised destruction of the metastatic liver lesions with sparing of the surrounding normal tissues. In addition, this method has minimal systemic toxic side-effects due to the localised coagulation necrosis. Various imaging methods are used to assess the success of thermal ablation. Ultrasound (U/S) is used to assess the procedure intraoperatively. U/S and Magnetic Resonance Imaging (MRI) is then used to monitor disease response in the post-operative period. Exudative-infiltrative changes occur in the lesions 2 days after the therapy which complicates the assessment of the zone of destruction on MRI. [¹⁸F]Fluorodeoxyglucose ([¹⁸F]FDG) Positron Emission Tomography/ Computed Tomography (PET/CT) is able to differentiate between viable and devitalised tissue therefore, we postulated that adding [¹⁸F]FDG PET/CT during the postoperative period could improve diagnostic certainty in this setting.

Methodology

Patients are routinely followed up with U/S and MRI on day 1, day 3 and day 5 after ablation. Delayed imaging with U/S and MRI is performed 2, 5/6, 9, 12, 18, 24, 30 and 36 months after the procedure. In this study PET/CT was added at the 2-3 month assessment in cases with questionable U/S and MRI findings.

Results

[¹⁸F]FDG PET/CT for the evaluation for equivocal lesions on U/S and MRI was introduced in our centre five years ago. During this time period more than 20 patients were evaluated with [¹⁸F]FDG PET/CT in addition to conventional follow-up.

Usually, complete ablation can be assessed up to two months after the procedure. On U/S areas of hyper, hypo and anechoic signal intensity are seen followed by compaction of the necrotic masses and the formation of a fibrotic capsule. In comparison CT scan at two months shows lesions with a lower density than metastases and they do not accumulate contrast during the venous phase.

In cases with incomplete ablation the interpretation of the CT findings is challenging. PET/CT can assess residual areas of metabolic activity in the thermal ablation zones. Residual normal liver uptake was assessed using the SUVmax of the avascular zone between the 6th and 7th segment, with a baseline SUVmax between 2.4 -3.7. Metabolically active lesions were detected if the lesions were bigger than 0.5 cm with a SUVmax 1.3 -1.4 higher than normal liver activity. Metabolic lesions as small as 2-3 voxels were detected. 18 F FDG- PET/CT was able to detect more than 30% of metabolically active lesions in comparison with conventional imaging methods.

Liver abscesses were one of the causes for false positive [¹⁸F]FDG uptake.

Conclusion

[18F]FDG PET/CT is recommended in cases with equivocal conventional imaging finding on the 2-month follow-up. This PET/CT study should not be performed earlier than 4-6 weeks after the thermal ablation. Further investigation of this method in a larger patient cohort is recommended.

Use of microwave radiolabelling method and rat brain biodistribution study of a new [^{99m}Tc]tricarbonyl complex as potential brain imaging agent

N. M. Saied, M. Saidi

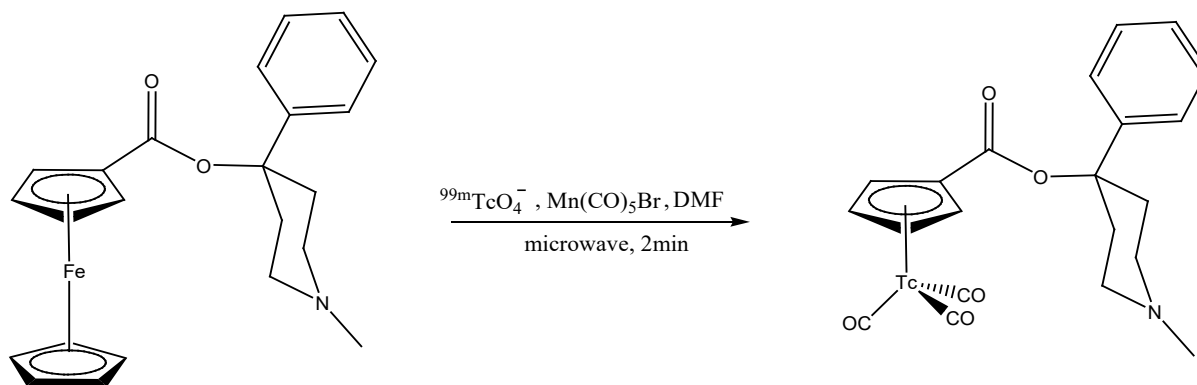
National Center of Nuclear Sciences and Technology, Tunisie

Background

Neuroimaging faces challenges in developing efficient and readily applicable radiotracers for effective brain imaging, wherein a critical obstacle lies in ensuring the radiotracers' ability to traverse the blood-brain barrier while maintaining specificity to target brain receptors.

Methodology

In this study, a novel lipophilic cyclic amine attached to cyclopentadienyl technetium-99m tricarbonyl (known as cytectrene), was successfully synthesized through a direct one-pot reaction. Using ferrocenoyl-1-methyl-4-phenyl-piperidinol-ester as the starting material, the synthesis demonstrated a 90% yield and maintained high radiochemical purity.



The synthesis involves dissolving the ligand and TcO₄⁻ in dimethyl formamide within a 5 ml vial, followed by exposure to microwave irradiation for 2 minutes at 600 watts. The resulting complex was efficiently purified using a preparative TLC method employing an ether/triethylamine (95:5) solvent system.

Results

The synthesis process is notably facile, highlighting the efficiency of this methodology. In biodistribution studies conducted in rats, the [^{99m}Tc]labeled cytectrene exhibited remarkable accumulation in the brain, reaching 2.3% of the injected dose. Moreover, the complex demonstrated high brain-to-blood ratios of 7.15 at 15 minutes post-injection. This confirms the capability of the complex to successfully cross the blood-brain barrier.

Conclusion

These findings underscore not only the simplicity and efficiency of the synthesis process but also the potential of the developed complex as a valuable agent in brain imaging. Further investigations are warranted to explore the full capabilities of this innovative agent for neurological studies.

Enhancement of Lesion Detectability and Shortening of Acquisition Time in Dynamic [¹⁸F]FDG PET using Principal Component Analysis: A Phantom Study

F. Bezoubiri¹, Y. Bouchareb², T. Zidi³, F. Kharfi⁴

¹ Radiological and Atomic Physics Department, Physics Division, Nuclear Research Centre of Algiers, Algiers, Algeria

² Sultan Qaboos University, College of Medicine & Health Sciences, PO. Box 35, Al-Khoud, Muscat, Oman

³ Atomic Energy Commission (COMENA), Algiers, Algeria

⁴ Department of Physics, Faculty of Sciences, Ferhat Abbas-Setif1 University, Campus El-Bèz, Sétif, Algeria. Laboratory of Dosing, Analysis and Characterization with High Resolution, Ferhat Abbas-Setif1 University, Campus El-Bèz, Setif, Algeria

Background

Dynamic PET imaging plays a key role in improving cancer diagnosis, assessing therapy response, and characterizing tumour lesions. However, it suffers from several limitations such as poor image quality and longer data acquisition time. This work aimed at improving image quality and shortening the total duration of the [¹⁸F]FDG study using Principal Component Analysis (PCA).

Methodology

The 4D-XCAT phantom combined with Time Activity Curves (TACs) was used to produce the dynamic activity maps. The TACs were calculated using a standard [¹⁸F]FDG two-tissue compartment model and [¹⁸F]FDG kinetic micro-parameters of different tissues, reported in the literature. Two spherical lesions of 9 mm diameter were inserted in the liver and the lung. STIR reconstruction software was utilized to generate [¹⁸F]FDG/PET dynamic frames. The PCA method was applied to the simulated dynamic [¹⁸F]FDG/PET frames generated at t=35-55min for lesion detectability and at different scanning times (11, 13, 15, 20, 25, 35, 40, 45, 50, and 55 min) for reduction of acquisition time. The estimated Principal Component Images (PCI1, PCI2 and PCI3) were visually assessed and compared to the SUMmed Images (SUMI), generated at t=35-55min. The Tumour-to-Background-Ratio (TBR) and Activity Line Profiles (ALPs) were considered in the quantitative assessment.

Results

For lesion detectability improvement, the visual assessment of PCIs shows that the lesion was better detected in the PCI2 and SUMI images, while no qualitative diagnostic information could be extracted from the PCI3 image. In PCI1, the lesion can be detected with lower activity in the lesion than in the surrounding tissue, for liver and lung. The quantitative analysis reveals that PCI2 provided better detectability of the lesion compared to PCI1 and SUMI, for the lesion inserted in the liver (TBRPCI2 = 4.05 ± 0.5, TBRPCI1 = -0.78 ± 0.01 and TBRSUMI = 3.09 ± 0.50). In the case of the lesion inserted in the lung, PCI2 has also shown better detectability than PCI1, but lower than SUMI (TBRPCI2 = 2.15 ± 0.05, TBRPCI1 = -0.85 ± 0.00 and TBRSUMI = 15.21 ± 3.50).

Concerning the reduction of the acquisition time, the quantitative assessment of PCIs shows that for the liver and lung the TBR estimated on PCI3 is higher than on PCI1 and PCI2 from timing 11 to 35 min, but is close to the SUMI for the liver and lower than SUMI for the lung (TBRPCI3(liver) = 2.49 ± 0.72 and TBRPCI3(lung) = 1.44 ± 0.06 at 25 min, whereas TBRSUMI (liver) = 3.09 ± 0.50 and TBRSUMI

(lung)= 15.21 ± 3.50). Overall, The TBRs estimated on PCIs for the liver are higher than those estimated for the lung for all times, except PCI2.

Conclusion

This study demonstrates that PCA may play an important role in improving lesion detectability and reducing of scanning time in dynamic [^{18}F]FDG/PET imaging, when the lesion is located in a tissue with high background.

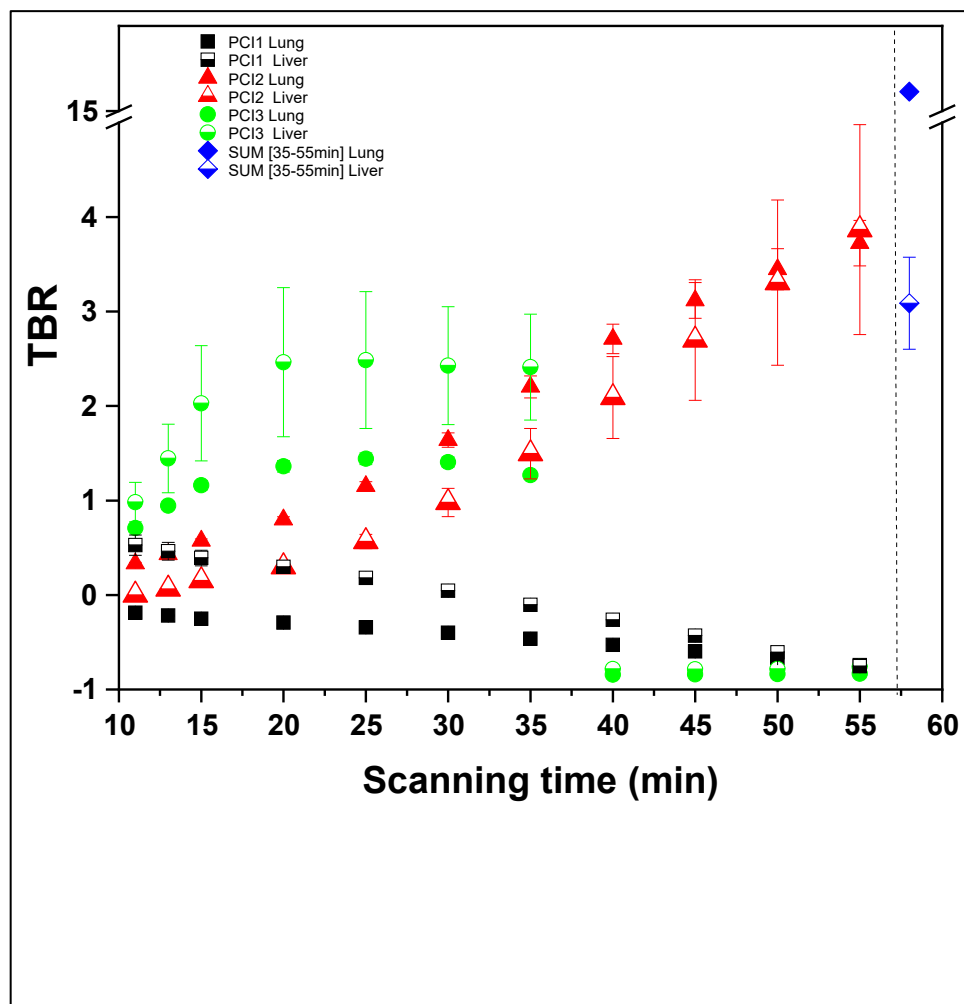


Figure 1. TBR calculated on PCI1, PCI2, PCI3 and SUMI as a function of scanning time, for lung and liver.

Contribution of Uruguay to education in Radiopharmacy: fostering the development of Nuclear Medicine in Latin America in the PET era

A. R. Rios, M. E. Tejería, M. T. Gretter

Área Radioquímica, Facultad de Química, Universidad de la República, Montevideo, Uruguay

Background

Nuclear Medicine development is highly dependent on the availability of high-quality radiopharmaceuticals. Technological complexity and legal requirements of radiopharmaceuticals preparation have increased significantly in the PET era. According to WHO's official documents (WHO Annex 2, Report 48 -TRS 986 and Annex 3 Report37 - TRS 908) the production of radiopharmaceuticals requires the supervision of qualified personnel with postgraduate training and appropriate experience in their function. Furthermore, the research and development of novel radiopharmaceuticals is highly dependent on basic knowledge in areas such as organic and inorganic chemistry, pharmaceutical technology, biochemistry, molecular biology, and animal science.

However, education in Radiopharmacy at pre and postgraduate level is almost non-existent in Latin America and professionals continue to be trained on the job without an adequate theoretical background.

Another challenge faced by the Latin American region is the need of generational renovation of professionals in Radiopharmacy.

Radiopharmacy in Uruguay has been historically developed in the University and educational offer at pre and postgraduate level has been developed during more than 50 years.

In the last years we have developed a series of new options for postgraduate and continuing education in the field. The Diploma of Specialization in Radiopharmacy offers a postgraduate program for specialization in Radiopharmacy. This diploma integrates comprehensive theoretical knowledge with the necessary practical experience to prepare professionals for specialized roles in this field. Admission to the program requires candidates to hold a university degree, with a minimum duration of four years, in Pharmacy, Chemistry, or Biochemistry, obtained from institutions in Uruguay or other countries. Applications from candidates with alternative qualifications are reviewed by a dedicated admission committee, and additional courses may be prescribed to supplement their foundational knowledge. The curricula comprises both theoretical and practical components, totaling approximately 300 hours of instruction. This includes hands-on training in conventional and Positron Emission Tomography (PET) Radiopharmacy, ensuring students gain practical expertise in both traditional and cutting-edge techniques. The courses can be partially performed virtually, thus facilitating the participation of foreign students. However, practical laboratory sessions and supervised practice are required to be completed in Uruguay, typically spanning a duration of 3-4 months. Additionally, partial validation of prior studies may be considered, allowing eligible students to receive credit for relevant coursework completed elsewhere.

In addition to our postgraduate program, we provide opportunities for continuous education through a variety of courses. These courses cover both fundamental topics such as the physics of radiation and the chemistry of radiopharmaceuticals, as well as applied subjects including legislation and clinical applications.

We also offer customized courses for institutions or private radiopharmaceutical firms.

Another contribution of our group was the participation in Arcal 6084 project that has pursued to strengthen the regional system of education of human resources through the training of your professionals that will constitute the initial seedbed of teachers in order to generate an educational offer in their countries in the future.

Conclusion

In conclusion, Uruguay has capitalized the accumulated experience to cooperate in overcoming the human resource development gaps in Latin America in a sustainable manner.

Aknowledgements

Centro Uruguayo de Imagenología molecular, CUDIM and Centro de Medicina Nuclear e Imagenología Molecular del Hospital de Clínicas.

Development of Cyclic Tetra Phosphonates Derivatives as Prospective Radiopharmaceutical Theranostics for Bone Metastasis

I. Daruwati¹, M. E. Sriyani¹, T. H. A. Wibawa¹, B. Hidayat², B. Darmawan², R. J. Sugiharti¹

¹ Research Center for Radioisotope, Radiopharmaceutical, and Biodosimetry Technology, Research Organization for Nuclear Energy, National Research and Innovation Agency (BRIN), Indonesia

² Department of Nuclear Medicine and Molecular Theranostics, Hasan Sadikin Hospital, Indonesia

Background

Various types of cancer such as breast, prostate, lung, and thyroid cancer can metastases to the bones. About 50-80% of breast and prostate cancers develop bone metastases. In nuclear medicine, bone scanning and therapy are usually performed with bisphosphonate radiopharmaceuticals. However, radioactivity also accumulates in organs other than bones. Phosphonate compounds enter the bone through absorption by hydroxy apatite where hydroxy apatite is part of the bone composition. The absorption of phosphonate compounds is influenced by the interaction of the phosphonate group in the phosphonate complex with calcium on the surface of hydroxyapatite. Therefore, the affinity of tetra phosphonates for bone is higher than bisphosphonates. This research has carried out the synthesis of Cyclic Tetra Phosphonates Derivatives compounds then optimized the radiolabeling using ^{99m}Tc for diagnosis and ^{186/188}Re as a therapeutic agent in bone metastases.

Methodology

This study includes optimization of CTTMP labeling with ^{99m}Tc and ^{188/186}Re using the direct reaction method, preclinical trials of radiopharmaceuticals, and clinical trials on volunteers. Labeling efficiency was determined by chromatographic methods; while preclinical tests were carried out using mice, rats and rabbits. Preclinical tests include biodistribution, blood clearance, and scanning with gamma cameras.

Results

Table 1. Optimized of radiolabeling CTTMP with ^{99m}Tc and ^{186/188}Re

Compound	Radiopharmaceuticals	
CCTTMP	^{99m} Tc-CTTMP	^{186/188} Re-CTTMP
pH	6-7	2
Radiochemical Purity	>95%	>90%

Table 1. Biodistribution of ^{99m}Tc-CTTMP the radiopharmaceutical in normal mice

Organ	% ID				
	10 min	1 h	3 h	5 h	24 h
Muscle	3.73	0.21	0.03	0.13	0.03
Bone	32.71	18.38	16.73	22.26	5.62

Blood	21.05	0.89	0.34	0.16	0.03
Intestines	4.59	0.51	0.31	0.13	0.03
Heart	4.28	0.41	0.28	0.08	0.06
Spleen	4.66	0.39	0.19	0.76	0.04
Kidney	28.91	3.84	1.67	1.68	0.52
Heart	6.18	0.35	0.07	0.05	0.02
Lungs	12.08	0.75	0.16	0.12	0.05
Stomach	7.54	0.61	0.16	0.13	0.07

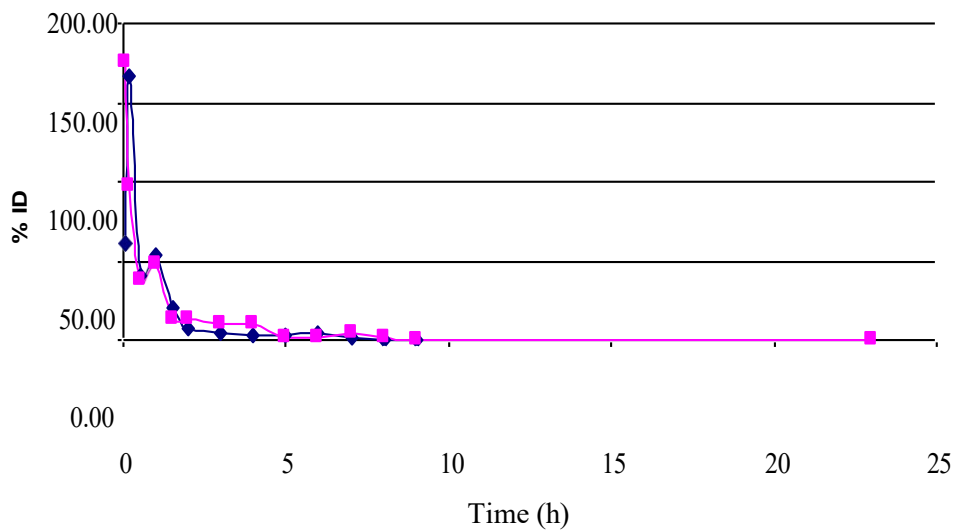


Figure 1. Blood Clearance of ^{99m}Tc -CTTMP after IV injections in normal mice

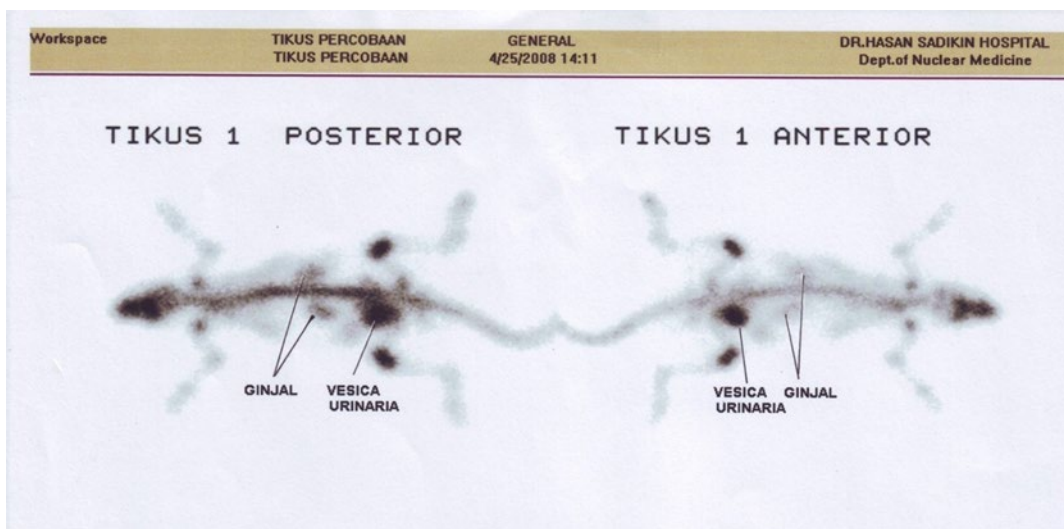


Figure 2. Static imaging of mice after 3 hours of injection with ^{99m}Tc -CTTMP radiopharmaceutical with a gamma camera

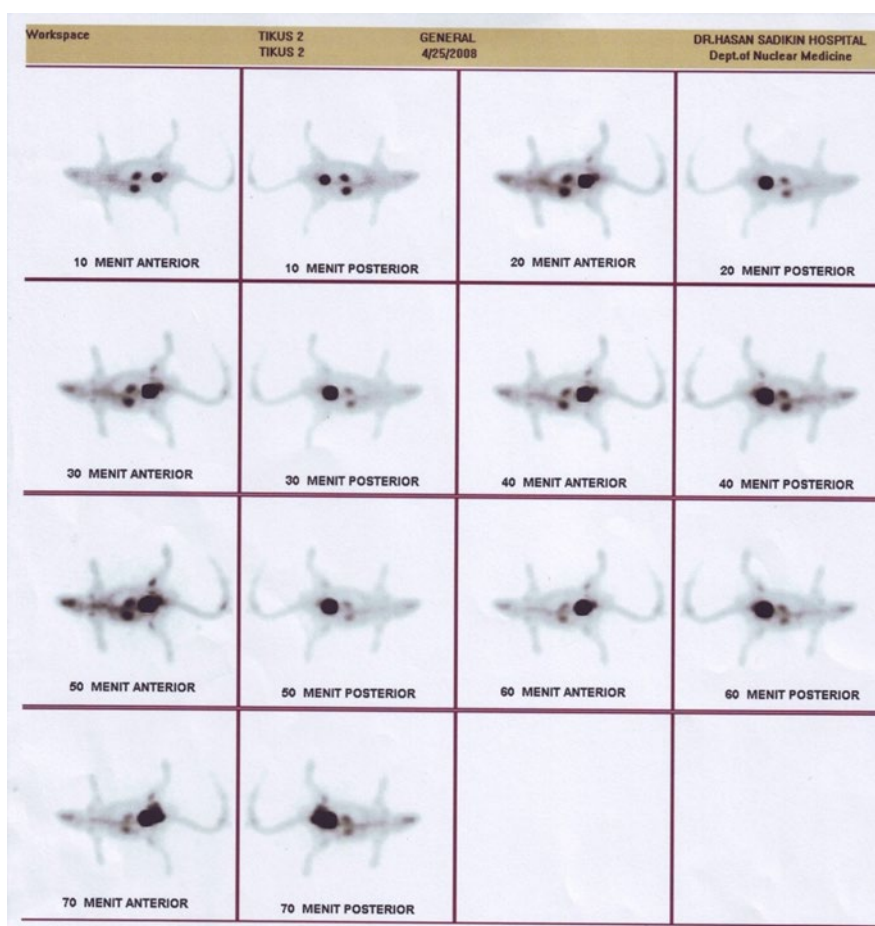


Figure 3. Dynamic imaging of white mice 3 hours after injection of ^{99m}Tc -CTTMP radiopharmaceutical with a gamma camera

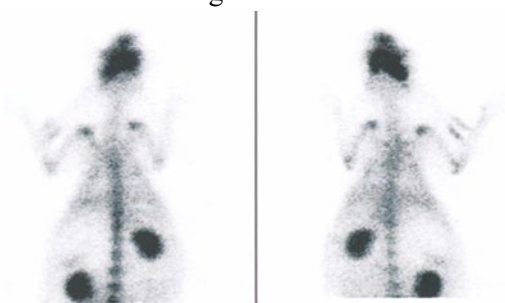


Figure 4. Static imaging of rabbits 3 hours after injection of ^{99m}Tc -CTTMP radiopharmaceutical with a gamma camera

Conclusion

The results showed that the labeling efficiency of CTTMP with ^{99m}Tc was >95 % with a composition of 100 mg of SnCl_2 , 500 mg of CTMP, pH optimum at 6-7 which was incubated in boiling water for 10 minutes, while $^{186/188}\text{Re}$ -CTTMP was carried out at pH 2 with KRK >90%. Preclinical tests showed that the radiopharmaceuticals accumulated in the bones were non-toxic, non-pyrogen, and excreted from the blood in about 2 hours and cleared from the kidneys in about 5 hours, respectively. From the preclinical tests that have been carried out above, it can be stated that this compound is safe and can be continued for clinical trials in humans.

Radiosynthesis of Brazilin with Iodine-131 as a Radiotheranostics Candidate and In Vitro Evaluation Against Cervical and Prostate Cancer Cell Lines

A. M. Forentin¹, I. Daruwati^{1,2}, V. Y. Susilo¹, W. Lestari^{1,2}, D. Ramadhani¹, A. Firmansyah^{2,3}, S. M. Faatin⁴

¹Research Center for Radioisotope, Radiopharmaceutical, and Biodosimetry Technology, Research Organization for Nuclear Energy, National Research and Innovation Agency (BRIN), Building 71, Kawasan Puspitek, Setu, Tangerang Selatan, Banten 15310, Indonesia

²Research Collaboration Center for Theranostic Radiopharmaceuticals, Jl Ir. Soekarno KM 21, Jatinangor 45363, Indonesia

³Indonesian College of Pharmacy (STFI), Jl. Soekarno Hatta No. 354, Bandung

⁴Department of Biomedicine, Faculty of Medicine, Andalas University, Jl. Limau Manis, Pauh, Padang, Sumatera Barat

Background

Plant-derived compounds exhibit a various range of structural varieties and possess unique pharmacological or biological properties. As a result, they have made a significant contribution to drug development, including radiopharmaceuticals, particularly for cancer diagnostics and therapy. The exploration of 125/131iodine radioisotopes for the synthesis of radiopharmaceuticals derived from natural compounds has not been thoroughly researched. Brazilin, derived from *Caesalpinia sappan* L., could induce apoptosis and reduce proliferation in many human cancer cell lines. However, there is a lack of data on its effects against cervical and prostate cancer. Indonesia's rich natural resources, particularly medicinal plants, are beneficial for the development of drugs, providing potential ligands for radiotheranostic candidates. This study focuses on an initial inquiry of radiosynthesis of brazilin with the iodine-131 or [¹³¹I]NaI. Furthermore, conduct an in vitro examination of brazilin's effects against Hela, LNCaP and DU-145 as cervical and prostate cancer cell lines.

Methodology

The radiosynthesis process involved the radiolabelling of the brazilin with the [¹³¹I]NaI isotope, which had a radioactivity range of 7.4 to 18.5 MBq. The radiolabelling process was conducted with brazilin (0.1 and 0.5 mg) and [¹³¹I]NaI at 25°C for 30 minutes using 0.05 mg of n-chlorosuccinimide as an oxidizing agent. Reactions were stopped using sodium metabisulfite. The radiolabelling result was characterised using electrophoresis methods with Whatman No. 1 paper as the stationary phase and 0.1 M phosphate buffer as the mobile phase. The electrophoresis was performed at 300 volts for 1 hour, and the radio TLC scanner was used to evaluate the percentage of [¹³¹I]I-brazilin. The biological activity of brazilin was assessed by measuring cell viability by the MTT assay and evaluating apoptosis using Acridine Orange/Propidium Iodide (AO/PI) staining. Cancer cell lines have been treated to different doses of brazilin ranging from 5.0 to 100.0 µg/ml over 24 hours. The IC₅₀ concentration from the cytotoxicity assay was utilized to evaluate apoptosis.

Results

Brazilin is a major compound isolated from the heartwood of *Caesalpinia sappan* L. Brazilin has a phenolic structure that's appropriate for labelling with radioisotopes, particularly [¹³¹I]NaI. Radiolabelling involves using n-chlorosuccinimide, which possesses the oxidizing capability of iodine,

to label the ligand. The radiolabelling studies demonstrated that varying reaction conditions can influence the radiochemical purity of [¹³¹I]-brazilin. The results indicated that the radiochemical purity was influenced by the quantity of ligand and the duration of incubation. The highest radiochemical purity achieved was 92.32% by the radiosynthesis of 0.5 mg of brazilin during a period of 30 minutes, as shown in Figure 1. The 0.1 mg of brazilin labelled with [¹³¹I]NaI for 15 and 30 minutes exhibited radiochemical purity above 50%, specifically 73.50% and 88.22, respectively. Brazilin was found to inhibit LNCaP and Du-145 by 50% at doses of 19.14 and 4.14 µg/mL, respectively. The IC₅₀ of brazilin against Hela cell lines was 40.04 µg/mL, as shown in Figure 2. The treated cells also exhibited morphological characteristics of apoptosis as validated by AO/PI staining, as shown Figure 3.

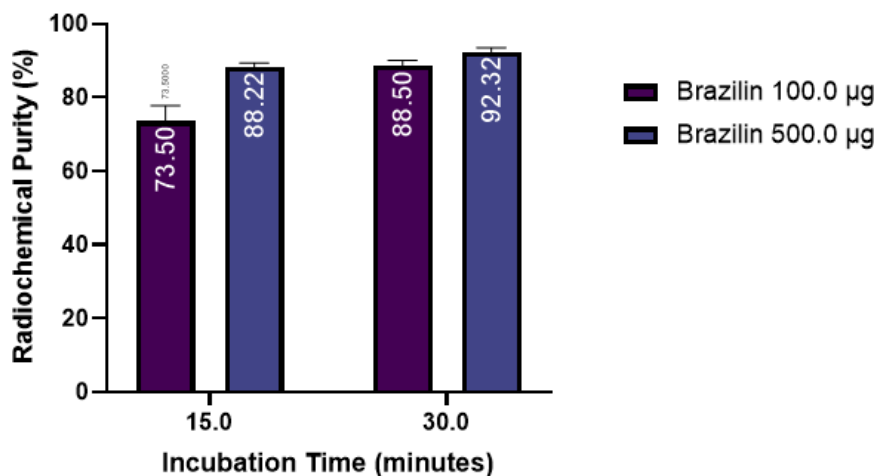


Figure 1. Radiochemical purity of [¹³¹I]-brazilin.

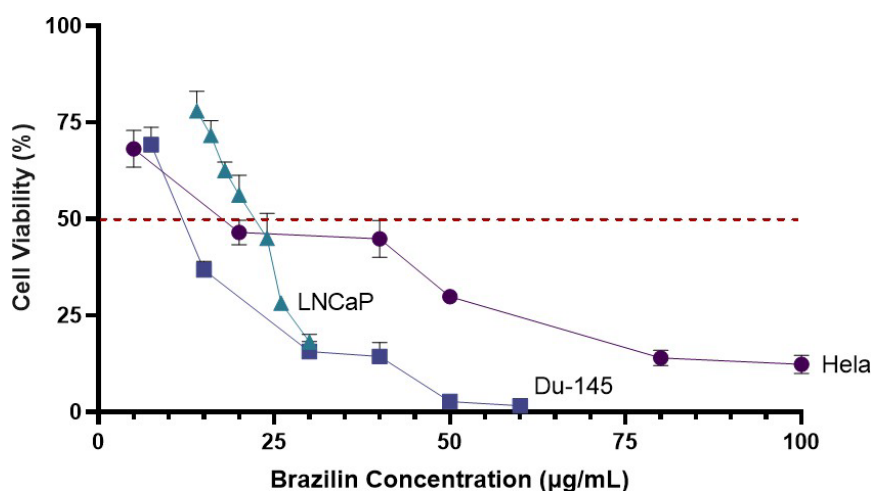


Figure 2. Cytotoxicity profile of Brazilin against Hela, LNCaP, and DU-145 cell lines

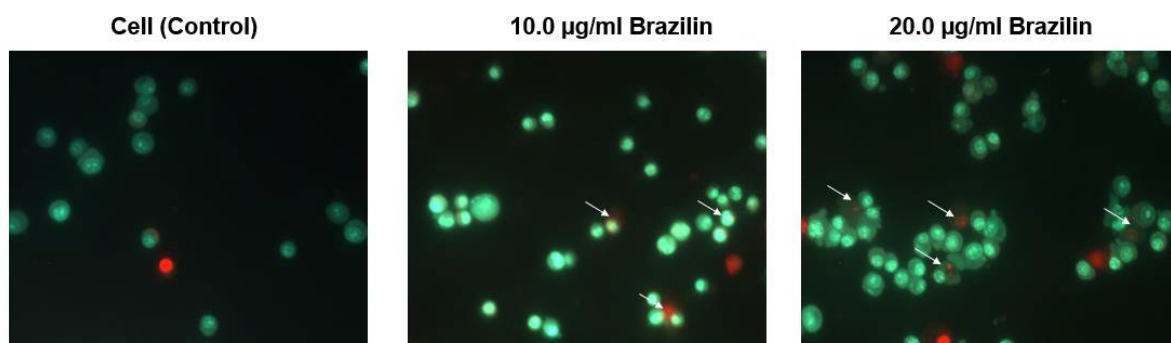


Figure 3. The morphological assessment of apoptosis was monitored using fluorescence microscopy. Red color indicated apoptosis phase and green was viable cells.

Conclusion

In conclusion, brazilin has been successfully labelled with [^{131}I]NaI with the radiochemical purity reach greater than 90%. Brazil showed potential cytotoxicity against prostate and cervical cancer cell lines by in vitro study. These results may hold great promise for the development of [^{131}I]I-brazilin as a radiopharmaceutical candidates. However, the radiosynthesis conditions must be optimized to improve the radiochemical purity, storage stability of [^{131}I]I-brazilin and the molecular mechanism of [^{131}I]I-brazilin must be investigated further.

Characterization of glucose transporters (GLUT 1 and 3) and hexokinase-2 (HK2) expressions in aggressive B-cell lymphomas and their associations with [¹⁸F]FDG PET semi-quantitative parameters

W. F. Alves¹, F. C. Neto^{1,2}, G. de Prince Garcia^{1,2}, M. Bonatelli¹, J. A. S. Otteiro¹, F. F. Barbin¹, E. C. A. Silva¹, C. M. Pinheiro^{1,2}

¹Barretos Cancer Hospital – Pio XII Foundation, Brazil

²Faculdade de Ciências da Saúde de Barretos (FACISB) Dr. Paulo Prata, Brazil

Background

Lymphomas are neoplasms derived from abnormal growth of B and T lymphocytes and natural killer cells, accounting for approximately 4% of neoplasms worldwide. Its treatment is mainly based on its histological/molecular classification and staging based on metabolic imaging findings from [¹⁸F]FDG PET/CT. Among all types of lymphomas, the group of aggressive B-cell lymphomas (BCL) has a greater diversity of response to treatment as it presents greater biological and genetic distinctions. In this context, the characterization of the expression of glucose transporters (GLUT 1 and 3) and hexokinase (HK2), some glycolytic metabolism proteins, and their associations with [¹⁸F]FDG PET semi-quantitative parameters can help to understand better the BCL microenvironment and the results could be used to search for new therapeutic approaches.

Methodology

This study is based on a retrospective collection of clinical data and analysis of tumour samples collected by excisional biopsies or core biopsies from 90 patients (over 18 years of age) with confirmed aggressive BCL (such as diffuse large B-cell lymphoma, follicular lymphoma, marginal zone lymphoma, MALT, etc) and who underwent staging [¹⁸F]FDG PET/CT before the start of treatment. The PET/CT images were evaluated using AW Server 2.0® and Fiji processing software by one nuclear physician (10 years experience). Immunohistochemistry was performed on histological sections of samples to characterize GLUT1 and 3 (membrane expression) and HK2 (cytoplasmic expression) in the tumour and stromal compartments. In the tumour compartment, the following semi-quantitative grading was used: 0: 0% positive cells; 1: <5% positive cells; 2: 5-50% positive cells; 3: >50% positive cells. The expression intensity of the marking was graded as 0: negative; 1: weak; 2: intermediate; 3: intense. The final grading was given by the sum of the extension and intensity parameters and grouped into negative (score of 0 or 2) and positive (score of 3 to 6). In the stroma, cases that showed staining in benign non-lymphomatous cells were considered positive, and cases with no staining or non-specific staining were negative.

Results

Of 90 patients, there were 51.1% men, 58.9% ≤ 60 years old, and 35.6% have Bulky lesions. The Ann-Arbor System/Lugano Classification's Stages I, II, III, and IV were 17.8%, 23.3%, 14.4%, and 44.4%, respectively. The tumoural expressions of GLUT1, GLUT3, and HK2 were 4.5%, 0.0% and 68.9%, respectively. For the stromal expressions, there were GLUT1 in 24.7%, GLUT3 in 45.6%, and HK2 in 82.8% of the cases. In the general context of the sample, the following mean values (minimum and maximum) of [¹⁸F]FDG PET were observed: SUV_{max} = 25.78 (3.70 - 51.26); SUV_{mean} = 12.50 (1.82 - 33.89); SUV_{peak} = 20.52 (3.08 - 44.78); MTV = 445.19 (1.77 - 4634.03); and TLG = 4674.43 (12.25 -

26963.87). There was no association between the stromal expressions of GLUT1 and 3 and tumour and stromal expressions of HK2 and the semi-quantitative parameters of the [¹⁸F]FDG PET. Figure 1 shows examples of the characterization of tumour GLUT1 and the presentation of the respective biopsy sites on [¹⁸F]FDG PET.

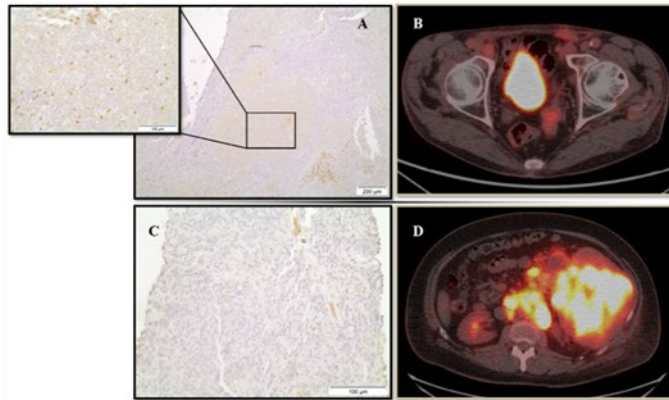


Figure 1. A. Immunohistochemistry with positive expression of GLUT1 in a patient with follicular lymphoma (magnification 200x). The labeling remained restricted to the lymphoid follicles (magnification 400x). B. On PET-CT, lymph node/thickening is observed in the left inguinal canal, with SUVmax = 3.7. C. Immunohistochemistry with no tumoral GLUT1 expression in a patient with DLBCL (magnification 400x). D. On PET-CT, intra-abdominal lymph node enlargement and splenomegaly are observed, with SUVmax = 40.38.

Conclusion

This study indicates that tumour expressions of GLUT1 and 3 do not appear to play a significant role in the metabolic remodelling of aggressive BCL and the uptake of [¹⁸F]FDG by neoplastic lesions. Although there was no significant association, higher stromal GLUT3 expression was observed in patients with hypermetabolic lesions on [¹⁸F]FDG PET. News studies that evaluate the tumour microenvironment in the context of proteins related to glycolytic metabolism and their associations with [¹⁸F]FDG PET will help to better understand tumour metabolic remodelling and allow new therapeutic approaches.

Adding Radiomics PET [¹⁸F]FDG increases accuracy to response prediction of aggressive B-cell B Lymphoma in a model based on machine learning: a pilot study

W. F. Alves¹, M. Furlan², F. C. Neto^{1,3}, G. de Prince Garcia^{1,3}, J. A. S. Otteiro¹, C. M. Pinheiro^{1,3}

¹Barretos Cancer Hospital – Pio XII Foundation, Brazil

²Instituto Tecnológico de Aeronáutica (ITA), Brazil

³Faculdade de Ciências da Saúde de Barretos (FACISB) Dr. Paulo Prata, Brazil

Background

Lymphomas are neoplasms derived from the abnormal growth of B and T lymphocytes and natural killer cells and account for approximately 4% of neoplasms worldwide. Its treatment is mainly based on its histological/molecular classification and staging based on metabolic imaging findings from [¹⁸F]FDG PET/CT. Among all types of lymphomas, the group of aggressive B-cell lymphomas has a greater diversity of response to treatment as it presents greater biological and genetic distinctions. Faced with this scenario, deepening knowledge regarding the molecular nature and its associations with imaging patterns in aggressive B-cell lymphomas can help in defining more efficient therapies. In this context, the evaluation of radiomics parameters from [¹⁸F]FDG PET has been gaining increasing prominence and this pilot study seeks to evaluate the benefit of adding radiomics values to a chemotherapy response prediction model based on artificial neural networks in aggressive B-cell lymphomas.

Methodology

The present study is based on a longitudinal design with retrospective collection of [¹⁸F]FDG PET parameters from 96 consecutive patients with pathological diagnosis of aggressive B-cell lymphomas, such as diffuse large B-cell lymphoma, follicular lymphoma, marginal zone lymphoma, MALT, etc. Staging images taken before the start of chemotherapy were analysed, from October 2016 to June 2020, on a single PET/CT equipment (Discovery 710, GE Healthcare, USA) and with the same acquisition protocol. The [¹⁸F]FDG PET/CT images were evaluated using AW Server 2.0® (GE Healthcare, USA) and Fiji (Open Source ImageJ software) processing software to collect semi-quantitative and radiomic parameters. PET/CT images to response assessment, based on the 5-point Deauville Score, were used to classify patients into responders (Deauville score = 1, 2 or 3) and non-responders (Deauville score = 4 or 5). Clinical and imaging data were grouped into 3 distinct categories: Category A (clinical data including age, LDH levels, ECOG, involvement of extranodal sites, staging, cells of origin), Category B ([¹⁸F]FDG PET semiquantitative parameters, including SUV_{max}, SUV_{mean}, SUV_{peak}, MTV and TLG) and Category C (radiomics parameters such as Entropy, Homogeneity, Contrast, ASM, Difference entropy, Difference variance, Correlation, Cluster prominence, Cluster shade, Measure of correlation 1, Measure of correlation 2, Inverse difference moment, Maximum probability, Sum average, Sum entropy and Sum variance). For the architecture of the artificial neural networks (ANN), the Multilayer Perceptron (MLP) model available in the SPSS 29.0 software was chosen. The configuration used for the training and testing sample was 70/30, with the neural model being run 30 times for each of the situations evaluated (210 times in total). To analyze the ANN models, the following adjustment indices were used: accuracy (ACC), ROC curve (AUC), sensitivity (S), specificity (E), G-mean, F1-score, positive predictive value (PPV) and negative predictive value (NPV).

Results

In the sample evaluated, 81.1% of patients were treated with R-CHOP as systemic therapy. In those undergoing radiotherapy (n = 33), the response assessment's PET/CT was performed after the end of all treatment in only 9 patients (27.2%). ANN models were created in 7 different situations, analyzing each category individually or making combinations between them. The ANN model that combined all categories (A + B + C) – Model 7 - had the best performance in the test phase for predicting response to treatment (S = 95.2%; E = 83.3%; ACC = 92.6%; G-mean = 89.1%, F1-score = 95.2%; PPV = 95.2% and NPV = 83.3%). The ROC curves and respective AUC values can be seen in Figure 1, highlighting Model 7 with AUC = 96.0%.

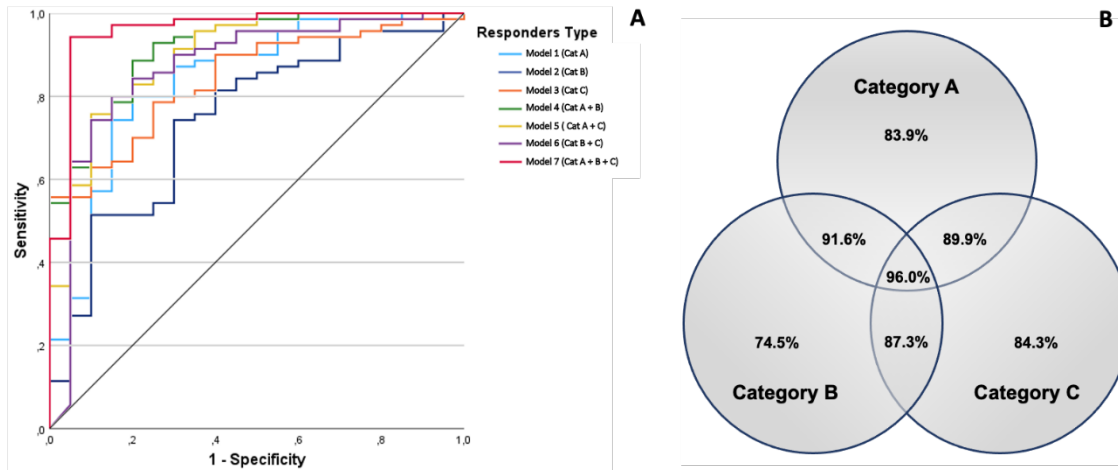


Figure 1. A. Graphical representation of the ROC curves of the evaluated models. B. Venn's diagram with the area under the curves ROC's values for the evaluated models.

Conclusion

According to the results observed in this pilot study, adding [¹⁸F]FDG PET radiomics parameters increases the accuracy of predicting response to treatment for aggressive B-cell lymphomas in a model based on artificial neural networks.

In Silico Study of Benzothiazole Derivatives in the Development of Hybrid (radio-fluorescent) Compounds for Imaging Guided Surgery Breast Cancer

E. M. Widayari^{1,2}, B. Permana¹, M. Santoso³, D. H. Tjahjono¹

¹ School of Pharmacy, Bandung Institute of Technology, Indonesia

² Research Center for Radioisotope, Radiopharmaceutical, and Biodosimetry Technology, National Research and Innovation Agency Indonesia

³ Research Center for Radiation Detection and Nuclear Analysis Technology, National Research and Innovation Agency Indonesia

Background

The use of radio-fluorescent hybrid compounds as surgical guides for cancer offers, the possibility of surgical procedures that achieve complete clearance of cancer cell tissue and improve safety by avoiding unnecessary damage to normal cells. Combining nuclear and fluorescent moieties in one targeting molecule/hybrid compound (radio-fluorescence) offers more valuable benefits than utilizing radiopharmaceuticals or fluorescence only. Benzothiazole derivatives have been reported to be highly efficacious moieties in the development of cancer candidates. To predict the best compound design based on time effectiveness, cost, and reduction of chemical waste, in silico studies need to be carried out.

Methodology

In the present study, a series of benzothiazole derivatives combine 2-benzothiazole-acetonitrile and 2-benzothiazole-amine with FITC fluorophore using linker intermediate and iodine-131 as radioisotope were designed and evaluated the binding affinity with estrogen receptor (PDB ID: 3ERT) by employing molecular docking and dynamic simulation. The molecular docking was performed with AutoDock 4.2, while molecular dynamics simulation was done using AMBER 22.

Results

Molecular docking simulations were performed for the compounds of ¹³¹I-BAF-01, ¹³¹I-BAF-02, ¹³¹I-BNF-01, ¹³¹I-BNF-02, and ¹³¹I-BNF-03 to interpret their activities based on their binding interaction with estrogen receptors. Five designed benzothiazole hybrids showed free binding energy of -5.96, -9.41, -9.29, -11.18, and -9.77 kcal/mol, respectively. Molecular Dynamic simulation of five designs showed that all the ligands were stable in the binding pocket of the receptor during simulation (200 ns) as indicated by the root-mean-square-deviation (RMSD) value. An analysis of protein residue fluctuation of hybrid compounds binding demonstrates that in all complexes, hybrid compounds produce minor fluctuation on amino acid residues. The molecular mechanics Poisson-Boltzmann surface area (MM-PBSA) free energy calculation shows that the binding affinities of hybrid compounds were comparable with tamoxifen (OHT) as a potential inhibitor. The result shows that both electrostatic and van der Waals interaction are the main forces that control the interaction of hybrid compounds with tamoxifen.

Conclusion

This study evaluated the binding of five designed hybrid compounds to estrogen receptors. It shows that all five benzothiazole derivatives hybrid compounds were able to bind to estrogen receptors and were

stable for 200 ns as observed by the molecular dynamic simulation. The binding affinities of ^{131}I -BAF01 and ^{131}I -BNF03 compounds were higher than tamoxifen so it is hoped that this hybrid compound can produce the desired pharmacological response as a surgical guide compound that can differentiate between cancer cells and normal cells and these two compounds will then be synthesized and tested both in vitro and in vivo.

Labeling of Penta-Gama-Vunon-1 (Pgv-1) With ¹³¹I Using CuSO₄.2H₂O and Centrifugation - A Facile Method with Potential For Radio-Iodination

M. Syaifudin¹, M. B. Febrian¹, M. Munir¹, A. Aries¹, A. M. Forentin¹, R. Y. Utomo², M. Ikawati², R. A. Susidarti², E. Meiyanto²

¹ Research Center for Radioisotope, Radiopharmaceutical and Biodosimetry Technology, Research Organization for Nuclear Energy, National Research and Innovation Agency (BRIN), Indonesia

² Cancer Chemoprevention Research Center, Faculty of Pharmacy, Universitas Gadjah Mada, Indonesia

Background

Curcumin analogues labeled with radio-halogens are useful for the imaging and treatment of some cancers, such as those of the breast. PGV-1, a curcumin analogue, has potent anticancer activity in some types of cancer models, such as breast, pancreatic, cervical, colon, and brain cancers by inhibiting cancer cell growth and inducing apoptosis. PGV-1 also showed a much better tumour-suppressing effect than that of curcumin and did not exhibit any harmful effects in the tested animals. The challenges are to increase its cytotoxic activities, confirm stability, and further explore their potential and feasibility to be used in therapy and diagnostic after being labeled with a radioisotope.

Methodology

Herein, we report an efficient method for the iodination of PGV-1 with CuSO₄.2H₂O followed by centrifugation of a mixture. For labeling, 1.5 mg of PGV-1 and 1.0 mg of CuSO₄.2H₂O were dissolved in 1 mL of isopropyl alcohol, mixed well, and then around 550 μ Ci of Na-¹³¹I was added. A mixture of CuSO₄.2H₂O and Na-¹³¹I (without PGV-1) was used as a blank solution (control). These mixtures were shaken for various times (1, 3, 5 h) at 700 RPM at 65°C, followed by centrifugation at 12,000 RPM for 5 minutes at RT. The radiochemical purity (RCP) in the supernatant was then measured with thin layer chromatography (TLC) using saline as a mobilizing agent, where 7 and 1 minute were the times for TLC running and radioactivity counting, respectively. The stability of the labeled compound was determined at 0, 20, 24 h, and 4 days at RT with a similar TLC method. The experiment was done in duplicate.

Results

Results showed that the RCP was 24.65%; 97.52%, and 80.02% for 1, 3, and 5 h of mixing times, respectively, indicating the optimal time for radio-iodine labeling of PGV-1 was 3 h. The blank solution also showed a similar pattern of RCP, where its percentage was altered with the time elapsed. The properties of solution were acidic (pH~5). Stability evaluation revealed that the labeled compound of 3 h shaking that resulted in highest RCP was quite stable at RT, where 97.52% at the beginning was decreased to 82% at 20 h, and was further decreased to 78% at 24 h, however, it was increased to 88.49% 4 days post labeling, possibly due to the radioactivity. It is suggested if sodium iodide is added to a copper sulfate solution, a redox reaction occurs in which the iodide ion converts cupric ion, to cuprous ion, before being oxidized to iodine which then easily react nucleophilically with hydrogen of ring of PGV-1 being labeled.

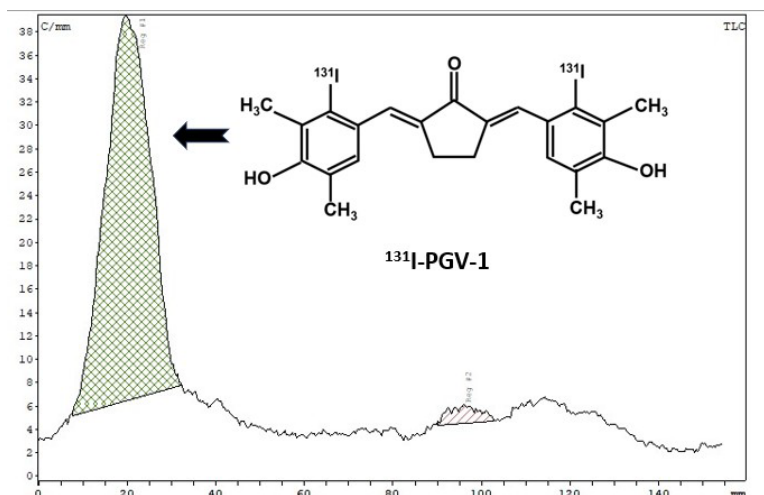


Figure 1. TLC results showing RCP 97.52% of labeled PGV-1 with iodine and its proposed chemical structure.

Conclusion

It was concluded that PGV-1 was simply radiolabeled with iodine in the presence of Cu as an oxidator, with a high RCP that was quite stable up to 24 h at RT that holds promise and facile for development into a method for radio-iodination.

Comparative performance of FDG PET/CT for end of anti-tuberculosis treatment response assessment in pulmonary tuberculosis patients with and without HIV infection

A. Ismaila¹, I. O. Lawal^{1,2}, G. O. Popoola³, M. Mathebula⁴, I. Moagi⁴, K. Mokoala¹, N. Moeketsi⁴, M. Nchabeleng⁴, C. Hikvam⁵, M. Hatherill⁵, B. P. Fourie⁶, M. M. Sathekge^{1,7}

¹ Department of Nuclear Medicine, University of Pretoria, South Africa

² Department of Radiology and Imaging Sciences, Emory University, United States

³ Saxon Court Lincolnshire Partnership NHS Foundation Trust (LPFT), Lincoln, United Kingdom

⁴ Department of Medical Microbiology and MeCRU, Sefako Makgatho University of Medical Science, South Africa

⁵ South African Tuberculosis Vaccine Initiative, Institute of Infectious Disease and Division of Immunology, Department of Pathology, University of Cape Town, South Africa

⁶ Department of Medical Microbiology, University of Pretoria, South Africa

⁷ Nuclear Medicine Research Infrastructure (NuMeRI), Steve Biko Academic Hospital, South Africa

Background

Pulmonary residual metabolic activity (RMA) is prevalent on FDG PET/CT imaging of patients who completed a standard course of anti-tuberculous therapy (ATT) for pulmonary tuberculosis (PTB). RMA has an association with tuberculosis relapse. We aimed to evaluate the impact of RMA on EOT FDG PET/CT in patients with PTB after completing a standard course of ATT amongst HIV-infected and uninfected patients.

Methodology

Approval for this study was granted by the Ethics Committee of the University Hospital of Pretoria. We prospectively recruited patients who were declared cured based on clinical and microbiological assessment after completing a standard course of ATT. All patients subsequently underwent [18F]FDG PET/CT within two weeks of completing ATT. We determined the proportion of patients who had RMA in the lungs as well as CT features suggestive of active PTB including lung consolidation, pulmonary nodules, lung changes in tree-in-bud pattern, hilar/mediastinal lymphadenopathy, and pleural effusion. All patients were followed up for 6 months to evaluate for relapse. Confirmatory bacteriologic testing was performed in patients with suspected relapse who demonstrated symptoms. In those who relapsed, a repeat FDG PET/CT imaging was subsequently performed.

Results

We studied 75 patients including 50 HIV-infected individuals with a mean age of 36.09 ± 10.49. Median CD4 count among HIV-infected patients was 255 cells/mm³ (IQR: 147–448). HIV viral load was 12497 copies (IQR:158-38841). HIV-infected patients had lower hemoglobin levels (13.07±1.78 g/dL versus 14.24±2.07, p=0.021) and higher C-reactive protein levels (5.70 versus 1.20, p=0.001) compared with HIV-uninfected patients. All other baseline clinical and demographic characteristics were not significantly different between the groups. Forty-one patients had RMA and its incidence was not significantly different between HIV-infected and uninfected patients (p=0.101). Thirty-four patients demonstrated complete metabolic response (CMR) to ATT. In the RMA group, 3 patients relapsed on

follow-up, whereas no tuberculosis relapse was demonstrated in those with CMR. Among the four CT features of active PTB, only metabolically active nodes were more prevalent among HIV-infected compared with uninfected patients (50.0% versus 5.9%, $p=0.003$) while the incidence of the other three CT features of active PTB was not significantly different between HIV-uninfected patients with RMA versus HIV-uninfected patients ($P>0.05$ in all cases).

Conclusion

FDG PET/CT imaging demonstrates a high prevalence of RMA among patients treated with a standard course of ATT for PTB, with a similar incidence between HIV-infected and uninfected patients. The risk of relapse within 6 months after completing ATT in patients with CMR is negligible. This study further iterates the potential of FDG PET/CT imaging in determining the optimal treatment duration in the management of patients with drug-sensitive PTB. However, tuberculosis relapse may be seen in 9% of patients within 6 months of completing ATT. The incidence of CT lung changes suggestive of active PTB was similar between the groups, indicating that the presence of HIV coinfection may not influence the interpretation of EOT FDG-PET/CT obtained for PTB treatment response assessment.

Single [¹⁸F]Fluoroestradiol ([¹⁸F]FES) negative FDG/NaF positive lesion as a predictive factor of molecular heterogeneity and hormonal treatment fail in metastatic estrogen positive (ER+) breast cancer patient. A case report.

N. Rasulova, E. A. Muhamed Hassanein, A. Alshammari, S. Contu, O. Ragab

Al-Adan Hospital, Kuwait

Background

While the [¹⁸F]FDG estimates the glucose metabolism and wide use in management of the breast cancer patients (BCP) for staging, restaging and follow-up, the [¹⁸F]FES is used for the detection of estrogen receptor status in patients with recurrent or metastatic ER+ breast cancer.

Aim: To estimate possibility of molecular heterogeneity by combined [¹⁸F]FES and [¹⁸F]FDG PET/CT scans and role of single FES negative metastases in its role in treatment response by follow-up FDG and NaF.

Methodology

A 29-year-old female with ER+ initially metastatic breast cancer, after excessive treatment for 2 years with almost metabolically negative bone metastases and mildly FDG-avid primary lesion, being on Femara, Zoladex and Xgeva, underwent [¹⁸F]FES and [¹⁸F]FDG scans, after discovering the new axillary metastases followed by series [¹⁸F]FDG and [¹⁸F]NaF for follow up scans.

Results

[¹⁸F]FES and [¹⁸F]FDG scans showed matching FES/FDG-avid primary right breast lesion and axillary lymph nodes (SUV_{max} FES/FDG for primary lesion 6.33/1.89 and axillary lymph nodes 7.58/6.15) as well as FES negative FDG-positive in newly developed bone lesion in the head of left femur (FDG SUV_{max} 3.65), confirmed by NaF PET/CT scan. Patient refused to change the therapy and on close follow up within one-month FDG showed a disease progression at the primary site (FDG SUV_{max} raised to 2.45, on further follow-up scans to 7.5), axillary lymph nodes became multiple with (SUV_{max} 6.58), and on NaF scan progression of the lesion in the head of left femur as well as reactivation of the old metastases. Farther follow up cases showed a disease progression on Faslodex, Xgeva and Afinitor and only when therapy was adjusted with Capecitabine the FDG scan showed disease regression.

Conclusion

A single FES negative/FDG positive lesion may indicate presence (appearance) of early metabolic heterogeneity and require the treatment modification in patient on hormonal treatment.

Initial experience in [¹⁸F]Fluoroestradiol ([¹⁸F]FES)/FDG PET/CT scan patterns in estrogen positive (ER+) breast cancer patients

O. Ragab, E. A. Muhamed Hassanein, A. Alshammari, S. Contu, N. Rasulova

Al-Adan Hospital, Kuwait

Background

About 75% of breast cancers are estrogen positive (ER+) at the time of diagnosis. However, in metastatic breast cancer, ER expression can be heterogeneous or may change over the time. In this case, [¹⁸F]FES/FDG could be useful to estimate ER expression and glucose metabolism.

Aim: To compare [¹⁸F]FES/FDG PET/CT patterns in initially ER+ breast cancer patients.

Methodology

3 ER+ breast cancer patients underwent both [¹⁸F]FES and [¹⁸F]FDG PET/CT. First patient 82-year-old left breast cancer being on Femara; Second patient 50-year-old on Femara, Abenaciclib and Xgeva and third 29-year-old patient being on Femara, Zoladex and Xgeva.

Results

Scans of the first patient showed partially matching FES/FDG uptake in the left breast lesion with FES/FDG SUV_{max} 5.99 and 6.44 respectively, likely representing the heterogeneity of breast lesion with partially presence and absence of estrogen receptors, further US showed mild decreased in size of the left breast lesion. In addition to a newly developed mismatched FES negative FDG positive right breast lesion, likely representing absence of estrogen receptors in the right breast: the further core biopsy showed the abscess with xanthomatous reaction in the right breast lesion.

Scans of the second patient showed matching low-grade FES/FDG uptake in the right breast lesion SUV_{max} 1.5 and 3.42 respectively, suggesting for low expression of ER. On follow up [¹⁸F]FDG PET/CT scan after 5 months there was a stable disease at the primary site with no worrisome hypermetabolic lesions to suggest locoregional or distant metastases.

Scans of the third patient showed matching FES/FDG uptake in the right breast nodule (SUV_{max} 6.33 and 4.76 respectively), matching FES/FDG uptake in right axillary lymph nodes the larger nodule FES/FDG (SUV_{max} 7.58 and 6.15 respectively), the smaller FES/FDG (SUV_{max} 3.38 and 2.14), and newly developed mismatched FES negative FDG positive bone lesion with SUV_{max} 3.65. In this patient expression of FES uptake at primary and metastatic axillary lymph nodes higher than FDG uptake. However, single FES-negative bone lesion was worrisome, representing absence of ER. On follow-up scans during one year with [¹⁸F]FDG and NaF there was significant disease progression till the patient switched the hormonal therapy into the chemotherapy.

Conclusion

Our initial experience showed 4 FES/FDG patterns: matching, partially matching with high ER expression, matching with low ER expression and mismatching FES/FDG pattern. The radiological and histopathological correlation in mis-matching patterns is needed to exclude other than molecular heterogeneity related to the loss/absence ER expression reasons at the primary site such as possibility of

having inflammatory/infection conditions. But the absence of ER related with true molecular heterogeneity is the signal for further disease progression.

PET/CT in diagnosis and staging of lung cancer

A. A. Khikmatov¹, S. S. Astasiev¹, G. G. Arifkhodzhaev²

¹ National Children's Medical Center, Uzbekistan

² Republican Specialized Scientific and Practical Medical Center for Surgery, Uzbekistan.

Background

To determine the role of positron emission tomography (PET) with computed tomography (CT) in improving the results of diagnosis and staging of lung cancer and to present diagnostic capabilities in the assessment of previously identified lesions in the lungs during and outside of screening according to the recommendations of Fleischner, British Thoracic Societies, Lung-Rads

Methodology

An analysis was carried out directly of the results of 46 patients who were treated in specialized departments of the Republican Scientific and Practical Medical Center of the Ministry of Health of the Republic of Uzbekistan in the period from 2022 to 2023. Under our supervision, there were 46 patients with various nosological forms: peripheral lung cancer - 24 patients, central lung cancer - 15 patients, NSCLC 7 patients. Staging according to TNM classification: T1N0M0 - 28 patients, T2N0M0 - 11 patients, T2N1M0 - 7 patients.

Examples are presented of assessing lesions suspected of lung cancer detected at early stages in patients under a screening program in the period from November 1, 2022 to December 31, 2023, according to existing international recommendations on the management of lesions and staging of lung cancer.

Results

Presented possibilities of PET/CT with 18F-Fluorodeoxyglucose (FDG) to determine the management tactics of patients with previously identified pulmonary nodules on time and outside of screening according to low-dose computed tomography (LDCT) and computed tomography (CT) of the chest according to recommendations Fleischner, British Thoracic Society (BTS), LungRads make it possible to differentiate with a high degree of certainty benign changes in the lungs according to the type of foci (fibrosis, intrathoracic lymph node, granuloma) and nodal changes characteristic of malignant processes (reactive in nature, primary, secondary lung cancer), based on such characteristics of foci as growth, structure, metabolic activity.

We studied [18F]FDG PET/CT characteristics for staging lung cancer.

Conclusion

Clinical studies demonstrate diagnostic methods PET/CT with [18F]FDG has great diagnostic capabilities. In visualizing lesions in the lungs at the earliest possible time, which makes it possible to establish stages and start treatment in a timely manner. In dynamics after chemotherapy (treatment effectiveness), and thus influence on the quality of life and improve the vital prognosis of patients with lung cancer.

Significance of positron emission tomography with computed tomography of the breast in the diagnosis of breast cancer

A. Khikmatov¹, S. Astasiev¹, G. Arifkhodzhaev²

¹National Children's Medical Center, Uzbekistan

²Republican Specialized Scientific and Practical Medical Center for Surgery, Uzbekistan

Background

For breast cancer (BC), a multimodal approach including positron emission tomography computed tomography (PET/CT) of the breast has been defined, especially when conservative surgery is being considered, as it is the most sensitive method for identifying additional sites of disease.

Methodology

Data from mammography "Siemens Nova 3000" (MG), ultrasound "GE Logiq P5" (US) and PET/CT with [¹⁸F]FDG "GE Discovery IQ" were compared with the morphological picture as the "gold standard". All patients underwent histological examination of the identified formations. 70 women aged from 21 to 56 years were examined. The average age of the patients was 39 years. In our studies, 21 (%) women had relatives who had breast cancer on the maternal side - of these, in 2 patients the mother suffered from bilateral breast cancer.

Results

In total, we identified 6 (8.6%) fibroadenomas, 25 (35.7%) cases of breast cancer, of which 2 (8.0%) were intraductal cancer, 9 (36.0%) were infiltrative lobular cancer, 14 (56.0%) - infiltrative ductal cancer. During clinical examination, breast cancer was not detected in 10 out of 25 cases. In MG, signs of breast cancer were detected in 16 (64.0%) of 25 patients. The main reason for false-negative results was the high radiological density of the breast in 7 (77.8%) patients, which is explained by the predominance of young women under 40 years of age in this group. False-negative ultrasound results occurred in 1 (4.0%) case with CADMG and in 5 (20.0%) cases with small sizes of detected formations, their deep localization and large volume of the breast. False-positive results with ultrasound occurred in 3 cases with hypervascularized fibroadenomas and in 1 case with a glandular lobule. FDG PET/CT revealed 18 breast cancers in 23 (92.0%) of 25; Congenital malformations were diagnosed in both cases. In addition, in 3 (12.0%) cases, PET/CT with [¹⁸F]FDG revealed breast cancer in women without clinical symptoms with negative results of MG and/or US (in one patient MG was not performed due to the presence of an implant, which increases the role PET/CT with [¹⁸F]FDG in women with endoprosthetics). PET/CT with [¹⁸F]FDG allowed not only to detect a greater number of cases of breast cancer (intraductal cancer) compared with MG and ultrasound, but also to diagnose breast cancer in clinically and radiologically hidden formations. Due to the low efficiency of standard examination methods (MG and US), there was a need to include an additional method that allows objective characterization of changes in breast tissue.

Conclusion

The PET/CT technique showed high sensitivity in detecting early breast cancer, regardless of the age of the patients. Our study, like many others, confirms the feasibility of using an integrated approach in the diagnosis of hereditary breast cancer using PET/CT along with MG and ultrasound.

Sestamibi parathyroid scintigraphy combined with SPECT CT in the preoperative localization of parathyroid ectopias: Report of five cases

N. I. Alaoui

Department of Nuclear Medicine, University Hospital Hassan II, Faculty of Medicine and Pharmacy, Sidi Mohamed Ben Abdellah University, Morocco

Background

The ectopic parathyroid adenoma is a source of topographic diagnostic difficulties especially for purely morphological examinations. The major interest of parathyroid scintigraphy in primary hyperparathyroidism is the localization of ectopias whose incidence is about 15%. SPECT CT allows 3-D localization of the parathyroid glands and gives more precise anatomic localization thus facilitating their surgical treatment. The aim of this work was to evaluate the value of a tomographic acquisition in addition to planar imaging in the context of the ectopic localizations of the parathyroid glands through 05 clinical cases explored isotopically.

Methodology

This is a retrospective study of 143 patients referred to the nuclear medicine department for preoperative assessment of a primary or secondary hyperparathyroidism. The acquisition protocol included planar images (technetium-99m thyroid scan, early and late technetium-99m Sestamibi cervicothoracic acquisition and a cervicomediastinal SPECT CT).

Results

Of the patients referred 61 had primary hyperparathyroidism, including 5 patients with parathyroid ectopia. They were 5 women aged between 26 and 70 years. They all had hypercalcemia associated with elevated PTH. Cervical ultrasound was positive in one patient while parathyroid scintigraphy showed parathyroid ectopia in all cases. The complement by SPECT CT allowed an optimal anatomical identification which optimized surgical management.

Conclusion

Preoperative imaging hyperparathyroidism's primary purpose is to determine precisely and reliably position and the reports of the pathological gland in order to guide the surgical procedure and to propose minimally invasive surgical approaches. technetium-99m MIBI planar parathyroid scintigraphy combined with SPECT CT plays a key role in the precise location of ectopic parathyroid which contributes to an elective and more rapid surgical resection of these lesion.

First results of radioiodine therapy in the Republic of Kazakhstan

K. Serikkanova¹, B. Atantayeva², N. Yesbolatova², B. Kaliyaskarova²

¹ Astana Medical University, Kazakhstan

² Center for Nuclear Medicine and Oncology, Kazakhstan

Background

Radioiodine therapy offers the most efficient and safe treatment for differentiated thyroid carcinoma with distant metastases and thyrotoxicosis.

The East Kazakhstan region has one of the first lines ranks in the incidence of malignant tumours in the country. More than 18 thousand patients are on files.

In June 2021, a radionuclide therapy unit was opened at the “Center of Nuclear Medicine and Oncology in Semey”. This is the first and only unit in the Republic of Kazakhstan, where the method of radioiodine therapy was implemented.

Methodology

Treatment is due to the use of the radiopharmaceutical "Sodium iodide I-131". This is a domestic medicinal radiopharmaceutical, created at the Institute of Nuclear Physics in Almaty and delivered weekly to the radioisotope therapy department on special transport.

The radioiodine therapy procedure involves patients receiving radioactive iodine I-131 by drinking it in the form of an aqueous solution that does not have any organoleptic properties. Next, patients are kept in specialized wards for 5-7 days, equipped with an autonomous ventilation and sewage system (“closed mode”). The patient is discharged when gamma radiation decreases to an acceptable level (20 mSv/h). Patients with thyroid cancer are additionally referred for a scintigraphy study to assess isotope inclusion and further treatment and observation are prescribed.

Results

Over three years (2021-2024), the number of cases treated was 1438, of which thyroid cancer was 974 (Figure1). In 2021, the total number of hospitalized patients with thyroid cancer and diffuse toxic goiter was 135 patients and 82 patients, respectively. In 2023, the total number of hospitalizations increased almost 3 times compared to 2021, and amounted to 445 cases of thyroid cancer and 160 cases of diffuse toxic goiter, respectively.

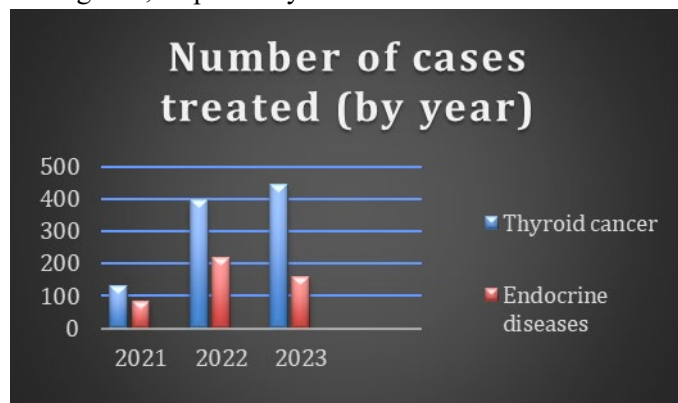
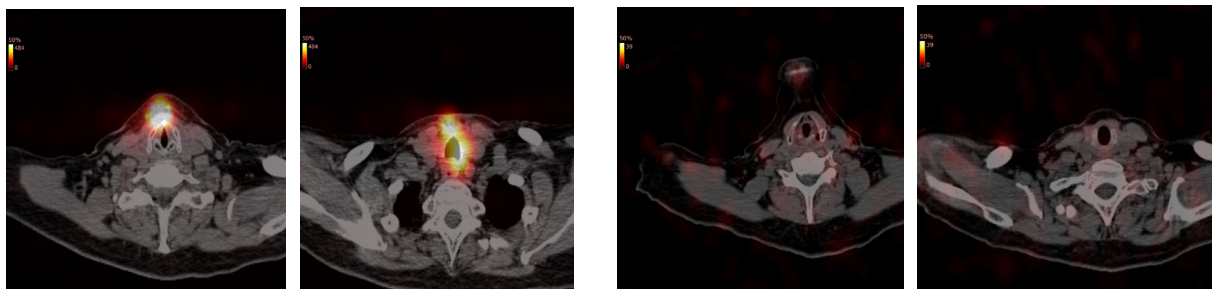


Figure 1. Number of cases treated (by 2021-2023 year).

According to the results of treatment of patients with thyroid cancer, 90% of patients showed an improvement in their condition. Scintigraphy of the whole body after courses of radioiodine therapy revealed a decrease or absence of accumulation of radioactive iodine in the isthmus bed and lobes of the thyroid gland (Figure2).



Whole body scintigraphy before radioiodine therapy

Whole body scintigraphy after 2 courses of radioiodine therapy

Figure 2. Whole body scintigraphy before radioiodine therapy and after 2 courses of radioiodine therapy.

According to the results of treatment of patients with thyrotoxicosis, 78% of patients had a hypothyroid state 6 months after courses of radioiodine therapy. Blood tests for thyroid hormones showed a decrease in free T4 and an increase in TSH. Euthyroidism was observed in 5% of patients. In 17% of patients, there was an improvement in blood parameters for thyroid hormones against the background of a hyperthyroid state.

The 5-year survival rate has not yet been assessed.

Conclusion

Radioiodine therapy has been proven to be an effective and safe treatment for thyroid cancer and thyrotoxicosis. The effectiveness of treatment was 90%.

The use of the radiopharmaceutical "Sodium iodide 131I oral solution" allowed patients to receive treatment within the country without traveling abroad.

This work is supported by the IAEA Technical Cooperation Project (KAZ6013)

Single Centre Data on Distribution of Mediastinal Masses

R. Jagtap, S. Solav

Dr Solav's Spectlab, India

Background

Mediastinal masses are located in one of its four compartments: superior mediastinum, anterior mediastinum, middle mediastinum and posterior mediastinum. There are very few studies on mediastinal masses from India, and most of those are from radiological databases. Here we present a retrospective study spanning from 2014 to 2023 at a stand-alone Nuclear Medicine Facility. We aimed to find the distribution of mediastinal lesions in our region.

Methodology

Retrospective data of PET/CT (positron emission tomography/computed tomography) scans done at our institute from January 2014 to July 2023 was collection. The studies included in the study were [¹⁸F]FDG (fluorodeoxyglucose) PET/CT, [⁶⁸Ga]-DOTANOC (DOTA-1-Nal3-octreotide) PET/CT, [⁶⁸Ga]Ga-FAPI (fibroblast-activation-protein inhibitors) PET/CT and Cardiac PET scans. Patients with histological and clinical diagnoses were included. Lung malignancies were excluded.

Results

A total of 1751 patients were included in the study. The largest group was of patients with lymphoma, consisting of 43.7% of patients. These included Hodgkin and Non-Hodgkin lymphomas. Metastases from primary at another site consisted of 23.1% cases. Primary oesophageal were 16.2% of cases. 9.6 % patients were of granulomatous aetiologies like tuberculosis and sarcoidosis. Thyroid malignancies were 3.5% and thymic tumours were 1.4% of the group. Other mediastinal masses were sarcomas, germ cell tumours, neurogenic tumours, mediastinal neuroendocrine tumours, aneurysms consisting of 0.7%, 0.6%, 0.5%, 0.17%, 0.11% of the cases respectively. 1 case of posterior mediastinal lipoma was detected incidentally which was 0.05% of the total number of the cases. Of all the 1751 cases, 186 patients had benign aetiologies which was 10.6% of the total number of cases. Rest of the 89.4% cases had malignant histology.

Conclusion

Our study demonstrated the distribution of mediastinal masses of various aetiologies. The cases were skewed heavily towards malignant histology. Benign granulomatous aetiology usually presented as pyrexia of unknown origin. Other benign mediastinal masses were usually incidentally detected. The location of the mediastinal mass and age of patient were of importance while considering the diagnosis and treatment of the patient.

FDG PET/CT response evaluation of multi-modality treatment options in NSCLC

G. Biswas, S. Panchadar, Z. Abdullah, R. A. Kordi, S. Mohammed, M. Garashi, E. A. Awadhi

Chest Diseases Hospital, Kuwait

Our aim was to evaluate the role of [18F]FDG PET/CT in assessing post-therapy response of patients with Non Small Cell Lung Carcinoma (NSCLC) who underwent treatment with multiple modalities.

Methodology

We performed baseline and post treatment follow up [18F]FDG PET/CT in 36 patients (24 males, 12 females), age: 45-84 years with primary Non Small Cell Lung Carcinoma (NSCLC). All of them were referred to our department for initial staging and assessing response following treatment after an interval of 6-18 months. 5 patients had surgery, 9 patients had chemotherapy, 1 patient had radiotherapy, 7 patients had targeted molecular therapy, 2 patients had immunotherapy, 3 patients had surgery and chemotherapy, 2 patients had surgery and radiotherapy, 3 patients had chemotherapy and immunotherapy, 2 patients had surgery, chemotherapy and radiation therapy, 1 patient had chemotherapy and immunotherapy and 1 patient had radiotherapy, chemotherapy and immunotherapy. We performed baseline and post treatment [18F]FDG PET/CT from vertex to mid-thigh in all the patients with a 64 slice, 16cms axial FOV (field of view) PET/CT camera (GE 710) 60 minutes after injecting a standard dose of 0.06mCi/kg of [18F]FDG. The images were reconstructed on an Advantage (GE) work station and analysed on a Hermes system by four independent PET/CT readers.

Results

Baseline FDG PET/CT showed disease restricted to lung in 15 patients, loco-regional lymph node metastasis in 11 patients, locally invasive disease in 3 patients and distant metastasis in 7 patients. Following treatment FDG PET/CT PERCIST 1 criteria showed CMR (complete metabolic response) in 8 patients (post treatment changes were observed in 2 patients), PMR (partial metabolic response) in 5 patients, SMD (stable metabolic disease) in 8 patients and PMD (progressive metabolic disease) in 15 patients.

Conclusion

Our study shows that [18F]FDG PET/CT can identify responders and non-responders in patients with NSCLC treated with multiple modalities including targeted molecular therapy and immunotherapy. This may help in designing new treatment options and continue existing ones to improve prognostic outlook in these patients.

Molecular response assessment following [¹⁷⁷Lu]Lu-DOTA-TATE therapy for advanced/inoperable grade 1/2 gastroenteropancreatic neuroendocrine tumours

A. Sood, P. Aggarwal, S. Satapathy, C. K. Das, B. R. Mittal

Post Graduate Institute of Medical Education and Research (PGIMER), India

Background

Peptide Receptor Radionuclide Therapy (PRRT) with [¹⁷⁷Lu]Lu-DOTA-TATE has become one of the main treatment modalities for advanced gastroenteropancreatic neuroendocrine tumours (GEP-NETs), due to its excellent efficacy and safety. The anatomical criteria for response assessment in GEP-NETs show significant limitations and inadequate treatment responses because of disease's indolent nature. An unmet need exists for better imaging biomarkers for early response assessment in NETs, where functional imaging modalities may be useful. This study evaluates the role of [⁶⁸Ga]Ga-DOTA-NOC PET/CT for response assessment in GEP-NETs using the adapted PET response criteria in solid tumours (PERCIST v1.0) and compares it with CT-based response evaluation criteria in solid tumours (RECIST v1.1).

Methodology

This was a prospective single-centre study. After informed consent, consecutive patients with somatostatin receptor-positive, advanced inoperable/metastatic grade 1/2 GEP-NETs were recruited from January 2020 to August 2022 and treated with [¹⁷⁷Lu]Lu-DOTA-TATE. [⁶⁸Ga]Ga-DOTA-NOC PET/CT was repeated 6-8 weeks after two and four cycles of treatment for response assessment. Best morphological response was assessed using RECIST 1.1. For molecular response, a single target lesion with maximum tracer uptake (SUL_{peak}) in each scan was evaluated and changes were assessed using adapted PERCIST. Complete response (CR) was defined as absence of any tracer uptake while a decrease in the SUL_{peak} of ≥30% was considered partial response (PR). Appearance of any new PET positive lesion or an increase in the SUL_{peak} of ≥30% was considered progressive disease (PD). Any case which did not meet any of these criteria was considered to be stable disease (SD).

Results

Fifty-five patients with a median age of 52 years (IQR: 40-61) with advanced GEP-NETs received a median cumulative activity of 29.6 GBq of [¹⁷⁷Lu]Lu-DOTA-TATE. Using CT-based RECIST criteria, 11/55 (20%) patients showed PR, 39/55 (70.9%) showed SD and PD was observed in 5/55 (9.1%) of the patients. Using PERCIST criteria, PR was noted in 21/55 (38.2%) patients, while 29/55 (52.7%) patients had SD and 5/55 (9.1%) patients showed PD. The concordance between the response criteria was 67.3%. Disagreement between the two criteria was noted, particularly for the stable lesions on CT. Of the 39 patients with SD on CT, 14 (35.9%) were re-classified as having PR and none (0) as PD

according to the PERCIST criteria (Table 1).

Best PET response \ Best CT response	PD	PR	SD	Total
PD	5	0	0	5
PR	0	7	4	11
SD	0	14	25	39
Total	5	21	29	55

Table 1: Comparison of responses according to RECIST 1.1 (rows) and adapted PERCIST 1.0 (columns)

Conclusion

GEP-NETs frequently show stable morphological responses on CT following [¹⁷⁷Lu]Lu-DOTA-TATE PRRT; however, PET-based criteria had incremental role in detecting partial responses in over a third of such patients. Molecular response assessment with [⁶⁸Ga]Ga-DOTA-NOC PET/CT using the PERCIST criteria, therefore, may be useful over conventional CT-based criteria, particularly for early treatment response assessment. However, long-term follow-up with overall survival is required to validate its applicability.

Follow up assessment on the first local theranostic intra-cavitary Yttrium-90 citrate colloid irradiation for refractory cystic craniopharyngioma

N. A. Razak

Hospital Kuala Lumpur, Malaysia

Background

Craniopharyngioma is uncommon benign intracranial tumour that may present in solid, cystic or mixed solid-cystic component. In some patients, the anatomical localisation makes the surgery or radiotherapy hazardous and impossible for treatment. We had the first local experience of treating a patient with refractory cystic craniopharyngioma using beta-emitting Yttrium-90 citrate colloid. This case report aims to discuss the follow up assessment of our patient succeeding six months of the irradiation therapy.

Case Presentation

A 43-year-old male who has underlying refractory cystic craniopharyngioma complicated with visual impairment and panhypopituitarism was referred to our department for intra-cavitary irradiation therapy. The theranostic irradiation therapy was performed with the initial diagnostic assessment using Technetium-99m MAA. Based on the diagnostic assessment, the patient was given 6.22mCi of Yttrium-90 citrate colloid via the Ommaya reservoir, to deliver a radiation dose of 300Gy to the tumour. He had no acute complications. However, the patient developed post therapy inflammatory reaction two weeks post therapy which resolved immediately after the initiation of dexamethasone. Post six months of therapy, we observed significant reduction on the aspirated cystic frequency and volume as well as major improvement on the visual function and hormonal level.

Conclusions

This case report highlights the preventable complication as well as the promising clinical outcome of our first local theranostic intra-cavitary Yttrium-90 citrate colloid irradiation therapy. However, further follow-up is necessary to assess the necessity of subsequent irradiation therapy in our refractory cystic craniopharyngioma patient.

Avidity of [⁶⁸Ga]Ga-Radiolabeled CXCR4 ligand in glioblastoma tumours (A preliminary report)

S. Farzanehfar, W. H. Sarhan, M. Abbasi, Y. Salehi

Tehran University of Medical Sciences, Iran

Background

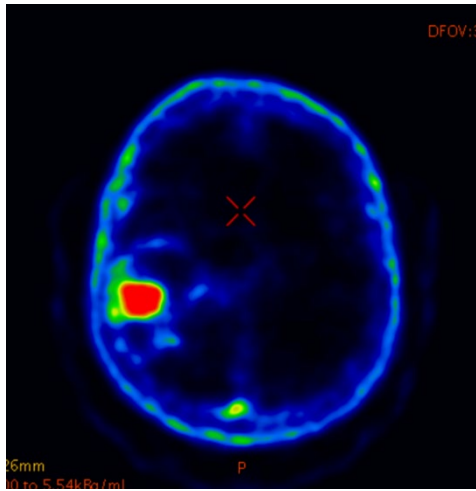
Glioblastoma Multiforme (GBM) harbors the most malignant potential and worst prognosis among adult's primary brain tumours. Chemokine Receptor-4 (CXCR4) is a member of the G protein-coupled chemokine receptor family. It has been reported CXCR4 overexpression association with tumour angiogenesis and poor patient's outcome. Recently a radiolabeled cyclic pentapeptide with high affinity to CXCR4 as [⁶⁸Ga]Ga-Radiolabeled CXCR4 ligand (Cixafor) was developed, which could be applied in PET/CT hybrid imaging characteristics as well as favorable human dosimetry has been developed. Considering previous reports of in vitro CXCR4 expression in glioblastoma multiforme cells, this study was conducted to evaluate its in vivo expression.

Methodology

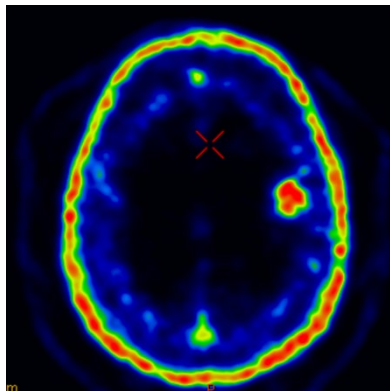
So far, we enrolled six patients with possible diagnosis of glioblastoma multiforme based on brain multi-parametric MRI findings. After signing the consent forms by the patients, the neurologist or neurosurgeon referred the patients for [⁶⁸Ga]Ga-Radiolabeled CXCR4 ligand (Cixafor) PET/CT imaging to the nuclear medicine department. Whole-body PET/CT studies were inspected visually for radiotracer biodistribution, overall tumour imaging characteristics and tumour maximum standardized uptake values (SUV_{max}). Two experienced nuclear medicine physicians drew three-dimensional volume of interest (VOI) around the respective lesions. For calculation of tumour to background ratios (TBR), similar VOIs were placed on contralateral brain tissue and liver parenchyma. After PET/CT imaging the patient underwent brain surgery based off routine institute protocol. Expert pathologist in the field examined tumours and IHC evaluation of CXCR4 ligand on tissue specimens after surgical resection were also done. Independent t-test were performed for evaluation of difference between the SUV of tumours with background and liver tissue as well as the CXCR4 expression in normal and tumoural tissue.

Results

In this preliminary study, glioblastoma multiforme tumours showed considerable difference between tumours SUV_{max} and background SUV_{max}.



Case 1, a middle-aged male known case of brain tumour (GBM), presented with recurrence symptoms one year after primary tumour surgical resection. [⁶⁸Ga]Ga-Radiolabeled CXCR4 ligand uptake is noted on the posterolateral margin of previous surgical bed.



Case 2, newly diagnosed brain tumour, highly suggestive of GBM based on MRI findings. PET/CT showed [⁶⁸Ga]Ga-Radiolabeled CXCR4 ligand uptake in the tumoural tissue which was confirmed GBM after surgical resection.

Conclusion

These results showed GBM tumours potentially express CXCR4 gene evaluated by high uptake of [⁶⁸Ga]Ga-Cixafor on PET/CT imaging.

Keywords: GBM, PET/CT, CXCR4, [⁶⁸Ga]Ga-Cixafor, SUV

Advancing Hybrid Imaging Capabilities through Innovative Collimator Design: A Comprehensive Assessment using MCNP Simulation

M. Mehrabi

Radiation Application Research School, Nuclear Science and Technology Research Institute (NSTRI), Iran

Background

Hybrid imaging, a powerful combination of single-photon emission computed tomography (SPECT) and other modalities such as computed tomography (CT) or positron emission tomography (PET), has revolutionized medical diagnostics by providing comprehensive and multi-dimensional insights into physiological processes. In hybrid imaging systems, the collimator plays a critical role in shaping the radiation field and ensuring accurate detection of gamma photons. Therefore, continuous advancements in collimator design are essential to optimize image quality and diagnostic accuracy in hybrid imaging. Collimator design for hybrid imaging involves striking a delicate balance between resolution and sensitivity. The choice of collimator geometry, material, and thickness significantly impacts the imaging performance. Consequently, a comprehensive assessment of collimator performance is necessary to fine-tune these parameters and improve hybrid imaging capabilities.

Methodology

To conduct a thorough assessment of collimator performance for hybrid imaging applications, a combination of experimental measurements and MCNP simulations was employed. Experimental measurements were carried out using a hexagonal collimator with varying thicknesses of a polyethylene dispersing environment. The full width at half maximum (FWHM) values were measured for both linear and point sources. These experimental results were then compared with the outcomes obtained from MCNP simulations, a widely used Monte Carlo code for modelling radiation transport. Additionally, the study investigated the impact of collimator penetration on gamma sources with energies of 140 keV and 511 keV. By analyzing the interaction of gamma photons with the collimator material, valuable insights were gained into the behaviour of collimator-detected radiation in hybrid imaging systems.

Results

The comparison between the experimental and MCNP simulation results demonstrated an exceptional level of agreement, with a discrepancy of less than 5%. The FWHM values obtained from the MCNP simulations closely aligned with the experimental measurements, providing strong validation of the simulation approach for hybrid imaging applications. This close agreement indicates the accuracy and reliability of the collimator design in accurately capturing and registering gamma radiation information in hybrid imaging systems.

Furthermore, the study revealed a significant correlation between FWHM values and the thickness of the dispersing environment as well as the energy of the gamma source. This correlation provides valuable insights into optimizing collimator parameters for enhanced resolution and overall imaging quality in hybrid imaging.

Conclusion

This comprehensive assessment of collimator design, utilizing a combination of experimental measurements and MCNP simulations, represents a significant advancement in hybrid imaging capabilities. The close agreement observed between the experimental and simulation results validates the effectiveness of the collimator design in accurately capturing and registering gamma radiation information in hybrid imaging systems.

The findings presented in this study serve as a valuable resource for researchers and practitioners seeking to design cutting-edge collimators for hybrid imaging. By optimizing collimator parameters based on the insights gained from this assessment, enhanced image resolution and diagnostic accuracy can be achieved in hybrid imaging applications. Future research endeavours can leverage the MCNP simulation process to further refine collimator design parameters, pushing the boundaries of hybrid imaging excellence and facilitating improved patient care through more precise and comprehensive diagnostics.

Evaluation of efficiency of [¹⁸F]FDG PET/CT Imaging in the detection of primary origin in patients with cancers of unknown primary (CUP)

A. Perveen, A. Fatima, A. Shami

INMOL Cancer Hospital, Lahore, Pakistan

Background

Carcinoma of unknown primary (CUP) is a heterogeneous group of metastatic malignancies in which a primary tumour could not be detected despite diagnostic evaluation. Due to its high sensitivity of detection of lesion, [¹⁸F]FDG PET/CT may be used an excellent imaging modality for detection of unknown primary tumour. The present study aimed to prospectively assess the role of [¹⁸F]FDG PET/CT in the detection of primary origin in patients with cancers of unknown primary (CUP)

Methodology

In this prospective, single-institutional study, [¹⁸F]FDG PET/CT was performed for 124 patients with CUP. These patients presented with metastatic lesions that were proven pathologically, radiologically and/or clinically suspected metastatic lesions of undetermined primary site. Clinical, surgical and histopathological findings and correlative imaging modalities were used to access the results of [¹⁸F]FDG PET/CT; the accuracy of [¹⁸F]FDG PET/CT was expressed in terms of sensitivity, specificity, positive and negative predictive value and accuracy.

Results

This study included 124 patients with CUP; [¹⁸F]FDG PET/CT positive lesions suggestive of primary malignant tumours were detected in 79 out of 175 patients. These lesions were pathologically proven to be malignant (true positive) in 76/124 patients (61.2%). 3/175 patients (2.4%) proved to be falsely positive after pathological assessment; 43/124 patients (34.6%) were negative for detection of primary malignancy all over the body by PET/CT (true negative) with 2/124 patients were found to be false negative (1.6%). PET/CT achieved a sensitivity of 97.4%, specificity of 93.4, positive predictive value to be 96.2%, negative predictive value to be 95.5% and accuracy to be 95.9 % in the detection of primary tumour location. The lung was found to be the most frequent site of primary tumour (26.3 %), followed by gastro-intestinal tract (19 %).

Conclusion

Based on the obtained results, the study showed that [¹⁸F]FDG PET/CT is an effective imaging modality for early detection of the site of primary tumour in patients with cancer of undetermined primary (CUP).

Keywords: [¹⁸F]FDG PET/CT, Carcinoma of unknown primary (CUP), primary malignant tumours

Practical implementation of Clinical internal dosimetry in nuclear medicine department at CHU Bab El Oued Methodology and first conclusions

S. Bouyoucef

Department of Nuclear Medicine CHU Bab El Oued Algiers, Algeria

Background

In Nuclear Medicine administered activity distributes in the body for diagnosis and therapy is always subject to discussion for internal dosimetry. Mainly radionuclide therapy which enters a new era with new treatments is strongly adopted everywhere for NET, Prostate and others too. Internal dosimetry for Beta and alpha particles emitters is becoming fundamental to assess treatment efficacy and potential toxicity.

Implementation of Internal dosimetry dosimetry is necessary to:

- Evaluate the treatment of - [¹⁷⁷Lu]Lu-PSMA therapy for metastatic prostate cancer and radionuclide therapy (RNT) with iodine-131 for metastatic thyroid cancer.
- Achieve the highest therapeutic efficacy by delivering maximum absorbed dose into the tumour lesions while sparing healthy tissues.
- Calculate accurate dosimetry needed in pre- and post-treatment in order to achieve desired radiation absorbed dose: minimum dose for maximum efficacy.
- To estimate the absorbed dose to ensure that the radiation doses to organs at risk (OAR), (kidneys, salivary and lacrimal glands) for [¹⁷⁷Lu]Lu-PSMA RNT is minimized and to (BM, RM and Salivary gland) for iodine-131 is under the acceptable limits.

Methodology

For calculating absorbed dose, a formalism called MIRD*-Scheme was developed in 1976 (summing over all organ contributions). Well-recognized MIRD dosimetry schema has been implemented with commercial software solutions of OLINDA/EXM (Hermes). Predictive dosimetry obtaining with distribution data 15mn and 1 h post [⁶⁸Ga]Ga-PSMA administration using PET imaging. Calibration of SPECT/CT was done appropriate collimators with 1.4 GBq of [¹⁷⁷Lu]Lu-PSMA and 111MBq of iodine-131. 6 Injected doses of [¹⁷⁷Lu]Lu-PSMA NCA for patients without dose escalation: 7,7 GBq. For each dose, internal dosimetry is performed. PECT/CT (Siemens Intevo, Prospecta or GE870D) and Whole-body scan and three bed SPECT/CT with Lutetium-177: 1 h and 72 hours (possible 48 h). Organ dosimetry was possible with 1 h and 72 hours SPECT/CT and better with 48 hours.

Results

Results of [¹⁷⁷Lu]Lu-PSMA treatment for the 6 doses were calculated in three patients. Normal values for the Drm were 0.06 to 0.16mSv/MBq, for the Right Kidney, the maximum dose estimated 2,8 mSv (0,38/GBq) and for the Left Kidney, the Maximum dose estimated was 3,2mSv (0,41/GBq). Also, dose delivered to the Parotid glands were equal to 18,6Gy/4 doses and salivary gland equal to 13,8Gy/4 doses. For Metastatic bones of thyroid cancer, poor responses to iodine-131 therapy can relate to either low iodine uptake or retention in thyroid cancer cells or to increased radio-resistance. For Both mechanisms are currently termed radioactive iodine (RAI)-refractory (RAI-R) thyroid cancer, the first reflects unsuitability for iodine-131 therapy that can be evaluated in advance of treatment whereas the

other can only be identified post therapy. Internal dosimetry may show under treated patients and also or over treated lesions mostly when lesion avidity is low.

Conclusion

Introduction of Internal dosimetry in a department of nuclear medicine is of high clinical value since it will allow a real predictive idea on the clinical response in patients treated by radionuclide therapy.

Calculation of S-values for organs from whole body XCAT phantom for Fluorine-18 positron-emitting radionuclide

A. Alem-Bezoubiri¹, M. Speiser², Y. Bouchareb³, H. Donya^{4,5}, F. Bezoubiri¹

¹Radiological and Atomic Physics Department, Division of Physics, Algiers Nuclear Research Center (CRNA), 02 Boulevard Frantz-Fanon, BP 399 Alger-RP, 16000, Algiers, Algeria

²Englewood Hospital and Medical Center, Englewood NJ, USA

³Sultan Qaboos University, College of Medicine and Health Sciences, Muscat, Oman

⁴Department of Physics, Faculty of Science, King Abdulaziz University, Jeddah, 21589, Saudi Arabia

⁵Department of Physics, Faculty of Science, Menoufia University, Shibin El-Koom 32511, Egypt

Background

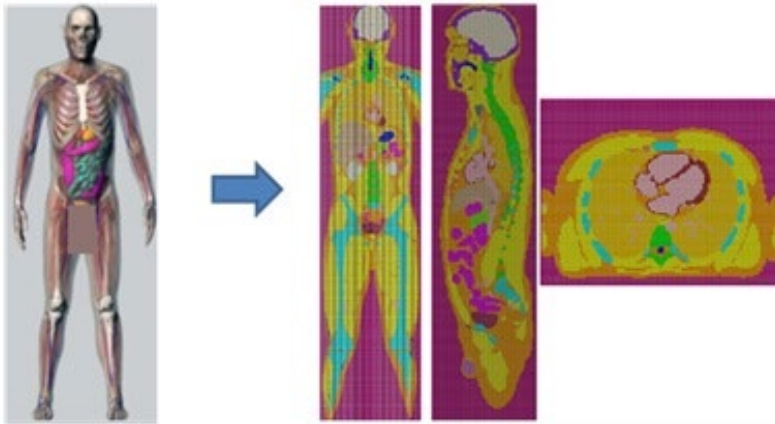
Stylized and voxelized phantoms have been used to estimate S-values for positron-emitting radionuclides. However, there is a lack of whole body computational phantoms. This study aims to address this limitation by constructing a multi-resolution whole-body phantom tailored for Monte Carlo simulations within the MCNP framework. Specifically, we converted the male XCAT phantom into MCNP format to calculate self-absorbed fractions (SAFs) and S-values for FLUORINE-18 positron-emitting radionuclide. Our results were compared with those from previously published phantoms studies, including the stylized MIRD.

Methodology

The Monte Carlo N-Particles eXtended (MCNPX) was employed to simulate radiation transport in the XCAT phantom, with DICOM images converted into MCNP format. Figure 1 illustrates the MCNP XCAT-adult male model, depicting transversal, sagittal, and coronal views. Utilizing this model, we computed SAFs and S-values (mGy/MBq*s) for different organs relevant to FLUORINE-18 PET imaging. Simulations involved uniformly distributing positrons, electrons, and photons within the source-structure, emitted isotropically within the XCAT phantom. Simulations were conducted on a workstation with 64 GB RAM and 20 physical CPUs, utilizing 6×10^7 particle histories. The photon-electron mode (mode p e) with cut-off energy of 1 keV was employed, utilizing the F8 tally for energy deposition in MeV. Thirteen organs are considered as source-structures and target-structures.

Results

The obtained S-values were compared with the MIRD-derived data, revealing substantial disparities exceeding 120% attributed to anatomical differences between the XCAT phantom and conventional mathematical models. This emphasizes the necessity of employing patient-specific computational models to ensure accurate radiation dosimetry in PET imaging. By accommodating individual anatomical variations, our approach enhances the precision of dose estimations, mitigating potential inaccuracies associated with standardized phantoms.



XCAT phantom

MCNP XCAT Geometry

Figure 1. Developed MCNP model of the XCAT phantom (Transversal, Sagittal and coronal views)

Conclusion

Our findings could have significant implications for risk assessment in nuclear medicine, demonstrating the complex relationship between radiation distribution and anatomical diversity. These insights could potentially enable clinicians to make informed decisions about radiation safety protocols during PET imaging procedures, thereby improving patient care. Ultimately, our hybrid phantom study represents a pivotal advancement in ongoing efforts in optimization of imaging protocols and improving outcomes in nuclear medicine practice.

A quantitative assessment addressing the role and value of different clinical Positron Emission Tomography reconstruction algorithms

L. Smith¹, T. Ebenhan¹, H. Ndlovu¹, K. Ramonaheng¹, M. Sathekge², C. Swanepoel¹

¹NuMeRI NPC, South Africa

²University of Pretoria/NuMeRI, South Africa

Background

Filtered Back Projection (FBP) is the most basic image reconstruction algorithm used for positron emission tomography (PET). It is also the only algorithm which allows an independent comparison of acquisition quality between vendors. Advances in system hardware and software now allows for a variety of other image reconstruction algorithms and applications to be used. These include iterative algorithms (OSEM/MOSEM), point-spread-function (PSF) and time-of-flight (TOF) features. Each of these applications can affect quantifiable data obtained from clinical acquisitions. We herein investigated the quantitative differences using alternate reconstruction algorithms by way of [¹⁸F]Fluorodeoxyglucose [¹⁸F]FDG/PET image analysis, thereby determining their role and value for the clinical setting.

Methodology

Retrospective data acquired on a Siemens Biograph Vision 450; equipped with a 64-slice Computed Tomography (CT) was used. Four random [¹⁸F]FDG scans were reconstructed using several reconstruction techniques, with CT attenuation correction. The images were evaluated to determine which reconstruction method was superior, with regards to the average Standardized Uptake Value based on bodyweight (bw) (SUVbwmean) concerning the physiological tissue biodistribution of [¹⁸F]FDG {heart; brain; liver; superior vena cava (svc) and brain:svc}.

Results

The FBP and the FBP+TOF pairing showed the highest noise and loss of resolution. In addition to this the highest standard deviations were also visualised for FBP+TOF as compared to FBP alone. Iterative reconstruction methods showed a significant difference when considering overall physiological function (SUV RATIObrain:svc) as is visualised in Figure 1.

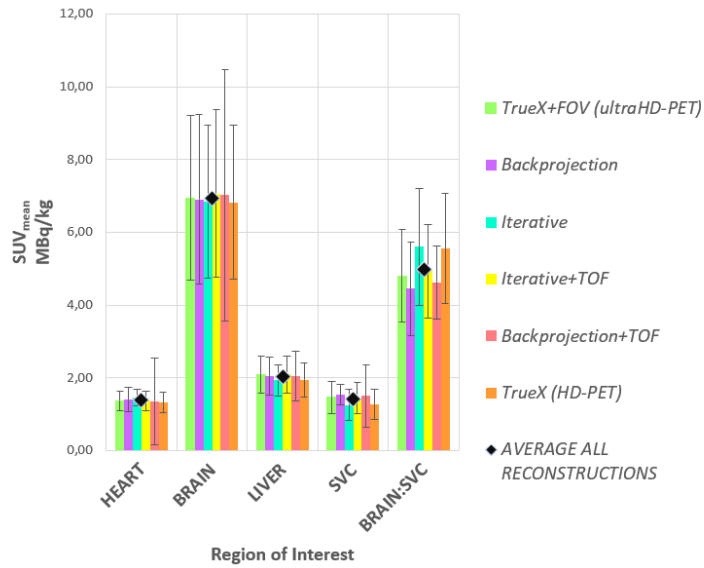


Figure 1. Summary of SUV_{mean} for each reconstruction method applied per region of interest in addition to the average of all regions.

Conclusion

FBP serves as a reference due to the reproducibility thereof between different vendors. It is however imperative that reconstruction parameters stay consistent within a department. The effects of different reconstructions must however be known to the reporting physicians.

Navigating radiolabeling challenges: Our experience with NOTA-pamidronic acid and [¹⁸F]AlF₂⁺ complexes alongside [⁶⁸Ga]Ga³⁺ ions

H. Hassan¹, M. F. Othman², I. H. N. Badi², W. H. B. W. Kamal³, H. R. A. Razak⁴, F. F. A. Saad¹

¹ Centre for Diagnostic Nuclear Imaging, Universiti Putra Malaysia, Malaysia

² Department of Pharmacy Practice, Faculty of Pharmacy, Universiti Teknologi MARA, Malaysia

³ Medical Technology Division, Malaysian Nuclear Agency (Nuclear Malaysia), Malaysia

⁴ Medical Imaging Program, Department of Health and Care Professions, Faculty of Health and Life Sciences, St Luke's Campus, University of Exeter, United Kingdom

Background

Recent years have witnessed a rise in the introduction of targeted radiopharmaceutical markers for Positron Emission Tomography (PET) for bone imaging. For instance, ⁶⁸Gabisphosphonates have attracted attention due to their strong affinity for bone minerals. Bisphosphonates (BPs) bind tightly to bone minerals through calcium coordination within the hydroxyapatite lattice, as opposed to fluoride binding. Pamidronic acid, among others, has the highest bone-binding affinity, making it a favoured bone targeting marker in our study.

Methodology

NOTA-pamidronic acid (NOTA-PAM) was prepared by conjugation of the NOTA chelator (1,4,7-triazacyclononane-1,4,7-triacetic acid) with pamidronic acid using the N-hydroxysuccinimide (NHS) ester strategy and validated by liquid chromatography-mass spectrometry (LC-MS/MS) analysis. The NOTA chelator was selected for its compatibility with [¹⁸F]AlF₂⁺ complexes and Ga³⁺ ions. The radiolabeling of NOTA-PAM was carried out with fluorine-18, using the aluminium fluoride (AlF) technique and with Ga-68. The radiolabeling conditions for both were further optimised by varying the amount of NOTA-PAM precursor used, reaction temperature and heating time. The efficiency of radiolabeling was evaluated using the radio-thin layer chromatography (TLC), and we compared the radiolabeling efficiency of [¹⁸F]AlF-NOTA-PAM with the ⁶⁸Ga-labeling of NOTA-PAM.

Results

The highest radiolabeling efficiency of [¹⁸F]AlF-NOTA-PAM was demonstrated at 95.50 ± 5.34% (n = 6) when the reaction mixture was heated at 100°C for 15 minutes and 500 µg of NOTA-PAM precursor was used. Similarly, the highest radiolabeling efficiency of [⁶⁸Ga]Ga-NOTA-PAM was shown to be 97.50 ± 0.40% (n = 6) under the same radiolabeling conditions. The results were expected as NOTA is a pentadentate with the configuration <<3N,2O>>, which forms an ideal octahedral complex with [¹⁸F]AlF₂⁺ and ⁶⁸Ga³⁺ ions. Nevertheless, we were puzzled by the radiolabeling efficiency results of [⁶⁸Ga]Ga-NOTA-PAM at room temperature. The radiolabeling efficiency of [⁶⁸Ga]Ga-NOTA-PAM at room temperature was less than 5% (n = 6). It is also known that BFC NOTA can be effectively radiolabeled with Ga-68 at room temperature. This was proven when we extended our radiolabeling experiment with [⁶⁸Ga]Ga-NOTA-NHS at room temperature. The efficiency of radiolabeling was 99.78 ± 0.01% (n = 6). It seems that radiolabelling of [⁶⁸Ga]Ga-NOTA-PAM requires heating to achieve excellent radiolabeling efficiency. The poor radiolabelling efficiency of [⁶⁸Ga]Ga-NOTA-PAM at room

temperature remained unexplained. Although we could postulate that the formation of a stable amide bond (CONH₂) from the conjugation of NOTA-NHS and pamidronic acid could affect the radiolabelling of NOTA-PAM at room temperature and therefore heating is required, this seems to have nothing to do with the coordination of the Ga³⁺ ions. The coordination of the Ga³⁺ ions occurred with the carboxylic acid group (OH) of the NOTA structure.

Conclusion

NOTA-PAM was successfully radiolabeled with [¹⁸F]AlF²⁺ complexes and ⁶⁸Ga³⁺ ions, with the highest radiolabeling efficiency of 97% achieved in [⁶⁸Ga]Ga-NOTA-PAM, followed by 95% achieved in [¹⁸F]AlF-NOTA-PAM.

Keywords: fluorine-18, Ga-68, aluminium fluoride (AlF), bisphosphonates, pamidronic acid, radiochemistry, radiopharmaceuticals, positron emission tomography

Staging FDG PET/CT in Newly Diagnosed Non-Small Cell Lung Carcinoma: Institutional Experience and Current Review of Clinical Characteristics and Scan Findings

S. Z. A. Hassan, R. D. Arunasalem, A. Z. Zanial

Nuclear Medicine Department, General Hospital Kuala Lumpur, Malaysia

Background

Fluorodeoxyglucose (FDG) PET/CT scan is extensively being applied in oncology including lung cancer staging and treatment response assessment by depicting glucose consumption of malignant cells. Non-small cell lung carcinoma (NSCLC) cases such as adenocarcinoma and squamous cell carcinoma (SCC) are more prevalent. We aimed to determine the FDG uptake avidity based on semiquantitative maximum Standardise Uptake Value (SUVmax) observed on staging FDG PET/CT of newly diagnosed NSCLC and the associated clinical factors.

Methodology

Cross-sectional review of 125 cases of biopsy proven lung cancer referred for oncological FDG PET/CT in a Malaysian tertiary referral institution over the past 2 years. Staging PET/CT scans (n=54) were included for analysis. Clinical parameters and PET/CT findings (SUVmax of primary lesion, presence of nodal and metastatic disease) were investigated. Data on SUVmax of primary lesion for SCC and adenocarcinoma was compared. Association between SUVmax of primary lesion and presence of extrapulmonary FDG-avid lesions was also determined.

Results

Males were predominant (60%). Average age was 62.5 years. Majority of cases were adenocarcinoma (65%) followed by SCC (22%) and others (13%). Mean tumour size was 5.1 cm. Lung SCC demonstrated intensely increased FDG uptake that was significantly higher compared to adenocarcinoma (average SUVmax 24.4 vs SUVmax 15.6, $p<0.05$). FDG-avid ipsilateral hilar nodal involvement seen in 63%, mediastinal nodes in 70% while distant metastatic disease in 33%. Patients having primary lesion with SUVmax 20.0 and above were significantly associated with larger tumour size and FDG-avid ipsilateral hilar nodal uptake ($p<0.05$).

Conclusion

Lung SCC was intensely FDG-avid and had higher SUVmax compared to adenocarcinoma. Primary lesions with SUVmax 20.0 and above were associated with larger tumour size and presence of hypermetabolic ipsilateral hilar nodal spread. Information obtained from this review will provide valuable insight into FDG PET/CT scan characteristics of newly diagnosed NSCLC cases in our institution that may influence not only scan reporting formulation but also patient management.

A sheep in wolf's clothing

L. Zaabar^{1,4}, A. Ghorbel^{2,4}, F. Abidi^{3,4}, C. Nasr^{2,4}, A. Zidi^{3,4}, A. Mhiri^{1,4}

¹ Nuclear Medicine Department, Salah Azaeiz Institute, Tunis, Tunisia

² Oncological Radiotherapy Department, Salah Azaeiz Institute, Tunis, Tunisia

³ Radiological Imaging Department, Salah Azaeiz Institute, Tunis, Tunisia

⁴ Faculty of Medicine of Tunis, Tunis El-Manar University, Tunisia

Background

[¹⁸F]FDG-PET/CT is recommended for the mapping of loco-regional neoplastic lesions, especially for distant lesions. The presence of metastases modifies therapeutic options. This is particularly important in patients with ENT sphere neoplastic pathologies. In these patients, FDG PET/CT has shown high diagnostic accuracy in staging, especially bone lesions detection. However, it is essential to be aware of possible false positives that can lead to incorrect staging of patients and loss of therapeutic opportunities.

The aim of this case presentation was to report a benign lesion mimicking a bone metastasis in nasopharyngeal carcinoma (NPC) patient, to highlight [¹⁸F]FDG-PET/CT variants and pitfalls in bone lesions. To our knowledge, it is the first case in the literature to report concomitant NPC with Fibrous Dysplasia of bone (FDB) revealed by a misleading excessive hypermetabolism on [¹⁸F]FDG-PET/CT.

Case Presentation

We reported a case of a 63-year-old male referred to us for his initial assessment of extension of a NPC classified T4N0M0 (partial encasement of the right internal carotid artery and invasion of the right posterior prevertebral muscles). [¹⁸F]FDG-PET/CT (23/8/2023) revealed a hypermetabolic tumoural process of the NP right posterolateral wall with extension towards the right parapharyngeal spaces, a lysis of the sphenoid bone (SUVmax=10.9), a secondary sectors II lymph node involvement bilaterally (SUVmax=7.8 on the left and 3.7 on the right). For distant locations, we found a single large "geographic" abnormal very hypermetabolic foci of the proximal part of the right femur (extended from the neck towards the trochanteric mass), with heterodense aspect of the bone structure but no cortical rupture (SUVmax=15.2; Reference Liver SUVmax=3.2), considered as a secondary single bone involvement of the right femur (T4N2M1). The patient underwent four cycles of chemotherapy. CT evaluation performed before planned concomitant radio-chemotherapy showed good partial tumour and lymph node response. The right femoral image was unchanged compared to the CT of the [¹⁸F]FDG-PET/CT, with diaphysometaphyseal and endomedullary location, extending towards the cortical bone, which is thinned, in ground glass like appearance, describing the almost pathognomonic appearance of FDB. FDB is a rare, benign, primary bone dysplasia characterized by progressive replacement of normal bone and marrow with fibrous connective tissue in either one (monostotic) or multiple (polyostotic) bones. The patient was retrospectively down staged as M0, but even had the scheduled concomitant radio-chemotherapy (because of T4 and N2 staging). He was in good health during the first follow up.

Conclusion

FDB presents a significant variability in the avidity of [¹⁸F]FDG, ranging from low to significant uptake, as seen in our case, greatly exceeding the hepatic metabolism uptake as reference. Similarly, this

variability is observed for the analysis of SUVmax values on late images (decreasing or increasing). It is very important to keep in mind that all bone «lesions» highlighted on [¹⁸F]FDG are not automatically linked to the same pathology, and that to label them it is necessary to carefully examine their morphological aspects associated with hybrid imaging.

Keywords: Fibrous dysplasia of bone, 18-Fluro-deoxy-glucose, Positron emission tomography/computerized tomography, Nasopharyngeal carcinoma, bone metastasis

Mesenteric inflammatory granuloma mimicking recurrence or metastatic disease on 18FDG-PET/CT in postoperative colorectal cancer patients

P. Corona, F. Arabolaza, Y. Blumenkrantz, G. Bruno, N. Bustos, C. Gonzalez, F. Matorra, S. Traverso

Fundación Centro Diagnóstico Nuclear, Argentina

Background

A significant percentage (approximately 40%), of patients who undergo surgical intervention for colorectal carcinoma (CRC), experience local or metastatic recurrence. An inflammatory granuloma at the surgical ligation site of the vascular pedicle may be misinterpreted as recurrence or metastatic disease on 18FDG PET/CT. The aim is to describe the characteristics of hypermetabolic mesenteric lesions detected on 18FDG-PET/CT in these patients.

Methodology

A retrospective analysis was conducted on a cohort of 45 postoperative CRC patients presenting focal 18FDG uptake at the surgical ligation site of the vascular pedicle. We employed an Apache Solr™ search engine (<https://solr.apache.org/>) to identify CRC patients, supported by a user-friendly web interface built with Ruby on Rails. To assess metabolic activity, visual parameters and the determination of SUVmax were taken into account.

Results

We included 18FDG-PET/CT studies conducted between March 2017 and November 2023, involving 45 patients, of whom 28 (62.2%) were men and had undergone surgery for CRC. These patients exhibited a hypermetabolic nodule at the site of surgical ligation of the vascular pedicle. In right-sided CRC (9 patients; 20%), this nodule was located in branches and tributaries of the superior mesenteric vessels, while in left-sided CRC (36 patients; 80%), it was associated with inferior mesenteric vessels. Although all 45 patients presented with similar findings, our analysis focused on the 17 patients (37.7%) who underwent two or more PET/CT studies to evaluate lesion evolution. The time interval between surgery and the initial PET/CT ranged widely from 2 to 84 months (mean: 14.7). Lesion size varied from 8 to 20 mm (mean: 12 mm), and initial SUVmax ranged from 1.6 to 6.3 (mean: 3.5). While 9 patients (52.9%) only had this finding, the remaining patients displayed additional hypermetabolic findings: 6 with distant metastases and 2 with non-neoplastic findings.

Over time, lesion morphology remained stable or reduced in size, and metabolic activity showed varied changes: 9 patients exhibited decreased SUVmax values, 5 experienced variable increases, and 3 showed complete metabolic resolution. The key diagnostic factor lies in the anatomical location of the lesion, correlating with the site of surgical ligation of the vascular pedicle.

Despite the absence of histological confirmation, patients demonstrated stability, reduction, or complete resolution of the lesions, with no instances of enlargement. The variable changes in metabolic activity suggest a chronic inflammatory nature, leading to the interpretation of a possible granuloma.

Conclusion

The identification of hypermetabolic nodular lesions on 18FDG-PET/CT, in conjunction with the surgical ligation site of the mesenteric vascular pedicle in CRC patients, may be misinterpreted as

recurrence or metastatic disease. However, the stability, reduction, or resolution observed in serial studies, along with the absence of size increase, supports the hypothesis of a chronic inflammatory process. We propose reporting these findings as mesenteric inflammatory granuloma, emphasizing that the diagnostic key lies in the anatomical location and is further supported by the temporal evolution of the lesions, thereby preventing erroneous diagnoses and unnecessary therapeutic interventions.

Radioiodine therapy in elderly patients with subclinical hyperthyroidism: Preliminary results

L. Zaabar^{1,2}, F. B. Amar¹, D. B. Sellem^{1,2}, A. Mhiri^{1,2}

¹ Nuclear Medicine Department, Salah Azaiez Institute, Tunisia

² Faculty of Medicine of Tunis, Tunis El-Manar University. Tunisia

Background

Radical treatment of subclinical hyperthyroidism (SHT) is essential in elderly patients vulnerable to potential cardiovascular risks.

The aim of this study was to describe the value of radioiodine therapy (RIT) in SHT in 65-year-old patients and over, based on the experience of the Nuclear Medicine Department at the Salah Azaiez's Institute.

Methodology

We conducted an observational descriptive retrospective monocentric study. We enrolled 65-year-old patients and over, treated with RIT for SHT (TSH <0.4 mUI/L controlled on two occasions at least one month apart with normal FT3 and FT4 levels) during January 2020-June 2022 period. We classified patients at three and/or six months after RIT into: Group1: effective therapy (G1a: achievement of euthyroidism; G1b: achievement of hypothyroidism); Group 2: equivocal result with hyperthyroidism present at three months and Group 3: therapeutic failure given the persistence of hyperthyroidism at 6 months.

Results

We enrolled 31 patients with mean age of 73.2±7.5 years and M/F sex ratio of 0.07. Cardiovascular history accounted for 71% of cases. SHT was discovered incidentally in 36% of patients, with 17 months old on average. RIT was performed for the first time in 94% of cases. The mean activity administered was 573.5±74 MBq of ¹³¹I, with a median of 555 MBq. For an average first check at 3.6 months after treatment, efficacy was noted in 77% of cases: G1a 16 cases (51%) and G1b 8 cases (26%). When Group2-patients were checked again, success rose up to 84% at six months. Group3 consisted of one Graves' disease case, one heteromulti-nodular goitre case, two cases of Graves' goitre and one toxic multinodular goitre case. RIT was effective in all cases not previously treated with antithyroid drugs.

Conclusion

Therapeutic effectiveness of RIT is evident. Obtaining hypothyroidism is one of therapeutic objectives, but could be avoided thanks to an adaptation of administered activities of Iodine 131, and not taking antithyroid drugs before treatment, which contributes to the significant improvement in patients' quality of life.

Keywords: Hyperthyroidism, Elderly, Therapy, Iodine

Quantitative assessment of reduced [68Ga]Ga-PSMA-11 administered dose – an exploratory investigation

C. Swanepoel¹, C. Davies¹, T. Ebenhan², M. Sathekge²

¹Nuclear Medicine Research Infrastructure, South Africa

²University of Pretoria/NuMeRI, South Africa

Background

Prostate-specific membrane antigen (PSMA) has become a key target to visualize and treat prostate cancer (PC). Internationally recognised guidelines for radiopharmaceuticals such as [68Ga]Ga-PSMA-11 recommend a patient dose range of 1.4-2.2 MBq/kg but it has been queried in the past by utilising whole-body list mode acquisition. These investigations have concluded that the prescribed dose should be adhered to for optimal diagnostic image quality. While the value of list mode acquisitions and subsequent computations should not be discarded, the increase in examination requests for staging and management of prostate cancer has necessitated further investigations to ascertain the feasibility of administering a decreased dose while still obtaining optimal diagnostics and comparable images. Should a lowered dose be deemed feasible, the benefits will include; decrease dose to patients and staff, decrease in departmental cost and ultimately a greater throughput of examinations.

Methodology

In this single centre, single arm study images were acquired on a Siemens Biograph64_Vision450 using continuous beam motion (CBM) [vertex to diaphragm 1.2 – 1.5min per bed; diaphragm to iliac crest – 2.5min/bed; iliac crest to mid-thigh 1 – 1.75min/bed] 60minutes post injection of [68Ga]Ga-PSMA-11. All images were corrected for attenuation and scatter and reconstructed iteratively using the same parameters (TrueX+FOV (ultraHD-PET) 3 Iterations, 5 Subsets). For data analysis the patient population was divided into two groups: GROUP 1: within reference range according to guidelines ([68Ga]Ga-PSMA-11 doses > (1.61±0.26MBq/kg)) and GROUP 2: below reference range ([68Ga]Ga-PSMA-11 doses < (1.05±0.08MBq/kg)). Patients with significant disease were excluded to minimise physiological variables. Regions of interest were drawn to organ and tissue that are clearly identified as expected (physiological) distribution of [68Ga]Ga-PSMA-11 [lacrimial glands, parotid glands, liver and kidneys]. Reference values were also obtained for blood pool and muscle [descending aorta and trapezius muscle]. The average standard uptake value (SUV_{mean}) per group was determined for each organ tissue and presented as a ratio to the blood pool. The initial sample size was n=20, equally divided between Group 1 and Group 2

Results

All acquired images were visually considered to be of good diagnostic quality by the departmental nuclear physicians. Quantitatively SUV_{mean} values in both groups showed similar results for areas of expected biodistribution. It should however be mentioned that the body weight in Group 2 patients (84 ± 11 kg) were significantly higher than that of Group 1 patients (69 ± 17 kg; p-value (two tailed) = 0.025)) and may account for the variance as shown in Figure 1.

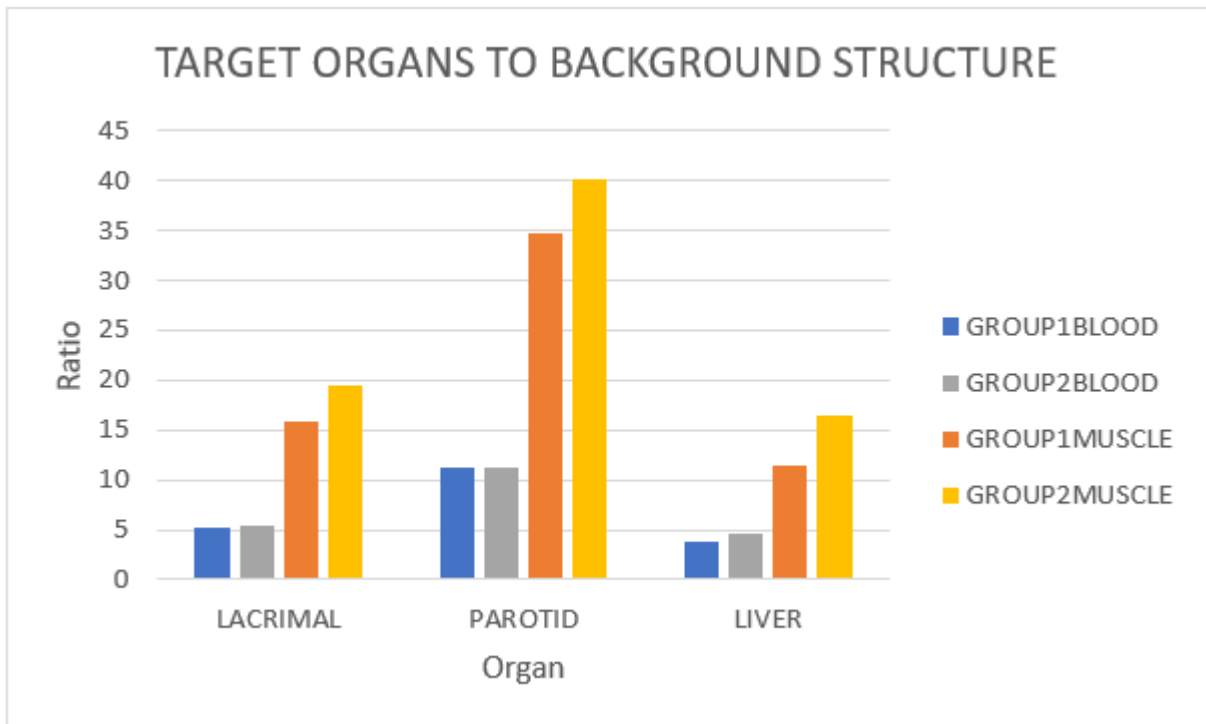


Figure 1. Tissue concentration ratio demonstrating $[^{68}\text{Ga}]\text{Ga-PSMA-11}$ uptake in two groups in areas of expected tracer biodistribution shown as a ratio to background tissues (blood pool and muscle).

Conclusion

A decrease in the administered doses of $[^{68}\text{Ga}]\text{Ga-PSMA-11}$ of up to 35% seems safe and feasible without creating major differences in the relative tissue concentration (physiological uptake) but a larger patient population may be investigated. The extent of the PC pathology, variations in individual excretory metabolism as well as compounding variations should be considered as it might add to slight variances seen.

Diagnostic Reference Levels Nuclear Medicine in Namibia: A Preliminary study

C. Kamerika¹, V. Uushona², R. Hamunyela³, P. Haiduwa¹

¹ Nuclear Medicine, Ministry of Health and Social Services, Namibia

² Matcon Knowledge Based Solutions, Namibia

³ University of Namibia, Namibia

Background

Nuclear Medicine is a branch of medicine that uses radionuclides to provide information about the function of a person's specific organs (diagnosis) or to treat disease (therapy). In most cases, the information is used by physicians to make a quick, accurate diagnosis of the patient's illness. The thyroid, bones, heart, liver, and many other organs can be easily imaged, revealing disorders in their function. In some cases, radiation can be used to treat diseased organs or tumours. The determination of diagnostic reference levels (DRLs) for nuclear medicine (NM) procedures has been proposed as one of several effective tools for optimization of medical exposure, including nuclear medicine examinations. The aim of the study was to establish DRL's in nuclear medicine from the administered activities of the radiopharmaceuticals Technetium-99m.

Methodology

The data for the administered activity of Tc-99m for the thyroid scan were collected from one center in Namibia from May to December 2023. The 75th percentile of the distribution and the average administered activity were calculated. A total of 125 procedures for thyroid scans were considered for the DRLs. The gathered data were analysed via Excel 2016 using descriptive statistics.

Results

The results showed that the administered activity of Tc-99m for thyroid scans ranged from 178 to 385 MBq, with an average of 308 MBq. The 75th percentile (315 MBq) of the distribution of administered activity represents the DRL.

Conclusion

This study presents the results of the first local DRLs for nuclear medicine. Further data should be collected at other Nuclear Medicine centers for the establishment of collective national DRLs.

Keywords: Tc-99m DRLs, Thyroid scan, Nuclear medicine

Impact of Patient Body Mass Index on the Patient Body Self Attenuation Factor in [¹⁸F]FDG PET-CT Examinations: A Pilot Study

Y. Lahfi, N. Alkerdi, T. Ayach

Protection and Safety Department, Atomic Energy Commission of Syria, Syrian Arab Republic

Background

Nowadays, the hybrid imaging PET/CT is widely used for several detection and monitoring cancers and other maladies. The association of this imaging modality with the production of high-energy radiation necessitates special radiation protection measures for the public and the staff. In spite of the fact that the occupational exposure is mainly related to the preparation and handling of the radiopharmaceutical doses. The close contact with the patient contributes also to staff and public radiation doses. The patient self-attenuation factor (PAF) was introduced to quantify the effect of a patient's body on the radiation absorption and scattering after being radioactively administrated. The aim of this study is to investigate the correlation between the patient self-attenuation factor and patient body mass index (BMI) in the [¹⁸F]FDG PET/CT examinations.

Methodology

A randomized sample of 15 patients administrated with [¹⁸F]FDG for PET-CT scan at PET&CT Advanced Clinic (in Damascus City) were monitored. The patient's age, height, weight, and the administered radioactivity were recorded and the patient' BMI was calculated. The radiation dose rate from unshielded [¹⁸F]FDG syringe just before patient administration at 1 meter was measured. The external radiation dose rate from the standing patient immediately post dose administration, in order to avoid correcting for radioactive decay, at a distance of 1 meter was measured at three different levels: head, thorax and knee and their average value was obtained. The patient self-attenuation factor was calculated as the ratio between the external dose rate measured from the patient with that measured from the unshielded [¹⁸F]FDG syringe. The annually calibrated radiation monitor TRACERCO T202 (UK) was used in this study as its measurement range from 0 to 10 mSv/h was suitable to measure the expected dose rate in the study.

Results

The average age and BMI of the patients' sample were 45.27 ± 16.97 years and 27.88 ± 6.29 kg/m² respectively. The administered [¹⁸F]FDG radioactivity was from 333 to 444 MBq, based on the applied patient preparation and imaging procedure guidelines. The average of the normalized measured external dose rate from the patient and from the unshielded [¹⁸F]FDG syringe were 0.10 ± 0.02 and 0.17 ± 0.01 μ Sv/h/MBq respectively. The average of the calculated patient body attenuation factor was 0.55 ± 0.11 . According to the World Health Organization's BMI classifications, the patients were assigned to one of four groups: Underweight, Healthy Weight, Overweight, or Obesity, and the average of the patients' PAF and BMI for each group were calculated. Additionally, in order to investigate the relationship between the both average values, the Pearson correlation coefficient R² value of the linear regression test was calculated. Its value of 0.83 indicates a good association between them as shown in the Figure 1.

Conclusion

The obtained relationship between the patient body attenuation factor and the patient body BMI could be taken into account in order to predict a more accurate estimation of the radiation dose from the patient especially when the close contact with the staff is needed. Consequently, the optimization of radiation protection for staff during PET/CT examinations will be positively impacted.

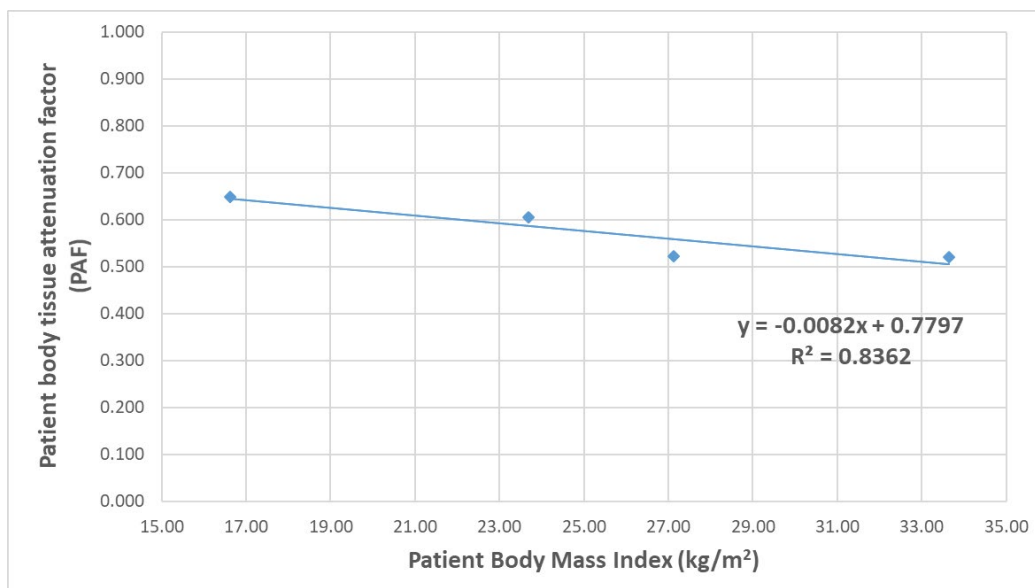


Figure 1. The relationship between patient body mass index (BMI) and the patient body tissue attenuation factor (PAF) in the four BMI classification groups

Side Effects of Radioactive Iodine Therapy on Reproductive Function in Differentiated Thyroid Carcinoma Patients: A Systematic Review

A. Elliyanti¹, Y. Kurniawati¹, Z. Aziza¹

¹ Department of Radiology, Division of Nuclear Medicine, Faculty of Medicine, Universitas Andalas, Indonesia

² Undergraduate Study Program of Medicine, Faculty of Medicine, Universitas Andalas, Indonesia

Background

Thyroid cancer is one of the most common cancers found in the endocrine system, and its incidence has increased rapidly over the past three decades. The treatment for patients with differentiated thyroid cancer (DTC) includes surgery, radioactive iodine (I-131) therapy, and L-T4 suppressive therapy. I-131 is indicated for intermediate and high-risk patients to improve survival rates. This study was to investigate the possible side effects of I-131 therapy on reproductive function in men and women with DTC.

Methodology

This study is a literature review of 17 research articles published between 2013 and 2023. PubMed, Science Direct, BMC, and Google Scholar are the database sources used. Articles are selected based on predefined eligibility criteria.

Results

Of the 17 articles reviewed, it was found that 13 articles discussed the side effects of I-131 therapy on women's reproductive function, and four articles discussed side effects on men's reproductive function. In women, the treatment decreases anti-Mullerian hormone (AMH) levels and changes in menstrual cycles in the first year, but it does not impact pregnancy in the following year. Meanwhile, in men, this therapy leads to an increase in Follicle Stimulating Hormone (FSH) and Luteinizing Hormone (LH), as well as changes in the quantity of sperm, morphology, and motility of sperm, improving within one year post-therapy.

Conclusion

The side effects of I-131 therapy on reproductive function are generally temporary, lasting approximately one year post-therapy, for both women and men.

Keywords: radioactive iodine therapy, reproductive function, differentiated thyroid carcinoma, side effects

Radiofluorination of PSMA-Targeted Radiotracers: A New Beginning of Prostate Cancer PET Imaging in Bangladesh

M. Anwar-Ul-Azim¹, Md. Jashim Uddin², S. C. Biswasarma², S. Islam², Md. Saiful Islam²

¹ Planning & Development Division, Bangladesh Atomic Energy Commission (BAEC), Bangladesh

² National Institute of Nuclear Medicine & Allied Sciences (NINMAS), BSMMU, Bangladesh

Background

⁶⁸Ga- labeled PSMA-targeted PET imaging probe become a part of routine clinical care for prostate cancer. Due to short half-life of Ga-68 and higher positron yield & lower positron energy of ¹⁸F-labeled radiotracers, ¹⁸F-labeled PSMA-targeted PET radiotracers may play an important role in the field of molecular PCa imaging. As the country's largest nuclear medicine service provider, our aim was to synthesis [¹⁸F]PSMA-1007 at the cyclotron (18/9 MeV, IBA) & Molecular Imaging facility of National Institute of Nuclear Medicine and Allied Sciences (NINMAS) of Bangladesh Atomic Energy Commission (BAEC) and to perform clinical trial of [¹⁸F]PSMA PET/CT for the first time in Bangladesh.

Methodology

[¹⁸F]Fluoride was produced by the ¹⁸O (p, n)fluorine-18 nuclear reaction using a cyclotron (18/9 MeV, IBA Belgium). [¹⁸F]PSMA-1007 was synthesized via direct substitution on IBA Sythera® autosynthesizer. [¹⁸F]F⁻ was trapped on the QMA-cartridge and subsequently was eluted with 0.075 M aqueous Tetrabutylammonium hydrogen carbonate (TBAHCO₃⁻) solution. Precursor (1.6 mg) in 2 mL of dimethyl sulfoxide (DMSO) was added to the reaction vessel and heated for 10 min at 5 °C. The reaction mixture was diluted with 4 mL 5.5% ethanol (EtOH) and the solution was passed through SPE and C18 cartridges into the waste. The product, [¹⁸F]PSMA-1007, was finally eluted with 5 mL 30% EtOH solution into the product vial by passing through a sterile Millex-Cathivex 0.22-µm filter and diluted with 15 mL 0.9% saline containing 100 mg sodium ascorbate, which was also passed through the sterile Millex-Cathivex GV 0.22-µm filter into the final product vial.

Results

[¹⁸F]PSMA-1007 was successfully synthesized with radiochemical yields of 46.85% and 40 minutes were required to complete synthesis. Synthesized [¹⁸F]PSMA-1007 was also passed all the quality control criteria, like appearance (colorless/clear), bacterial endotoxin test (0.2024 EU/mL), pH (6.5), radiochemical purity (96.1%), half-life (108 min), gamma-ray energy (511 KeV), filter integrity test (62 psi), tests of residual DMSO (100 ppm) & Ethanol (256 ppm), sterility test (no turbidity growth), etc. [¹⁸F]PSMA-1007 PET/CT study of four (04) patients were successfully done as trial.

Conclusion

The successful synthesis, quality control and clinical trial of [¹⁸F]PSMA-1007 at NINMAS lead to a new beginning in the field of prostate cancer PET imaging in Bangladesh.

Keywords: PSMA, [¹⁸F]PSMA-1007, prostate cancer; PET/CT imaging, quality control.

From Negative to Positive: F18 Choline Sheds Light on a Parathyroid Adenoma: A First in the Philippines - A Case Report

E. Cruz, I Bandong, C.T. Azarraga

Department of Nuclear Medicine and Theranostics, St. Luke's Medical Center Quezon City, Philippines

Background

The parathyroid glands play a crucial role in calcium regulation through parathyroid hormone (PTH) production. Hyperparathyroidism, characterized by excessive PTH, leads to elevated calcium levels and symptoms like bone pain and fatigue with parathyroid adenomas as the primary cause in up to 85% of cases. Diagnosis involves measuring serum calcium and PTH levels, followed by imaging with neck ultrasonography and dual tracer radio-isotope scintigraphy. Some noted limitations in the initial imaging modalities include operator-dependent limited sensitivity in neck ultrasonography, poor spatial resolution, and poor sensitivity in the mitochondria-poor adenomas in the dual tracer scintigraphy. Other modalities such as thin-section Computed Tomography (CT), and Magnetic Resonance imaging (MRI) are available as well, however, these lack sensitivity and subject the patients to high radiation exposure, thus leading to the exploration of other alternative imaging options such as the use of the positron emitter F18-Choline.

Case Report

This case report describes a 24-year-old female with borderline elevated calcium levels and a suspected parathyroid adenoma. Initial imaging with the dual tracer scintigraphy Tc99m-Perchnetate and Tc99m-sestamibi accompanied by SPECT/CT and subtraction method was negative for a parathyroid adenoma, however a suspicious nodular structure was seen on ultrasonography. Due to the high clinical suspicion and by the patient's request, further imaging evaluation was done. A subsequent 18F-Choline PET/CT identified an 18F-Choline-avid lesion, inferior to the right thyroid lobe, highly suggestive of a parathyroid adenoma. The patient is currently awaiting possible parathyroidectomy. This is the first recorded 18F-Choline PET/CT usage for a parathyroid adenoma in the country and highlights the potential of 18F-Choline PET/CT as a sensitive and specific imaging modality in cases where conventional imaging is inconclusive.

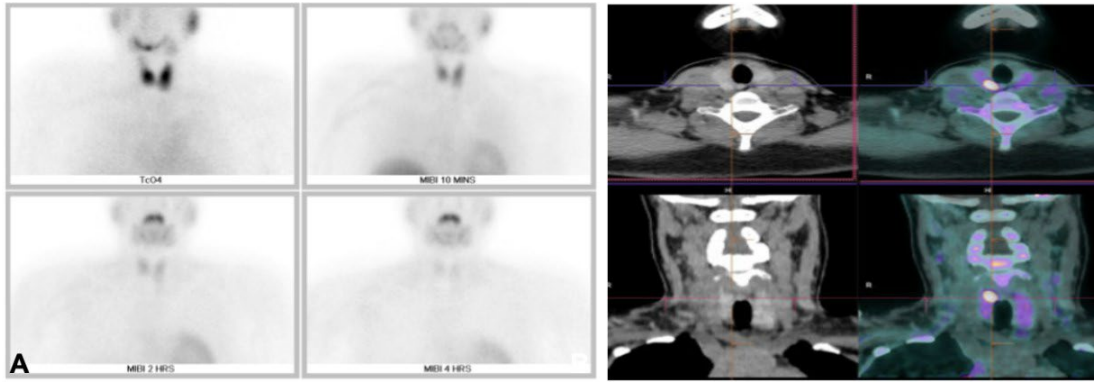


Fig 1. Dual tracer Tc99m-Pertechnetate and Tc99m-Sestamibi. F18-Choline PET/CT images of a 24-year-old female with high clinical suspicion of a parathyroid adenoma. (A) No sestamibi-avid focus in the dual phase dual tracer scintigraphy. (B) F18-Choline-avid lesion inferior to the right thyroid lobe raises suspicion of a parathyroid adenoma

Conclusion

F18-Fluoromethylcholine PET/CT is a highly sensitive and specific imaging test that may be used in negative scintigraphic parathyroid scans for patients with high clinical suspicion of a parathyroid adenoma.

Treatment of thyroid cancer at the National Oncology Center of Nouakchott and radiation protection measures

M. L. Dieng

National Oncology Center of Nouakchott, Mauritania

Background

Iodine 131 is one of the isotopes of iodine, emitting β and γ radiation, with a half-life of 8 days. Its complex radiation consists mainly of β radiation with a maximum energy of 606 keV, an average energy of 192 keV, and a tissue penetration depth (R90) of 0.8 mm, as well as γ radiation of 364 keV. Treatment with iodine or radiotherapy refers to the administration, usually orally, of iodine 131 in the form of sodium iodide (NaI). Iodine 131 treatment is also used for indications other than thyroid cancer: - diffuse or nodular hyperthyroidism (GMN and NT). - goitres without hyperthyroidism, for mass reduction in case of surgical contraindication. Iodine 131 treatment for thyroid cancers is performed in two distinct situations:

Surgical removal of the tumour is complete, and the treatment aims to destroy the post-operative thyroid remnants and to detect and treat any infra-clinical and infra-radiological metastases.

Surgical removal of the tumour is incomplete and/or the cancer has metastasized, the treatment aims to destroy the metastatic foci and the residual local tumour that retains iodine.

Methodology

We treat patients with goitre, hyperthyroidism, and differentiated thyroid cancers.

For patient measurement, we used the RDS 31 radiometer, which detects gamma and X-ray radiation with an energy range of 15 keV-7 MeV and a dose rate between 0.01 μ Sv/h and 100 mSv/h, and the LB 124 SCINT D.

For patients with goitre and hyperthyroidism, the activity varies between 20 and 30 mCi, while for differentiated thyroid cancers, we administer between 30 and 100 mCi.

Patients with differentiated cancers are hospitalized for a maximum of 3 days.

Results

Over the past three years, we have treated 98 thyroid cancers and 180 hyperthyroidism cases. The dose rate limit is set at 20 μ Sv/h, and the majority of patients are hospitalized for a maximum of 3 days. Most patients return for a second or third treatment, and some even more. It is too difficult to determine an effective period for iodine 131 as it depends on the biological periods of each patient, which vary depending on many parameters (elimination time, weight, height, water or beverages consumed...). Since the capsule is initially ingested, it will inevitably go to the digestive system first before migrating more or less to the thyroid area, explaining the differences in observed effective periods between the thyroid and abdomen (but this difference is not too significant). The urinary stock in each patient's bladder and by default the amount of water they drank during hospitalization directly influences these parameters. This distribution of iodine is observed again at the end of hospitalization when the patient undergoes a scan for control.

Conclusion

Radioactive iodine 131 is used to treat overactive thyroid gland disorders, and it is an effective treatment method. It is not just about treating patients because we use iodine 131, which is radioactive and also emits γ radiation. It is therefore important to respect radiation protection rules to avoid irradiating the patient's surroundings. The decree of January 21, 2004, of the French regulations presents the mandatory elements that must be included in the recommendations given to the patient to limit the exposure of people who will be in contact with them. These recommendations must be given to the patient by their doctor before treatment. Treated patients also produce waste (solid and liquid), which must be properly managed after their release according to the decree of July 23, 2008, laying down the technical rules to be met for the disposal of effluents and waste contaminated by radionuclides. It is important to perform pre-therapeutic dosimetry to establish the maximum activity to be administered, considering the red marrow as the organ at risk. We plan to implement internal dosimetry through our cooperation with the IAEA.

Machine learning can predict M1 disease in treatment-naïve prostate cancer patients undergoing 68Ga-PSMA-11 PET/CT

R. Wakankar¹, B. Khangembam¹, A. R. Chanu², K. M¹, C. J. Das³, C. Patel¹, R. Kumar¹

¹ Department of Nuclear Medicine, All India Institute of Medical Sciences, India

² Department of Physical Medicine and Rehabilitation, All India Institute of Medical Sciences, India

³ Department of Radiodiagnosis and Interventional Radiology, All India Institute of Medical Sciences, India

Aim

To evaluate the feasibility of a machine learning (ML) approach employing routine clinical, regional imaging, and laboratory parameters for predicting distant metastasis (M1 disease) in treatment-naïve prostate cancer patients undergoing 68Ga-PSMA-11 PET/CT.

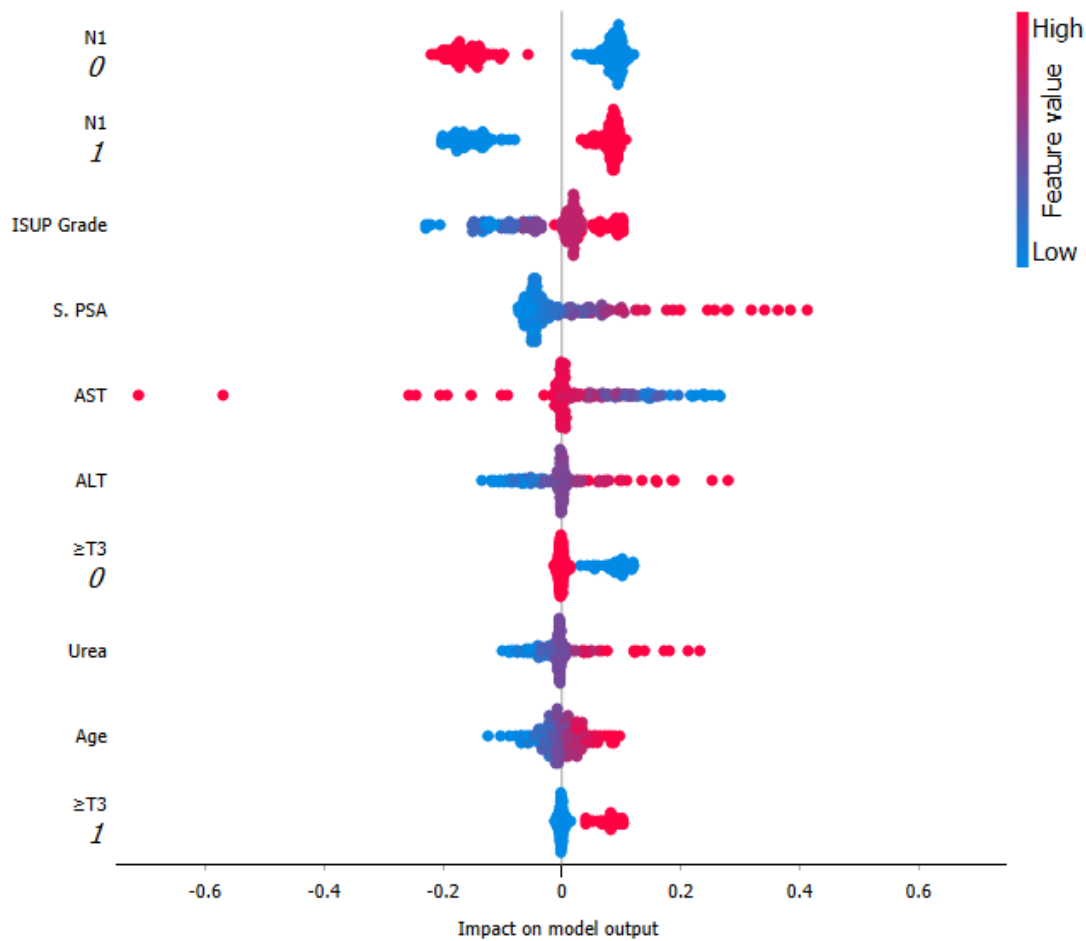
Methodology

Data from pathologically confirmed treatment-naïve prostate cancer patients, who had baseline 68Ga-PSMA-11 PET/CT scans between January 2018 and September 2023, constituted the training set. M1 disease was determined on 68Ga-PSMA-11 PET/CT. Various routine clinical, regional imaging and laboratory parameters were collected for each patient. Data preprocessing involved feature imputation and selection, with the 5 highest-ranked features based on Gini Index scoring chosen for cross-validation using a Logistic Regression (LR) model. The LR model incorporated Ridge (L2) regularization, $C=1$, and no class weights. The generalization of the model was assessed by testing it on an unseen dataset of prospectively enrolled patients from October 2023 to February 2024. Performance metrics included Area Under the Curve (AUC), classification accuracy (CA), F1 score, precision, recall, and specificity. Feature importance was determined by measuring the decrease in AUC after permuting each feature's values. For transparency and interpretability, SHAP (SHapley Additive exPlanations) values were assessed and presented as SHAP Beeswarm and Force Plots. A nomogram was developed, incorporating the five most crucial parameters for predicting M1 disease.

Results

The training set comprised 184 male patients with a mean age of 68 ± 8 years, while the testing set included 30 patients with a mean age of 67 ± 9 years. No statistically significant difference in the proportion of M1 disease was observed between the two groups ($P = 0.331$). Among the 16 patient-related parameters, serum total protein, albumin, and alkaline phosphatase (ALP) showed differences between the groups ($P \leq 0.008$). The 5 top-ranked parameters based on Gini Index scoring were N1, ALP, ISUP Grade, primary tumour $\geq T3$, and serum prostate-specific antigen (PSA). In cross-validation, the Logistic Regression (LR) model exhibited an AUC of 0.893, with CA, F1 score, precision, recall, and specificity values of 0.832, 0.831, 0.784, 0.884, and 0.786, respectively. The 5 most impactful features for predicting M1 disease, determined by the decrease in AUC after feature permutation, were N1, serum aspartate transaminase (AST), PSA, primary tumour $\geq T3$, and ISUP Grade. When tested on the unseen dataset, the LR model yielded an AUC of 0.928, with CA, F1 score, precision, recall, and specificity values of 0.833, 0.857, 0.833, 0.882, and 0.769, respectively. The SHAP Beeswarm plot

highlighted N1, ISUP Grade, and PSA as the most crucial features, providing a clear pattern of model interpretability. The 5 best-ranked features based on absolute importance employed by the constructed nomogram for predicting M1 disease were AST, PSA, serum alanine transaminase (ALT), urea, and creatinine.



Conclusion

Machine learning can predict M1 disease in treatment-naïve prostate cancer patients using routine clinical, imaging, and laboratory data. The model's robustness and generalizability offer insights for planning patient management during diagnostic workups. Integrating the model and nomogram into clinical practice could enhance decision-making and optimize patient care.

Evaluation of occupational exposure in the production and use of radiopharmaceutical products in Syria

A. Bitar, M. Maghrabi, H. Sharaf, A. Daoud, H. Al-Hinawy

Atomic Energy Commission of Syria, Damascus, Syria

Introduction

In 1997, the Atomic Energy Commission of Syria (AECS) installed Syrtic-1 facility for the production of first generation of sterile Mo-99/Technetium-99m generator in Syria. IBA Cyclone 30 accelerator was installed at AECS in 2001 for the production of [¹⁸F]DG, Tl-201, Ga-67, and I-123. The I-131 was prepared using a dispensing system at AECS from 2002 to 2018. Researches and trials were also carried out using other radioisotopes such as Sr-90 / Y-90. The individual monitoring service (IMS) at AECS is the sole service provider in the country, and is monitoring currently about 2000 workers in different fields. This study evaluates the effective doses received by about 160 workers, from 1998 to 2023, in the production facilities at AECS (Syrtic & Cyclone) and in Al-Bairouni University Hospital (AUH) in Damascus.

Methodology

The routine external monitoring is assured by using HARSHAW TLD and FOMA film. Internal monitoring is also offered by AECS to many workers either using NaI(Tl) or HPGe detector on thyroid, or measuring the activity in urine and/or nasal samples. The personal dose equivalents Hp(10) were recorded for each worker, and the committed effective doses (CED) were calculated after each measuring of internal contamination.

Results

The figure shows the cumulative recorded Hp(10) during the respective period of work for the chosen workers in Syrtic facility whose average annual dose is more than 2 mSv. The workers ID5 and ID7 received relatively high doses at the beginning of Syrtic project. Their annual doses in the years 1999, 2000, 2001 were (8.6 mSv, 5.7 mSv, 4.4 mSv) and (8.3 mSv, 7.4 mSv, 3.7 mSv), respectively. After improving the shielding of hot cells and the work procedures, their annual doses were reduced to less than 3 mSv. The average annual doses for most workers in Cyclone facility were below 2 mSv. Actually, the procedures of handling the radioisotopes in Syrtic and Cyclone facilities are done remotely in well designed hot cells. Therefore, the routine and special internal monitoring showed very low CEDs for all monitored workers. Also, there were no significant recorded doses for extremities and eye lens. The calculated CEDs for chosen workers in AUH, during an internal monitoring for Technetium-99m, I-123, and I-131, ranged from 0.13 mSv to 3.20 mSv. Following the results of monitoring, many recommendations were given to the workers in AUH to reduce external exposure and internal contamination. In fact, AUH is handling daily high number of patients with limited number of staff. Also, the lack of radiation protection knowledge affected the radiation exposure of workers.

Conclusion

The recorded whole body and extremity doses were significantly below the recommended dose limits, 20 mSv and 500 mSv per year, respectively, for the monitored workers in Syrtic and Cyclone facilities. This proves that the radiation protection program followed in these facilities complies with the radiation

protection requirements according to ALARA principle. Though the recorded doses for workers in AUH didn't exceed the dose limits, however, the radiation protection procedures need to be improved.

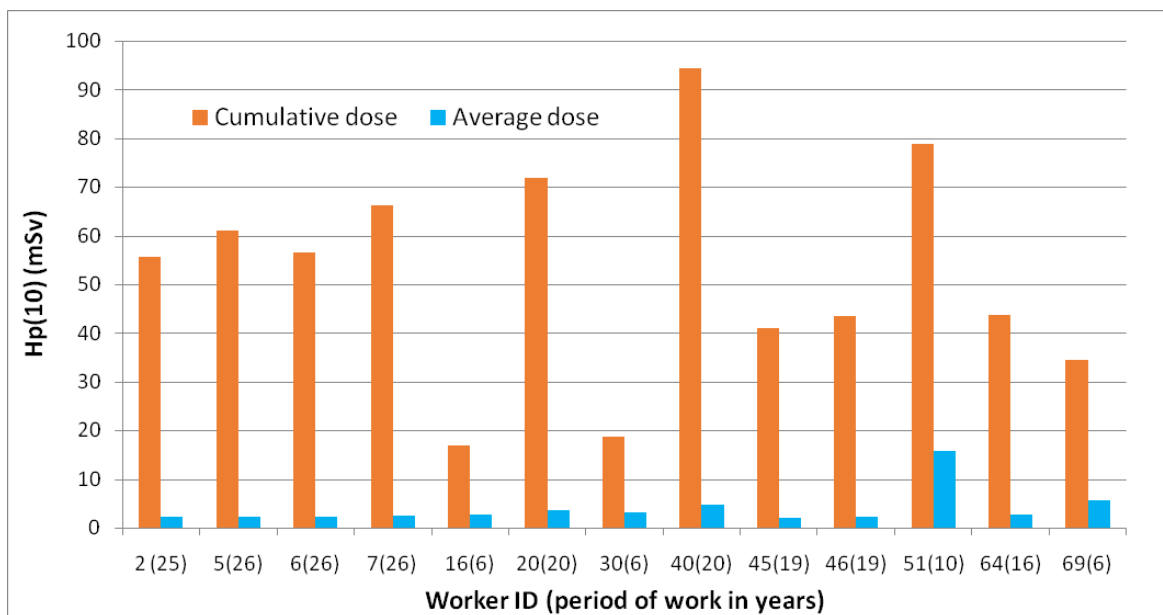


Figure 1. Cumulative recorded Hp(10) and average annual dose for chosen workers in Syrtic facility

Low Activity of [^{99m}Tc]Pertechnetate as Anti-inflammatory Agent in Dermatitis of BALB/c Mice

H. Budiawan

Department of Nuclear Medicine, Hasan Sadikin General Hospital, Indonesia

Background

The radiobiological effects caused by low-dose radiation are distinct from that of high-dose radiation. Low-dose X-ray radiation therapy (LD-RT) was proposed to modulate uncontrollable inflammation in pneumonia and may exert anti-inflammatory effects and raised the attention for the treatment of COVID-19 pneumonia during the hyper-inflammatory state. Due to the possession of similar properties, gamma photon might also have the similar anti-inflammatory effects as X-ray does. Several in vitro and animal studies concluded that gamma photon was useful as anti-inflammation agent. This study was aimed to prove that relatively low-dose radiation of [^{99m}Tc]pertechnetate might have a role as anti-inflammatory agent and useful in treating dermatitis in BALB/c mice.

Methodology

Topical 1-chloro-2,4-dinitrobenzene 99% was used to induce dermatitis on the back of mice. Three groups of BALB/c mice were treated with patches (diameter of 1 inch) for 72 hours containing 37 MBq, 111 MBq, and 222 MBq respectively, one group treated with topical hydrocortisone, and one group was left untreated.

Results

Two weeks later the post-treatment dermatitis was evaluated. Treatment with 37 MBq [^{99m}Tc]pertechnetate showed the best results visually. Immunohistochemistry studies with interleukin 6 (IL-6) and tumour necrosis factor alpha (TNF- α) also showed that the lowest immuno-expression was observed from samples treated by 37 MBq, almost similar with the effect of topical hydrocortisone. Treatment with 111 MBq and 222 MBq revealed more intense immunoexpression.

Conclusion

Relatively lower activity of [^{99m}Tc]pertechnetate is potential to be used as anti-inflammatory agent, while higher activity may induce hyperinflammation.

Keywords: [^{99m}Tc]pertechnetate, anti-inflammatory effect, dermatitis

Predictive Value of [¹⁸F]F-PSMA-1007 PET/CT Quantitative Parameters for Lymph Node Involvement in Intermediate to High-Risk Prostate Cancer and its Potential to Improve Patient Selection for Extended Pelvic Lymph Node Dissection

J. E. V. Ahumada, F. O. G. Perez, S. D. G. Rueda, E. M. Sánchez, Q. G. P. Cortés, F. A. S. Solís

Instituto Nacional de Cancerología, Mexico

Background

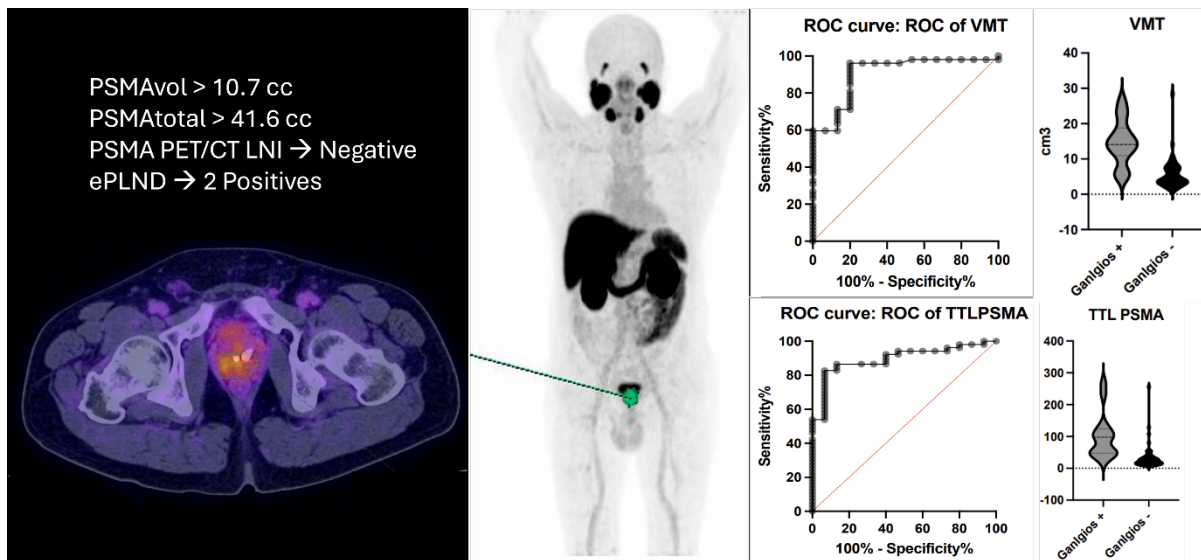
Accurate primary staging of prostate cancer (PCa) is important for individualized treatment planning. Current guidelines recommend PSMA PET/CT which has demonstrated higher accuracy than conventional imaging for disease localization and high specificity for the detection of pelvic lymph node metastases in patients undergoing radical prostatectomy. Despite the advances in molecular imaging, radical prostatectomy with extended pelvic lymph node dissection (ePLND) represents the gold standard for nodal staging in PCa, however, ePLND is associated with potential complications, such as lymphoceles, lymphedema and thromboembolic events. [¹⁸F]PSMA PET/CT has not reached satisfactory detection of micrometastasis; therefore, cancer centers perform ePLND based on clinical nomograms to predict lymph node involvement (LNI), even in the absence of positive findings on staging imaging. Assessment of the primary tumour by molecular imaging may be a potential tool to predict nodal metastasis in PCa patients. The aim of this study is to investigate whether quantitative parameters on [¹⁸F]F-PSMA-1007 PET/CT could predict LNI in patients with intermediate and high-risk PCa and assess the added value of PSMA PET/CT in comparison with current clinical nomograms for risk assessment of nodal disease.

Methodology

[¹⁸F]PSMA PET/CT scans of 67 patients that underwent radical prostatectomy and ePLND from 2018 to 2023 were reviewed for qualitative assessment of suspicious nodes and quantitative parameters of the primary tumour (SUV_{max}, PSMA_{total} and PSMA_{vol}). PET parameters to predict nodal metastasis was assessed with receiver operating characteristics (ROC) analysis. A multivariable logistic regression model combining PSA, Gleason score, visual nodal status on PET and primary tumour PSMA_{vol} developed by Muehlematter et al. (www.psm-pet.com/predict/) was used and compared with two clinical nomograms: MSKCC and Bringanti.

Results

Overall, pathology of ePLND revealed 25 pelvic metastatic lymph nodes in 14 patients. [¹⁸F]F-PSMA-1007 PET visual analysis correctly detected suspicious nodes in 6 patients, yielding a sensitivity of 43%; specificity of 98%; PPV 86% and NPV 87%. The area under the ROC curve for primary tumour PSMA_{vol} was 0.9 (CI 95%; 0.82-0.98; p<0.0001) and for PSMA_{total} 0.89 (CI 95%; 0.81-0.97; p<0.0001). The optimal cut-off for nodal involvement was PSMA_{vol} >10.7 cc (sensitivity 96%; specificity 80%) and PSMA_{total} >41.6 cc (sensitivity 82%; specificity 93%) with an increased likelihood ratio of 4.8 and 12.4 respectively. PSMA SUV_{max} showed not statistically significance. The PET model including PSA, Gleason score and quantitative PET parameters had a higher accuracy compared with the other two clinical nomograms.



Conclusion

Our results indicate that quantitative parameters derived from [¹⁸F]F-PSMA-1007 may improve LNI prediction in intermediate to high-risk PCa patients, even in the absence of positive findings on staging imaging. Also, when combined with clinical parameters, PSMA PET/CT quantitative parameters of the primary tumour showed a tendency to improve patient selection for ePLND over the currently used clinical nomograms.

Diagnostic Performance of Novel [18F]PSMA-1007 PET/CT on the Assessment of Prostate Cancer: National Experience in CUDIM in 237 Patients

G. d. S. Loureiro, I. Cordero, A. Banchemo, A. Quagliata, E. S. Quevedo, V. Trindade, J. P. Leiva, J. G. Gonzalez, P. Duarte, O. Alonso

Nuclear Medicine and MI Centre, University of Uruguay and Centro Uruguayo de Imagenología Molecular (CUDIM), Uruguay

Background

As the novel tracer [18F]PSMA-1007 had demonstrated interesting properties for the diagnostic evaluation of prostate cancer (PCa),

Aim

To determine its clinical value of (detection rates) [18F]PSMA-1007 in different clinical scenarios.

Methodology

A sample of 237 patients (median age:70.22, range:49-89 years; median PSA level:16.17 ng/mL, range:0.03-659 ng/mL; Gleason Score >6) at initial staging (n=54, 22.7%) or with biochemical recurrence/restaging (n=180, 75.9%) after radical prostatectomy (n=82, 45.5%) or radiotherapy/hormonotherapy/QT (n=98, 54.4%) were included between Jun/2020-Feb/2024. 3 patients (1.4%) were evaluated for treatment of [¹⁷⁷Lu]PSMA-617.

All patients underwent a routine PET/CT scan with [¹⁸F]PSMA-1007.

Consent to publish and informed consents were obtained from all individual participants included in the study.

Results

[¹⁸F]PSMA-1007 showed hepatobiliary clearance with high uptake in the liver and gallbladder, while limited uptake was noted in the kidneys and urinary bladder, which was an advantage in the detection of retroperitoneal pathological nodes.

In the whole population [¹⁸F]PSMA-1007 PET/CT demonstrated abnormal findings in 181/237 patients (positivity rate: 76.3%). Discriminating by scenario, the positive rate for Initial Staging and Biochemical Recurrence scenarios were 83 and 74 % (45/54 and 133/180 patients) respectively.

Globally, the lesions were detected by the radiopharmaceutical in the following sites: bone (n=75 patients), lymph-nodes (n=69 patients) and prostate gland (n=132 patients). Unusual sites of metastases were found on lungs (n=8), rectum (n=2), spleen (n=2), bladder (n=2), suprarenal gland (n=1), muscle (n=1), liver (n=2) and ureter (n=1).

At least one suspicious lesion for PCa metastasis was detected in 118 (49.7%) of 237 patients.

In the primary staging group, [¹⁸F]PSMA-1007 PET/CT detected distant metastases in 23/54 patients, both in lymph nodes (15 patients, 27%) and in bone lesions (17 patients, 32%). Notably, therapy planning was modified in 42% of patients.

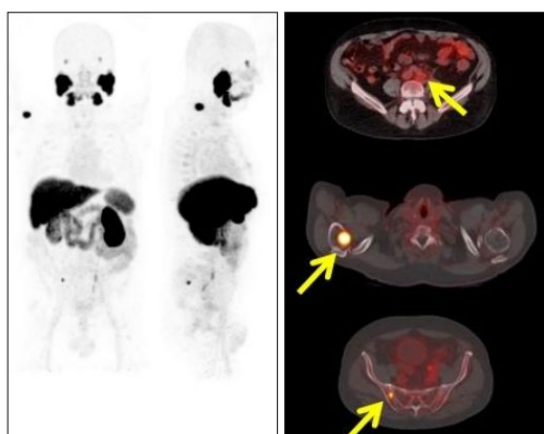
In patients undergoing RBQ/restaging, metastases and/or PCa recurrence were detected in 93 (51%) of 180 in the following sites: prostate (n=87, 48%), lymph nodes (n=54, 30%), bone (n=55, 30%), and in other organs or systems – chop - (n=19, 10%).

In RBQ scenario even at low PSA values (PSA<1 ng/ml), prostate tumour activity and extra-prostate metastases were detected in 14 and 20 patients respectively (detection rate 30% and 43%).

The smallest size of a lesion detected was 3.6 mm.

Lowest detected PSA value was 0.03 ng/ml. The detection rates for extrapelvic disease (metastases) for PSA levels 0-<0.5, 0.5<1, 1<2, 2<5 and >5 ng/mL were 58%, 56%, 62%, 79% and 87% respectively.

In the “Theranostic” scenario (n=3), the PET/CT images confirmed PSMA expression in metastatic lesions and post-therapy SPECT/CT images performed 48 hours after the injection of 7GBq of [¹⁷⁷Lu]PSMA-617 allowed follow up.



MIP and PET/CT images in primary staging showing unexpected metastases. Therapy planning was modified in 4% of the sample.

Conclusion

[¹⁸F]PSMA-1007 demonstrates clinically relevant information for the detection of lesions in the diagnosis and follow-up of Pca patients that conditions clinical behaviour. Its detection ability is not affected by PSA levels which is an advantage in the range of early biochemical relapse. Low urinary excretion of [¹⁸F]PSMA-1007 presents a clear advantage for the pelvic interpretation.

[¹⁸F]PSMA-1007 and [¹⁷⁷Lu]PSMA-617 seem to be a potential theranostic tandem.

Role of FDG PET/CT in staging NSCLC – review of a single institution in Johannesburg, South Africa

O. Mbakaza, B. Kagodora, M.-D.-T. Vangu

Charlotte Maxeke Johannesburg Academic Hospital, University of the Witwatersrand, South Africa

Background

Revised eighth edition of the TNM staging for lung cancer that was released in 2017 included updates for both T and M descriptors. A new M1b descriptor that defines ‘a single extrathoracic metastasis’ is of a particular attention because individuals with this descriptor have a better survival despite the presence of a metastatic disease when opposed to those with multiple extrathoracic metastases. Positron emission tomography/computed tomography (PET/CT) with 18F-fluorodeoxyglucose ([18F]FDG) is today a standard in the care of lung cancer and plays a central role in the management of non-small cell lung cancer (NSCLC). The aim of this study is to describe findings of F-FDG PET/CT during staging.

Methodology

This is a retrospective analysis of data from patients that were referred at the CM Johannesburg Academic Hospital (CMJAH) from 2017 to 2021. The size and activity of the primary site (PS) was measured, and their location defined. The frequency of lymph nodes involvement and metastatic disease spread was measured and their [18F]FDG activity assessed with the use of maximum standardized uptake value (SUVmax).

Results

Data from 24 female (24.24%) and 75 male (75.76%) patients were reviewed. The mean age \pm SD was 60.55 ± 9.77 years. Most PS were identified in right upper lobe of the lung (RUL) and had median size = 4.5 cm (IQR1=3.06 cm & IQR3=6.49 cm) with median SUVmax =12.4 (IQR1=8.4 & IQR3=17.9). Presence of distant metastases was noted in 26 patients (26.3%) and the adrenal was gland the sole metastasis in 5 patients (5.05%), and brain being the sole metastasis in 3 patients (3.03%). Metastases were highly associated with the PS seen in the left upper lobe (LUL), $p=0.01$. Metabolically active mediastinal lymph nodes noted in 64 patients (64.7%). Their median size was 1.9 cm (IQR1= 1.4 cm & IQR3= 2.3 cm, with median SUVmax= 8.3 (IQR1=5.4 & IQR3=11.5). Forty-four patients (44.4%) showed evidence of active hilar nodes with median size= 1.5 cm (IQR1=1.1 cm & IQR3=2.3 cm), and median SUVmax= 4.4 (IQR1= 3.2 & IQR3= 7.4). Primary sites in RUL had a very highly significantly association with mediastinal lymph nodes ($p=0.009$). Supraclavicular lymph nodes were noted in 24 patients (24.2%) and had a median size= 1.4 cm (IQR1=0.9 cm & IQR3=2.6 cm) with median SUVmax=4.9 (IQR1=3.5 & IQR3=9.4).

Conclusion

[18F]FDG PET/CT is currently the imaging modality of choice for the assessment of metastatic disease in NSCLC. Detailed mapping (size and metabolic activity) of visualized metastases together with involved intra and extrathoracic nodal disease is feasible with the use of [18F]FDG PET/CT at staging. This study demonstrated the role that this molecular imaging modality plays in staging NSCLC. It can direct biopsy to the most avid lymph nodes to enhance patients’ management. In individuals without

evidence of metabolically active mediastinal nodes, surgical resection of PS may be safely considered or conducted without the need of an invasive mediastinal staging. Derived quantitative parameters on PET/CT with F-FDG may be of tremendous value in predicting disease outcomes.

Initial Institutional experience on Role of Radioguided surgery in Giant Cell tumour (GCT)

R. Suthar, G. Bavaliya, N. Bharwani, J. Gandhi, S. Pandya, A. Salunke, O. Sinha

The Gujarat Cancer and Research Institute, India

Background

Radioguided surgery (RGS) is a time tested method surgery. It all started in way back when first radioguided surgery was performed using a beta emitter molecule in brain.

Radioguided surgery of para thyroid gland using Tc Sestamibi (MIBI) have performed by many centers previously. Except sentinel nodes dissection, parathyroid surgery is one of most explore part using gamma probe and RGS.

MIBI being a non specific tumour molecule, it is very well localized in GCT. Negative margin in GCT surgery is most import prognostic factor and this is totally dependent to skill of surgeon. And due to varied experience among surgeon recurrence rates in GCT ranges varies on long range from 5-45%. Hence it is reasonable to assume that MIBI guided surgery shall very well demarcate the margin of active tumour and can achieve better adequacy of curettage margin clearance in surgery.

Here in this abstract we sharing initial experience of 3 such patients.

Study Design

Investigator initiated interventional Pilot study, Ethical approval granted by Institutional Review committee (IRC) no: EC/03/2023.

All individuals aged >18 years with biopsy-proven giant cell tumours (GCT) of bone who are scheduled to undergo curettage surgery

Study Methodology

The patient received an injection of 10 mCi of Tc-99m MIBI on the day of the surgery. Two hours post-injection, planar imaging was conducted to confirm the concentration of the tracer. The surgical procedure was carried out under the guidance of a gamma probe. Background counts were meticulously recorded in the adjacent, most prominent subcutaneous bone, specifically the medial malleolus in these three patients.

Sequential tissue samples were systematically collected from the tumour sites mentioned in mentioned in Table. The counts obtained are meticulously documented in the specified manner, as outlined in Table.

Results

All three patients presented with a primary giant cell tumour (GCT) located in the proximal tibia. In all cases, concentration of 99mTc MIBI was observed in the primary tumour, and none of the patients exhibited abnormal tracer concentration in distant locations. The surgeries were conducted under the guidance of a gamma probe.

Patient No.	Tumour Site	Background counts	Counts at tumour entry	Counts of tumour bulk	Counts of most deepest cavity
01	Tibia	10	60	61	10
02	Tibia	12	67	70	15
03	Tibia	12	65	67	15

Tissue samples for histopathology examination with corresponding counts rate were obtained from three distinct sites:(refer to Table). Three samples were collected from each patients. All of the tissue samples displayed counts higher than the background, correlating with tumour positive histopathology reports.

Conclusion

GCT tumour is very well demarcated with intravenous ^{99m}Tc MIBI hence it can achieve better adequacy of curettage margin clearance in surgery.

However, further larger sample size follows up needs to compare rate of recurrence from standard recurrence rate.

Evaluation of Quality Assurance Program (QAP) in Nuclear Medicine for Malaysia's Medical Institution

M. N. M. Kamari, Z. Kayun

Medical Radiation Surveillance Division, Ministry of Health, Malaysia

Background

The quality assurance program ensures that the entire radiological system and associated equipment are functioning efficiently and effectively. Implementation of Quality Assurance Program (QAP) in government hospital started since 1987 for radiology service involving 14 state hospitals and 2 district hospitals. In 2017, Ministry of Health Malaysia (MOH) made QAP as a mandatory requirement for nuclear medicine service for the government and private hospitals to improve the quality of services in nuclear medicine. MOH has taken a proactive step by conducting a study on implementation of QAP in Nuclear Medicine from 2022 until 2023.

Objectives

The study is aimed to identify the effectiveness of the QAP program that has been implemented and potential improvement that can be made. Several medical institutions have been chosen as a location for the research such as Sunway Medical Centre, KPJ Ampang Puteri Specialist Hospital, Sultan Abdul Aziz Shah Hospital, Beacon Hospital and Sarawak Heart Centre.

Methodology

The research was then assessed through questionnaires, interviews, observations and document review.

Results

From the results, majority of the premises successfully implemented the QAP program as stated in the QAP Implementation Manual. However, there is an improvement needed such as on Indicator-Rate of Repeat Studies and Training records (CME/CPE) for each personnel whereby these records need to be well maintained and monitored from time to time. Besides that, Quality Audit Manager and the Internal Quality Audit group can also be introduced to help coordinate the implementation of QAP at each premises.

Conclusion

In conclusion, the implementation of the QAP program has successfully improved the quality of services in nuclear medicine as well as being able to optimize the production of clinical information through the effective use of radioactivity.

Diagnostic Performance of [^{99m}Tc]UBI (29-41) SPECT/CT In Infectious Diseases

S. Saeed, J. K. Maitlo

Pakistan Institute of Engineering & Applied Sciences (PIEAS), Pakistan Atomic Energy Commission (PAEC), Pakistan

Background

Ubiquicidin (UBI) 29-41 is a cationic, synthetic antimicrobial peptide fragment that binds preferentially with the anionic microbial cell membrane at the site of infection. It is a part of human innate immunity.

Labelled with ^{99m}Tc, it is increasingly used as an infection specific imaging agent.

Aims: The study was conducted to evaluate the potential role of [^{99m}Tc]UBI (29-41) SPECT/CT in diagnosing invasive fungal chest infections, diabetic foot and orthopaedic implant infections.

Methodology

21 patients (Males = 17, females = 4, mean age = 53 years and range = 25-80) suspected of having fungal chest infections, 41 patients (Males = 34, females = 7, mean age = 56 years and range = 40-76) suspected of having diabetic foot osteomyelitis and 14 patients (Males = 11, females = 3, mean age = 43 years and range = 12-77) suspected of having orthopaedic implant infections were included in this study. A dose of 407 MBq (11mCi) of [^{99m}Tc]UBI (29-41) with high specific activity (407MBq/0.5ml) was injected to patients with suspected fungal chest infection patients, diabetic foot and orthopaedic implant infection patients. In suspected fungal chest infection patients, anterior and posterior whole body projections were acquired at 30minutes post radiotracer injection followed by static spot views of suspicious area. Immediate 1 minute dynamic study was followed by spot views at 15-30minutes and SPECT/CT at 30-45minutes in suspected diabetic foot and prosthetic implant infection patients. The scans were interpreted as true or false positive and true or false negative on the basis of bone biopsy/pus culture, history, clinical examination and follow up.

Results

The technetium-99m UBI (29-41) scintigraphy results for fungal chest infection are 42% sensitivity, 50% specificity, 89% positive predictive value, 8% negative predictive value with 43% diagnostic accuracy. Sensitivity, specificity, PPV, NPV and diagnostic accuracy for diabetic foot infection are 100%, 86%, 97%, 100% and 98% respectively. The technetium-99m UBI (29-41) imaging results for orthopaedic implant infection are 91% sensitivity, 100% specificity, 100% positive predictive value, 75% negative predictive value with 93% diagnostic accuracy.

Conclusion

The labeled antimicrobial peptide technetium-99m ubiquicidin (29-41) is a specific imaging agent and shows promising results for diagnosis of diabetic foot infections and orthopaedic implant infections. However it is not suitable for invasive fungal chest infection diagnosis.

Use of interim PET/CT (iPET/CT) in the detection and determination of early responders in the management of advanced Hodgkins lymphoma (HL)

Satish Panchadar, Gautam Biswas, Saqr Mohammad Asaad, Zainab Abdullah, Masoud Garashi, Rawand Al Kordy, Eiman Al Awadhi

Chest Diseases Hospital, Kuwait

Aim

The objective was to evaluate whether early response assessment in advanced HL by interim PET/CT after 2 cycles of chemotherapy could predict positive treatment outcomes and disease free status post-therapy.

Methodology

We analysed 39 patients with biopsy proven HL (23males, 16females) in the age group of 33 to 72 years. All patients had both baseline and interim PET/CT studies using standardized protocol with a 64slice, 16cms axial field of view GE 710 PET/CT camera. A standard dose of 0.06 mCi of FDG per kg/body weight used and vertex to mid-thigh images acquired after an uptake phase of 60mins. Three independent PET/CT qualified and experienced physicians did reconstruction, analysis and interpretation on Advantage (ADW) and Hermes workstations. Based on Lugano classification, 13patients had disseminated disease (stage IV); 17patients had stage III (1) and 9patients had stage III (2). iPET/CT was performed after 2 cycles of chemotherapy (ABVD) and patients followed up for 15 months.

Results

Statistical analysis performed with statistical package for social sciences (SPSS). Differences between responders tested with paired t-test in the same patient. The p values <0.05 were considered to indicate statistical significance. Maximum standardized uptake values (SUVmax) with visual Deauville 5point scores incorporated into Lugano classification were used to assign responses as partial response (PR), complete response (CR), stable disease (SD) and progressive disease (PD). 14patients with stage III (1), 2from stage III (2) and 3from stageIV (total 19patients; 48.71%) showed partial response with Deauville score of 4-5, no new lesions, reduced FDG uptake from baseline study. 1 patient (2.56%) from stage III (2) showed complete response with Deauville score of 1-3, no new lesions, no bone marrow involvement and remaining 9 patients (23.07%) from combined stageIII(1) and (2) showed stable disease with Deauville score of 4 or 5, no change in FDG uptake from baseline, no change in bone marrow involvement and no new lesions. 10 patients (25.64%) from stageIV showed disease progression with Deauville score of 4 or 5, increased FDG uptake from baseline and appearance of new lesions, necessitating change in treatment strategy.

Conclusion

Our study indicates that early interim chemotherapy response evaluation using iPET/CT could stratify patients into responder's versus non-responders in advanced HL, thereby affecting treatment strategies. In our study 48.71% of patients showed early response with complete response in 1patient (2.56%) and disease progression in 25.64%, leading to change in treatment strategies. These responses from interim

PET/CT showed high degree of agreement with end-of-treatment PET/CT. Of late, the role of iPET/CT is being widely recognized in guiding treatment strategies of advanced HL. With precise early prediction of response-to-therapy, sorting of patients can be done into the ones who can be rescued completely with standard regular therapy or less intensive/toxic regimens from the ones who may have to be switched to alternative and/or more aggressive treatment strategies to improve outcomes. Recently, a phase III trial showed that if interim PET/CT is negative after two cycles of ABVD, bleomycin can be stopped (i.e., de-escalation to AVD) without compromising efficacy. In general, iPET/CT tailored-risk and response-adapted approach could become the standard of care to achieve a higher cure rate with a lower risk of treatment related morbidity/mortality.

Evaluation of the Whole Body Computed Tomography scanning parameters in PET/CT

N. Salkica, A. Beganović, A. Skopljak-Beganovic, H. Čorović, S. Hadžimusić

Clinical Center of the University of Sarajevo, Bosnia & Herzegovina

Background

Computed tomography (CT) is an essential modality used for attenuation correction of PET images. Besides this, CT gives morphological information of the pathological process seen on PET images. This information can be obtained in a process called fusion of the CT and PET images. The vast majority of PET/CT studies use low dose CT parameters for attenuation correction and fusion of the PET and CT. Nevertheless, patient dose due to whole body CT is comparable to dose resulting from [¹⁸F]FDG intake. Hence, special attention needs to be given to the optimization of scanning parameters, as they are sometimes not appropriate for different patient sizes. Many studies highlight problems in attenuation correction of PET images when inadequate CT parameters are used for different patient's body size. The aim of our research was to evaluate the current low dose CT protocol used for PET/CT studies, and provide a tool for quality control of CT scanning protocols used in PET/CT.

Methodology

We performed prospective study for 50 oncology patients who underwent [¹⁸F]FDG PET/CT study. Our patients have been divided into groups based on their body mass index (BMI). A Python script was created to extract necessary data values from DICOM header, including patient data (gender, height and weight, age, etc.), scanning parameters (tube voltage and current for each slice, pitch, tube rotation time, collimation etc.), and exposure data (CTDI and DLP).

Results

The results indicate that automatic tube current used in the evaluated protocol fails to achieve optimal values due to a set maximum at 200 mA. Overweight and obese patients receive dose lower than optimal in high attenuation areas, such as breasts in female patients, or abdomen for both genders. Similarly, for underweight patients included in the study, tube current cannot go below 10 mA, which is the minimum current that CT can produce.

Conclusion

Due to negative effects on CT image quality and/or patient dose, optimisation of the low dose CT protocol for patients with extreme weight is highly recommended. This is especially true for CT images in PET/CT studies due to the possible impact on SUV measurements and diagnosis. In the study, we identified the situations when the alternative scanning protocol based on patient's BMI must be used. Further investigations could go in direction of evaluating the resulting image quality and its impact on SUV calculations.

Keywords: CT, PET/CT, BMI, [¹⁸F]FDG, SUV

Cross calibration Correction Factor (CCCF) of a PET/CT system using manufacturers' guidelines and comparing it with the IAEA SUV calculation: An IALCH experience

T. Mkhize^{1,2}, D. Seabi^{1,2}

¹ Inkosi Albert Luthuli Central Hospital, South Africa

² University of KwaZulu-Natal, South Africa

Background

NEMA acceptance tests are a well-established tools for assessing the performance of a PET/CT system. The advantage of these tests are that they are independent of multiple factors that may affect the system, but usually they are tested annually in most cases. Cross calibration correction factor (CCCF) tests are usually performed once a year, with the factor being checked daily using a daily quality assurance phantom to assure system performance. The test is done to cross calibrate the PET/CT system to the dose calibrator used for measurements of activity. The objective of this study is to confirm our PET/CTs CCCF value and to compare this with the IAEA SUV calculation.

Methodology

CCCF test was performed following the manufacturers' protocol on our Biograph mCT S(64) PET/CT system (Siemens Healthineers, Erlangen, Germany) using a 4000ml phantom injected with ≈ 1.59 mCi of F-18 activity. The activity was measured using a Curiementor 4 (PTW, FreiburgLorracher Strasse, Germany) dose calibrator. From the workstation interface the following information was entered in the PET cross calibration tool: measured dose, measured dose assay time, residual dose, residual dose assay time, and phantom volume. A scan of the phantom with one bed position and 100 000 000 counts was made (with a delay time of 31 minutes from measurement to scan). These values were also used to calculate the IAEA SUV value. The acquired images were analysed on the workstation tool (See Figure 1).

Results

12 regions of interests (ROIs) were drawn within the phantom image and the concentrations for each ROI were recorded as "Measured Specific Activity", the average Measured Specific Activity was recorded as 12472.58 Bq/ml (See Figure 1). The CCCF was computed as 0.97, whilst the calculation using the IAEA SUV was 1.02.

Conclusion

From the results, the CCCF was calculated using the manufacturers' tool and the value was within the acceptable range. The IAEA SUV value was calculated (accounting for the decay correction) and its value was also within the acceptable range. These tests are very important for the role of PET/CT in quantitative imaging. Regular checks of the CCCF is advised annually and after a source change.

PET Cross Calibration

E-18 Phantom Information

Measured Dose: 1.60 mCi Time: 14:21:00
 Residual Dose: 0.11 mCi Time: 14:24:00
 Net Dose: 1.59 mCi Time: 14:21:00
 Phantom Volume: 400.0 ml

Scan Information

Scan Start Time: 14:51:52 Delay to Scan Start: 30.87 min

Calculated Specific Activity

Calculated Specific Activity @ Scan Start: 12106.92 Bq/ml

Measured Specific Activity

ROI	Activity	ROI	Activity
ROI #1	12290.61 Bq/ml	ROI #2	12457.23 Bq/ml
ROI #3	12125.53 Bq/ml	ROI #4	12498.95 Bq/ml
ROI #5	12551.82 Bq/ml	ROI #6	12465.52 Bq/ml
ROI #7	12550.10 Bq/ml	ROI #8	12487.92 Bq/ml
ROI #9	12535.23 Bq/ml	ROI #10	12496.45 Bq/ml
ROI #11	12501.59 Bq/ml	ROI #12	12479.64 Bq/ml

Measured Specific Activity @ Scan Start: 12472.69 Bq/ml

Dose Cross-Calibration Factor

CCCF: 0.97

IMPORTANT!
 Remember to update Dose Cross-Calibration Factor using
 Options -> Configuration -> PET QC Configuration

Figure 1.

SPECT/CT Whole-Body Bone Scan Time Optimization Using Image Quality: A phantom Study in IALCH

T. Mkhize^{1,2}, D. Seabi^{1,2}, S. Zwane¹

¹ Inkosi Albert Luthuli Central Hospital, South Africa

² University of KwaZulu-Natal, South Africa

Background

Single-Photon emission computed tomography (SPECT) is an imaging technique that allows in vivo measurements of 3-dimensional (3D) distribution of gamma photon emitting tracers. Technetium-99 metastable is the most commonly used SPECT imaging radionuclide. SPECT acquisition parameters play a major role on image quality and should be chosen carefully. Acquisition times range from 15-25 minutes per bed position, which tend to discourage whole-body (WB) SPECT imaging which often tend to need 3-5 bed positions. The reduction in acquisition times per bed position can reduce artefacts, improve patient comfort and improve patient throughput especially in a resource constrained centre. The prospect of scan time reduction should not reduce image quality. The objective of the study was to investigate the impact of acquisition time and reconstruction parameters on image quality for a bone scan protocol and investigate the possibility of reducing our current times on the bone scan protocol.

Methodology

A 9.8 l PTW PET emission Phantom (acc NEMA NU2-2007) with 6 fillable spheres was used (the 37mm sphere was damaged, but the other 5 spheres were used). 5.95 mCi Tc-99m activity measure on a Curiemeter 4 (PTW, Freiburg, Germany) dose calibrator. The activity was mixed with 1.2 l of water to give an activity concentration of 183 kBq/ml, which was used to fill the 5 spheres (10ml, 13ml, 17ml, 22ml and 27ml). The remainder of the activity was used to give a background activity concentration of 22 kBq/ml. The hot-sphere-to-background ratio was 8:1. An Intevo SPECT/CT (Siemens Healthineers, Erlangen, Germany) dual camera was used to acquire 3 scans of times “5 seconds, 8 seconds and 15 seconds (Current protocol)” per projection for a 120 projections (Total time: 15 minutes, 8 minutes and 5 minutes, per bed position). The acquired scans were analysed using MIMS software v7.2 with OSEM variable reconstructions and variable Gaussian filters, with respect of time. Image quality parameters analysed were Contrast Recovery (CR), Contrast to noise ratio (CNR) and Background variability (BV), all with respect to time.

Results

The first part of the study was to take the longest scan time and develop a reconstruction protocol to use for all the subsequent times. RC showed a slight improvement with increased Iterations but the improvement decreases with decreasing sphere size. BV reduced with increasing filter sizes, but increases with increasing Iterations. CNR increased with increasing filter and a reconstruction protocol of 8 iterations, 8 subsets and 4mm Gaussian filter was chosen. Using this protocol for the other times, with respect to image quality. RC improved slightly as time increased, BV decreased with increasing time and CNR improved with increased time with a levelling from 8 minutes.

Conclusion

The results showed the effect of image quality with respect to time, from our results it was shown that the 8 minutes scan protocol fared well with comparison to the 15 minute departmental protocol. This could reduce our WB scan times by up to 40 - 50%.

Importance of SPECT/CT Imaging in the Follow up of Differentiated Thyroid Carcinoma and additional value of 20 days-levothyroxine withdrawal

G. d. S. Loureiro^{1,2}, K. Bayardo¹, T. Arias¹, M. T. Negreira³, P. Orellano³, S. Rodriguez¹, B. Mendoza³, J. C. Hermida¹, O. Alonso^{1,2}

¹ Nuclear Medicine and MI Centre, University of Uruguay, Uruguay

² CUDIM - Molecular Imaging Uruguayan Center, Uruguay

³ Cátedra de Endocrinología y Metabolismo, del Hospital de Clínicas Montevideo, Uruguay

Background

To describe the benefit of SPECT/CT in the follow-up of patients with differentiated thyroid cancer (DTC), given indeterminate findings in the whole-body scanning (WBS) with 131I.

As induced hypothyroidism by 4-6 weeks discontinuation of Levothyroxine (to reach TSH \geq 30 uIU/ml) can produce adverse effects, in a subpopulation we aimed to dose it also at day 20.

Methodology

From November/2014 to Jun/2023, 281 WBC studies were carried out with 131I in patients with DTC (at least 6 months after the administration of a therapeutic dose of 100-200 mCi of 131I).

72 hours after oral administration of 3-5 mCi of 131I, images of the whole body and neck (AP and PA) were acquired.

30 patients (11%) with indeterminate or suspicious findings in the TBC underwent a SPECT/CT study of the region of interest using a Mediso AnyScan16 device and the results were analysed.

All patients suspended LT4 30 days before TSH dosage and WBS. In a 20 patient-subpopulation, TSH was also dosed also on day 20 and quality of life was assessed.

Results

26/30 patients (87%) were female and 4/30 (13%) were male. The average age was 49 years (range 27-79).

The Tg value ranged between 0.04 and 5000 ng/ml.

19/30 patients (63%) have normal values of antithyroglobulin antibodies (VN: <40 IU/ml), while the rest (n=11/30; 37%) are above the range or without data.

All patients had a TSH value <30 IU/ml as a requirement.

10 (33%) of the patients were low risk, 16 (53%) were intermediate risk and 4 (13%) high risk.

An abnormal alteration in 131I uptake ("positive study") was observed in 17/30 patients (57%; 15 remnants, 5 lymph-nodes).

9 patients (30%) showed uptake in thyroid remnants, which defined the surgical procedure, making it possible to coordinate a new therapeutic dose.

In 7 patients (23%) doubtful findings were found on the planar image. SPECT-CT was able to determine the etiology and topography of these uptakes: physiological salivary gland (n=7), esophagus (n=2), thyroglossal duct (n=1), physiological uptake in the source bronchus (n=2), uptake in breast (n=1) and peritoneal nodule (n=1).

In the subpopulation the TSH prior to the suspension of LT4 had a mean value of 0.9uIU/ml, standard deviation +/- 0.67.

On the 20th day, 19 patients increased TSH to ≥ 30 uIU/ml, with a mean of 62.6 uIU / ml (Range: 48.54-76.66). On day 30, all patients had a TSH had >100 uIU/ml.

The symptoms of hypothyroidism registered on day 30 were significantly more severe in relation to day 20.

Conclusion

The indication of SPECT/CT in WBC with ^{131}I is relevant because it allows defining the structures involved, whether pathological or physiological, achieving better staging and adapting the therapeutic approach to the findings found.

According to our results, suspending LT4 20 days prior to DTC evaluation is enough to raise TSH to a value ≥ 30 uIU/ml, and can reduce the undesirable symptoms of acute hypothyroidism that occurs after 30 days.

New radiolabelling strategies for the development of radiotracers for PET infection images

M. T. Gretter, E. S. Quevedo, G. Ceccetto, J. G. Giglio

Facultad de Química – Udelar, Uruguay

Background

Opportunistic infections pose a significant challenge to public health, and the accurate detection and localization of infections in the early stages of the disease are crucial for effective patient management and cost containment. Defensins, plant antimicrobial peptides (AMPs), have garnered attention due to their activity against both plant and human pathogens. Within our research group, we have identified a synthetic short analogue of a defensin that retains the active site of the peptide. This analogue has been selected as a pharmacophore for the development of a potential detection agent for identifying hidden infection foci.

Objective

Development and evaluation of a radiolabelled peptide with Ga-68 and fluorine-18 as potential radiotracer for the detection of hidden infection sites through PET images.

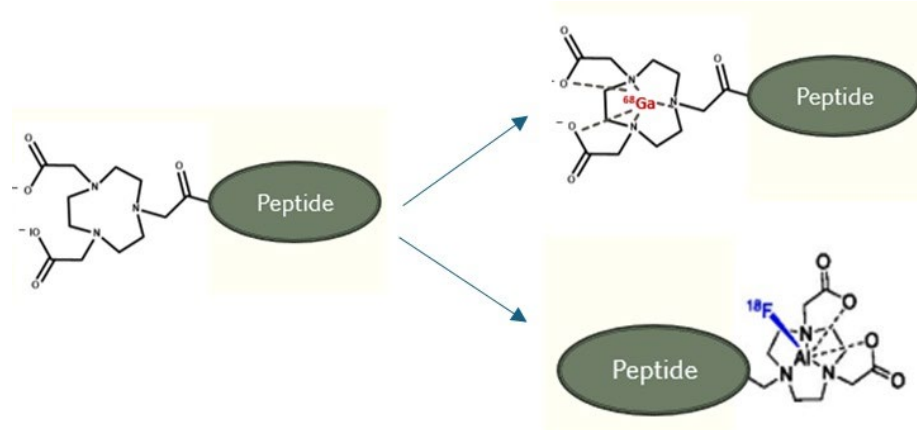
Methodology

The synthetic EcgDf1(10) short analogue was derivatized with the bifunctional chelating agent 1,4,7-triazacyclononane-1,4,7-triacetic acid (NOTA) through a lysine linker in the amino-terminal group. This strategy allows radiolabelled with Ga-68 and fluorine-18 to obtain [⁶⁸Ga]Ga-NOTA-K-GHCRGFRRRC and [¹⁸F]F-NOTA-K-GHCRGFRRRC respectively. Labelling conditions were optimized, the radiolabelled complex was purified and relevant physicochemical characteristics as stability, plasma protein binding and lipophilicity were evaluated. To determine the capacity to bind to different pathogenic microorganism in vitro behaviour was assessed against *C. albicans*, *A. niger* and *S. aureus* cultures. Complementary biological evaluation was conducted in nude female mice. Lesion in the left foreleg were induced in four groups of animals namely: G0=sham, G1=sterile inflammation, G2=*C. albicans* infection, and G3=*A. niger* infection. Image and biodistributions were performed at 2 hours post injection of complex into lateral tail vein.

Results

[⁶⁸Ga]Ga-NOTA-GHCRGFRRRC, was obtained with a radiochemical purity higher than 95% and its stability in milieu was assessed up to 3hs. The competition assay against 10-fold molar excess of DTPA revealed that the complex is stable during the 2hs of study. Lipophilicity studies revealed the complex has a hydrophilic behaviour (Log P: -2.4 ± 0.3), and plasma protein binding is of $42,8 \pm 1,7\%$. In vitro binding assays to microorganism cultures, showing that [⁶⁸Ga]Ga-NOTA-K-GHCRGFRRRC has higher specific binding to *C. albicans* and *A. niger*. There was no specific binding to *S. aureus* according to the microbiological profile of this peptide. Biodistribution indicate urine elimination and no in vivo degradation. Image acquisition revealed clear discrimination between lesion and healthy tissues infected with *C. albicans* and *A. niger*. Infection model reaching a lesion/muscle ratio of $4,5 \pm 0,5$ for *C. albicans* and $5,3 \pm 0,6$ for *A. niger*, statistically different from sterile lipopolysaccharide inflammation of $2,1 \pm 0,2$.

[¹⁸F]AlF-NOTA-GHCRGFRRRC was obtained with high radiochemical purity (>90% after purification) and its physicochemical characteristics are currently being evaluated.



Conclusions

The [⁶⁸Ga]Ga-NOTA-GHCRGFRRRC complex presents appropriate physicochemical characteristics and specific binding to pathogenic fungi. Biodistribution profile indicates urine elimination and no in vivo reoxidation. PET/CT image and lesion/muscle ratio significantly distinguish infection from sterile inflammation.

In case of [¹⁸F]AlF-NOTA-GHCRGFRRRC, complex was successfully synthesized, and its main physicochemical characteristics are under evaluation.

Acknowledgements: CSIC-Project2104, ANII Postgraduate Scholarship POS_NAC_2023_1_177796, PEDECIBA.

An Unconventional Detour: Utility of IJ Catheter as Vascular Access for RBC Labeling in Gastrointestinal Bleeding Scintigraphy with SPECT/CT - A Case Report

M. G. Tumaming¹, I. Bandong²

¹St. Luke's Medical Center Quezon City, Philippines

²Philippine Society of Nuclear Medicine, Philippines

Background

Gastrointestinal bleeding remains the most common gastrointestinal symptom as a cause of hospitalizations in the United States. Due to its high mortality rate, especially in the elderly, prompt identification of the possible source of bleeding is crucial. Upper gastrointestinal endoscopy is the initial diagnostic test to identify and control the bleeding. In addition, gastrointestinal bleeding scintigraphy may play a role, especially in those presenting with intermittent bleeding. It has a high sensitivity of up to 93% and can detect bleeding rates as low as 0.05 mL/min to 0.1 mL/min. Adding hybrid SPECT/CT imaging increases its diagnostic ability by accurately identifying the bleeding site compared to planar images alone. One of its drawbacks is the presence of free pertechnetate due to poor labeling efficiency, which may result in false-positive findings. The objective of the study is to describe the utility of Internal Jugular (IJ) catheter as vascular access for gastrointestinal bleeding scintigraphy radiolabeling in detecting active gastrointestinal bleeding.

Case Report

This is a case of a 91-year-old female presenting with recurrent upper gastrointestinal bleeding and anaemia, and underwent esophagogastroduodenoscopy, hemoclipping, mesenteric angiogram with embolization of the gastroduodenal and left gastric arteries, and multiple blood transfusions. Recurrence of melena was noted despite medical and surgical management. Gastrointestinal bleeding scintigraphy was performed to evaluate other possible sites of bleeding. Due to the patient's poor peripheral venous access, an unconventional route through IJ catheter was used to administer stannous ions, extract blood, and reinject the [^{99m}Tc]labeled RBCs. Dynamic images show a focus of increased tracer uptake in the mid-abdomen at the 10th minute of the study, increasing in intensity, followed by anterograde movement towards the left lower quadrant, consistent with active gastrointestinal bleeding. SPECT/CT further localizes the bleeding to the stomach, duodenum, and proximal jejunum. No undue tracer uptake in the thyroid and salivary glands is seen in the static images of the neck.

Central venous access catheters are not routinely used as a route of administration since stannous ions may bind to the tubing, reducing the administered amount. Stannous ion is used as a reducing agent for technetium-99m to allow binding to haemoglobin; thus, too little stannous ion may be insufficient to reduce [^{99m}Tc]pertechnetate (VII) to a lower oxidation state, adversely affecting RBC labeling. Despite the use of IJ catheter in administration of the various components in labeling RBCs, sufficient radiolabeling was done evidenced by the absence of thyroid gland activity. The sites of active bleeding were also accurately identified with the aid of SPECT/CT.

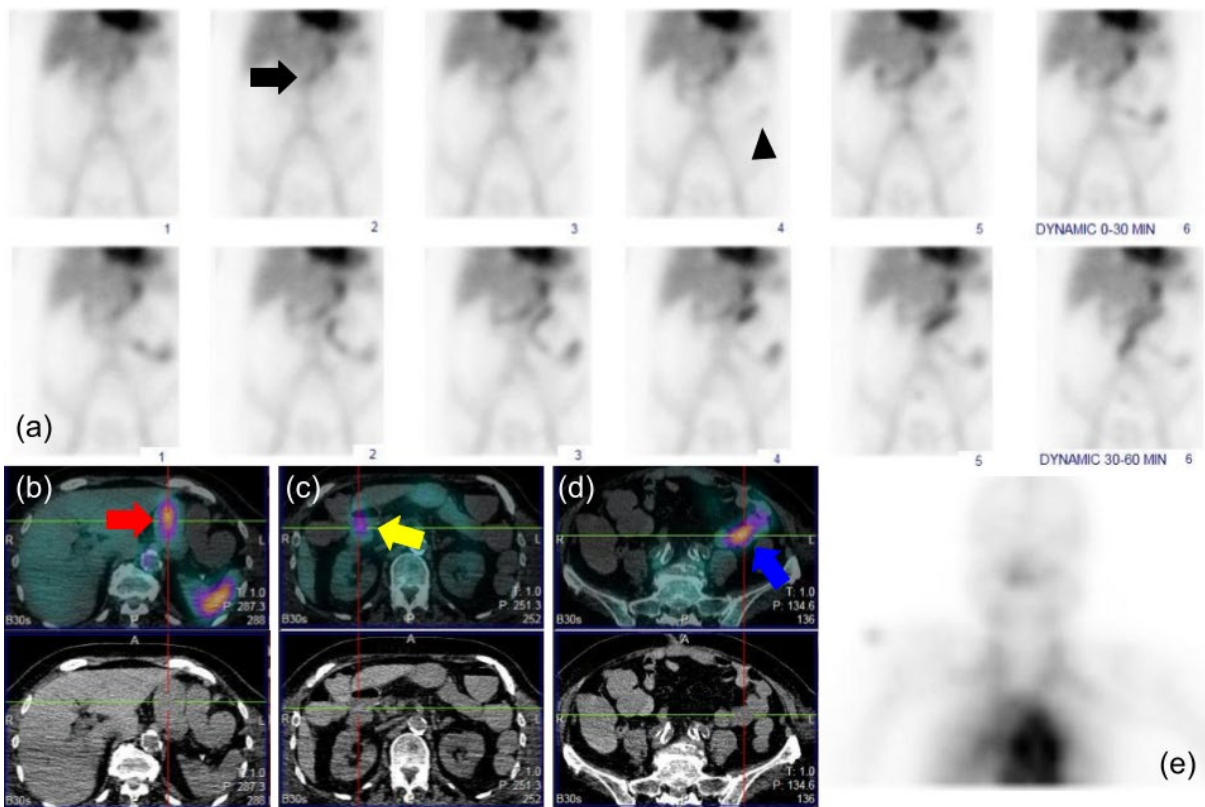


Figure 1. (a) Gastrointestinal bleeding scintigraphy dynamic imaging sequence (5 min/frame) show a focus of increased tracer uptake in the mid-abdomen (arrow) at the 10th minute of the study, increasing in intensity, with antegrade movement towards the left lower quadrant seen by the 20th minute (arrowhead). (b) (c) (d) Fused SPECT/CT images localize the bleeding sites to the stomach (red arrow), duodenum (yellow arrow) and the proximal jejunal (blue arrow) segments. (e) Anterior static image of the neck shows no tracer uptake in the thyroid and salivary glands to denote the presence of free pertechnetate.

Conclusion

Gastrointestinal bleeding scintigraphy with SPECT/CT using IJ catheter as vascular access for radiolabeling may be used to detect and localize active bleeding sites, especially in patients with poor peripheral venous condition.

Comparative study in estimation of radiation exposure and Equivalent dose during dispensing and injection of [18F]FDG using dose calibrator with and without lead ring

M. K. Chauhan^{1,2}, M. V. Manikandan^{1,2}, A. Suresh^{1,2}, J. P. Kumar^{1,2}

¹ Mahamana Pandit Madan Mohan Malviya Cancer Centre, India

² Homi Bhabha Cancer Hospital, India

Background

In Nuclear Medicine, open radiation sources are handled by radiation worker. Our purpose of the study is to estimate the radiation exposure and equivalent dose received by nuclear medicine staff while dose dispensing and injection of [18F]FDG with and without lead ring around dose calibrator.

Methodology

The dose calibrator used was VIK 202 model procured from COMECER, which has the capacity of measuring activity up to 2.0Ci. It has lead shielding of 3.0mm. The instrument used for measuring radiation exposure was SE International Inspector survey meter with model name Ranger, which has the capacity of measurement of radiation exposure from 0.001 μ R to 100mR/hr. For measuring equivalent dose, Pocket Dosimeter was used which has measuring range from 1 μ Sv/h to 100Sv/hr. These each measurement was measured in two different institute. One Institute has Dose Calibrator which was surrounded by Lead rings which are 5.0 cm thick. The other institute have Dose calibrator which was not surrounded by Lead rings. [18F]FDG was dispensed by a radiation worker in a dose calibrator. The radiation exposure was measured at 1 meter distance by using a radiation survey meter for both dose calibrator. The measurements were collected for 11 days for handling different amount of activity of [18F]FDG and average number of PET/CT performed.

Results

The Radiation exposure measured for average activity of 2.64mCi, 3.13mCi, 4.6mCi, 5.48mCi, 6.46mCi, 7.38mCi and 8.86mCi in without lead ring was 2.2mR/hr, 2.5mR/hr, 4.03mR/hr, 4.78mR/hr, 5.69mR/hr, 6.47mR/hr and 7.71mR/hr And for the lead ring was 0.126mR/hr, 0.138mR/hr, 0.189mR/hr, 0.219mR/hr, 0.271mR/hr, 0.304mR/hr and 0.359mR/hr respectively.

Equivalent Dose

For Dose Calibrator not surrounded by lead ring, the radiation worker dispensing the [18F]FDG getting average 14 μ Sv/hr for avg. 12 times of dispensing for handling avg. dose of 103mCi while radiation worker on injection duty getting 16.6 μ Sv/hr for same. For Dose calibrator surrounded by lead ring, the radiation worker dispensing the [18F]FDG getting avg. 11 μ Sv/hr for avg. 13 times of dispensing for handling 107mCi while radiation worker on injection duty getting 13 μ Sv/hr for the same. It was observed that the equivalent dose received by radiation worker during [18F]FDG dispense (in dose calibrator which was surrounded by lead rings) and injection was comparatively low with the other.

Conclusion

Handling the open sources in nuclear medicine without radiation protecting accessories gives unwanted exposure to radiation worker. In institute where they do not have such protecting accessory, the person who is dispensing the activity should left the room after dispensing the activity. Otherwise, that person

may get unwanted exposure during injection. So, during injection time only that person who is injecting should be available. It is very important to work in nuclear medicine with radiation protecting accessories. It minimizes the radiation exposure to radiation workers who will work for a long time in the radiation field.

[⁶⁸Ga]Ga-FAPI-2286: production and quality control methodology using cyclotron produced Ga-68 in a liquid target

J. G. Giglio, J. Vasquez, K. Zirbesegger, A. Boné, L. Tajam, I. Kreimerman, M. P. Pereira, C. Cabillón, A. Blengio, M. Bentura, F. Zoppolo, V. Trindade, G. Falasco, L. Urrutia, P. Duarte, J. P. Gambini, E. Savio

Departamento de Radiofarmacia, Centro Uruguayo de Imagenología Molecular (CUDIM), Montevideo, Uruguay

Background

Fibroblast activation protein (FAP) is a selective marker of cancer-associated fibroblasts. FAP overexpression has been detected in different tumours, making it an attractive target for both diagnosis and therapy. Among FAP inhibitors, FAPI-2286 presents high affinity ($K_d=1.1$ nM) and higher retention in the tumour compared to other derivatives.

The aim of this work was to perform the optimization of the production of [⁶⁸Ga]Ga-FAPI-2286 using Ga-68 produced in cyclotron (General Electric PETtrace, 16.5MeV) with liquid target (Stracotek Co. mod. SC-65), by the reaction $Zn-68(p,n) Ga-68$ irradiating enriched zinc nitrate ($[^{68}Zn]Zn(NO_3)_2 > 99\%$ - CMR) in solution (irradiation 53 minutes at 45 μA).

The purification of the Ga-68 produced was performed on a Synthra RN plus Research platform designed for fluorine-18 labeling using Triskem ion exchange columns (ZR-R10-5 and TK200-R10-5) adapting the module for this process according to the scheme presented in Figure 1.

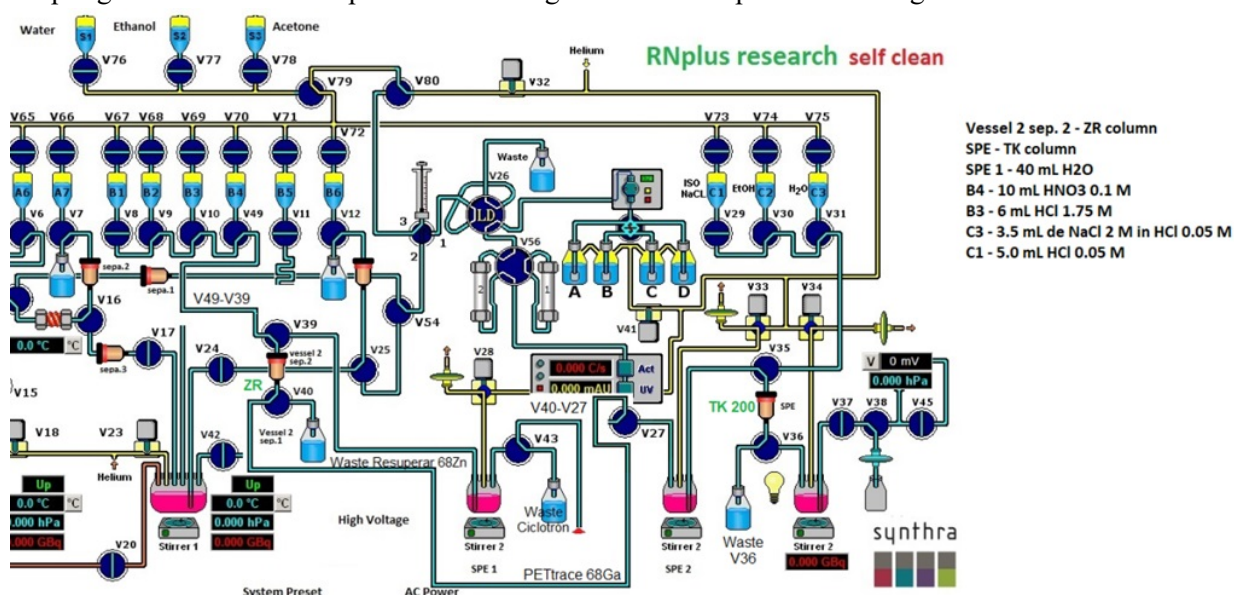


Figure 1. Ga-68 purification module connections.

The purified Ga-68 was controlled according to the European Pharmacopea for Ga-68 produced by accelerator.

After purification on the Synthra platform, labeling was performed on an iQS® Ga-68 FLUID MARKING MODULE (ITM), using a solution of the precursor FAPI-2286 (MCE) in acetate buffer at pH 4.2, to be finally formulated in a 0.9% NaCl solution containing 10% ethanol.

Radiochemical purity was determined by HPLC using a Mancherrey - Nagel column (EC250/4.6 NUCLEODUR 100-5 C18ec) and a gradient with 0.1 % trifluoroacetic acid in water and 0.1 % trifluoroacetic acid in acetonitrile in conjunction with iTLC with 1 M ammonium acetate and methanol (1:1). The other controls of residual solvents, radionuclide purity, pyrogens, sterility, etc. were performed according to the European Pharmacopoeia.

Applying this methodology of using a platform designed for fluorine-18 labeling for the purification of Ga-68, it was possible for us to safely and reproducibly obtain 2700 ± 185 MBq (73 ± 5 mCi) (n=5) of purified Ga-68 and then transfer it to the IQS module for the FAPI-2286 labeling. This allowed us to work safely with high activity, avoiding the problems of handling the high activity at the end of irradiation due to the ^{13}N and ^{11}C produced during irradiation.

The labeling on the module was carried out in a similar way to other Ga-68 brands, allowing the radiopharmaceutical to be obtained at the end of the synthesis with purity greater than 90%, in agreement all the requirements environment under GMP environment for clinical purposes.

In conclusion, this work allowed us to obtain a radiopharmaceutical for clinical use using Ga-68 produced from cyclotron in a robust and safe manner under GMP conditions.

Differences in Cardiac Glycolytic Metabolism According to Gender and Cardiovascular Risk Factors in Cancer Patients

S. Brandão, J. Sobrinho, E. Leão, B. Accioly, V. Menezes, M. Becker, F. Mourato

Hospital das Clínicas da Universidade Federal de Pernambuco, Brazil

Background

The increase in life expectancy in cancer patients has reinforced the importance of evaluating other factors that contribute to increased cardiovascular morbidity and mortality. In this sense, strategies that allow early diagnosis of cardiotoxicity related to oncological therapies are useful for preventing these complications. Positron Emission Tomography combined with Computed Tomography (PET/CT) using Fluorodeoxyglucose F-18 (FDG) is an examination that assesses glycolytic metabolism and is routinely used in the workup of neoplasms. Studies have shown the potential of PET/CT in identifying patterns of myocardial FDG uptake associated with cardiotoxicity, as well as with comorbidities that increase the risk of cardiovascular and cardiac toxicity, such as diabetes and hypertension. This study aimed to evaluate the association between myocardial FDG uptake and clinical-epidemiological data of cancer patients.

Methodology

A cross-sectional, retrospective study where clinical-epidemiological data and myocardial FDG uptake of patients referred for FDG PET/CT oncological study in a public and university nuclear medicine service in the Northeast of Brazil were evaluated. The examinations were carried out from January to August 2023. Patients were grouped according to the absence (G1) or presence (G2) of myocardial FDG uptake, whether focal, heterogeneous, or diffuse, and the clinical-epidemiological data were compared between them. Significant myocardial FDG uptake was considered if greater than the blood pool in the aorta. A p-value <0.05 was considered statistically significant.

Results

Data from 645 patients were evaluated, 449 (69.6%) female, mean age 54 ± 15 years, 244 (38.5%) hypertensive, 130 (20.4%) diabetic, and 71 (11%) with dyslipidemia. One hundred and fifty-six (24.2%) patients had breast cancer, 140 (21.7%) lymphoma, 88 (13.6%) melanoma, 82 (12.7%) cervical, 58 (9%) lung, and 121 (18.8%) had other types of cancer. Treatment response evaluation (42.9%), restaging (24.8%), staging (19.2%), and control (13.1%) were the clinical indications for the examination. Regarding myocardial FDG uptake, 265 patients (41.1%) presented uptake. In the univariate analysis, diabetes was more frequent in G1 (23% x 16.6%, $p=0.0487$), while male gender (25.52% x 37.35%, $p=0.0013$) and hypertension (35.37% x 43.02%, $p=0.052$) were more prevalent in G2. In logistic regression analysis, male gender (OR:1.80; 95%CI: 1.27-2.56, $p=0.0009$) and hypertension (OR:1.70; 95%CI: 1.19-2.41, $p=0.005$) were independent risk factors for the presence of myocardial FDG uptake, while diabetes was the only factor associated with the absence of uptake (OR: 0.53; 95%CI: 0.34-0.82; $p=0.003$).

Conclusion

In oncological patients who underwent FDG PET/CT examinations, myocardial FDG uptake was more prevalent in men and hypertensives. Meanwhile, diabetes was an independent

predictor of the absence of uptake. These results point to differences in cardiac glycolytic behaviour according to gender, the presence of hypertension, and diabetes. These differences may be involved in the myocardial mechanisms of metabolic response to toxicity to oncological treatment.

Qualitative [¹⁸F]FDG PET/CT in Predicting Clinical Outcomes of Post-surgical Differentiated Thyroid Cancer Patients with Elevated Thyroglobulin and Negative Radioiodine Whole-Body Scan

L. Ngoc Ha, N. Thi Phuong, M. Hong Son

Department of Nuclear Medicine, Tran Hung Dao Hospital (Hospital 108), Vietnam

Background

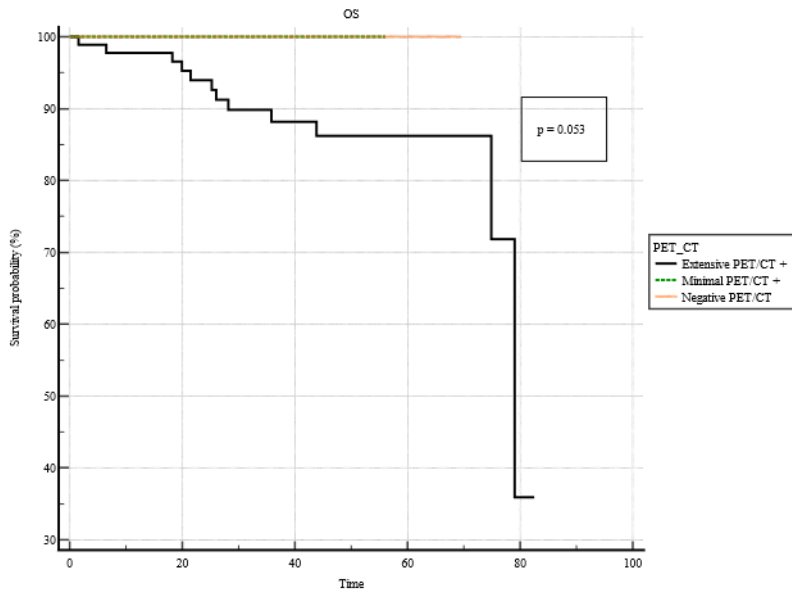
[¹⁸F]FDG PET/CT has been widely used as a diagnostic tool in detection and localization of recurrent non-avid radioiodine lesions in post-operative differentiated thyroid cancer (DTC) patients with elevated serum thyroglobulin but negative radio-iodine whole-body scan syndrome (TENNIS). The aim of our study was to evaluate the role of [¹⁸F]FDG PET/CT in prediction on outcomes of these DTC patients.

Methodology

Post-operative DTC patients with TENNIS syndrome were collected in the department of nuclear medicine, Hospital 108 from 2019 to 2023. All selected patients underwent [¹⁸F]FDG PET/CT with standard protocol following EANM guideline for tumour imaging version 2.0. The imaging characteristics were classified into three categories: (i) negative [¹⁸F]FDG PET/CT uptake, (ii) minimal [¹⁸F]FDG PET/CT uptake, (iii) extensive [¹⁸F]FDG PET/CT uptake. All patients were followed-up during 33 months (1.57 – 88.5 months). Progression-Free Survival (PFS) and Overall Survival (OS) were the end point of the study. The prognosis of different [¹⁸F]FDG PET/CT uptake pattern on PFS and OS was illustrated by Kaplan-Meier survival analysis. The independent factors predicting PFS and OS were determined by univariate and multivariate analysis using logistic regression.

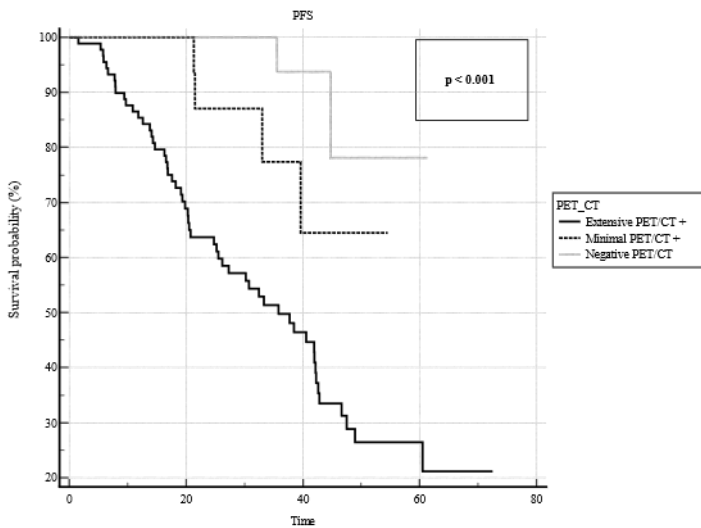
Results

There were 164 consecutive patients, 51.2% female and 48.8% male with median of age 50.1 (range 16-79). The most common histopathologic type was papillary accounting for 87.8%. The median time of follow-up was 33.3 months, (range 6.57 – 82.5). There was 36.6% (70) progressive cases and 12 (7.35%) death. Negative and minimal [¹⁸F]FDG PET/CT uptake patients had longer PFS than intensive uptake with 57.1 months, 46.2 months and 37.6 months respectively ($p < 0,001$). 1-year OS and 5-year OS in extensive PET/CT uptake patients was 97.8 % and 86.2 % respectively which were significantly lower than that of negative and minimal uptake ($p = 0.053$). In multivariate analysis, pulmonary, bone metastases and intensive PET/CT uptake were independent factor predicting PFS. Bone metastases was the factor could predict OS in multivariate analysis.



	1 year	2 ^{sd} year	3 rd year	5 th year
Negative PET/CT -	-	-	-	-
Minimal PET/CT +	-	-	-	-
Extensive PET/CT +	97.8 %	94 %	88.2 %	86.2 %

Figure 1. Kaplan–Meier Overall Survival curves for different patient’s group based on the extent of avid-[18F]FDG lesion in PET/CT imaging.



	1 st year	2 ^{sd} year	3 rd year	4 th year	5 th year
Negative PET/CT -	-	-	93.8 %	78.1 %	-
Minimal PET/CT +	-	87.1%	77.4 %	64.5 %	-
Extensive PET/CT +	85.4 %	63.7 %	49.8 %	28.9 %	26.4 %

Figure 2. Kaplan–Meier Progression-free survival curves for different patient’s group based on the extent of avid-[18F]FDG lesion in PET/CT imaging.

Conclusion

The minimal and negative [¹⁸F]FDG PET/CT uptake had better prognosis than others pattern of [¹⁸F]FDG uptake in PFS and OS. Bone metastases was only the independent factor that could predict both PFS and OS. Intensive PET/CT uptake was independent factor for predicting PFS.

Keywords: [¹⁸F]FDG PET/CT, prognosis, PFS, OS, TENNIS, differentiated thyroid cancer

Diagnostic Value of Antithyroglobulin Antibodies in the Detection of Recurrent Differentiated Thyroid Carcinoma: A Meta-Analysis

A. Apostol

Philippine Heart Center, Philippines

Background

Well-differentiated (follicular and papillary) thyroid carcinoma accounts for the majority of thyroid malignancies and is among the most curable neoplasms. About 5% to 20% of survivors develop local or regional recurrences while <5% to 10% develop distant metastases, generally in the first years of follow-up. After diagnosis of local relapse, the mortality rate is 12% and increases to 43% after distant metastases develop. Because of the long-term risk of recurrence and the importance of timely detection, diagnostic follow-up of well-differentiated thyroid carcinoma is life-long and must be very sensitive, in which serial thyroglobulin and anti-thyroglobulin determination are currently used. However, there is no general consensus as to whether the measurement of thyroglobulin antibodies is significant for the evaluation of possible interference with thyroglobulin measurement or whether thyroglobulin antibody measurement complements the thyroglobulin recovery test. Thus, we aim to determine the diagnostic accuracy of antithyroglobulin antibodies in predicting recurrent differentiated thyroid carcinoma.

Methodology

Search Strategy: A comprehensive search of PubMed and Google Scholar were undertaken. Citation searches, manual searches and screening of references of included studies were done. **Selection Criteria:** Cross-sectional and longitudinal diagnostic studies that utilized antithyroglobulin antibodies as a predictor of recurrent differentiated thyroid carcinoma. **Data Collection and Analysis:** The authors searched citations that correlated with the criteria using a data collection form generated in Review Manager. The methodological quality was then assessed using Quality Assessment of Studies of Diagnostic Accuracy (QUADAS). Hierarchical summary receiver operating characteristic (HSROC) meta-analytical tool was used to estimate summary receiver operating characteristic (ROC) curves.

Results

Eight studies with 2116 participants with 182 patients with recurrent differentiated thyroid carcinoma were included. Pooled sensitivity and specificity were 63% and 79% respectively. SROC shows an overall area under the curve (AUC) of 0.712.

Conclusion

Antithyroglobulin antibody has the ability to predict recurrent differentiated thyroid carcinoma, furthermore, it has a complementary role to thyroglobulin in the detection of differentiated thyroid carcinoma and tumour recurrence was more frequent in patients with elevated levels or a trend towards increasing levels.

Keywords: Diagnostic Accuracy, Recurrent Differentiated Thyroid Carcinoma, Recurrent Papillary Thyroid Carcinoma, Recurrent Follicular Thyroid Carcinoma, Antithyroglobulin Antibody

Biological Evaluation of ^{113}mIn –DOTA-RGDFK as SPECT imaging agent on Cancer Cells Expressing $\alpha\text{v}\beta\text{3}$ Integrin

F. Badipa¹, B. Alirezapour¹, H. Yousefnia¹, F. Bolorinovin¹, F. M. Sedeh²

¹ Radiation Application Research School, Nuclear Science and Technology Research Institute, Iran

² Nuclear Agriculture Research School, Nuclear Science and Technology Research Institute, Iran

Background

The phenomenon of angiogenesis as a very effective factor on the growth and spread of cancer cells is the molecular interactions between the components of the extracellular matrix and vascular cells. Among the different integrin's expressed on the surface of cells, $\alpha\text{v}\beta\text{3}$ integrin has a specific expression pattern during angiogenesis. Integrin $\alpha\text{v}\beta\text{3}$ is a critical receptor that affects tumour growth and invasion, metastasis, and angiogenesis. Aims of this study are optimization of the peptides radiolabeling by Indium-113m radionuclide and production of suitable radiopharmaceuticals for imaging studies of the $\alpha\text{v}\beta\text{3}$ Integrin expressing cancers.

Methodology

For the ^{113}mIn labeling Briefly, 20 nmol of DOTA-RGDFK peptide was dissolved in 20 μL of ultrapure water and incubated with 4 mCi (148 MBq) of ^{113}mIn for 15 min at 95°C , $\text{pH}=3.5$. After 15 min the reaction was stopped with 8 ml of WFI water and for more purification the product passed through C18 cartridge. ^{113}mIn –DOTA-RGDFK product was then evaluated by analytical RTLC, the radioactive peak containing desired product was collected. Stability test was checked in the human serum and in PBS buffer, radiolabeling yield, radiochemical purity, cell studies on U-87 MG cell lines, biodistribution study in normal rats (n=3) at 15, 30, 60 and 120min (expressed as %ID/g) and imaging study were examined.

Results

The percentage of radiochemical purity was 100%. 78% radiolabeling yield. In the stability studies section, which were performed in PBS buffer and human blood serum in 0, 60, 90 and 120 minutes. In general obtained result showed that, the stability of the labeled peptide in PBS buffer is higher than human serum in all times of the study, but overall, in both compounds, the stability has been decreased over time, the result indicated radiochemical purity of 96% in PBS buffer and 94% in human serum after 120 min. Constant values of $K_d = 17.8 \pm 2.9$ nM was obtained indicating the high affinity of ^{113}mIn –DOTA-RGDFK towards U-87 MG cell line overexpressed $\alpha\text{v}\beta\text{3}$ receptors. Biodistribution study was performed in normal Balb/c mice at time intervals (15, 30, 60, and 120) minutes after the injection, expressed as percentage of injected dose per gram of tissue (%ID/g), biodistribution study and imaging study of free ^{113}mIn and ^{113}mIn –DOTA-RGDFK showed similar accumulation pattern to the other radiolabeled RGDFK compounds.

Conclusion

^{113}mIn –DOTA-RGDFK is a potential compound for SPECT imaging of the cancer cells expressing $\alpha\text{v}\beta\text{3}$ integrin.

Keywords: Arg-Gly-Asp (RGD), Integrin, Angiogenesis, $\alpha\beta 3$ Integrin

Nerve-Wracking Discovery: Value of Fluorine-18 FDG PET/CT in Detection and Treatment Monitoring for Neurolymphomatosis - A Case Report

R. B. Ma-alat¹, M. G. Tumaming¹, I. Bandong²

¹St. Luke's Medical Center Quezon City, Philippines

²Philippine Society of Nuclear Medicine, Philippines

Background

Perineural invasion (PNI) is an uncommon and pathophysiologically ambiguous pathway of metastasis wherein cancer cells invade in, around, and through nerves. It has been seen in different malignancies including head and neck, pancreatic, and prostate cancers, as well as in lymphomas. The finding of PNI is an ominous harbinger associated with elevated tumour recurrence rates and poor prognosis. Neurolymphomatosis is a type of PNI wherein lymphoma directly invades the peripheral nervous system. Its prevalence only ranges from 0.2% to 3%, most commonly seen in B-cell non-Hodgkin lymphoma, in particular diffuse large B-cell lymphoma. Definitive diagnosis still relies on nerve biopsy, which is an invasive procedure and carries a significant risk of nerve damage. Thus, imaging modalities such as MRI and Fluorine-18 FDG PET/CT scan are greatly utilized for diagnosis, as well as in assessment of treatment response. However, MRI is less specific for neurolymphomatosis, and similar findings may also be seen in other conditions like inflammatory radiculoneuropathy. This study highlights the value of Fluorine-18 FDG PET/CT scan in detection and monitoring of treatment response for neurolymphomatosis in a patient initially suspected to have recurrent prostate cancer.

Case Report

This is a case of a 70-year-old male who was diagnosed with prostate carcinoma and underwent radiotherapy in 2017. Six years later, he presented with chronic low back pain radiating to the right lower extremity. MRI was done and showed a thickening with increased abnormal signals of the bilateral L4 and L5 exiting nerve roots and bilateral sacral nerve roots, for which post-radiation changes and inflammatory plexopathy are considerations. Whole-body Fluorine-18 FDG PET/CT was then performed and showed increased metabolic activity along the course of the bilateral L4-L5 and L5-S1 nerve roots, as well as hypermetabolic enhancing intra-abdominal mass, hypermetabolic heterogeneously-enhancing bilateral testes, enlarged on the left, hypermetabolic prominent bilateral seminal vesicles and bilateral spermatic cords, hypermetabolic iliac chain lymph nodes, and hypermetabolic foci in the appendicular skeleton. The initial impression was tumour recurrence with loco-regional spread and distant metastases. However, the PSA level is low. Biopsy of the intra-abdominal mass and left radical orchiectomy were then performed and showed diffuse large B-cell lymphoma. Patient underwent chemotherapy and had a follow-up PET/CT scan to evaluate treatment response. It showed metabolic resolution along the course of the bilateral L4-L5 and L5-S1 nerve roots, supporting the diagnosis of neurolymphomatosis. Regression to resolution of metabolic activity in the other aforementioned lesions was likewise noted.

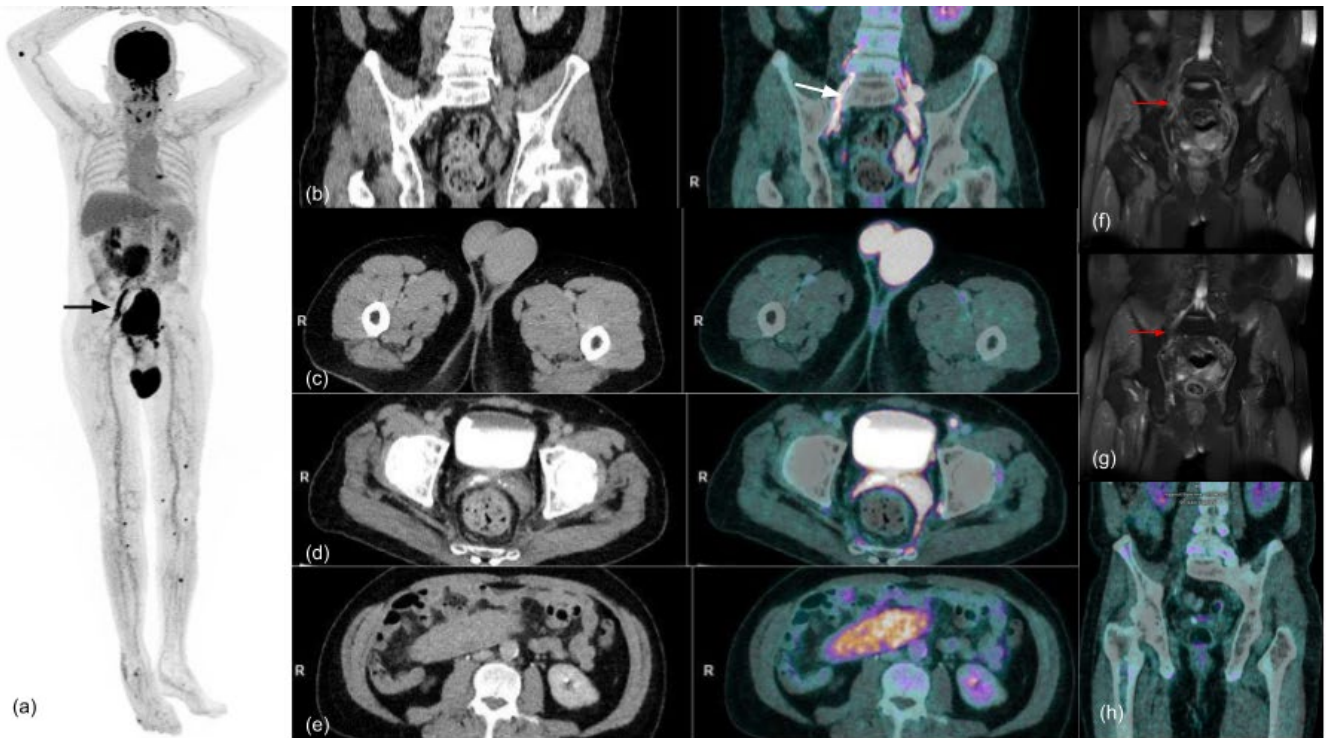


Figure 1. (a) Initial ^{18}F -FDG PET MIP and (b) coronal fused PET/CT show increased FDG activity along the course of L4-L5 and L5-S1 nerve roots. (c) (d) (e) Axial fused PET/CT shows increased FDG activity in the bilateral testes, seminal vesicle, spermatic cord, and intraabdominal mass. (f) and (g) Representative coronal T2FS images show thickening and T2 heterogeneous signals of the bilateral L4-L5 and L5-S1 exiting nerve roots most evident on the right (red arrow). (h) Post-treatment coronal fused PET/CT shows metabolic resolution in the regions of L4-L5 and L5-S1 nerve roots.

Conclusion

Fluorine-18 FDG PET/CT scan is a highly sensitive imaging modality used for the detection and therapeutic monitoring of neurolymphomatosis, particularly in patients presenting with non-specific MRI findings, also eliminating the risk of neurologic deficit from nerve biopsy.

Development and Clinical Applications of Copper-64 Based Theranostic Radiopharmaceuticals in Iran

Behrouz Alirezapour, Fatemeh Hooshmandan, Samaneh Zolghadri

Radiation Application Research School, Nuclear Science and Technology Research Institute, Iran

Cancer is a major disease which has become the biggest threat to human health due to its difficult early detection, diagnosis, and treatment. In the Islamic Republic of Iran, cancer is the third leading cause of death, and according to the global cancer statistics in 2018, about 110 000 cancer cases occurred and about 56 000 patients died. In order to strengthen the capacity of the country's health system to combat this problem, there is a focus on strengthening the capacity in the area of research and development as well as production and quality control of new generation theranostic radiopharmaceuticals, such as PET and therapeutic radiopharmaceuticals based on peptide as well as monoclonal antibodies (mAbs) through different national/international projects, with the aim of effective clinical use of theranostic new generation radiopharmaceuticals at the national level. During past 3 decades, nuclear medicine has flourished as vibrant and independent medical specialty in Iran. Since that time, more than 220 nuclear physicians have been trained and now practicing in nearly 224 centers throughout the country. Recently, positron emission tomography (PET) has been initiated in the country using the most important PET tracer, i.e. fluorine-18, Ga-68 and Cu-64 based radiopharmaceuticals. The advances of radiopharmaceutical sciences in Iran have been recently reported at international levels, with great position compared to other countries in the Middle East. In this abstract, the status of production, availability and clinical applications of the different types of the [⁶⁴Cu]-based radiopharmaceuticals in the country has been presented. Copper-64 has several unique attributes that make it a multi- purpose radionuclide with many potential applications. It has a complex decay scheme, with electron capture, beta-emission, and positron emission branches, and it may be described as the archetypal “theranostic” radionuclide, producing excellent PET molecular imaging at low administered doses without major dosimetry or radiobiological concerns, and having potential for radionuclide therapy at high doses with radionuclide distribution and accurate dosimetry possible using PET imaging during therapy. The most important production routes are via Ni-64(p,n) and Zn-68(p,αn) routes in small or medium-size cyclotrons or both. Owing to suitable half-life (12.7 hours), it can be used in the development of small size to large-size targeting molecules such as peptides and also full size monoclonal antibodies. Table 1 demonstrates the status of some of recently developed tracers based on the copper-64 radionuclide in the country under clinical evaluations with completed preclinical data.

Table 1: The Status of [⁶⁴Cu]Labeled Compounds Under Clinical Evaluations with Completed Preclinical Studies in the Country.

No.	Tracer	Molecule Type	Target/Application
1	[⁶⁴Cu]PR81	Antibody	MUC-1 positive tumours
2	[⁶⁴Cu]trastuzumab	Antibody	Her2 positive tumours
3	[⁶⁴Cu]PSMA	Peptide	Metastatic Prostate Cancer
4	[⁶⁴Cu]DOTATATE	Peptide	Neuroendocrine Tumours
5	[⁶⁴Cu]NODAGA-RGD-BBN (Heterodimer)	Peptide	GRPR Positive Tumours

Impact of Q clear filter on PET CT imaging in lymphoma patients

R. Elsheikh, M. E. Elkut

Faculty of Applied Health Sciences Technology, MUST University, Egypt

Background

Positron Emission Tomography/Computed Tomography (PET/CT) serves as a pivotal tool in nuclear medicine for assessing metabolic activities associated with oncological and neurological conditions. Recent advancements in reconstruction algorithms have introduced the Bayesian penalized likelihood (BPL) approach, exemplified by Q.Clear, aimed at enhancing precision and specificity in tumour identification and staging.

Methodology

This study encompassed PET/CT images from 50 patients diagnosed with lymphoma, acquired using a GE Discovery IQ5 PET/CT scanner following established weight-based protocols and FDG administration. Sinograms underwent reconstruction employing an Ordered Subsets Expectation Maximization (OSEM) protocol augmented with the Q.Clear algorithm, utilizing a beta factor of 350. Visual analysis of resulting images was conducted by two experienced Nuclear Medicine and Radiodiagnosis consultants.

Results

Comparison between Q.Clear and OSEM reconstruction methods revealed disagreement in Deauville Score (DS) assessments in 11 cases (15.7%). Q.Clear reconstruction prompted a DS elevation from 3 to 4 in 3 patients (4.3%), consequently impacting the categorization into positive PET findings. Statistical analysis demonstrated a significantly higher DS with Q.Clear compared to OSEM ($p < 0.001^*$), as well as elevated Standardized Uptake Value (SUV) measurements for lymphoma lesions ($p < 0.001^*$).

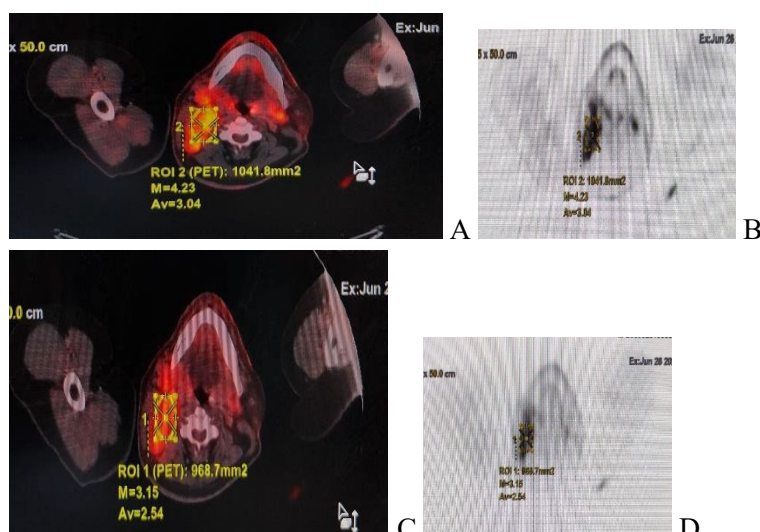


Figure 1. Measuring SUV_{max} at lymphoma lesion, (A&B). For Q.Clear measuring (C&D) for MAC-OSEM measuring.

Conclusion

The utilization of the Q.Clear reconstruction algorithm demonstrates a notable enhancement in clinical image quality and accuracy in diagnosing lymphoma lesions. Despite augmenting SUV values for hypermetabolic results, Q.Clear maintains background values unchanged, thus offering substantial benefits for clinical interpretation and patient management.

Potential of Artificial Intelligence in PET Imaging for Dose Reduction using Deep Learning Reconstruction

M. Vangu¹, K. Purbhoo²

¹ Charlotte Maxeke (CM) Johannesburg Academic Hospital, University of the Witwatersrand, South Africa

² Chris Hani (CH) Baragwanath Academic Hospital, South Africa

Background

Positron emission tomography/computed tomography (PET/CT) plays a central role in the management of cancer. However, the radiation exposure to patients from the radiopharmaceutical and the CT remains of concern in clinical practice. We decided to test the hypothesis that a reduced FDG dose will not affect the diagnostic quality of PET imaging when a deep learning reconstruction algorithm. DLR is intended to reduce noise from FDG/PET images by using a deep learning technique to produce better signal to noise ratio (SNR), where the neural network is trained to learn the noise from low-count FDG images by using high-count FDG images as gold standard. The aim of this study is to evaluate the SNR performance of DLR in clinical practices then to obtain an optimized protocol with reduced dose (equivalent time/bed position's reduction) for an oncological FDG scanning when using DLR.

Methodology

This prospective trial was done in two phases to obtain high quality and diagnostic images with a reduced (dose level of phase2 is decided based on result of phase1) dose of FDG in clinical PET protocol. Study participants were administered with a standard FDG dose (approximately 5.6 MBq/kg (0.15 mCi/kg) as per EANM Dosage Calculator. The whole-body FDG oncological imaging was acquired in a PET/CT system (uMI 550, United Imaging Healthcare, Shanghai, China), and 3.0 mins per bed and overlap >35% were used. Each participant's whole-body FDG images were reconstructed into 3 bedtime configurations (3.0 mins, 1.5 mins and 1.0 min) using DLR and OSEM with gaussian smooth (3 mm) respectively. Paired t-test was used to compare the SNRs.

Results

Fifty participants entered Phase 1 trial and data from 44 [mean age \pm SD = 53.3 \pm 17.4 years, range: 12 years to 82 years; median weight = 70 kg (IQR=60 kg & IQR3=78 kg), range: 39 kg to 112 kg; and median BMI=24.4 (IQR1=21.8 & IQR3=26.6)] were analysed. The mean injected FDG dose was 377.77 \pm 69.56 MBq (10.21 \pm 1.88 mCi). DLR's SNRs are all significantly higher than OSEM's SNRs ($p < 0.0001$) for all bedtimes. The mean SNR for DLR is 1.28, 1.34, 1.33 times higher than OSEM for corresponding bedtime of 3.0mins, 1.5mins to 1.0min. The SNR of DLR 1.0 min bedtime is 1.02 times higher than OSEM 3.0 mins bedtime. The DLR SNR over body weight also follows the same inverse square power relationship of the OSEM. The visual observation is also consistent with the statistical results and shows improved quality of output images, particularly in participants with high body mass index (BMI). A Phase 2 directly comparing 20 same participants at two time points (T1 & T2 within a week period) validated the outcomes of Phase 1 study.

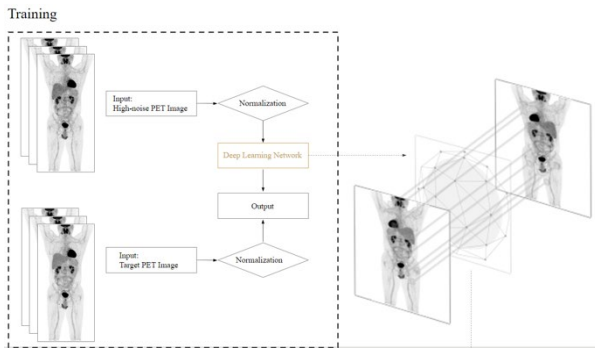


Figure 1: Showing a summary of neural network training on improving SNR

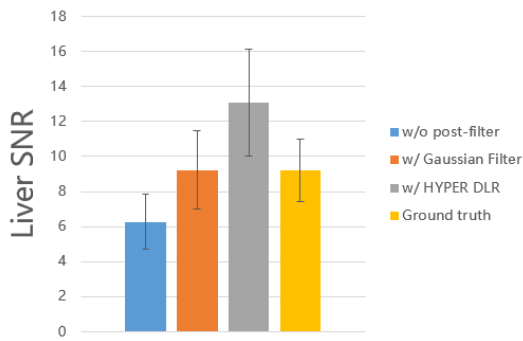


Table 1: Showing that HYPER DLR has better outcome.

Conclusion

The DLR for oncological FDG imaging is feasible with 1/3 reduction of equivalent FDG dose from the standard dose used in clinical OSEM protocol. A multicenter evaluation of our results would be advisable to consider route usage of dose reduction.

Exploring the Neuroprotective Potential of a Novel Third-Generation TSPO Ligand in Tauopathy

T. A. Kumar^{1,2,3}, A. K. Mishra², M. R. Zhang³

¹ Department of Chemistry & Nuclear Medicine, Babasaheb Bhimarao Ambedkar University, India

² Division of Cyclotron and Radiopharmaceutical Sciences (DCRS), Institute of Nuclear Medicine and Allied Sciences (INMAS), DRDO, India

³ Department of Advanced Nuclear Medicine Sciences, Institute for Quantum Medical Science, National Institutes for Quantum Science and Technology, Japan

Background

The 18kDa Translocator protein (TSPO), formerly recognized as the peripheral benzodiazepine receptor (PBR), has been considered a positron emission tomography (PET) biomarker for various types of neuroinflammation. While it has been demonstrated that TSPO ligands may decrease the level of beta-amyloid peptide associate in Alzheimer's but their role for tau pathology remains unexplored. To investigate this aspect, we conducted an analysis of the influence of the third-generation TSPO ligand, BBMP regarding the progression of the tau transgenic mice neuropathology.

Methodology

In pursuit of this objective, we conducted an analysis of the impact of the third-generation TSPO ligand BBMP (2-(5-Bromo-2-oxo-1,3-benzoxazol-3(2H)-yl)-N-methyl-N-phenylacetamide) on development of neuropathology in TauTg. Analysis were made through MR and PET imaging and immunohistochemistry/autoradiography.

Results

The in vivo animal neuro-imaging results were corroborated with immunohistochemistry to analyse markers associated with inflammation (TSPO, Controller of the complement cascade (1q / C1q), microglial tauopathy marker (AT8) and the neuronal survival (NeuN), in the brain sections obtained from the mice that underwent scanning. The administration of BBMP significantly reduced atrophy during the 6 to 10-month period, resulting in a 50% reduction in cortical and hippocampal volumes in comparison to TauTg mice administered with the vehicle

Administering BBMP to TauTg mice resulted in a decrease in average concentration levels of the three assessed inflammatory markers. Distance-based redundancy analysis revealed a strong correlation (80%) between the variation in inflammatory markers among groups and C1q (0.996). The indicators of neuroinflammation/degeneration in cortex and hippocampus exhibited a negative association with inflammatory markers.

Conclusion

In conclusion, our data point to a safeguarding role of new generation TSPO ligands in tauopathies, with the potential to lower neuroinflammation/degeneration, and brain atrophy.

Developing PET Infection Imaging Agent for Visualizing Bacterial Peptidoglycan Assembly

P. C. Koatale^{1,2}, M. M. Welling³, S. Mdanda^{1,2}, A. Mdlophane^{1,2}, J. Takyi-Williams⁴, C. Durandt⁵, I. van den Bout^{6,7}, F. Cleeren⁸, M. M. Sathekge^{1,2}, J. R. Zeevaart^{1,2,9}, T. Ebenhan^{1,2,9}

¹ Department of Nuclear Medicine, University of Pretoria, Pretoria, 0001, South Africa

² Nuclear Medicine Research Infrastructure (NuMeRI), Steve Biko Academic Hospital, South Africa

³ Interventional Molecular Imaging Laboratory, Department of Radiology, Leiden University Medical Center, The Netherlands

⁴ Pharmacokinetic and Mass Spectrometry Core, College of Pharmacy, University of Michigan, United States of America

⁵ Institute for Cellular and Molecular Medicine, South African Medical Research Council Extramural Unit for Stem Cell Research and Therapy, Department of Immunology, University of Pretoria, South Africa

⁶ Department of Physiology, University of Pretoria, South Africa

⁷ Centre for Neuroendocrinology, University of Pretoria, 0001 Pretoria, South Africa

⁸ Radiopharmaceutical Research, Department of Pharmacy and Pharmacology, University of Leuven, Belgium

⁹ Radiochemistry, The South African Nuclear Energy Corporation (Necsa), South Africa

Background

The limitation of deoxy-2-[18F]-fluoro-D-glucose ([18F]FDG) to discriminate infection from inflammation limits the diagnostics power that Positron Emission Tomography – Computed Tomography (PET/CT) can offer. As a result, improvements in diagnostic strategy will require the development of targeted radiotracers that can allow the detection of infections with high specificity and selectivity. The peptidoglycan is a unique and integral structure of a bacterial cell wall composed of alternating N-acetylglucosamine and N-acetylmuramic acid amino sugars cross-linked by oligopeptides. The ability of bacteria to recycle exogenous amino acids and amino sugars for peptidoglycan biosynthesis has been extensively investigated using optical imaging. In particular, fluorescent murine tripeptide alanyl-gd-glutamyl-l-lysine-N-7-nitro-2,1,3-benzoxadiazol-4-yl (AeK–NBD) was effectively utilised by to study peptidoglycan recycling pathway in gram-negative bacteria. These results provided proof of concept for using murine tripeptide for in vivo localization of bacterial infection using PET/CT which has not been reporting elsewhere to our knowledge. In this study, using a similar approach we report the development of L-alanine-γ-D-glutamine-L-lysine (AeK) conjugated with DOTA trans-chelator for complexation with Gallium-68 [68Ga] and in vitro characterization.

Methodology

The DOTA-AeK tripeptide was radiolabelled with [68Ga] to produce [68Ga]-DOTA-AeK followed by solid-phase purification using C-18 Sep-Pak cartridge and quality control using radio-iTLC and HPLC. Plasma stability and protein binding tests were carried out to determine the physicochemical properties of [68Ga]-DOTA-AeK. Bacterial incorporation of [68Ga]-DOTA-AeK was investigated in live and head-killed *Escherichia coli* (*E.coli*) and *Staphylococcus aureus* (*S.aureus*) over 2 hrs. Using a similar

approach, fluorescent NBD-AeK was included as a reference control using flow-cytometry and confocal imaging for sample analysis.

Results

An easy-to-implement radiolabelling and purification procedure of [68Ga]-DOTA-AeK was established with radiochemical purity (RCP) of $\geq 95\%$. The radiotracer remained stable in plasma with no protein binding observed. The findings of this study demonstrated that AeK is a PG biosynthesis targeting molecule (even when conjugated to NDB) with high fluorescence intensity reported for both live *E. coli* and gram-positive (*S.aures*) strains which was significantly decreased in heat-killed cells (P-value < 0.05). Unfortunately, no conclusive intracellular uptake pattern of [68Ga]-DOTA-AeK was observed for both *E. coli* and *S.aures* cells live and heat-killed bacterial strains (P > 0.05).

Conclusion

Finally, our study well demonstrates proof that the intracellular corporation of AeK is necessary for successful bacteria-specific imaging using PET/CT. Therefore, Ga-68 is not a suitable radioisotope for tracing bacterial uptake of AeK tripeptide as it requires trans-chelation with a bulky metal chelator such as DOTA. An alternative to optimization is to explore diverse chemical structures of AeK that will allow complexation with fluorine-18 and C-11 which was a limitation in this study due to lack of infrastructure.

Correlation between the metabolic parameters and tumour biomarkers in Non Small Cell Lung Cancer (one centre study results)

S. Kukava, M. Baramia, N. Esvanjia, S. Kakhadze, A. Kukhashvili, N. Otkhozoria, S. Tsitsilashvili, G. Tsivtsivadze

Department of CT and PET/CT; Todua Clinic Tbilisi, Georgia

Background

Lung cancer is one of the most commonly diagnosed cancers worldwide, accounting for 11.4% of all cancer diagnoses and remains the leading cause of cancer-related mortality, accounting for 18.0% of overall cancer mortality.

There have been important improvements in the treatment of the advanced-stage lung cancer in the past years. Immune checkpoint inhibitors targeting the PD-1/PD-L1 play an important role in the adjuvant and metastatic treatment of non-small cell lung cancer (NSCLC). PD-L1 positive patients with high PD-L1 expression can benefit from immunotherapy and have a better survival rate.

Metabolic parameters, showing glucose metabolism and tumour heterogeneity (such as SUVmax, SULpeak, TLG, MTV) have been studied to predict PD-L1 expression, however, controversial results have been reported.

The aim of our study was to find the correlation between metabolic parameters and tumour biomarkers, and identify the subgroup of patients who can benefit from the novel immunotherapy treatment.

Methodology

We conducted a retrospective analysis of 14 patients with non-small-cell lung cancer diagnosed at our institution during the years 2022 to 2023. All patients underwent [¹⁸F]FDG PET/CT scans prior to treatment, and pathology reports, including PD-L1 status, were available for analysis. PD-L1 Positivity was defined as a proportion of PD-L1-positive tumour cells >1%. Proportion of PD-L1-positive tumour cells ≥50% was defined as high expression. [¹⁸F]FDG PET/CT scans were obtained on 16-slice PET/CT scanner with 5-rings system. Visual and semi-quantitative assessment (SUVmax value measured) were made by two physicians.

Results

Patient characteristics: 11 males, 3 females, age range 45 -78, mean age 64. All patients were diagnosed with NSCLC (11-adenocarcinoma, 2-squamous cell carcinoma, 1-undifferentiated NSCLC). Among the NSCLC patients 8 (57.1%) were PD-L1 positive. Of these, 4 specimens (50%) had low PD-L1 expression levels (1–49%) and 4 (50%) had high PD-L1 expression levels (>50%). High PD-L1 expression was seen in adenocarcinoma.

The SUVmax was higher in the PD-L1-positive subgroup of 8 patients, with a mean SUVmax of 16.5, while in patients with high PDL-1 expression (>50%) mean SUVmax was 22. However, in 6 patients with negative PD-L1 status, the SUVmax remained elevated, averaging 12.2. If we were to adopt an SUVmax value of 12.5 as the cut-off threshold, the accuracy, specificity and sensitivity to predict PDL-1 expression would be 50%. Yet, focusing solely on patients with high PDL-1 expression (PD-L1≥50%), the sensitivity within this group would increase to 75%.

Gender	Age	Morphology	SUV _{max} in either primary focus or lymph node	PDL 1 status
M	45	adenocarcinoma	SUV _{max} 28 (primary)	100%
M	54	adenocarcinoma	SUV _{max} 4 (primary)	10%
M	64	adenocarcinoma	SUV _{max} 8 (primary)	0%
M	62	adenocarcinoma	SUV _{max} 14 (lymph node)	0%
M	78	squamous cell carcinoma	SUV _{max} 15 (primary)	30%
M	73	adenocarcinoma	SUV _{max} 31 (primary)	70%
M	75	adenocarcinoma	SUV _{max} 17 (primary)	0%
M	75	adenocarcinoma	SUV _{max} 18 (primary)	0%
M	54	undifferentiated NSCLC	SUV _{max} 10 (primary)	0%
M	62	adenocarcinoma	SUV _{max} 6 (primary)	0%
F	72	adenocarcinoma	SUV _{max} 11 (lymph node)	95%
F	57	adenocarcinoma	SUV _{max} 19 (primary)	100%
F	62	adenocarcinoma	SUV _{max} 12 (primary)	1 %
M	67	Squamous cell cancer	SUV _{max} 12 (primary)	15%

Conclusion

[18F]FDG uptake in NSCLC and metabolic parameter, like SUV_{max}, correlates with PD-L1 expression and slightly differs between high and low PD-L1-expressing individuals. The metabolic parameter can be used to select patients who can benefit from immunotherapy, however patients with negative PDL -1 status can still have high SUV_{max} values. SUV_{max} is may not be a robust parameter to select patients for immunotherapy. Taking into consideration tumour heterogeneity, other metabolic parameters, such as metabolic tumour volume (MTV) can be investigated. Limitations of our study include retrospective nature, and a small number of patients, one of the reasons being the lack of availability of [18F]FDG PET/CT and PD-L1 histopathological analysis for our population.

Optimizing metastatic workup in treatment-naïve prostate cancer patients: a machine learning-driven nomogram to reduce superfluous 68Ga-PSMA-11 PET/CT

R. Wakankar¹, B. Khangembam¹, A. R. Chanu², K. M¹, C. J. Das³, C. Patel¹, R. Kumar¹

¹ Department of Nuclear Medicine, All India Institute of Medical Sciences, India

² Department of Physical Medicine and Rehabilitation, All India Institute of Medical Sciences, India

³ Department of Radiodiagnosis and Interventional Radiology, All India Institute of Medical Sciences, India

Aim

To evaluate the feasibility of a machine learning-driven nomogram utilizing routine clinical, regional conventional imaging, and laboratory biomarkers to reduce superfluous 68Ga-PSMA-11 PET/CT for metastatic workup in treatment-naïve prostate cancer patients.

Methodology

Data from pathologically confirmed treatment-naïve prostate cancer patients, who underwent 68Ga-PSMA-11 PET/CT between January 2018 and September 2023 constituted the training set. M1 disease was determined on 68Ga-PSMA-11 PET/CT. Routine clinical, regional conventional imaging, and laboratory biomarkers viz., age, ISUP Grade, serum prostate-specific antigen (PSA), serum alkaline phosphatase (ALP), primary tumour stage, and regional nodal status (the latter two, determined on regional conventional imaging) were retrieved. Data preprocessing included feature imputation using average/most frequent values, and these six features were utilized for cross-validation employing a Naïve Bayes model, which discretized numeric values into four bins with equal frequency. The model's generalization was evaluated on an unseen testing set of prospectively enrolled patients from October 2023 to February 2024. Performance metrics included Area Under the Curve (AUC), classification accuracy (CA), F1 score, Precision, Recall, and Specificity. Feature importance was determined by measuring the decrease in CA after permuting each feature's values. Calibration curve with sigmoid calibration and performance curve with probability thresholds were plotted. For transparency and interpretability, SHAP (SHapley Additive exPlanations) values were assessed and presented as SHAP Beeswarm plot. A nomogram was developed, incorporating the five best-ranked features for predicting the absence of M1 disease on 68Ga-PSMA-11 PET/CT.

Results

The training set comprised 184 male patients with a mean age of 68 ± 8 years, while the testing set included 30 patients with a mean age of 67 ± 9 years. No statistically significant difference in the proportion of M1 disease was observed between the two groups ($P = 0.331$). Among the six parameters considered, ALP showed a significant difference ($P = 0.002$). On cross-validation, the Naïve Bayes model displayed good performance metrics (AUC: 0.874, CA: 0.804, F1: 0.811, Precision: 0.837, Recall: 0.786, Specificity: 0.826). The absence of regional nodal metastasis (N0) emerged as the most impactful feature for predicting the absence of M1 disease, as confirmed by the decrease in CA after feature permutation. On the unseen testing set, the model exhibited commendable performance metrics (AUC: 0.928, CA: 0.867, F1: 0.846, Precision: 0.846, Recall: 0.846, Specificity: 0.882). The SHAP Beeswarm plot highlighted N0, ISUP Grade, and PSA as pivotal features, elucidating the model's interpretability. The five best-ranked features based on absolute importance employed by the

constructed nomogram for predicting the absence of M1 disease were N0, ISUP Grade, ALP, primary tumour <T3, and PSA. The absence of regional nodal metastasis, ISUP Grade 3, ALP 123 –220 IU/L, primary tumour <T3, and PSA 13.4 –24.6 ng/ml had a total nomogram point of 3.0 with a probability of 96% for predicting the absence of M1 disease on 68Ga-PSMA-11 PET/CT.

Conclusion

A machine learning-driven nomogram utilizing routine biomarkers can predict the absence of M1 disease in treatment-naïve prostate cancer patients. Its robustness and generalizability suggest potential for reducing superfluous 68Ga-PSMA-11 PET/CT in metastatic workup.

Quantitative analysis of the contrast of liver lesions in relation to glycolytic activity and parenchymal clearance with [¹⁸F]FDG PET/CT. Contribution of the study in dual protocol

M. Portillo, S. Hasi, A. Liaudat, S. Collado, M. Mussio, S. Racioppi

Servicio de Medicina Nuclear, Imágenes Moleculares y Terapia Metabólica, Instituto Alexander Fleming, Buenos Aires, Argentina

Background

In 2020, 130,878 new cases of cancer occurred in Argentina, 52.7% in women. Considering tumour sites, breast cancer was the largest cancer, accounting for 16.8% of all new cases. It is the leading cause of death in women with 19.4% of all cancers and an age-adjusted rate of 15.9/100,000 women. Survival at 5 years varies depending on the extent of the disease. Initial staging of breast cancer is performed to detect the extent of the disease at the loco-regional and distant level. Liver metastases have a prevalence of approximately 13% in series of newly diagnosed breast cancer and up to 61% in necropsies, their confirmation is an important prognostic factor and of relevance in therapeutic options. [¹⁸F]FDG PET/CT has been shown to be very useful in the staging of breast cancer patients. Our objective is to evaluate the contrast ratio of liver lesions versus the surrounding parenchyma with dual protocol in [¹⁸F]FDG PET/CT studies.

Methodology

126 [¹⁸F]FDG PET/CT studies were retrospectively analysed for staging female patients with breast cancer. Late acquisitions of the abdomen were made for better characterization and contrast with the liver parenchyma of secondary involvement in this location. The acquisition of the [¹⁸F]FDG PET/CT was performed by administering an activity of 0.1mCi/kg of body weight and initiating the acquisition of the PET image at 60±10min. The studies were carried out on a General Electric PET/CT Discovery 710. In all cases, intravenous contrast media of 0.1mL/kg body weight were administered in the portal phase to better characterization of parenchymal liver lesions.

Results

Sixty liver lesions were noted. The SUV_{max} was determined and the contrast ratio with the surrounding parenchyma was calculated. The SUV_{max} decreased in 81.7% of ROIs made at the liver parenchyma and 68.3% of the lesions increased between early and late acquisition. 85% of the lesions increased the contrast between both images. Of the 51 lesions that increased their contrast ratio, 13.7% less than 5%; 39.3% between 5% and 10%; 37.2% between 10% and 20% and 9.8% more than 20%.

Twenty-seven lesions had a contrast difference of less than 10% (mean 6.6) and the average time in which the images were made was 63.3 minutes, while 24 lesions had a contrast difference of more than 10% (average 15.4) and the average time was 74.3 minutes. The lesions increased their uptake according to the average post-acquisition time.

Conclusion

The analysis reflects the variability of the contrast of the liver lesions in relation to glycolytic activity and parenchymal clearance, with a direct effect on the interpretation of the images, with a better characterization of the hepatic metastatic involvement given the contrast established in the dual protocol.

Hybrid imaging in monitoring and treatment tailoring of malignant melanoma for improving prognosis

L. Chavdarova¹, V. Georgiev², I. Gavrilova³, E. Piperkova¹

¹ Clinic of Nuclear Medicine, University Specialized Hospital for Active Treatment in Oncology – Sofia, Bulgaria

² Clinic of Surgery, University Specialized Hospital for Active Treatment in Oncology – Sofia, Bulgaria

³ Clinic of Dermatooncology, University Specialized Hospital for Active Treatment in Oncology – Sofia, Bulgaria

Background

Contemporary immune- and target-therapies in malignant melanoma (MM) show big promise for improving outcome. The correct timing for their initiation at micrometastatic disease, e.g. in a positive sentinel lymph node (SLN), appears critical for future therapy success.

The aim of our study was to standardize diagnostic hybrid approach in MM and elaborate precized indications and timings for SPECT/CT and PET/CT imaging, with special regard to adjuvant treatment tailoring.

Methodology

We conducted a prospective single-centre study in the period 02.2020-07.2022 on 77 patients (41 female, 36 male, 28-83y) with verified early-stage MM, before definitive re-excision of primary lesion. Planar sentinel lymph node scintigraphy (SLSc) with targeted SPECT/CT was performed in all patients, followed by intraoperative gamma-probe-guided biopsy of SLN (SLNB). [18F]FDG-PET/CT was based on elaborated clinical indications. Pre-SLNB-PET/CT was indicated in case of ultrasound-suspicious regional LN, patient- or primary lesion-associated risk factors. In case of micrometastasis-positive (+)SLN, patients were upstaged in stage III and tailored to adjuvant immune or target-therapy. Post-SLNB PET/CT was indicated in all (+)SLN cases, with follow-up PET/CT-scans every 3-6 months, to discriminate between “no evidence of disease” (NED), progressive disease (PD) or treatment effect with respective therapeutic change.

Results

SLSc-SPECT/CT recognized SLN in all pts, gamma-probe showed 100% detection rate. SPECT/CT found 11,3% more SLN than planar imaging. In 26% of patients SPECT/CT detected more than one route of lymphatic drainage. SPECT/CT helped in the differentiation of transient lymph depots in 5 and in-transit SLN in 1 patient.

In 20,78% of patients (+)SLN was verified, with upstaging in stage III. In regression analysis higher T-stage correlated with 2,4-fold higher chance for (+)SLN. The highest SLN-number was found in torso-lesions, followed by head-and-neck and extremities. In 1 patient with left lumbar region primary, SPECT/CT found a (-)SLN in left axilla and a 4mm in-transit (+)SLN in subcutaneous lumbar region. Pre-SLNB-PET/CT was performed in 6 patients, showing no sign of metastatic disease. Post-SLNB-PET/CT was performed in 26 patients, 9 with (+)SLN. In 20 patients PET/CT showed NED, 5 - PD, 1 - with suspicious finding. PD-lesions were as follows: 1 patient with a single in-transit lesion, 2 with

metastatic regional LN, 2 with systemic disease. All PD patients were assigned to adjuvant-therapy with PET/CT follow-up.

A PET/CT-follow-up study for all (+)SLN patients (as of 02.2024) is ongoing. According to latest data, PET/CT with up to 5 consecutive scans tailored therapeutic approach: 12 patients were assigned to immune-therapy, 3 to targeted therapy, 2 to radiotherapy, 2 to lymph node dissection.

Conclusion

Hybrid imaging supports individualized treatment tailoring in MM. For better clinical understanding of its role, a specified and standardized hybrid diagnostic algorithm is needed. SLS_c-SPECT/CT is essential for correct staging of early MM and appoints the prognosis-critical early start of adjuvant therapy. [18F]FDG-PET/CT should be implemented in early-stage MM in cases of clinical suspicion or patient/lesion associated risk factors. In our proposed algorithm, patients with (+)SLN should be monitored closely including post-SLNB-PET/CT. Follow-up PET/CT should be further implemented to assess therapy response and side effects.

Prognostic Value of [¹⁸F]FDG PET/CT Metabolic Parameters in Rectal Cancer

R. Milardović¹, N. Bešlić¹, N. Salkica², L. Džananović³

¹ Nuclear Medicine, Clinical Center of Sarajevo University, Bosnia and Herzegovina

² Clinic of Radiology, Clinical Center of Sarajevo University, Bosnia and Herzegovina

³ Department of Epidemiology and Biostatistics, Faculty of Medicine of Sarajevo University, Bosnia and Herzegovina

Background

Colorectal cancer (CRC) is the third most common cancer worldwide, and it represents a versatile genetic group with prognosis dependent on its molecular features. [¹⁸F]FDG PET/CT is a hybrid diagnostic imaging tool used for staging, restaging, treatment response evaluation and radiation planning. It is hypothesized that PET/CT can also be used to determine prognosis in some cancer types, including CRC. Tumour glycolysis in a tumour volume is quantified and expressed by metabolic PET/CT parameters such as SUV_{max}/SUV_{mean}, MTV and TLG, which are potential prognostic biomarkers, whose association with survival is actively researched for their prognostic significance. Prognostication is used for guiding both clinical decisions of physicians and personal decisions of patients, and as such, it facilitates decision making and management strategies. Strengthening of precision medicine as a new medical model requires a solid system of prognostic factors to be developed and validated.

Methodology

A descriptive, cross-sectional study of 63 patients previously diagnosed with rectal cancer, treated with surgery and selectively chemo/radiotherapy, and whose clinical findings, imaging results or increasing CEA raised suspicion for relapse or metastatic disease. Patients were referred to [¹⁸F]FDG PET/CT between January 2020–February 2024, and vendor software was used to generate threshold-based ROIs followed by semiquantitative analysis of PET/CT parameters (SUV_{max}/SUV_{mean}, MTV and TLG). As a gold standard, pathohistology or clinical follow-up data were used. The cut-off values of SUV_{max}, MTV, and TLG were determined by analyzing the ROC curves that were plotted to estimate the most discriminating cut-off value for each parameter and maximize the difference between true positives (sensitivity) and false positives (i.e. Youden's index) in predicting survival. The patients were divided into two groups (low vs. high) based on the cut-off value for each factor. By dichotomising each parameter, the Kaplan–Meier survival curves were generated. Progression-free survival (PFS) is defined as a period to an endpoint (relapse or metastasis) or termination of study without progression of disease. A log-rank test was used to compare progression-free survival (PFS) between each pair of groups. In each analysis, a value of $p \leq 0.05$ was considered significant. All analyses were performed using MS Excel 2019 and IBM SPSS Statistics 27.0.

Results

The cut-off values for SUV_{max}, MTV and TLG determined from the ROC curves were 11.55 g/ml (AUC=0.589, 95% confidence interval (CI)=0.443-0.735), 9.33cm³(AUC=0.487, 95% CI=0.336-0.639), and 40.55 (AUC=0.523, 95% CI=0.368-0.679), respectively. Patients were divided into a low and a high group for each factor based on the cut-off values. The low and high SUV_{max}, MTV and TLG groups included 46 and 17, 35 and 28, and 31 and 32 patients, respectively. The median survival time in

the low and high SUV_{max}, MTV, and TLG groups were 17 and 10 months ($p=0.205$), 17 and 13 months ($p=0.195$), and 19 and 13 months ($p=0.05$), respectively, demonstrating significantly lower duration of PFS in patients with high TLG only.

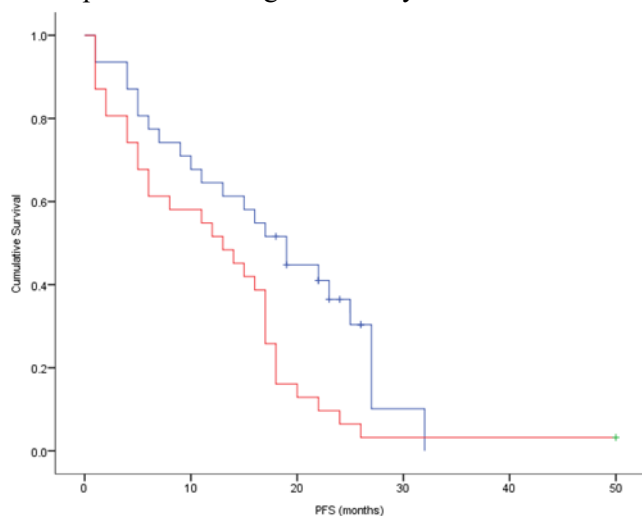


Figure 1. Progression-free survival curve for rectal cancer according to total lesion glycolysis (TLG) ($p=0.015$) Patients were dichotomised according to the cut-off value for each parameter; blue line: low group, red line: high group.

Conclusion

The results of our study suggest that TLG, unlike SUV_{max} and MTV, as the metabolic and volumetric PET/CT parameter significantly associates with PFS, and could be appropriately considered a prognostic biomarker for PFS in rectal cancer.

Pioneering PET Scans: Unveiling Cancer Treatment Responses and Demographics in Nigeria's Oncology Landscape

V. Isibor¹, A. Adeniji², A. Adetugbobo³, A. Alabi¹, M. Bashir¹, F. Fagbemide³

¹ Department of Radiation Oncology, Lagos University Teaching Hospital, Nigeria

² MeCure Oncology Centre, Nigeria

³ NSIA-LUTH Cancer Centre, Lagos University Teaching Hospital, Nigeria

Background

The utilization of PET/CT scans in cancer management is gaining prominence worldwide. In Nigeria, there's a scarcity of studies exploring the implementation of PET/CT scans and the subsequent comparison of RECIST (Response Evaluation Criteria in Solid Tumours) and PERCIST (PET Response Criteria in Solid Tumours) criteria for treatment response assessment. This study aims to report the LUTH experience with utilization of PET CT scans in staging and monitoring treatment response as well as basic demographics of the patients.

Methodology

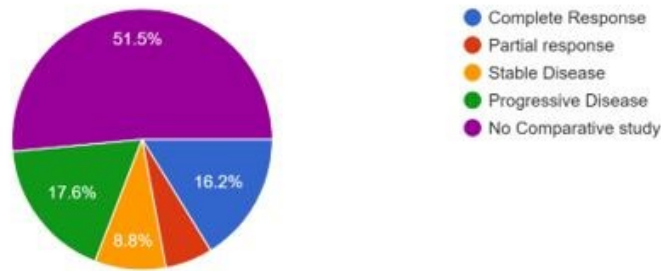
A retrospective review of 213 cancer patients attending the oncology clinic at LUTH was conducted. All patients underwent PET/CT scans at Mecure laboratory (a privately owned laboratory providing diagnostic services and only PET centre in West Africa) in Lagos, Nigeria. CT or MRI scans were performed at various labs. Demographic data including age, gender, and cancer type were collected. Treatment modalities such as surgery, chemotherapy, and radiotherapy were administered based on patient characteristics. RECIST and PERCIST criteria were employed to assess treatment response. The discordance between the two criteria was analysed to evaluate discrepancies in treatment response evaluation.

Results

Among the 213 patients, the majority were females (58%) with a median age of 58 years (range: 16-81 years). Breast cancer was the most prevalent cancer type (35.66%), followed by Prostate Cancer (24.3%) and lung cancer (4.2%). PET/CT scans were performed in Nigeria for all patients in this report, signifying the pioneering nature of this study. Majority of PET scans were done to monitor treatment response -31.4%. PERCIST values of Complete Response was seen in 2 (1.4%), Partial Response in 1 (0.7%), Progressive disease in 3 (2.1%) and Stable disease in 4 (2.8%). All the remaining patients had only one PET study and as such a comparison could not be made to assign PERCIST criteria. CT scans were the commonest imaging modality done in about 80% of patients. RECIST values of Complete response was seen in 11 (7.7%), Partial Response in 4 (2.8%), Progressive Disease in 12 (8.4%) and Stable Disease in 6 (4.2%). A significant number of patients had only one study with reasons varying from still undergoing treatment etc.

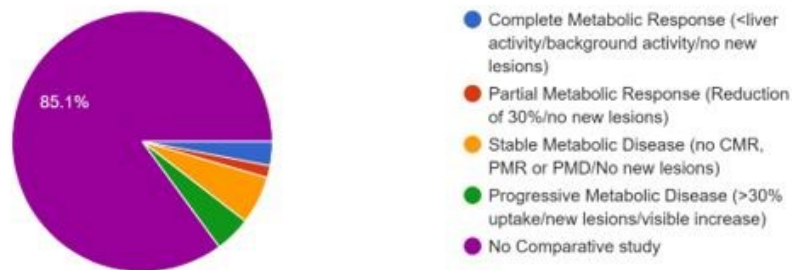
RECIST Criteria

68 responses



PERCIST Criteria

67 responses



Conclusion

More research and follow up needs to be done to monitor and improve discordance in imaging data when reporting with RECIST and PERCIST criteria. Future research will also look into barriers to accessing imaging like PET scans, MRIs, CTs, payment plans, factors that affect the discordance between RECIST and PERCIST like multimodal treatments etc. The observed discordance highlights the need for a comprehensive approach in evaluating treatment response, considering both imaging criteria to optimize clinical decision-making and patient care. Further research should focus on refining criteria and establishing standardized protocols to enhance the accuracy and reliability of treatment response assessment in the Nigerian oncology setting.

Susuk – The Mystical Metallic Foreign Bodies Observed on Oncology FDG PET/CT Scan: Case Series and Pictorial Review

R. D. Arunasalem, S. Suhaili, A. Z. Zaniah

Nuclear Medicine Department, General Hospital Kuala Lumpur, Malaysia

Background

FDG PET/CT has become an important investigation tool in the field of oncology for various indications and disease related assessment. We may encounter unexpected findings such as incidentalomas or even artefacts during PET/CT examinations. Susuk are tiny mystical metallic talismans inserted subcutaneously in certain body areas. In order to highlight their appearance on hybrid imaging, we present case series and pictorial review of 2 oncology patients who were noted to have susuk or charm needles observed on FDG PET/CT scan.

Case Report

Case 1: 57 years old lady with recurrent ovarian carcinoma involving large bowel post-surgical interventions and chemotherapy who presented with rising tumour marker and new right mesenteric mass and segment VII liver lesions. FDG PET/CT (June 2021) showed hypermetabolic metastases in right hemipelvis and liver. Additionally, non FDG-avid multiple subcutaneous tiny needles were seen in the face, anterior chest wall, pelvis and gluteal regions. She voluntarily disclosed the information on susuk use to the attending imaging department personnel.

Case 2: 56 years old lady with advanced papillary thyroid carcinoma post-thyroidectomy associated with lung and liver metastases. Serum thyroglobulin was persistently raised despite several radioiodine therapies. FDG PET/CT (August 2021) showed hypermetabolic metastases in the right lung, neck and pelvic nodes and multiple bones. Ametabolic tiny multiple subcutaneous metal pins are seen in her face, chin and right gluteal region in this patient but she was unaware of their existence. Upon questioning, she claimed that susuk may have been inserted at very young age. Although these charm needles caused some localised attenuation, the overall image qualities of FDG PET/CT scan of both patients were satisfactory.

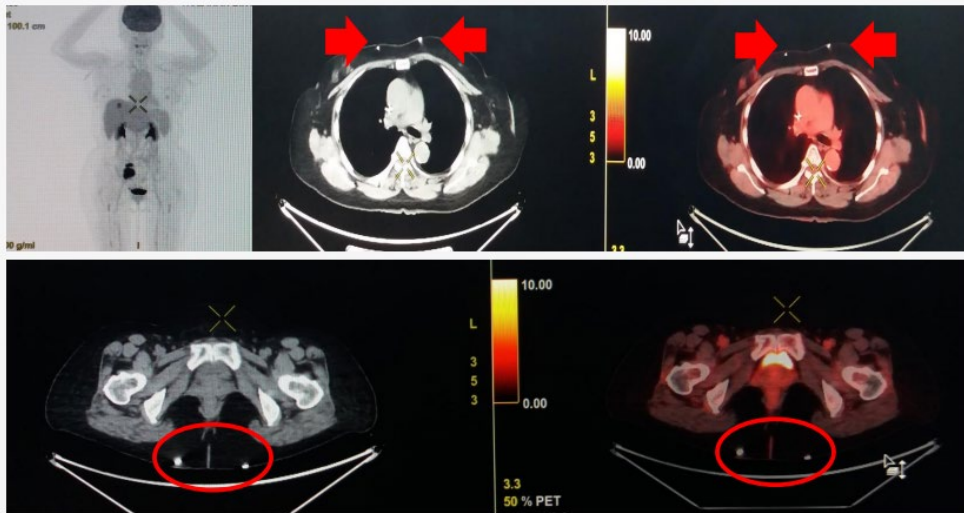


Fig. 1: FDG avid liver and right pelvic lesions. Susuk needles causing local metal artifact including at the anterior chest wall (arrows) and gluteal regions bilaterally (circles).

Conclusion

We need to recognise charm needles seen on hybrid imaging particularly oncology FDG PET/CT as they would cause localised metal attenuation artifact that may potentially affect image quality and interpretation in some cases.

Detection of higher prevalence of lymph node metastasis in prostate cancer in patients with type 2 diabetes by PET/CT with 18F / 68Ga-PSMA

R. Hernández-Álvarez¹, V. O. Cortés-Hernández², A. A. García-Reséndez³, E. Rivera-López⁴

¹ Imagen Molecular Aplicada San Luis Potosí y Aguascalientes, Mexico

² Hospital Infantil Teletón Oncológico, Querétaro, Mexico

³ Hospital Regional de Alta Especialidad del Bajío, Guanajuato, Mexico

⁴ Hospital Central “Dr. Ignacio Morones Prieto”, San Luis Potosí, Mexico

Background

Unlike other malignancies, prostate cancer has a lower incidence in diabetic patients, however, survival is lower in these patients and the conditioning mechanisms of this evolution are not yet fully understood. There is limited evidence that lymph node dissemination is more frequent in diabetic patients.

Objective

We compared the uptake patterns of 18F / 68Ga-PSMA in diabetic and non-diabetic patients.

Methodology

97 PET / CT studies with 18F / 68Ga-PSMA (21 of type 2 diabetic patients and 76 of non-diabetic patients) were analysed by three certified nuclear oncologists performed between October 2018 and April 2020 in four PET / CT centers in Mexico (Imagen Molecular Aplicada of Aguascalientes and San Luis Potosí, Hospital Infantil Teletón Oncológico and Hospital Regional de Alta Especialidad del Bajío), to determine the metastatic sites of each subgroup and establish if there is a significant difference in lymph node dissemination.

Results

Odds ratios (OR) and 95% CI were used to estimate the association between the presence of type 2 diabetes mellitus and lymph node spread in patients with prostate cancer. P values for different factors were calculated using the chi-square test and Fisher's exact test. Diabetic patients had a significantly higher prevalence of lymph node metastases ($p = 0.016$, OR = 3.229, IC 1.076-10.068), especially at extrapelvic lymph nodes ($p = 0.0158$, OR = 3.577, IC 1.037-12.180). The rest of the neoplastic activity sites did not show significant differences.

Conclusion

Our findings suggest that the diagnosis of type 2 diabetes mellitus should be considered as a risk factor for developing lymph node disease, especially extrapelvic. This potential fact must be weighed at the time of therapeutic planning and for the choice of the radiotracer for molecular imaging, which will ultimately lead to improved financial toxicity and time optimization.

Exploring the Utility of PET/CT Imaging in Monitoring Treatment Response and Managing Breast Cancer in Resource-Limited Settings: A Nigerian Perspective

V. Isibor¹, A. Adeniji², A. Alabi³, C. Njoku¹, G. Oluyede¹

¹ Department of Radiation Oncology, Lagos University Teaching Hospital, Nigeria

² MeCure Oncology Centre, Nigeria

³ NSIA-LUTH Cancer Centre, Lagos University Teaching Hospital, Nigeria

Background

Breast cancer is the malignancy with the highest incidence in Nigeria. It poses a significant health challenge, compounded by expensive treatments and high mortality rates. Late presentation and limited access to advanced diagnostic tools further worsen the burden of the disease. Positron Emission Tomography-Computed Tomography (PET/CT) imaging has emerged as a valuable tool for monitoring treatment response in breast cancer patients. However, its utility in the Nigerian context requires exploration due to the unique challenges faced in resource-limited settings. PET/CT scans are currently only offered in 1 private facility in Lagos state.

Methodology

A retrospective analysis was conducted on breast cancer patients in the Oncology clinic at the Lagos University Teaching Hospital. They were referred for PET/CT scans at Mecure Labs in Lagos, Nigeria between 2021 and 2024. The patients' clinical data, including demographics, tumour characteristics, treatment regimens, and PET/CT findings, were collected and analysed. PET/CT scans were evaluated for metabolic response using the PERCIST criteria.

Results

A total of 50 breast cancer patients were referred for the PET Scan, males being 2 (4%) and with a median age of 52years. 96% of the tumour types were invasive ductal carcinoma. The majority of patients presented with advanced-stage disease (56%). PET/CT imaging revealed 4% of patients exhibited metabolic response following primary treatment, while 2% showed stable disease, and 2% displayed disease progression.. Additionally, PET/CT imaging facilitated the detection of distant metastases when requested after CT and MRIs had been done.

Conclusion

The use of PET/CT imaging in monitoring treatment response in breast cancer patients in Nigeria demonstrates promising results. Despite the challenges posed by the highest incidence rates of breast cancer in Nigeria, along with expensive treatments and high mortality, PET/CT provides valuable information regarding metabolic changes within tumours, aiding clinicians in optimizing treatment strategies and predicting patient outcomes. Early identification of treatment responders allows for timely adjustments in therapy, potentially improving survival rates and quality of life. Furthermore, PET/CT plays a crucial role in detecting occult metastases, guiding clinicians in the management of advanced disease. However, challenges such as cost, availability, and expertise in interpreting PET/CT scans remain significant barriers to widespread adoption in resource-limited settings like Nigeria. Collaborative efforts between healthcare providers, policymakers, and stakeholders are necessary to

address these challenges and enhance the accessibility and affordability of PET/CT imaging for breast cancer patients in Nigeria.

Idiopathic Granulomatous Mastitis: How to identify it by Imaging Features?

L. Elsayed¹, A. Radwan², M. Abdo¹, R. Elsheikh³, M. Metawee⁴, S. Sami⁵

¹Theodor Bilharz Research Institute, Egypt

²National Cancer Institute, Egypt

³Faculty OG Applied Health Sciences Technology, Egypt

⁴Egyptian Ministry of Health, Egypt

⁵Baheya Foundation, Egypt

Background

Idiopathic granulomatous mastitis (IGM) is a chronic inflammatory disease of the breast with obscure etiology that mimics invasive carcinoma both clinically and radiologically. Since the disease can mimic both clinically and radiologically breast cancer and other inflammatory breast conditions and has a completely different management plan, there is an urge for proper and rapid diagnosis. A multimodality imaging approach and characterization of imaging features are essential in making this correct diagnosis.

Aim

The aim of this study is to assess the different radiological findings and eliciting the typical appearance of idiopathic granulomatous mastitis. We highlighted the various findings by different imaging techniques.

Methodology

This study included 41 patients examined by different imaging modalities and later pathologically all cases proved to have IGM. The initial modality was selected depending on the age of the patient and then complementary studies were tailored according to each patient condition and availability.

Results

In our study, IGM appears as a unilateral disease in (92.7%), and of bilateral distribution in (7.3%), manifested by conventional MG as breast asymmetrical density in (77.1%), and mass densities in (22.9%) with about (17.1%) had associated architectural distortion.

On U/S it appeared as multiple hypoechoic lesions/pockets in (73.2%) with tubular extensions in (65.9%) and abscess with sinus formation and skin opening in (70.7%) of the patients. Associated oedema of the surrounding tissues was in (78%), Skin thickening in (53.7%) and reactive ipsilateral axillary lymph nodes in (80.5%). On Doppler application mean RI calculated was 0.51 in (34.1%). On Contrast studies (68.8%) of the patients showed combined mass and non-mass enhancement patterns and (25%) showed non mass enhancement pattern. All patients were pathologically proven to have IGM.

Conclusion

The imaging findings of idiopathic granulomatous mastitis overlap with those of malignancy. The most common presentation is a focal asymmetric density on mammography and an irregular hypoechoic mass with tubular extensions on ultrasound, combined mass and non-mass enhancement. Core biopsy is typically diagnostic.

Keywords: Granulomatous mastitis, IGM, multimodality approach, histopathology, focal asymmetry, hypoechoic pockets, non-mass enhancement

Gated SPECT MPI and [18F]FDG PET Cardiac Hybrid Imaging for Myocardial Viability Assessment – The Initial Experience in a Single Institute of Bangladesh

T. Mandal¹, S. M. F. Begum², S. Sultana¹, M. A. B. Siddique¹, P. Mutsuddy¹, P. Akhter¹

¹ National Institute of Nuclear Medicine & Allied Sciences, Bangladesh

² Bangladesh Atomic Energy Commission, Bangladesh

Background

Cardiac Positron Emission Tomography (PET) is a newer modality in Bangladesh to assess the myocardial viability providing valuable information about the functional status of the heart. The initial experience of Gated SPECT MPI and 18F- FDG PET hybrid cardiac imaging in single institute of Bangladesh will be highlighted in this study.

Methodology

The study includes 35 patients who referred for myocardial viability assessment 18F FDG PET cardiac scan from January 2022 to December 2023 in National Institute of Nuclear Medicine and Allied Sciences, Dhaka, Bangladesh.

Gated SPECT- rest MPI prior to PET imaging is done to detect area of hypoperfusion and wall motion abnormality. If not contraindicated, stress/rest MPI is done to detect reversible defect or ischemia. Non-gated PET cardiac imaging with 18F fluorodeoxyglucose (FDG) is done after good patient preparation according to American Society of Nuclear Cardiology (ASNC) imaging guidelines/SNMMI procedure. Interpretation is made by analyzing [18F]FDG metabolic images alongside SPECT perfusion images. A mismatch defect between perfusion and metabolism indicates potentially viable hibernating myocardium, while matched defects suggest non-viable tissue. Normal perfusion and metabolism indicate healthy, viable myocardium.

Results

A total 35 patients were enrolled in the study. Among them most of the patients (n-26) were interpreted as mixed pattern (both hibernating and non-viable myocardium) while seven (n-7) patients showed non-viable myocardium. One patient was normal and one showed hibernating pattern. All the patients are contacted over telephone for their wellbeing and treatment plan. Almost all the patients with non-viable myocardium were given conservative treatment. The patients having viable myocardium who underwent revascularization were followed up by echocardiogram for improvement of wall motion.

Conclusion

The regular implementation of 18F FDG PET cardiac viability scans at NINMAS represents a notable progression in cardiac imaging, offering the potential to guide therapeutic interventions through the assessment of myocardial viability.

Limitations

The outcome evaluation is limited due to the small dataset. However, a more extensive evaluation is planned for the future with large group of patients.

PSMA PET volume metrics as predictor to [¹⁷⁷Lu]Lu-iPSMA radioligand in patients with metastatic castrate resistant prostate cancer.

I. S. Gallardo¹, F. O. G. Perez¹, E. M. Sánchez¹, M. A. O. Casas²

¹Instituto Nacional de Cancerología, Mexico

²ABC Hospital, Mexico

Background

[¹⁷⁷Lu]Lu-PSMA-617 therapy has demonstrated excellent clinical and biochemical responses, variables related to tumour burden have demonstrated to provide a prognostic value, PET PSMA can give us information about extension of disease through estimation of total tumour burden (PSMA TTB) using algorithms of auto segmentation based in artificial intelligence. In other neoplasms PSMA TTB has proved to be a prognostic biomarker.

Aim: To estimate the prognostic value of PSMA TTB pre therapy with [¹⁷⁷Lu]Lu-PSMA-617 in metastatic Castrate Resistance Prostate Cancer (mCRPC).

Methodology

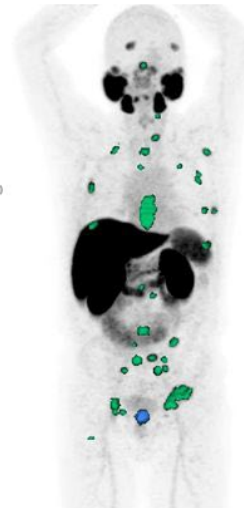
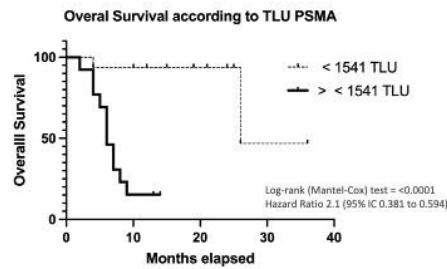
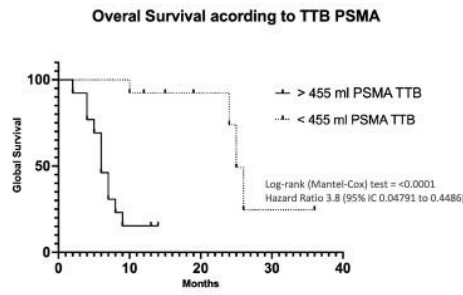
29 male patients from the National Cancer Institute of Mexico and the American British Cowdray Hospital with diagnostic of mCRPC were included in this analysis, age mean was 69 +/- 7.6 years (range 61-78), all patients had baseline PSMA-1007 and were treated with at least 2 or 3 previous lines of therapies with taxanes, ARPi's or 223Ra. In all patients were estimated volumetric parameters as PSMA-TV (total tumour volume) and PSMA TLU (total lesion uptake), using lesion ID (MIM Software Inc.). ROC curves were used to define a cut-off for PSMA TTB (total tumour volume) and PSMA TLU and Kaplan Meier analysis for estimating global survival and Pearson coefficient to estimate correlation between PSA and TTB and TLU.

Results

Haematological toxicity (G1 & G2) was observed in 70.3 % (n=19) patients and G3-G4 in 30.3 % (n=10). Mean PSMA TTB 399.6 cm³ +/- 413.5 cm³ mean PSMA TLU 5369 +/- 5612.7. Mean PSA pre therapy was 72.2 ng/mL +/- 559.3 (range 19-949 ng/ml). 6 patients received 1 cycle (7.4 GBq), 6 patients; 2 cycles (14,8 GBq), 4 patients; 3 cycles (22.2 GBq), 7 patients; 4 cycles (29.6 GBq) and 5 patients; 5 cycles (37 GBq). Cut-off of 455 cm³ for PSMA TTB and 1542 SUV_{max}cm³ for PSMA TLU using ROC curves were used to establish groups according to prognosis. Patients with PSMA TTB > than 455 cm³ has mean survival of 6.2 mo and < than 455 cm³ had has mean survival of 13.6 mo. Patients with values PSMA TLU > than 1542 SUV_{max}cm³ has mean survival of 8.1 mo, and patients < than 1542 SUV_{max}cm³ has mean survival of 11.6 mo. Pearson correlation coefficient between PSMA and PSMA TTB was 0.7278 and 0.922 for PSMA TLU, both volumetric parameters with statistically significance (p<0.05).



Patient #12
 PSMA-TTB 1056.78 ml
 PSMA TLU 4074.59 ml
 Overall Survival: 6 months



Patient #23
 PSMA-VOL 138.35 ml
 PSMA TLU 491.06 ml
 Overall Survival: still alive

Conclusion

PSMA TTB and PSMA TLU estimated with semi-automatic artificial intelligence algorithms have a good correlation with tumour markers such as PSA, this volumetric metrics such as tumour volume or Total lesion uptake, efficiently define subgroups of patients who will have unfavourable prognoses due to all the variables inherent to a high tumour burden, in addition, potentially they could include risk variables to consider them in response prediction models.

A Case Report of Incidental Thyroid Cancer Metastasis Detected in a 68Ga-PSMA PET/CT Scan of a Prostate Cancer Patient: Predicting RAI-Refractoriness

I. F. Gries

St. Lukes Medical Center BGC, Philippines

Background

Differentiated thyroid carcinoma (DTC) in Filipinos is linked to a more aggressive recurring behaviour, leading to higher morbidity rates. It is crucial to be vigilant and improve the quality of diagnosis, treatment, and prognosis of thyroid cancers in the Philippines. With the advent of 68Ga-PSMA PET/CT, multiple studies have described incidental uptake in the thyroid gland. Such finding may represent both benign and malignant etiologies, which warrant further clinical investigation. Presently, there is limited evidence on the potential of 68Ga-PSMA PET/CT scan as a prognostic biomarker in DTC, and opinions on its use in thyroid cancers, specially compared to [18F]FDG PET/CT scan, are varied. We aim to highlight the significance of simultaneous cancers identified by 68Ga-PSMA PET/CT scan, compare its benefits to an iodine-131 total body scan, examine its predictive value in radioactive iodine-refractory DTC (RAIR-DTC), and explore how PSMA radioligand therapy (PRLT) can enhance treatment protocols in the future.

Case Report

A 57-year-old male, diagnosed with prostate adenocarcinoma (Gleason score 4+3=7, ISUP group 3) who underwent a 68Ga-PSMA PET/CT (Figure 1) showed PSMA receptor-overexpressing lesions in the prostate and left lower lung nodule, measuring 2.5 x 2.1 x 2.0 cm. After biopsy, histomorphology and immunohistochemical staining of the lung nodule favoured metastatic thyroid carcinoma. Total thyroidectomy revealed papillary thyroid microcarcinoma, and the patient subsequently underwent RAI therapy. Post-therapy total body scan (Figure 1) showed functioning thyroid tissue remnants in the anterior neck with a non-iodine-avid left lung nodule. The increase in thyroglobulin hormone levels (from 26.82 to 561 ng/ml over a four-month period) led to a second round of radioactive iodine treatment which showed successful ablation of the neck remnants, however with persistent non-radioiodine concentration in the known lung metastasis. Follow-up 68Ga-PSMA PET/CT (4 months since the first scan) revealed decreased PSMA expression in the prostate and stable PSMA uptake in the lungs with interval increase in size and number on CT. Patient is maintained on Pamorelin and starting on Lenvatinib.

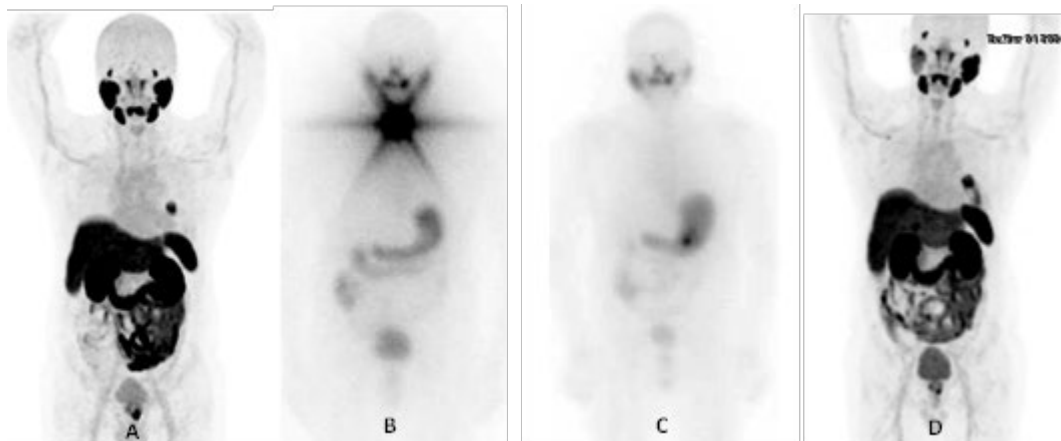


Figure 1. A) PSMA receptor-overexpressing lesions in the prostate and left lower lung nodule B) Functioning thyroid tissue remnants in the anterior neck with a non-iodine-avid left lung nodule and C) Successful ablation of the neck remnants and persistent non-radioiodine concentration of left lung nodule. D) Interval decrease of PSMA receptor-overexpressing lesions in the prostate while stable PSMA uptake in the lung nodule.

Conclusion

This case indicates that ^{68}Ga -PSMA PET/CT scan may be able to detect radioiodine resistance at an early stage and stratify patients in need of close monitoring, further evaluation, and other treatment options.

Application of 18F FDG-PET/CT scan for Evaluation of Ovarian Malignancy: Experience in a Tertiary Hospital

P. Akhter, F. Begum, T. Mandal, P. Mutsuddy, S. M. A. Rahman, M. A. B. Siddique

Nuclear Medicine, Bangladesh

Introduction

Widely used imaging modalities for ovarian malignancies are ultrasound, CT and MRI. Recently fluorine-18-fluoro-2-deoxy-D-glucose ([18F]FDG PET CT) scan shows increasing clinical application to supplement conventional imaging modalities to assess ovarian malignancies. This study was done to see the clinical use of [18F]FDG PET CT in evaluation of ovarian malignancies.

Methodology

Women with ovarian malignancies who were referred to PET/CT division of NINMAS for 18F- FDG PET/CT scan in between January 2023 to December 2023 were included in this study. This retrospective study was carried out to assess the primary disease, staging, metastases, recurrence or to see the therapy response. Patients age, sites of primary malignancy, metastases, maximum standardized uptake value (SUVmax) were evaluated.

Results

A total of 36 patients with ovarian carcinoma were included in this study. Age ranged from 39 to 74 years with an average of 52.07 ± 11.8 and most common age group was in between 51 to 60 years (36.11%). Histopathologically serous adenocarcinoma (21), mucinous adenocarcinoma (05), clear cell carcinoma (05), endometrioid carcinoma 03 and germcell tumour (02). Most of the patients came after surgery; nineteen patients came for follow up evaluation, 15 to see therapy response and only two patients came for base line scan without prior treatment. Primary malignancy was detected in two cases, residual disease in one, recurrence in one, metastases was detected in 13 cases. Rest of 19 patients showed good therapy response without any suspicious FDG uptake. In case of ovarian carcinoma most common metastatic site was abdominopelvic lymph nodes (10 cases) followed by peritoneal seeding (04 cases), hepatic (02 cases), lung (02 cases) and skeletal (one case). No individual factor was found independently associated with sites of metastases.

Conclusion

In this study patients with ovarian carcinoma referred mainly to see therapy response. Significant number of patients showed metastases on 18F- FDG PET/CT scan after standard treatment protocol. [18F]FDG PET CT scan provide significant impact on patient management by improving staging of the cancer, detecting early metastases or recurrent disease, and influencing patient selection for further treatment.

Keywords: [18F]FDG PET/CT, ovarian malignancy.

Development of [⁶⁸Ga]Ga-Deferoxamine-B as a novel agent for PET imaging of *Vibrio cholerae* infection

S. Zolghadri, F. Mohammadpour-Ghazi, H. Yousefnia

Radiation Application Research School, Nuclear Science and Technology Research Institute (NSTRI), Iran

Background

Cholera is an acute fatal disease caused by intestinal infection with the toxigenic bacterium *Vibrio cholerae*. This is an endemic illness in 69 countries including Asia, Africa, and the Americas with 1.3 billion people at risk, Sub-Saharan Africa being the worst. The early and accurate detection of the disease can effectively prevent its prevalence and help to manage the patients. Today, the high sensitivity and accuracy of the positron emission tomography (PET) make it an ideal imaging tool of different malignancies and infections. Due to the high existence of iron-specific chelators on the bacterial cells compared to normal cells, and the special physical and chemical characteristics of Gallium-68, [⁶⁸Ga]Ga-deferoxamine-B ([⁶⁸Ga]Ga-DFO-B) was prepared at optimized condition and evaluated as a new PET tracer for detection of *Vibrio cholerae* infection.

Methodology

⁶⁸Ga was eluted by a 0.1 mM HCl solution from an in-house Germanium-68/Gallium-68 generator (~370 MBq/mL). The radionuclide, chemical and radiochemical purities of [⁶⁸Ga]GaCl₃ were checked by gamma spectrometry, inductively coupled plasma (ICP), and instant thin layer chromatography (ITLC) methods, respectively. Various parameters affected on the labeling, including pH, temperature, time and DFO-B concentration, were changed to optimize the labeling procedure. The radiochemical purity (RCP) of the final product was checked using ITLC and high-performance liquid chromatography (HPLC). The stability of the final complex was assessed in PBS and human serum up to 120 min post-incubation. Partition coefficient, uptake, and competition assays were studied in vitro. Eventually, the biodistribution of [⁶⁸Ga]Ga-DFO-B was evaluated in normal and cholera mice models using organs %ID/g calculation and imaging.

Results

[⁶⁸Ga]Ga-DFO-B radiolabeled compound was prepared with RCP > 99% (ITLC & HPLC). The stability assessment of the complex in PBS buffer (4 °C), and human blood serum (37 °C) showed the radiolabeled compound had the stability >96% at least for 2 h. The partition coefficient of the complex showed the high hydrophilic nature of [⁶⁸Ga]Ga-DFO-B, which results in a fast blood clearance and rapid urinary tract excretion of the complex. The results demonstrated the high in vitro and in vivo uptake of the *Vibrio cholerae* strain could be significantly decreased in presence of an excess of iron-DFO-B.

Conclusion

The results showed that [⁶⁸Ga]Ga-DFO-B radiolabeled complex can be considered as a high potential agent for PET imaging of *Vibrio cholerae* infection, however more biological data are still needed.

[^{113m}In]In-BPAMD: A New Agent for SPECT Imaging of Bone Metastases**H. Yousefnia, S. Zolghadri, A. Karimian, B. Alirezapour**

Radiation Application Research School, Nuclear Science and Technology Research Institute (NSTRI), Iran

Background

Cancer is one of the most common reasons of death worldwide. The correct and early diagnosis is an effective way to manage the patient's treatment and reduce its mortality. Skeletal metastases are observed in various cancers, including lung, prostate, and breast malignancies. Today, ^{99m}Tc-methylene diphosphonate (^{99m}Tc-MDP) is widely used for single photon emission computed tomography (SPECT) imaging of skeletal metastasis. Due to the suitable physical and chemical properties of ^{113m}In and its availability in the form of ¹¹³Sn/^{113m}In generator, [^{113m}In]In-(4-{{(bis(phosphonomethyl)) carbamoyl)methyl} -7,10-bis(carboxymethyl)-1,4,7,10-tetraazacyclododec-1-yl) acetic acid ([^{113m}In]In-BPAMD) complex was developed as a new bone-seeking agent for SPECT imaging of the bone metastases.

Methodology

^{113m}In was eluted from an in-house made ¹¹³Sn/^{113m}In generator by 0.05 M HCl in 2 mL. The radionuclide, radiochemical, and chemical purities of the eluate were checked by gamma spectrometry, instant thin layer chromatography (ITLC), and inductively coupled plasma (ICP) methods, respectively. The BPAMD was labeled with ^{113m}In in the optimized conditions. The radiochemical purity of the final complex was measured by Radio TLC (RTLTC) using different mobile phases. The stability of the radiolabeled complex was checked in PBS (4°C), room temperature, and human blood serum (37°C) for 2 h. Hydroxyapatite (HA) binding of the [^{113m}In]In-BPAMD complex was studied in the presence of various amounts of HA. The final complex was injected into a normal rat and the biodistribution of the compound was assessed in different intervals.

Results

The gamma spectrometry of the elution showed the radionuclide purity >99.99% for the eluate. The radiochemical purity of the generator eluate was >99%, and the total chemical impurity of the solution was less than 1 ppm. [^{113m}In]In-BPAMD complex was prepared with radiochemical purity > 99% at optimized conditions. The compound was stable, in PBS, human serum, and at room temperature at least for 2 h. The HA binding assay of the final complex demonstrated the major portion of the complex was bound to the HA in vivo, even at a small amount of the HA. The biodistribution of the complex in rat organs showed the main portion of the remained activity in the body was accumulated in the bone.

Conclusion

The total characteristics of the complex showed [^{113m}In]In-BPAMD complex has a high potential to serve as a new bone-seeking agent for SPECT imaging of bone metastases, however, more biological data still is needed.

Once in a Brachial Plexus: A Case Report of Metastatic Brachial Plexopathy in a 61-year-old female Breast Cancer Patient

J. Purugganan¹, I. Bandong²

¹ St. Luke's Medical Center Quezon City, Philippines

² Philippine Society of Nuclear Medicine, Philippines

Introduction

Brachial plexopathy is a rare but important complication that causes pain and disability in cancer patients. It is a rare condition with an incidence of less than 0.5%. Metastatic breast and lung cancers are the most common non-traumatic causes of brachial plexopathy, after radiation induced fibrosis. This is to determine the importance of PET/CT in the detection of rare perineural spread of breast cancer

Case Report

This is a case of a 61-year-old female who was diagnosed with breast carcinoma in 2006 with recurrence in the neck in 2018. Re-evaluation with PET/CT scan in 2020 revealed suspicious perineural invasion of the brachial plexus (Figures 1 and 2).

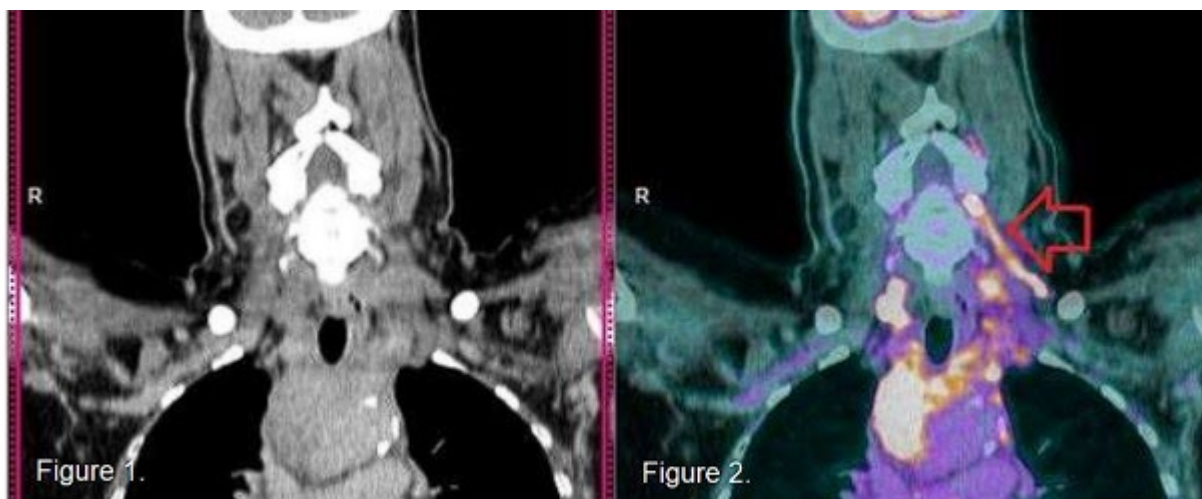


Figure 1 and 2. Coronal images of neck region of PET-CT. Linear FDG uptake is seen along the left lateral neck extending into the left neural and lateral aspect of the spinal canal at the level of C3-C4 and C4-C5 (red arrow).

Discussion

The typical occurrences of brachial plexopathies resulting from tumour recurrence or metastases are more frequently observed in the local spread of breast tumours compared to other types of carcinomas. Brachial plexopathies manifest with various associated complications including pain, restricted shoulder movement, malignant lymphedema, Horner syndrome, and neuropathies. The prevalence of cancer-associated plexopathy is approximately 0.4% in patients with cancer and 2–5% in those treated with radiotherapy. The addition of separately performed PET to diagnostic CT improved staging by 21%, while integrated PET was 34% more accurate than diagnostic CT alone.

Conclusion

This case demonstrates a rare incidence of perineural metastatic spread of known cancer, for which medical imaging, particularly nuclear imaging in partnership with radiologic imaging is key in evaluating spread of disease to help aid in treatment of patients for a better prognosis. The consequences for late detection of metastatic brachial plexopathy is debilitating and could cause great pain and loss of quality of life for these patients. PET/CT is a sensitive diagnostic imaging that could help in diagnosing rare perineural spread of metastasis, that is otherwise undetectable in CT scan alone.

[¹⁸F]FDG PET/CT versus [^{99m}Tc]HMPAO-WBC SPECT/CT in Diagnosis of Suspected Left-Ventricular-Assist-Device or Prosthetic Vascular Graft Infection

A. Štrok¹, K. Šenica¹, D. Š. Planjšek¹, A. Sočan¹, M. Logar², J. Kšela³, L. Ležaić¹

¹ Department of Nuclear Medicine, University Medical Centre Ljubljana, Slovenia
Clinic for Infectious Diseases and Febrile Illnesses, University Medical Centre Ljubljana,

² Solvenia

³ Cardiovascular Surgery, University Medical Centre Ljubljana, Slovenia

Background

The number of left ventricular assist device (LVAD) implants for the treatment of advanced heart failure as well as the use of prosthetic vascular grafts (PVG) for various indications is continuously increasing. A severe complication following insertion of these devices is infection, which remains a diagnostic challenge. Radionuclide imaging of infectious processes plays a pivotal role in diagnosis of prosthetic valve endocarditis, but for other device-related infections the precise role of individual molecular imaging modalities remains to be established.

The aim of our study was to evaluate two molecular imaging techniques, namely [¹⁸F]FDG PET/CT and [^{99m}Tc]HMPAO-WBC SPECT/CT in patients with suspected LVAD or PVG infection.

Methodology

Patients with suspected LVAD or PVG infection who underwent both [¹⁸F]FDG PET/CT (1 hour after injection) and technetium-99m HMPAO-WBC-SPECT/CT (4 and 20 hours after reinjection) in time span of <14 days were retrospectively analysed. 6 patients had LVAD and 21 patients had PVG suspected infection. The results of [¹⁸F]FDG PET/CT and [^{99m}Tc]HMPAO-WBC-SPECT/CT were analysed separately by experienced nuclear medicine physicians. The final diagnosis was based on a composites standard of truth comprising of positive haemoculture, positive bacteriological culture from the site of infection and patient follow-up (clinical, repeated imaging).

Results

27 patients (5 women and 22 men, mean age 62 years) were included in our prospective study. 17 of them had infection. With [¹⁸F]FDG PET/CT 6 patients were correctly diagnosed as positive, 1 patient as false positive (FP), 1 patient as false negative (FN), 4 patients as true negative (TN) and 15 results were equivocal. With [^{99m}Tc]HMPAO-WBC -SPECT/CT 15 patients were correctly diagnosed as positive, 1 patients as FP, 1 patient as FN, 9 patients as TN and 1 result was equivocal. Sensitivity, specificity, positive predictive value, negative predictive value and accuracy of each imaging modality were 88%, 60%, 79%, 90% and 78%, respectively, for [¹⁸F]FDG PET/CT; and 88%, 90 %, 94 %, 82 % and 89%, respectively, for [^{99m}Tc]HMPAO-WBC-SPECT/CT in patient-based analyses.

Conclusion

[^{99m}Tc]HMPAO-WBC-SPECT/CT offers higher specificity than [¹⁸F]FDG PET/CT, therefore a sequential strategy for the diagnosis of suspected LVAD or PVG infection has been proposed and consists of performing [¹⁸F]FDG PET/CT first, following [^{99m}Tc]HMPAO-WBC-SPECT/CT when results of [¹⁸F]FDG PET/CT are inconclusive appears feasible.

A Comparative Analysis of F-18-PSMA-1007 and Ga-68 PSMA-11 for Prostate Cancer: A retrospective study

A. Ghujeh¹, S. Nair¹, M. Altinyay¹, A. A. A. Rahim¹, F. Alves², H. Fayad¹

¹ Hamad Medical Corporation, Qatar

² CIBIT/ICNAS, Institute for Nuclear Sciences Applied to Health, University of Coimbra, Portugal

Background

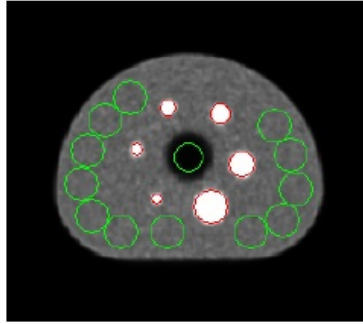
Prostate-specific membrane antigen (PSMA) imaging, using radiotracers such as F-18-PSMA-1007 (F-18) and Ga-68 PSMA-11 (Ga-68), has emerged as a pivotal tool in prostate cancer diagnosis including both detection and especially staging. This study compares the advantages and disadvantages of each isotope, focusing on their physics attributes and clinical imaging performance. These insights will contribute to a deep understanding of the isotopes performance and guide their application in patient personalized and precision medicine.

Methodology

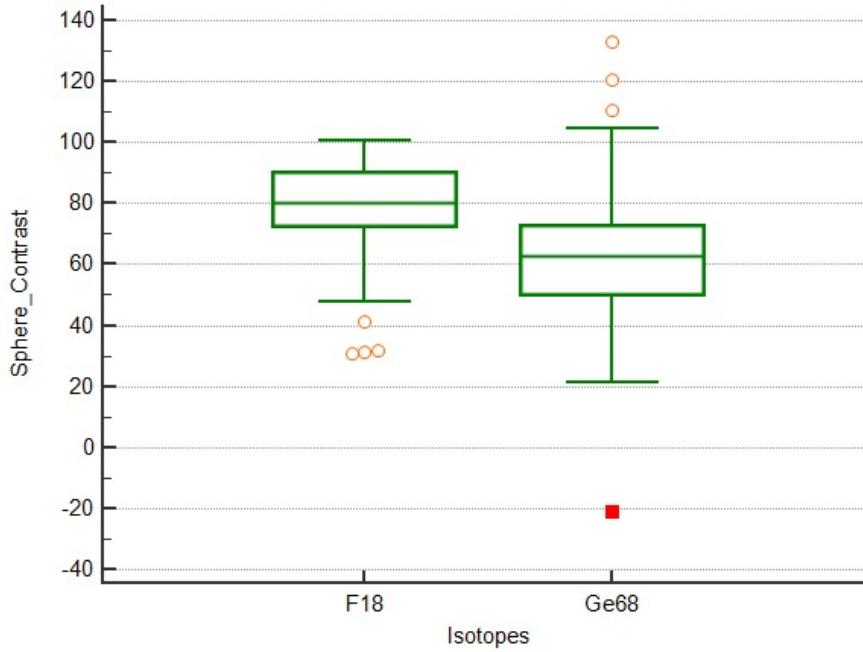
This study comprises two tasks. Firstly, a comprehensive analysis of F-18 and Ga-68 physics features was conducted, including spatial resolution, contrast sensitivity, and background variability. Spatial resolution was assessed using the NEMA L-shape phantom holder, measuring Full Width at Half Maximum (FWHM) at different location (at the center (0 cm) of the scanner Field of View, (0, 20 cm) position and (20, 0 cm) position. Contrast percentage evaluation utilized the NEMA body phantom, employing radioisotope concentration ratio of 4:1. A total of 44 acquisitions were performed obtaining a total of 264 measurements for both Ga68 and F18. Background variability, indicative of imaging noise, was measured based on the same previous NEMA body acquisitions using the part of the phantom without spheres. In all studies mean \pm standard deviation is reported. Moreover, statistical analysis, including the one-way ANOVA test, was applied for robust evaluation. A p-value of less than 0.05 is considered statistically significant. Secondly, images from six patients scanned for initial staging were reviewed by two Nuclear Medicine experts. Regions of interest were delineated on prostate lesions and on the liver, operating as background, to determine the SUV max and SUV mean respectively. Then the Tumour to background ratio is calculated by having the ratio of the two above values.

Results

Spatial resolution revealed a mean of 4.2 ± 0.7 and 4.9 ± 1.5 for F-18 and Ga-68 respectively (p-value of 0.002). Regarding contrast percentage, for the biggest sphere having a 37 mm diameter, F-18 yielded a mean of $95.9 \pm 3.7\%$, compared to $83.4 \pm 11.3\%$ for the Ga-68 (p-value < 0.001). The overall mean contrast percentage showed a mean of $78.2 \pm 16.6\%$ and $62.2 \pm 18.8\%$ for F-18 and Ga-68 respectively (p-value < 0.001 , Fig 1). Moreover, background variability testing revealed values of 1.7 ± 0.7 and 2.0 ± 0.6 for F-18 and Ga-68 respectively (however p-value of 0.178). Regarding the clinical measurements the background variability range was 4.1 % to 9.34% for F-18 PSMA patient scans compared to Ga-68 PSMA scans (6.99% to 11.46%). Additionally, the contrast ratio of tumour to liver (background) had values of 0.42 to 3.79 for F-18 and 1.31 to 4.48 for Ga-68.



A. Spheres and background regions



B. Anova one way analysis of Variance comparison graph regarding sphere contrasts showing separation between Ga68 and F18

Conclusion

This study underscores the superiority of F-18 over Ga-68 in terms of spatial resolution, contrast, and background variability. Although conclusions can be raised on phantom studies, clinical images only suggest better background variability for F-18 compared to Ga-68, along with higher contrast ratios. Future work will consist of increasing the number of patients to draw conclusions on either radiopharmaceuticals choice or the optimal use.

Optimized production of ^{177}Lu -Curcumin as a possible theranostic agentS. Vosoughi¹, N. Salek², S. S. Arani², A. B. Samani²¹ Radiation Application Research School, Nuclear Science and Technology Research Institute (NSTRI), Iran² Nuclear Fuel Research School, Nuclear Science and Technology Research Institute (NSTRI), Iran**Background**

Among the different effective agents, Curcumin has been recognized as a potential cancer chemoprevention agent. It was observed that curcumin suppresses the expression of estrogen receptors and epidermal growth receptors, which are cancer-associated growth factors. Radiolabeling curcumin by ^{177}Lu can be developed for radiotherapy in a wide range of cancers. In this way, the binding affinity of radio-complex to tumour cells leads to the death of the tumour cells and preservation of the non-targeted tissues. ^{177}Lu , with relatively mild β^- -emission with maximum energies of 497 keV (78.6%), 384 keV (9.1%), and 176 keV (12.2%) and a long half-life of 6.7 days, has the advantages of a higher injected dose amount and long retention of radiation in tumours but lower irradiation of adjacent normal tissues. Moreover, the emission of proper gamma photon energies of 113 keV (6.4%) and 208 keV (11%) with relatively low abundances of ^{177}Lu , enables its use in the imaging and dosimetry assessment of patients before and during treatment without requiring a surrogate tracer. In this study, the possibility of radiolabeling curcumin with n.c.a ^{177}Lu was investigated.

Methodology

Neutron irradiation of enriched ^{176}Yb (NO_3)₃ target (10mg) was performed to produce n.c.a ^{177}Lu in a quartz ampoule with a thermal neutron flux of $1 \times 10^{14} \text{ ncm}^{-2}\text{s}^{-1}$ for 5 days at the Tehran Research Reactor. Due to the ^{174}Yb content in the target, ^{175}Yb ($T_{1/2} = 4.185$ days) was also produced and used as a tracer for Ytterbium. For the ^{177}Yb ($T_{1/2} = 1.9$ h) to decay, the irradiated target was cooled for 3 days. The bombarded target was then dissolved in 0.1 M HNO_3 for the EXC separation method. The acidic solution (1mL) of $^{177}\text{LuCl}_3$ (0.6–1.8 GBq) was transferred into a 3 mL-borosilicate vial. Then, curcumin (10 μL) in pure ethanol (0.1 mg/mL) was added to the lutetium-containing vial followed by the addition of acetate buffer pH 5 (450 μL). The reaction mixture was stirred at 95 °C for 1 h in a water bath. The radiochemical purity of the final solution was checked by RTLC. Finally, the prepared complex was analysed by different quality control tests.

Results

The radiochemical purity of n.c.a ^{177}Lu -curcumin was more than 95% as determined by RTLC. The stability of up to 48h was observed for the prepared complex in serum. The partition coefficient was calculated for the compound ($\log P = -0.31$). Evaluating biodistribution in tumoural C57 nu/nu mice exhibited high tumour uptake (average ID/g%=2.79) (Fig.1).

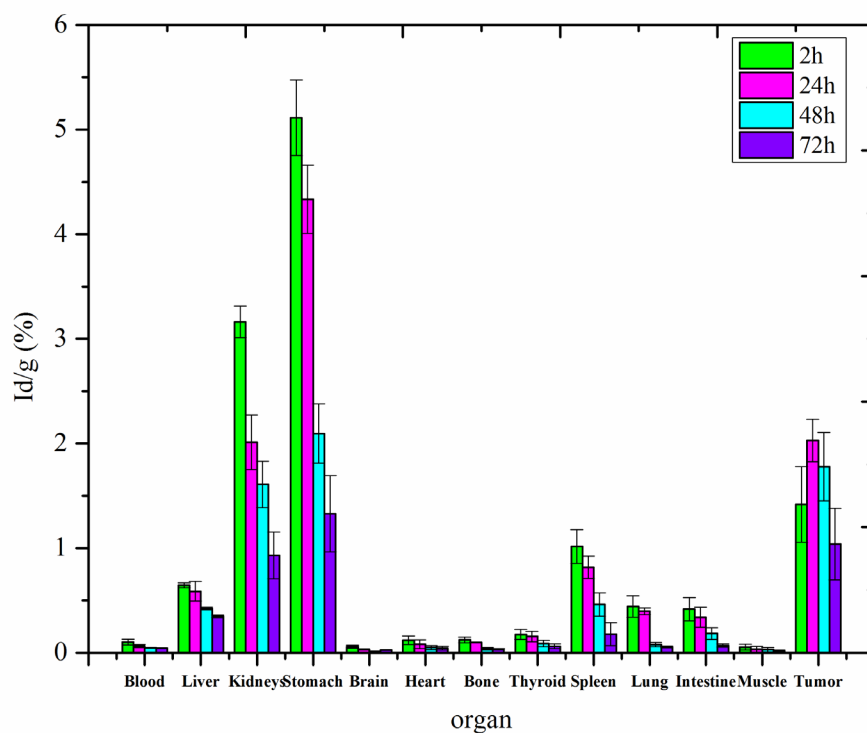


Figure 1. Percentage of injected dose per gram (%ID/g) of n.c.a. ^{177}Lu -curcumin at 2 h, 24 h, 48 h and 72 h post-injection

Conclusion

^{177}Lu , as a prospective reactor-produced radionuclide, is highly promising in targeted therapy. The ligand complexation with ^{177}Lu and targeting of the particular organ with radio-complex was the purpose of this study. The promising results showed that n.c.a. ^{177}Lu -curcumin can be considered as a possible radiopharmaceutical agent for theranostic applications.

Artificial Intelligence for the Stratification of Breast Cancer Using $^{18\text{F}}$ FDG PET/CT**M. A. Hossain¹, S. I. Chowdhury²**¹ Department of Physics, University of Rajshahi, Bangladesh² Institute of Nuclear Medicine and Allied Sciences, Bangladesh Atomic Energy Commission, Bangladesh**Background**

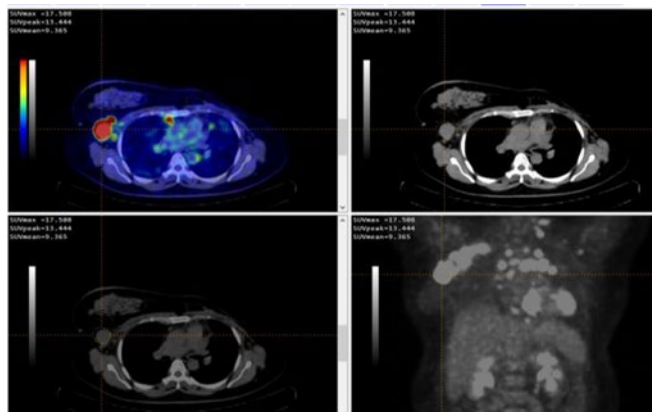
While PET/CT is a standard tool for measuring breast cancer, subtypes are not automatically classified by it. Thus, the purpose of this research is to use artificial intelligence to assess the clinical subtypes of breast cancer according to the significance of tumour markers.

Methodology

This research was conducted at Institute of Nuclear Medical Physics, Savar, Bangladesh, Bangladesh Atomic Energy Commission. In our nuclear medical facility, 122 breast cancer patients (training, testing) had $^{18\text{F}}$ FDG PET/CT to identify the various subtypes of the disease. $^{18\text{F}}$ FDG-18 injections were administered to the patients before to the scanning process. We carried out the scan according to protocol. Based on the tumour marker value, the artificial neural network's output layer uses the softmax function with cross-entropy loss to detect different subtypes of breast cancer.

Results

With an accuracy of 95.77%, the result illustrates the ANN model for k-fold cross validation. The mean values of specificity and sensitivity were 0.955 and 0.958, correspondingly. AUC on average was 0.985.

**Figure 1.** $^{18\text{F}}$ FDG-PET/CT for breast cancer.**Conclusion**

Subtypes of breast cancer can be categorized using the suggested model. The PET/CT may be updated to diagnosis breast cancer subtypes using the appropriate tumour maker value when the suggested model is clinically implemented.

Advancing Cancer Management in Burundi: The Crucial Role of Nuclear Medicine in the Present and Future

C. Uwizeyimana

Ecole Normale Supérieure, Burundi

Background

Cancer incidence and mortality rates in Burundi are alarming, with an estimated 7,929 new cases reported in 2020 (Globocan 2020). Among these cases, cervical cancer, breast cancer, prostate cancer, Kaposi's sarcoma, and oesophageal cancers emerged as the leading types. The high burden of cervical and breast cancers on women necessitates urgent interventions to enhance cancer management and reduce associated morbidity and mortality.

According to the Bujumbura Pathology Centre (BUJAPATH) report, women are more affected with a high burden of cervical and breast cancer, and many men are being diagnosed with prostate cancer in Burundi.

A total of 847 patients have consulted the oncology service at only Centre Medico-Chirurgical de Kinindo (CMCK), Bujumbura: Only 289 out of 847 (34%) were treated by chemotherapy. 49 out of 289 (17%) are children and 240 (83%) are adults. The majority of cancer patients pay the cost of diagnostic tests & treatment by themselves (in Public, Private and abroad), A small number of patients are assisted by the Ministry of solidarity. Some cases of Leukaemia and other patients have been sent abroad for treatment particularly for Radiotherapy treatment. In a study realized by the General Directorate of Health Services, 18.4% of cases transferred abroad for treatment in 2016-2017 were due to tumour cancer.

The role of nuclear medicine and benefits in cancer management in Burundi:

Integrating nuclear medicine into the existing cancer management infrastructure can yield several benefits. Firstly, it allows for precise diagnosis, facilitating early detection and timely intervention. This is especially crucial for cervical and breast cancers, which are prevalent in Burundi. Nuclear medicine techniques such as positron emission tomography (PET) can provide valuable information on tumour characteristics and metastasis, guiding treatment decisions.

The introduction of nuclear medicine therapies, such as targeted radionuclide therapy, can expand treatment options for cancer patients in Burundi. These therapies deliver radiation directly to cancer cells, minimizing damage to healthy tissues. This approach can be particularly valuable for patients who are unable to access or afford external radiation therapy abroad.

To fully leverage the potential of nuclear medicine, strengthening human resources is essential. Increasing the number of nuclear medicine specialists, radiologists, and medical physicists will enhance the capacity to deliver high-quality nuclear medicine services. Training programs, collaborations with the IAEA will contribute to building a skilled workforce in the field of nuclear medicine.

Conclusion

The burden of cancer in Burundi calls for urgent action to improve cancer management and reduce morbidity and mortality rates. The introduction of targeted radionuclide therapy offers expanded treatment options, especially for patients who lack access to external radiation therapy. However, realizing the full benefits of nuclear medicine requires strengthening human resources through increased

training and collaboration with organizations like the IAEA, and would enhance ability to provide high-quality cancer care and reduce the burden of the disease.

Preliminary results from a trial of a standardized intravenous insulin protocol for the management of unexpected hyperglycemia before [18F]FDG PET scans

A. Singhal, A. Venugopal, N. A. Damle, Y. Gupta, B. Khangembam

Department of Nuclear Medicine, All India Institute of Medical Sciences, India

Background

[18F]FDG is the most commonly used radiotracer for Positron Emission Tomography-Computed tomography (PET/CT) imaging in various oncological and non-oncological indications. [18F]FDG is an analogue of glucose and undergoes competition at a molecular level with the latter for uptake in cancer or healthy cells through glucose transporters (GLUTs). The 2015 EANM procedure guidelines for [18F]FDG PET/CT in tumour imaging recommend rescheduling the patient if the plasma glucose level is higher than or equal to 200 mg/dL. Few studies have investigated the utility of using insulin to correct glucose levels, but the procedure is not yet validated. The aim of this study was to evaluate an intravenous insulin protocol to perform diagnostic quality imaging in patients who present with unexpected hyperglycemia on the day of PET scan.

Methodology

32 cancer patients who demonstrated plasma glucose levels between 200 to 350 mg/dL before their scheduled PET/CT examination were prospectively enrolled in the study. All these participants were administered regular human insulin through intravenous route with the dose determined using a sliding scale depending on the level of glycemia. Sequential glucose monitoring was done at every 15-minute interval and [18F]FDG was injected intravenously at a prefixed interval of 60 minutes post-insulin administration, in patients who had their glucose level reduced to below 200 mg/dL. In all patients who underwent PET/CT imaging, the biodistribution of [18F]FDG was graded using a visual ordinal scale (Score 0: Normal biodistribution; 1: Mild muscular uptake; 2: Moderate uptake in more than one muscle group; 3: Moderate diffuse uptake in muscles; 4: Diffuse intense muscular uptake). Patients with acceptable biodistribution (scores 0 to 2) were distinguished from those with abnormal distribution and non-diagnostic imaging (scores 3 or 4). The latter group of patients were rescheduled to appear for imaging at a later date with better glycemic control using prevailing standards.

Results

32 patients (11 males, 21 females) with age 55.5 ± 7.5 years (range 43 – 73 years) presented with plasma glucose levels in a range of 200 to 340 mg/dL (mean glucose 251 ± 36.5 mg/dL). One patient could not achieve glycemia reduction below 200 mg/dL despite an adequate dose of insulin and was rescheduled and excluded from the analysis. The remaining 31 patients who underwent PET/CT scans experienced a reduction in glucose level of 107.6 ± 44.6 mg/dL. 27 (87%) patients demonstrated a normal to near-normal [18F]FDG biodistribution (scores 0 to 2) on imaging. The remaining 4 (13%) patients showed altered biodistribution (scores 3 or 4). Of the 27 patients with acceptable biodistribution, 17 (63%; 53% of the total sample) patients showed normal (score 0) distribution of [18F]FDG. The other 10 patients had near-normal tracer biodistribution with acceptable image quality for routine diagnostic purposes.

Conclusion

The proposed protocol for intravenous use of regular insulin shows high efficacy in obtaining diagnostic quality [18F]FDG PET imaging in hyperglycemic patients not otherwise fit for the examination as per prevailing international guidelines.

Multimodality Imaging for Evaluating Response to Neoadjuvant Chemotherapy in Locally Advanced Breast Cancer

S. M. F. Begum¹, S. H. Dinu², K. Hosain³, T. Mandal³, P. Mutsuddy³, K. K. Nath³, M. A. B. Siddique³

¹Member (Planning), Bangladesh Atomic Energy Commission, Bangladesh

²Ministry of Health and Family Welfare, Bangladesh

³National Institute of Nuclear Medicine & Allied Sciences, Bangladesh Atomic Energy Commission, Bangladesh

Background

Breast cancer is the most common malignancy among Bangladeshi female which accounted for 6808 total deaths in 2020 according to World Health Organization (WHO). Many patients identified at more advanced stage of the disease attributed by diverse number of socioeconomic factors. Fate of the disease finally depends on proper management i.e. precise diagnosis and appropriate treatment. Neoadjuvant chemotherapy (NACT) is the treatment of choice in many patients of the country particularly in locally advanced breast cancer (LABC). NACT is used to downstage the disease and to reduce or eliminate micro metastasis. However, therapeutic response following the NACT is the prognostic indicator for subsequent management of these patients leading to personalized therapy. Final response can be evaluated by invasive post-surgical histopathological findings. But the non-invasive imaging modalities like MRI, CT and PET can play a crucial to evaluate therapy response. Conventional imaging modalities have limitations as these depend on changes of size and morphology. On the other aspect functional imaging techniques are superior as they identify vascular, biochemical, metabolic, and molecular changes of cancer cells. Even PET is superior to other modalities as metabolic change can be identified before the morphological changes, by determining the metabolic tumour volume and demarcating the viable tumour from fibrous tissue. MRI is well practicing tool in Bangladesh and PET-CT is a relatively newer modality for the huge population of our country.

Aim

A recently completed IAEA Coordinated Research Project (IAEA-CRP project- E13044) is contributing to approach the LABC patients to assess the response to NACT by performing both MRI and PET; before and after NACT by using RECIST 1.1 and PERCIST criteria then were compared with histopathological findings.

Methodology

A total of 32 patients with LABC were enrolled; among them 11 cases were dropped out and excluded from the study. Total 21 patients' data were analysed.

Results

The sensitivity, specificity, and accuracy of F-18 FDG PET were 83.33%, 100%, 95.24% and MRI were 100%, 80% and 85.71% respectively.

Conclusion

F-18 FDG PET-CT demonstrated greater specificity and accuracy than MRI; nevertheless, both PET-CT and MRI characteristics may be predictive in identifying therapeutic responders and non-responders after NACT. PET also provides valuable information by the whole-body survey by detecting presence of distant osseous or non-osseous metastases. The outcome from this research will provide the opportunity in appropriate application of these modalities and guide the clinician in optimal cancer management for female breast cancer patients of our country.

Key words: Neoadjuvant chemotherapy (NACT), locally advanced breast cancer (LABC)

Experience in establishing a nuclear medicine facility in Mauritius; A Medical Physicist Perspective

S. Baichoo

Nuclear Medicine Department, J. Nehru Hospital, Mauritius

Background

Mauritius established its Nuclear Medicine Department in 2008. The establishment of the department was made possible through a collaborative effort between the Medical Physicist (advisor to the project), the Government of Mauritius, and the International Atomic Energy Agency (IAEA). With the support of various national and regional technical cooperation projects facilitated by the IAEA, the department procured a gamma camera in 2009, and personnel were trained through fellowships and training courses. Fifteen years later, Mauritius has achieved significant progress in its nuclear medicine services. The introduction of PET/CT and SPECT/CT hybrid imaging capabilities in the public healthcare sector was facilitated by the construction of a new cancer hospital. The integration of these advanced modalities involved meticulous planning and coordination at all levels to ensure successful implementation within the facility.

Methodology

The shielding calculations for the nuclear medicine facility were conducted in accordance with the methodology outlined in the AAPM TG-108 for PET/CT. Various IAEA publications, including Safety Report 58, SSG-46, and Human Health Series 11, were consulted to facilitate the planning of nuclear medicine services.

Result

For the licensing purposes of the radiation practice, radiation protection aspects had to be ensured and communicated to the regulatory body in the form of Safety Assessment Reports. This process consists of two stages: shielding calculations and layout, and operationalization. The design of the nuclear medicine facility emphasizes radiation protection, with reinforced concrete walls of varying thickness throughout the facility. Access to the department is limited to patients and nuclear medicine staff, requiring a key code at the main entrance. The layout of the facility has been designed to have an optimised patient flow, emphasizing a controlled environment. Laboratory areas, including the radioactive waste room, physics laboratory, and radiopharmaceutical laboratory, are restricted to limited staff. The radiopharmaceutical laboratory incorporates HEPA filters in the air exhaust systems. To manage waste, active toilets in the PET uptake room and SPECT/CT post-injection waiting room channel waste to a delay tank for collection, ensuring safe disposal practices.

Future Directions

The next significant advancement in nuclear medicine in Mauritius entails establishing a radionuclide therapy facility. This endeavour will necessitate highly skilled personnel and a meticulously designed facility to address all radiation safety requirements associated with such a specialized service.

Conclusion

This marks a pivotal moment in Mauritius' healthcare landscape, as we embark on a groundbreaking development. Given the complexities of radiation licensing processes, guidance from the International Atomic Energy Agency (IAEA) has been instrumental in the success of our new cancer hospital. There is a recognized need for ongoing improvements in hospital practices and regulatory frameworks. The lessons learned from this initial experience will undoubtedly inform and enhance future endeavours, particularly with the impending introduction of radionuclide therapy services. Continuous education of hospital staff remains paramount in optimizing safe radiation practices within our facilities.

The Value of Delayed Imaging in Detection of Biochemical Recurrent Prostate Cancer using Gallium-68 Prostate Specific Membrane Antigen (PSMA) PET/CT

N. A. Denil, S. Z. A. Hassan, M. M Manap, N. S Ali

¹ General Hospital Kuala Lumpur, Malaysia

² National Cancer Institute, Malaysia

Background

Ga-68 prostate specific membrane antigen (PSMA) PET/CT has shown high detection rate in recurrent prostate cancer with significant clinical impact on treatment allocation. The study is to evaluate the significance of additional delayed imaging in Ga-68 PSMA PET/CT in detection of prostate cancer lesion in biochemical recurrent prostate cancer.

Methodology

This study included 87 prostate cancer patients referred for Ga-68 PSMA PET/CT for suspicion of relapse based on detectable or rising PSA level after radical prostatectomy or radiation therapy. Biochemical recurrence is defined by PSA level >0.1 ng/mL after radical prostatectomy ; or 3 successive rise or absolute increase of 2 ng/mL above nadir following radiation therapy. Imaging consisted of whole-body PET/CT conducted at 1-hour post injection (1 h p.i) and 3-hour post injection (3 h p.i). The lesions detected were categorized as local recurrence, lymph node, bone or other soft tissue organ metastases. The lesions detected in the early images were compared with the late images in terms of number of lesions detected and maximum standardized uptake value (SUVmax) according to the suggestive anatomical field.

Results

Ga-68 PSMA PET/CT showed high detection rate with a total of 158 PSMA positive lesions identified in 73 out of 87 patients (84%). The mean PSA of the positive scans was higher than that of negative scans (mean PSA 5.11 ng/mL vs 2.82 ng/mL) ($p = 0.17$ by Mann-Whitney U-test). Higher SUVmax were observed in most pathologic lesions between 1 h p.i. and 3 h p.i. scans ($p < 0.001$ by Wilcoxon Signed Ranks Test in local recurrence, pelvic and extra pelvic nodes and bones) with the highest average SUVmax was seen in bone metastases (SUVmax 16.3 at 1 h p.i. vs. SUVmax 22.1 at 3 h p.i.) The lowest average SUVmax were observed in soft tissue visceral metastases (SUVmax 5.2 at 1 h p.i. vs. SUVmax 7.3 at 3 h p.i.) ($p = 0.110$). The study demonstrated that the delayed imaging at 3 hour p.i. was helpful for 8 % of the patients. The suspicious lesions detected during 1 hour imaging were later confirmed as malignant with the increased in SUVmax. ($p < 0.001$)

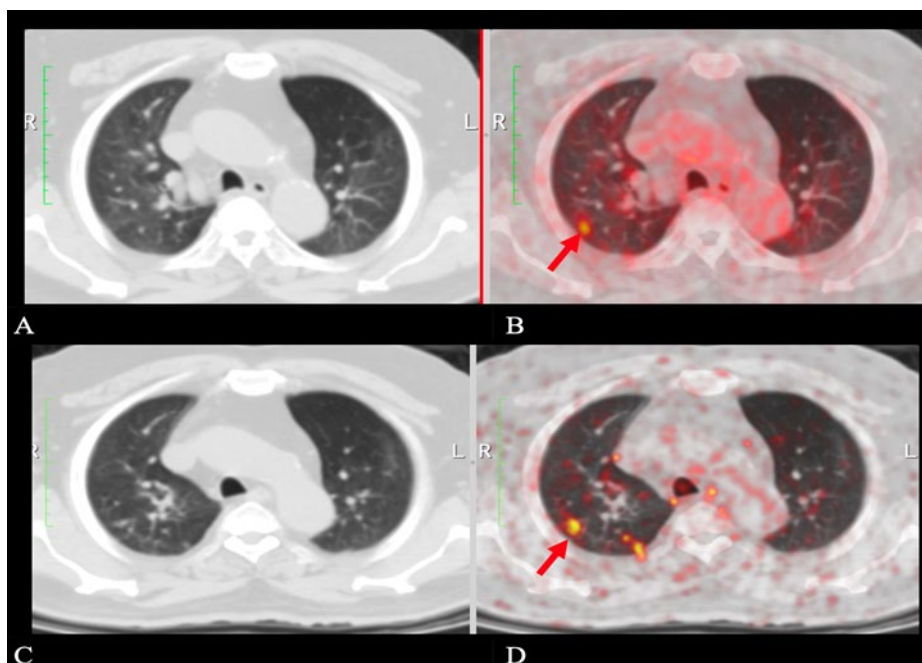


Figure 1. Patient post external beam radiotherapy. Ga-68 PSMA PET/CT at 1 h p.i.(A [low dose CT at 1 h p.i.] and B [fusion PE/CT at 1 h p.i.] and at 3 h p.i. (C [low dose CT at 3 h p.i.] and D [fusion PET/CT at 3 h p.i.]). Red arrows point to PSMA uptake at the right upper lobe suspicious of prostate cancer recurrence at 1 h p.i. with increasing uptake and contrast in late scans (SUVmax 2.9 at 1 h p.i. and 4.8 at 3 h p.i.).

Table 2. Comparison of number of PMSA-positive lesion and SUVmax between 1-hour post injection and 3-hour post injection Ga-68 PSMA PET/CT. Wilcoxon Signed Ranks test showed significant difference in median between the two-imaging time (p value of < 0.001)

PSMA-positive lesion location	Number of PSMA-positive lesions (n, %)	Hour	SUVmax*		p-value ^a
			Median	Quartile	
Local recurrence	50/158 (32 %)	1	12.0	(8.0, 22.0)	<0.001
		3	18.6	(11.0, 31.8)	
Pelvic node	42/158 (26 %)	1	11.3	(6.5, 19.8)	<0.001
		3	18.4	(10.4, 30.9)	
Extra-pelvic node	23/158 (14 %)	1	11.6	(3.9, 21.6)	<0.001
		3	15.9	(7.1, 42.7)	
Bone metastases	31/158 (20 %)	1	16.3	(5.4, 26.4)	<0.001
		3	22.1	(9.5, 54.5)	
Soft tissue organ	12/158 (8 %)	1	5.2	(3.1, 7.4)	0.110
		3	7.3	(3.0, 14.4)	

*Data SUVmax skewed to the right
^ap value < 0.05 is considered significant (Wilcoxon Signed Ranks Test)

Conclusion

With delayed Ga-68 PSMA PET/CT imaging, there is a higher degree of confidence to clarify malignant lesions when it is supported by an increase in the SUVmax value especially in the surgical bed and irradiated pelvis. It is also important that clinician understand that some prostate cancer lesions may exhibit low PSMA expression and therefore a significant increase in SUVmax value on delayed images may assist the clinician in the final interpretation which may lead to disease upstaging and change in treatment plan.

Impact Of FDG PET CT On Management Of Patients With Treatment Naive HCC Intended For Local Surgical/Ablative Or Embolisational Therapies

M. Sarma, W. M Jose, Binoj S T

Amrita Institute of Medical Sciences, India

Background

2-deoxy-2-[fluorine-18]fluoro-D-glucose ([18F]FDG) PET CT has shown mixed utility in the detection of primary Hepatocellular cancer (HCC) with sensitivities of around 55-64%. FDG PET CT is more useful in detection of regional and distant extrahepatic metastases. We intended to study the impact of FDG PET CT on those patients intended for local management of treatment naïve primary HCC (local surgical/ablative or embolisational therapies).

Methodology

FDG PET CT scans of 61 consecutive patients of treatment naïve HCC acquired between 2010 and 2020 who were intended for local surgical/ablative or embolisational therapies were retrospectively reviewed to look for change in management following the findings in FDG PET scan. Data on patient characteristics, initial plan of management, findings on FDG PET CT, subsequent management, change in management if any and the reason of change in management were collected.

Results

There was overall change in management in 18 out of 61 patients (29%). Most of the patients plan changed to systemic therapy because of detection of metastatic lesions (10 out of 18 patients). Plan changed to palliative therapy in 2 patients. In 2 patients, TACE was planned instead of surgery while in another 2 patients plan was changed to extended hepatectomy. In another 2 patients, the initial plan of surgery was dropped and patient was lost to subsequent management. Detection of distant metastases (7 out of 18 patients), portal vein involvement (4 out of 18), IVC thrombus (1 out of 18), lymphnodal metastases (2 out of 18) and other lobe of liver involvement (4 out of 18 patients) on FDG PET CT were the reasons leading to management changes.

Conclusion

Inspite of its low sensitivity of detecting primary HCC, FDG PET can bring about change in management in a significant number of patients intended for local surgeries/ablative or embolisational therapies.

Added value of SPECT-CT MPI in diagnosis of ischemia and atherosclerotic coronary artery disease

N. Kostova¹, A. Celikic¹, D. PopGjorceva², E. Vrajnko¹, M. Zdravkovska², M. Vavlukis¹, V. Majstorov²

¹ University Clinic of Cardiology, Ss Cyril and Methodius University in Skopje, Faculty of Medicine, North Macedonia

² Institute for Pathophysiology and Nuclear Medicine, Ss Cyril and Methodius University in Skopje, Faculty of Medicine, North Macedonia

Background

SPECT CT MPI is a hybrid nuclear imaging technique that enables collecting, calcium score, myocardial perfusion, and LV functional data.

Our study aimed to analyze data collected with SPECT CT MPI, specifically coronary calcium score, myocardial perfusion and left ventricular function with coronary anatomy as defined with invasive coronary angiography.

Methodology

We designed a single-center cross-sectional observational cohort study. All patients who were reported to our laboratory for SPECT CT MPI, without known coronary artery disease (CAD), and who subsequently underwent invasive coronary angiography (ICA) (in three months at longest), were subjected to comparative analysis for their demographic and clinical data, based on what SCORE2 and pretest probability was calculated, Agatston calcium score, myocardial perfusion, and LV function. Patients were comparatively analysed with respect to PCI treated CA (PCI-CA), and/or coronary atherosclerotic disease as detected (CATHD) by ICA. Comparative statistic methods (Chi square, Student t-test, Univariate analysis, correlations, and ROC curves) were undertaken. Statistical significance was determined at the level of 0.05.

Results

85 patients at mean age 60.9±11.0 y., 45 (52.9%) females and 40 (47.1%) males. CATH patients Significant positive correlations were found for CATHD with male gender ($r=.339^{**}$, $p=0.002$), pre-test probability for CAD($r=.366^{**}$, $p=0.001$), LVES volumes at rest and after stress ($r=.247^{*}$ and $.320^{**}$ with $p=0.024$ and 0.003 respectively), EF after stress ($r=-.215$, $p=0.050$), and Agatston calcium score ($r=.516^{**}$, $p=0.0000013$). While, PCI-CA was correlated with advanced age ($r=.357^{**}$, $p=0.001$), male gender ($r=.225^{*}$, $p=0.038$), pre-test probability ($r=.532^{**}$, $p=0.000003$), and coronary calcium score ($r=.497^{**}$, $p=0.000001$). Same findings were confirmed with ROC curve analysis (images attached). In multivariate analysis three independent predictors associated with CATHD were: male gender (OR 4.13, $p=0.008$); presence of ischemia (OR 4.13, $p=0.060$), and Agatston CAC score ($p=0.005$). Furthermore, independent variables associated with PCI-CA were pre-test probability, and Agatston CAC score, although presence of ischemia and EF at rest were in the final step of the model, however demonstrating no statistical significance as independent predictors.

Table 1. Distribution of patient's variables based on presence of CATH

Variable	CATH present	N	Mean	Std. Deviation	sig(P)
age	0	45	59.31	9.53	ns
	1	40	62.80	12.32	
BMI	0	45	30.34	5.01	ns
	1	40	29.64	4.76	
Pre-test probability	0	45	13.78	10.30	0.006
	1	40	20.25	10.72	
Ischemia (% of LV mass)	0	45	10.04	9.35	ns
	1	40	11.70	12.57	
LVEDv (rest)	0	45	103.07	31.93	ns
	1	39	109.59	30.83	
LVESv (rest)	0	45	35.04	21.88	ns
	1	39	42.54	25.15	
EF (rest)	0	45	65.29	7.98	ns
	1	39	62.46	9.28	
LVEDv (stress)	0	44	101.52	37.66	ns
	1	40	111.43	38.89	
LVESv (stress)	0	44	34.61	27.51	0.093
	1	40	44.95	28.13	
EF (stress)	0	44	65.45	8.14	0.077
	1	40	62.03	9.40	
Agatston CAC score	0	45	46.89	117.68	0.000025
	1	40	367.65	466.23	

2. Multivariate logistic regression analysis (binary logistic, method backward conditional)

Model summary: Chi-square 33.272, $p < 0.000$, percent correct prediction 75.6

B		S.E.	Wald	df	Sig.	Exp(B)	
Step 1 ^a	age	-.014	.044	.100	1	.752	.986
	female0/mail1(1)	-1.164	.936	1.548	1	.213	.312
	0low/1inter/2high/3verhigh			1.339	2	.512	
	0low/1inter/2high/3very high(1)	.685	1.063	.415	1	.519	1.985
	0low/1inter/2high/3very high(2)	-.217	.890	.059	1	.807	.805
	Pre-test probability	.008	.045	.031	1	.859	1.008
	Presence of ischemia	-1.264	.933	1.835	1	.176	.282
	Ischemia (% of LV mass)	-.054	.044	1.479	1	.224	.947
	LVEDv (rest)	-.002	.044	.002	1	.969	.998
	LVESv (rest)	.046	.099	.220	1	.639	1.047
	EF (rest)	-.015	.126	.014	1	.905	.985
	LVEDv (stress)	-.015	.022	.477	1	.490	.985
	LVESv (stress)	-.014	.045	.098	1	.754	.986
	EF (stress)	.003	.083	.001	1	.971	1.003
	Agatston CAC score	.006	.002	6.189	1	.013	1.006
	Constant	2.638	7.828	.114	1	.736	13.982
	Step 10 ^a	Male gender	1.498	.565	7.033	1	.008
Presence of ischemia		1.419	.781	3.303	1	.060	4.13
Ischemia (% of LV mass)		-.054	.035	2.420	1	.120	.947
Agatston CAC score		.006	.002	7.999	1	.005	1.006
Constant		.877	.683	1.650	1	.199	2.403

Table 3. Distribution of patient's variables based on presence of PCI-CA

Variable	CATH present	N	Mean	Std. Deviation	sig(P)
age	0	45	59.31	9.53	ns
	1	40	62.80	12.32	
BMI	0	45	30.34	5.01	ns
	1	40	29.64	4.76	
Pre-test probability	0	45	13.78	10.30	0.006
	1	40	20.25	10.72	
Ischemia (% of LV mass)	0	45	10.04	9.35	ns
	1	40	11.70	12.57	
LVEDv (rest)	0	45	103.07	31.93	ns
	1	39	109.59	30.83	
LVESv (rest)	0	45	35.04	21.88	ns
	1	39	42.54	25.15	
EF (rest)	0	45	65.29	7.98	ns
	1	39	62.46	9.28	
LVEDv (stress)	0	44	101.52	37.66	ns
	1	40	111.43	38.89	
LVESv (stress)	0	44	34.61	27.51	0.093
	1	40	44.95	28.13	
EF (stress)	0	44	65.45	8.14	0.077
	1	40	62.03	9.40	
Agatston CAC score	0	45	46.89	117.68	0.000025
	1	40	367.65	466.23	

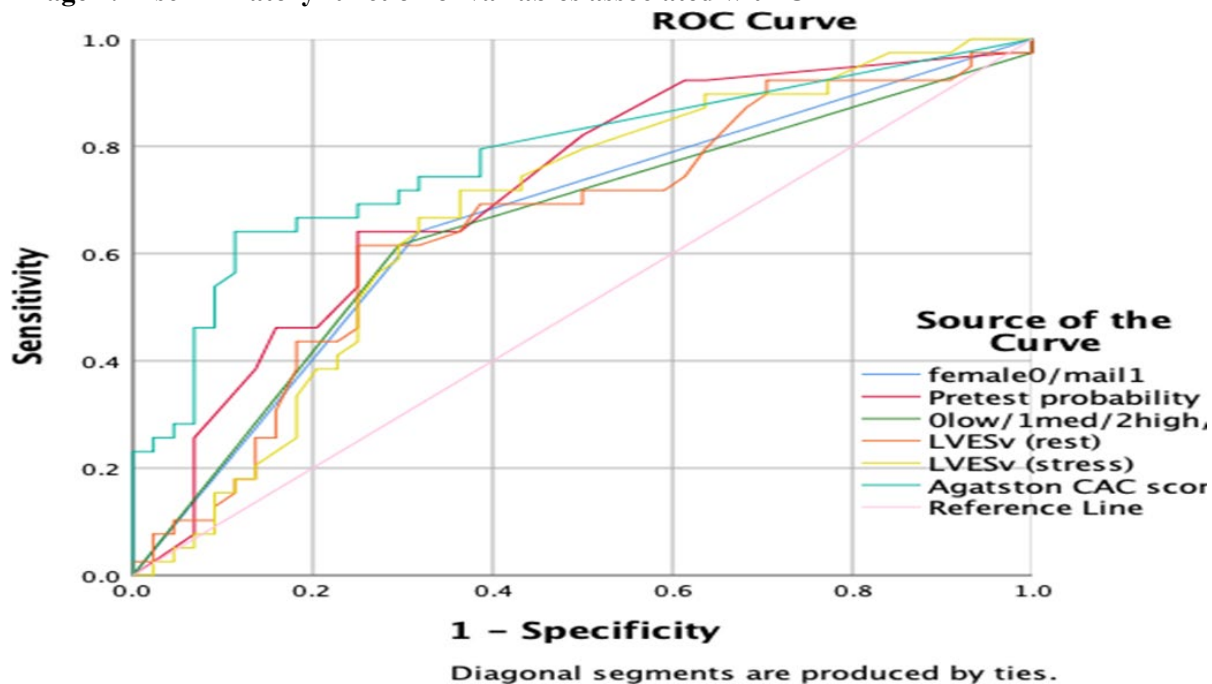
Table 5. Significant correlation coefficients for any CATHD degree of stenosis (part A), and for PCI-CA treated stenosis (part B)

Part A CATHD	Gender (male)	Pretest probability	LVESv (rest)	LVESv (stress)	EFs	Agatston CAC score
Correlation (r)	.339**	.366**	.247*	.320**	-.215	.516**
Significance (p)	.002	.001	.024	.003	.050	.0000013

Part B PCI-CA	age	Gender (male)	Pretest probability	Agatston CAC score
Correlation (r)	.357**	.225*	.532**	.497**
Significance (p)	.001	.038	.000003	.000001

Legend: CATHD -coronary artery atherosclerotic disease; PCI-CA-coronary artery treated with stenting; LVESv- left-ventricular end-systolic volume (at rest, and after stress);EF-ejection fraction;

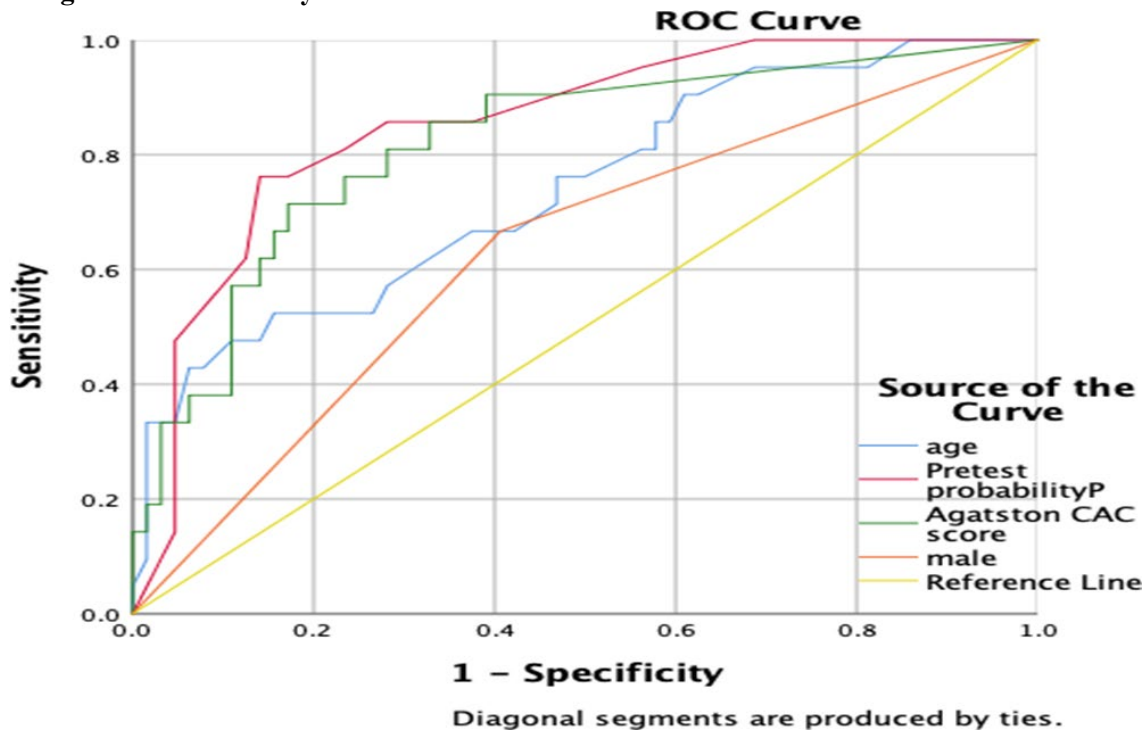
Image 1. Discriminatory function of variables associated with CATHD



Area Under the Curve

Test Result Variable(s)	Area	Std. Error ^a	Asymptotic		
			Sig. ^b	Lower Bound	Upper Bound
Male gender	.661	.061	.011	.543	.780
Pre-test probability	.716	.057	.001	.604	.827
SCORE2 categorical	.651	.062	.018	.530	.772
LVESv (rest)	.656	.061	.014	.537	.776
LVESv (stress)	.677	.060	.006	.560	.794
Agatston CAC score	.779	.052	.000	.676	.881

Image 2. Discriminatory function of variables associated with PCI-CA



Area Under the Curve

Test Result Variable(s)	Area	Std. Error ^a	Asymptotic Sig. ^b	Asymptotic 95% Confidence Interval	
				Lower Bound	Upper Bound
age	.739	.064	.001	.614	.864
Pre-test probability	.853	.046	.000	.764	.943
Agatston CAC score	.820	.054	.000	.714	.926
Male gender	.630	.070	.075	.493	.767

Conclusion

Hybrid SPECT MPI by combining data from myocardial perfusion, LV function, and coronary calcium score, accompanied with demographic data (advanced age and male gender), and calculated pre-test clinical probability for CAD, greatly complement, and/or predict ICA findings, which makes it valuable tool in the hands of cardiac imagers.

[¹⁸F]FDG PET/CT for Follow-up of Blastic Plasmacytoid Dendritic Cell Neoplasm/BPDCN/-differential diagnosis between lung involvement and atypical pulmonary infection

E. Dimitrova, P. Bochev, G. Mateva

Acibadem City Clinic Mladost, Sofia, Bulgaria

Background

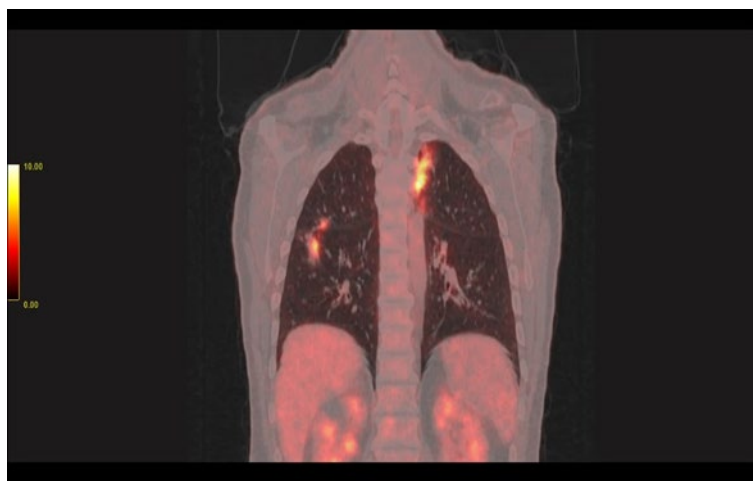
Blastic plasmacytoid dendritic cell neoplasm is a rare hematologic malignancy. Skin lesions are the most frequent initial presentation of the disease, followed by extra-cutaneous manifestations- lymphadenopathy, splenomegaly and hepatomegaly, as well as lung involvement. The diagnosis is made by skin biopsy and immunochemistry. Immunohistochemistry must show positive for CD4, CD56, CD123 and TCL1. Since the malignancy is FGD-avid, PET/CT is valuable tool for the evaluation of the extent of disease, or treatment response and for follow-up.

Case Report

The aim of this case report is to present a rare case in which PET/CT questions the differential diagnosis between lung involvement and lung infection in a patient with BPDCN.

We report a case of a male patient diagnosed with BPDCN in July 2022. The initial manifestation was multiple purple-brown patches cutaneous lesions on the face, trunk and extremities as an initial presentation. Apart from the skin involvement there was also initial bone marrow involvement. The patient successfully responded to non-Hodgkin lymphoma treatment (Hyper CVAD) and the follow-up PET/CT was negative.

In October 2023, the patient underwent allogenic stem cell transplantation (ASCT). Four months later his condition was reevaluated with [¹⁸F]FDG PET/CT. The scan revealed several metabolically active lung lesions bilaterally, most of them subsolid.



No other FDG-positive lesions were present on the whole body scan. No reappearance of the skin lesions was observed on clinical examination.

Lung involvement is not typical for BPDCN, however it is not completely impossible site of engagement.

Given the immunocompromised status of the patient due to the recent ASCT and the appearance of lung lesions, it is highly likely the etiology of the changes to be associated with infection, most likely atypical. However lung involvement from the hematologic malignancy cannot be completely ruled out, especially putting into consideration the presence of a few solid lung nodules.

The patient was referred to pulmonologist for microbiological testing and evaluation of the need for subsequent biopsy of the lung lesions.

The patient was tested for various bacterial and fungal pathogens and was positive for *Aspergillus*.

Conclusion

In conclusion we would like to stress on the importance of interpreting the PET/CT findings, taking into account the clinical status of the patient and the expected evolution of the disease.

Incremental Role of Whole-Body [¹⁸F]FDG PET/CT to assess extra cranial involvement in Cavernous Sinus Syndrome

H. Singh¹, R. A. Mahdi², A. Takkar³, C. K. Ahuja⁴, R. Kumar², S. Bansal⁵, D. Chatterjee⁶, B. R. Mittal², V. Lal³

¹Post Graduate Institute of Medical Education and Research (PGIMER), Chandigarh, India

²Department of Nuclear Medicine, PGIMER, Chandigarh, India

³Department of Neurology, PGIMER, Chandigarh, India

⁴Department of Radiodiagnosis and Imaging, PGIMER, Chandigarh, India

⁵Department of ENT, PGIMER, Chandigarh, India

⁶Department of Histopathology, PGIMER, Chandigarh, India

Background

A wide range of pathologies ranging from inflammation to infection, and from benign to malignant neoplasms can cause Cavernous Sinus Syndrome (CSS). Extensive clinical, imaging, laboratory and Histopathological work-up are necessary to clinch the etiological diagnosis in majority of cases. Still, the cause may not be ascertained in many, leading to empirical treatment. ¹⁸F-Fluorodeoxyglucose ([¹⁸F]FDG) uptake can be seen in neoplastic as well as infective/inflammatory pathologies. The present study aims to assess utility of [¹⁸F]FDG PET/CT in detection of extra cranial sites of involvement and guiding biopsy in CSS.

Methodology

Forty-eight adult patients who presented with CSS (defined as “involvement of two or more cranial nerves (which pass through CS) or oculosympathetic fibres on the same side, or involvement of only cranial nerve in combination with a radiologically confirmed cavernous sinus lesion”) were prospectively recruited. Whole-body [¹⁸F]FDG PET/CT was performed in all patients after clinical, imaging and laboratory work-up. Presence, site and number of extracranial lesions on [¹⁸F]FDG PET/CT was documented. Histopathology was taken as gold standard. “Consensus Diagnostic Criteria for Neurosarcoidosis” from the Neurosarcoidosis Consortium Consensus Group was used to diagnose Neurosarcoidosis. “2020 revised comprehensive diagnostic (RCD) criteria” was used for IgG4- Related disease. Modified ICHD-III criteria were used for diagnosis of Tolosa Hunt Syndrome.

Results

The mean age of patients was 46.4 years (18-75 years), with 25 male (52%) and 23 females (48%). The most common symptom was headache, followed by diplopia. [¹⁸F]FDG PET positive extra cranial lesions were detected in 23 patients (48%). A total of 260 extra cranial lesions were detected. The most common sites of involvement were lymph nodes (14 patients), followed by lung (n=11), bones (n=5), paraspinal soft tissue (n=3), liver (n=2), perivascular thickening (n=2), lacrimal, tongue, nerve root thickening, myocardium, thyroid, adrenal and prostate (n=1 each). Biopsy was done from FDG positive extra cranial sites in 9/48 (18.7%) patients: lymph nodes (n=3, TB and n=1, sarcoidosis), liver lesion and lacrimal gland in one patient each (sarcoidosis), skeletal lesion (n=1, Ewing’s sarcoma), lung lesion (n=1, adenocarcinoma) and tongue lesion (n=1, squamous cell carcinoma). In six patients (12.5%), biopsy was done from the local site in CS or paranasal sinus [fungal (n=3), hypertrophic pachymeningitis (n=1), IgG4-RD (n=1), and meningioma (n=1). In four patients, the final diagnosis was

possible IgG4-RD (n=3) and Tolosa Hunt Syndrome (n=1). In the remaining four patients, the extra cranial lesions were found to be incidental co-existing pathology: Lung nodules, skeletal, prostatic and seminal vesicle lesions due to tuberculosis in a patient with pituitary adenoma, Non-specific mediastinal lymph nodes in a meningioma patient, FDG avid incidental thyroid nodule in a patient with fungal CSS and Pheochromocytoma in a case of meningioma.

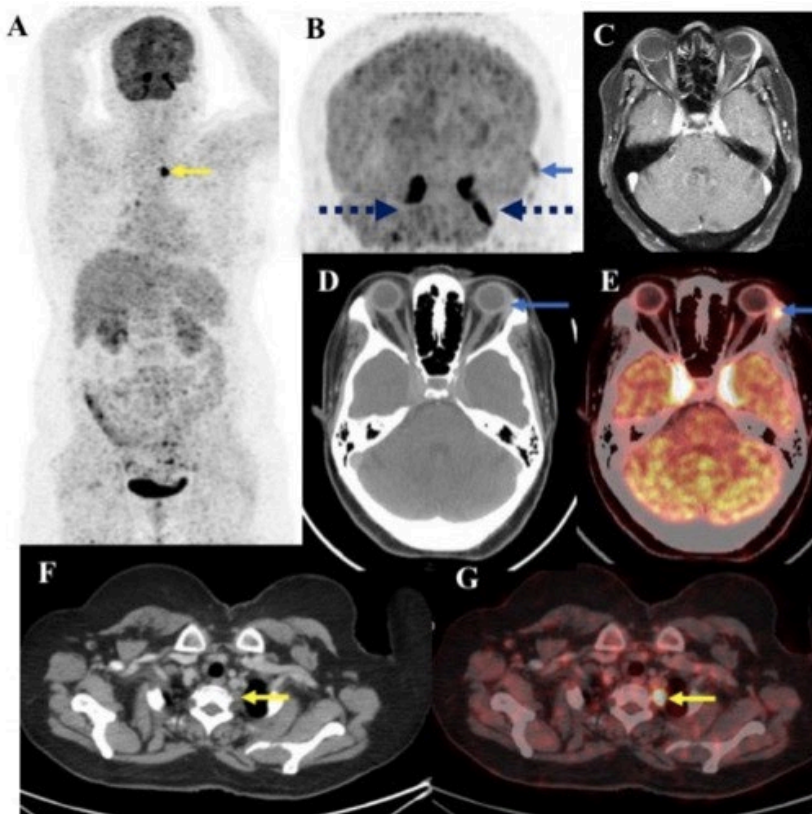


Figure 1: A 58-year-old female presented initially with headache and diplopia followed by numbness on left half of face, facial deviation, ptosis and bilateral diminution of vision. Maximum intensity projection (MIP) image of whole body (A) and dedicated brain image (B) with CT and fused PET/CT images showing increased FDG uptake in the bilateral cavernous sinuses (SUV_{max} 41.9; dashed arrows in B, E). T1 post contrast MRI (C) showing enhancement in the bilateral cavernous sinuses. FDG avid bulky left lacrimal gland (SUV_{max} 11.0) was noted (solid blue arrow B, D-E), biopsy from which revealed granulomatous inflammation suggestive of sarcoidosis. FDG avid centimetric paravertebral soft tissue was also noted at upper dorsal vertebral level in the whole-body MIP and transaxial fused PET/CT and CT images (SUV_{max} 24.5, yellow arrow, A, F-G)

Conclusion

Whole-body [^{18}F]FDG PET/CT can detect extra cranial sites of involvement in a significant percentage of patients with Cavernous Sinus Syndrome and can be used to guide biopsy to reach an etiological diagnosis. [^{18}F]FDG PET/CT may also detect clinically significant coexisting pathologies in a small subset, which can impact patient management.

Rapid and accurate estimation of voxel S-values for personalized dosimetry in PET/CT using deep learning

M. Karimipourfard¹, S. Sina^{1,2}, H. Mahani³, M. H. Sadeghi¹

¹ Department of Ray-Medical Engineering, Shiraz University, Iran

² Radiation Research Center, Shiraz University, Iran

³ Radiation Applications Research School, Nuclear Science and Technology Research Institute, Iran

Background

Molecular imaging plays a central role in the early diagnosis of cancer, selection of suitable treatment, and follow-up. Radiation burden to the patient is, however, a main concern, particularly in multimodality imaging like PET/CT. Personalized dosimetry in PET/CT imaging is of the essence to optimize imaging protocols and estimate the risk of radiation. While the Monte Carlo (MC) method is considered the gold standard in such tasks, it suffers from an extensive computational burden hampering its clinical usage. The problem is more challenging in image-based dosimetry where accurate dose estimation is mandated at the voxel level. To this end, the present study aims to exploit a deep learning (DL) model to approach the problem and facilitate rapid and accurate estimation of voxel S-value map in patient-specific internal dosimetry for [18F]FDG PET/CT.

Methodology

To do so, whole-body unenhanced [18F]FDG PET/CT scans of 50 patients were collected using Philips's Ingenuity PET/CT scanner. The PET and CT images were resampled and registered before feeding to both the GATE simulator and the DL model. The liver, kidney, bladder, heart wall, lungs, pancreas, stomach, and spleen were segmented on PET/CT images, as well (Figure 1) and the segmented PET and CT images were imported to the GATE v8.2 as voxelized source and phantom, respectively. The GATE simulation was performed to calculate the MC-derived S-value map and construction of the ground truth. The pretrained p2p-U-Net-GAN model was then utilized to predict the S-value map from the PET/CT image of each patient. To further enhance the performance of the DL network, optimal hyperparameters were selected based on Taguchi's method. Three key metrics including structural similarity index (SSIM), peak signal-to-noise ratio (PSNR), and mean squared error (MSE) were evaluated and reported.

Results

The findings confirm that the optimized p2p-U-Net-GAN gives rise to rapid and accurate estimation of S-value maps for all patients by providing acceptable performance metrics (Figure 2). By optimizing the hyperparameters of the p2p-U-Net-GAN, improved performance of the DL model is obtained in terms of accuracy and convergence speed. The difference between the MC- and DL-calculated S-values falls within the range of 0.2% to 3.3%, with the largest deviation observed in the stomach region. For the same level of accuracy, the MC method requires over 72.0 h to compute voxel S-values for a typical PET/CT image, whereas DL can predict the output in 10.0 min.

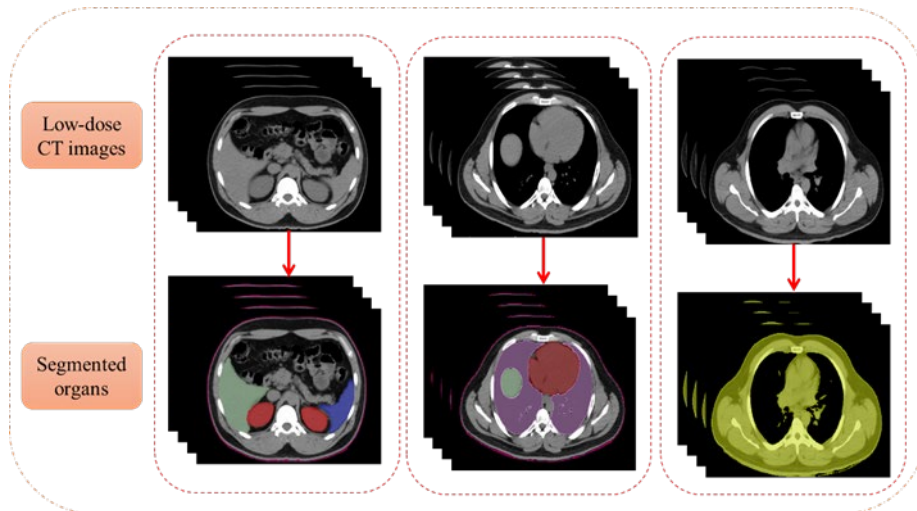


Figure 1. Segmentation of the organs of interest on PET/CT images.

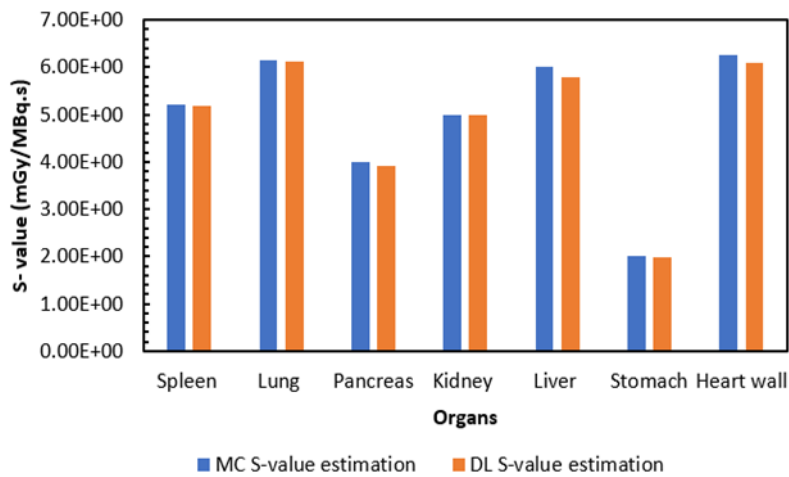


Figure 2. Comparison of the DL-derived organs' S-values with the MC-derived ones.

Conclusion

When compared to the well-established MC method, the optimized p2p-U-Net-GAN offers similar accuracy with substantially improved efficiency and speed. Therefore, it can be the method of choice for rapid and accurate prediction of voxel S-values for clinical patient-specific internal dosimetry in PET/CT scanning.

Correlation between [⁶⁸Ga]PSMA-11 PET/CT total tumour volume (PSMA TV) and serum PSA in carcinoma prostate patients at initial staging as a tool to predict prognosis and tumour burden

P. Verma^{1,2}, S. Basu^{1,2}, V. Dhawan³, B. K. Soni⁴

1 Radiation Medicine Centre, Bhabha Atomic Research Centre, India

2 Homi Bhabha National Institute, India

3 Department of Urology, INHS Asvini, India

4 Department of Radiodiagnosis, INHS Asvini, India

Background

[⁶⁸Ga]PSMA-11 PET/CT has been shown to be of immense value in staging and restaging of carcinoma prostate. In the current era of personalized medicine, it becomes important to quantify disease burden and predict treatment response in individual patients. Our study is directed in helping us formulate the tools which can guide the clinician in decision making for personalized treatment options. The objective of this study was to evaluate whether [⁶⁸Ga]PSMA-11 PET/CT tumour volume (PSMA TV) is associated with clinical parameters and laboratory parameters in carcinoma prostate patients at initial staging.

Methodology

We retrospectively evaluated the [⁶⁸Ga]PSMA-11 PET/CT scans performed for initial staging of prostate cancer patients from January 2022 to January 2024. Total body volume of PSMA-avid tumour lesions (PSMA TV) was calculated semi-automatically by drawing region of interest (ROI) over the PSMA avid lesions on the scan using the software Synapse 3D (Fujifilm). In non-metastatic patients, the ROI was drawn on the prostate lesions and PSMA TV was calculated, while for metastatic patients, the ROI on each metastatic site was calculated and TV was added up for each patient. Spearman's rank correlations between PSMA TV and clinical, laboratory parameters (age, total serum PSA levels, and the Gleason score) and with the highest SUVmax in a patient were analysed.

Results

There were a total of 29 patients with [⁶⁸Ga]PSMA-11 PET/CT scan performed for initial staging. PSMA TV ranged from 31 ml in non-metastatic patient with S.PSA 12 ng/ml to 9500 ml in a patient with multiple metastases and S.PSA 296 ng/ml. We observed a significant correlation between PSMA TV and total serum PSA values, PSMA SUVmax and Gleason's score ($p < 0.05$).

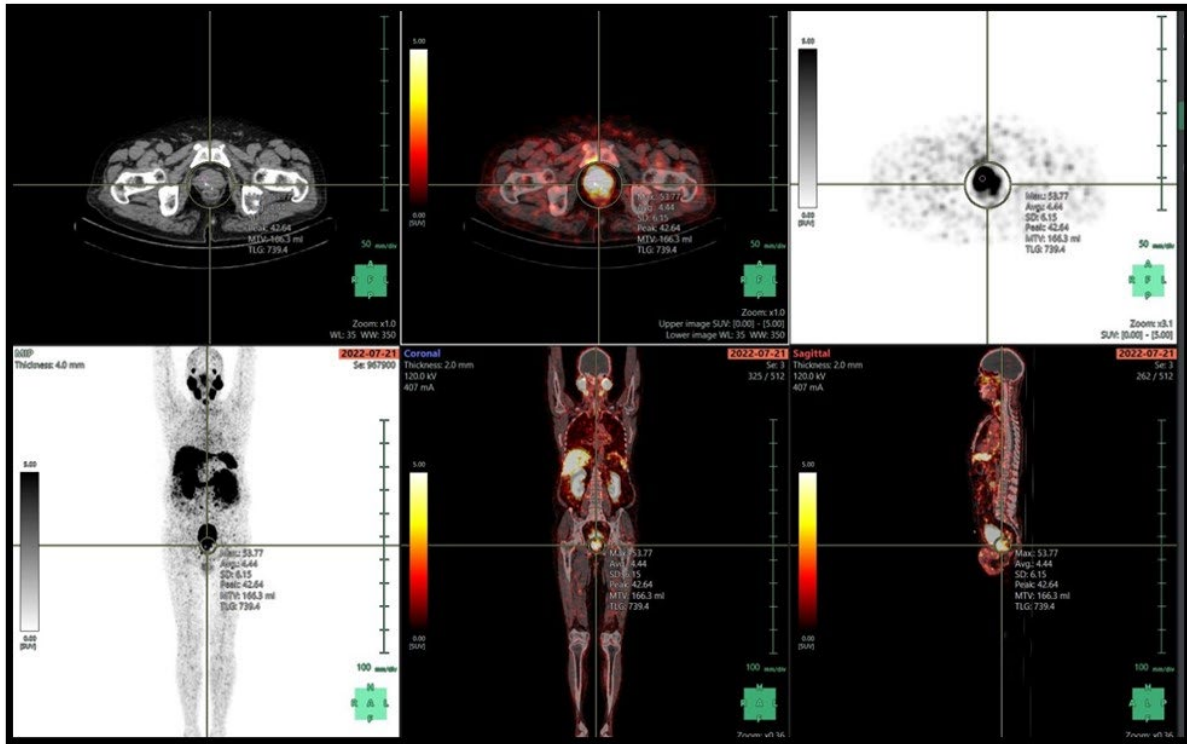


Figure 1. [^{68}Ga]PSMA-11 PET/CT images of 70 years old patient with carcinoma prostate, S.PSA 29.1 ng/ml, Gleason's score 8, SUVmax 53.77 and PSMA TV calculated as 166.3ml.

Conclusion

PSMA TV has a significant correlation with serum PSA values, PSMA-SUVmax and Gleason's score in carcinoma prostate patients. Therefore, PSMA TV may be a potentially parameter to predict prognosis and tumour burden. Additionally, it may help in objectively assessing treatment response on PSMA PET/CT, if imaging is repeated after therapy.

⁶⁸Ga-PSMA-11 PET/CT and ¹⁸F-Fluorocholine PET/CT in assessment and clinical decision making of recurrent prostate Cancer: A crossover trial

M. S. Akbari^{1,2}, M. Hacker³, W. Loidl⁴, W. Langsteiger^{3,5}, M. Beheshti¹

¹ Division of Molecular Imaging and Theranostics, University Hospital Salzburg, Paracelsus Medical University, Austria

² Research Institute for Nuclear Medicine, Department of Nuclear Medicine, Tehran university of Medical Sciences, Iran

³ Division of Nuclear Medicine, Department of Biomedical Imaging and Image-Guided Therapy, Medical University of Vienna, Austria

⁴ Department of Urology, Ordensklinikum, Austria

⁵ Department of Nuclear Medicine & Endocrinology, PET/CT Center LINZ, Ordensklinikum, Austria

Objectives

While ⁶⁸Ga-labelled prostate-specific membrane antigen-11 (⁶⁸Ga-PSMA-11) positron-emission-tomography/computed-tomography (PET/CT) proved its high diagnostic accuracy in the assessment of recurrent prostate cancer (PCa) patients, there are only few prospective studies addressed its role in clinical decision making comparing to ¹⁸F-Fluorocholine (¹⁸F-FCH) PET/CT. This study aims to evaluate the impact of PET/CT using ⁶⁸Ga-PSMA-11 and ¹⁸F-FCH in clinical management of recurrent PCa and correlate imaging findings with clinical characteristics of the disease.

Methodology

Forty-six PCa patients (mean age 68.3±6.3 years) with biochemical recurrence after treatment were enrolled in this prospective crossover trial. In 27 (59%) patients, no systemic treatment (androgen deprivation therapy and/or chemotherapy) was performed after radical treatment (radical prostatectomy ± radiotherapy). PSA value was ≤1, > 1 ≤ 2, and > 2 ng/ml in 29 (63%), 5 (11%) and 12 (26%) of cases, respectively. All patients underwent both ⁶⁸Ga-PSMA-11 and ¹⁸F-FCH PET/CT within a maximum interval of 15 days. Clinical decision making was done in an interdisciplinary meeting considering the PET/CT findings based on blinded-reading and a consensus meeting for final interpretation of the detected lesions. Histopathology and/or clinical and imaging follow-ups were defined as reference standard.

Results

In the lesion-based analysis, 136 malignant lesions were detected by both imaging modalities. ⁶⁸Ga-PSMA-11 and ¹⁸F-FCH PET/CT detected 130 and 65 lesions with a sensitivity of 96% and 48%, respectively (P-value < 0.001). In addition to higher detection rate of ⁶⁸Ga-PSMA-11, tumour to background and semi-quantitative PET parameters were significantly higher in 54 (41.2%) congruent lesions detected on both imaging modalities (mean SUV_{max} 12.81±13.5 on ⁶⁸Ga-PSMA PET versus 6.35±4.89 on ¹⁸F-FCH PET). From 77 (56.6%) incongruent lesions, ⁶⁸Ga-PSMA-11 PET/CT exclusively detected 71 (52.2%) lesions [Local recurrence: 2 (2.59%), regional Lymph Node: 18 (23.4%), distant Metastases: 51 (66.2%)], while only 6 (4.4%) lesions were seen on ¹⁸F-FCH PET/CT [regional Lymph Node: 3 (5.1%), distant Metastasis: 3 (5.1%)].

In patient-based analysis, 68Ga-PSMA-11 and 18F-FCH PET/CT were positive in 35 and 26 patients, respectively. Both imaging modalities were negative in 10 patients. 68Ga-PSMA-11 PET/CT upstaged the disease in 16 (34.8%) patients, more prominently in M staging. However, PET/CT imaging led to major treatment change in 4 (8.7%) patients, of which only in one patient 18F-FCH PET/CT had a superior impact.

Conclusion

68Ga-PSMA-11 PET/CT revealed higher diagnostic performance to 18F-FCH PET/CT in recurrent PCa patients, even in cases with very low PSA levels (i.e. ≤ 1 ng/ml). Moreover, it led to more accurate staging and clinical management of the disease. 18F-FCH PET/CT may play a complementary role only in rare selected high-risk cases even with ongoing ADT, showing negative 68Ga-PSMA-11 PET/CT.

Keywords: Positron emission tomography/computed tomography (PET/CT); Prostate cancer; Biochemical recurrence; ^{18}F -Fluorocholine; ^{68}Ga -PSMA-11.

Disclosure

This study was funded by TELIX pharmaceuticals Limited, Melbourne, Australia.

Unusual metastatic sites and presentations of differentiated thyroid cancer

P. Verma^{1,2}, G. Malhotra^{1,2}, R. Rao¹, S. Sonavane^{1,2}, S. Basu^{1,2}

¹ Radiation Medicine Centre, Bhabha Atomic Research Centre, India

² Homi Bhabha National Institute, India

Background

Differentiated thyroid carcinoma usually manifests as an indolent cancer with good prognosis. However, rarely uncommon sites of metastatic involvement can worsen the prognosis and require aggressive therapeutic approach. The aim of the study was to evaluate the frequency of unusual sites of involvement in differentiated thyroid cancer to increase clinical awareness about the same.

Methodology

We screened our database of 2349 differentiated thyroid carcinoma patients who presented in our clinics (along with their imaging findings of 131 I scintigraphy and 18-F FDG PET/CT scans) from January 2020 till December 2022 for presence of rare sites of metastases. These were found in 19 patients (0.8%) comprising 8 females and 11 males.

Results

Table 1: Summarizes the clinical details of 19 patients of DTC with unusual sites of metastases being highlighted.

Sr. no.	Age	Sex	Presentation	Diagnosis	Unusual metastatic site
1	69	F	Anterior neck swelling	Papillary thyroid carcinoma.	Brachial plexus, tumour thrombus in superior vena cava (SVC)
2	51	M	Cognitive and behavioural changes	Multifocal follicular variant of papillary carcinoma	Brain, adrenal
3	69	F	Anterior neck swelling	Invasive follicular carcinoma thyroid	Kidney
4	34	M	Hematuria	Papillary thyroid carcinoma with tall cell features	Urinary bladder
5	68	M	Anterior neck swelling	Differentiated papillary carcinoma of thyroid.	Cerebellar and cerebral (brain)
6	55	M	Right breast lump	Papillary thyroid carcinoma, follicular variant.	Breast

7	60	F	Anterior neck swelling	Follicular variant of papillary carcinoma	Adrenal, large intestine.
8	59	M	Anterior neck swelling	Follicular carcinoma thyroid	Mandible
9	63	m	Anterior neck swelling	Papillary thyroid carcinoma	Subcutaneous skin deposits, muscle
10	68	F	Anterior neck swelling	Follicular carcinoma thyroid	Subcutaneous skin deposits
11	65	M	Anterior neck swelling	Papillary thyroid carcinoma.	Axillary node, subcutaneous deposit
12	57	M	Left breast lump	Follicular variant of papillary carcinoma	Breast
13	46	F	Anterior neck swelling	Widely invasive follicular variant of papillary carcinoma.	Liver, right parotid
14	54	M	Anterior neck swelling	Invasive encapsulated follicular variant of papillary thyroid cancer	Kidney
15	48	F	History of craniotomy and left breast lump.	Follicular carcinoma thyroid	Petrous temporal bone and breast
16	41	M	Anterior neck swelling	Papillary thyroid carcinoma.	Sella
17	77	M	Low back ache	Follicular carcinoma thyroid	Nasal bone
18	50	F	Low back ache	Invasive encapsulated follicular variant of papillary thyroid carcinoma	Liver
19	51	F	Swelling in the forehead	Follicular carcinoma thyroid	Brain

The frequency of unusual sites of involvement in the present cohort of patients was as follows: brain- 2, adrenal -2, subcutaneous deposits-3, breast-3, axillary node-1, liver-2, unusual bone site-4, parotid-1, brachial plexus-1, SVC-1 , urinary bladder -1 , cerebellum -1 , large intestine -1 and muscle- 1 .

Conclusion

Rare metastases are diagnosed late, which may result in poor prognosis & outcome. Metastases of thyroid carcinoma to the brain, kidney, adrenal, urinary bladder and colon are rare and often associated with poor prognosis. The awareness of these rare sites of involvement should alert the treating physician to look for early clinical signs and initiate timely management.

Follicular thyroid carcinoma: A case of persistently elevated serum thyroglobulin levels with negative 131I-whole body scan (WBS) and [18F]FDG PET scan leading to delayed detection of lung metastasis

S. Sharmin, A. Akhter, M. Hossain, R. Afrin, S. Hossain, F. Rahman, S. Islam, S. K. Biswas, R. Begum, J. A. Haque

Institute of Nuclear Medicine and Allied Sciences (Dhaka), DMCH Campus, Bangladesh
Atomic Energy Commission (BAEC), Bangladesh

Background

Here we present a case of follicular thyroid carcinoma having persistently raised serum Tg level with negative 131I-WBS and [18F]FDG/PET scan but delayed detection of lung metastasis in post therapy scan (PTS).

Case Report

A 52-year-old female patient of well differentiated follicular thyroid carcinoma underwent total thyroidectomy and then referred to nuclear medicine department for radio-iodine ablation therapy. Post-surgery evaluation showed no residual thyroid tissue or enlarged cervical lymph nodes on neck ultrasound, no remnant thyroid tissue at technetium-99m Thyroid scan, serum thyroglobulin level: 0.32 ng/ml, TSH level >30 mIU/L. She underwent radio-iodine ablation with 100 mci of 131I. Her post therapy scan showed focal area of good tracer uptake at thyroid bed. Her first WBS after one year of therapy was negative, Tg level: 0.05 ng/ml and TSH:80.68 mIU/L. 2nd WBS was also negative with mildly raised Tg level: 7.21 ng/ml and TSH: 14.18 mIU/L and negative neck USG for locoregional recurrence. In this long term follow up period between 2nd and 3rd WBS, clinically she was disease free with slight variation of serial Tg level ranging from 4.02 to 11.21 ng/ml and thyroglobulin antibody (TgAb): 15.0 IU/ml. After 5 years of 2nd WBS, 3rd WBS was also found negative, TSH: 55.6 mIU/L but markedly raised Tg level > 500 ng/ml, and no evidence of local recurrence at neck USG. [18F]FDG/PET scan was done for evaluation of metastatic foci but there was no FDG avid lesion or any other abnormal uptake. Only few (three to four) tiny non-FDG avid hyperdense lung nodules (3 to 6 mm in size) were found. 2nd therapy 150 mci 131I was given due to high Tg level. PTS showed faint radiotracer uptake in neck, but Tg is consistently high in subsequently follow up. Then WBS was done showed faint radiotracer concentration in thyroid bed with high Tg level. Then, CT scan of chest showed multiple small lung nodules in both lungs. Patient treated with 3rd therapy with 200 mci 131I & post therapy scan showed focal increased uptake in thyroid bed, bilateral diffuse lung uptake with increased focal radiotracer uptake in apical region of right lung, focal increased uptake in left pelvic region. Finally, this patient is diagnosed as lung metastasis & Tg again reported high after 3rd therapy.

Conclusion

The presenting case reflects a definitive entity of thyroid cancer showing raised Tg level but negative WBS and [18F]FDG/PET scan. However, 131I treatment being considered in case of persistently high Tg level.

Effect of digital reconstruction of multi-view planar bone scan images on first impression reporting whole-body SPECT/CT

P. Jarusevicius, D. Vajauskas

Lithuanian University of Health Sciences Hospital Kaunas Clinics, Lithuania

Background

Prostate cancer takes 2nd place as the most frequently detected cancer in men, according to the Global Cancer Observatory. In cases of metastatic prostate cancer, most common involvement is in the skeletal system. Bone scintigraphy with Technetium-99m labelled diphosphonates is most used to detect bone metastases. Correct lesion identification is important to evaluate possible progression as per PCWG2 criteria. With novel imaging techniques such as CZT digital ring-based solid-state detector gamma cameras, bone scans became faster and more convenient to evaluate. Advanced reconstruction modes such as multi-view planar (MVP) images allow for easy detection of lesions and evaluation of the extent of the metastatic process, while maximum intensity projection (MIP) images allow for quick and accurate correlation with SPECT/CT images. The goal of our study was to retrospectively investigate and compare the diagnostic performance of MVP whole-body bone scans versus digital 3D whole-body SPECT/CT in detecting metastatic spread to the bones for prostate cancer patients.

Methodology

This was a retrospective analysis of 50 bone scan performed between January 2021 to September 2022 in Nuclear medicine department of Lithuania Health Sciences University Hospital Kaunas Clinics. All patients had confirmed prostate cancer and at least two bone metastases. Bone scans were performed on Veriton-CT (Spectrum dynamics), 360° CZT gamma camera. Whole-body SPECT/CT acquisition was performed after 2 hours of [^{99m}Tc]MDP injection with low dose CT, acquisition time at 210 sec. per bed position. Hybrid 3D images were reconstructed with an ordered-subset expectation maximization (OSEM)-3D algorithm (2 iterations with 4 subsets) images were corrected for attenuation and scatters, point spread function value was applied, and displayed with voxels of 2.46 × 2.46 × 2.46 mm. Multi view planar (anterior and posterior view) whole-body images were retro reconstructed from digital 3D whole-body SPECT/CT images. SPECT/CT and MVP imaging data were assessed independently by two experienced physicians.

Results

The lesions were divided into 5 sites: skull, spine, chest, pelvis, and limbs (arms and legs together). MVP bone scan and SPECT/CT results were compared using Spearman's correlation coefficient. In all sites the physician's 1 and physician's 2 evaluation scores correlated: skull 0.803, spine 0.950, chest 0.875, pelvis 0.940, limbs 0.975 and whole-body 0.838. Only for 2 (4%) males additional screening was recommended to accurately interpret pathological findings on whole-body SPECT/CT. The downside of MVP images were lytic metastases and lesions with no [^{99m}Tc]MDP uptake, such metastases without osteoblastic activity. Therefore, MVP can only be used as an additional tool and can't replace SPECT/CT images.

Conclusion

This study demonstrated high correlation between MVP whole-body bone scan and digital 3D whole-body SPECT/CT. These findings suggests that MVP whole-body bone scan is easy to read and can give correct first impression on primary evaluation of osteoblastic bone metastasis with accuracy comparable to 3D SPECT/CT imaging, when images were processed and reconstructed to their maximum quality.

PET/CT and stand-alone MRI comparison study; synergistic roles of PET/CT and MRI in the staging and restaging of cancer of the rectum

P. Nemataduni, A. Gutta, N. Nyakale

Sefako Makgato Health Science University, South Africa

Background

Suboptimal anatomical correlation in cancer of the rectum due to lack of soft tissue delineation in the pelvis from computed tomography (CT) has limited the role that 18F-fluoro-2-deoxy-D-glucose positron-emission tomography (FDG-PET), computed tomography (CT) plays in the assessment lower gastrointestinal malignancies. Accurate assessment is hampered by physiological 18F-fluorodeoxyglucose (FDG) uptake in the bowel. Technological advancements have made PET/CT and magnetic resonance imaging (PET/MRI) a feasible alternative to PET/CT and stand-alone MRI for colon cancer. This is however impractical in developing countries. The purpose of this study is to compare PET/CT and stand-alone MRI findings in patients with rectal cancer

Methodology

This is a retrospective study of 23 patients with biopsy-verified rectal adenocarcinoma or neuro endocrine tumour and underwent a minimum of one FDG-PET/CT and stand-alone MRI examinations. Some of the patients had staging PET/CT and some did not. These patients were all referrals from the colorectal unit of the surgical department, at the Dr George Mukhari academic Hospital, a South African tertiary institute.

Results

Twenty-three patients were included in the study. 61% of the patients were referred for PET/CT staging and 39% (9) did not benefit from initial staging. 65 % of the patients had surgery and 35 % were deemed unresectable. In terms of surgical management, 100% of patients with T2 tumour staging had surgery, 56% of those with stage T3 did not have surgery and 44% had surgery, while in the T4 group, 84% of the patients were deemed unresectable and only 16% had surgery. A comparison between tumour stage and total lesion glycolysis (TLG) did not yield any significant results. However, majority of patients (34%) with local and distant metastases demonstrated high TLG of more than 150g. Prior PET/CT staging, the tumours were clinically defined as tumours limited to the rectum, recto-anal and recto sigmoid. Patients whose initial tumour staging was limited to the rectum, had 80% of the tumour remaining within the rectum and 20 % with no residual disease on PET/CT. Those with initial stage in the recto sigmoid, 67 % had tumour confined to the recto sigmoid and 33% demonstrated previously unknown disease beyond the recto sigmoid (p=002). The patients with tumour at initial staging in the recto anal were found to have 75 % remaining within the recto anal and 25 % had external sphincter of the bladder involvement. The overall p value in this group was p=0.001 demonstrating the ability of PET/CT to upstage patients.

PET/CT vs MRI findings demonstrated analogous results in 91% of patients but MRI was able to further identify extensive disease in 56% of patients. The time taken between PET/CT and MRI ranged from 1 to >6months. The delay can be attributed to backlog and equipment down time.

Conclusion

PET/CT and stand-alone MRI provide a more detailed assessment of the local staging of rectal cancers as well as local extension into adjacent structure. MRI has demonstrated its ability to identify lesions that may have been radio occult on CT in PET/CT imaging and also upstage the patients.

First experience in setting-up cyclotron and PET/CT in Mongolia

S. Erdenechimeg, O. Dorjsuren, M. Enkhjargal, B. Otgonpurev, U. Tugsuu

Nuclear Medicine Center of Second State Central Hospital, Mongolia

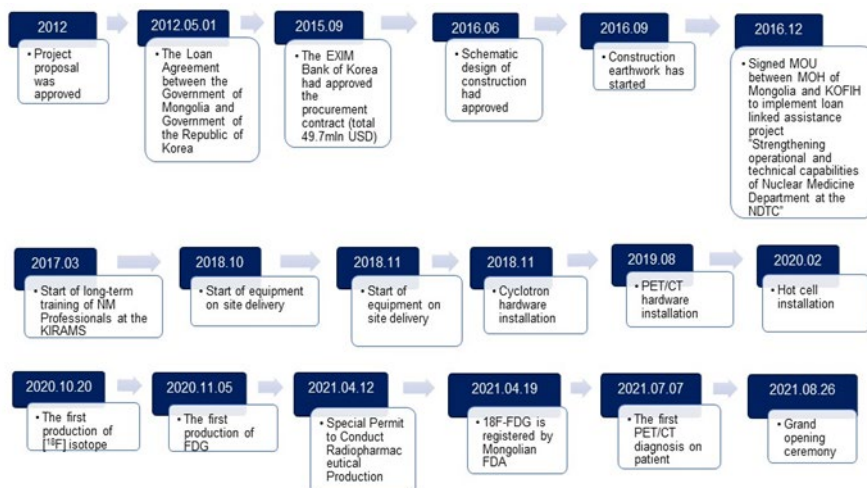
Background

In 2021, Mongolia's medical landscape entered a new phase with inauguration of the first cyclotron (9.6 MeV GE MINITrace Qilin) and PET/CT scanner (GE Discovery IQ) scanner at the Nuclear Medicine Center of Second State Central Hospital, officially opened on August 26th, 2021. This center's cyclotron based radiopharmaceutical facility design and operation management were organized per the International Atomic Energy Agency guidelines to achieve GMP compliance. The objectives of this study were to provide an overview and share some information on the initial experience of ([18F]-FDG) production and PET/CT results in Mongolia.

Methodology and Results

Since the grand opening, the Center has conducted approximately 300 [18F]-FDG radiopharmaceutical productions over 28 months, with an average radioactivity of [18F] isotope from cyclotron 1200 ± 50 mCi; and an average yield of [18F]-FDG $70 \pm 5\%$ at the end of synthesis, with the decay uncorrected. Quality control reports covering 9 types of tests show no failed production batches, with all tests meets USP requirements, including radiochemical purity exceeding 99% by TLC, acceptable residual concentration of acetonitrile and ethanol solvents, and pH range of 5.5 to 7. These quality measures ensure that the synthesized [18F]-FDG meets all USP requirements and is suitable for patient injection, with no reported immediate or subsequent side effects thus far. In the clinical field, the PET/CT facility has performed over 1826 scans on various cancer patients ranging from 2 months to 80 years old. The scan indications for staging, restaging, treatment response and follow-up were 19%, 29%, 18,7% and 29,3 %, respectfully. While among the total patients 2% was for screening purpose. Based on cancer types, referral cases cover a diverse of cancer types, with lymphoma (14,7%), stomach cancer (13,5%), breast cancer (11,7%), HCC & cholangiocarcinoma (10,2%), lung cancer (8,4%), colorectal cancer (8,8%), soft tissue cancer (5,7%), ovarian cancer (3,3%), cervix uteri (4,9%), endometrial cancer (2,5%), malignancy unknown primary (4,4%), head and neck cancer (3,5%), RCC (3,1%), brain tumour (2.6%), oesophageal cancer (2,2%), pancreas cancer (0.9%) and thyroid cancer (0.1%).

Milestones



Conclusion

In conclusion, the quality of synthesized $[^{18}\text{F}]$ -FDG met all USP requirements. PET/CT was mainly used for restaging and follow-up, with the most common referral pathologies being lymphoma, gastric, and breast cancer. The on-site cyclotron sets the stage for new opportunities that will provide an important impetus for further developments in the clinical and radiopharmaceutical fields as well in theranostics.

Optimization of the [18F]FDG administration in PET/CT : a pharmaco-economic study and a Tunisian practical dose management tool

H. Trabelsi¹, M. Somai², I. Slim², A. Mhiri²

¹ Radiopharmacy Department of Salah Azaiez Institute, Tunisia

² Nuclear Medicine Department of Salah Azaiez Institute, Tunisia

Background

In Tunisia, industrial production of [18F]FDG started in 2019. The growing popularity of PET/CT resulted to a significant increase of its request and consequently an increase in orders for [18F]FDG doses to meet patient needs.

This increase has led our department to an inevitable rise in associated costs, in addition to a 40% increase of the dose cost by 2021. In this context, a pharmaco-economic evaluation seemed essential to us considering economic conditions of our country.

For this purpose, we have developed a tool for optimizing [18F]FDG injection during a day of PET activity, to maximize efficiency and cost-effectiveness of using this radiopharmaceutical.

Methodology

To optimize the use of FDG injection during a day of PET activity we have carried out a descriptive study in Nuclear Medicine department of Salah Azaiez Institute. To this end, we developed an Excel spreadsheet designed to maximize the efficient use of the multidose vial received, taking into account activity and radioactive decay.

Results

We developed a calculation table considering the number of patients /day and their respective weights. This table integrates various predefined parameters such as injection and acquisition times, ordered dose and activity to be injected. Using this tool, it was possible for us to automatically calculate the residual activity by considering activity received, doses injected, radioactive decay and usable volume. Real-time adjustments are made to assess the number of feasible patients. In the event of unforeseen circumstances, two patients were put on hold at home. This tool allowed us to effectively optimize the use of FDG doses, thus avoiding any waste since no ordered dose was lost.

7-3-2024

Image modality	Patient N°	Full Name	Weight (Kg)	Age	Social security	Address	Diabetes	Examination time	Dose (MBq/kg)	Injection time	Total activity at injection time (MBq)	Volume (ml)	Patient activity (MBq)	Volume to inject (ml)	Total volume remaining (ml)	Residual usable volume (ml)	Remaining activity (MBq)	Usable activity (MBq)	Time between injection and PET scan	Time in PET room
Standard	1	Olfa Horchani	58	33	CNAM	Tunis	No	00:30	3	07:45	4700	9.5	174	0.4	9.1	8.5	4526	4209	01:00	08:45
Standard	2	Zohra Ben Mansour	49	75	CNAM	Tunis	No	00:30	3	08:15	3745	9.1	147	0.4	8.8	8.1	3598	3336	01:00	09:15
Standard	3	Chebbi Hayet	80	60	CNAM	Tunis	No	00:30	3	08:45	2977	8.8	240	0.7	8.1	7.4	2737	2520	01:00	09:45
Standard	4	Imen Hammami	70	41	CNAM	Nabeuk	No	00:30	3	09:15	2265	8.1	210	0.7	7.3	6.7	2055	1875	01:00	10:15
Standard	5	Toumi Aicha	65	50	Indigent	Zaris	No	00:30	3	09:45	1700	7.3	195	0.8	6.5	5.9	1505	1357	01:00	10:45
Standard	6	Mondher Saidani	72	42	CNAM	Tunis	No	00:30	3	10:15	1246	6.5	216	1.1	5.4	4.7	1030	907	01:00	11:15
Standard	7	Fatma Ghazouani	68	69	CNAM	Tunis	No	00:30	3	10:45	852	5.4	204	1.3	4.1	3.4	648	546	01:00	11:45
Standard	8	Chammakh Zakaria	19	10	CNAM	Nabeul	No	00:30	3	11:50	430	4.1	57	0.5	3.5	2.9	373	305	01:00	12:50
Standard	9	Jmil Hatem	80	40	CNAM	Tebourba	No	00:30	3	12:20	309	3.5	240	2.8	0.8	0.1	69	13	01:00	13:20
Date	Ordered activity (MBq)	Calibration time	Volume ordered (ml)	Half-life ordered (min)																
7-3-2024	4500	08:00	10	109.8																

Conclusion

This tool allowed us to optimize the activity administered while maintaining good image quality for diagnosis.

PSMA PET total tumour burden (TTB) as a prognostic biomarker in de novo metastatic hormone-sensitive PC (mHSPC)

F. G. Perez, M. A. Jimenez-Rios, F. L. Ramírez, I. S. Gallardo, A. Scavuzzo, N. Sobrevilla-Moreno, L. Torres-Agreto

Instituto Nacional de Cancerología, Mexico

Background

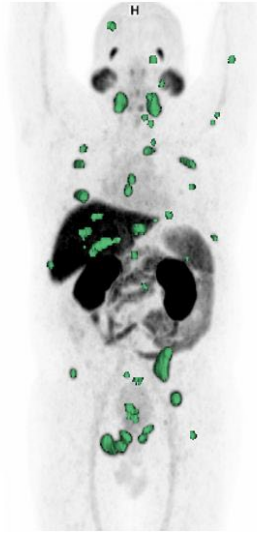
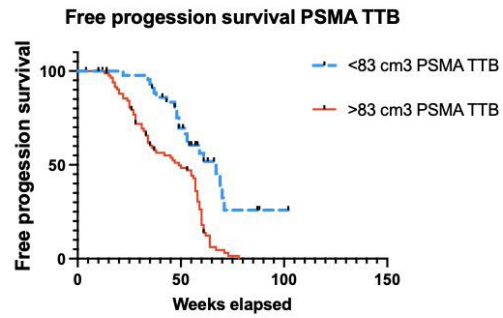
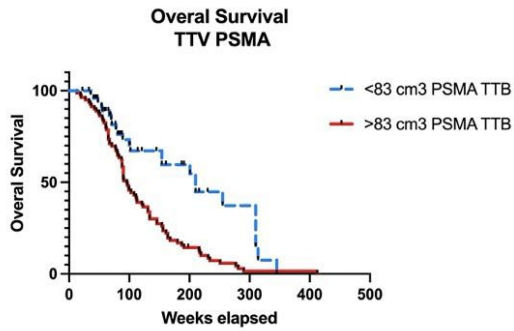
De novo mHSPC represents at least 10% of all prostate cancer diagnoses and may be underdiagnosed in low- and middle-income people due to limited access to molecular imaging and inefficient screening programs. Unfortunately, the presentation of this disease could be responsible for approximately 50% of deaths associated with prostate cancer, the behaviour of this presentation is variable and although molecular predictors such as transcriptomic profiling have been described, it still requires further validation, the PSMA PET/CT provides information on the aggressiveness of the disease based on molecular characteristics of the neoplasia, and has proven to be highly efficient in staging evaluating systematically extension of disease, making possible to calculate the total tumour burden (PSMA TTB) and providing useful information to choose patients who could benefit from more aggressive therapeutic schemes.

Methodology

Baseline [¹⁸F]F-PSMA-1007 PET scans of patients with histopathological corroborated diagnosis of prostate cancer, considered as high volume according to PSMA PET/CT imaging between 2017 to 2020 were retrospectively analysed using an automated algorithm to estimate PSMA TTB, patients were divided into two groups according to the optimal cutoff values of PSMA TTB and was estimated the progression-free survival after initial therapy and overall survival with Kaplan-Meier curves, also was performed a correlation index between tumour burden and prostatic specific antigen.

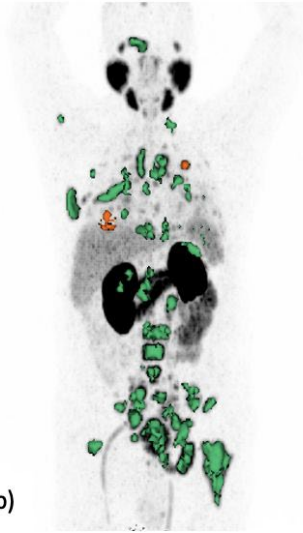
Results

67 patients considered high volume according to the CHAARTED (Chemohormonal Therapy Versus Androgen Ablation Randomized Trial for Extensive Disease in Prostate Cancer) definition and treated with docetaxel and androgen deprivation therapy were included with a mean age of 68.4 years (+/- 4.8), the mean PSA value at diagnosis was 89.9 ng/dL (range 19.8-317.4). The mean PSMA TTB was 176.1 cm³ (range 21.3 ml-1873.1 ml), patients were stratified using an optimal ROC curve cutoff of 83 ml to calculate progression-free survival after initial therapy and overall survival using Kaplan-Meier curves. Pearson index between PSMA TTB and prostate-specific antigen was statistically significant ($r = 0.671$, $p < 0.0001$). The mean PFS for the group of patients with PSMA TTB < 83 ml and > 83 ml was 64.8 and 48.4 weeks respectively, Hazard ratio 2.7 ($p = 0.0001$ 95% CI log-rank test 1.8 to 4.5); The mean OS for the group of patients with PSMA TTB < 83 ml and > 83 ml was 97.5 and 208.1 weeks respectively with HR of 2.2 ($p = 0.0014$ 95% CI 1.8-3.5 log-rank test).



a)

PSMA TTB 41 ml
 Overall Survival: 310 weeks
 Free progression survival: 218 weeks



b)

PSMA TTB 195 ml
 Overall Survival: 110 weeks
 Free progression survival: 71 weeks
 Vicesal disease

Conclusion

PSMA TTB acts as a prognostic biomarker in overall and progression-free survival, providing information on the biological behaviour of high-volume disease, it has a strong assessment with PSA the main marker of tumour burden in prostate cancer. Decision making for the use of new therapeutic regimens is based on tumour volume, PSMA TTB could allow stratification of patients susceptible to this type of therapy.

Incidental diagnosis of Diffuse Idiopathic Skeletal Hyperostosis (DISH) by hybrid SPECT/CT imaging, in a prostate cancer setting

E. H. A L. Bathily^{1,2}

¹Nuclear Medicine Department, Idrissa Pouye General Hospital / Biophysics and Nuclear Medicine Laboratory, Cheikh Anta Diop University, Dakar, Senegal

²Biophysics and Nuclear Medicine Department, Bicetre Hospital, Paris, France

Background

The value of bone scintigraphy in the assessment of prostate cancer lies in its high sensitivity and early detection of bone metastases. However, the tracers most often used, technetium-99m-labelled biphosphonates, bind to the skeleton according to osteoblastic activity and the rate of bone turnover. This mechanism is not specific to any particular pathological process. SPECT/CT allows better localization of abnormalities, which can help differentiate malignant from benign lesions. This is the case for the spine, where the frequency of both metastases and benign abnormalities is high, especially in elderly patients. We report on the contribution of SPECT/CT in the fortuitous discovery of a DIHS case, in a patient referred for extension workup of prostate cancer.

Methodology

This was a 64-year-old patient referred for a bone scan as part of a prostate cancer extension work-up, with a Gleason 8 score (4+4) and a PSA level of 4.58 ng/ml. A whole-body scintigraphy was performed 3 h 4 min after IV injection of 702 MBq of [^{99m}Tc]HDP Technescan. The examination was completed by a CT-coupled Thoraco-Abdomino-Pelvic (TAP) tomoscintigraphy, using a SPECT/CT, GE (General Electric) Discovery 870, commissioned in August 2019.

Results

Bone scintigraphy revealed no hyperfixation of the entire axial and appendicular skeleton, suggesting bone metastasis. On the other hand, complementary SPECT/CT acquisitions had revealed multi-staged thoracic intervertebral osteophytic bridges lateralized to the right, as well as multiple ossifications of the ischial entheses and anterosuperior iliac spines, suggestive of a diffuse idiopathic skeletal hyperostosis syndrome (DISH) (Figure 1). Hybrid imaging was therefore necessary to establish the final diagnosis in this patient, thus avoiding any confusion with a metastatic lesion in this field.

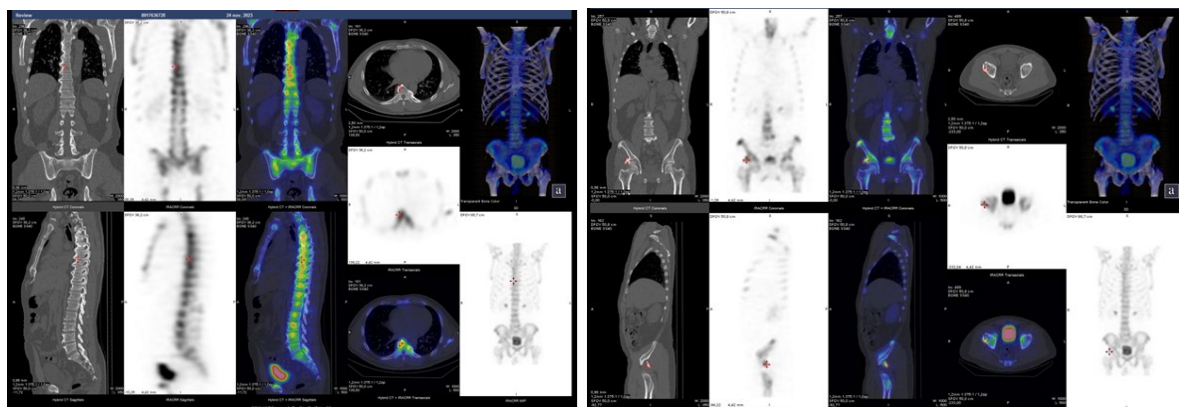


Figure 1: SPECT/CT acquisitions suggestive of DISH: multi-staged thoracic intervertebral osteophytic bridges lateralized to the right and multiple ossifications of the ischial entheses and anterosuperior iliac spines.

In addition, planar acquisition also showed hyperfixation in the large joints (shoulders, knees, ankles) corresponding to degenerative arthrosis (Figure 2).

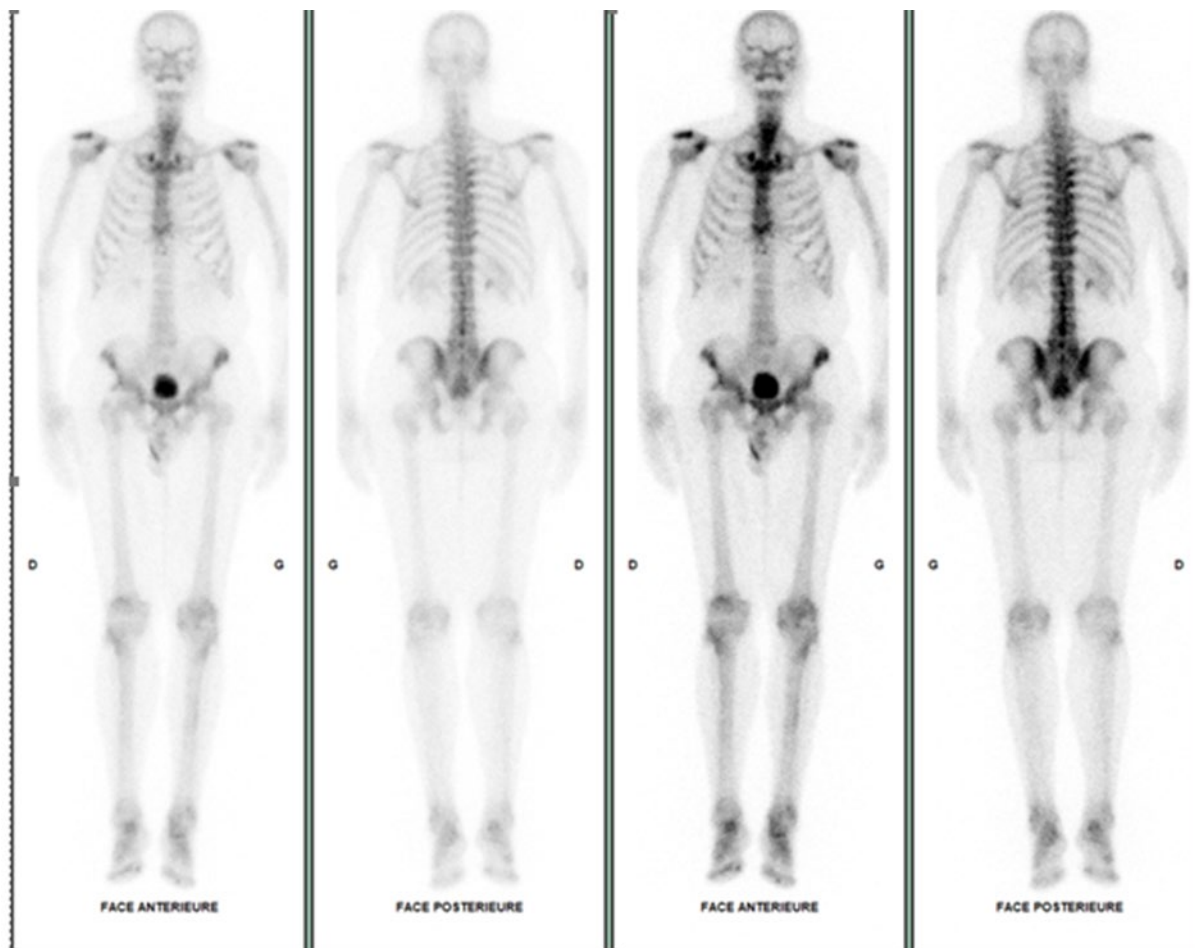


Figure 2: Whole-body planar acquisition without bone metastasis, with degenerative damage to large joints (shoulders, knees, ankles)

Conclusion

SPECT/CT, which provides fused functional and anatomical images, enables precise localization of abnormalities, and the additional information provided by this technique can also be useful for the diagnosis of benign pathology, as illustrated in this case.

Keywords: Diffuse Idiopathic Skeletal Hyperostosis, SPECT/CT, prostate cancer terrain

Hybrid Imaging and Theranostics

D. Verganelakis¹, M. L. Georgosopoulou²

¹ ELPIDA, Children's Hospital, Greece

² National and Kapodistrian University of Athens, Greece

Background

Radioisotopes and radiopharmaceuticals in Theranostic Nuclear Medicine and innovation techniques in production of imaging/therapy radiopharmaceuticals are referred here.

Advances in medical knowledge and better realizing disease processes are directing the search for early diagnosis/imaging methods and new therapy choices.

Greater quantities of radioisotope products in centers around the world are necessary. There is also a shift towards reduced dependence on long-distance transport of radioisotope products.

Clinicians increasingly seek to noninvasively inspect of tumour phenotypes and estimation of functional and molecular responses to therapy.

Theranostics — the combination of diagnostic imaging with targeted therapy — is becoming more widely applied. The study of theranostics combines molecular imaging with targeted radionuclide therapy, which involves the use of small molecules, peptides and/or antibodies as carriers for therapeutic radionuclides.

Theranostics (or theragnostics) combines molecular imaging (hybrid studies by PET/CT or SPECT/CT) with targeted radionuclide therapy, typically with radionuclides that emit α , β or Auger-radiation.

Radioactive isotopes are used in radioligand therapy to target cancer cells. Radioligand is a radioactive biochemical substance used for diagnosis or for research-oriented study. The radioisotopes are produced in special nuclear reactors or generators, then transported to a production facility where the radioisotope is connecting to the cell-targeting compound. SPECT/CT and PET/CT hybrid studies are critical for use in medical conditions where isotopes detect life-threatening.

When radioligands attach to certain types of cancer cells in the body, there is a high possibility of obtaining the proper diagnosis or treatment. Radioactive medical isotopes, specific medical isotopes utilized in cancer therapeutics that effectively emit alpha (α) or beta (β) radiation, for very short periods, are applied to destroy cancer cells inside tumours.

For therapeutics, high Linear Energy Transfer (LET) radiations such as alpha (α), beta (β^-) or Auger electrons are utilized to kill cancerous cells locally, while saving the normal tissues surrounding the malignant tumour cells.

Personalized cancer treatment obtained via Targeted Radionuclide Therapy (TRT) is of growing importance. Radionuclides with theranostic properties are proved to be clinically effective and widely used because diagnostic imaging and therapy are completing using a single preparation that avoids additional procedures and unnecessary radiation burden to the patient. Imaging diagnosis is used to determine an optimal treatment modality and can help monitor and evaluate medical treatment progress. Radiopharmaceuticals for theranostics use either the same radiopharmaceutical, which emits rays for diagnosis and particles for treatment, or two radiopharmaceuticals (one for diagnosis and the other for treatment). Radiopharmaceuticals for theranostics have developed rapidly in recent years with great progress in treating tumours and other diseases.

Radiation protection is of high concern in a production facility. There are regulations concerning the management of radiation. Instruments are required to measure the levels of radioactivity in a laboratory to ensure it is always restricted.

We indicate that the field of Radiopharmaceutical Therapy is expanding, and new standards and reliable applications are produced.

Comparing Characteristics of Differentiated Thyroid Cancers Across Age Groups. A population-based study from the Department of Nuclear Medicine at Ibn Rochd Hospital

H. Tabitha, A. Guensi, K. Bendahou

Hassan II University, FMPC, Laboratory of Cellular and Molecular Inflammatory, Degenerative and Oncologic Pathophysiology, Morocco

Background

Differentiated Thyroid cancer exhibits variations in clinical presentation, histological features, and outcomes across different age groups. Understanding these differences is essential for management approaches and improved patient care. This study aimed to compare the characteristics and outcomes of differentiated thyroid cancers (DTCs) among teenagers, adults, and elderly patients.

Methodology

A cross-sectional study was conducted at the Department of Nuclear Medicine, Ibn Rochd Hospital Hassan II University, analyzing data from patients diagnosed with DTC between 2004 and 2012. We utilized the WHO classification of age groups (Adolescents: Ages 10 to 19 years old. Adults: Ages 20 to 59 years old. Elderly or Geriatric: Ages 60 years and older). Clinicopathological variables, including gender, family history of thyroid cancer, histological type, tumor characteristics, metastatic status, treatment modalities, and survival outcomes, were compared across three age groups. Statistical analysis was done using the Chi-square test, and we calculated survival using the Kaplan-Meier method. We utilized the software of JAMOVI 2.3.17,

Results

The analysis included 1366 patients, 28 teenagers, 1173 adults, and 158 elderly. Gender distribution showed that female predominance 82.1% of teenagers were female as 90.4 % of adults and 84.8 of elderly. Family history of thyroid cancer was more prevalent among teenagers (7.1%) compared to adults (1.2%) and absent in the elderly (0%) ($p < 0.005$). Papillary thyroid carcinoma (PTC) was the most common histological type across teenagers, adults, and the elderly, with similar proportions of 89.3 %, 93.9% 89.2% respectively. Follicular thyroid carcinoma accounted 5.7 % in adults, and 10.8 % in the elderly. The mean thyroglobulin levels were 277 ng/ml in adolescents, 105 ng/ml in adults and 302 ng in the elderly. Teenagers had Tumor smaller than 4 cm in 85% of cases compared to 87.1% in adults and 80.5% in the elderly ($p < 0.001$). Vascular invasion was present in 7.1% of teenagers, 5.3% of adults, and 13 % of the elderly ($p < 0.001$). Extrathyroidal extension (ETE) was present in 7.1%, 4.3%, and 13.7% of teenagers, adults, and the elderly, respectively ($p < 0.001$). Additionally, adenopathy invasion was positive in 4% of teenagers, 2.7% of adults, and 1.5% of the elderly ($p < 0.654$). The metastatic occurrence at diagnosis was 0%, 0.3%, and 3.5% in teenagers, adults, and the elderly, respectively ($p < 0.001$). Classification into risk groups per ATA guidelines varied significantly ($p < 0.001$), with 64.3% of teenagers classified as low risk, compared to 85.8% of adults and 68% of the elderly. While 3.7% of teenagers are classified as high risk, compared to 6.5% of adults and 19% of the elderly. Treatment modalities also showed differences, with higher utilization of Itra therapy among teenagers (96.3%) compared to adults (86.4%) and the elderly (87.6%).

Conclusion

Survival outcomes differed significantly, with teenagers and adults demonstrating higher rates of complete remission (Teenagers: 100%, Adults: 90.2%, Elderly: 63%) and superior 5-year survival rates (Teenagers: 82.1%, Adults: 79%, Elderly: 62.7%) compared to the elderly ($p < 0.001$).

Dual Tracer Imaging for Suspicious Thyroid Nodules: Exploring ^{99m}Tc Pertechnetate and ^{99m}Tc-MIBI Uptake Patterns and Their Clinical Significance

A. Akhter, S. Sharmin, R. Afrin, S. Islam, T. Biswas, F. Rahman, S. Hossain, M. Hossain, S. Biswas, R. Begum, J. A. Haque

Institute of Nuclear Medicine and Allied Sciences, Dhaka, Bangladesh Atomic Energy Commission, Bangladesh

Background

Thyroid nodules are a common clinical concern, with a substantial portion being benign, but necessitating careful evaluation to differentiate them from potentially malignant lesions. Nuclear medicine techniques have evolved to include dual-tracer imaging, utilizing both ^{99m}Tc Pertechnetate and ^{99m}Tc-methoxyisobutylisonitrile (^{99m}Tc-MIBI, sestamibi) radiopharmaceuticals, to enhance the diagnostic accuracy of thyroid nodule assessment.

Methodology

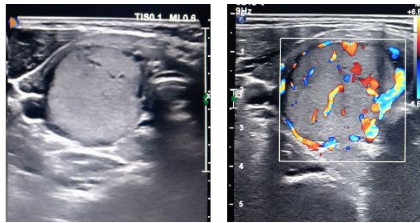
In this retrospective study, ten patients (M/F ratio: 3:7, age range: 16-65 years), with suspicious thyroid nodules identified via ultrasound underwent dual-tracer imaging with ^{99m}Tc Pertechnetate and ^{99m}Tc-MIBI SPECT CT on separate days. Biochemical parameters and histopathological findings were analysed.

Results

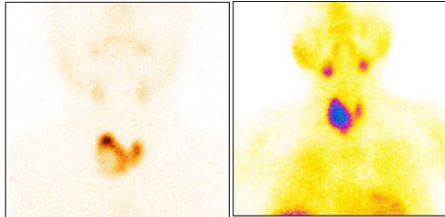
Among the ten cases, five (50%) were diagnosed with malignant nodules, while the remaining five were benign. Malignant nodules displayed diverse uptake patterns. Two cases exhibited a mismatch pattern, presenting cold lesions on ^{99m}Tc Pertechnetate and intense nodule uptake on ^{99m}Tc-MIBI SPECT-CT, accompanied by elevated thyroglobulin levels. One case was histologically confirmed as well differentiated papillary microcarcinoma (pT1aN0M0) with additional adenomatous goitre (TSH: 11.46 mIU/L, thyroglobulin level 75 ng/ml, normal range <50 ng/ml) and another one was classic variety of papillary thyroid carcinoma (pT2N0M0) with markedly raised thyroglobulin level (>500 ng/ml), normal TSH level. Third malignant nodule showed match pattern, reduced patchy uptake on ^{99m}Tc Pertechnetate and persistent faint nodule uptake on ^{99m}Tc-MIBI SPECT-CT, markedly elevated thyroglobulin levels (>500 ng/ml), and classic papillary thyroid carcinoma (pT3aN0M0) on histopathology. An increased heterogeneous uptake pattern was observed on dual tracer imaging in a 65-year-old male patient of thyroid lymphoma having mildly elevated thyroglobulin levels (80 ng/ml) and high TSH (60 mIU/L). The last case of malignant nodule was a 27-year-female, exhibited cold uptake on both scans with a normal thyroglobulin level and moderately differentiated medullary thyroid carcinoma (pT2NxMx) on histopathology.

Benign nodules displayed mainly concordant uptake patterns on dual-tracer imaging, with one case exhibiting focal intense MIBI uptake coupled with normal ^{99m}Tc uptake and normal thyroglobulin levels, diagnosed as lymphocytic thyroiditis on histopathology. Two cases showed focal nodule uptake on both scans, consistent with follicular adenoma and thyroglobulin level 56 ng/ml & 94 ng/ml respectively. The remaining benign case displayed large complex nodule on ultrasound, reduced uptake on ^{99m}Tc Pertechnetate, though diffuse uptake on early ^{99m}Tc-MIBI scan, three hours delayed SPECT

CT revealed complete washout with raised thyroglobulin levels (237 ng/ml), normal TSH and nodular goitre with cystic changes on cytological examination.

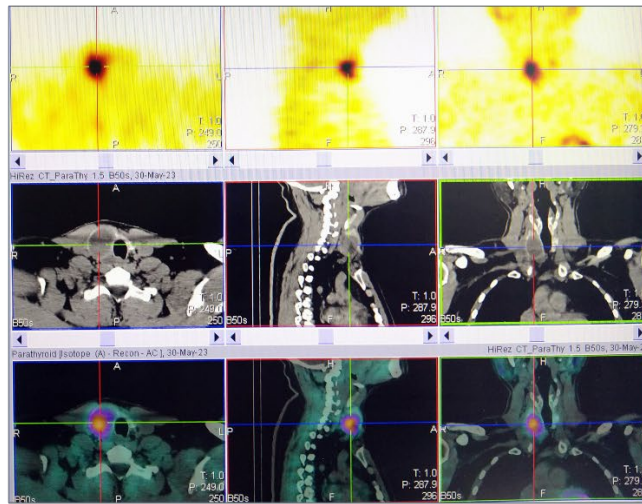


USG: Solid echogenic vascular nodule



**^{99m}Tc Thyroid scan
(cold nodule right)**

**^{99m}Tc-MIBI Scan
(Hot nodule)**



**^{99m}Tc-MIBI SPECT CT Delayed Scan
(solid nodule with intense uptake)**



**Post-operative specimen:
thyroid gland
with nodule.
H/P: Papillary
Microcarcinoma**

Conclusion

The integration of ^{99m}Tc Pertechnetate and ^{99m}Tc-MIBI as dual-tracer imaging facilitates refined decision-making in thyroid nodule management. Mismatch or discordant uptake patterns with markedly elevated thyroglobulin levels and raised TSH level warrant further diagnostic evaluation, potentially including fine-needle aspiration cytology or surgical intervention, to assess malignancy suspicion. Concordant low uptake patterns should also raise concerns. Conversely, concordant uptake patterns may indicate eligibility for conservative management strategies. This approach empowers clinicians to navigate between accurate diagnosis and appropriate intervention, optimizing patient care outcomes.

Diagnostic efficiency of [18F]FDG PET/CT for detection of primary site in patients with Cancer of Unknown Primary (CUP) – multicenter experience in Bangladesh

R. Afrin¹, S. M. F. Begum¹, S. Biswas¹, R. Islam², S. Sharmin¹, F. Rahman¹, S. Hossain¹, A. Akhter¹, M. Hossain¹, J. A. Haque¹

¹Institute of Nuclear Medicine and Allied Sciences, Dhaka, Bangladesh Atomic Energy Commission

²Department of Biochemistry and Molecular Biology, Jagannath University

Background

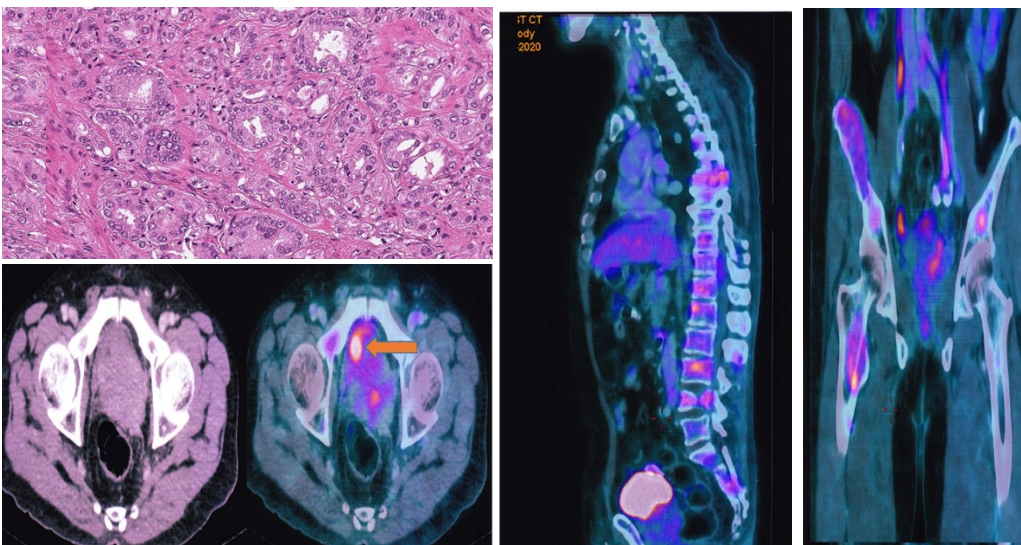
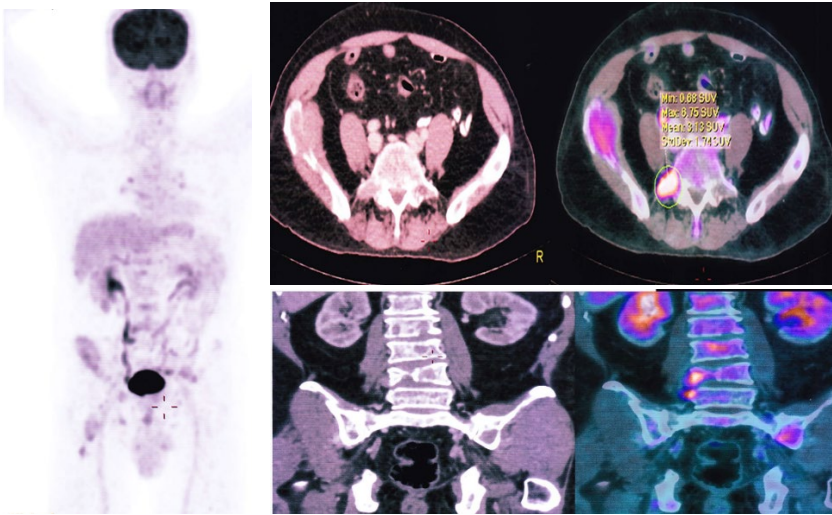
Cancer of unknown primary (CUP) is defined as the presence of histologically proven metastatic disease for which the site of origin cannot be identified at the time of diagnosis. CUP is one of the ten most frequent cancers and is the fourth most common cause of cancer-related deaths. Conventional imaging modalities can detect primary site in less than 30% of CUP patients this may negatively affect patient management. Clearly, there is a need for an alternative, non-invasive imaging modality with a high diagnostic efficiency. From Bangladesh perspective there is very few published data regarding the role of PET/CT in unknown primary. This diagnostic accuracy test study was conducted to assess the role of 18 F- FDG PET/CT in the detection of primary tumour in cases of metastasis of undetermined primary site.

Methodology

The study was carried out for 60 months in two centers of Dhaka, Bangladesh, (one government tertiary referral hospital and one private PET/CT center). A total 270 patients (aged between 30 and 84 years) were included by purposive sampling. Patients having at least one biopsied metastatic lesion, radiologically and/or clinically suspected metastatic lesion(s) were included. But patients with uncontrolled diabetes and known primary cancer were excluded. State of the art FDG PET- CT scan was acquired from vertex to mid-thigh in a whole-body PET/CT scanner.

Results

In our study population 53% were male, 47% were female. FDG PET/CT can detect primary site in 74% cases. Maximum 41% patients were in age group 60 to 69 years. 55% patients had metastatic adenocarcinoma, 23% metastatic squamous cell carcinoma at the time of presentation. The most common primary site detected by FDG PET- CT was in lungs. FDG PET detected other sites of metastases, 38% presented with abdominal lymph nodes, PET/CT achieved a sensitivity of 98%, and specificity of 94%, accuracy of 97%, PPV 98% and NPV 94% in detection of unknown primary tumour location.



- A 60 -year-old male patient diagnosed as metastatic adenocarcinoma involving right ileum.
- PET/CT detect primary malignant lesion in prostate, Histopathology confirmed adenocarcinoma.
- MIP, axial CT, fused PET/CT images also revealed hypermetabolic skeletal metastases.

Conclusion

PET/CT, using the radiotracer ¹⁸F-Fluorodeoxyglucose ([¹⁸F]FDG), can be an excellent problem-solving tool in patients with CUP.

Keywords: CUP, [¹⁸F]FDG PET/CT

Estimation liver-lung shunt fraction (LSF%) on [^{99m}Tc]MAA SPECT/CT using automated CNN-based segmentation in hepatocellular carcinoma (HCC) patients before trans-arterial radiation embolization (TARE): a pilot study

H. Le Ngoc, M. Mai

Tran Hung Dao Hospital (Hospital 108), Việt Nam

Background

Currently, commercial software is a manual tool for estimating quantitative liver lung shunt fraction on [^{99m}Tc]MAA SPECT/CT however it consuming time and not popular because of economic issues. The aim of this study is using automated CNN-based segmentation method to improve the limitation of manual method using commercial software.

Methodology

We collected thirty-four [^{99m}Tc]MAA SPECT/CT DICOM imaging of HCC patients and proceeded by CNN based segmentation to assess LSF%, along with the manual method performed by experienced nuclear medicine doctors using commercial software. The CNN-based segmentation method was developed by Hanoi Technology Institute.

Results

There was 91.2% of male patients with median age 63 (range from 45-80). Most of the tumours were located on the right liver. Regarding characteristics of tumours, necrosis and heterogenous [^{99m}Tc]MAA's distribution were 67.3% and 73.5% respectively. The mean \pm SD of LSF % estimated by commercial software was not a significant difference from CNN based method ($5.4 \pm 3.9\%$ vs $5.9 \pm 3.9\%$, $p=0.058$). The median time for estimation LSF% on automated CNN-based method was 1.05 minutes which was significantly lower than commercial software ($p<0.001$). The agreement between LSF% between two methods was moderate (Kappa = 0.62) in estimation LSF%. The region of interest (ROI) of lungs and livers drawn by automated method matched with manual method was 56%. Gastric and spleen were the organs defined wrongly by the automated method.

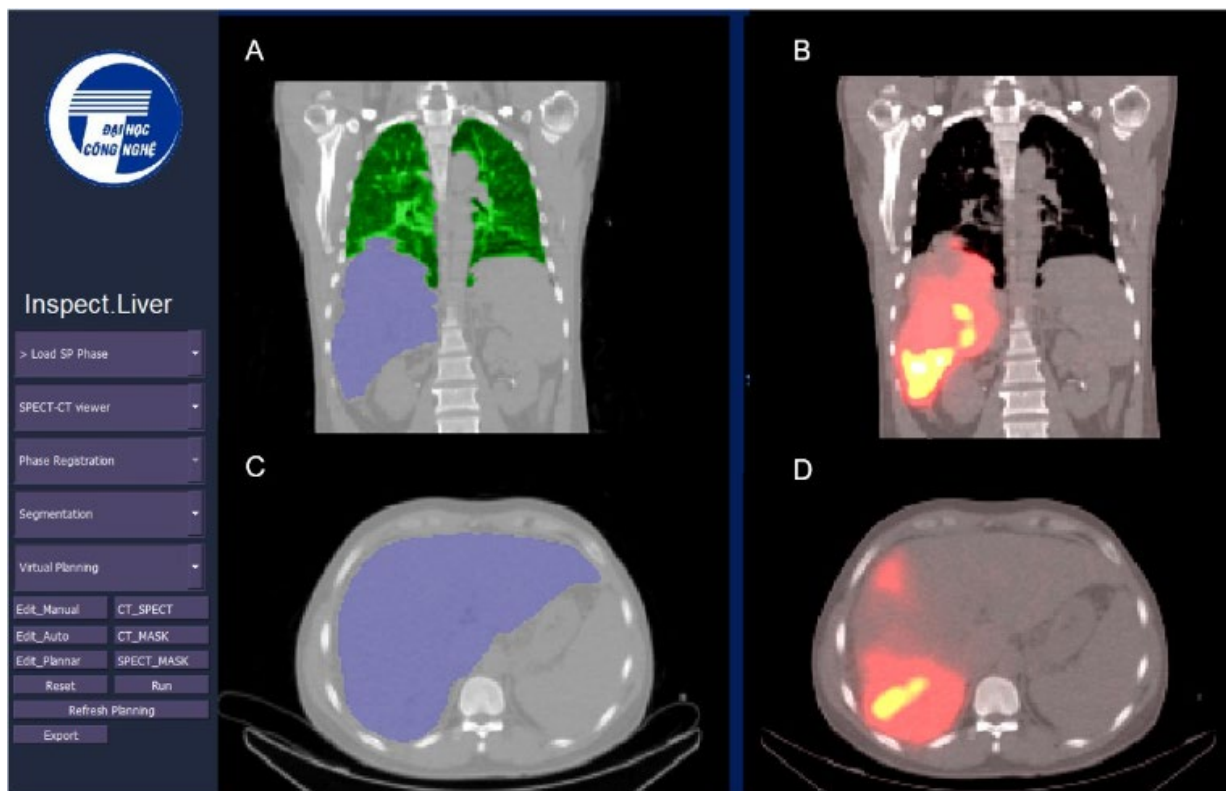


Figure 1. Estimation LSF% by automated CNN- based segmentation. Definition of liver and lung ROIs on sagittal imaging (A) correlated with fused $[^{99m}\text{Tc}]\text{MAA}$ and CT imaging (B). Recognition liver border on CT image (C) in comparison with fused $^{99\text{mTc}}\text{-MAA}$ and CT imaging (D).

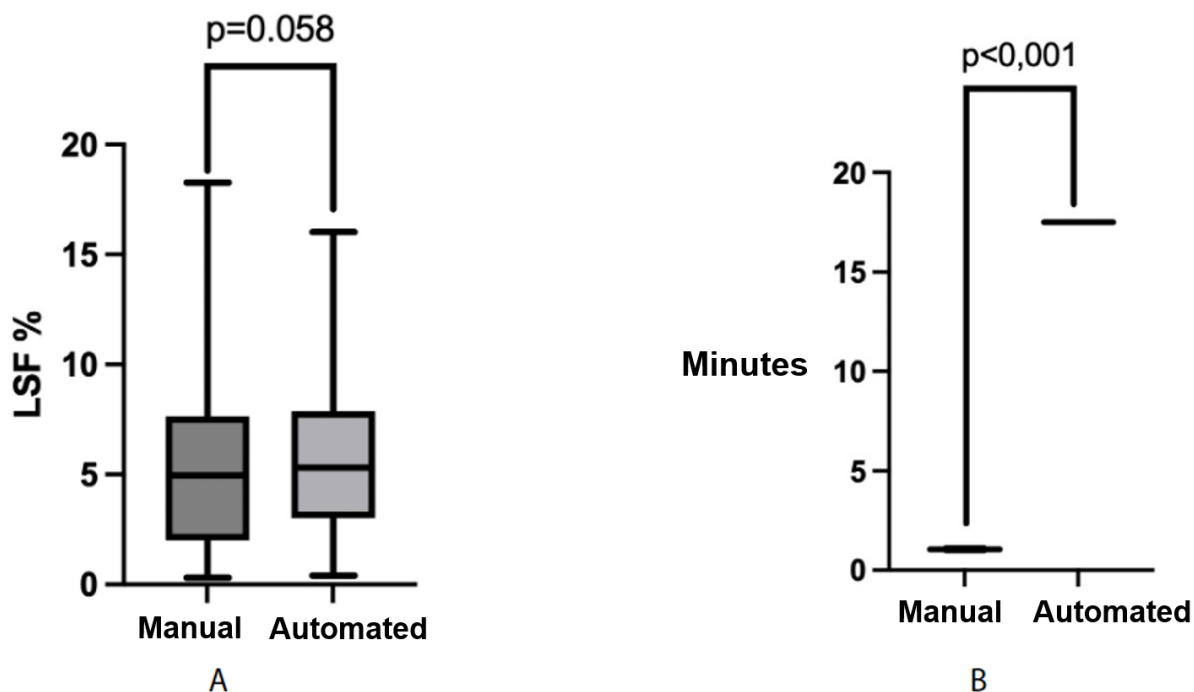


Figure 2. (A): Comparison LSF% performed by manual commercial software and automated CNN-based segmentation method, (B): Comparison consuming time of LSF% estimation performed by manual commercial software and automated CNN-based segmentation method.

Conclusion

Automated CNN-based method provided additional value in assisting nuclear medicine doctors to estimate LSF% with the similar results meanwhile shortened the time for performing in comparison with manual method.

Accuracy of SPECT/CT in Localizing Abnormal Parathyroid Gland in Patients with Primary Hyperparathyroidism

M. Hossain, R. Afrin, S. Sharmin, A. Akhter, S. Hossain, F. Rahman, R. Begum, S. K. Biswas, J. A. Haque

Institute of Nuclear Medicine and Allied Sciences, Dhaka, Bangladesh Atomic Energy Commission, Bangladesh

Background

Successful minimal-access parathyroid exploration and reoperative surgery of the parathyroid gland requires accurate preoperative localization of the diseased gland. The objective was to evaluate the accuracy of [^{99m}Tc]sestamibi SPECT/CT in localizing abnormal parathyroid glands in patients with primary hyperparathyroidism who were scheduled for surgery and to compare among the different modalities of parathyroid imaging to determine the superiority of one over another.

Methodology

A cross sectional analytical study was performed at the Institute of Nuclear Medicine and Allied Sciences for a period of one year. Purposive sampling was done. A total number of 43 (32 females and 11 males) diagnosed cases of primary hyperparathyroidism with a mean age of 42.3 ± 16.1 years were evaluated. Established cases of secondary hyperparathyroidism, End-Stage Renal Disease, pregnant and lactating women were excluded. High Resolution Ultrasound (HRUS) of neck, planar parathyroid scintigraphy, SPECT and SPECT/CT were performed on each patient. Findings of each individual technique were reviewed blindly, and comparison was made among the different modalities regarding localization and detection of abnormal gland. Surgical location and histopathology findings served as the standard. The imaging results were compared with the operative results to determine sensitivity, specificity, PPV, NPV and accuracy for each method.

Results

Out of 43 patients of primary hyperparathyroidism, 34 cases had abnormal parathyroid glands on surgery (25 cases of single adenoma, 3 cases of double adenoma, 1 case of ectopic gland and 5 cases of hyperplastic parathyroid glands). Nine patients showed no hyperactive parathyroid tissue. HRUS of neck, planar, SPECT and SPECT/CT scans were true positive in 15, 21, 30 and 31 patients respectively among 34 surgery positive cases. It revealed 91.17% sensitivity for SPECT/CT whereas HRUS of neck, planar and SPECT showed 44.1%, 61.7% and 88.2% sensitivity respectively (Chi-square test was done to measure the level of significance; P-value for SPECT and SPECT/CT = 0.001, HRUS = 0.10, Planar = 0.05). Out of 3 cases of double adenomas, HRUS detected 1 case and planar imaging detected 2 cases. SPECT and SPECT/CT identified all 3 cases. Among 3 cases of primarily failed parathyroidectomies, HRUS, planar, SPECT and SPECT/CT scans detected 1, 1, 2 and 3 cases respectively. Sonography and planar scintigraphy were unable to detect the ectopic gland (mediastinal), but it was identified successfully by SPECT and SPECT/CT. The statistical findings of SPECT and SPECT/CT were almost similar, but the latter provided superior topographic information with 88.37% diagnostic accuracy.

Conclusion

Hybrid SPECT/CT combines the three-dimensional functional information of SPECT with the morphologic information of CT, and it is superior to HRUS of neck, planar imaging and SPECT alone. Even though SPECT/CT has almost similar identification sensitivity to SPECT; it provides detail anatomic information in case of both ectopic or eutopic diseased gland including previously failed parathyroidectomy. The study highly recommends the use of SPECT/CT in preoperative parathyroid localization.

Primary Intracranial Neuroendocrine Tumour : The First Brain Tumour Imaging Experience with 18F-FDOPA PET/CT Scan in Indonesia

J. I. Pribadi, A. R. Dewi, Y. Tuti

Department of Nuclear Medicine, Dharmais National Cancer Center Hospital, Indonesia

Background

18F-Fluoro-dihydroxyphenylalanine (18F-FDOPA) is a radiopharmaceutical analogue of L-DOPA, metabolized in the same catecholamine 400iosynthesis pathway. 18F-FDOPA actively transported to the cell by large amino acid transporter (LAT), undergoes decarboxylation by aromatic l-amino-acid decarboxylase (AADC), and stored in vesicles. In neuroendocrine tumours (NET), the increased transport and AADC activity result in intracellular retention of metabolized 18F-FDOPA and positive signals on PET images. We have been used 131I-MIBG for diagnostic patient with NET in our hospital. However, it has several limitations, such as limited spatial resolution, limited sensitivity for small lesions, prolonged acquisition sessions, limited tomographic field-of-view, need for pharmacological thyroid protection, and inconvenience of a 2-days schedule. Currently, magnetic resonance imaging (MRI) and computed tomography (CT) are the preferred techniques for evaluating central nervous system (CNS) involvement, nuclear medicine procedures such as meta-iodobenzylguanidine (MIBG) scans have limited diagnostic relevance in detecting CNS lesions.

Case Report

21-year-old female with an intracranial tumour and an unknown primary following craniotomy biopsy, with histology and immunohistochemistry revealed two possibilities for origin: solid papillary carcinoma or neuroendocrine tumour. The patient performed an [18F]FDG PET/CT scan examination to determine the primary location; the results revealed ametabolic mass in left frontoparietal and no abnormal hypermetabolic lesion in the other areas of the body suggesting malignancy. We recommended 18F-FDOPA PET/CT scan examination during the tumour board, and they agreed; this was Indonesia's first experience evaluating tumours in the CNS with 18F-FDOPA. Patient fasted for 4 hours, there was no premedication with Carbidopa, and we did not perform the early imaging acquisition. The 18F-FDOPA PET/CT scan was carried out 60 minutes following the slowly intravenous administration 250 MBq of 18F-FDOPA. The findings revealed pathological intense tracer uptake mass in the left frontoparietal, but no pathological tracer uptake in other areas of the body. The final diagnosis was a primary intracranial neuroendocrine tumour; this was an extremely rare case.

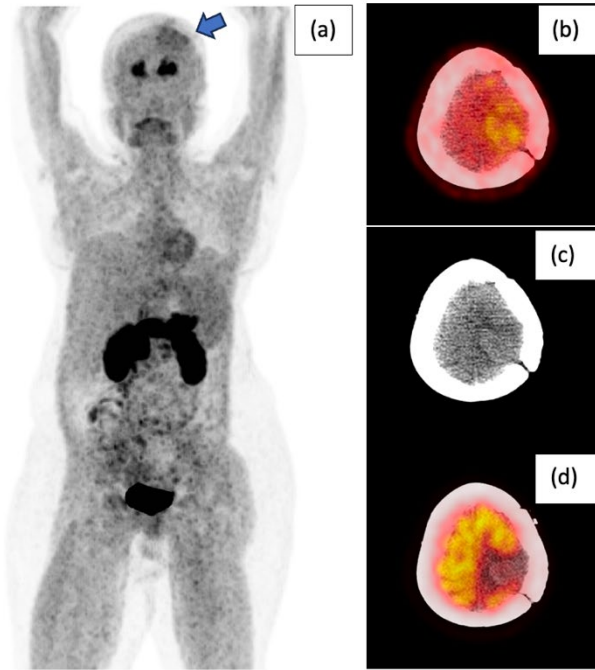


Fig. 1 FDOPA PET/CT scan of 21 years old female intracranial neuroendocrine tumor patient (**a**, **blue arrow**) shows intense tracer uptake mass in the left frontoparietal (**b,c**). FDG PET/CT scan shows amebolic mass in the left frontoparietal (**d**).

Conclusion

^{18}F -FDOPA PET/CT can be performed to help confirm an accurate diagnosis of neuroendocrine tumour CNS lesions in areas where ^{18}F FDG PET/CT scan or MIBG scan have diagnostic limitations.

Perspective of SPECT-CT Hybrid Modality in High Intact Parathyroid Hormone level - A Single Institute Experience

S. Reza¹, R. Perveen¹, T. Begum², N. N. Sayem³

¹ National Institute of Nuclear Medicine & Allied Sciences, Bangladesh

² Dhaka Medical College and Hospital, Bangladesh

³ National Heart Foundation Hospital and Research Institute, Bangladesh

Background

This study analysed the relationship between high intact parathormone (iPTH) levels with hybrid modality single photon emission computed tomography/ computed tomography (SPECT/CT) images in diagnosis the causes of hyperparathyroidism.

Methodology

100 patients as per physician advised underwent methoxyisobutyl isonitrile (MIBI) using SPECT/CT imaging between January 2023 and December 2023 in National institute of Nuclear Medicine and Allied Sciences (NINMAS). The SPECT/CT equipment used in this study was Symbia T16 (Siemens, Germany), which combines 16-slice multidetector CT and SPECT. 740 MBq of 99mTc-MIBI was injected intravenously in all patients. Early and delayed neck and upper thorax planar images were acquired 10 and 120 minutes after the injection, respectively. SPECT/CT acquisition was performed between 125 to 130 minutes after obtaining the delayed planar image. Overall, 38 projections (128×128 matrix) were acquired (25 seconds each), with a total duration of 15 minutes for the whole SPECT/CT procedure. CT was performed immediately after SPECT imaging. The main CT parameters were 130 kV, 25 mAs, and a 1.2 mm slice thickness; no intravenous contrast medium was used. SPECT/CT data were analysed on a Syngo workstation, which provided transaxial, coronal, and sagittal slices of SPECT, CT, and fused SPECT-CT data.

Results

Out of 100 patients, 56.0% of the patients were female and the mean (SD) age of the patients was 40.9 (15.3) years with minimum and maximum ages being 11 years and 78 years respectively. There is 40 patients had iPTH level >200 pg/ml, among them SPECT/CT identified 14 patients as positive for parathyroid adenoma and 26 patients identified as negative cases. In SPECT/CT positive cases the median value of iPTH level was 506.2 pg/ml with a minimum and maximum were 20.1 pg/ml and 1630 pg/ml respectively, and on the other hand, in SPECT/CT negative cases the median value of iPTH was 130.9 pg/ml with a minimum and maximum were 10.2 pg/ml and 2939 pg/ml. The differences of iPTH between the positive and negative SPECT/CT were statistically significant ($p = 0.001$) with 95% confidence level. A non-parametric, Mann-Whitney U test was done to measure the level of significance.

Serum iPTH level (Normal level 15 to 65 pg/ml) SPECT-CT p value#

Positive Negative

Mean \pm SD 533.0 \pm 338.7 283.3 \pm 473.6

Median 506.2 130.9

Min-Max 20.1-1630.0 10.2-2939.0

Mean Rank 69.8 45.7 0.001

Mann-Whitney U test was done to measure the level of significance.

Serum <u>iPTH</u> level (Normal level 15 to 65 <u>pg/ml</u>)	SPECT-CT		p value [#]
	Positive	Negative	
Mean ± SD	533.0 ± 338.7	283.3 ± 473.6	
Median	506.2	130.9	
Min-Max	20.1-1630.0	10.2-2939.0	
Mean Rank	69.8	45.7	0.001

Table: Serum iPTH level correlation with SPECT-CT positive and negative adenoma cases.

Conclusion

This small-scale retrospective study showed that positive cases can be found at any age group, with female predominance. Statistically it was proven that when there was raised iPTH level was found, SPECT/CT was also become positive in some of those cases. Hybrid SPECT/CT MIBI scan plays an important role for specific localization of parathyroid tissue.

131Iodine-RAI Theranostics of Differentiated Thyroid Cancers. The pioneer of Radionuclide Theranostics in Mauritius & A IAEA Fellow take-home mission!

P. Ramdass

Department of Nuclear Medicine, Jawaharlal Nehru Hospital, Mauritius

Background

Thyroid Cancers are the most common endocrinological malignancies globally and in Mauritius. The 2020 report of the National Cancer Registry demonstrated a prevalence of 1.39% and an incidence of 0.04% of Thyroid cancers with a ratio F:M 2:1

In Mauritius, the management of Thyroid Cancers started in the late 1970's by the Oncology Unit and included post-operative 131I- RAI Ablation followed by exogeneous thyroxine therapy. In cases of clinically/radiologically determined metastatic/recurrent disease, additional RAI doses were randomly administered up to a cumulative dose limit of 1000mCi. Correlation with tumour marker levels (TSH-stimulated serum Thyroglobulin levels) and RAI diagnostic/ post-therapy imaging was not an established practice. Hence the treatment of DTCs was for decades carried out without optimal staging/restaging nor risk-adapted 131I-RAI dose determination.

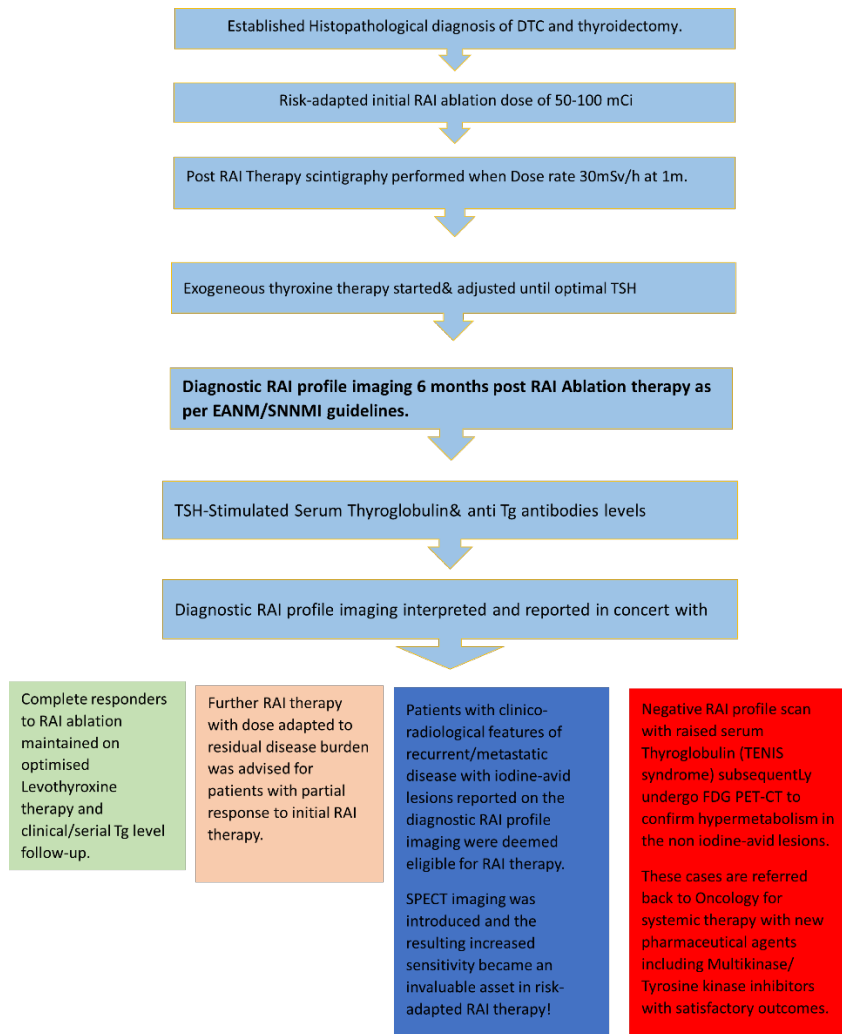
With the acquisition of the first Gamma Camera (Siemens Single-head Gamma Camera) In 2001 and then of a Mediso Dual-Head Gamma Camera in 2009 from the IAEA, few post RAI-therapy scintigraphies were performed in a random referral pattern. It was only in 2016, following an IAEA fellowship award under the aegis of IAEA MAR6015, that the Head of Department and the IAEA Fellow initiated the evidence-based RAI Theranostics of thyroid cancers. The project evolved gradually with fluctuations associated with logistic factors but was fully established by 2022.

Methodology

A concise Standard-of-care management scheme with standards of procedure based on international guidelines was proposed and a collaboration was established between the Department of Nuclear Medicine of J. Nehru hospital and the Department of Oncology& Radiotherapy of Victoria Hospital. RAI diagnostic and post-therapy Imaging studies were performed by the NM team while in-patient RAI therapies were under the care of the Oncology team.

Results

From 2016 to date, a total of 153 RAI scintigraphies were performed. The majority of patients were in the 3rd-4th decade of life and average gender ratio F:M was 3:1. 42 patients received 1-3 RAI therapies in a systematic manner and in compliance to international standards of practice. 31 patients achieved complete response to RAI ablation and 7 cases of metastatic disease demonstrated good partial response to RAI therapy. 3 patients were diagnosed with tumour dedifferentiation and subsequently received TKI systemic therapies with favourable outcomes. One patient demised from RAI refractory disease progression.



Conclusion

The most laudable outcomes of this successful pioneer Theranostics project have been:

- the avoidance of unnecessary RAI therapies when not indicated.
- the accurately risk-adapted RAI therapies to patients with residual/recurrent/metastatic disease.
- the great paradigm shift of the detection of cases of dedifferentiation, previously misdiagnosed as disease free status, and their timely change in management.
- the bridging of pre-existing gaps between NM and Oncology via multidisciplinary team meetings enabling a more productive collaboration.

It is hoped with much enthusiasm that under the new IAEA National Tc project for the establishment of Theranostics in Mauritius, a ‘state of the art’ Unit will be created to allow the NM team to take over the holistic management and follow-up of patients with thyroid carcinomas.

Diagnostic Reference Levels in Skull Radiography: Insights from Sri Lanka

S. Welarathna^{1,2}, S. Velautham¹, S. Sarasanandarajah³

¹ Department of Physics, University of Peradeniya, Sri Lanka

² Postgraduate Institute of Science, University of Peradeniya, Sri Lanka

³ Peter MacCallum Cancer Institute and RMIT University, Australia

Background

The complex anatomy of the head and the presence of radiosensitive organs nearby require a cautious approach during skull radiography. Generally, the lifetime attributable risk of cancer mortality per 100,000 for all cancers in skull radiography is higher than in cervical spine radiography, underscoring the need to minimise radiation exposure and potential stochastic effects for patients. Diagnostic reference levels (DRLs) are valuable for optimising radiation dose and ensuring image quality, particularly for patients who may receive unexpectedly high doses. This study aimed to propose institutional DRLs (IDRLs), multicentric DRLs (MCDRLs), and achievable doses (ADs) for adult patients undergoing skull radiography in selected hospitals in Sri Lanka.

Methodology

This prospective cross-sectional observational study was conducted in six major tertiary care hospitals (HA-HF) in Sri Lanka with 240 adult patients (≥ 18 years) referred for skull anteroposterior/posterior (AP/PA) and lateral (LAT) examinations. Patient demographics, exposure parameters (kVp and mAs), and patient dose indicators were collected from all participants. Patient dose indicators were measured in terms of kerma-area product (PKA) using a VacuDAP Bluetooth PKA meter. IDRLs were determined as the 50th percentile of the PKA distribution in each hospital. ADs were defined as the 50th percentile of the median PKA values for all hospitals, while MCDRLs were set as the 75th percentile of the median PKA values for all hospitals. The Kruskal-Wallis test was used to examine the differences in PKA across all hospitals. A p-value less than 0.05 was considered statistically significant.

Results

The mean kVp values for skull AP/PA ranged from 69.9 (HE) to 74.0 (HF), while mean mAs values ranged from 26.6 (HF) to 37.4 (HA). In contrast, for skull LAT, mean kVp values ranged from 65.4 (HF) to 72.6 (HA), while mean mAs values ranged from 17.6 (HF) to 26.3 (HE). Hospital HA had the highest, and HF the lowest mean PKA values for both skull AP/PA (1.26 and 0.56 Gy cm², respectively) and LAT (0.84 and 0.40 Gy cm², respectively) examinations. Despite the minimal influence of patient body size on skull size, significant variations in PKA, kVp, and mAs were observed across all hospitals. The proposed IDRLs for hospitals HA, HB, HC, HD, HE, and HF were 1.15, 0.64, 0.88, 0.89, 0.61, and 0.53 Gy cm², respectively, for skull AP/PA and 0.80, 0.39, 0.72, 0.74, 0.60, and 0.36 Gy cm², respectively, for skull LAT examinations. The proposed ADs and MCDRLs for skull AP/PA were 0.76 and 0.89 Gy cm², respectively, and for skull LAT were 0.66 and 0.74 Gy cm², respectively. Significant differences ($p < 0.05$) in median PKA were observed for both skull AP/PA and LAT examinations across all hospitals.

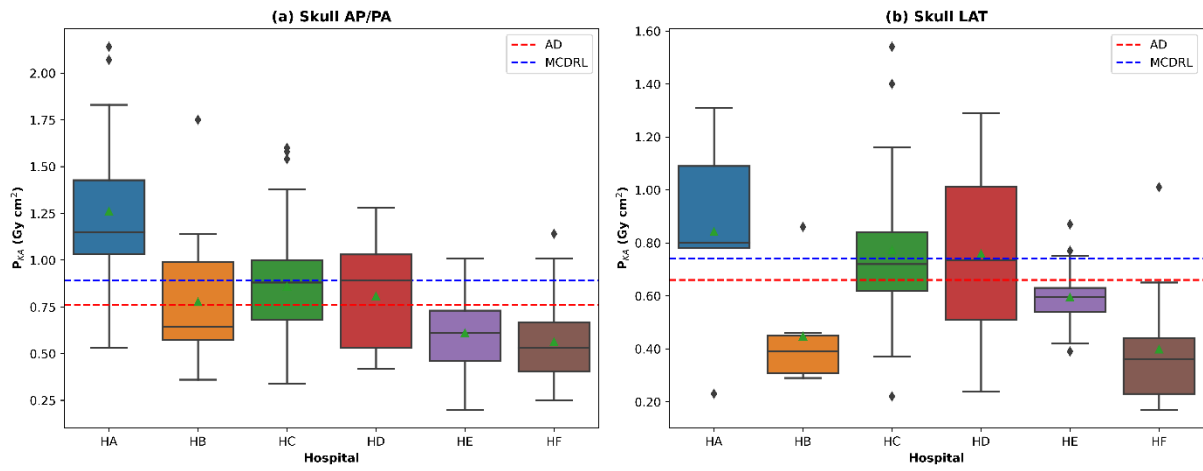


Figure 1. Boxplots of PKA distribution across hospitals for skull (a) AP/PA and (b) LAT examinations.

Conclusion

Significant differences in PKA, kVp, and mAs observed across all hospitals highlight the need for standardised skull radiography examination protocols. In the absence of national DRLs in Sri Lanka, the proposed ADs and MCDRLs can serve as national benchmarks that can aid medical professionals and policymakers in effectively optimising dose management practices.

Preclinical Evaluation of [⁸⁹Zr]Zr-DFO-Bevacizumab for PET imaging of VEGF-expressing tumours

H. Yousefnia, F. Mohammadpour-Ghazi, S. Zolghadri

Radiation Application Research School, Nuclear Science and Technology Research Institute (NSTRI), Iran

Background

Cancer is the prominent cause of death and early detection is critical to reduce cancer morbidity and mortality. Radioimmunosciintigraphy (RIS) utilizing monoclonal antibodies (mAbs) radiolabeled with suitable radionuclides is recognized as a particular and accurate approach for detection of cancer. Position emission tomography (PET) is known as ideal method for imaging of various malignancies. Among the PET radionuclides, the long half-life of ⁸⁹Zr (78.41 h), compatible with the biological half-life of antibodies. This study aimed to evaluate [⁸⁹Zr]Zr-Bevacizumab as a powerful tool for detecting tumours overexpressing vascular endothelial growth factor receptors (VEGFRs).

Methodology

⁸⁹Zr was produced by the bombardment of ⁸⁹Y₂O₃ pellet target with 15 MeV proton energy (current: 25 μA, time: 5 h). ⁸⁹Zr and the target materials were separated by ZR resin. The radionuclide, chemical and radiochemical purities of [⁸⁹Zr]Zr-oxalate were checked by gamma spectrometry, inductively coupled plasma (ICP), and instant thin layer chromatography (ITLC) methods, respectively. Various parameters affected on the labeling, including pH, temperature, time and mAb concentration, were changed to optimize the labeling procedure. The radiochemical purity (RCP) of the final product was checked using ITLC. The stability of the final complex was assessed in PBS and human serum up to 48 h post-incubation. The in-vitro cell studies on SKOV3 cell lines and the biodistribution in tumour bearing mice were also studied.

Results

The radiolabeled compound was prepared with the radiochemical purity >99% and specific activity of 74 GBq/g. the radiolabeled compound showed the stability > 91% even after 48 h both in PBS buffer and human serum. The cellular studies on SKOV3 cell lines indicated that the radioimmunoconjugate has the high specific binding to the cells overexpressed VEGFR. The radiolabeled compound was accumulated in the tumour site, and retained for longer time. The tumour to non-tumour ratios for [⁸⁹Zr]Zr-Bevacizumab would increase over the time.

Conclusion

The results showed that this radiopharmaceutical can be considered as a suitable PET agent for imaging of VEGF-expressing tumours such as ovarian cancer.

Primary Lung Cancer Associated with COVID-19 Infection: Diagnostic Challenges and Role of PET/CT Scan: One Case Report

S. K. Biswas, A. Akhter, F. Rahman, M. Hossain, R. Afrin, R. Begum, S. Hossain, S. Sharmin, T. Biswas, J. A. Haque

Bangladesh Atomic Energy Commission, Bangladesh

Background

Cancer patients usually more vulnerable for developing different form of infections, particularly during Corona pandemic, COVID 19 infection became very serious in case of associated lung cancer, moreover the disease expanded very rapidly. Due to overlapping symptoms and diagnostic features in CT scan different challenges came forward for proper diagnosis and management of lung cancer at that period. PET/CT scan showed the unique potential for evaluating extension of lung cancer whenever it was associated with concomitant COVID 19 infection. Here we would like to depict one case report to unravel the impact of PET/CT scan for proper diagnosis of lung cancer associated with COVID 19 infection.

Case Report

One 54 years old male presented with fever, cough and dyspnoea on 10th July 2021, considering COVID 19 pandemic he underwent different tests. His corona test was positive and his chest CT scan revealed inflammation in both lungs with ground glass opacity showing discrete crazy-paving appearance associated with airspace consolidation that was typical of COVID 19 infection. In addition one Bronchogenic growth (32x46x47mm) was evident at left perihilar region, resulting in partial encasement of left principal bronchus and left pulmonary vessels with mediastinal lymphadenopathy. CT guided FNAC showed non small cell carcinoma. For proper staging he underwent PET/CT scan on 4th August 2021, and revealed left perihilar enhancing hypermetabolic (SUVmax: 13) soft tissue mass (45x26.5x35mm)-compatible with cytologically proven malignant neoplastic lesion, left paravertebral mass just above the diaphragm with intense FDG uptake (SUVmax: 9.2) & hypermetabolic lesions noted in right 3rd & 4th ribs (SUVmax: 6.3) involving intercostal muscles and in the pericardium (SUVmax: 7.3)-suggesting metastases, however there was no hypermetabolic mediastinal lymphadenopathy. Ground glass opacity and mild hyper attenuated areas also noted with minimal FDG uptake (SUVmax: 2.2) which was due to concomitant COVID pneumonitis.

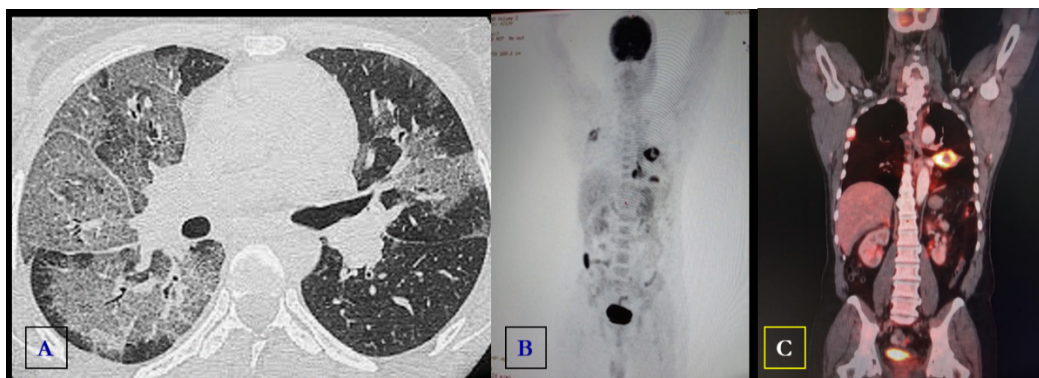


Figure. (A) CT Scan of chest showing inflammation in both lungs with ground glass opacity and discrete crazy-paving appearance associated with airspace consolidation, typical of COVID 19 infection. Bronchogenic growth also evident at left perihilar region. Three weeks later MIP (B) & fusion images (C) of PET-CT scan revealed hypermetabolic left perihilar and left paravertebral soft tissue mass compatible with cytologically proven malignant neoplastic lesion, hypermetabolic lesions in right 3rd & 4th ribs involving intercostal muscles, pericardium-signify metastases.

Conclusion

PET/CT scan findings explored many things for proper diagnosis and staging, and consequently opened the window for thinking much more about rapid disease progression of primary lung cancer whenever it is associated with COVID 19 infection which already been depicted in many literatures.

The efficacy of F-18 PSMA -1007 PET/CT to diagnose biochemically recurrent Adenocarcinoma prostate: Indian Perspective

A. Vyas¹, A. T. Vyas²

¹ Max Super Speciality Hospital, Vaishali, India

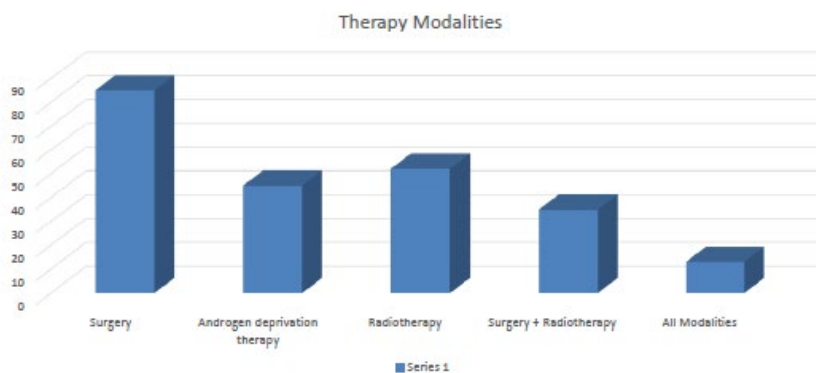
² Janakpuri Super Speciality Hospital, India

Objective

The tracers targeting transmembrane protein -prostate-specific membrane antigen (PSMA), like F-18 PSMA 1007 and Ga-68 PSMA, have changed the diagnostic protocol of patients with adenocarcinoma prostate, significantly. The aim of this study was to evaluate the efficacy of the F 18-PSMA 1007 PET/CT to diagnose patients with recurrent adenocarcinoma prostate in India.

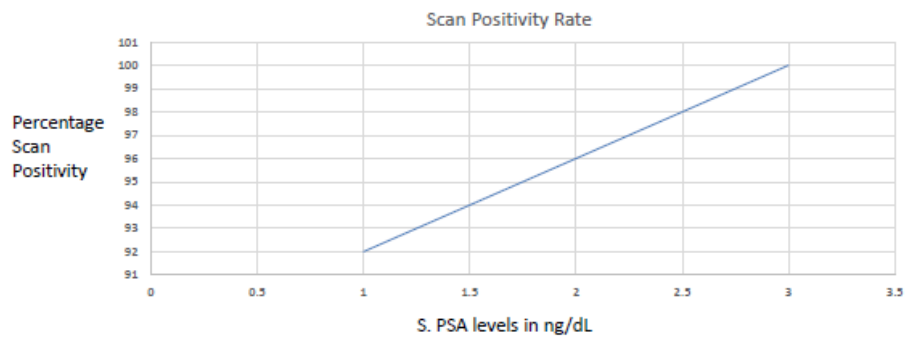
Methodology

The retrospective analysis of 120 adenocarcinoma prostate patients, who presented with biochemical relapse (mean age 65 ± 9.6 years) and were referred for F-18 PSMA PET/CT. Whole-body PET/CT imaging (from vertex to mid-thigh) was performed in all patients 60 min after injection of 370 ± 50 MBq F18-PSMA. 85 %, 45% and 52 % of the patients had received prostatectomy (surgery), androgen-deprivation therapy, and radiotherapy of the prostate bed respectively. Radiotherapy of the prostate in addition to surgery in 35 patients (35%). Thirteen patients (13%) had received all three therapy modalities. The efficacy of F-18 PSMA1007 PET/CT scan to diagnose recurrent disease was compared with biopsy (if available), S. PSA levels and 3 monthly follow up.



Results

Out of 120 patients, 115 (96 %) patients showed positive finding on F-18 PSMA1007 scan. The overall median PSA level was 1.1 ng/ml (range 0.02–60.3 ng/ml). Scan positivity rates were 92%, 96% and 100% respectively with PSA levels ≤ 0.50 , 0.51–2.5 and > 2.5 ng/ml. Overall PET positivity in these patients was 94.1 % (113/120). Two patients showed false positive PSMA uptake in mediastinal lymph nodes.



Images

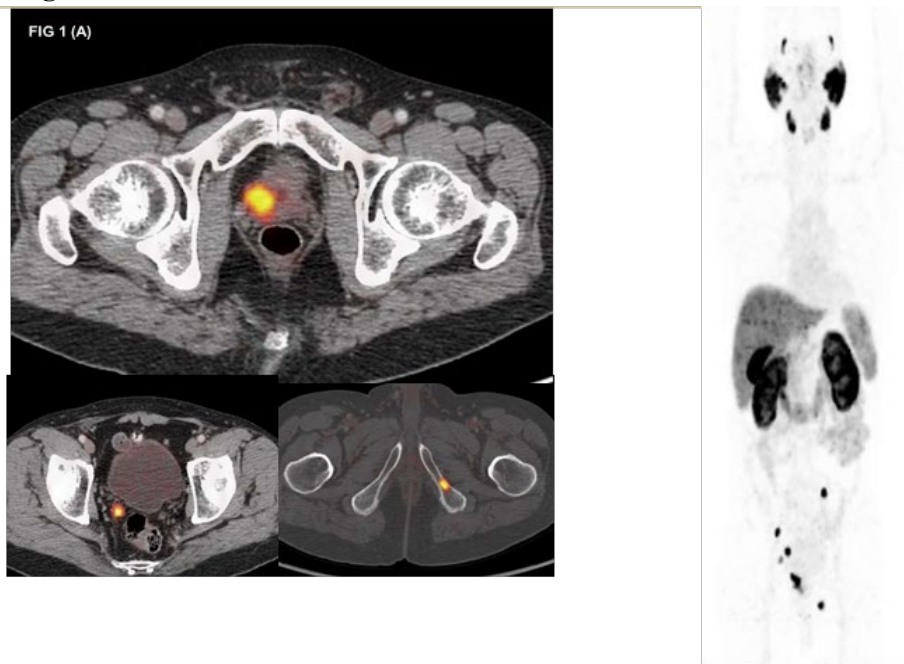


Figure 1. (A) axial & coronal MIP (B) image shows recurrent adenocarcinoma carcinoma prostate. Fused PET/CT images shows recurrent disease in prostate, right seminal vesicle and left ischiopubic bone metastases.

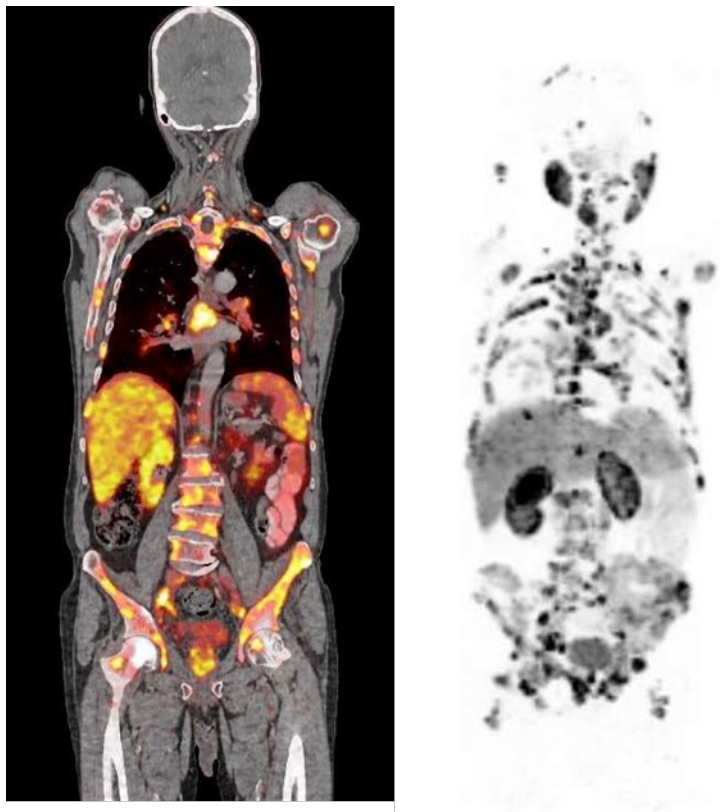


Figure 2. (A) and (B): 68 Yr-old male with adenocarcinoma of the prostate presented with prostatic involvement, retroperitoneal lymph nodes and extensive skeletal metastases. Patient was initially treated with ADT followed by radiotherapy. Present PSMA PET/CT shows recurrent disease involving prostate with multiple skeletal metastases.



Figure 3. (A) & (B): Coronal (A) & Sagittal (B) image showing a PSMA avid lesion in prostate. Patient was treated with bilateral orchidectomy followed by ADT.

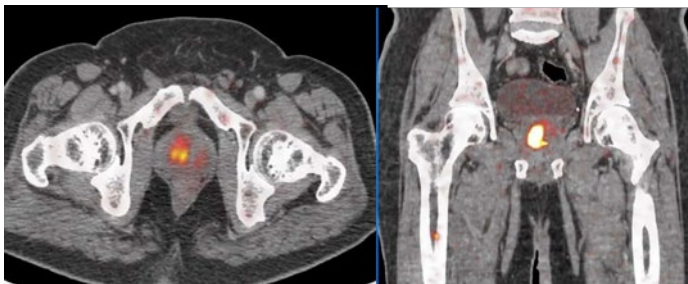


Figure 4. (A) & (B): Recurrent adenocarcinoma prostate. Transaxial and coronal sections of pelvis in a 74 yrs old male with hypermetabolic PSMA avid lesion in prostate. No other PSMA avid lesion in rest of the body.

Conclusion

F-18 PSMA 1007 PET/CT can diagnose recurrent adenocarcinoma prostate in a significantly high percentage of patients with early biochemical relapse, Positive predictive value of F-18 PSMA PET/CT was found significantly high with low PSA level ≤ 0.5 ng/ml, and this may positively impact early detection. Large prospective studies are required. Availability of F-18 PSMA-1007 is better choice in India as it is cyclotron produced tracer.

Role of FDG PET/CT in Response Assessment of Ewing's Sarcoma Family of Tumours

A. T. Vyas¹, A. G. Vyas²

¹ Janakpuri Super Speciality Hospital, India

² Max Super Speciality Hospital, Vaishali, India

Background

Ewing sarcoma was first described by James Ewing in 1921, after observing radiosensitivity in a subgroup of bone tumours.

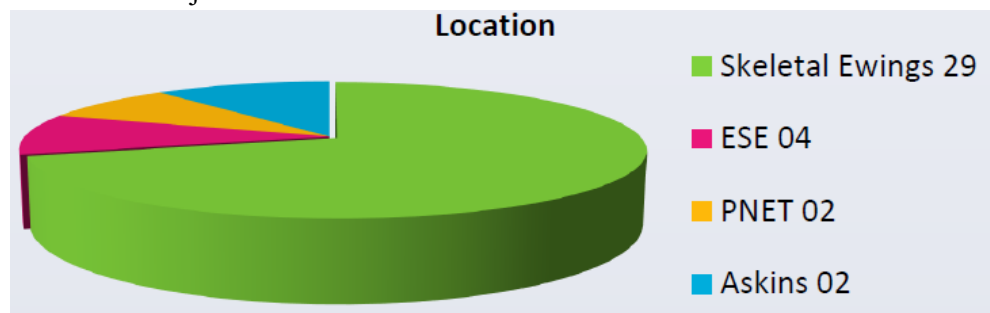
The Ewing sarcoma family of tumours includes Ewing sarcoma, Extraskeletal Ewing sarcoma, peripheral primitive neuroectodermal tumour, neuroepithelioma, and Askin tumour (tumour of the chest wall).

Purpose

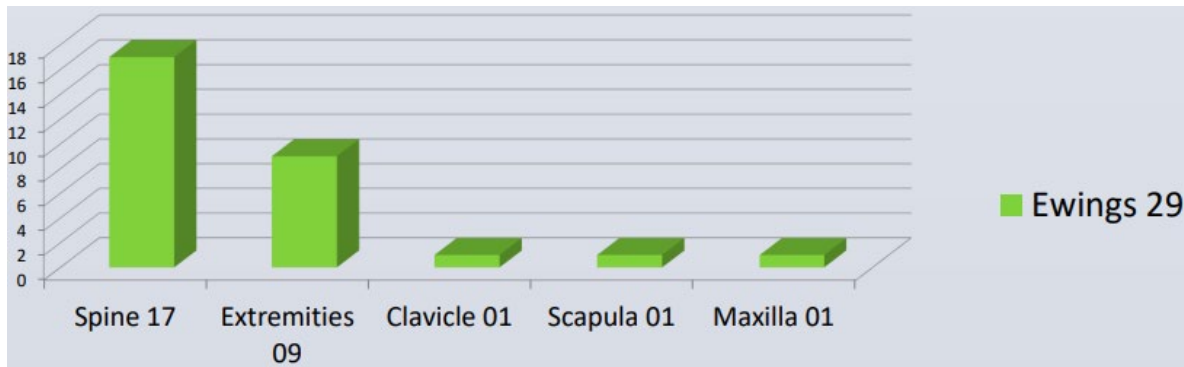
To determine the role of FDG PET/CT in response assessment of Ewing's Sarcoma Family of Tumours (ESFT).

Methodology

37 patients (30 males, 7 females, age range 3-45 years, median 20 years) of histopathologically proven ESFT were subjected to serial FDG PET/CT.



Response was assessed by PERCIST criteria after completion of treatment (surgery for resectable tumours & chemotherapy / radiotherapy for advanced tumours). Data was interpreted using qualitative (compared to liver & mediastinal blood pool) & semi-quantitative (Standardized Uptake Value-SUVmax) methods. PET/CT represents a non invasive means of estimating histologic tumour grade & can be used to detect response prior to anatomical imaging. Resolution of metabolic activity was used as a marker of response. Correlative imaging, clinical follow up 1 year and /or biopsy results whenever available were used as the reference standard.



Results

Out of 37, there were 29 cases of skeletal Ewings sarcoma (ES), 4 cases of Extraskkeletal Ewings (ESE), 2 cases of Askin's tumour & 2 of PNET. There were 17 (45.9%) cases of stage II, 1 (2%) of stage III & 19 (51.3%) of stage IV. Typically a mixed sclerotic-lytic lesion with associated soft tissue component and variable heterogeneous FDG uptake is seen in most of the cases. SUVmax of primary lesion ranges from 2.5 to 19.3 with mean of 6.1. Out of 26 patients there was complete metabolic response in 9 (34.6%), partial metabolic response in 7 (26.9%), stable disease in 1 (3%) & progressive disease in 9 (34.6%) cases respectively.

Images

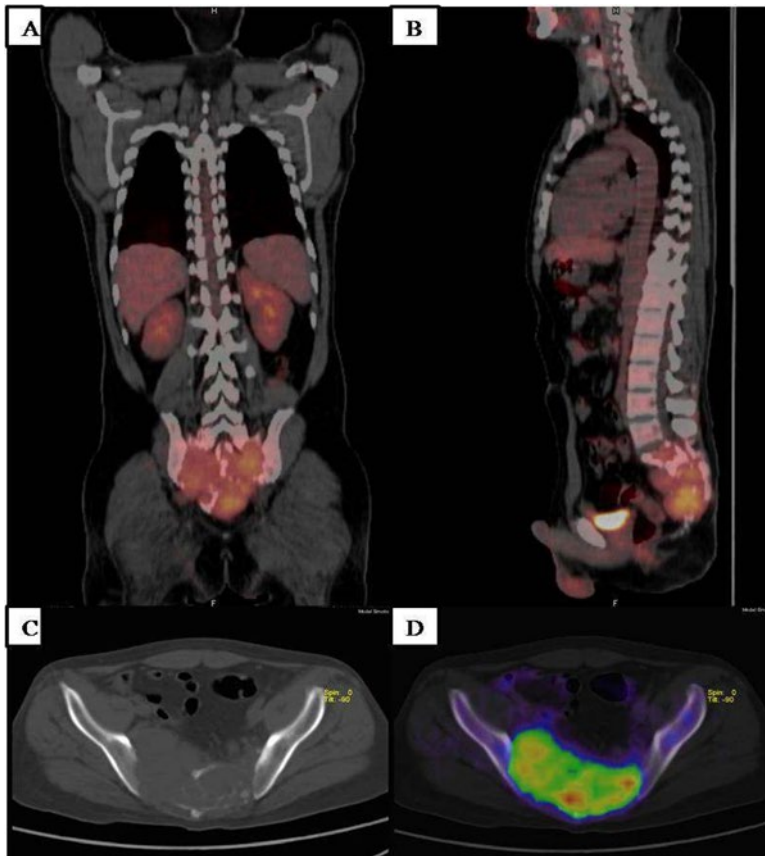


Figure. (A) & sagittal (B) image shows destructive lytic lesion involving sacrum and Rt iliac bone with associated soft tissue component (C), Transaxial NCCT (D) Fused PET/CT sagittal image at the same level depicts a region of hypermetabolic activity corresponding to biopsy-proven Ewing sarcoma.

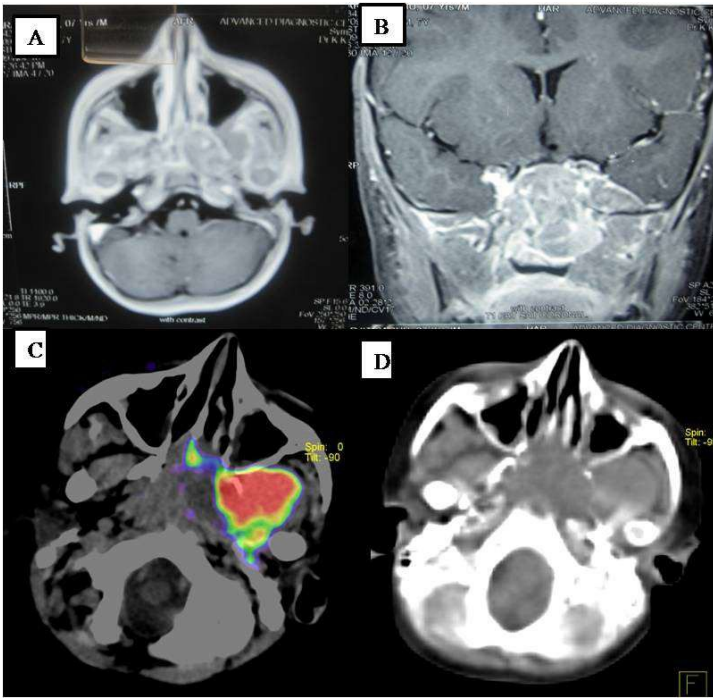


Figure. (A) CECT heads & neck of a 7 yrs old child showing an enhancing lobulated mass involving the Lt masticator space, nasopharynx , sella & parasellar area. (B) MRI (C) transaxial PET/CT scan of the child showing mass involving Left masticator space nasopharynx, sphenoid sinus with intracranial extension & causing erosion of Lt pterygoid plate. Focal area of hyper metabolism in the region of Lt masticator space & rest of the mass shows hypometabolism.

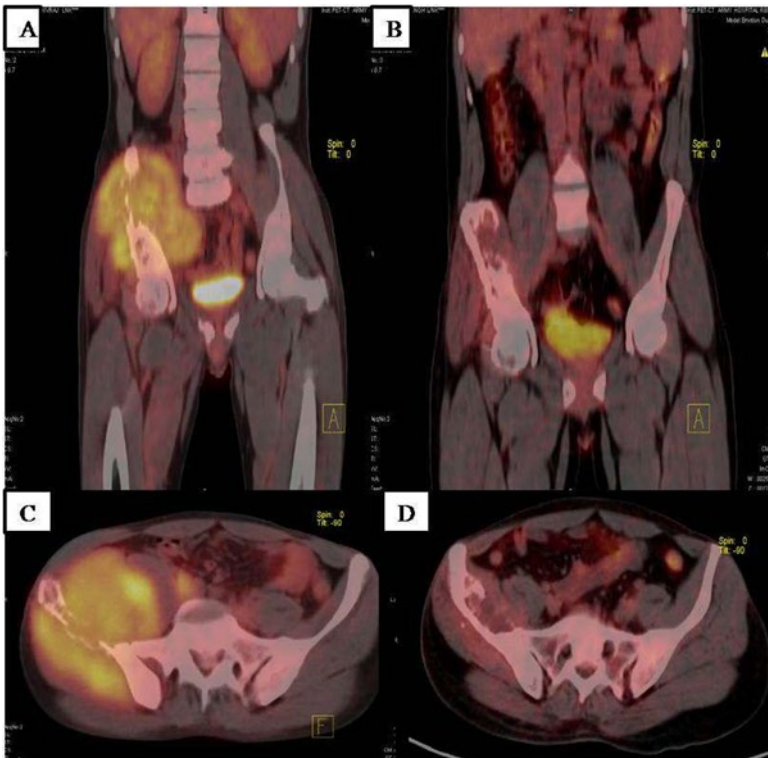


Figure. Response assessment (A) (C) Pretherapy scan: Expansile lytic lesion in right illiac bone with large soft tissue component involving the gluteal muscles.

(B) (D) Post therapy scan: Diffuse FDG uptake in the region of right iliac bone & adjacent muscles (iliacus & gluteus minimus)- Post Radiotherapy changes.

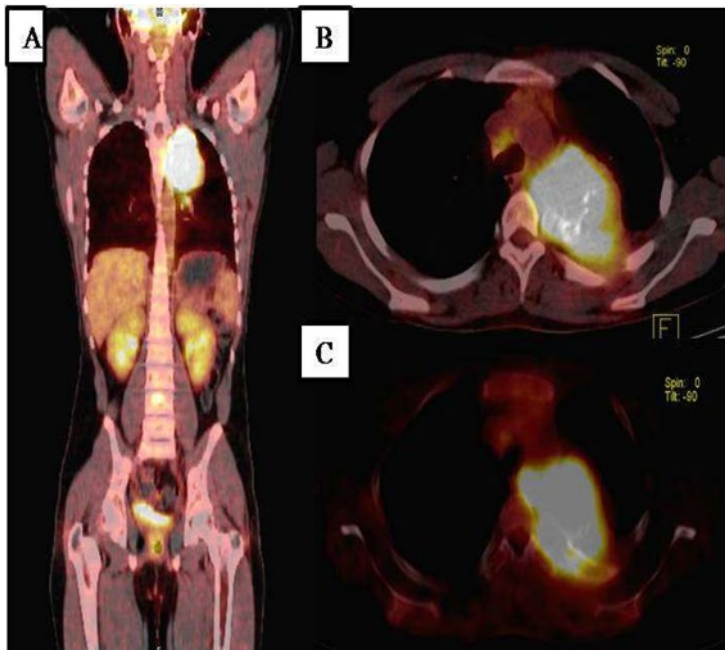


Figure. 15-year-old male with history of Ewing sarcoma (A) Coronal 1st PET/CT for staging showed left paravertebral lesion arising from left 3rd & 4th ribs with soft tissue component , mediastinal nodal & skeletal (LV-4) metastases.

(B) Transaxial image showing soft tissue density lesion arising from left 3rd & 4th ribs with a large soft tissue component (C) erosion of rib.

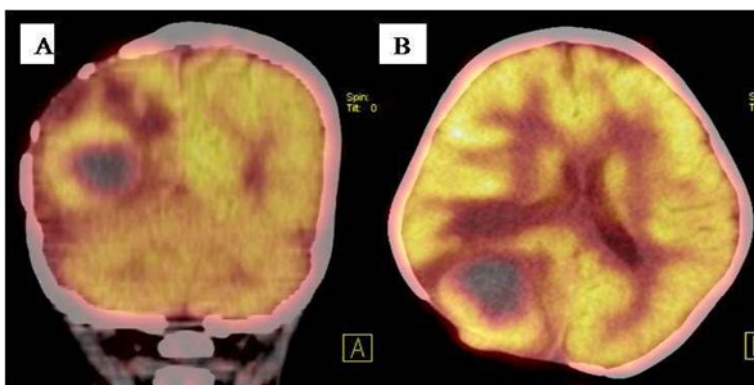


Figure. (A) & (B) : Rt parieto-occipital craniotomy status. Coronal (A) & transaxial (B) image showing a well defined, lesion in the Rt parietooccipital region . The lesion is showing peripheral FDG uptake and central areas of hypometabolism with surrounding perilesional oedema- Recurrent PNET

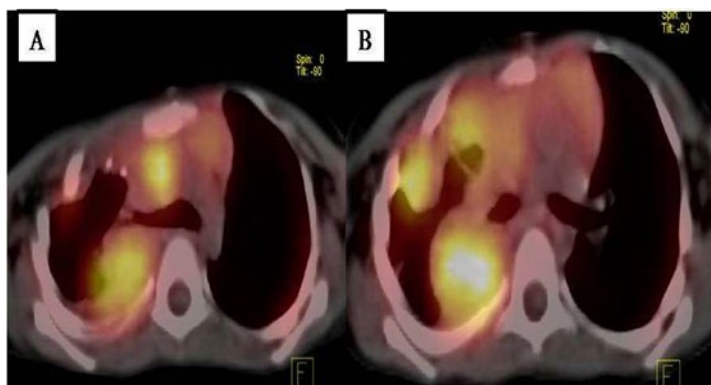


Figure. (A) & (B) Askin's tumour (optd) - Transaxial sections of mediastinum in a 4 yrs old child with askin`s tumour showing hypermetabolic pleural based lesions abutting the Right anterior chest wall and eroding Right 2nd to 6th ribs.

Conclusion

FDG PET/CT may be helpful tool for staging & restaging of ESFT as well as for localization of distant metastases. In addition to this it may be a valuable tool in response assessment of all the types of Ewing sarcoma family of tumours by using qualitative & semi-quantitative (SUVmax) methods. This suggest the need of a large prospective study with serial evaluations & pathological correlations.

Keywords: Ewings sarcoma, Ewing sarcoma family of tumours, FDG PET/CT in Ewings Sarcoma.

A New Strategy to increase the number of clinically qualified personnel in the area of Nuclear Technology in Cameroon

F. P. Ekoume^{1,2,3}, O. Samba^{1,2}

¹Yaounde General Hospital, Cameroon

²University of Yaoundé I, Cameroon

³Catholic University of Central Africa, Cameroon

Background

New developments in radiation imaging and radiotherapy require increased numbers of specialized and qualified personnel. Human health is the second priority of Cameroon's programme framework with the IAEA for 2024 to 2029. The government has chosen to increase the number of Nuclear-Technology (NT) staff three-fold and to expand their scope of practice. This paper aims to share the experience of the new strategic approach in Cameroon.

Methodology

Awareness of careers in the Nuclear-Technology team was raised for potential students and key role-players in Cameroonian relevant ministries. This was done through seminars, conferences and the introduction of new academic and clinical training programs both at undergraduate and specialization level for both private and public institutions. The purpose was to then recruit qualified specialist lecturers for the establishment of the new programs and create new opportunities of employment.

Results

1. Awareness campaigns: 300 brochures (French and English) related to roles, responsibilities and education of medical physicists (MP), radiation imaging specialists, radiotherapy specialists and radiopharmacists were distributed at the universities. In addition, a yearly congress was organized in radiology where ongoing research was presented. Seminars in related fields were arranged.
2. Academic and clinical programs were introduced at level 1 medical-schools, 1st year specialization medical doctors curricula as well as at undergraduate and postgraduate medical schools of engineers. These programs have included on the job training, more practical courses and internships which have considerably increased the number of person academically and clinically qualified.

To date two Radiation-oncologists, one MP, two radiopharmacists and three Radiation-therapy technologists were all trained and recruited. There is ongoing CPD and recruitment of personnel to be academically and clinically qualified in NT. A minimum of 250 new learners enrolled each year to the programs.

Level of study	Course name	Additionally introduced course
Medical doctor Specialization & PhD in Nuclear Technologies	Medical Physics	Advance medical physics link to patient dose (diagnostic reference levels/optimization of doses)

Applied to medicine	Radiopharmacy II	Advance radiopharmacy & radioth�ranostique principle
	Nuclear medicine	Scintigraphic imaging: principles and applications Gamma Camera SPECT, introduction to PET, molecular imaging
	Radiotherapy	Basic principles of radiotherapy, radiobiology, gamma ray production, radiation protection and dosimetry
Postgraduate pharmacist	Radiopharmacy II	Advance radiopharmacy & radioth�ranostique principle
1 st year medical school	Medical Physics	Basic of medical physics
	Radiopharmacy	Introduction to radiopharmacy
Engineers in nuclear technology	Medical Physics	Principle of equipment in radiation imaging and radiotherapy
	Radiopharmacy	Principle of equipment in radiopharmacy

Table 1: Example of additionally introduced courses

Conclusion

The new strategy has increased staff number three times during the last 6 years. There is a growing number of learners in the fields each year showing that the strategy is working and could help to fulfil the objective of building human capacities and addressing the need to fill the gap of qualified specialist in the domain of NT in Cameroon.

A rare case of primary synovial sarcoma of prostate with no distant metastases, staging by F-18 PSMA 1007 scan - case report & review of literature

A. T. Vyas¹, A. G. Vyas²

¹ Janakpuri Super Speciality Hospital, India

² Max Super Speciality Hospital, Vaishali, India

Objective

Synovial sarcoma arising from the prostate is extremely rare. Synovial sarcoma of the prostate is usually identified at late stage and usually with distant metastases. Treatment of synovial sarcoma of prostate is challenging as non-specific clinical symptoms, imaging and treatment protocols. We report a case of primary synovial sarcoma of prostate in a 40 year male. Staging was done by F-18 PSMA1007 PET-CECT scan. Findings revealed PSMA avid heterogenous enhancing localised to prostate with no distant metastases. Patient underwent radical prostatectomy, followed by radiotherapy.

HPE

- Tumor histologic type - Synovial sarcoma, monophasic.
(IHC:- Tumor cells are positive for BCL2, CD99, TLE-1 and focally for Cytokeratin. Tumor cells are negative for CD34, S100 and SMA. Ki-67 proliferation index is 10-15%. Few entrapped prostatic glands are positive for Cytokeratin).
- FNCLCC Grade - Grade 2 (3+1+0 = 4).
- Mitosis count - 6-8/10 hpf.
- Necrosis - Absent.
- Perineural infiltration - Absent.
- Overall Percentage of Prostate Gland Involved by Tumor - Approximately 60% of total tissue is involved by the tumor.
- Extraprostatic Extension (EPE) - Multiple foci of focal extension identified.
- Location of Extraprostatic Extension - Localised on the right side(Lateral, anterior and posterior).
- Capsular breach - Three capsular breach identified (possibly iatrogenic as per clinical details).
- Lymph-vascular Invasion - Absent.

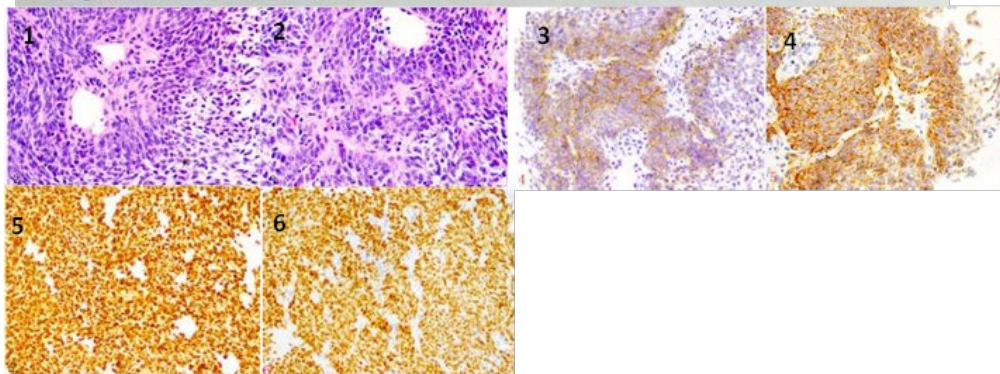


Figure 1. HE staining image with magnification: the tumour tissue grows around blood vessels with cell atypia, has a fine chromatin,

Figure 2. HE staining image 2, magnification: the collagen fibers and mucus-like matrix in the interstitium of tumour cells.

Figure 3. CD99 immunocytochemistry result, 400× magnification: cytoplasmic staining was positive.

Figure 4. Bcl-2 immunohistochemical staining results, it was diffusely positive, mainly positive for cytoplasmic staining.

Figure 5. SS18-SSX immunohistochemical staining result, : the antibody was diffusely positive.

Figure 6. SSX immunohistochemical staining result, : the antibody was diffusely positive.

Review of Literature

SSs generally occur in the soft tissues of the limbs, especially in large joints. SSs that occur in the prostate are very rare. Through a literature search, we found that 10 cases of prostate SS were clearly diagnosed by molecular studies in the English literature. The earliest case of SS of the prostate was reported by Iwasaki et al. in 1999 in the American Journal of Surgical Pathology. ***Together with our report, there were a total of 11 cases reported of monophasic sarcoma prostate.***

For most of the cases reported, the main treatment method is radical surgical resection, supplemented with radiotherapy and chemotherapy according to the degree of the tumour. However, based on previously reported cases, it was found that the prognosis of prostate SS is generally poor, and the survival time of prostate SS is relatively short, with the longest survival time being 32 months. The 18 months reported in our case was relatively long. In terms of treatment, due to the extremely low incidence of SS of the prostate, there is still no consensus on the best treatment plan for prostate SS.

Thus, surgical resection remains a positive method. Whether chemotherapy can benefit patients remains unknown, and more cases are needed to establish a more scientific diagnosis and treatment plan.

Images

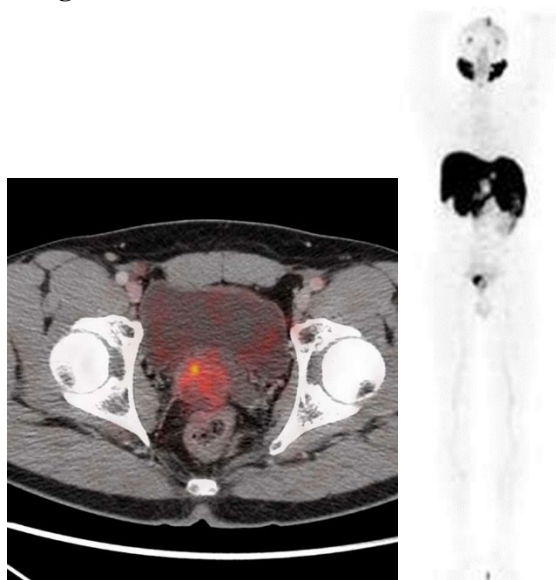


Figure. (A) axial & coronal MIP (B) image shows synovial sarcoma prostate. Fused PET/CT images shows PSMA avid lesion with areas of necrosis within involving prostate. No distant metastases seen.

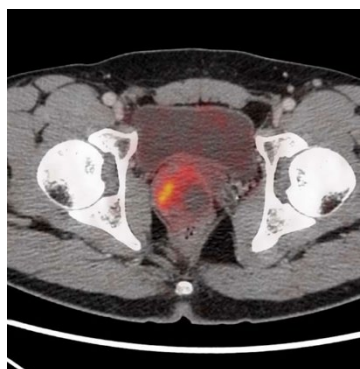


Figure. (C): 40 Yr-old male synovial sarcoma presented with prostatic involvement. Patient was underwent radical prostatectomy followed by radiotherapy.

Present PSMA PET/CT shows disease involving prostate with no metastases.

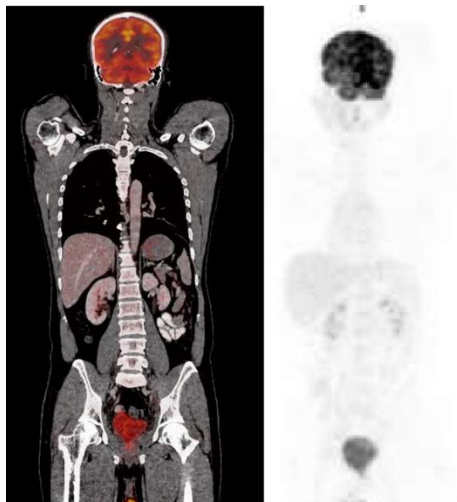


Figure. (D) & (E): Coronal (A) & (B) image showing FDG PET/CT Post radical prostatectomy. No FDG avid lesion is seen in the body.

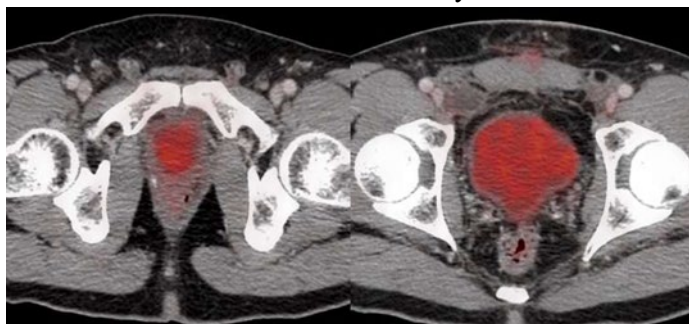


Figure. (F) FDG PET/CT Post radical prostatectomy. No FDG avid lesion is seen in prostatic bed or rest of the body.

A Rare Case of Primary Synovial Sarcoma of Prostate with No Distant Metastases, Staging By F-18 PSMA Scan- Case Report

A. T. Vyas¹, A. G. Vyas²

¹ Janakpuri Super Speciality Hospital, India

² Max Super Speciality Hospital, Vaishali, India

Background

Primary pulmonary synovial cell sarcomas are rare (less than 0.5% of pulmonary malignancies), which are designated as mesenchymal tumours (WHO classification). Primary pulmonary synovial sarcoma is usually identified at a late stage and with distant metastases.

Purpose

To diagnose and stage a rare case of primary synovial sarcoma (PPS) of prostate with F-18 PSMA Scan.

Methodology

PSS are rare mesenchymal tumours, representing less than 0.1% of primary prostate malignancies in adults [1].

It originated from the mesoderm in the reproductive tract, and its risk factors may be related to prostatitis, perineal trauma, previous prostate biopsy, and radiation induced. Treatment of synovial sarcoma of prostate is challenging as non-specific clinical symptoms, imaging and treatment protocols.

Case Study

A 40 year old male underwent F-18 PSMA PET/CT scan (from vertex to mid-thigh), 60 minutes after the injection of tracer.

Findings revealed PSMA avid disease localised to prostate with no distant metastases. S. PSA levels were 0.12 ng/dL (within normal range) [3-5]. Treated with radical prostatectomy with pelvic lymph nodal dissection. Biopsy and final histopathology revealed primary synovial sarcoma of the prostate p T3N0M0.

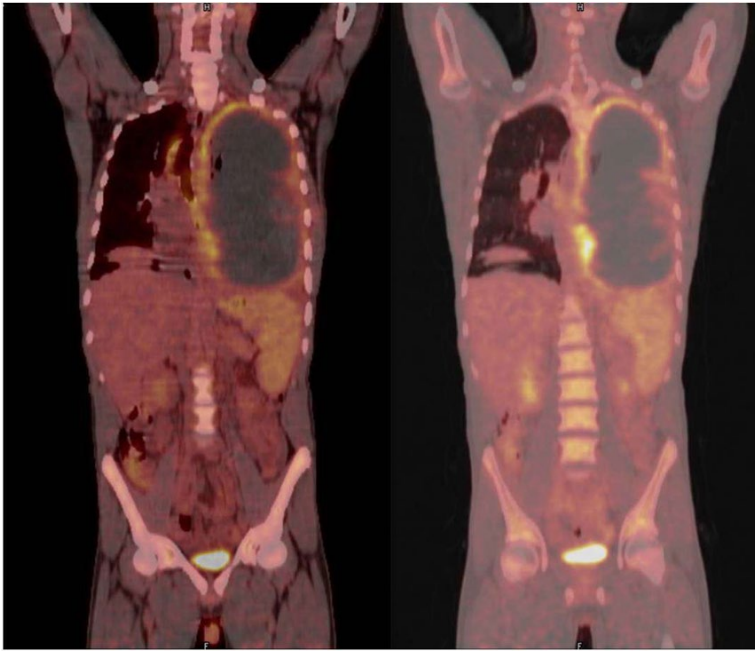


Fig 2: Coronal PET/CT images in soft tissue & lung window showing a large pleural based soft tissue density lesion filling almost the entire left hemithorax with peripheral FDG uptake with central area of hypometabolism and mediastinal shift to right

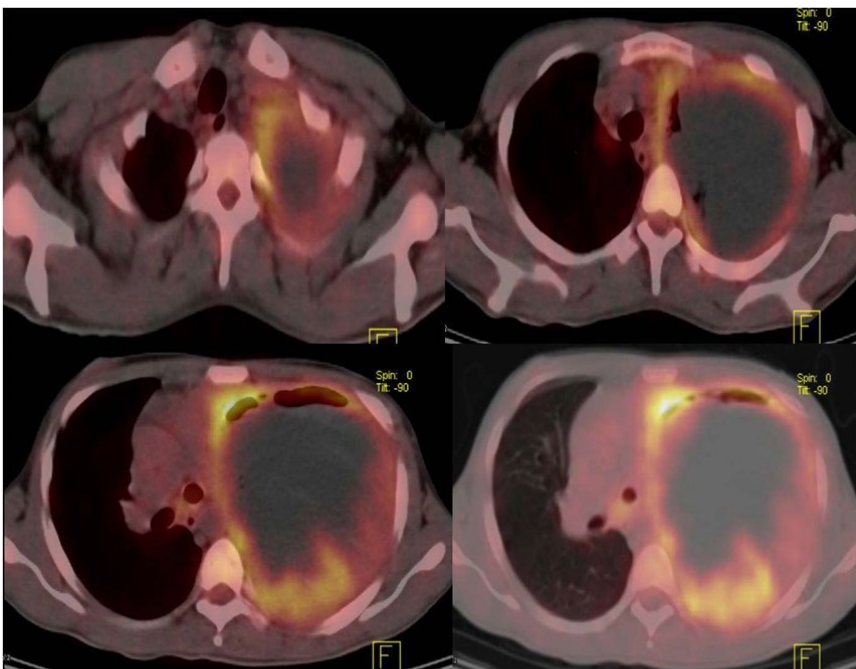


Fig 3: Transaxial PET/CT images in soft tissue & lung window. showing. a large pleural based soft tissue density lesion, starting from the apex of lung, filling almost the entire left hemithorax with peripheral FDG uptake with central area of hypometabolism and mediastinal shift to right.

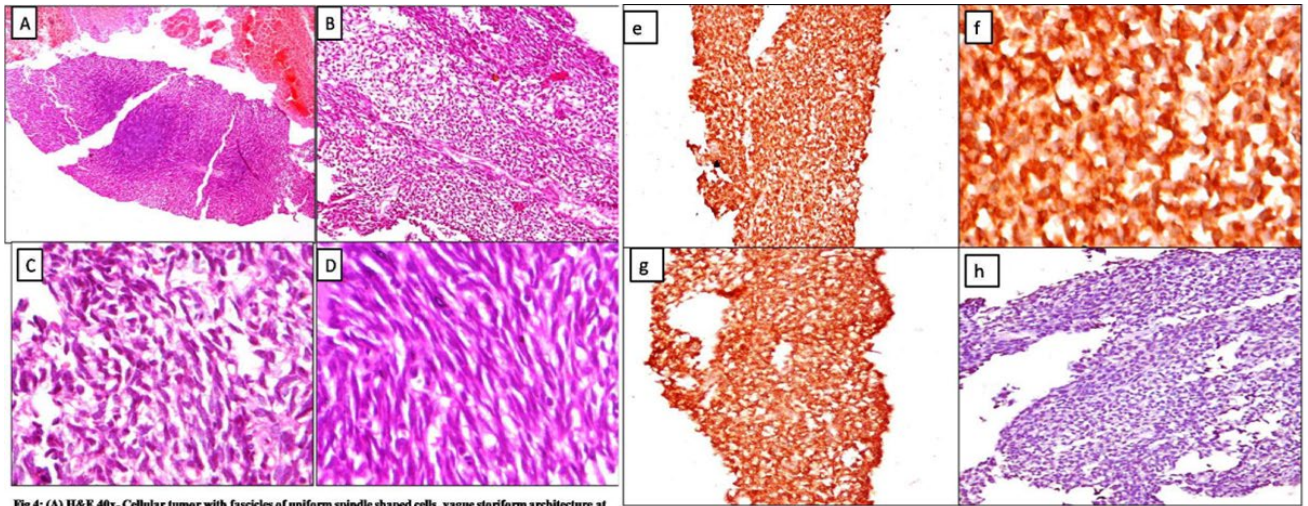


Fig 4: (A) H&E 40x- Cellular tumor with fascicles of uniform spindle shaped cells, vague storiform architecture at places, (B) H&E 100x- Hypercellular and hypocellular areas (marbled appearance), (C) H&E 400x- Uniform plump spindle shaped cells, (D) H&E 400x- Monomorphic uniform spindle shaped cells-no mitosis.

Fig 4: IHC (e) Vimentin -Strong positivity, (f) 400X : bcl2 Strong positivity , (g) CD99: Strong positive, (h) H&E 100x- Negative for CK, EMA, CEA, S100, SMA, CD34, Calretinin

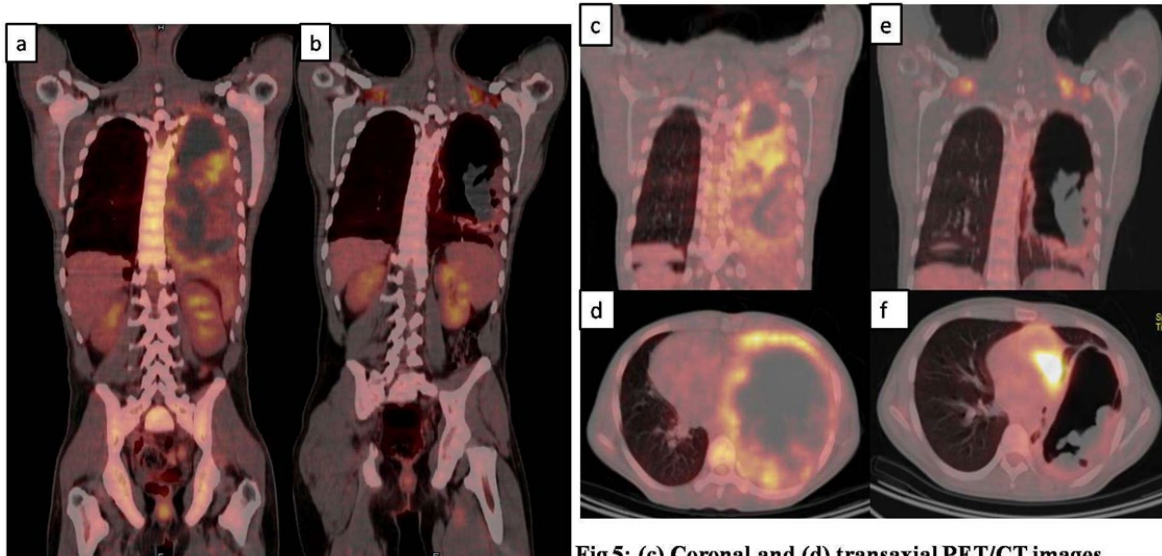


Fig 5: Coronal PET/CT images (a) pretherapy scan- mass lesion in left lung and (b) posttherapy showing significance response to chemotherapy and residual disease in left lung

Fig 5: (c) Coronal and (d) transaxial PET/CT images Pretherapy scan- mass lesion in left lung and (e) Coronal and (f) transaxial PET/CT images Posttherapy showing significance response to chemotherapy and residual disease in left Lung

Conclusion

We present this case with particular emphasis on rare presentation of F-18 PSMA avid sarcoma prostate and role of F-18 PSMA PET/CT in its staging. Further studies with large number of cases may be done.

Not all that Glitters is Gold- a case report of false positive PSMA uptake detected on SPECT/CT

O. Kolade^{1,2}, A. Brink³, K. Hlongwa², S. More²

¹Department of Nuclear Medicine, University College Hospital, Ibadan, Nigeria

²Division of Nuclear Medicine, University of Cape Town, South Africa

³Division of Human Health Department of Nuclear Sciences and Applications, International Atomic Energy Agency (IAEA)

Background

[99mTc]Tc- Prostate Specific Membrane Antigen (PSMA) scintigraphy is an affordable and accessible alternative to PSMA positron emission tomography (PET), especially in resource limited settings where PET/CT units may be out of reach. [99mTc]Tc-PSMA SPECT/CT though less sensitive has comparability with PSMA PET/CT. It is important to note that PSMA uptake is not limited to prostate cancer cells but can also be present in a host of other tumours due to neovascularisation-related PSMA upregulation, as well as in some benign conditions.

Case report

A 67-year-old male with high-risk prostate cancer (PSA: 30.3 ug/L, Gleason score: 3+3) who underwent [99mTc]Tc-PSMA scintigraphy for staging. Whole-body planar and SPECT/CT images (from vertex to mid thighs) were acquired in line with departmental protocols. On review of planar images, focal PSMA uptake (lesion:liver uptake ratio 0.25) seen in the right hemi-thorax was reported as a rib metastasis (images A & B- tip of arrows on anterior and posterior views). On SPECT, the lesion was determined as being in lung rather than rib and deemed a lung metastasis (C - crosshairs on trans-axial and coronal views). However, this right lung lesion on SPECT/CT (D) with corresponding CT findings (E) revealed spiculated margins. This lesion was therefore considered suspicious for a second primary malignancy. A CT-guided lung biopsy confirmed a primary lung adenocarcinoma. Staging [18F]-FDG PET done showed FDG-avidity in the right upper lobe lesion (SUVmax 17) with subcarinal nodal metastasis (F – maximum intensity projection).

Discussion

PSMA uptake in non-prostate malignancies is an established pitfall for PSMA radioligand imaging. These include breast, lung, thyroid, and colorectal cancers more commonly, as well as neuroendocrine tumours and lymphomas less frequently. PSMA uptake is also described in benign neoplastic and non-neoplastic conditions including meningiomas, schwannomas, thymomas, parathyroid adenomas, as well as in Paget's disease, haemangiomas, lung infections, in osteodegenerative change, and in sympathetic ganglia. It is therefore imperative that Nuclear Medicine Physicians are aware of these pitfalls when interpreting PSMA radioligand imaging.

Hybrid imaging, as demonstrated with SPECT/CT, provides the added benefit of anatomical correlation, and as reported in this case, it was valuable in the detection of a potential false positive. Therefore, given the potential of PSMA uptake in non-prostate cancer malignant and benign conditions, SPECT/CT is essential for increasing the specificity of findings on PSMA scintigraphy thus avoiding the pitfalls, and increasing accuracy of the reporting Nuclear Medicine Physician.

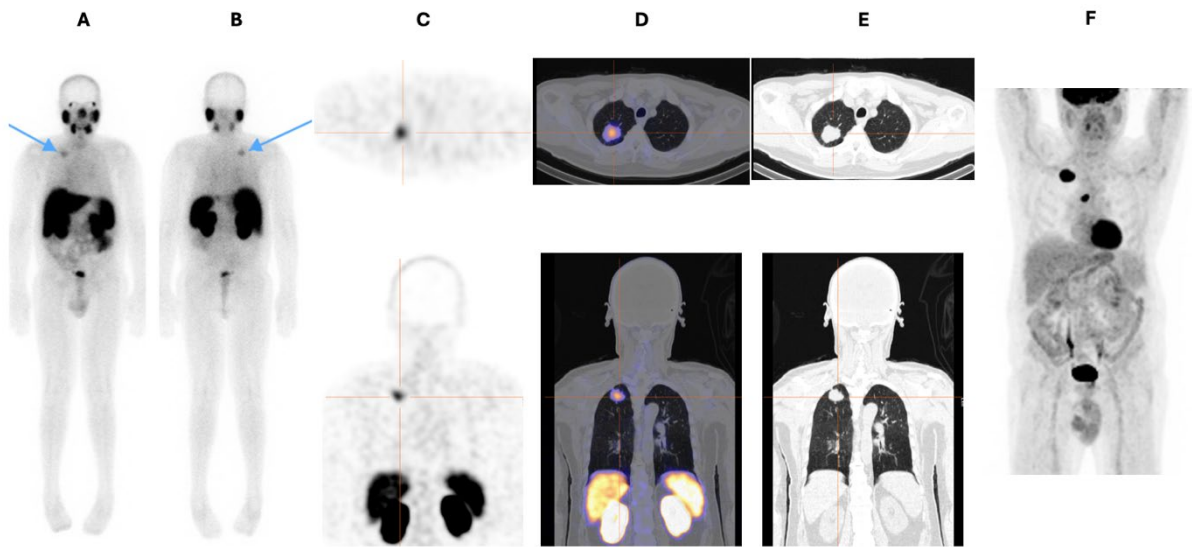


Figure 1. [99mTc]Tc-PSMA Planar, SPECT, and SPECT/CT images (A-E) showing right upper lobe lung lesion (A-E). [18F]FDG PET showing avidity in the right upper lobe lesion and subcarinal nodal metastasis (F).

Prognostic value of several [¹⁸F]FDG PET/CT SUV delineation methods in Diffuse large B-cell lymphoma

A. Doma¹, B. Jezeršek Novaković¹, A. Studen²

¹ Oncology institute Ljubljana, Faculty of medicine, University of Ljubljana, Slovenia

² Fakulteta za matematiko in fiziko Univerze v Ljubljani, Slovenia

Background

PET quantitative parameters Metabolic Tumour Volume (MTV) and Total Lesion Glycolysis (TLG) have shown promise in predicting cancer patient outcomes. However, the prognostic value of these parameters is substantially influenced by the chosen standardized uptake value (SUV) threshold. This retrospective study aims to determine the impact of different SUV delineation methods on prognostic performance of MTV and TLG in Diffuse large B-cell lymphoma (DLBCL) patients.

Methodology:

Manual segmentation of pathological lesions on baseline [¹⁸F]FDG-PET/CT images was performed by an experienced nuclear medicine physician using Slicer3D suite.

The delineation of lesions and 3 and 5 year overall survival (OS3, OS5, respectively) prognostication was performed for four SUV cutoff values: fixed absolute thresholds 2.5 and 4.0 (MTV25, TLG25, MTV4, TLG4, respectively), mean liver SUV+2x standard deviation (MTL2SD, TLG2SD), and >41%SUVmax (MTV41, TLG41); p<0.05 was considered statistically significant.

Results

Included were 186 stage 2-4 DLBCL patients with standard treatment; mean age 67.5 years (range 20-85), OS3 78% and OS5 65%.

Receiver-operating characteristic (ROC) analysis for predicting overall survival at OS3 and OS5 demonstrated moderate to good discriminative ability (Figure 1). Area under the curve (AUC) values ranged from 0.66 (TLG4, p=0.0066) to 0.75 (IPI, p<0.0001) for OS3 and 0.67 (TLG4, p=0.005) to 0.77 (IPI, p<0.0001) for OS5. All AUC values were statistically significant (p< 0.05) except for SUVmax at both OS3 and OS5 (p=0.66, p=0.68, respectively). IPI consistently achieved the highest AUC for both OS time points.

In survival analysis, patients who met any of criteria: MTV2.5≤399cm³, MTV4≤214cm³, MTV2SD≤399cm³, MTV41≤150cm³, TLG2.5≤2562, TLG4≤2347, TLG2SD≤2474, TLG41≤1199, or IPI≤3 showed better OS3 (p=0.005, p=0.003, p=0.002, p=0.001, p<0.001, p=0.003, p=0.001, p=0.006, and p<0.001, respectively). Criteria associated with better OS5 were: MTV2.5≤395cm³, MTV4≤256cm³, MTV2SD≤390cm³, MTV41≤139cm³, TLG2.5≤2561, TLG4≤2347, TLG2SD≤2584, TLG41≤1199, or IPI≤2 (p=0.001, p=0.002, p=0.001, p=0.001, p<0.001, p=0.001, p<0.001, p=0.003, and p<0.001, respectively).

Strong correlation existed between MTV25, MTV4, MTV2SD, MTV41, TLG25, TLG4, TLG2SD, TLG41 (Pearson-coefficient range: 0.75-0.99, all p<0.001), however moderate correlation was seen between IPI and all MTV and TLG values (Pearson-coefficient range: 0.44-0.51, p<0.001).

In Cox proportional hazard multivariate analysis of IPI, disease stage, WHO status, SUVmax, MTV25, MTV4, TLG25 and TLG4, no factor achieved statistical significance for OS3 or OS5, however IPI showed a trend towards significance ($p=0.09$).

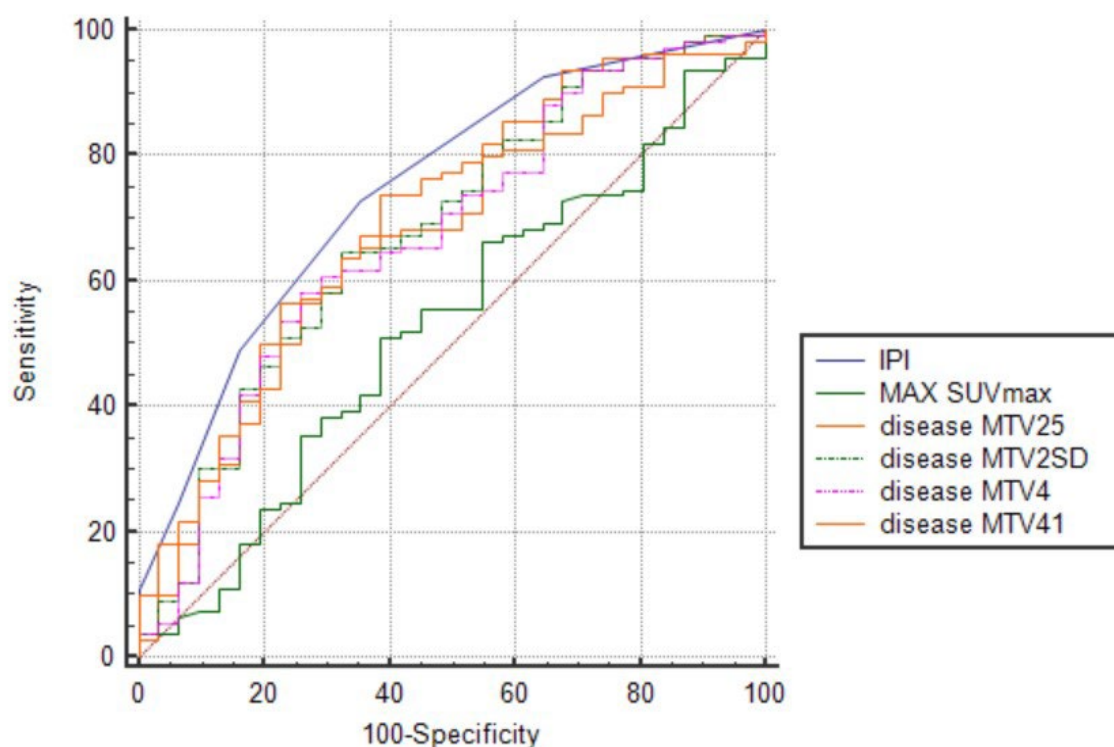


Figure 1: ROC of several parameters for OS3

Conclusion

Higher MTV and TLG are associated with significantly poorer OS at both 3 and 5 years, regardless of the method used to define the tumour volume. IPI demonstrates the strongest association with OS. A fixed SUV4 threshold offers a simpler approach for manual segmentation and avoids misinterpretations of physiological tracer uptake. This method holds promise for achieving optimal results when implementing future automated delineation techniques.

Should [18F]FDG PET/CT replace 99m Tc-MDP bone scintigraphy in the management of breast cancer patients with suspected skeletal metastases?

M. Patel, L. Harry, T. Nxasana, L. Gabela, S. Masikane, V. Pillay, B. Hadebe, M. Vorster

University of Kwa Zulu Natal / Inkosi Albert Luthuli Hospital, South Africa

Background

Breast cancer, being the leading cause of cancer related death in women worldwide, is also a significant cause of mortality. It most frequently disseminates to bone. Morbidity from bone metastases, can be prevented by obtaining accurate, early diagnosis for preliminary staging, planning of treatment, treatment monitoring, restaging and prediction of survival in these patients. 99m Tc-MDP bone scintigraphy for the staging work-up of breast cancer patients, is still used in many centres in South Africa, likely due to the relatively low cost, availability, and physician familiarity with this imaging modality. [18F]FDG PET/CT scans are more sensitive in detecting lytic lesions and purely marrow involvement in addition to soft tissue metastases, which can also be detected. The aim of this cross-sectional study is to compare the detection of suspected metastatic skeletal lesions in both 99m Tc - MDP bone scintigraphy and [18F]FDG PET/CT scans and its impact on management.

Methodology

Sixty-six (66) breast cancer female patients, with a mean age of 54 years, underwent both a [18F]FDG PET/CT scan and 99m Tc-MDP bone scintigraphy, performed within 42 days, between January 2017 and December 2023. A lesion-by-lesion analysis was done for comparison, retrospectively, and any change in stage and management was recorded.

Results

A total of 164 lesions were detected on 99m Tc-MDP bone scintigraphy and 332 lesions were detected on [18F]FDG PET/CT scans which led to a change in management of 17 patients with 99m Tc-MDP bone scintigraphy and 22 patients with [18F]FDG PET/CT scans. Of the sixty-six (66) patients, 71.4% (n=45) of patients had invasive ductal carcinoma (IDC), 25.4% (n=16) had invasive breast cancer no specific type 4(IBC-NST), 3.2% (n=2) had invasive lobular cancer (ILC) and 6.5% (n=3) of patients had missing histological results. For molecular subtypes, 33.3% (n=9) with triple negative (basal like), 10.5% (n=6) HER2 enriched, 49.1% (n=28) Luminal B and 7% (n=4) Luminal A. With regards to tumour stage(T), 56.1% (n=37) had T4 lesions, 16.7% (n=11) had T3 lesions, 21.2% (n=14) had T2 lesions and 6.1% (n=4) had T1 lesions. For lymph nodal staging, there were 12.1% (n=8) for N0, 48.5% (n=1) for N1, 27.3% (n=18) for N2, 9.1% (n=6) for N3 and 3% were unknown. In terms of metastases, 13.6% (n=9) had no metastases, 16.7% (n=11) had known metastases and 69.7% had metastatic status unknown. [18F]FDG PET/CT scans detected 19.7% (n=13) lung, 71.2% (n=47), 12% (n=8) liver and 3% (n=2) adrenal soft tissue metastases.

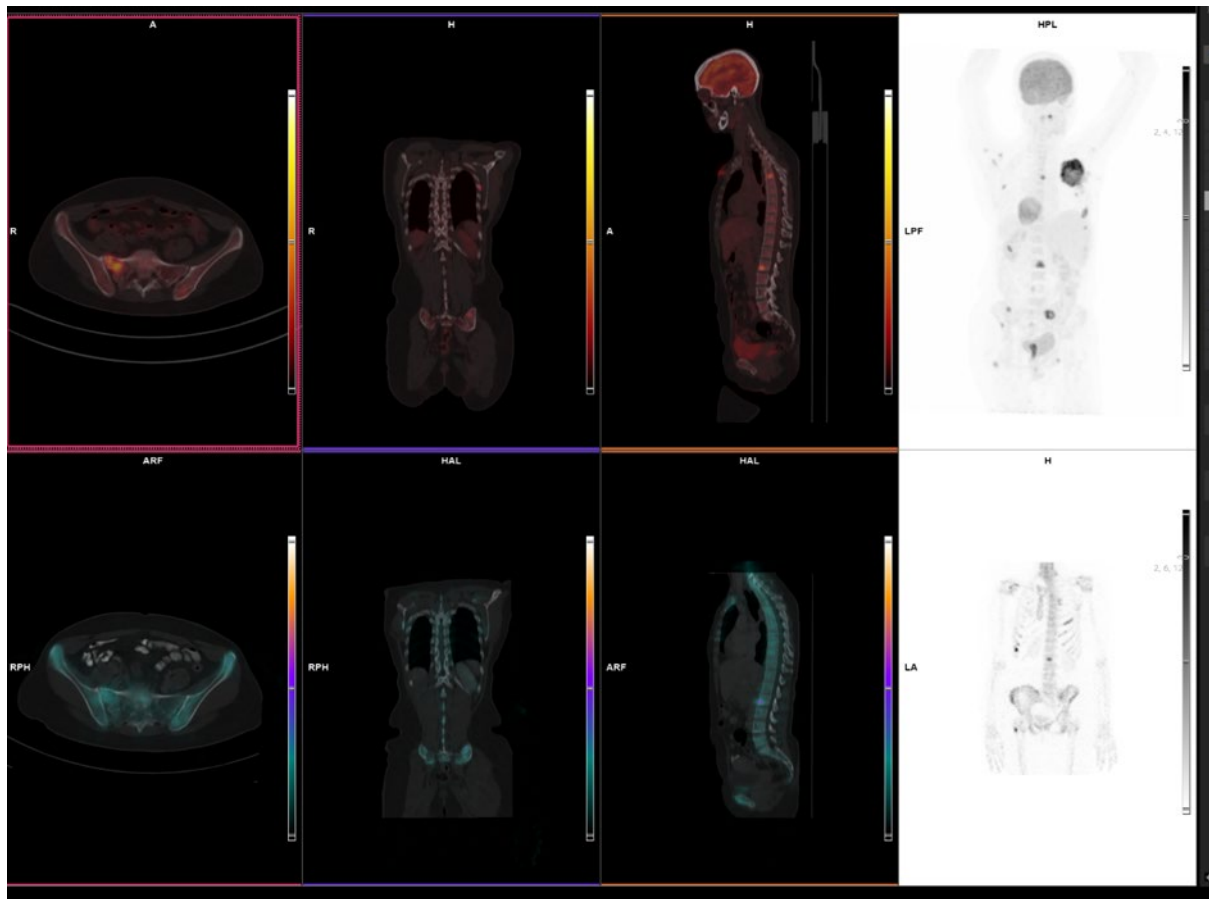


Figure 1. 43-year-old female diagnosed with breast cancer. Images demonstrating more skeletal lesions on FDG PET/CT (row above) in comparison to bone scan (row below).

Conclusion

[18F]FDG PET/CT scans proved to be the superior modality in detecting skeletal and other soft tissue distant metastases. [18F]FDG PET/CT scans detected 49% more skeletal lesions than bone scans. However, in this limited sample, FDG resulted in an upstaging and change in management of only an additional 5 patients (7.57%) in comparison to 99m Tc-MDP bone scintigraphy.

Comparison between the European and the ACR Thyroid Imaging Reporting and Data Systems

C. J. E. Chammakhi, A. Souid

Habib Thameur Hospital, Tunis, Tunisia

Objective

The aim of this study was to evaluate the diagnostic efficiency of the European TI-RADS score proposed by Russ G et al in 2017 and the new TI-RADS score proposed by the American College of Radiology (ACR) in 2017 by comparing TI-RADS categories with histopathological results in operated patients.

Methodology

Eighty-three patients with 129 nodules were operated between January 2018 and December 2019. All of our patients were explored by a US scanning and nodules were scored with a flowchart based on a EU TI-RADS version.

Based on ultrasound data, patients were also classified according to the new TI-RADS proposal of the ACR in 2017. The sonographic findings, the EU TI-RADS and the ACR TI-RADS categories were compared with the final histopathological results. The EU and the ACR TI-RADS classifications were then compared.

Results

Between the different US suspicious features evaluated, the solid composition had the highest sensitivity (80.7%) and negative predictive value (NPV) (89.3%), however irregular or lobulated margins had the highest specificity (94.1%) and positive predictive value (PPV) (57.1%).

The PPV was 7.1%, 8.6%, 21.9%, 45%, and 80% for of the EUTI-RADS categories I, II, III, IV, and V respectively. The sensitivity was 76.9%, the specificity was 64%, the NPV was 91.6%, and the accuracy 67%. The PPV of the ACR TI-RADS was 9.1%, 5.3%, 9.8%, 30.4%, and 50% for respectively TR1, TR2, TR3, TR4, and TR5 nodules. Sensitivity, specificity, NPV, and accuracy were: 92.3%, 27.2%, 93.3%, and 41%. The cut-off value of the ACR score combining the highest sensibility and specificity was 5 ($p=0.001$). When comparing the 2 classification systems, the difference was not significant for the sensitivity, however the EU TI-RADS was significantly more specific.

Conclusion

Between the US suspicious features, irregular margins had the highest odds ratio. The sensibility of the ACR TI-RADS was higher with no significant difference between the 2 classifications, however the EU TI-RADS was significantly more specific (64%).

Analysis of semi-quantitative PET/CT parameters in the evaluation of indeterminate pulmonary nodules

C. V. Díaz Shuňa, J. Kubinyi

Regional Hospital of Liberec, Czech Republic

Background

Lung cancer represents a significant public health issue in the Czech Republic. Based on data provided by the National Institute of Public Health, while there has been some stabilization in lung cancer incidence in recent years, it remains a matter of considerable concern. Positron emission tomography combined with computed tomography (PET/CT) is a hybrid imaging technique that provides combined information about metabolic activity and anatomy. However, imaging techniques like PET/CT often find accidentally indeterminate lung nodules (ILN), that cannot be definitively classified as benign or malignant. For this reason, in the post-processing of PET/CT studies, semiquantitative methods are used to measure the accumulation of Fludeoxyglucose (FDG). One of these methods is the standardized uptake value (SUV), which provides a numerical value for the FDG accumulation levels in the nodule.

Methodology

A total of 310 patients with a diagnosis of non-small cell lung cancer (NSCLC) were retrospectively analysed, who underwent [18F]FDG PET/CT at our hospital centre between October 2023 and February 2024. The aim of the study was to evaluate the usefulness of semi-quantitative PET/CT parameters in the differentiation of benign and malignant lung nodules. From the image analysis, lung nodules were detected using clinical parameters such as SUV_{max} , and SUV_{peak} , identifying ILN in 210 patients.

Results

ILN were identified in 210 patients (113 men and 97 women), representing 67.74% of the analysed patients. During the analysis with SUV_{max} and SUV_{peak} , 83 patients (39.52%) with ILN, $SUV_{max} < 2.5$ and $SUV_{peak} < 2.32$ were identified, reported as benign, suggesting future radiological controls. 127 patients reported with malignant ILN, 74.02% have an $SUV > 4.1$, and $SUV_{peak} > 4.05$, and 25.98% have an $SUV > 2.5$ and $SUV_{peak} > 2.61$.

Conclusion

Visual analysis of lung PET/CT studies allows us to identify ILN in both the parenchymal and mediastinal areas of the lung, and the analysis of semi-quantitative PET/CT parameters (SUV_{max} and SUV_{peak}) are useful to differentiate nodular benignity or malignancy.

[⁶⁸Ga]Ga-PentixaFor PET/CT for imaging of chemokine receptor 4 expression in patients in triple negative breast cancer

B. Hadebe^{1,2,*}, L. Harry^{1,2}, L. Gabela^{1,2}, S. Masikane^{1,2}, M. Patel^{1,2}, S. Zwane^{1,2}, N. Ndlovu^{1,2}, T. Nxasana^{1,2}, V. Pillay^{1, 2}, I. Buccimaza³, T. Buthelezi-Zulu⁴, N. Maphumulo², M. M. Sathekge⁶ and M. Vorster^{1,2}

¹Department of Nuclear Medicine, College of Health Sciences, University of KwaZulu Natal

²Inkosi Albert Luthuli Central Hospital, South Africa

³Department of Surgery, College of Health Sciences, University of KwaZulu Natal, South Africa

⁴Department of Radiation Oncology, College of Health Sciences, University of KwaZulu Natal, South Africa

⁵Department of Medical Physics, Inkosi Albert Luthuli Central Hospital, South Africa

⁶Department of Nuclear Medicine, Faculty of Health Sciences, University of Pretoria, South Africa

Background

Triple-negative breast cancer (TNBC) is a highly aggressive breast cancer subtype which lacks progesterone and estrogen receptors and has low HER2 expression with severely limited therapeutic possibilities. Chemokine receptor-4 (CXCR4) is overexpressed in breast cancer and promotes tumour proliferation and metastasis by increasing the number of blood vessels in tumours. Preclinical studies of TNBC, CXCR4 expression correlates with poorer prognosis and visceral metastasis. [⁶⁸Ga]Ga-PentixaFor non-invasively detects CXCR4 expression in vivo using molecular imaging. The aim of this study was to assess the diagnostic performance of CXCR4-directed PET imaging in patients with triple negative breast cancer using the novel PET probe [⁶⁸Ga]Ga-PentixaFor and to compare this novel tracer with ¹⁸F-2-fluoro-2-deoxy-D-glucose ([¹⁸F]FDG).

Methodology

21 patients with primarily diagnosed triple negative breast cancer underwent [⁶⁸Ga]Ga-PentixaFor PET/CT. Images were analysed visually and semi-quantitatively for CXCR4 expression and standardized uptake values (SUV_{max}), metabolic tumour volume (MTV) and total lesion glycolysis (TLG) and tumour-to background ratios (TBR) of tumour lesions were measured and correlated with ¹⁸F-2-fluoro-2-deoxy-D-glucose ([¹⁸F]FDG, n= 19) and CXCR4 immunohistochemistry (IHC) staining (n=13).

Results

[⁶⁸Ga]Ga-PentixaFor PET/CT was visually positive in all cases, however [¹⁸F]FDG PET demonstrated higher SUV_{max} in the primary lesions in all patients compared to [⁶⁸Ga]Ga-PentixaFor PET. The majority of the patients had locally advanced disease, 11 (57.9%) had T4 disease and 6 (31.6%) had T3 disease. 17 (89%) patients had nodal metastasis. 10 (53%) were HIV positive. 12 (80%) patients had Bloom-Richardson grade III disease, 3 (20.0%) had grade II disease. 14 (73.7%) had a Ki67 of > 70%. The median SUV_{max} for [⁶⁸Ga]Ga-PentixaFor was 7.10 (5.95-9.63) and 17 (5.86-77.9). The median SUV_{mean} (Q1-Q3) for [⁶⁸Ga]Ga-PentixaFor was 4.12 (3.17-5.23) and 9.84 (7.78-14.6) for [¹⁸F]FDG. Metastasis to the skull and brain were more clearly visualised on [⁶⁸Ga]Ga-PentixaFor PET/CT compared to [¹⁸F]FDG

due to the lower background activity in these organs however this did not change the stage of disease. All 21 patients underwent chemotherapy, seven patients had complete metabolic response to therapy, 3 had stable disease, 5 had partial response and 4 patients had disease progression. One patient demised before completing chemotherapy. In this small sample, there was no significant correlation between [⁶⁸Ga]Ga-PentixaFor PET parameters and treatment response or CXCR4 IHC stains.

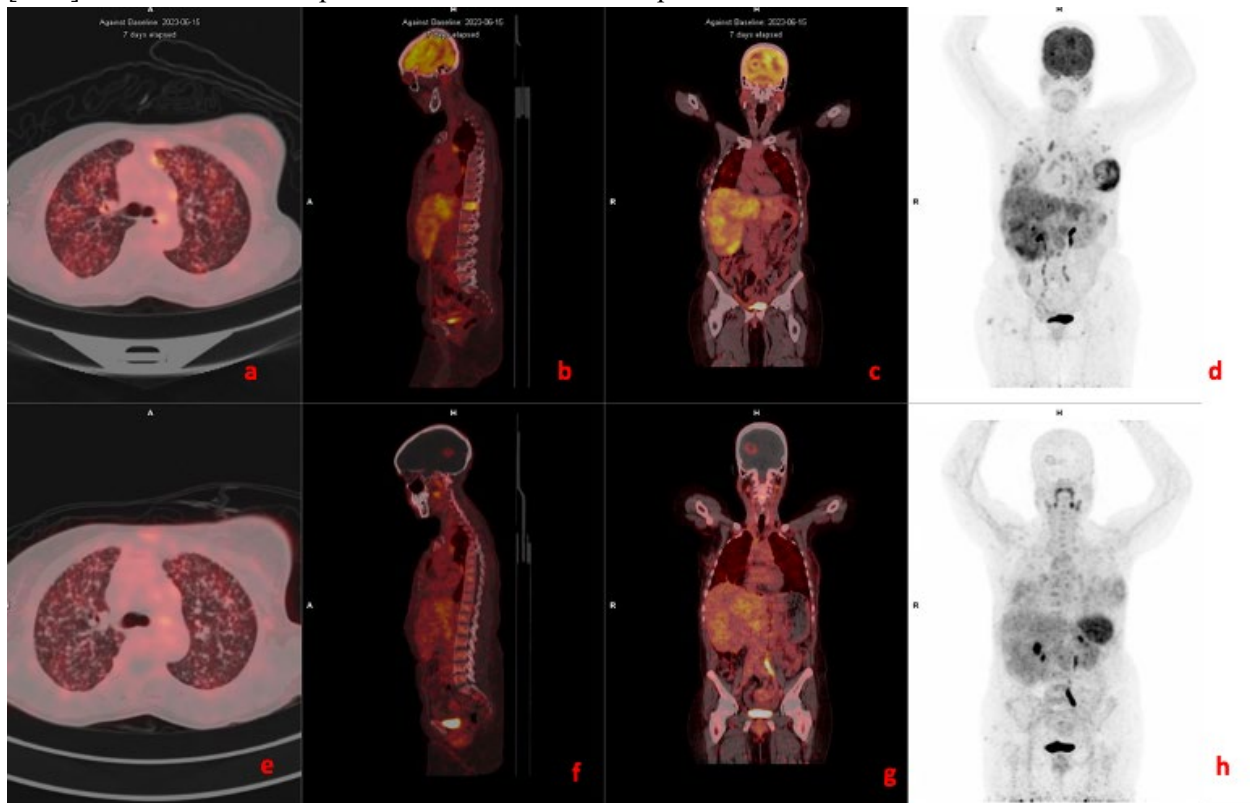


Figure 1: A 41-year-old female with metastatic invasive ductal breast cancer TNBC who underwent [⁶⁸Ga]Ga-PentixaFor (lower panel) and [¹⁸F]FDG PET/CT (upper panel). Axial, coronal, and sagittal fused [⁶⁸Ga]Ga-PentixaFor PET/CT images demonstrated lung (a, e); brain (b, f), bone (b, f) and liver (c, g). The brain and liver metastases which were more clearly visualized on [⁶⁸Ga]Ga-PentixaFor compared to [¹⁸F]FDG PET/CT whereas the metastasis to the vertebra were clearly visualised on [¹⁸F]FDG PET/CT and missed [⁶⁸Ga]Ga-PentixaFor.

Conclusion

Our findings confirm the ability of CXCR4-directed PET imaging to detect TNBC; however, tracer accumulation is significantly lower on [⁶⁸Ga]Ga-PentixaFor compared to [¹⁸F]FDG PET/CT. Moreover, there is better visualisation of skull, brain and liver metastasis on [⁶⁸Ga]Ga-PentixaFor compared [¹⁸F]FDG PET. CXCR4-targeted PET imaging cannot replace [¹⁸F]FDG PET as a diagnostic tool for breast cancer imaging but may have a role in non-invasively selecting patients with triple negative breast cancer eligible for therapies targeting CXCR4.

Value of Computed Tomography Scanner in Neoplastic Colonic Obstruction: Predictive Factors for Emergency Surgery

C. J. E. Chammakhi, S. Chaker

Habib Thameur Hospital, Tunis, Tunisia

Background

Acute bowel obstruction is the most common complication of colonic tumours and is the leading cause of emergency surgery in this population. Emergency treatment can be either exclusive medical or medical and surgical. The aim of our work was to identify the computed tomography scanner (CT-scan) factors predictive of emergency surgery.

Methodology

We conducted a retrospective study at the radiology department of Habib Thameur Hospital that included all patients admitted in emergency for occlusive syndrome due to neoplastic colonic origin between 2012 and 2020. We included all patients who were admitted in emergency and had an abdominal CT scan on admission. We consulted patients' medical records and provided a review of their abdominal scans to identify factors predictive of emergency surgery during neoplastic colonic occlusions.

Results

Among 37 cases, the most frequent tumour site was the sigmoid colon. Parietal enhancement defect was the most common CT sign of severity in our population with 13.5% (n=5) followed by co pneumoperitoneum. Concerning the signs of digestive distress, the CT-scan and intraoperative data were concordant in 85% (n=22) of the patients. Seventy percent of the patients underwent emergency surgery and the discharge stoma was the most common procedure performed. We compared the CT-scan data of patients who had exclusive medical treatment in the emergency department with those who had emergency surgery. The analytical study showed that respective thresholds of 60 mm and 70 mm for tumour size and caecum diameter may be predictive of the use of emergency surgery (respective p values 0.025 and 0.011). The continent nature of the ileocecal valve was non-significantly associated with emergency surgery.

Conclusion

In the case of neoplastic colonic obstructions, apart from CT-scan signs of severity highlighting digestive parietal ischemia, a tumour size greater than 60 mm and caecum diameter greater than 70 mm could be an indication for emergency surgery.

A comparison of ^{68}Ga -PSMA PET/CT-based split renal function to $^{99\text{m}}\text{Tc}$ -MAG3 renography in patients with metastatic castration-resistant prostate carcinoma treated with ^{177}Lu -PSMA

L. Gabela^{1,2}, L. Harry^{1,2}, T. Nxasana^{1,2}, N. Ndlovu^{1,2}, T. Mkhize^{1,2}, V. Pillay^{1,2}, S. Masikane^{1,2}, M. Patel^{1,2}, B. Hadebe^{1,2}, N. E. Nyakale³, M. Vorster^{1,2}

¹ Department of Nuclear Medicine, College of Health Sciences, University of KwaZulu Natal, South Africa

² Inkosi Albert Luthuli Central Hospital, South Africa

³ Department of Nuclear Medicine, Sefako Makgatho Health Science University, South Africa

Background

Physiological PSMA expression in the cells of the proximal renal tubules and consecutive radiopharmaceutical binding and retention could potentially lead to radioligand therapy induced nephrotoxicity. Thus, patients with metastatic castrate resistant prostate cancer undergo $^{99\text{m}}\text{Tc}$ -Mercaptoacetyltriglycine (MAG3) renal scintigraphy to assess kidney function and to exclude renal obstruction as part of their workup for PSMA targeted radioligand therapy (RLT). The $^{99\text{m}}\text{Tc}$ -MAG-3 renal scintigraphy often requires an additional visit to the nuclear medicine department and patients spend 30 – 90 minutes in the department which is inconvenient and takes up camera time. In addition, patients are subjected to a baseline ^{68}Ga -PSMA PET/CT to assess for PSMA positive disease prior to targeted radioligand therapy. The aim of this retrospective cross-sectional study was to compare $^{99\text{m}}\text{Tc}$ -MAG-3 based split renal function (SRF) with ^{68}Ga -PSMA derived SRF.

Methodology

This retrospective cross-sectional study included 28 patients with histologically proven metastatic castration-resistant prostate cancer (mCRPC) who received ^{177}Lu -PSMA-617. A comparison between the split renal function using ^{68}Ga -PSMA PET/CT and $^{99\text{m}}\text{Tc}$ -MAG-3 derived split renal function was done in 56 kidneys (n=56). The SRF on ^{68}Ga -PSMA was calculated using the volume and the average standard uptake value (SUV_{mean}) within each VOI calculated as previously described by Roser et.al 16:

SRF

$$= (\text{VOLUME}_{\text{right}} * \text{SUV}_{\text{mean}_{\text{right}}}) / (\text{VOLUME}_{\text{right}} * \text{SUV}_{\text{mean}_{\text{right}}} + \text{VOLUME}_{\text{left}} * \text{SUV}_{\text{mean}_{\text{left}}})$$

Paired tests and correlation coefficients were used to compare the ^{68}Ga -PSMA and $^{99\text{m}}\text{Tc}$ -MAG-3. A visual comparison of kidney morphology on both studies was also performed.

Results

The median SRF of the right kidney was 49.9% (range: 3-91%) using ^{68}Ga -PSMA PET/CT and 50.5% (range: 0-94%) with $^{99\text{m}}\text{Tc}$ -MAG3 scintigraphy. Notably there was a strong correlation, between SRF measurements obtained from PSMA and $^{99\text{m}}\text{Tc}$ -MAG3 with a Pearson correlation coefficient of 0.957 ($p < 0.001$). Both $^{99\text{m}}\text{Tc}$ -MAG3 and ^{68}Ga -PSMA PET/CT studies identified morphological renal abnormalities, there were 9 hydronephrotic kidneys, 4 shrunken kidneys and 1 obstructed kidney and there was a strong positive correlation between ^{68}Ga -PSMA kidney morphology and $^{99\text{m}}\text{Tc}$ -MAG3 renal scintigraphy kidney morphology, with a correlation coefficient of 0.93.

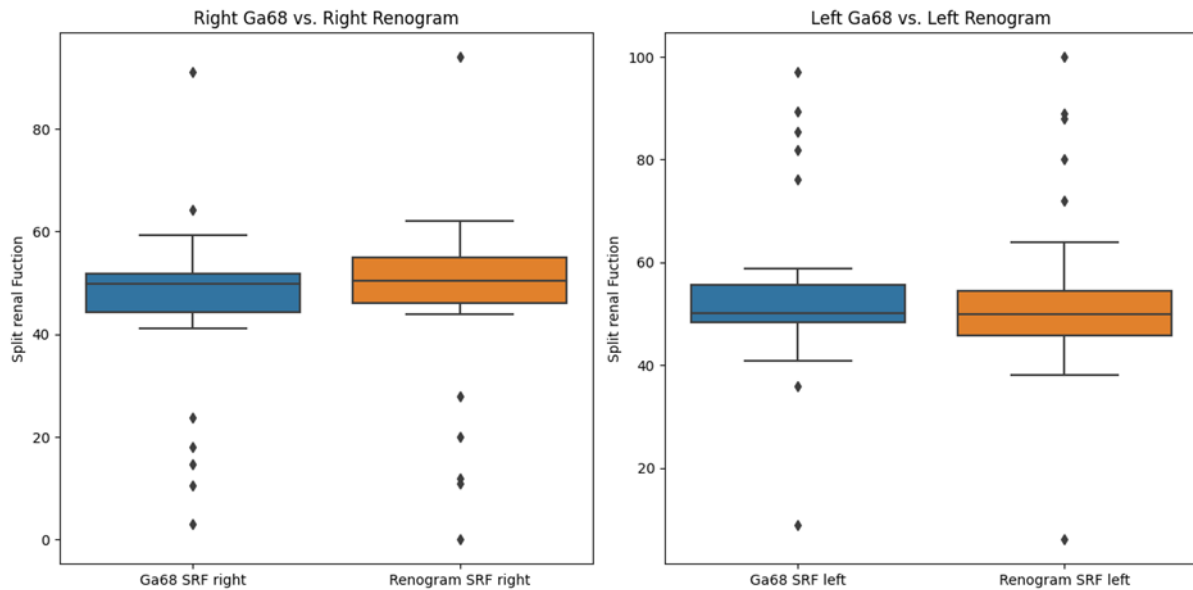


Figure 1. Boxplot showing the recorded differences between the renogram and the PET data. The SRF is centrally located with a few outliers.

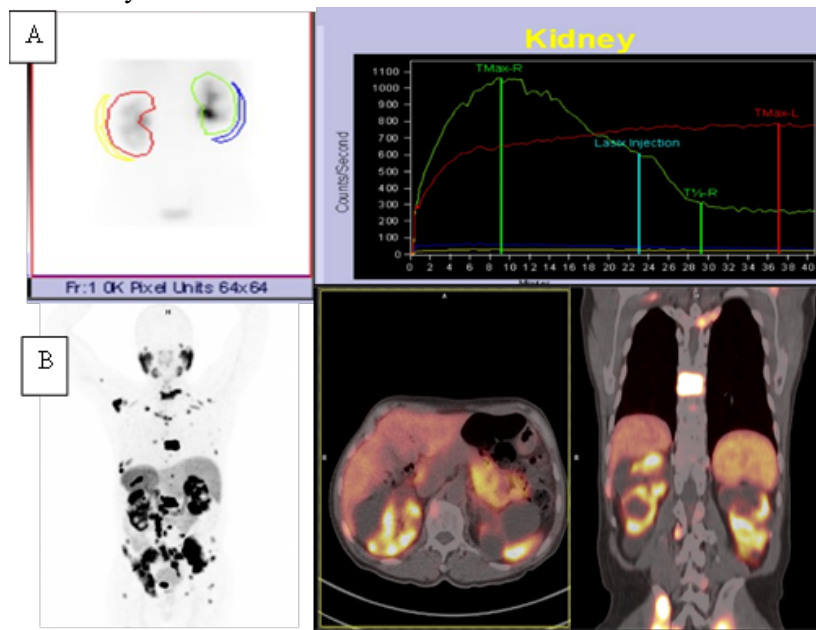


Figure 8. ^{99m}Tc -MAG3 renogram images (A) showing left kidney obstruction. ^{68}Ga -PSMA PET/CT images (B) showing multiple kidney cysts bilaterally with decreased tracer uptake and a stasis of radiotracer in a dilated collecting system.

Conclusion

PSMA derived split function demonstrated a high correlation with renal function assessed on diuretic ^{99m}Tc -MAG3 renograms. PET-derived split renal function may therefore be considered as an alternative to diuretic renogram based split function. Furthermore, both ^{99m}Tc -MAG3 and ^{68}Ga -PSMA PET/CT studies identified morphological renal abnormalities such as hydronephrosis, shrunken and obstructed

kidneys. This correlation underscores the potential utility of ^{68}Ga -PSMA imaging as a valuable tool for assessing kidney morphology as an alternative to renogram split function in clinical practice.

Keywords: PET/CT; ^{68}Ga PSMA-11; $^{99\text{m}}\text{Tc}$ -MAG3; kidney; renal function

F18-FDG PET/CT Imaging in Patients with Suspected LVAD-specific Infection

C. K. Akca, F. A. Görtan, A. Yıldırım, E. Özdemir

Ankara City Hospital, Turkey

Background

Left ventricular assist devices (LVAD) are used as destination therapy or bridge to transplantation in patients with end-stage heart failure. LVAD-specific and LVAD-associated infections cause a high risk of morbidity and mortality in patients with long-term LVAD support. Detection of LVAD infections with conventional imaging methods is a challenging process. Previous studies have shown that F18-FDG PET/CT imaging is useful in the detection of LVAD infections. The aim of this study was to demonstrate the benefits of F18-FDG PET/CT imaging in patients with suspected LVAD-specific infection.

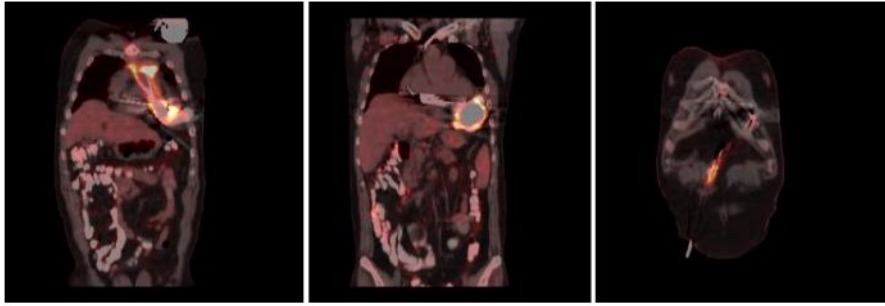
Methodology

31 F18-FDG PET/CT scans of total of 26 patients (23 M - 3 F) referred to our clinic with suspicion of LVAD-specific infection between January 2020 and February 2024 were retrospectively evaluated. All patients had clinical and/or laboratory findings of infection and positive wound and/or blood cultures. Patients underwent a cardiac preparation protocol with a low carbohydrate diet 1 day before the examination and the regular fast of 6 hours. The F18-FDG PET/CT scan was performed 60 minutes after administration of 2.2 Mbq/kg. The PET/CT images were evaluated on AC and NAC images. Uptake higher than background activity on AC images considered positive if it persisted on NAC images. If there was no increased uptake around the LVAD components on NAC images, the uptake on AC images was considered to be secondary to attenuation correction and evaluated as negative. For localization of LVAD-specific infection, the LVAD was subdivided into 4 components 1- Driveline entry point 2- Driveline pathway 3- Pump Pocket+ Inflow Cannula 4- Outflow Cannula

Results

A total of 31 examinations performed in 26 patients were evaluated retrospectively. The mean patient age was 41.7 ± 17.6 years. The interval from LVAD implantation to PET/CT examination was 850 ± 632 days.

The most common focus of infection was found to be the Driveline entry point in % 88 exams. 2nd most common site was found to be around the Driveline Pathway in % 42 of the cases. Central infection in Pump + Inflow Cannula and Outflow Cannula found in %39 and % 13 cases respectively. The wound culture result from the Driveline entry point was positive in % 88 cases and the blood culture result was positive in 45% cases. Staph Aureus (MSSA & MRSA) was the most common infectious agent in wound and blood cultures. The sensitivity of the F 18 FDG PET/CT imaging in the detection of Driveline entry point infections was 95%, specificity was 60% and positive predictive value was 90.5%.



LVAD component	SUVmax
Driveline entry point (N:26)	7.2+2.8 (3.1-13.8)
Driveline pathway (N:13)	9.4+3.9 (4.9-17.6)
Pump Pocket+ Inflow Cannula (N:12)	9.4+3.3 (6.6-18.8)
Outflow Cannula (N:4)	8.5+5.3 (3.1-20.2)

Conclusion

In this study, the most common focus of infection was found to be the Driveline entry point, consistent with the literature. The sensitivity of the test in the detection of Driveline entry point infections is 95%, specificity is 60% and Positive Predictive Value is 90.5%. F 18- FDG PET/CT imaging provides significant information about presence and the localization of infection. F 18- FDG PET/CT is a technique with high diagnostic value in the detection of Driveline entry point infections in LVAD patients.

Assessing the Utility of Hybrid Multiphase Contrast FDG PET/CT Protocol in Patients with Muscle-Invasive Bladder Cancer: Single Center Initial Experience

S. Taywade, S. Kumar, S. Tripathi, S. Sahu, T. Yadav, D. Datta, R. Kumar, A. S. Sandhu, G. R. Choudhary

All India Institute of Medical Sciences - Jodhpur, India

Background

Urinary bladder cancer represents a prevalent malignancy globally, characterized by notable morbidity and mortality rates. For the initial staging of muscle-invasive bladder cancer (MIBC), contrast-enhanced computed tomography (CECT) of the abdomen and thorax is commonly preferred. However, FDG PET/CT imaging emerges as a valuable adjunct, furnishing crucial information for staging, restaging, treatment response assessment, and prognostication. However, it may not be feasible and advisable to perform both CECT and FDG PET/CT in all the patients. We tried to combine different phases of CECT along with FDG PET/CT and studied its impact on staging of MIBC patients. The primary objective of our study was to compare diagnostic accuracy of FDG PET/CT to that of conventional imaging for detecting distant and nodal metastases.

Methodology

In this prospective study, total 58 patients with histopathologically proven MIBC patients were recruited. These patients underwent novel multiphase contrast protocol FDG PET/CT. The non-contrast phase, venous phase and delayed phase of CECT was incorporated into whole body FDG PET/CT without additional CT sequencing. The CECT and FDG PET/CT scans were reported separately by experienced radiologist and Nuclear Medicine physician respectively. The results of novel imaging protocol were evaluated and compared with conventional approach.

Results

Both modalities showed concordant findings in 48/58 patients. However, 10/58 patients showed discordant results. Among patients with concordant findings 45 showed locoregional lymph nodal metastasis, 15 showed lung nodules suspicious for metastases and 7/48 revealed skeletal metastasis on both CECT and FDG PET/CT. Amongst discordant cases (10/58), two patients (2/10) were identified with bone metastases solely on CECT, with one of them also showed lung metastasis on CECT alone. 1/10 patient exhibited lung and supraclavicular lymph node involvement exclusively on CECT. Lung (1/10) and locoregional lymph node (1/10) metastases were detected only on CECT scans for one patient each. On the other hand, FDG PET/CT revealed lung metastases in two patients (2/10), bone metastases in one patient (1/10), adrenal metastasis (1/10) and paraaortic lymph node (1/10) involvement in one patient each which were not detected through CECT. Notably, discrepancies between CECT and PET/CT findings were relatively less and predominantly in assessment of skeletal and lung metastases. Overall, the results of novel protocol were comparable with conventional imaging approach.

Conclusion

This novel hybrid imaging protocol integrates all the sequences of CECT and whole body FDG PET/CT in a single study without compromising the acquisitions of either. It is an amalgamation of superior

loco-regional tumour delineation on CECT and higher detection of metastatic sites on FDG PET/CT. Moreover, it limits the repeated use of contrast preventing the potential renal damage. It also reduces patient radiation doses by decreasing the number of CT sequences. Overall, this combined approach enhances the confidence of the clinician by providing detailed & better insights into local as well as distant disease extent in a single study. This hybrid multiphase contrast FDG PET/CT protocol enhances the patient care, clinical outcomes and could impact management of patients with MIBC significantly.

3D Phantom modelling and printing for use in Nuclear Medicine quality control

H. Fayad¹, T. Torfeh², A. Ghujeh¹, A. A. Al Rahim¹, M. H. Kharita¹, R. Hammoud³, N. Al-Hammadi³

¹ Hamad Medical Corporation, Qatar

² National Center for Cancer Care and Research, Qatar

³ Department of Radiation Oncology, National Center for Cancer Care and Research, Hamad Medical Corporation, Qatar

Background

Quality control (QC) is a critical aspect of nuclear medicine practice ensuring that equipment and procedures used to diagnose and treat patients are accurate and reliable. This includes acceptance testing as well as regular calibrations. Acceptance and annual testing are usually based on international guidelines from National Electrical Manufacturers Association (NEMA) and use different types of phantoms acquired within clinical conditions. Some of these phantoms are available commercially but are sometimes expensive and some of them need to be fabricated in house. The goal of this study is to use 3D printing in order to create one phantom to be used in the System Alignment NEMA test (Center of Rotation).

Methodology

A 3D phantom was designed based on NEMA specifications and printed using the MakerBot Replicator Z18 3D printer. The phantom, as shown in figure 1, contains 3 bars that can fit one capillary tube each. Horizontal distances between the end point of the tallest bar and the other two bars are 5 and 10 cm respectively. The vertical distance between bars were 7.5 cm. We tested the 3D printed phantom on a GE SPECT CT (870 DR) installed in the MINM department in Hamad General Hospital. 3-point sources (around 2 mCi each), with a maximum dimension of 2 mm was prepared inside three capillary tubes which were placed inside the three bars. The printed phantom was positioned in the plane of the three-point source holders parallel to the plane of the table and the central point source at the center of field of view (figure 2). A SPECT acquisition is then performed, and the Center of Rotation is calculated based on NEMA guidelines.



Printed 3D phantom (left) and phantom positioning (right)

Results

Using the phantom, System alignment / COR results indicate a COR error of 3.22 mm, a COR deviation between heads of 5.94 mm, an axial deviation 0.43 mm and a relative axial misalignment of 0.32mm. These values fit within machine specifications.

Conclusion

Our 3D printed phantom is a valuable and cost-effective tool for measuring system alignment/COR. It represents an economical solution, and its straightforward design makes it easy to print.

Increased Sensitivity and Specificity of Prone 18 FDG PET CT in Breast Cancer Response to Treatment Assessment

M. Agolti

Centro de Medicina Nuclear, Clinica Modelo, Argentina

Background

[18F]Fluorodeoxyglucose (FDG) positron emission technology/computed tomography (PET/CT) is a commonly used modality for the restaging of breast cancer (BC). Superior sensitivity and specificity of prone FDG PET/CT image acquisition in comparison to its supine equivalent has been described in the initial staging of BC, probably due to it allows a better separation of deep breast structures from the chest wall and better relaxation of the pectoral muscles. Our aim is to determine if there is a change in restaging/response to treatment evaluation in both positions, regards local relapse, intramammary, internal mammary and axial lymph nodes.

Methodology

In this retrospective analysis we included 141 female patients, with average age of 55 years old, treated with surgery; radiotherapy or neoadjuvant treatment (when indicated), we performed conventional supine [18F] FDG PET/CT images and after 1 hour we performed prone thorax images with a styrofoam device, we have designed, with a minimum extra radiation dose (CT low dose). We excluded 4 patients for involuntary movements. We compare the number of increased uptake breast lesions, the differences in Standard Uptake Value (SUV), the number of axillary lymph nodes, their SUV, the intramammary and internal mammary lymph nodes when seen.

Results

We found 63 increased uptake images in breast in prono position and 55 in supine position, we assumed as relapse, according to biopsy and follow up. Regards the SUV in Prono acquisition the medium SUV was 3,77 and in supine images the medium SUV was 3,20 with statistical significance (less than 0,05; in this case $p=0,001$) according to Wilcoxon Test. Regarding Axillary nodes we found 37 in supine position and 41 in prono. We found only 4 intramammary lymph nodes one of them that was less than 1 cm size was not seen in supine images and one internal mammary lymph node in one patient with clear increased uptake in prone (SUV Max 2,5) regards to supine acquisition (SUV Max 1,8) which allowed better visualization. Two cases had seromas and adjacent to them solid increased uptake images were seen only in prono acquisition.

Conclusion

Prono images in treated breast cancer showed relapse in 8 patients that weren't seen in conventional images, showing a change in stratification in 12,7% of the cases. Regards lymph nodes metastasis we found no significative change in axillary nodes; regards intramammary and internal mammary lymph nodes, it showed increased sensibility (change staging in 33.3%), although the number of patients (6) may not be significative. A very important issue is that this technique means minimum extra radiation (1.5mSv) and changes stratification in more than 10% of the patients.

Radiochemical yields of fluorine-18 radiopharmaceuticals using a new high-power target with niobium insert, one year experience at UNAM

M. J. Mendoza-Figueroa, E. Zamora-Romo, H. Gama-Romero, F. Trejo-Ballado, R. Tecuapetla-Chantes, U. Rabadán-Domínguez, G. Contreras-Castañón, A. Zárate-Morales, A. Flores-Moreno, M. A. Ávila-Rodríguez

Unidad Radiofarmacia-Ciclotrón, Facultad de Medicina, Universidad Nacional Autónoma de México, Mexico

Background

The Radiopharmacy-Cyclotron Unit of the National Autonomous University of Mexico is the main producer of PET-radiopharmaceuticals in Mexico. More than thirty thousand unidoses of different radiopharmaceuticals are annually provided to over twenty hospitals and diagnostic centers located in Mexico City and other surrounding cities. Since the early 2000s this Unit has operated a self-shielded 11 MeV cyclotron that has been upgraded on three occasions. The most recent upgrade included a single BTI target for fluorine-18 production, increasing by twofold the production yield of [¹⁸F]F⁻. Herein we present the radiochemical yields (RCY) of three highly demanded radiopharmaceuticals obtained for one year with the new and replaced target.

Methodology

A high-power (>1.3 kW) target (BTI) for the production of [¹⁸F]F⁻ with capability to withstand up to 120 μA of beam current was installed on December 2022 by replacing the rotating target changer of the Eclipse HP cyclotron by a single target port. The insert of the BTI target is machined in Niobium with a cavity of 2.3 ml, volume similar to the replaced Eclipse target (Siemens), but the latter with an insert cavity of tantalum and a maximum current of 60 μA (660 W). Both targets use a Havar window. [¹⁸F]F⁻ was produced in both targets for the routine synthesis of [¹⁸F]FDG, [¹⁸F]PSMA-1007 and [¹⁸F]AlF-NOTA-Octreotide in a cassette based synthesizer (AiO, Trasis). The production yields of these radiopharmaceuticals using [¹⁸F]F⁻ from both targets were analysed for a one year period.

Results

The production yield of [¹⁸F]F⁻ was increased by twofold when running the BTI target at 120 μA, as compared with the yield of the Eclipse target, but for routine production the BTI target is run with a current of 100-110 μA. Table below summarizes the RCY and production yields of the evaluated radiopharmaceuticals.

	RCY* (%)		Average production yield (GBq)		Average [¹⁸ F]F ⁻ starting activity (GBq)	
	BTI	Eclipse	BTI	Eclipse	BTI	Eclipse
[¹⁸ F]FDG	79.3 ± 5.4 (n=381)	76.2 ± 7.5 (n=280)	127.9±28.4	82.9±27.4	196.0±41.4	132.6±41.8
[¹⁸ F]PSMA-1007	44.7 ± 7.9 (n=58)	47.7 ± 11.0 (n=44)	70.3±17.7	44.8±13.2	206.9±49.2	126.5±37.8

[¹⁸F]AIF- NOTA- Octreotide	22.4 ± 6.1 (n=29)	25.9 ± 6.6 (n=26)	32.7±10.5	23.3±7.4	183.4±34.4	115.9±16.3
--	----------------------	----------------------	-----------	----------	------------	------------

*Decay corrected.

Conclusions

There were no statistically significant differences in the RCYs of the evaluated radiopharmaceuticals when using of [¹⁸F]F- from the BTI and the Eclipse target, however the production yields significantly increased due to the higher current used in the BTI target, which is of great help to meet the high demand of the evaluated radiopharmaceuticals.

Perfusion scintigraphy in the study of myocardial viability: Results of the first study from a Mauritanian center

B. A. Horma^{1,3}, L. Zaabar^{2,4}

¹ Nuclear Medicine Department of the National Oncology Center, Nouakchott, Mauritania

² Nuclear Medicine Department, Salah Azaeiz Institute, Tunis, Tunisia

³ Faculty of Medicine of Nouakchott, Mauritania

⁴ Faculty of Medicine of Tunis, Tunis El-Manar University, Tunisia

Background

The Nuclear Medicine Department of Nouakchott was opened at the National Oncology Center in 2015. Myocardial scintigraphy with [^{99m}Tc]MIBI was introduced in 2020 and thanks to the involvement of several cardiology departments from several countries, the number continues to increase, we reached 45 examinations in 2023 between viability scintigraphy and ischemia research.

The aim of our study was to highlight our first results of evaluating the role of myocardial scintigraphy in myocardial viability.

Methodology

We conducted a retrospective study including 13 patients (10M and 3W, sex Ratio M/W=3.33), aged 35 to 81 years (Mean 56.6 years ±11.85). They were referred to us for a myocardial viability scintigraphy (MVS) with [^{99m}Tc]MIBI.

Results

6/13 patients had respectively 2 and 3 cardiovascular risk factors. Chest pain was present in 12/13 patients, mainly atypical (8/12). The electrocardiogram (ECG) was abnormal in all patients, including: myocardial infarction (5/13), ST+ (4/13) and ST- (4/13). Coronary angiography (CA) was performed in 10/13 patients, positive in all of them, located in the anterior interventricular artery (AIV) in 5 patients, the circumflex (Cx) in 2, the right coronary artery (RCA) in 1 patient and trivessels in 2 patients. MVS was normal (viability preserved in 7/13 (54%). For the other 6, it was localized at the AIV in 1 patient, RCA in 3, RCA+Cx and AIV+CX in 1 patient respectively. Left ventricular ejection fraction (LVEF) ranged from 25% to 53% (35.6%±8.9%), distributed as: <30%: 4 patients, 30-40%: 6 patients, 40-50%: 2 patients, >50%: 1 patient.

The comparison of MVS with ECG more frequently found an ECG (+) Vs MVS (-) discordance in 7/13 patients (54%). Comparison of MVS to CA found discordance in 6/10 (CA (+) Vs MVS (-). Elsewhere, for the 4 concordant (positive) MVS, the affected territories matched in 2 patients, were different in 1 patient, and for the last one there was an additional lesion. The comparison of MVS with the association of 2 positive parameters (chest pain and ECG+) was mainly in discordance (7/12). the comparison of MVS with the combination of 3 positive parameters (chest pain (+) + ECG (+) + CA (+) was also mainly in discordance (6/9). The correspondence between positive MVS and LVEF was negative in 3/4 patients with LVEF<30%; positive in 4/6 with LVEF between 30-40%, and negative in the patient with LVEF >50%.

In total, MVS was abnormal in 33% of patients, indicating non-viability of the downstream myocardial tissue and thus avoiding an unnecessary revascularization procedure.

Conclusion

Diagnostic value of MVS is robust in predicting functional recovery after revascularization since in our series, as in the literature, it avoided unnecessary revascularization in 33% of patients with non-viable myocardium. Our small experience with the isotopic study of myocardial viability should be continued while enriching it with other studies involving a larger number of patients.

Development of a Classification System for Drug Related Problems for Radiopharmaceutical Use

M. F. Othman¹, M. H. A. Rahim², N. Daud¹

¹ Universiti Teknologi Mara, Malaysia

² Malaysian Ministry of Health, Malaysia

Background

Radiopharmaceuticals played a pivotal role in modern medical diagnosis and treatment. However, their usage was associated with unique drug-related problems (DRPs) that necessitated a specialised approach to pharmaceutical care. These radiopharmaceutical-related problems encompassed aspects such as production, quality control, administration, and radiation, setting them apart from non-radiopharmaceutical DRPs. Existing classifications had failed to adequately address the distinct challenges and complexities posed by radiopharmaceutical, underscoring the need for an innovative solution.

Objectives

To develop a classification system that identified DRPs in patients undergoing radiopharmaceutical treatments.

Methodology

A DRPs classification system that had been systematically adapted and modified based on the development of the Pharmaceutical Care Network Europe (PCNE) framework, which consisted of: 1) Defining the DRPs to create the definition for radiopharmaceutical-related problems (RRPs); 2) Identifying RRP based on previous studies; 3) Classifying RRP into the classification to create new domains and subdomains in addition to describing the nature of radiopharmaceutical use; and 4) Validating the content of the classification with a panel of experts. A core team consisting of three pharmacists with nuclear medicine practice backgrounds and one nuclear medicine specialist evaluated the content of the modified PCNE classification. Then, face-to-face interviews with a questionnaire were conducted with an expert panel consisting of 10 practicing pharmacists from multidisciplinary settings and 1 nuclear medicine specialist to validate the first version of the RRP classification system were done. The expert panel provided feedback, ratings, and recommendations to upgrade the classification accordingly.

Results

Major modifications were made to the to the PCNE classification to produce the RRP classification with primary domains and subdomains to suit the radiopharmaceutical characteristics and radiopharmaceutical use process. The new classification system comprised five domains for Matters, four for Reasons, four for Actions, and two for Decisions. The system encompassed 14 grouped subdomains for Matters, 36 for Reasons, four for Actions, and four for Decisions. The percentage of overall agreement in the validation study was 76%. The percentage showed that the strength of agreement requiring further optimisation.

Conclusion

A classification system for DRPs related to radiopharmaceutical use was developed based on the PCNE classification. The validation studies demonstrated a strength of agreement for the overall developed classification, although further restructuring of the classification is required.

A Comparative Study of Methods Used for Size-Specific Dose Estimate (SSDE) of CT Scans

A. Abuhaimed¹, K. Almuqbil¹, A. Abanomy¹, Y. Alashban¹, C. Martin²

¹ King Abdulaziz City for Science and Technology, Saudi Arabia

² University of Glasgow, Scotland

Background

Size-specific dose estimate (SSDE) of CT scans has become an essential dose index that is utilized in many clinics around the world to estimate and optimize doses of CT patients. To assess the SSDE of a patient, the body size is required to be determined accurately. Several methods are suggested, with the method based on attenuation of the scan area known as water-equivalent diameter (D_w) being the recommended method by the American Association of Physicists in Medicine (AAPM). However, several practical challenges make the assessment of D_w difficult at some clinics. Recently, a method based on using electron densities of the scan area tissues has been suggested. This work aims to investigate this method to determine the body size.

Methodology

The electron density method is based on measuring the length of each tissue in the lateral and the anterior-posterior directions at the center of the scan area. Each length is, then, multiplied by the corresponding electron density, from which the size of the patient's body is determined. Images of 350 adult and paediatric patients who underwent CT body scans were collected retrospectively from a local hospital. The images were analysed using a MATLAB code to measure the body size of each patient enrolled in the study. The body sizes were assessed by the code using the D_w and the electron density methods. Two different ways were used for the electron density method: (1) by using the tissue lengths and electron densities in the lateral and the anterior-posterior directions, and (2) by assuming that minimal tissue variations were present in the anterior-posterior direction, thus, the length in this direction was measured without applying the electron densities, and only the tissue lengths and electron densities were considered for the lateral direction.

Results

The body sizes of the patients measured by considering electron densities of the lateral and the anterior-posterior directions were in the ranges of (12.6 – 32.0 cm), (13.1 – 39.0 cm), (12.3 – 36.9 cm), and (14.6 – 39.1 cm) for chest, abdomen-pelvis, and pelvis, and CAP, respectively. These ranges did not differ significantly from those determined by using only electron densities of the lateral direction, which were (12.4 – 31.0 cm), (12.5 – 38.7 cm), (12.0 – 36.3 cm), and (14.3 – 38.0 cm), respectively. By comparing the ranges determined by the electron density method to those of the D_w method, it has been found that the use of electron densities in the lateral direction provided a better assessment of D_w for most cases as compared to those based on the two directions.

Conclusion

The results show that the use of electron densities of the scan area tissues could be utilized as an alternative method to measure the patient body size for SSDE if tools required for the D_w method are

not available. The comparisons between the two ways of the electron density method revealed that the use of electron densities of the lateral direction would give a reasonable accuracy for the body size.

Improving research infrastructure of PET imaging by using straightforward Gallium-68 kit radiopharmaceutical preparation

T. Ebenhan^{1,2,3}, J. Suthiram³, C. Davis^{2,4}, B. Marjanovic-Painter³, J. R. Zeevaart^{1,3,4}, M. M. Sathekge^{2,4}

¹University of Pretoria, Pretoria, South Africa

²Nuclear Medicine Research Infrastructure (NuMeRI), NPC, Pretoria, South Africa

³Necsa, Radiochemistry, Pelindaba, South Africa

⁴Nuclear Medicine and Steve Biko Academic Hospital, Pretoria, South Africa

Background

Radiochemistry has made tremendous impact in operations for Nuclear Medicine by developing user-friendly strategies that involve the straightforward compounding of radiopharmaceuticals with technetium-99m for SPECT imaging. This provided a improved infrastructure and safe-to-inject radiopharmaceuticals from radiosynthesis kit starting material that allowed for a facile radiopharmaceutical production and multi-dose administrations into patients. The emergence of generator produced gallium-68 has sparked renewed interest in the latter kit production approach, but this time for PET imaging. It is plausible that Ga-68 radiopharmaceuticals can be prepared from kits containing lyophilized starting material for “shake-and-bake” radiolabeling. Both Necsa and the Nuclear Medicine Department at Steve Biko Academic lead this project to develop various kits for an improved Ga-68-PET imaging workflow.

Methodology

Kit material was developed and tested in-house (kits batches containing buffer and ligand in the same vial). Straightforward use of fractionated Ga-68 eluate was tested over time. The parameters per kit radiosynthesis were tailored for each compound (see. Table 1). ITLC and HPLC radioanalysis were performed for product quality assurance. The kit performance and robustness were documented (pH, dose number and yield, purity, critical parameter, trends) for each Ga-68-radiopharmaceutical.

Results

Optimization of radiolabeling parameters led to Ga-68-radiopharmaceuticals with >95% RCP, quantitative labelling efficiency at lower temperatures (NODAGA-conjugated compounds) or after max. 15 min at 95 degrees Celsius incubation (PSMA-11, DOTA-pentixafor, NOTA-UBI29-41). Minor radiolabeling inconsistencies occurred with DOTA-substance-P and DOTA-TATE, mainly at times of prolonged generator use (quality of eluted Ga-68-activity). Table 1 summarized the main application option based on the current status of the kit development – imaging of infection (UBI) as well as cancer staging, recurrence, and monitoring of radiotheranostic efficacy were successfully performed in different patient population of varying sizes. Kit preparation all warranted expected dose numbers, improved radioanalytical product quality and radiolabeling robustness over the lifespan of the kit batches.

Table 1: Overview of Ga-68 radiolabeling kits developed in South Africa

Ga-68 radiopharmaceutical	Research Status	Research study size	RCY (%)
DOTA-pentixafor	radiopharmaceutical development	Not tested	69 – 90%
DOTA-substance-P	ready for clinics	Not tested	77 – 94%
NODAGA-zoledronate	ready for clinics	patient case series	82 – 93%
NODAGA-c(RGDyK)	exploratory / FIH	small patient population (>50)	79 – 93%
NOTA-UBI29-41 [#]	exploratory / FIH	small patient population (>50)	76 – 93%
DOTA-TATE	clinical routine	large patient population (>100)	89 – 97%
HBED-PSMA-11	clinical routine	high-throughput patient population (>1000)	90 – 98%

Footnotes: FIH: first-in-human, # tracer suggested for imaging of infection.

Conclusion

A successful South African initiative featuring seven different kit preparations is presented allowing facile support of radiotheranostics and imaging of infection. Except for Ga-68-HBED-PSMA-11 and Ga-68-DOTA-TATE, kit performances must be still tested for larger research patient populations.

In pursuit of an appropriate use criteria of using [¹⁸F]FES PET/CT in the management of ER positive breast cancer: a work in progress in a tertiary care cancer institute in India

P. Choudhury, S. Chowdhury, M. Gupta, R. Kumar, V. Zamre

Rajiv Gandhi Cancer Institute & Research Centre Delhi, India

Background

Oestrogen receptor (ER) is highly expressed in 70-80% of breast malignancies. ER expression or its absence plays a central role in the oncogenesis of breast cancer (BC) and is both prognostic and predictive biomarker. Molecular imaging with [¹⁸F]Fluoroestradiol ([¹⁸F]FES) positron emission tomography (PET) computed tomography (CT) targets oestrogen receptor and may have a higher incremental value in guiding management by increasing specificity.

Methodology

We enrolled 37 female and 1 male breast cancer patient as a part of an ongoing prospective study and performed both [¹⁸F]FDG and [¹⁸F]FES within 1 week. Whole-body [¹⁸F]FDG and [¹⁸F]FES study was performed by the standard protocol from base of skull to mid-thigh. In addition, a regional image of the breasts was performed in prone position by the hanging technique (device supplied by IAEA as a part of another CRP). The study was approved by the scientific committee (Res/SCM/53/2022/67) and the institutional review board IRB (RGCIRC/IRB-BHR/112/2022) of the institute. Lesion detection sensitivity was compared for a total number of lesions, excluding hepatic lesions by McNemar test. [¹⁸F]FES PET/CT was taken as reference in case of indeterminate lesions. The incremental value was reported by identifying FES exclusive lesions. Spearman rank test was used to co-relate ER expression value and maximum standardized uptake value (SUV_{max}).

Results

38 ER positive breast cancer patients with 312 lesions were analysed. 247 lesions were detected by FDG. FES detected 150 lesions. Number of lesions seen only with FDG was 150 and with FES was 78. The sensitivity of FES was better when hepatic lesions were excluded. Overall FES impacted 20% of patient management. FDG has better sensitivity than FES which depends on the percentage of ER expression and guides management with better lesion characterization. This is especially true for characterizing mediastinal lymph nodes which are commonly FDG positive due to granulomatous involvement especially in the Asian subcontinent. FES can also detect the level of hormonal suppression during treatment and can better guide management and can appear as discordant findings in FDG and FES studies.

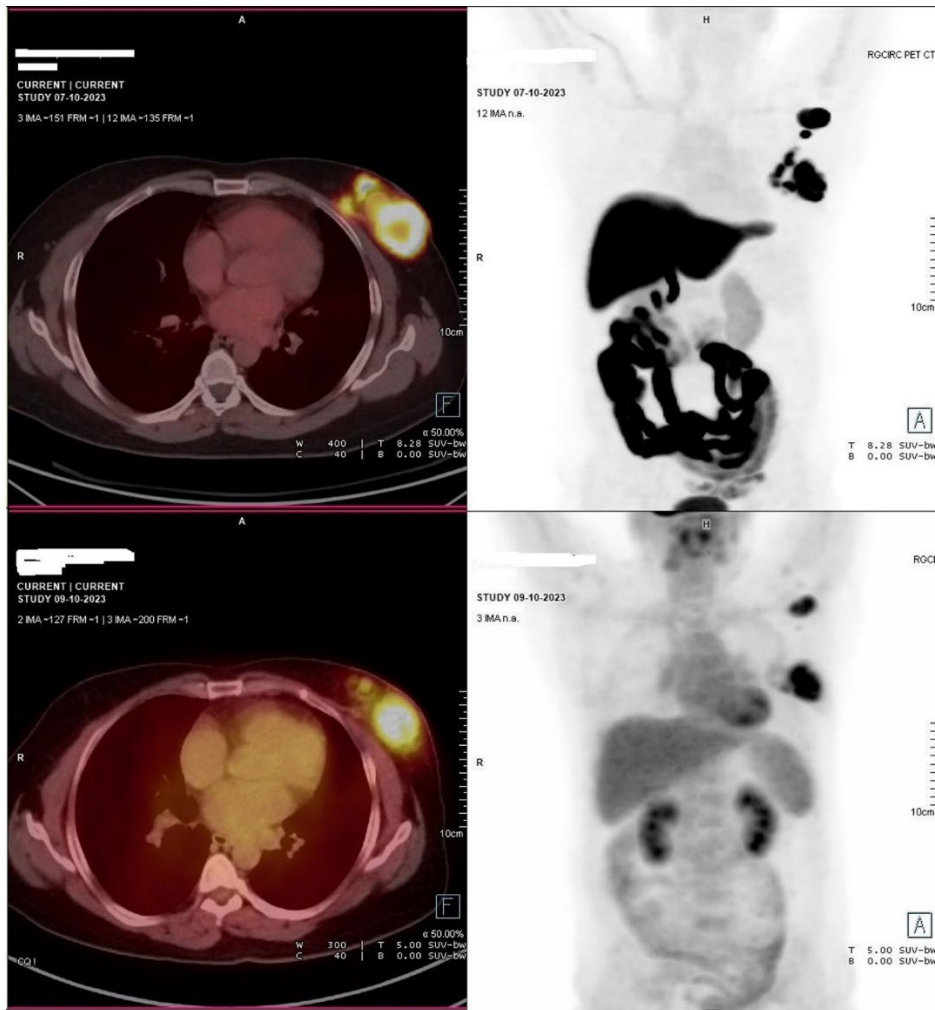


Figure 1: A 50-year-old case of invasive breast carcinoma on the left side with axillary lymphnodal metastasis. ER=100% expression: strong. $[^{18}\text{F}]$ FES scan shows FES avid breast lesion and axillary lymph nodes, more in avidity and number than the $[^{18}\text{F}]$ FDG study.

Conclusion

We conclude that as a proof of concept, at this point of time, a dual tracer imaging in breast cancer will be helpful in characterization of indeterminate lesions, detection of heterogeneity in ER expression in metastatic lesions and guide adequacy of hormonal treatment in breast cancer.

Development of Samarium-153 Loaded Radiotracer for Gamma Scintigraphy of Whole Gastric-Intestinal Transit Study

Y. H. Wong¹, A. Kasbollah², M. N. B. M. Shah³, B. J. J. Abdullah¹, C. H. Yeong¹

¹School of Medicine, Faculty of Health and Medical Sciences, Taylor's University, 47500 Subang Jaya, Selangor

²Malaysian Nuclear Agency, 43000 Kajang, Selangor, Malaysia

³Department of Biomedical Imaging, University of Malaya Medical Centre, 59100 Kuala Lumpur, Malaysia

Background

Constipation is affecting a quarter of human population at any one time in all age groups. However, a proper gamma scintigraphic study of whole gastrointestinal (GI) transit is rarely performed in Malaysia due to the lack of suitable radiopharmaceutical. Hence, this study was undertaken to develop a suitable radiotracer formulation for gamma scintigraphy study of whole GI transit.

Methodology

Firstly, non-radioactive samarium oxide ($^{152}\text{Sm}_2\text{O}_3$, 5%, w/v) was incorporated into biocompatible polystyrene (PS) through solvent evaporation technique, producing $^{152}\text{Sm}_2\text{O}_3$ -loaded radiotracer of 600–800 μm . The formulation was then activated in a nuclear flux of $5.0 \times 10^{12} \text{ n.cm}^{-2}.\text{s}^{-1}$ for 5 minutes to produce radioactive ^{153}Sm ($E\gamma = 103 \text{ keV}$, $E\beta_{\text{max}} = 807.6 \text{ keV}$, $t_{1/2} = 46.3 \text{ hours}$). Physicochemical characterization, gamma spectrometry and in-vitro retention efficiency in simulated gastric fluid (SGF) and simulated intestinal fluid (SIF) were carried out to study the properties and stability of the radiotracer before and after neutron activation. Scanning electron microscope (SEM) and particle size analysis showed that the size, shape and surface morphology of the particles remained the same after neutron activation.

Results

The synthesized ^{153}Sm -loaded PS radiotracer achieved specific activity of $57.20 \pm 1.96 \text{ MBq.g}^{-1}$ after 48 hours. According to gamma spectrometry, no long half-life radioimpurities was found in the samples. The physicochemical properties of the ^{153}Sm -loaded PS radiotracer remained the same after neutron activation. The ^{153}Sm -loaded PS radiotracer achieved a retention efficiency of more than 95% in both SGF and SIF over 120 hours.

Conclusion

In conclusion, a biocompatible ^{153}Sm -microspheres radiotracer has been successfully developed for whole GI transit study. The proposed formulation is relatively cheaper, easier to be produced and reduces radiation exposure to staff compared to the standard ^{111}In formulation. Further studies are needed to validate the in-vivo performance of the formulation for clinical applications.

Keywords: GI motility and transit, Samarium-153, Radiotracer, Gamma Scintigraphy

White blood cell scintigraphy as a possible alternative to arthrocentesis in patients with suspected periprosthetic infection of the knee

R. M. A. Amorese, E. Noriega-Álvarez, J. C. R. Gómez, F. J. P. Pardo, M. D. L. N. Sicilia Pozo, M. D. P. Talavera Rubio, V. M. P. García

University Hospital of Guadalajara, Spain

Objectives

To analyse whether ^{99m}Tc-HMPAO- white blood cell (WBC) scintigraphy can be an alternative to avoid arthrocentesis (ATC) in patients with suspected periprosthetic knee infection (PKI).

Methodology

Retrospective study of patients (p) with suspected PKI referred to the nuclear medicine service between January/2017 and May/2022. All patients underwent planar GLM imaging at 30 minutes p.i., at four hours p.i. and the latest at eight hours p.i. (all with time decay corrected acquisition), as well as tomographic images (SPECT/CT) at 8h. Any WBC scintigraphy with a progressive increase in the intensity of leukocyte uptake was considered positive and negative in the absence or progressive decrease of the same. WBC results were compared with the final diagnosis with ATC to determine sensitivity, specificity, accuracy and positive/negative predictive values of WBC, as well as kappa index.

Results

We analysed 34 patients (16 women, mean age 71 years) with knee prostheses who underwent WBC and ATC. The final diagnosis showed PKI in 14 patients and ruled it out in 20p. On the other hand, GLM was positive in 11p and negative in 23 patients (3 patients were false negatives, although imaging could not be performed at 8 hours). Sensitivity: 78.6%; specificity: 100%; positive predictive value: 100%; negative predictive value: 87% and diagnostic accuracy: 91.2%. Comparing the final diagnosis with GLM, considerable agreement was obtained with kappa index = 0.812 ($p < 0.0001$) and $\chi^2 = 23.23$ ($p < 0.0001$).

Conclusions

WBC scintigraphy's high specificity, positive predictive value and diagnostic accuracy denote its value as a non-invasive technique to confirm PKI, representing a reliable alternative to an invasive procedure such as the ATC. However, prospective studies with a larger sample size are required.

¹⁷⁷Lu-PSMA first successful therapy performed in East Africa: A case report from Mulago National Referral Hospital, Kampala, Uganda

R. E. A. Kuru¹, J. M. Sebikali², S. Sibiya³

¹ Mulago National Referral Hospital, Kampala

² Mbarara University of Science and Technology, Mbarara, Uganda

³ NTP Radioisotopes SOC Ltd, Uganda

Background

¹⁷⁷Lu-PSMA radioligand therapy (RLT) is an important form of treatment for prostate cancer (PCa) patients. Its availability is predominantly in resource rich and adequately resourced and (equipment) established regions/ or countries unlike the east African region which is resource and equipment constrained.

Case Report

A 69-year-old man in 2015 with total PSA (TPSA)=75ng/mL was diagnosed with adenocarcinoma prostate, Gleason 7 (4+3) following prostate biopsy. On 17th November 2015, a ^{99m}Tc-MDP bone scan (whole body) done showed no bone metastases. He then underwent a robotic radical prostatectomy with good recovery post-surgery. Histology report of the post-surgical prostate tissue – adenocarcinoma prostate Gleason 9 (4+5) and circumferential margins involvement by tumour. He then had injection Zoladex and adjuvant external beam radical radiotherapy (EBRT) to the pelvis. Since 2016 TPSA had been stable below 0.2 ng/mL until November 2022 when TPSA had increased to 0.61ng/ml, doubling in just 3 months in keeping with biochemical recurrence. A ⁶⁸Ga-PSMA PET/CT scan performed showed ⁶⁸Ga-PSMA avid prostate cancer metastases in infra and supradiaphragmatic lymph nodes.

Therapy and Imaging

Following the PET/CT study and report in March 2023 as well as consideration of the therapy options, the patient was treated successfully with ¹⁷⁷Lu-DOTA-iPSMA 9-months (delayed) later. The procedure was conducted in the nuclear medicine department of Mulago national referral hospital, Kampala, Uganda by a multidisciplinary team that comprised of Ugandans and a South African. Planar and SPECT images post-therapy were obtained using Mediso Any scan® at 6- and 24-hours' time points to evaluate ¹⁷⁷Lu-DOTA-iPSMA uptake and for dosimetry purpose. The patient was discharged after the 24 hours imaging with a radiation of 4.0 μSv/hour at 1-metre distance.

Conclusion

¹⁷⁷Lu-PSMA RLT is an important treatment option for prostate cancer patients. However, its access is very limited in resource limited/constrained areas. Our case is an excellent example of how RLT can be rolled-out/made available to patients who qualify and need this form of treatment among prostate cancer patients in resource constrained regions like Uganda.

Keywords: Radioligand therapy (RLT), ¹⁷⁷Lu: Lutetium-177, Prostate specific membrane antigen (PSMA), Prostate cancer, East Africa, Uganda

Aggressive Unusual Pleural Metastasis in a 35-Year-Old Female with Osteosarcoma of the Right Tibia

J. A. Haque, A. Akhter, S. Sharmin

Institute of Nuclear Medicine and Allied Sciences, Dhaka, Bangladesh Atomic Energy Commission, Bangladesh

Background

Osteosarcoma, a primary malignant tumour of the bone, commonly metastasizes to the lungs, but pleural involvement is exceptionally rare. This rarity poses unique diagnostic challenges due to atypical presentations and potential misinterpretations of imaging and cytological findings.

Case Report

A 35-year-old female with a history of osteosarcoma of the right tibia underwent two cycles of chemotherapy followed by above-knee amputation and subsequent right hip disarticulation, though documentation was not provided. Despite discontinuing treatment, she presented five years later with respiratory distress and right hip pain. CT chest revealed a pleural-based mass in the right lung field with associated calcified plaques. Planar bone scan demonstrated abnormally increased radiotracer uptake in the right chest, with intense focal uptake at the lower zone. Regional SPECT CT revealed a large lobulated solid mass occupying most of the right lung, with a thick rim of calcifications showing intense radiotracer uptake. Fine-needle aspiration cytology (FNAC) initially yielded nonspecific chronic pleuritis without malignant cells, potentially due to inadequate sampling.

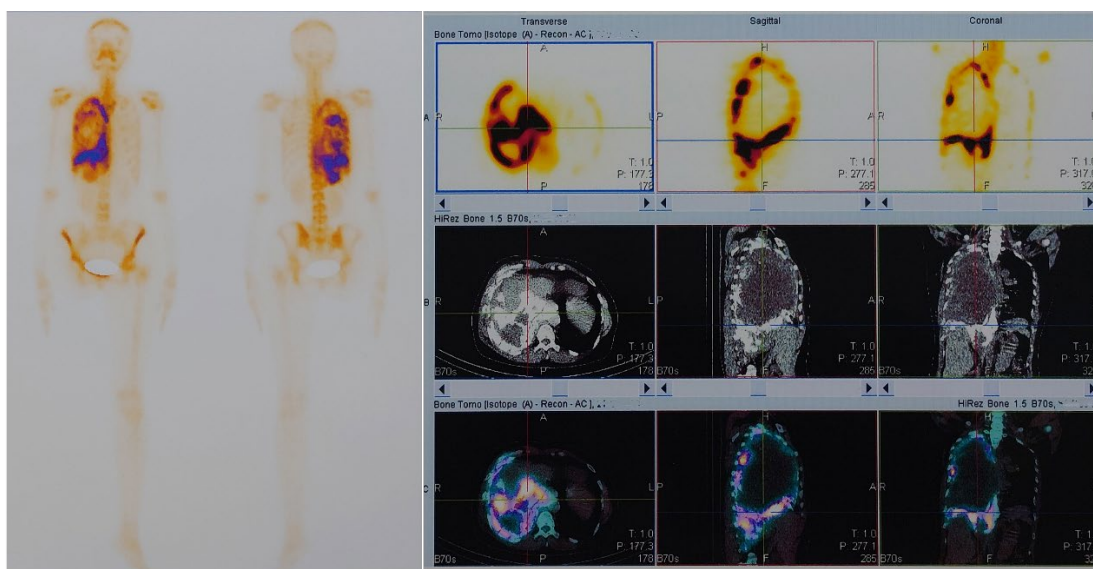


Figure: Planar bone scan and Chest SPECT CT revealing pleural based calcified mass with intense ^{99m}Tc -MDP accumulation.

Conclusion

This case underscores the rarity of pleural metastasis in osteosarcoma and the diagnostic challenges it presents. Clinicians should maintain a high suspicion for metastatic disease in patients with a history of

osteosarcoma and respiratory symptoms. Comprehensive evaluation, including histopathological examination and correlation with imaging studies, is crucial for accurate diagnosis and management. Further research is needed to understand the mechanisms underlying the metastatic spread of osteosarcoma to unusual sites such as the pleura.

Peritoneal carcinomatosis from a recurrent retroperitoneal malignant peripheral nerve sheath tumour revealed on FDG PET/CT

K. B. Ahmed, H. Noomen, W. Amouri, S. Charfeddine, K. Chtourou

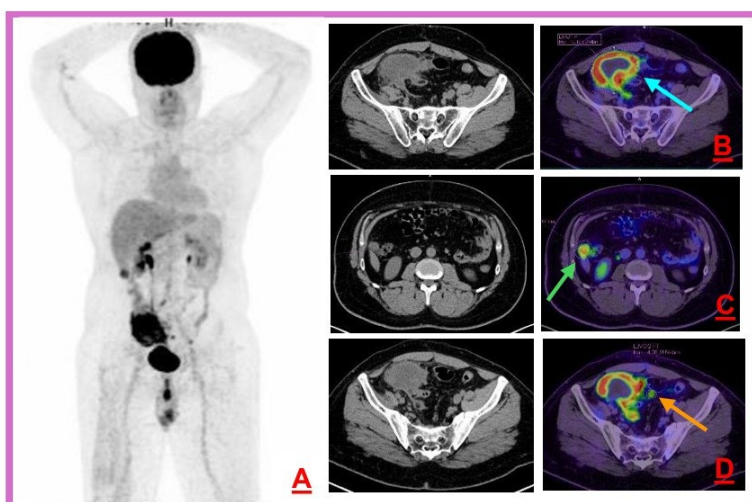
Nuclear Medicine Department, Habib Bourguiba Hospital, SFAX, Tunisia

Background

Malignant peripheral nerve sheath tumours (MPNSTs) are rare, arising from a peripheral nerve or in extraneural soft tissue which shows high metastatic potential and poor prognosis. MPNSTs are aggressive soft tissue sarcomas (STS), accounting for 2–3% of all STS. The term MPNST replaces many previously used names including malignant schwannoma, neurofibrosarcoma and neurogenic sarcoma. They can arise de-novo or through malignant transformation in neurofibromatosis (NF-1) syndrom.

Case Report

Here we report the case of 28-year-old male patient, with no previous medical history, diagnosed in January 2023 with retroperitoneal right-sided paravertebral MPNST at L4-L5. He was treated by surgery followed by chemotherapy and radiotherapy. Six months later, on a follow-up CT scan, a large peripherally enhancing collection was found in the right iliac fossa. A relapse of his tumour was then advanced. For a restaging aim, a 18 FDG PET/CT was therefore requested. The exam was performed on a PET/CT Siemens Biograph-64 after 6 hours of fasting and 60 minutes after injection of 8 mCi of 18 FDG. The right iliac fossa collection showed an intensely and heterogeneously hypermetabolic wall (SuvLbmmax=10.2). In addition, hypermetabolic subhepatic and mesenteric nodules were identified (SuvLbmmax=4.2), suggestive of peritoneal carcinosis. The patient underwent further surgery, and the anatomicopathological examination confirmed local and peritoneal recurrence of his high grade MPNST.



18 FDG PET/CT of a 28-year-old male patient diagnosed with recurrent retroperitoneal malignant peripheral nerve sheath MPNST (A) and axial pelvic image (B) showing hypermetabolic wall of a collection located in the right iliac fossa (blue arrow) while the other axial images (C+D) showed a hypermetabolic subhepatic nodule (Green arrow) associated to another hypermetabolic mesenteric nodule (orange arrow) suggestive of peritoneal carcinosis.

Conclusion

MPNSTs are soft-tissue neoplasms that usually arise from the peripheral nerves, mostly from the major nerve trunks, such as the sciatic nerve. Up to 60% of patients with MPNST present with recurrence after surgery, and 30% to 60% develop metastases. Accurate staging of MPNST is crucial for treatment planning and prognostic stratification. The current case demonstrates the importance of the additional information provided by the FDG PET/CT about unknown peritoneal metastases , thereby leading to an optimal therapeutic approach.

[⁶⁸Ga]CBP8-PET imaging of patients with TB as an early predictor of lung fibrosis- A preliminary analysis.

M. Vangu¹, S. Montesi², G. Bisson³, S. Auld⁴

¹ CM Johannesburg Academic Hospital, University of the Witwatersrand, South Africa

² Harvard University, Boston, MA, USA

³ University of Pennsylvania, Philadelphia, PA, USA

⁴ Emory University, Atlanta, GA, USA

Background

Tuberculosis (TB) causes pulmonary inflammation and damage that limits respiratory health well beyond treatment completion. Indeed, up to half of all TB survivors have long-term pulmonary impairment. Despite a growing awareness of the long-term sequelae of TB, there are no interventions known to treat or prevent post-TB lung disease (PTLD), largely because there is a critical knowledge gap with respect to the risk factors and pathological drivers of fibrosis in the lungs. Fibrosis also occurs in the context of pulmonary TB and can lead to PTLT, which is defined as respiratory impairment after TB cure. [⁶⁸Ga]CBP8 (Gallium-68 labelled collagen binding probe 8) is a molecular imaging probe, which selectively binds collagen type I. Collagen deposition is a pivotal event in several human conditions including fibrosis (lungs, liver and kidneys) and also in cardiovascular diseases. We aim to preliminarily estimate the variability of [⁶⁸Ga]CBP8-PET measurements in the lungs of adult patients being treated for pulmonary TB and correlate uptake with both high-resolution chest CT (HRCT) scans and the measured biological biomarkers as a predictor of lung fibrosis.

Methodology

This is an early analysis of a cross-sectional part of a long term longitudinal prospective study of individuals with pulmonary TB. We have so far enrolled 138 participants of whom, 39 underwent PET imaging with [⁶⁸Ga]CBP8 and 128 underwent HRCT. Sputum and plasma cytokines, including luminex analytes on limited samples as well as uptake on PET imaging were analysed. Attempt for lung segmentation on PET was done using an AI based theranostic tool for oncology as an extrapolation to measure both SUVs (max and mean) and the measures for burden of disease activity, both the metabolic lesion volume (MLV) and total lesion activity (TLA) as adjusted from oncology use.

Results

Preliminary data analysis shows a dominance of male gender (81%) participants. Collagen uptake is seen in lung lesions and cavities visualized on HRCT. Lower SUVs consistent with limited published literature was noted with median SUV_{max}=1.526 (median in healthy volunteers for SUV_{max}=0.48). Almost no collagen uptake seen in the unaffected lung fields. Higher levels of cytokines are noted in sputum as compared to plasma. HIV+ individuals showed a positive linear correction on measured cytokines (r=0.75, p=0.066) as opposed to HIV- individuals with a negative correlation (r=0.56, p=0.042).

Conclusion

PET activity in lung lesions translates collagen deposition that will be correlated with both long-term changes on HRCT and all measured biomarkers. The longitudinal results will confirm if early deposition

of collagen is an imaging marker to predict lung fibrosis following treatment of individuals with pulmonary TB. This will be assessed both visually and using the average SUVs as well as the volumetric metabolic parameters, namely the MLV and TLA.

Myocardial perfusion imaging evaluated by single photon emission tomography in post-COVID-19 patients without known coronary artery disease according to sex

A. P. Barragán, C. J. Hiciano, L. V. López

National Medical Center "November 20th" ISSSTE, Mexico

Background

Myocardial ischemia may contribute to morbidity and mortality in post-COVID-19 patients. After recovery, chest pain, shortness of breath, and fatigue may occur and be confused with symptoms of ischemic disease. Single-photon emission computed tomography (SPECT) is a non-invasive, useful diagnostic imaging technique.

Purpose

To evaluate myocardial perfusion SPECT (MP-SPECT) findings in a group of post-COVID-19 patients without known coronary artery disease (CAD), according to sex.

Methodology

The results of 106 rest-stress Tc99m mibi MP- SPECT from patients without known CAD, with symptoms of suspected ischemic heart disease and a history of COVID-19 lasting more than one month of evolution were evaluated retrospectively. The severity of COVID-19 disease, myocardial ischemia (mild, moderate, severe), and sex-related differences were analysed. Statistical analysis: frequencies and percentages, median and/or mean, chi2 test.

Results

Mean age 56 ± 14 years, 55% were men, 71% with > 2 cardiovascular risk factors (CVRF), 60% with dyspnoea and chest pain. Mild COVID-19 was the most common disease (61%) in each sex, followed by moderate (29%) and severe (9%). MP-SPECT: 52% with ischemia, 67% in men. Moderate ischemia (60%) was more frequent, both in men (62%) and women (56%). There is no significant difference between the severity of COVID-19 disease ($p= 0.94$) and ischemia ($p= 0.64$) with sex. Table 1.

Table 1: Baseline clinical characteristics of patients with COVID-19 according to sex. CVRF; cardiovascular risk factors, MP-SPECT; myocardial perfusion single positron computed tomography.

	Men 59 (55%)	Women 47 (55%)	Total 106
Age	56 ± 12	56 ± 14	56 ± 13
Cardiovascular Risk Factors (CVRF)			
Arterial Hypertension	34 (58%)	33 (68%)	67 (63%)
Dyslipidemia	28 (47%)	22 (45%)	50 (47%)
Diabetes Mellitus	23 (38%)	16 (33%)	39 (36%)
Smoking	10 (17%)	6 (13%)	16 (15%)
Obesity	21 (35%)	19 (40%)	(28%)
≥ 2 CVRF	43 (73%)	33 (68%)	76 (71%)
COVID-19			
COVID-19 mild	36 (61%)	29 (62%)	65 (61%)
COVID-19 moderate	17 (29%)	14 (30%)	31 (29%)
COVID-19 severe	6 (10%)	4 (8%)	10 (9%)
MP-SPECT			
Without ischemia	22 (43%)	29 (57%)	51 (48%)
With ischemia	37 (67%)	18 (33%)	55 (52%)
Mild ischemia	13 (35%)	7 (39%)	20 (36%)
Moderate ischemia	23 (62%)	10 (56%)	33 (60%)
Severe ischemia	1 (3%)	1 (5%)	2 (4%)

Conclusion

Abnormal MP-SPECT is present in more than half of patients with history of COVID-19, predominantly in men with moderate ischemia. Despite these findings, there were no significant differences related to COVID-19 and ischemia severity with sex. Ischemia could be influenced by CVRF and accelerated by COVID-19 disease. It is necessary to carry out a timely non-invasive diagnostic evaluation to reduce cardiovascular morbidity and mortality in this group of patients.

First use of Seracam[®] hybrid optical-gamma camera for sentinel lymph node imaging in breast cancer management

M. N. M. Musidek¹, N. A. Hao¹, M. N. M. Shah¹, Y. C. Hong², A. C. Perkins³

¹ Faculty of Medicine, Universiti Malaya, Kuala Lumpur, Malaysia

² School of Medicine, Faculty of Health and Medical Sciences, Taylor's University, Subang Jaya, Malaysia

³ Radiological Sciences, School of Medicine, University of Nottingham, United Kingdom

Background

Radioguided sentinel lymph node biopsy (SLNB) procedure is a vital procedure in breast cancer management. Standard care involves the use of dual technique (radiopharmaceutical and blue dye techniques) to localise the sentinel lymph node intraoperatively. The emergence of a hybrid optical-gamma camera (Seracam[®]) offers hybrid optical-gamma images at the patient bedside. This study aims to assess the imaging performance of Seracam[®] in breast cancer patients undergoing sentinel lymph node imaging procedure.

Methodology

The camera underwent characterisation and routine quality control tests in clinical settings. Eligible patients were recruited from the Nuclear Medicine Department, University Malaya Medical Centre. Following administration of the routine radiopharmaceutical at the primary tumour site with the activity either 37 MBq (1-day protocol) or 370 MBq (2-day protocol) of [^{99m}Tc]Tc-nanocolloid, standard nuclear medicine imaging such as planar lymphoscintigraphy or SPECT/CT were conducted. Seracam[®] acquired image data at the region of interest with a 10-minute acquisition time using a 1 mm diameter pinhole collimator. Image data from Seracam[®] were processed and analysed using ImageJ software v1.53e and compared with the image data produced by the standard nuclear medicine imaging.

Results

Quality control tests including system uniformity, spatial resolution, sensitivity, count rate capability and image fusion, met performance standards set by the manufacturer. Ten (10) breast cancer patients were recruited. Seracam[®] has demonstrated the capabilities of localising sentinel node preoperatively compared to standard imaging. Challenges arose in localising sentinel lymph nodes with limited radioactivity uptake and higher source-to-collimator distances.

Conclusion

Seracam[®] demonstrates feasibility for sentinel lymph node imaging procedure in breast cancer patients, providing real-time high-resolution hybrid optical-gamma images at patient bedside. Further investigations into optimising the device for sentinel lymph node biopsy procedure during surgical procedure is warranted.

Keywords: hybrid optical-gamma camera, sentinel lymph node, breast cancer

Usefulness of [18F]FDG PET/CT as a Prognosis Tool in Patients with Natural Killer Extranodal Nasal T-Cell Lymphoma, A Series of Cases

L. F. P. Escalante, M. I. R. Montecinos

Oncoservice, Bolivia

Background

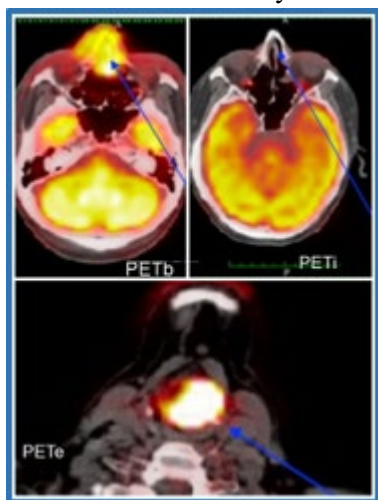
Nasal extranodal T/NK cell lymphoma constitutes 1.5% of cases of peripheral T cell lymphoma. The value of PET/CT-[18F]FDG in these cases is still under study. The cases of six patients affected by this lymphoma are presented in which the technique was applied to study its value as a prognosis tool.

Description

Case 1 and 2: 60-year-old woman, treated with multiple chemotherapy, comes for restaging. The study shows absence of lesions suggestive of lymphoproliferative activity. 29-year-old male with injury to the right nasal cavity, undergoing chemotherapy. Come to monitor response to treatment. The PET/CT study did not show lesions suggestive of malignancy. Both patients are monitored and remain free of disease.

Cases 3 and 4: 57-year-old male, presented for baseline PET/CT. A lesion is observed in the frontal region with SUVmax of 18.7 with extension to the nasal turbinates and multiple laterocervical lymphadenopathy. He receives treatment and returns for control where the lesion with lower metabolism is observed. He went to PET/CT at the end of treatment and showed a new epiglottic lesion with SUVmax of 20.1, supra- and infradiaphragmatic lymphadenopathy, and spinal infiltration. 33-year-old man treated with chemotherapy. A PET/CT was performed for restaging, which showed involvement of the left maxillary sinus with an SUVmax of 4.6. A 2nd PET/CT was performed, which showed an increase in SUVmax metabolism of 20 and new inguinal lymphadenopathy. Last PET/CT shows new lesions on the palate and supraclavicular lymphadenopathy. Both patients died.

Cases 5 and 6: A 79-year-old man, with baseline PET/CT showing a lesion in the left nasal cavity up to the soft palate with SUVmax of 19.2 with involvement of the left maxilla, in addition to multiple laterocervical and hiliomediastinal lymphadenopathy. 32-year-old man treated with chemotherapy and radiotherapy. PET/CT was performed for restaging, which showed a lesion in the oropharyngeal mucosa that extended to the larynx with SUVmax of 12.7. Both patients died.



Conclusion

PET/CT with [18F]FDG is a useful technique in the initial staging, restaging and prognosis of patients with extranodal nasal T/NK cell lymphoma. In the first cases that reported absence of disease, it was found that they currently remain stable and disease-free. The following two cases, which have more than three studies, allow us to evaluate the behaviour of the disease, given that each control showed the presence of new lesions and increased metabolism of the target lesions; Likewise, the PETi allowed modifications to be made in the treatment. The last two cases show us target lesions with significant avidity for the radiotracer and high SUVmax values that may be related to a poor prognosis. The four cases that presented an average SUVmax value of 18 died, so, according to the literature studied, it is concluded that the application of the technique is important during the different stages of the disease, as well as to define the prognosis of the patients. Patients.

Monte-Carlo-based SPECT/CT Reconstruction for Quantitative Cardiac Imaging

M. Ljungberg¹, L. Torres², P. Knoll³

¹ Medical Radiation Physics, Lund University, Sweden

² Nuclear Medicine Service, Center of Isotopes (CENTIS), Cuba

³ Medical Radiation Physics, International Atomic Energy Agency, Austria

Background

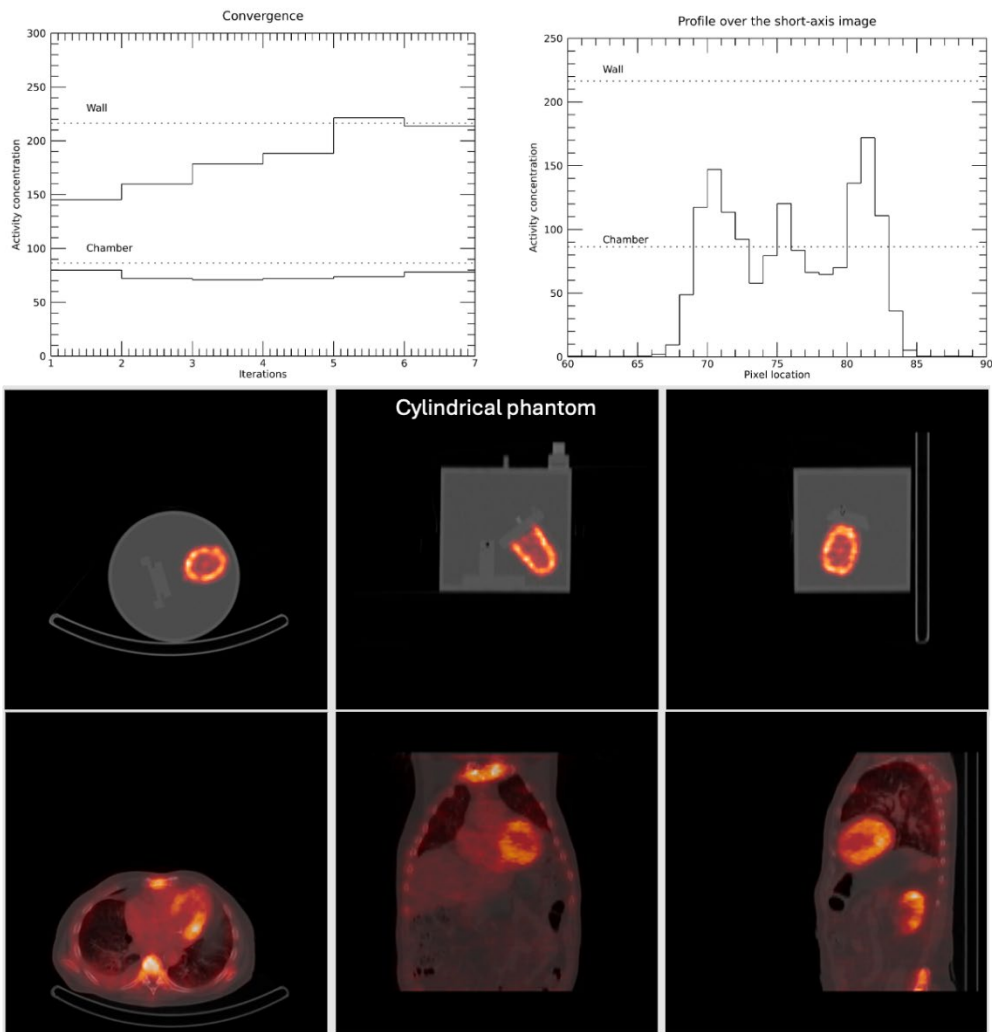
An iterative reconstruction method includes a model of the SPECT camera and patient to mimic the radiation transport. From an initial source estimate, calculated SPECT projections are compared to measured ones by the ratio of their voxel values and the ratios are reconstructed and used to update the estimate until the ratios are converging to unity. An accurate model is therefore very essential because if it is inaccurate when modelling the radiation transport, the iterative procedure will still find a converged solution but that will not be the correct distribution. Thus, the more accurate the model is, the better are SPECT images expected to be. Clinical systems often have approximations in their models due to practical reasons. One common way of estimating the contribution of scatter is to use scatter windows below the main photo window. However, the result will be scatter estimates based on different type of photons, scattered in wider angles as compared to those that have generated event in the photo window. An alternate is to model the system by a full Monte-Carlo-based procedure.

Methodology

The program SIMIND was used to create a full MC-based reconstruction program (Gustafsson 2018), where photons are followed explicitly in a CT-model of a patient towards the camera. This includes simulation of scatter photons relevant for the photo-peak window and scatter in the crystal. Results were validate by reconstructing a cardiac insert, filled with 216.4 MBq/ml in the wall and 86.3 MBq/ml in the chamber, located in a cylindrical water-phantom. SPECT/CT projections were acquired with an Mediso AnyScan (120 projections around 360°) and reconstructed with 4iters, 10subs to reorientated to short-axis images. Noise was regularized by a median-root prior using a beta-value of 0.3. Chamber activity concentration was obtained by averaging 9 voxels around the axial center of the chamber. Wall activity concentration was calculated by averaging voxels segmented from a threshold of 95% of maximum. In addition, an example of patient study administered with 99m-Tc was reconstructed using the same parameters.

Results

The activity concentration in wall and chamber for the phantom measurement were 222.6 and 84.7 kBq/mL, respectively, which compare well with measured activity of 216.4 and 86.3 kBq/mL. Phantom and patient images are show in the figure together with plots of convergence and activity distribution.



Conclusion

Results show that MC-based reconstructions produce estimates of activity concentration close to those measured by an activity meter and because the reconstruction is fully quantitative, no calibration factor obtained from a well-calibrated source are needed. This is because the model is accurate in the radiation transport and thereby internally preserve the relation between detected events (counts) and the underlying activity. Therefore, this MC-based reconstructions are applicable to other radionuclides of more complicated decay-schemes, such as ^{177}Lu , ^{131}I , ^{123}I and alpha-emitting radionuclides. Ongoing research include comparative studies of MC reconstruction with different SPECT/CT systems and quantification methods.

Tumour imaging study using radiolabelled quercetin: synthesis, biological distribution, and quality control in mice

M. H. Sanad^{1a,1b}, H. M. Eyssa⁴, F. A. Marzook^{1a}, N. M. El Bakary³, A. Massoud²

^{1a} Labeled Compounds Department, Hot Laboratories Center, Egyptian Atomic Energy Authority, Egypt

^{1b} Department of Physics and Engineering Mathematics, Faculty of Engineering, Ain Shams University, Egypt

² Nuclear Chemistry Department, Hot Labs Center, Egyptian Atomic Energy Authority, Egypt

³ Radiation Biology Department, National Center for Radiation Research and Technology, Egyptian Atomic Energy Authority, Egypt

⁴ Radiation Chemistry Department, National Center for Radiation Research and Technology (NCRRT), Egyptian Atomic Energy Authority, Egypt

Background

In this study, ^{99m}Tc-tricarbonyl was successfully employed as a precursor for the labelling of quercetin. The quantity of the quercetin, the pH of the solution, the reaction temperature, and lastly the impact of time on the formation of the complex all played a role in adjusting the radiolabeling reaction. At ideal conditions, the reaction's maximum yield was 98.5%. Using thin-layer chromatography (TLC) and high-performance liquid chromatography (HPLC), the radiochemical purity of the ^{99m}Tc-tricarbonyl quercetin complex was evaluated. Before being used in a biological study, the ^{99m}Tc-tricarbonyl quercetin complex's stability in plasma and saline was assessed. At various time intervals up to 3 hours, the biological distribution of the complex in Albino mice having solid tumour-bearing was examined. After 60 minutes post-injection, solid tumour cells began to accumulate a significant amount of ^{99m}Tc-tricarbonyl quercetin complex, according to the biological distribution study. Based on the Target/Non-Target ratio, it may be confirmed that it is possible to use the ^{99m}Tc-tricarbonyl quercetin combination in mice carrying solid tumours.

Keywords: Quercetin, [^{99m}Tc]tricarbonyl precursor, ⁴⁷⁷abelling, tumour, imaging

Two cases of different [99mTc] PYP scan phenotype of Danon disease

M. Kalnina, L. Bondare, A. Rudzitis, A. Strengē

ARS Nuclear Medicine Clinic, Latvia

Background

Hypertrophic cardiopathy in young adults is not common and requires a multidisciplinary approach. The LAMP2 gene mutation-based rare and fatal disease Danon disease is one of the differential diagnoses. It is a multisystemic condition with predominant involvement of the heart and is mostly presented in childhood. Males are believed to be typically more severely affected. Early identification and imaging play a crucial role in improving patient survival and facilitating genetic counselling. There is a lack of data on the possible different imaging phenotypes in which nuclear molecular imaging may play a role.

Case Presentation

We present two examples of young people, one male and one female, both diagnosed with Danon disease. These cases exhibit distinct clinical courses and show varying imaging results.

The 19-year-old male patient had a positive family history with three relatives who died at a young age. He has been suffering from hypertrophic cardiomyopathy since early childhood, and at the age of 16, he underwent ICD implantation. The patient did not report any complaints of shortness of breath, chest pain, palpitations, oedema, dizziness, loss of consciousness, or any other symptoms. The patient did not restrict their physical activities. During the physical examination, he had a high level of load tolerance. The patient's heart rhythm was normal, with a rate of 50 bpm. A systolic murmur was detected. He had an MRI, which revealed hypertrophied myocardial walls, with the LV wall measuring 19 mm. In addition, he underwent a PYP scan, which revealed a somewhat increased Grade 1 uptake in the LV walls with a H/CL ratio of 1.46.

The disease in a 22-year-old female patient exhibited a clinically more severe course. The patient was referred to the hospital multiple times. She experienced frequent periods of weariness, dyspnea, palpitations, and chest discomfort. These symptoms were a result of her previously diagnosed LV hypertrophy. A diagnosis of storage disease was considered following the use of multimodal imaging techniques. Although she had experienced heart failure since childhood, it was not until she reached young adulthood that the correct diagnosis was made, thanks to the availability of genetic testing in the country. She underwent medical therapy and subsequently obtained an LVAD implantation. She is currently on the waiting list to be considered as a candidate for a heart transplant. Throughout the progression of the disease, PYP scintigraphy showed a high level of uptake in the heart, which was more significant than the uptake in the ribs. The heart-to-contralateral (H/CL) ratio was measured at 1.52.

Danon disease might potentially give false-positive results in [99 mTc] PYP scans in individuals with amyloid hypertrophic cardiomyopathy. However, it is not commonly utilized for patients with vacuolar myopathies. Our findings indicate that the level of PYP uptake is associated with the progression of Danon illness and could potentially serve as a prognostic indicator for future patient outcomes. We recommend considering [99 mTc] PYP SPECT/CT scans for patients with myocardial storage disorders in their diagnostic pathway to explore their potential role, which may extend beyond current clinical practice.

Heterogeneity of PD-L1 expression: Correlation of immunohistochemical PD-L1 expression and genetic profile with [^{99m}Tc]Tc-iPD-L1 SPECT/CT in patients with metastatic non-small cell lung cancer

E. M. Sánchez, L. A. C. Miranda, G. Ferro-Flores, F. O. G. Perez, S. D. G. Rueda, I. S. Gallardo

Instituto Nacional de Cancerología (INCan), Mexico

Background

Lung cancer is one of the most frequently diagnosed neoplasms and is the leading cause of cancer death worldwide. This neoplasm modulates the immune response through the expression of PD-L1 and PD-L2, these ligands target the surface receptor of the programmed cell death protein (PD-1), which is expressed on the surface of T cells, B cells and NK cells. Recently, therapies with specific antibodies against PD-1 or PD-L1 have achieved significant clinical responses in non-small cell lung cancer patients. There are no immunohistochemical biomarkers with adequate prediction of selection and response because the expression of this receptor is dynamic and highly heterogeneous. Molecular imaging has helped to complement the study and characterization of neoplasms, recently it has been used a cyclic peptide inhibitor of PD-L1 (iPD-L1) radiolabelled. The aim of this pilot study is to analyze the correlation of [^{99m}Tc]Tc-iPD-L1 SPECT/CT with [¹⁸F]FDG PET/CT and the immunohistochemical expression of PD-L1 to demonstrate its high heterogeneity, in order to improve sampling and its possible role as a biomarker of selection and response to immunotherapy.

Methodology

We evaluated prospectively 10 patients with a diagnosis of histologically and immunohistochemistry confirmed non-small cell lung carcinoma, with a profile of oncogenic driver mutations, [¹⁸F]FDG PET/CT and [^{99m}Tc]Tc-iPD-L1 SPECT/CT. Performing a qualitative and semiquantitative analysis with volumetric parameters with the subsequent correlation between these, the immunohistochemistry results, and the tomography used to take the biopsy in order to verify that the sampling sites match with the uptake sites. We subsequently classify uptake patterns in peripheral, homogeneous and patchy.

Results

We include 7 woman and 3 men with mean age of 62 y/o (range 44 to 90). 8 patients had adenocarcinoma and 2 squamous cell carcinomas. All patients were stage IV, 50% (n=5) had EGFR mutation, 40% (n=4) were wild-type and 10% (n=1) ALK (+). MTV with FDG and iPD-L1 in the primary tumour showed a statistically significant correlation (r: 0.81, p=0.0038). Immunohistochemistry was performed with Sp263 assay of which 2 patients had positivity of 20%, 1 of 1% and the remaining patients (n=7) 0%. 9/10 patients had peripheral uptake pattern with iPD-L1 and 6/10 with FDG, 1/10 patients had patchy pattern with iPD-L1 and 0/10 with FDG and none had homogenous uptake pattern with iPD-L1 and 4/10 with FDG. In 5 patients, biopsy sites did not correlate with areas of iPD-L1 uptake due to a peripheral uptake pattern, explaining negative immunohistochemistry. There was no correlation between patterns or intensity of PD-L1 imaging with oncogenic driver mutation.

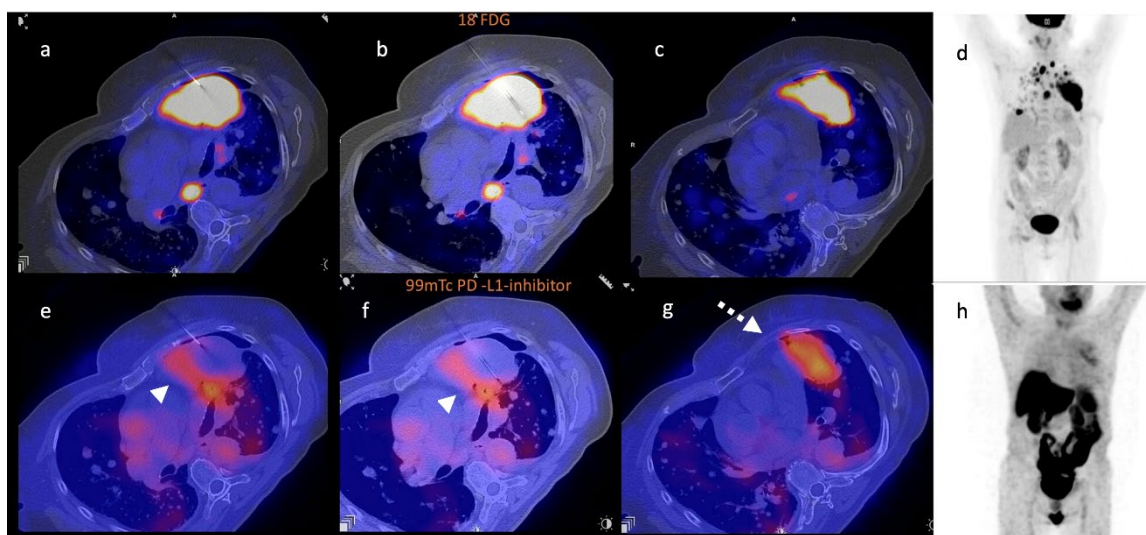


Figure 1: A 70-year-old woman diagnosed with poorly differentiated lung adenocarcinoma, mutated EGFR (exon 19 deletion) and IHC for PD-L1 with negative results. [^{18}F]FDG PET/CT guided biopsy with distal end of coaxial needle in solid and hypermetabolic portions of left lung tumour (a-b). Retrospective co-registration of the inhibitor directed at PD-L1 (technetium-99m SPECT/CT) with the CT used for the biopsy, in which an absence of radiotracer concentration is observed at the biopsy sites (e-f). The expression of PD-L1 is heterogenous, dynamic and is not necessarily related to hypermetabolism, in such a way that the low immunoreactivity could be related to a failure in sampling and not to the real behaviour of the tumour, because the portion with greater reactivity is found in the medial peripheral (head arrow) and caudal portion of the tumour (g) (dotted arrow).

Conclusion

Our results indicate a high intratumoural heterogeneity evaluated with [$^{99\text{m}}\text{Tc}$]Tc-iPD-L1 SPECT/CT that does not fully correlate with [^{18}F]FDG PET/CT, which is routinely used in biopsy guidance. There is evidence of clinical response to immunotherapy in patients with even 0% immunoreactivity; our preliminary findings may help explain this type of response and its possible discrepancy in biopsy sites. Therefore, this new imaging tool could adequately guide us in taking biopsy samples and be a potential diagnostic biomarker for selection and response to immunotherapy.

An unusual metastatic retroperitoneal mass from a recurrent basaloid squamous cell carcinoma of the larynx detected by [¹⁸F]FDG PET/CT

K. B. Ahmed, H. Noomen, W. Amouri, S. Charfeddine, K. Chtourou

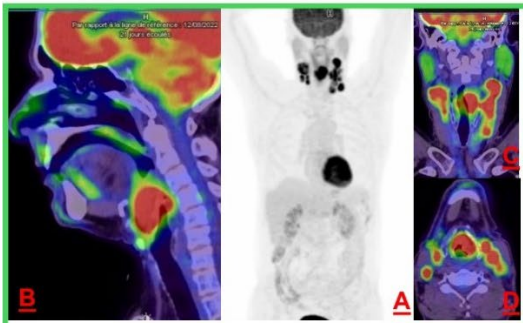
Nuclear Medicine Department, Habib Bourguiba Hospital, SFAX, Tunisia

Background

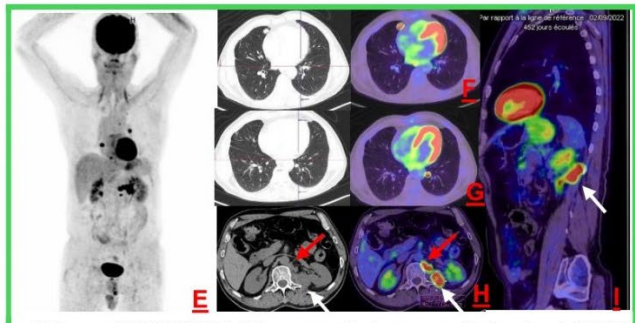
Basaloid squamous cell carcinoma (BSCC) is an aggressive subtype of squamous cell carcinoma. Laryngeal BSCC is extremely rare, accounting for less than 1 % of all laryngeal cancers. Recurrence of this tumour within the first year of the postoperative period is as high as 30%. The incidence of distant metastases in BSCC are scarce and when present, most commonly involve the lung. We hereby present an unusual case of recurrent laryngeal BSCC, metastatic to the lung and to the retroperitoneal pararenal region after 1 year of total laryngectomy followed by radical chemo-radiation to the head and neck region.

Case Report

Here we report the case of 63-year-old male patient, diagnosed in august 2022 with a basaloid squamous cell carcinoma nearby HPV-related carcinoma in situ of the larynx. He had an initial [¹⁸F]FDG PET/CT to evaluate the locoregional tumour extension and occult metastases. The exam was performed on a PET/CT siemens biograph-64 after 6 hours of fasting and 60 minutes after injection of 7 mci of [¹⁸F]FDG. The examination revealed intense hypermetabolism of the supraglottic mass reaching the base of the tongue (SUVLbm-max= 13.2) associated with bilateral hypermetabolic cervical lymph nodes (SUVLbm-max=15.6 in the left upper jugular region) and the rest of the whole body study was without abnormality. He was then treated by total laryngectomy followed by chemotherapy and radiotherapy. One year later, on a follow-up CT scan, suspicious pulmonary nodules were identified. A recurrence of his tumour was then advanced. For a restaging aim, a [¹⁸F]FDG PET/CT was therefore requested. The examination showed bilateral hypermetabolic pulmonary nodules in favour of their metastatic origin (SUVLbm-max= 9.2 in the S5 of the middle lobe). In addition, a retroperitoneal hypermetabolic mass in the left pararenal space (SUVLbm-max=7.7) associated with satellite latero-aortic nodes (SUVLbm-max= 8.2) were identified. The patient underwent a CT guided biopsy of this misrecognized mass, the anatomopathological results of which came back in favour of metastasis of his high-grade basaloid epidermoid carcinoma of the larynx simulating small-cell carcinoma.



Baseline 18F-FDG PET/CT MIP (A) of a 64-year-old male patient with hypermetabolic basaloid squamous cell carcinoma of the larynx seen in the sagittal image (B) with bilateral hypermetabolic cervical lymph node extension in the frontal (C) and axial (D) images



Follow-up 18F-FDG PET/CT of the same patient one year after treatment, MIP (E) showing hypermetabolic lung nodules visible on different levels of axial PET/CT and CT sections (F+G). An unknown hypermetabolic left-sided pararenal mass (white arrow) associated with satellite latero-aortic nodes (red arrow) was also revealed visible in the axial (H) and sagittal (I) CT and PET/CT images.

Conclusion

In laryngeal BSCC, [¹⁸F]FDG PET/CT is known to be superior to neck MRI in terms of achieving higher accuracy in detecting nodal metastasis. The overall incidence of distant metastases is reported to be around 8.5% in cancers of the larynx, with the lung being the most commonly affected site, followed by the bones and liver. Unusual sites of metastases such as skin, muscles, endocardium and kidney have been also described. To our knowledge, this case report highlights the first documented occurrence wherein [¹⁸F]FDG PET/CT played a pivotal role in the detection of an uncommon site of tumour spread, the retroperitoneal pararenal region. Previous studies have suggested that HPV-positive laryngeal BSCC presented a more disseminated metastatic pattern with the involvement of unusual anatomical locations of metastases. It is therefore crucial to increase awareness of similar cases, advocate for the implementation of whole-body molecular imaging to ensure early recognition of occult metastases and achieving favourable outcomes in patients affected by this challenging condition.

Analysis of false results in the staging of primary lung cancer using noninvasive CT and [18F] FDG PET

M. Kalnina, M. Gaidukova, K. Gulbe, J. Kedrova, A. Krams, R. Mikilps-Mikgelbs, G. Petersons, I. Silins

Background

The aim of this study was to find out how useful diagnostic computed tomography and [18F] FDG PET/CT are for finding early stages of non-small cell lung cancer in lymph nodes in the hilar and mediastinal regions at a single hospital.

Methodology

We conducted an analysis of the data from 104 patients, both male and female, who underwent surgical procedures to remove lung adenocarcinoma and squamous cell carcinoma. The age of the patients varied between 45 and 82 years. Before the surgery, the patients underwent staging using contrast-enhanced CT and [18F] FDG PET/CT. The scanning was conducted utilizing a cutting-edge digital detector PET/CT camera that had remarkably high sensitivity. The false-negative and false-positive outcomes were analysed separately, and their individual diagnostic contributions to each other were observed.

Results

The diagnostic CT had a sensitivity of 16.6%, a specificity of 88.8%, a positive predictive value of 33%, a negative predictive value of 76%, and an accuracy of 43.6%. The PET results were as follows: 33.3%, 81%, 37.5%, 89%, and 45.3%, respectively. Only 36% of patients displayed a discrepancy between their pathological N stage and the N staging determined by CT scans. Out of all these CT false negative patients, only one had a more precise N staging at PET. The findings concerning false negatives in CT and false negatives in FDG PET/CT were almost identical in the same group of patients for both procedures. These two modality-negative patients were all men with squamous cell carcinoma. An association was also discovered between CT and PET in false-positive lymph nodes.

Conclusion

Our data indicate that PET/CT has a remarkably high negative predictive value when used for the nodal staging of primary lung cancer. Still, our research has shown that the wrong N staging of primary lung cancer can happen even when using a very sensitive digital PET/CT detector and a contrast CT. This is true even when dealing with a highly metabolically active carcinoma. The fusion of diagnostic CT and [FDG] PET/CT data still demonstrates a significant proportion of false negative results. From our point of view, males with squamous cell carcinoma are at higher risk of two-modal false-negative results. They have the highest risk of a false negative N staging and need to go through extra invasive staging with mediastinoscopy or endobronchial ultrasound-guided transbronchial needle aspiration.

Experience in establishing the Zirconium-89 Infrastructure required for a South African Research Programme

T. Ebenhan, J. R. Zeevaart

¹University of Pretoria/Necsa/NuMeRI, South Africa

²Radiochemistry, The South African Nuclear Energy Corporation (Necsa), Pelindaba, 0240, South Africa

Background

Zirconium-89 has a relatively long half-life of 78.4 hours which suits explicit investigations that require an extended imaging window using PET. Whilst radiopharmaceutical development in South Africa would benefit from a sustainable supply of Zirconium-89, only import and no local production has occurred in the country to date. Through the involvement of the South African Nuclear Energy Corporation (Necsa) in the IAEA Coordinated Research Project concerning the production of Zirconium-89 and the development of Zirconium-89 radiopharmaceuticals, a significant benefit for pioneering research can be expected. Therefore, a research portfolio of projects utilizing the supplied Zirconium-89 was proposed. We herein report on our experience in establishing the Zirconium-89 infrastructure specifically required for the South African research program (2018–2023) from and for Africa and beyond.

Methodology

This research development program comprises of four major projects: namely i) intellectual contribution to a basic infrastructure project allowing the prospective production of Zirconium-89 activity from solid target (from 2025), ii) the launch of more facile radiolabeling of blood elements, iii) inauguration of two relevant Zirconium-89-antibodies and promotion of their clinical availability for immune-PET of cancer, and iv) master radiolabeling of specific cells of different origin. Project design also included technical transfer or development of radiosynthesis protocols (varying degree of radiochemistry optimization involved).

Results

The new Nuclear Medicine Research Infrastructure featuring an 18 MeV cyclotron that will allow solid target production of Zirconium-89 is currently housed in a state-of-the-art research laboratory complex. As on demand, secure Zirconium-89 supply was supported by the IAEA, so far, a method was developed that does not require an incubation step for [⁸⁹Zr]Zr-Df-Bz-NCS complex formation which improved [⁸⁹Zr]-labelling of blood elements and also other cells by 45 min. RCY levels varied between 60-85%, but all had >95% purity. Preliminary labelling of other cells still requires protocol optimization (< 45% yield, low specific activity). Also, knowledge on antibody labelling (h-R3, HER2) was achieved using different chelation agents (DFO (*), DOTA), and testing route of tracer injection and resulting changes to biodistribution, to discover new opportunities for detection of abdominal cancer types. In addition, research activities were extended to new antibody labelling which yielded the novel prototype radiopharmaceutical [⁸⁹Zr]Zr-Pf-mAbF (preclinical assessment successfully completed) for prospective imaging malaria infected pathology.

Conclusion

Due to the latter described concerted efforts, significant impact was made in securing the basic supply of Zirconium-89 and relevant Zirconium-89 radiopharmaceuticals with relevance to the Sub-Saharan African continent. New collaborations are desired to foster further development needs demanded by the clinical setting in Nuclear Medicine. Such future collaboration and funding support for Zirconium-89 based research emerging in South Africa, with its unique patient population and disease focus, is expected to provide substantial innovation.



Added value of third reading on a double reading system in the final report of PET/CT studies in a Private Institution. Initial experience, benefits, and future

M. G. Gama Moreno¹, S. J. Anaya González², J. A. Castro Sánchez², B. Conde Castro, C. Galindo Sarco, A. P. Gaxiola Mascareño², M. C. Gutiérrez Rivera², D. J. Jimenez Arenas, A. K. Miranda Playas²

¹ Telerad Salud Digna A.C., Mexico

² Unidad PET/CT Facultad de Medicina, Universidad Nacional Autónoma de México, Mexico

³ Centro de Monitoreo Clínico Telerad Salud Digna A.C., Mexico
Investigación Imagenología, Mexico

Background

The final report of the PET/CT studies is the main means of communication between specialists or subspecialists in molecular imaging with the referring physician, and is part of the decision making for staging, treatment, evolution, and response to therapy. PET/CT study is one of the most complex techniques of molecular imaging in both anatomical and metabolic findings, requiring certain degree of expertise and knowledge in the area. The concept of double reading of studies varies among specialists. The arguments in favour are the reduction of errors and increasing the quality of the final report, against the fact that it consumes time, increases delivery times, and requires multiple resources, both human and technical.

Having a third reader in PET/CT studies can be helpful when there are discrepancies or conflicting findings. The third reader can evaluate the entire study and analyze specific disagreements to make a final decision on whether the reported findings are present or not. This approach can improve the quality of interpretation and help experts reach a consensus, which ultimately leads to better diagnostic quality in the report. As a result, the patient benefits, and there is a reduction in complaints from patients or medical colleagues. Additionally, this approach can increase knowledge and provide feedback to healthcare professionals in the field.

Objectives

- To illustrate how incorporating a third reader in the interpretation of PET/CT studies in a private institution can lead to a reduction in diagnostic errors, an improvement in the quality of the final report, and positive feedback between subspecialist physicians.
- To know how the use of a third reader in the interpretation of PET/CT studies can potentially decrease complaints from patients or referring physicians.

Methodology

The PET/CT studies were conducted according to international recommendations for the acquisition of positron emission tomography and computed tomography. Additionally, they were reviewed by a radiologist or nuclear medicine specialist to ensure quality control. The first and second readings of PET/CT are performed by a radiologist and a nuclear medicine specialist, respectively. The third reading is performed by a radiologist who specializes in PET/CT and occurs in two different situations. First, it is performed upon request in cases of discrepancies between the first two readers. Second, it is carried

out after the report has been completed by the first two readers to identify relevant findings that could have been missed before the final report is delivered to the patient.

Results

By analyzing the results of the study, we demonstrate that having a third reader can be a valuable tool in improving the accuracy of diagnostic findings. The process of having a third reader evaluate the study as a whole and specifically analyze discrepancies can lead to a more informed and accurate interpretation, which ultimately benefits the patient.

Conclusion

In conclusion, we hope that our study will provide evidence of the benefits of incorporating a third reader in PET/CT studies in private institutions and encourage healthcare professionals to consider this approach in their own practices.

Treatment of Differentiated thyroid cancer using Radioactive Iodine-131 in Mulago National Referral Hospital, Nuclear Medicine Department, Experiences and Challenges

E. A. Kuru Richard

Mulago National Referral Hospital, Nuclear Medicine Department, Uganda

Background

Uganda has one Nuclear Medicine Unit equipped with a Dual head SPECT gamma camera. With increasing prevalence of cancer diseases, the number of patients referred for cancer screening at the Nuclear Medicine Department has increased considerably. For optimal patient evaluation there is need to use both SPECT and PET/CT imaging. Unfortunately, in our setting, there is no PET/CT, therefore we only use SPECT gamma camera with [^{99m}Tc]MDP as a first line diagnostic tool for the exclusion of metastases as part of the investigation strategy in cancer patients referred for radionuclide imaging whereas assessment of Differentiated thyroid cancer(DTC) with Nuclear medicine techniques using Iodine-123 and-131 possess a big challenge due to the costs importing the radioisotopes.

According to IAEA-TEC Doc-1608, despite the thyroid nodules being common thyroid cancer is relatively rare with overall incidence of cancer in cold nodule being 5 to 15% and the annual incidence rate in different parts of the world ranges from 0.5 to 10 cases per 100,000 populations with the papillary thyroid cancer being the most type of the thyroid cancer.

However, challenges still exist in patient selection, pre-treatment thyroid stimulating hormone (TSH) stimulation, dose decision as well as in the treatment for Iodine-131 refractory DTC.

Objective

The aim of this case study was to present challenges and strategies on radioiodine treatment for differentiated thyroid cancer in Nuclear Medicine Department, Mulago national referral Hospital.

Methodology

All patients referred to the nuclear medicine department were assessed by the Nuclear medicine physician before scheduling for radioactive iodine-131 ablation.

A total of 10 patients were assessed. All the patients were performed diagnostic CT scans of the Head, Neck and Chest.

TSH were assayed in all the patients and other blood work ups too.

Results

Of the 10 patients 4 had TSH less than 0.1, 8 patients both diffuses Metastatic lung nodules and Neck Nodular involvement in the diagnostic CT scans.

Challenges

- ✓ Most of the patients had advanced thyroid cancer disease who could not undergo surgery hence needed Thyrogen 0.9mg injectables.
- ✓ We needed Thyrogen 0.9mg to raise the TSH levels which is not available in the country and those who obtained paid heavily for the costs.
- ✓ Some of the patients had comorbidities such as diabetes hence required steroids hence made the patients difficult to manage during treatment.

- ✓ Cost of radioactive iodine -131 is very high due to shipment costs most patients cannot afford.
- ✓ Follow ups are not easier as some of these patients once improved travelled back to rural areas with poor communications hence showed up after disease had reoccurred.

Conclusion

Thyroid cancer is present in the country, but its prevalence is currently unknown.

All cases with DTC who presented to the Nuclear Medicine department were in advanced stages.

Radioactive Iodine-131 is still the choice of treatment for DTC, however, most patients cannot afford the treatment.

Most of the patients treated had comorbidities however, they have undergone successful treatment.

GROSEM: Gradient Descent based OSEM, a new image reconstruction algorithm for non-linear projection models

E. Vijande, M. Namías

Fundación Centro Diagnóstico Nuclear, Argentina

Background

Image reconstruction is the processing step required to obtain the transaxial views of a ET or CT study from the measured projections. OSEM is one of the most frequently used reconstruction algorithms for nuclear medicine imaging. One of OSEM's limitations is that it needs a linear projection model for it to be able to apply the backprojection step in each iteration before updating the image estimate. To surpass this limitation, we propose a new OSEM inspired algorithm that performs the backprojection step implicitly via the minimization of a loss function with stochastic gradient descent and applying gaussian filtering to the gradient.

Methodology

Reconstructions with both OSEM and GROSEM were performed over the simulated projections of an already reconstructed PET/CT study. The used projection operator models the acquisition of a SPECT system. Both algorithms were tested using the same linear projection operator, which was also used to calculate the corresponding projections from the reference volume. Tests were done over a range of cases with different levels of Poisson noise and fixed resolution loss of FWHM [mm]= $5+0.02D$, with D being the distance from the source to the detector plane. Poisson noise simulation was done over scaled versions of the original images in order to test different noise levels.

Structural similarity index measure (SSIM) and mean squared error (MSE) between the reconstructions and the original volume were used as quantitative metrics of performance. All reconstructions were performed using 3 subsets and 30 iterations. Every noise case was evaluated over 50 samples and the Wilcoxon signed-rank test was employed for hypothesis testing.

Metrics were calculated for each of the 30 iterations of the reconstruction process and using as ROI the voxels which are inside of the patient's body. Algorithm comparison was done using only the iteration which achieved the best metric so as to compare the best results of each algorithm.

Results

For both SNR=25dB and SNR=15dB, OSEM achieved a higher SSIM ($p<0.001$) and a lower MSE ($p<0.001$) than GROSEM. While for SNR=10dB and SNR= 5dB, GROSEM achieved a higher SSIM ($p<0.001$) but also a higher MSE ($p<0.001$) than OSEM. Highest SSIM in OSEM was achieved at iterations 17, 5, 3, and 1, for SNR=25dB, 15dB, 10dB and 5dB respectively.

Convergence speed for GROSEM was slower with maximum SSIM achieved at iterations 30, 21-22, 15-16, 7-9 for the same noise scenarios. Five iterations after its minimum, MSE rose: 2.0-3.7% for GROSEM and 64.6-70.8% for OSEM with SNR=5dB. 3.4-4.2% for GROSEM and 23.4-27.3% for OSEM with SNR=10dB.

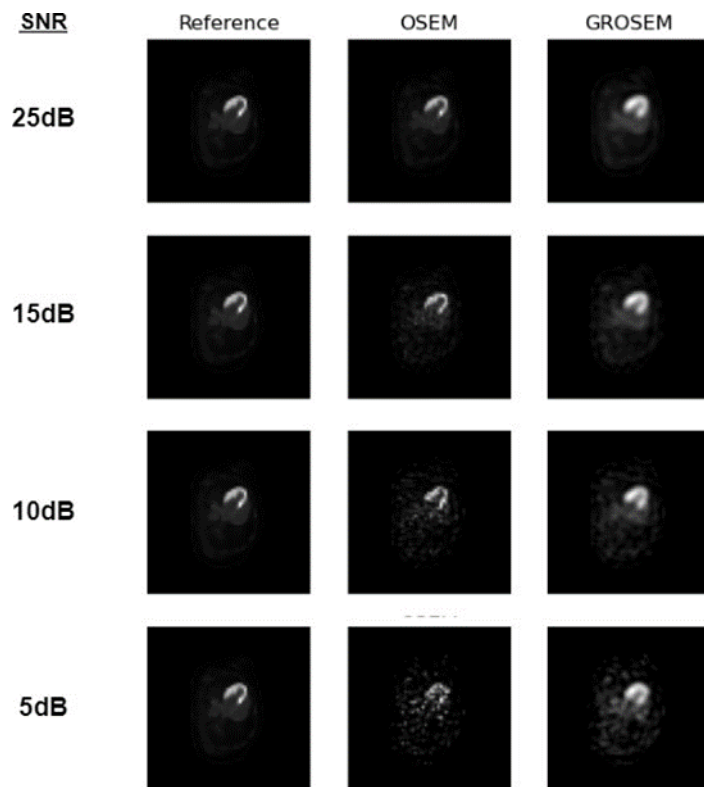


Figure 1: View of one of the heart slices for the different reconstruction methods at iteration 30. The reference taken as the true image (left), OSEM reconstruction (middle) and GROSEM reconstruction (right)

Conclusion

GROSEM could successfully perform the reconstruction of a real case PET/CT with simulated depth dependant resolution loss and different poisson noise scenarios while allowing for the possibility of a non-linear projector. OSEM seems to perform better than GROSEM in low noise scenarios ($SNR > 10dB$). In high noise scenarios ($SNR \leq 10dB$) GROSEM achieves smoother and less noisy images than OSEM, as shown in its higher SSIM, but at the price of lower resolution and higher MSE. Convergence for GROSEM was slower than OSEM but also suffered from less noise amplification.

Thyroid Papillary Microcarcinomas: Clinical Features, Prognosis and Survival in Moroccan patients

H. Tabitha, A. Guensi, K. Bendahou

Hassan II University, FMPC, Laboratory of Cellular and Molecular Inflammatory, Degenerative and Oncologic Pathophysiology, Morocco

Background

Papillary thyroid microcarcinoma (PMC) is defined as a variant of papillary carcinoma whose size is less than or equal to 1 cm. It generally has a good prognosis. However, even if the tumor is small, it can be very aggressive, leading patients to undergo more invasive treatment. This study aims to identify the clinicopathological characteristics, treatment modalities, prognosis, and survival of papillary microcarcinoma in Moroccan patients.

Methods

We conducted a retrospective analysis of patients diagnosed with thyroid cancer between 2004 and 2012 at the Department of Nuclear Medicine at Ibn Rochd Hospital Hassan II University. Clinicopathological data, including age, gender, familial history of thyroid cancer, mode of discovery, histological variants, tumor characteristics, metastatic status, treatment modalities, and survival outcomes, were collected and analyzed.

Results

The study included a total of 242 patients, with 79% aged less than 55 years old and 21% aged 55 or above. Gender distribution showed 92% female and 8% male with a sex ratio of female to male of 11.1. Regarding familial history of thyroid cancer, only 2% reported a positive history and none of our patients had a history of cervical irradiation. Fortuitous discovery of thyroid cancer was noted in 14% of cases and 86% of thyroid mass (72% a solitary nodule, 28% a multinodular goiter). All patients had undergone a total thyroidectomy. Among the tumor variants, the follicular variant was as frequent as the classical one each accounting for 50%. An undifferentiated component was shown in only 0.41%. Tumors encapsulated were found in 26% of cases. Multifocality was present in 7%, while vascular invasion was seen in 1.23%. Node involvement was present in 2.1% of cases. Metastasis at diagnosis was observed in only 0.41% (one patient, localization in the skull). The average of Thyroglobulin was 27.8 ng with maximum values ranging from 0.01 to 1954. Radioiodine therapy was indicated in 64% of patients. Complete remission was shown in 87%, recurrent disease in 3%, and bone and lung metastases in 1.65% each. Five-year and ten-year survival rates were respectively 97% and 95%. Eight patients died at the end of the study. Causes of death varied: 37.5% attributed to COVID-19, followed by bone and lung metastasis each accounting for 25% and 12.4% with an unknown cause.

Conclusion

Our study sheds light on the clinical and pathological features of papillary microcarcinoma, demonstrating its good prognosis and excellent response to treatment, with high 5- and 10-year survival rates. Nevertheless, 50% of deaths were attributed to bone and lung metastasis, reflecting the aggressive nature of certain tumors. We recommend that further research should focus on understanding the predictive factors of poor prognosis in patients with PMC, to ensure risk-adapted management.

[^{99m}Tc]Tc-iPSMA-BN: A Novel Molecular Bispecific Heterodimer in Metastatic Castration Resistant Prostate Cancer with Homologous Recombination Repair Germline and Somatic Mutations: A Pilot Study

S. D. G. Rueda¹, G. Ferro-Flores², F. G. Perez¹, E. M. Sánchez¹, Q. G. P. Cortés¹, J. V. Ahumada¹

¹Instituto Nacional de Cancerología de Mexico, Mexico

²Instituto Nacional de Investigaciones Nucleares

Background

Prostate cancer (PC) is male's second most common malignant neoplasia worldwide. Once "castration resistant" status has been established, therapeutic options are limited. Theragnosis with PSMA radiotracers is nowadays widely accepted in international guidelines due to its high therapeutic efficiency. In some clinical scenarios, dual PET/CT scan with PSMA and FDG is required to confirm tumour heterogeneity and disease aggressiveness, this approach is expensive and non-viable for developing countries. [^{99m}Tc]iPSMA-BN is a novel heterodimer molecule which is composed from iPSMA and bombesin: a gastrin releasing peptide receptor analog overexpressed in primary PC tumours and metastasis, it has influence over androgen receptors and its splice variants through nuclear-factor-kappa-beta, involved into developing castration resistance and progression. This pilot study further investigates the diagnostic accuracy of [^{99m}Tc]iPSMA-BN versus [¹⁸F]PSMA-PET/CT, in metastatic castration resistant PC (mCRPC), evaluates molecular heterogeneity receptors intra and interpatient status.

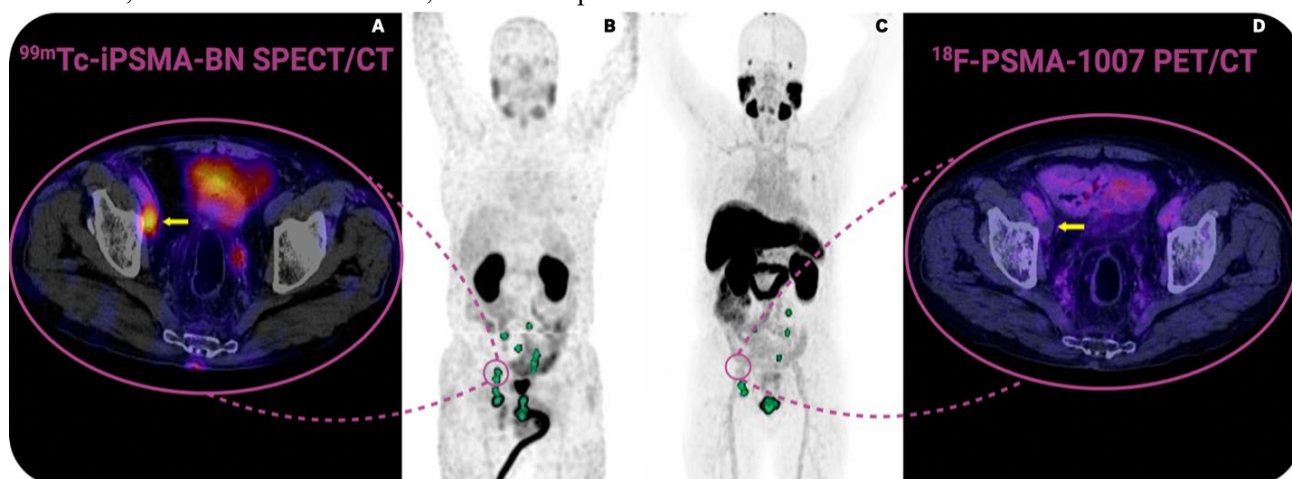
Methodology

This pilot study has five mCRPC patients, who had an ISUP grade ≥ 3 , distant metastatic known disease, previous ADT, at least 1 taxane-based chemotherapy, for evaluation to receive RLT; all of the patients had a recent [¹⁸F]PSMA-PET/CT study and were enrolled to this prospective study on their behalf. For standardizing measurements, target-to-background ratio(TBR), lesion detection rate was obtained for both PSMA PET and heterodimer SPECT.

Results

Mean age:69.8 years (range 58–77),40% of patients had ISUP grade 4 and 60% grade 5 at diagnosis, median PSA at diagnosis:57 ng/dL, median PSA at time of study: 111ng/dL(range 4.0–440.6). 107 lesions were observed by computed tomography, 97 with PSMA-PET and 87 with heterodimer SPECT, divided into:44 bone lesions, 21 locoregional (LRLN)and 23 non-locoregional (NLRLN) lymph nodes, as well as 6 visceral lesions(4 lung nodules and 2 mesenteric implants).In two patients more lesions were visualized with SPECT heterodimer rather than with PSMA-PET, divided as follows: 1 LRLN,1 NLRLN and 1 lung nodule(N= 7vs6, 3vs2 and 2vs1, respectively), histopathology reports from this patient were a dedifferentiated sarcomatoid variant and an acinar adenocarcinoma ISUP grade 5 since diagnosis. NKX3.1 immunohistochemistry was performed and reported as positive, additionally PSA at the time of the study in this patient was 4.0ng/dL, which supports the loss of cellular differentiation and further PSA production; interestingly this was the patient in whom we found a better lesion detection rate and higher TBR in the SPECT versus PET study (86.66%vs73.33% and 207vs25.31, respectively). The second patient, there was no difference in lesion detection rate between PET and SPECT

radiotracers, but TBR was higher for SPECT than PET (39.25vs29.5). 40% of the patients had no HRR mutations, while 60% had: CHEK2, BRCA and p53 mutations.



Patient 5 was diagnosed with prostate adenocarcinoma in 2013, ten years later, in 2023 underwent for the second time through a TURP procedure, with a histopathology report of "sarcomatoid differentiation" and extense necrosis, IHC demonstrated prostate origin with positive NKX3.1. A and B are ^{99m}Tc -iPSMA-BN SPECT/CT axial fusion and maximum intensity projection (MIP) images, respectively, showing a lymphadenopathy in right obturator chain with high focal concentration of the heterodimer, while C and D images are MIP and axial fusion ^{18}F -PSMA-1007 PET/CT projections, respectively, showing no concentration whatsoever of the radiopharmaceutical in the previously mentioned lesion, denoting a more aggressive and higher grade, less differentiated spectrum of the malignancy, matching the latter histopathology report.

Conclusion

Novel heterodimer [^{99m}Tc]iPSMA-BN appears to have better lesion detection in those patients in which an aggressive histologic transformation has occurred, those in which PSA is no longer a suitable tumoural marker representing tumour burden. There needs to be more studies performed with a broader number of recruited patients, but this is a promising alternative for not only diagnostic purposes with a wider availability and a more economic option, but also for patients to undergo radionuclide therapy and not be excluded from this treatment modality.

The role of [^{99m}Tc]Tc-PSMA in patients with biochemical recurrent prostate cancer with low PSA levels

A. Ankrah, S. Teye, C. Korsah, M. Yartey, E. Hammond

National Centre for Radiotherapy and Nuclear Medicine, Ghana

Background

Imaging of biochemical recurrence has improved tremendously with PET-based PSMA imaging. However, PET/CT imaging is unavailable in some places, especially developing countries. [^{99m}Tc]Tc-PSMA is a SPECT-based tracer that may be used in place of the PET-based tracer, but there is a concern that its role may be limited due to the better spatial resolution of PET/CT.

Aim: We examine the role of [^{99m}Tc]Tc-PSMA in patients with biochemical recurrence.

Methodology

We retrospectively recruited 22 patients with biochemical recurrent prostate cancer and PSA levels less than 10ng/ml. We recorded the PSA levels and treatment the patients had previously received for prostate cancer. We injected all patients with [^{99m}Tc]Tc-PSMA, and we performed whole-body planar and SPECT/CT after 2 to 4 hours.

Results

14 (63.6%) of patients previously had prostatectomy, while 8 (36.4%) of the patients had brachytherapy for prostate cancer. The PSA levels ranged from 0.36 to 10ng/ml, with a median of 4.3ng/ml. We detected recurrent disease in the prostate bed in all patients. In five of these patients (22.7%), the disease extended into the seminal vesicle and in two (1%) patients, bone metastasis was detected. We detected a metastatic lymph node in one patient (0,5%).

Conclusion

[^{99m}Tc]Tc-PSMA performs well in disease detection in patients with biochemical recurrence and low PSA levels.

FDG PET/CT in the initial staging of DLBCL: Preliminary results from the Salah Azaïez Institute experience

F. B. Amar, I. Yeddes, I. Meddeb, H. Rokbani, M. Somai, O. B. Hamida, I. Slim, A. Mhiri

Nuclear Medicine Department of the Salah Azaïez Institute, Tunis, Tunisia

Background

[18F] Fluoro-deoxyglucose (FDG) positron emission tomography/computed tomography (PET/CT) is the current state-of-the-art imaging in Diffuse Large B-Cell Lymphoma (DLBCL).

At diagnosis, FDG/PET/CT plays a central role in treatment decisions. In fact, accurate staging is crucial not only for appropriate therapy selection but also in prognostic assessment.

The aim of our study was to describe the contribution of FDG/PET/CT in DLBCL staging since its introduction in Tunisia.

Methodology

Our study was observational descriptive retrospective monocentric. Adult patients followed for DLBCL, referred to the Nuclear Medicine Department of the Salah Azaïez Institute for staging by FDG/PET/CT between November 2019 and July 2022 have been enrolled.

we compared the results of FDG/PET/CT with those of CT in the identification of lymphomatous nodal and extra-nodal involvement. for the specific case of bone marrow involvement, we compared the results of FDG/PET/CT with those of Bone Marrow Biopsy (BMB).

To evaluate the statistical significance between diagnostic modalities p-value was set at 0.05.

Results

We included 49 patients. The average age was 54 ± 12 years [21-75 years]. The sex-ratio was 0.2 M/F. The difference between FDG/PET/CT and CT was significant ($p < 10^{-4}$) for the assessment of lymph node and extra-nodal involvement, excepted the lung involvement ($p = 0.63$). Concordance between FDG/PET/CT and BMB was noted in 87% of cases, with no significant difference between the two modalities ($p = 0.73$). Thus FDG/PET/CT was behind the stage Ann Arbor migration in 41% of cases, including 31% of up-staging leading to a therapy change in 10% of cases. A significant difference was noted when comparing the international prognostic index before and after FDG/PET/CT ($p < 10^{-4}$).

Conclusion

The use of FDG/PET/CT at diagnosis led to a significant change in the evaluation of initial involvement. FDG/PET/CT better define prognostic subgroups and thus facilitate patient's management avoiding under and over-treatment. Baseline FDG/PET/CT remains indispensable for optimal assessment of response to treatment.

Evaluation of Tumour Uptake of [68Ga]Ga-FAPI-04 in Patients with Various Cancers

E. Lischinsky, J. P. Gambini, A. Banchemo, A. Quagliata, J. P. Leiva, I. Cordero, J. Giglio, E. Savio, O. Alonso, P. Duarte

Centro De Medicina Nuclear E Imagenología Molecular Del Hospital De Clínicas (CMNIM),
Montevideo, Uruguay

Background

Fibroblast activation protein (FAP) is a human enzyme that exhibits increased expression in the stroma of various malignant tumours. It is also observed in over 90% of activated stromal fibroblasts in all human carcinomas. Specific inhibitors of fibroblast activation protein (FAP), labeled with different radionuclides, are being evaluated for the diagnosis of different tumours, with highly encouraging clinical and preclinical results.

The aim of this study is to quantify tumour uptake in [68Ga]Ga-FAPI-04 PET/CT for various primary and metastatic tumours.

Methodology

[68Ga]68Ga was obtained from a generator (ITM) with activity levels ranging from 100-700 MBq. Labelling was carried out with the following parameters: 25-30 micrograms of FAPI-04; pH 4.0-4.5; incubation temperature 100 °C; incubation time 10 min. The radiotracer was prepared in a GMP environment, with radiochemical purity exceeding 95% and meeting all quality assurance system specifications.

[68Ga]Ga-FAPI PET/CT scans were requested by various referring physicians based on individual clinical indications that were considered insufficiently covered by [18F]FDG PET/CT or other imaging modalities. All PET/CT scans were performed 1 hour after the injection of [68Ga]Ga-FAPI-04 (102-209 MBq).

Fifteen patients with primary tumours were identified. Tumour uptake was quantified using the maximum standardized uptake value (SUV_{max}). Images were reconstructed using the iterative method (OSEM) with time-of-flight (TOF) correction. Two nuclear medicine physicians independently conducted visual image analysis. These studies were approved by the Ethics Committee.

Results

Fifteen patients with different tumour entities were evaluated (Table 1). Primary and secondary lesions with [68Ga]Ga-FAPI-04 uptake (SUV_{max} 27.7 – 4.1; average 13.8; mean 12.5; SD 6.2) were identified, with the highest uptake found in hepatobiliary cancer and the lowest uptake in pancreatic cancer (Table 1). Low uptake was observed in brain, muscle and blood.

Primary Tumor	Highest Lesion Uptake	⁶⁸ Ga-FAPI-04 SUVmax
Anal Canal Cancer	Left iliac wing lesion	12.3
Breast Cancer	Metastatic tumor in LLL	11.3
Colorectal Cancer	Abdominal wall metastases	9.2
Gastric Cancer	Gastroesophageal lesion	17.2
Hepatobiliary Cancer	Liver tumor	27.7
Hodgkin Lymphoma	Mediastinal mass	7.9
Non-small Cell Lung Cancer	Right hilar mass	22.9
Non-small Cell Lung Cancer	Right hilar mass	19.7
Non-small Cell Lung Cancer	Mass in LUL	12.5
Oat Cell Small Cell Lung Cancer	Mediastinal mass	12.3
Pancreatic Cancer	Peripancreatic diffuse uptake	4.1
Penile Cancer	Left superficial inguinal adenopathy	6.8
Tracheal Squamous Cell Carcinoma	Right paratracheal adenopathy	16.5
Urothelial Carcinoma	Left external iliac adenopathy	13.5
Vulvar Cancer	Mass in left iliac fossa	13.1

Table 1. Patient sample with primary cancer type, lesions with most intense ⁶⁸Ga-FAPI-04 uptake in PET/CT, and measured SUVmax for each lesion. Sorted by SUVmax values (decreasing).

Conclusion

In all studied patients, variable uptake of [⁶⁸Ga]Ga-FAPI-04 with different intensities was observed, indicating differences in the tumour microenvironment among the various evaluated tumours. Tumour uptake of [⁶⁸Ga]Ga-FAPI-04, coupled with low uptake in the brain, muscle, and blood, highlights its potential for tumour detection, as well as its possible role in oncologic therapy when labelled with theranostic radionuclides, such as [¹⁷⁷Lu]LuCl₂.

**The importance of a diagnostic scan in the management of differentiated thyroid cancer:
A case of metastatic papillary microcarcinoma**

S. Teye¹, N. Malan², M. Vangu²

¹ Ghana Atomic Energy Commission Hospital, Ghana

² Department of Nuclear Medicine and Molecular Imaging, CM Johannesburg Academic Hospital, University of the Witwatersrand, South Africa

Background

Papillary microcarcinoma (PMC) is defined as papillary thyroid carcinoma (PTC) measuring ≤ 1 cm. This definition is independent of the presence of high-risk features such as nodal metastasis, distant metastasis, extrathyroidal extension and histological subtype.

The mainstay of management of PTC is surgery with or without radioactive (RAI) treatment. PMCs are generally regarded as low risk / indolent disease.

The recent increase in the incidence of thyroid cancer is in part attributed to the rise in the identification of low-risk PMCs, and a major clinical issue has thus arisen: how should these low-risk PMCs be managed? This unusual case illustrates the value of RAI diagnostic scan in staging of patients with PMC and thus assist in their management, that is, observation without treatment, active surveillance or treatment of micro metastatic disease or known disease.

Aim

To demonstrate the value of radioiodine (RAI) diagnostic scan in the management of PMC.

Methodology

We report the case of a 36-year-old female who presented with an incidental finding of an anterior neck swelling. Neck ultrasound showed multiple left thyroid nodules. FNA of the largest nodule was consistent with papillary thyroid cancer.

The histology report following the total thyroidectomy, showed a solid variant of papillary microcarcinoma with no capsular or lymphovascular invasion (pT1aNx, stage 1-AJCC 8th edition). With sufficiently elevated TSH, a 2mCi RAI diagnostic scan showed a focus of uptake in the anterior neck, in the midline of the abdomen, as well as to the left of the urinary bladder. SPECT/CT localized the uptake in the neck region to the left thyroid bed, in the abdomen to the L3 vertebra bone with extension to the right pedicle and to the left iliac bone (Figure 1a, b, c and d). The patient was upstaged to cT1aN0M1, stage 2 (AJCC 8th edition) and treated as a case of metastatic PMC.

Conclusion

Diagnostic scans with radioactive iodine in patients with differentiated thyroid cancer is incalculable, this may even assist in microcarcinomas by improved patient management because of clinically relevant downstaging and upstaging.

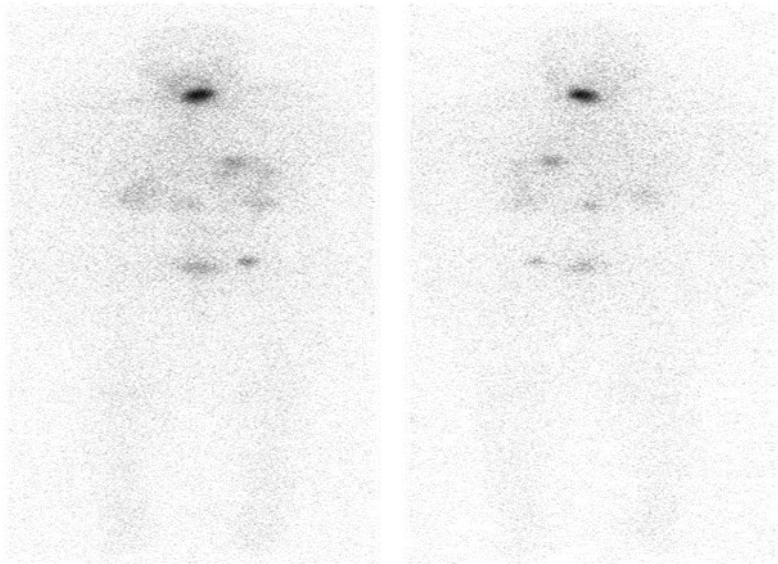


Figure 1

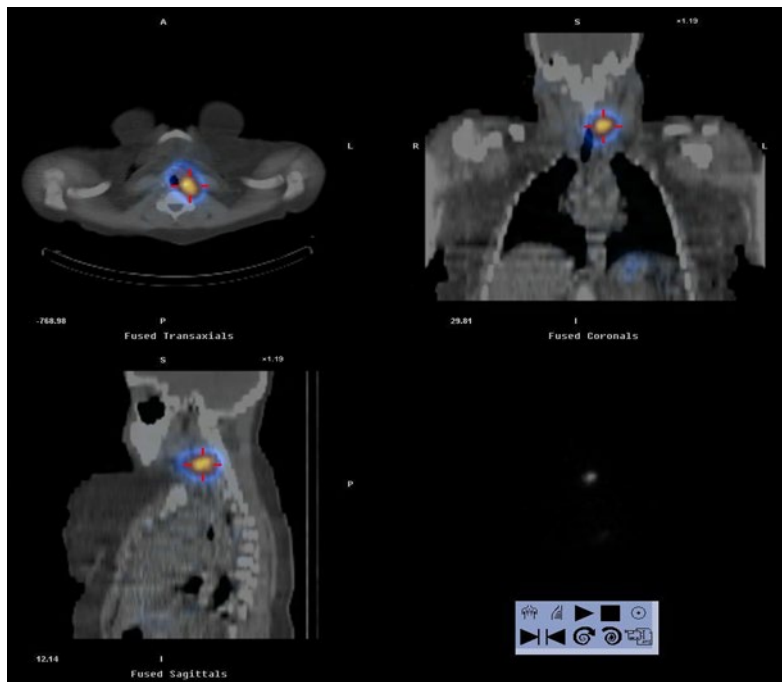
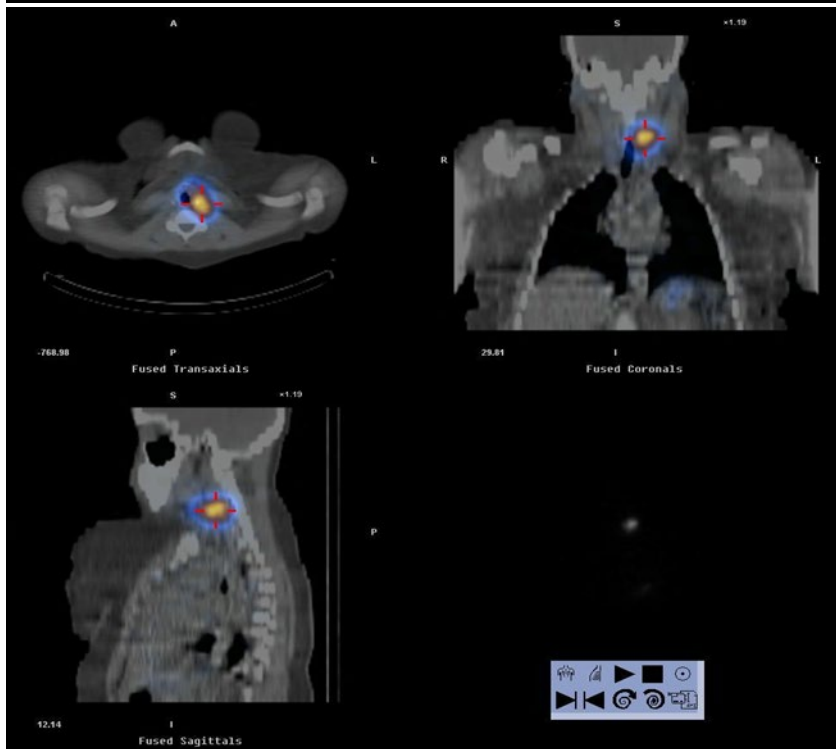
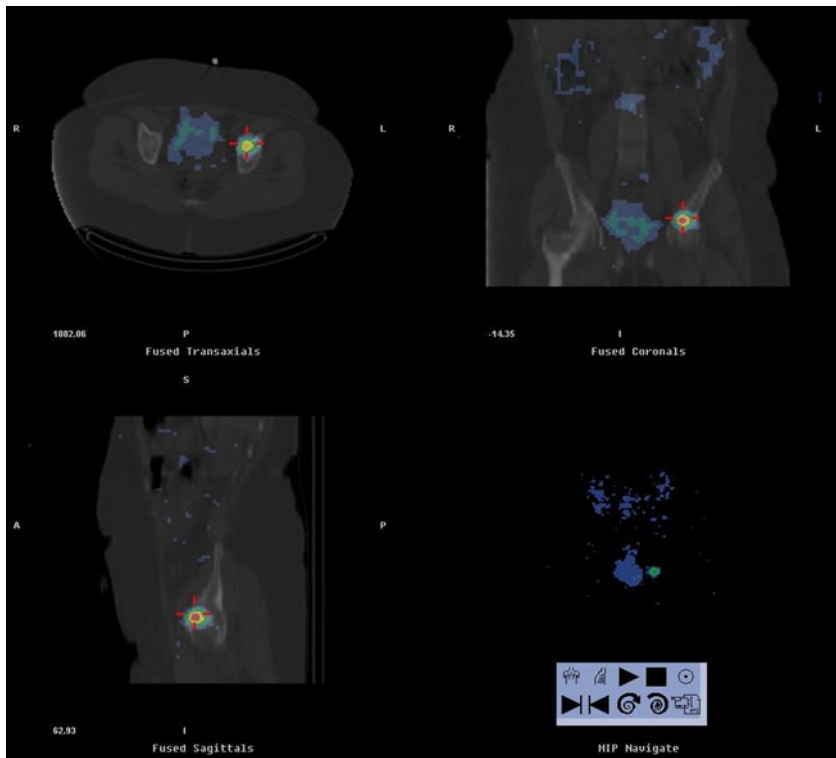


Figure 1b



Functional Imaging the Neuroendocrine tumour (NET), with PET/CT Al[18F]F-NOTA-Octreotide in Mexico.(CT Scanner Lomas Altas)

E. A. Hernández, J. S. Andonaegui, S. C. Alvarez

CT Scanner Lomas Altas, Mexico

Background

Neuroendocrine tumours (NET), are a heterogeneous group of neoplasms that arise from neuroendocrine cells and affect the diffuse neuroendocrine system, including pancreatic NET, small intestine (SI-NET), lung NET, medullary thyroid carcinoma (MTC), pheochromocytoma, and paraganglioma. These tumours present in widely variable ways, in which imaging plays an important role. Managing patients with NETs is complex and requires referral to high volume centers with appropriate expertise to ensure favorable outcomes. PET/CT plays an increasingly crucial role in every step of their management and outcome. The choice of radiopharmaceutical depends heavily on tumour grade and clinical presentation (diagnostic vs theranostic). Somatostatin receptor (SSTR) PET has shown significant improvement over conventional imaging (CI). Currently, it is recommended by all guidelines to use the SSTR-based imaging options including SSTR-PET/CT or SSTR-PET/MRI, or octreotide SPECT/CT. Appropriate SSTR-PET tracers include ⁶⁸Ga-DOTATATE, ⁶⁸Ga-DOTATOC, or ⁶⁴Cu-DOTATATE.

The short half-life, increasing costs, and regulatory issues significantly limit the availability of approved imaging agents of ⁶⁸Ge/⁶⁸Ga generators in Mexico.

Al[18F]F-NOTA-Octreotide provides a similar biodistribution and tumour uptake, can be produced on a large scale and may improve access to precision imaging.

Methodology

Considered PET scans with Al[18F]F-NOTA-Octreotide of patients with histopathologic confirmed diagnosis of NETs, between December 2021 and January 2023, were analysed descriptively, and retrospectively.

Patients were categorized into six groups based on diagnosis, metastatic disease, previous PET/CT with ⁶⁸Ga-DOTA-NOC, SULmax primary lesion and lutetium treatment.

Results

42 patients with a mean age of 61.5 years (+5.1) were included, comprising 25 males and 17 females. Eight had a diagnosis of pancreatic NET, 18 intestine (I-NET), 9 lung (L-NET), 2 vesical (V-NET), 1 pheochromocytoma, and paraganglioma, 1 parotid NET, and 3 had a unknown primary tumour.

PET/CT demonstrated a local tumour in 11 patients, with a SULmax tumour uptake of 9.5 (+ 2).

Metastatic disease was observed in 11 patients, 2 with bone involvement, 6 lung metastases, 13 with liver metastases, 11 with lymph node involvement, and 2 with peritoneal implants. Twelve patients had a previous PET/CT with ⁶⁸Ga-DOTA-NOC where the primary lesion's result was similar to Al[18F]F-NOTA-NOC. Four patients had lutetium treatment.

Conclusion

PET/CT with Al[18F]F-NOTA-NOC has a high affinity for SSTR2 and SSTR5, favorable biodistribution, high tumour uptake, and has proven to be safe in clinical applications for patients diagnosed with NETs.

Bone scans with SPECT/CT in benign bone disease, the added value in a referral tertiary children's hospital in South Africa

K. Hlongwa¹, A. Brink², M. Jassen¹, S. More³, F. Smith¹

¹Red Cross War Memorial Children's Hospital and University of Cape Town, South Africa

²Nuclear Medicine and Diagnostic Imaging Section, Division of Human Health, International Atomic Energy Agency, Vienna, Austria

³Division of Nuclear Medicine, University of Cape Town, South Africa

Background

Musculoskeletal pain is one of the most common indications to paediatric orthopaedics centers/clinics and can often be managed symptomatically or with further intervention. In a resource-limited setting, x-rays are used as first-line conventional imaging. Access to a skilled ultrasonographer, computed tomography (CT), and magnetic resonance imaging (MRI) is not always readily available. The role of SPECT/CT in paediatric populations is becoming beneficial in guiding the management of patients in orthopedic clinics.

We aim to review its added value in the largest referral children's hospital in Africa.

Methodology

We reviewed the records of patients with non-specific limb/bone pain who were referred for bone scans with SPECT/CT between 1 March 2020 and 29 February 2024. All patients had an x-ray at the time of referral. We excluded patients referred for non-benign pathology. A positive bone scan was defined as a study that was either single or dual-phase positive, or a cold area surrounded by an increased rim of uptake on planar imaging with the finding localized and/or characterized on SPECT/CT imaging.

Results

A total of 53 patients had bone scans with SPECT/CT imaging over the referral period. 41 patients were included in the review and 12 were excluded due to non-benign pathology. The patients' mean age was 6,9 years (range 7 months to 14 years). 19 patients were female and 22 were male. 33/41 (80%) patients had positive scans on bone SPECT/CT. 8/41 (20%) patients had normal (negative) scans. We were able to localize the source of bone pain on SPECT/CT alone in 23/41 (56%) which aided in further management of the patients. X-ray findings were congruent with bone scan SPECT/CT in 10/41 (24%) patients. Diagnostic bone SPECT/CT was followed up with an X-ray and/or ultrasound for patients who received further management.

Conclusion

SPECT/CT was useful in localizing the source of bone pain in children with non-specific symptoms referred to our hospital.

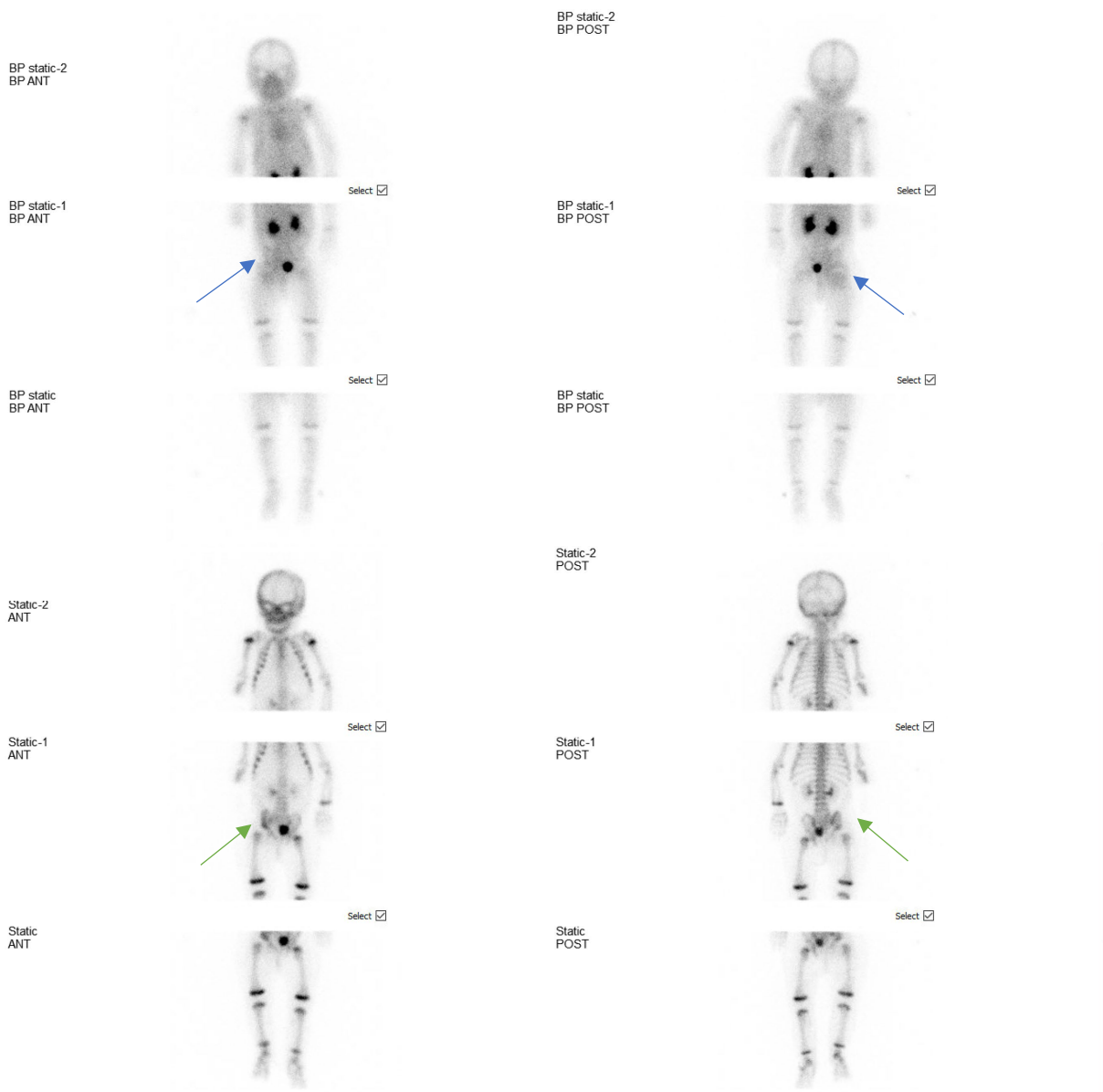
Table 1: Positive bone scan findings

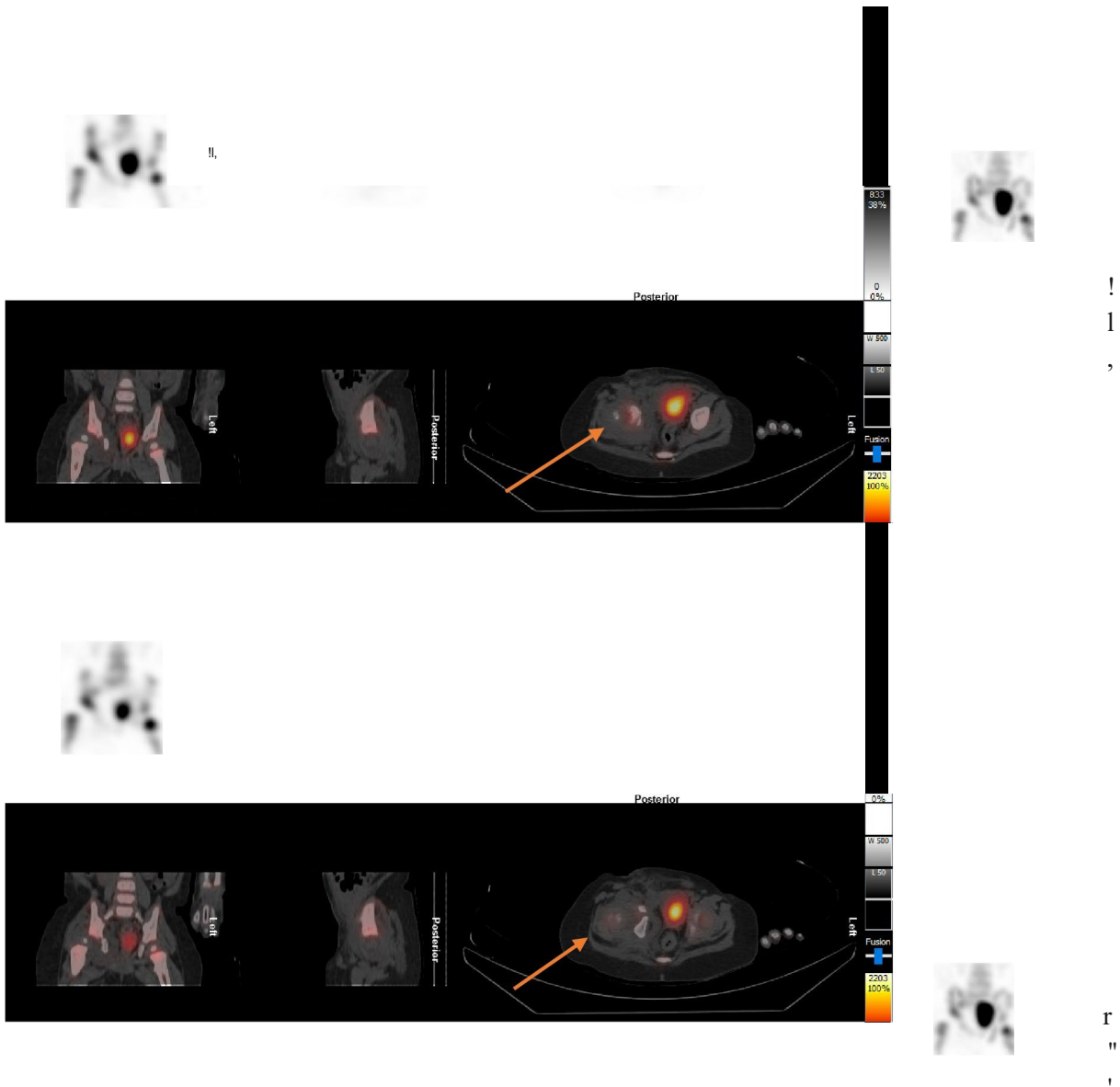
Positive finding	No of patients
Osteomyelitis	10
Sacroiliitis	6
Cellulitis	3

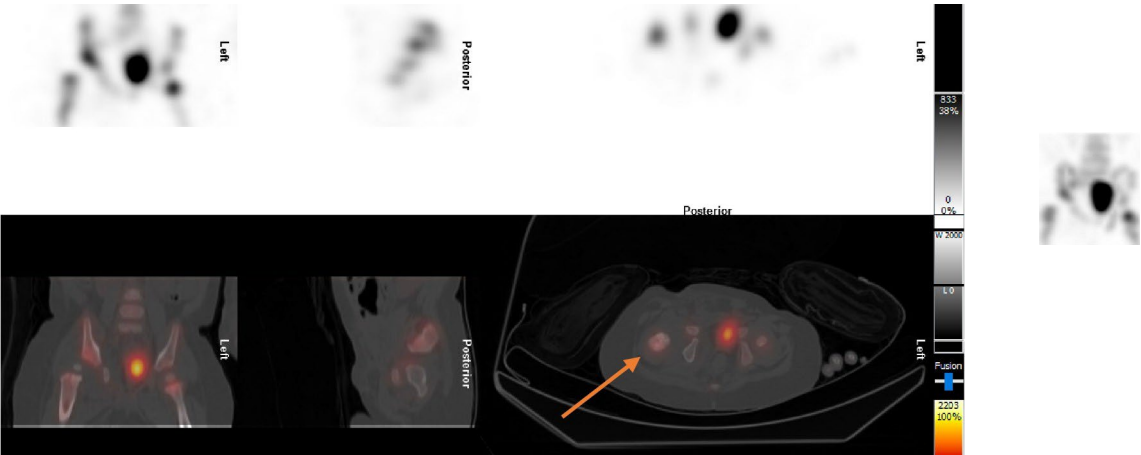
Septic arthritis	4
Myositis	1
Osteoid osteoma	1
Collection/abscess	4
Fractures	4

Images

9-month-old male with decreased range of motion in the right leg. Blood pool images demonstrate abnormally increased uptake in the right hip on the anterior images and a cold centre is seen on the posterior images (blue arrows). Delayed images demonstrate asymmetry in the hips (green arrows). There is a widened right hip joint with a cold area in the region of the right femoral head. Pelvic SPECT/CT demonstrates a fluid collection in the right hip (orange arrows). Findings of septic arthritis in the right hip.







IAEA-CN-326/368

Initial experience with ^{68}Ga -FAPI-04 PET in patients with urological tumours

F. Savio, A. Banchemo, I. Cordero, P. Duarte, J. P. Gambini, J. G. Giglio, J. P. Leiva, E. Lischinsky, A. Quagliata, E. Savio, V. Trindade, L. Urrutia, G. dos Santos Loureiro

Centro Uruguayo de Imagenología Molecular (CUDIM), Uruguay

Background

Bladder and penile cancer are frequent in oncological practice. The objective of this work is to report our initial experience in the diagnosis of these urological tumours with ^{68}Ga -FAPI-04.

Methodology

^{68}Ga was obtained from a generator (ITM). Activity levels ranged from 100-700 MBq. Labeling was carried out with the following parameters: 25-30 micrograms of FAPI-04; pH 4.0-4.5; incubation temperature 100 °C; incubation time 10 min. The radiopharmaceutical was prepared in a GMP environment, with a radiochemical purity greater than 95% and meeting all the specifications of the center's quality assurance system.

Eight patients over 18 years of age were included, with a confirmed histopathological diagnosis of urological neoplasia (5 bladder cancer and 3 penile cancer). Patients had to have recent conventional imaging studies (computed tomography, nuclear magnetic resonance, bone scintigraphy). They could have received previous oncospecific treatment (surgical, intravesical BCG, chemotherapy, etc.). All 8 patients underwent a positron emission tomography (PET) study fused with low-dose computed tomography (CT) without contrast medium. All PET/CTs were performed 1 h after injection of ^{68}Ga -FAPI-04 (102-209 MBq). Images were reconstructed using the iterative method (OSEM) with time-of-flight (TOF) correction. Two nuclear medicine physicians performed the visual analysis of the images separately. These studies were approved by the Ethics Committee.

Results

In the biodistribution of the radiotracer we find a low level of uptake in the brain, muscle and blood. It was observed that lymph nodes and bone tissue were the most affected regions, with lesions detected in all patients with penile cancer (2/2). Furthermore, it was found that 50% of patients with bladder cancer (3 of 6) had lesions in lymph nodes and bone tissue. The bladder showed a lower frequency of lesions, with 16.7% of bladder cancer patients (1 of 6) and 50% of penile cancer patients (1 of 2) showing involvement. Respectively, the prostate also showed a frequency of 16.7% of lesions in patients with bladder cancer (1 of 6).

Conclusion

Our results suggest that FAPI is a promising tool for the detection of lymph node and bone lesions in patients with penile and bladder cancer. Studies with a larger number of patients are needed to confirm these results and determine the usefulness of FAPI in the follow-up and prognosis of these patients.

IAEA-CN-326/369

Mixed pancreatic carcinoma evaluated by dual PET/CT protocol with [¹⁸F]-AIF-NOTA-Octreotide and [¹⁸F]FDG: Series of interesting cases

J. S. Andonaegui, E. A. Hernández, S. Carrillo

C.T. Scanner Lomas Altas, Mexico

Background

Pancreatic tumours are rare, constitute less than 1% of all malignant neoplasms and can arise from either the exocrine component (ductal and acinous cells) or the endocrine component (neuroendocrine cells). Acinous cell carcinomas may contain neuroendocrine cells in up to 40% of cases; but these occur in less than 25% of the tumour. When neuroendocrine cells occupy more than 25-30%, the tumour is called mixed endocrine and acinous cell carcinoma of the pancreas. Cellular differentiation is the similarity between tumour cells and islet of Langerhans cells; It is classified as a well-differentiated tumour (NET grade 1,2 and 3) and a poorly differentiated tumour (CNE grade 3). Tumour grade is the aggressiveness of the tumour in terms of growth and ability to spread; It is established based on the mitosis index per field (<2, 2-20, >20) and the Ki67 index (<3, 3-20 and >20).

A unique characteristic of neuroendocrine tumours (NEN) is the overexpression of somatostatin receptors (SSTR) on the surface of tumour cells, mainly somatostatin receptor type 2 (SSTR2), which facilitates their molecular diagnosis, using linked somatostatin analogues. to radionuclides. Of the radionuclides used in PET, [⁶⁸Ga]DOTA-peptide is currently the standard for imaging the somatostatin receptor in patients with neuroendocrine tumours. Fluor 18 is the most used radionuclide in PET examination, since somatostatin analogues labeled with it have better resolution potential than with Gallium-68, in addition, [¹⁸F]FDG evaluates glycolytic metabolism in aggressive and poorly differentiated NEN. [¹⁸F]-AIF-NOTA-Octreotide its first results in humans are recorded by Long et al; It may be an alternative due to its production performance, availability, longer half-life and improvement in spatial resolution, in addition to showing favorable safety, biodistribution and dosimetry profiles with high tumour uptake and a high tumour-to-background ratio; Its diagnostic importance is due to its greater sensitivity in the detection of less aggressive and well-differentiated NEN.

Case Presentation

5 cases of interest of patients with a diagnosis of mixed pancreatic carcinoma, who have the histopathological diagnosis, are correlated.

Results

The imaging findings of [¹⁸F]-AIF-NOTA-OC and [¹⁸F]FDG were compared with each other and with histopathological information. Lesions that presented an activity greater than the physiological uptake of the affected organ lesion were considered a pathological lesion. [¹⁸F]-AIF-NOTA-OC allowed us to obtain better images of the region of the cellularly well-differentiated tumour, while [¹⁸F]FDG was related to poorly differentiated tumours.

Discussion

The dual FDG-Octreotide PET protocol is a valuable molecular imaging tool to evaluate this rare entity, with few cases reported in the literature. They have a predominantly acinous growth pattern. 60% of cases are located in the head of the pancreas and are often diagnosed in middle-aged people (58 years).

[¹⁸F]AIF-NOTA-octreotide has better performance because it is more affordable, presents safety for the patient and does not have significant changes in images with other radionuclides, which is why it represents an alternative to Ga-68 SSA, the current gold standard for NEN.

IAEA-CN-326/370

Evaluation of Dosimetry Software Programs for Lu-177 Radiopharmaceutical Therapy Using Voxelised Phantoms**K. Ramonaheng¹, C. Swanepoel¹, C. Davis¹, H. D. Raan¹, H. Ndlovu², J. V. Staden², L. Smith¹, M. Qebetu¹, M. Sathekge¹**¹Nuclear Medicine Research Infrastructure and University of Pretoria, South Africa²University of the Free State, South Africa**Background**

The use of voxel-based phantoms and Monte Carlo (MC) simulations in virtual dosimetry presents the advantage of establishing a gold standard against which absorbed doses can be benchmarked, ensuring dosimetry accuracy. Additionally, these reference values aid in assessing the accuracy of absorbed dose methodologies across various software programs. Lutetium-177 (Lu-177) has gained interest and importance in the realm of Radionuclide Therapy (RPT) due to its favorable decay properties and theragnostics applications. This study aimed to compare the accuracy of absorbed doses calculated using LundADose and OLINDA/EXM 1.0 for Lu-177.

Methodology

The accuracy assessment was conducted based on Lu-177-DOTATATE distributions of three voxel-based phantoms. SPECT projection images were simulated at time intervals of 1, 24, 96, and 168 hours after administration, followed by reconstruction using LundADose. The reconstruction process entailed 3D OS-EM reconstruction incorporating CT-based attenuation correction, effective source scatter estimation, and collimator detector response correction. Mono-exponential curves were applied to the bio-kinetic data for organs including the kidneys, liver, spleen, and tumours, resulting in SPECT time-integrated activity (SPECT-TIA). These SPECT-TIA values were used to calculate mean absorbed doses using both LundADose (LND-DSPECT) and OLINDA (OLINDA-DSPECT) for the respective organs. The accuracy of the mean absorbed doses obtained from the reconstructed SPECT images of the phantoms was compared to the true MC absorbed doses, determined from a true dose image and direct MC transport. The true dose images were derived from pre-defined true activity images, which were used to obtain TRUE-TIA values. These, along with direct MC simulations, were used to compute the true doses (MC-DTrue). The dosimetry accuracy was evaluated by comparing LND-DSPECT and OLINDA-DSPECT to MC-DTrue.

Results

LND-DSPECT overestimated the mean absorbed dose compared to MC-DTrue by up to 6.59%. This overestimation was attributed to spill-out activity from the reconstructed LND-DSPECT, resulting in a higher dose contribution than MC-DTrue. Conversely, OLINDA-DSPECT generally underestimated (< 8.11%) absorbed doses compared to MC-DTrue. The overestimation may arise from differences in geometry between the voxel-based phantoms used in this study and the geometric reference phantoms employed in OLINDA. Despite attempts to normalize organ masses between our phantoms and OLINDA models, the geometric differences in shape remain unaccounted for.

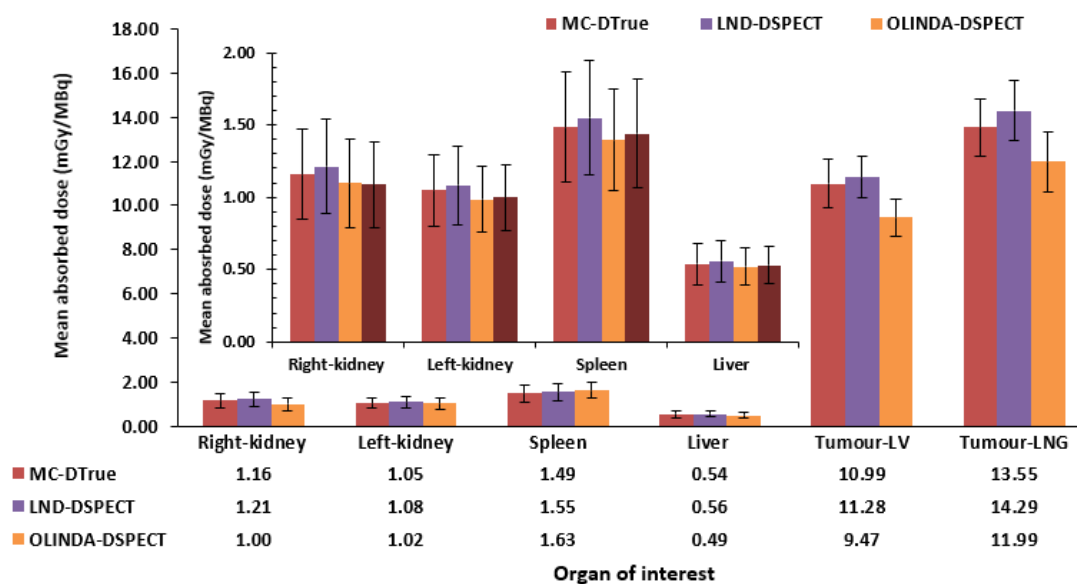


Figure 1. Mean absorbed doses for the right-kidney, left-kidney, spleen, liver and tumour-LV (tumour adjacent to the liver) and tumour-LNG (tumour between the lungs) with a zoom-in of the data shown in the upper left section. Doses were computed from true activity images using direct Monte Carlo (MC) transport (MC-DTrue) and from reconstructed SPECT images using LundADose (LND-DSPECT) and OLINDA/EXM 1.0 (OLINDA-DSPECT).

Conclusion

An accuracy of better than 10% implies that the mean dose values obtained with LND-DSPECT and OLINDA-DSPECT closely approximate the true values. The mean absorbed doses from both software programs and the gold standard were comparable, indicating the reliability of the results. This study will be valuable for optimizing Lu-177 dosimetry in clinical applications. The overall accuracy between the two software programs, which is less than 10%, is considered acceptable by other researchers conducting similar investigations.

IAEA-CN-326/371

Nuclear medicine hybrid imaging role in Erdheim Chester disease: a case report

O. B. Elkilani, H. Boudriga, T. Dardouri, M. Nourira, K. Chatti

University Hospital Sahloul Sousse, Tunisia

Background

Erdheim Chester disease (ECD) is an extremely rare blood cell malignancy with significant mortality rates. We report the case of a man who benefited from a bone scan in order to consolidate the suspicion of ECD.

Case Report

We report the case of a man, aged 39 y/o, with history of diabetes insipidus, hypogonadotropic hypogonadism, who was admitted for acute chest pain irradiating to the back alongside a fever of 39°C. A thoracic CT angiography, done for suspecting aortic dissection in the diagnosis but showed an aspect of “hairy kidneys” suggesting ECD. A thoraco-abdomino-pelvic CT showed signs of upper mediastinal, nodal, cardiac and renal involvement.

A 99mTc-HDP bone scan revealed a marked uptake in the sphenoidal bone and mandible, alongside a bilateral grossly symmetrical uptake in the lower femoral extremities, tibial bones and ankles which are typical of ECD. SPECT – CT revealed a rarefaction of bone density of the sphenoidal bone along with fields of osteocondensation of high uptake within lower femoral and tibial bones further suggesting ECD.

A 18FDG PET CT was done and revealed multisystemic involvement: signs of disease activity within the brain, retroorbital, heart, mediastinal and axillar lymph nodes, kidneys, adrenal glands, testis, bones, fat tissue and abdominal-pelvic wall.

A cerebral MRI revealed bilateral retro-orbital masses, a hypothalamic mass, absence of post-hypophysis, pachymeningitis and intrasinusal masses.

The patient was treated with a four-month course of PEGylated interferon and 6 months course of corticosteroids.

A PET CT 3 months after the end of the corticosteroid course revealed a partial response with signs of persistent activity especially in the brain, retroorbital regions, whereas pericardial, nodal, parietal, testicular and osseous affections responded well to treatment.

Figure 1. Initial bone scan 99mTc-HDP

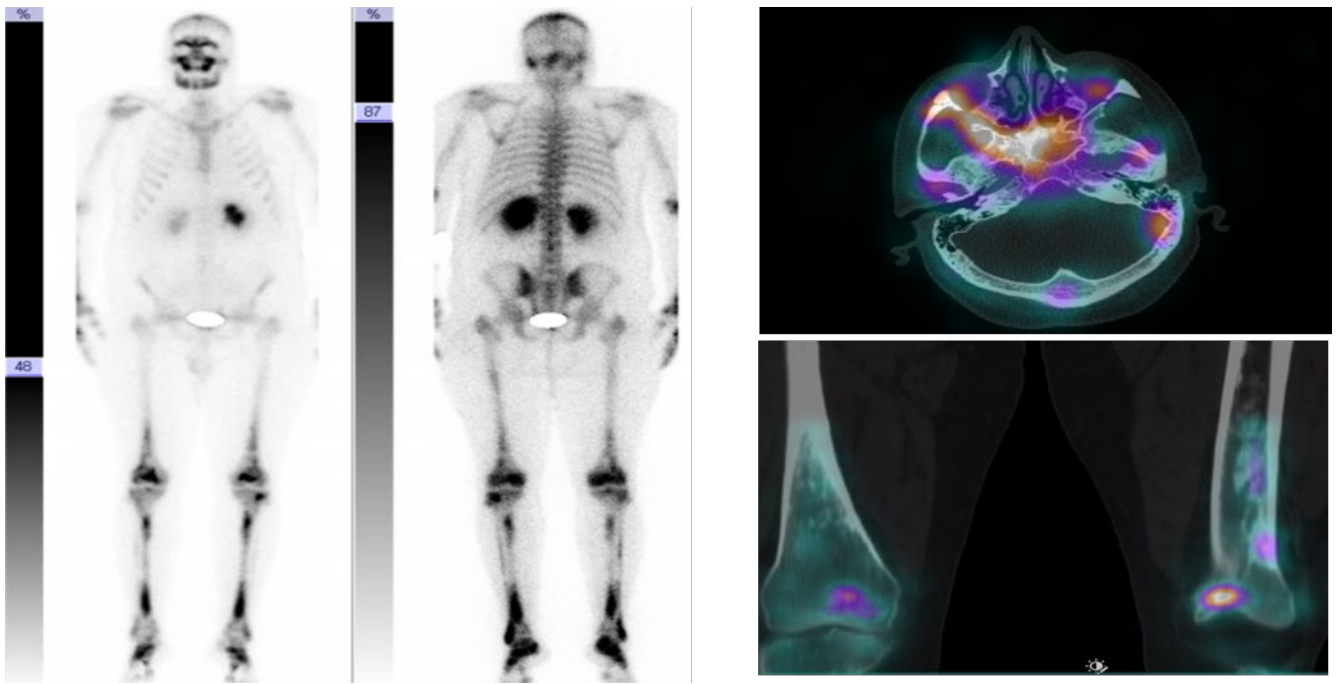
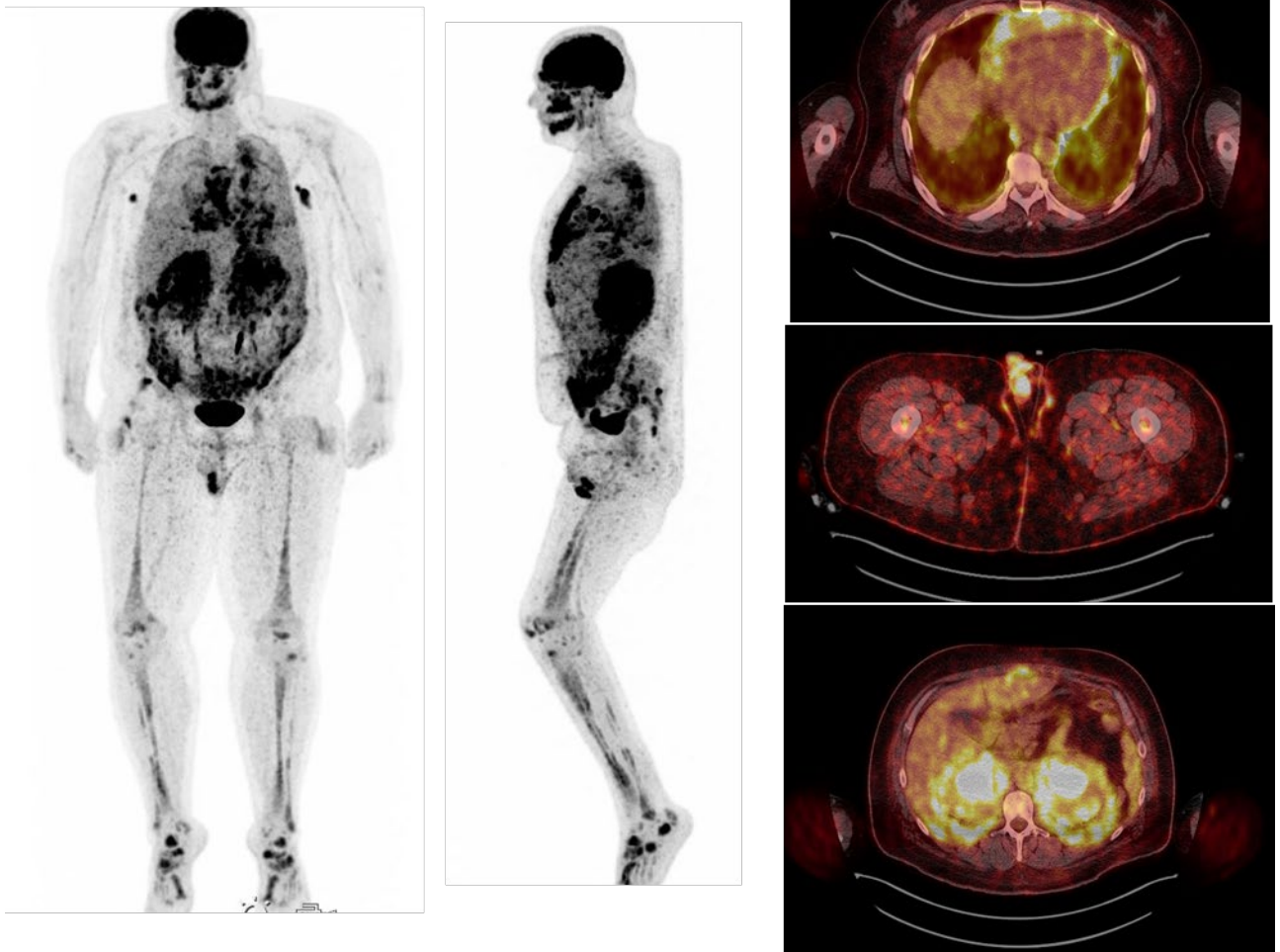


Figure 2. Initial ^{18}F FDG PET CT



Conclusion

Erdheim Chester disease is a rare haematological malignancy with poor prognosis, 99m Technetium bone scan is very helpful in the diagnosis, 18FDG PET CT is useful in evaluated systemic involvement and therapy response.

IAEA-CN-326/372

Impact of ^{18}F FDG-PET CT on the management of patients with locally advanced cervical carcinoma about 28 patients

O. B. Elkilani, M. Noura, T. Dardouri, K. Chatti

Department of Nuclear Medicine, University Hospital Sahloul Sousse, Tunisia

Background

Positron emission tomography coupled with computed tomography using ^{18}F -fluorodeoxyglucose (^{18}F FDG-PET CT) is a relatively novel modality of imaging in Tunisia, permitting both functional and anatomical studying of many types of malignancies. We report the first experience of evaluation of the impact of this modality on the initial management of 28 patients with locally advanced cervical carcinoma in Tunisia.

Methodology

We conducted a study, on patients with proven locally advanced cervical carcinoma, who benefited from a ^{18}F FDG-PET CT between November 2019 and June 2023 and didn't undergo any treatment; only conization is authorized. We excluded patients who had incomplete medical files and those who died before any treatment has begun. We analysed the programmed management modalities before PET CT and the change of the modalities after the PET CT. We classified it into intermodality change or intramodality change.

Results

We obtained 28 cases who complied to the inclusion criteria. The analysis of the impact on the treatment plan revealed that treatment modality didn't change in 20 cases (71.4%); whereas it changed in 8 cases (29.6%). For patients with impact on the management modalities, two had intermodal switch which consisted in the inclusion of neo-adjuvant mostly to reduce the size of lymph node metastasis to prevent digestive toxicity of radiotherapy, and 6 had intramodal change, which consisted in nodal boost irradiation in 4 cases, and enlargement of irradiation field in the two other cases.

Results summary			
No change			20
Change	Total		8
	Intermodal change	Adjunction of Neo-adjuvant chemotherapy	2
		Nodal Boost	4
	Intramodal change	Enlargement of field	2

Table : Summary of the results of this study

Conclusion

^{18}F FDG-PET CT plays an important role in the management of cervical carcinoma, by establishing a more precise staging and more accurate mapping of lymph node and visceral metastases.

IAEA-CN-326/373

Impact of ¹⁸FDG-PET CT in redefining the initial staging of cervical carcinoma. First tunisian experience, about 38 patients

O. B. Elkilani, M. Nourira, T. Dardouri, K. Chatti

Department of Nuclear Medicine, University Hospital Sahloul Sousse, Tunisia

Background

Cervical cancer is associated with a significant morbidity and mortality worldwide; both are linked tightly to the stage of the disease which can be inaccurate using conventional imaging techniques. Positron emission tomography coupled with computed tomography using ¹⁸F-fluorodeoxyglucose (¹⁸FDG-PET CT) is used widely to assess the extension of various types of cancer. We conducted in our institution a study to evaluate the impact of ¹⁸FDG-PET CT in the re-evaluation of initial staging among 38 patients with cervical cancer.

Methodology

We conducted a study on patients, with histologically proven cervical carcinoma, stage IB2 or higher according to FIGO 2018 classification for cervical cancer, who benefited from a ¹⁸FDG-PET CT between November 2019 and June 2023. We analysed age, clinical signs, histological type, pre PET stage using data from magnetic resonance imaging results and computed tomography results and post PET stage using ¹⁸FDG-PET CT results for each patient. We excluded patients with a synchronic cancer or with incomplete results.

Results

Thirty-eight patients fitted in the study. The mean age was 61.29 years. Regarding histological features 33 patients (86.8%) had squamous cell carcinoma, followed by adenocarcinoma in 3 patients (8%), 1 had adenosquamous and the other had adenosarcoma. For pre TEP stages: IIB stage was the most common 12 patients, followed by IIIC1 in 11 patients, IVA in 7 patients, IVB in 4 patients, IIA1 in 2 patients, stage IB2 and IIIB was present in 1 patient each. For post TEP stages IIIC1 become the most common in 15 patients followed by IVA in 7 patients, IIB in 6 patients, IVB in 5 patients, IIIC2 in 3 patients, stages IIIA and IIA1 had one patient each. This leads to changing of the staging in 15 cases (39.4%), which was an upstaging in 13 (34.5%) and a downstaging in 2 (5.2%). The upstaging was mostly linked to the discovery of locoregional nodal involvement in 10 cases and distant metastases in the 3 other patients.

Figure 1. Stages of patients before benefitting from PET

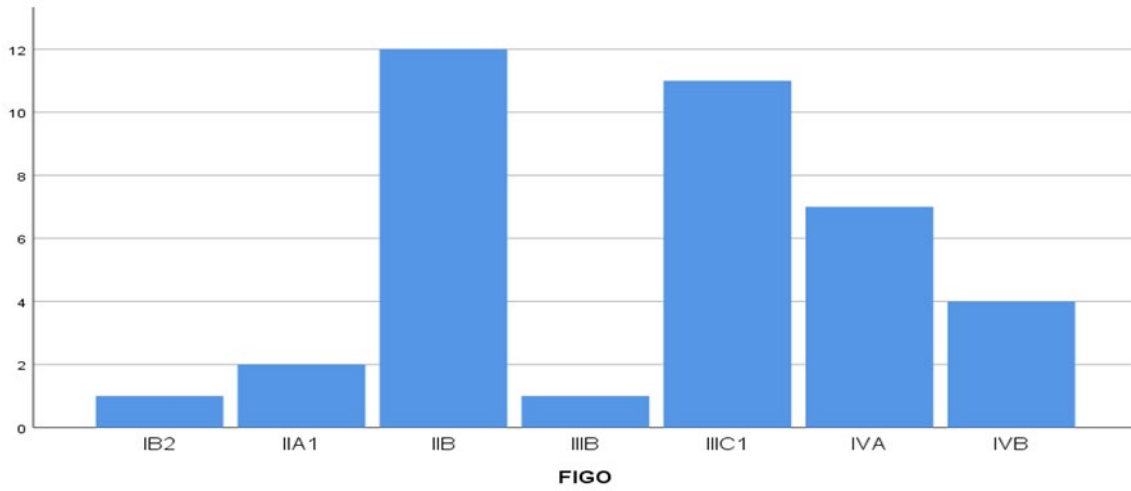
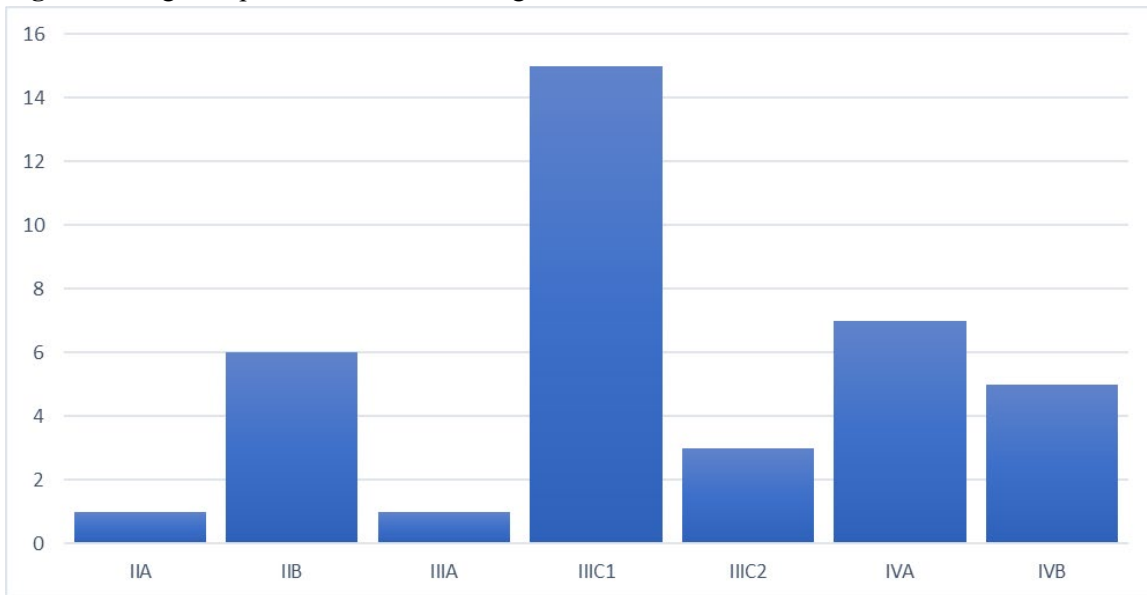


Figure 2. Stages of patients after benefitting from PET



Conclusion

Establishing an accurate stage for cervical cancer is crucial for identifying prognostic features and choosing therapeutic strategy. ¹⁸F-DG-PET CT plays an important role in evaluating the cancer extension, especially regarding nodal and distant metastases.

IAEA-CN-326/374

Case Report: Value of ^{11}C -Methionine and ^{68}Ga DOTA-TATE PET/CT in a patient with Ectopic Cushing's Syndrome

E. Lischinsky, A. Damian, A. Quagliata, F. Feo, A. Lujambio, R. Ferrando

Centro De Medicina Nuclear E Imagenología Molecular Del Hospital De Clínicas (CMNIM), Montevideo, Uruguay

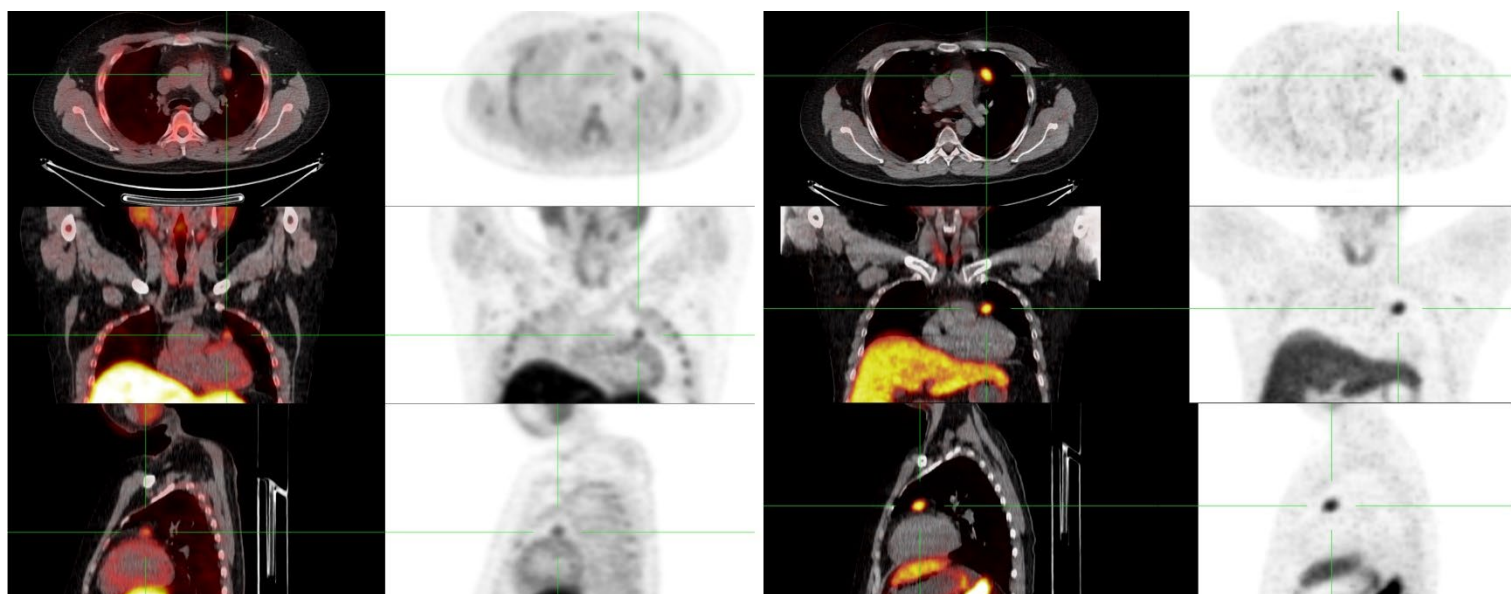
Background

Cushing's Syndrome (CS) is a rare condition characterized by elevated cortisol secretion, with a reported incidence of 2-3 cases per million inhabitants. Approximately 10-15% of CS cases correspond to the ectopic form, caused by extra-pituitary tumours secreting ACTH. PET/CT with somatostatin analogs, ^{18}F FDG, or ^{11}C -methionine can be useful in locating the primary tumour, although the role of molecular imaging in the diagnostic algorithm for these patients is still under discussion.

Case Report

This is a report of a 29-year-old male with ACTH-dependent Cushing's Syndrome, who was initially studied with conventional and magnetic resonance imaging which reported a pituitary adenoma and subsequently underwent pituitary tumour surgery, with inconclusive pathological findings. Persistent hypercortisolism with repercussions such as osteonecrosis of the right hip and hypertension prompted further evaluation.

A PET/CT with ^{11}C -methionine revealed normal aminoacid metabolism for age in the sella turcica and a mediastinal nodular lesion measuring 14 x 17 mm with increased radiotracer uptake (Figure 1). The study was complemented with ^{68}Ga DOTA-TATE PET/CT, showing an increased expression of somatostatin receptors in the lesion (Figure 1). The patient underwent surgery with resection of the mediastinal nodular lesion, confirmed as an ACTH-secreting tumour in the pathological findings, with good clinical response and outcome.



IAEA-CN-326/375

Prognostic Value of 123I-mIBG scintigraphy in children with high-risk neuroblastoma after intensive first-line treatment protocols in in Al-Assad University Hospital, local Experience

M. Zein

Al-Assad University Damascus, Syria

Background

Neuroblastoma is one of most malignancy seen in young children. Different prognosis can be observed, ranging from spontaneous regression to aggressive metastatic tumours with fatal outcomes despite multimodality therapy. Patients are divided into risk groups on the basis of age, stage, and biologic tumour factors. Although multiple clinical and imaging tests are needed for accurate patient assessment. Iodine 123 (123I) metaiodobenzylguanidine (MIBG) is the first-line functional imaging agent used in neuroblastoma imaging.

Purpose

Evaluate the prognostic value of 123I-mIBG scintigraphy in children with high-risk neuroblastoma after intensive first-line treatment protocols in in Al-Assad University Hospital.

Methodology

32 patients suffering from high-risk neuroblastoma referred to Al-Assad University Hospital during the period between January 2018 and January 2023. All children had initial 123I-mIBG scintigraphy for staging, also after 4 courses and after 6 courses of treatment.

The presence of any 123I-mIBG positive tumour tissue was correlated with event-free survival (EFS) and overall survival (OS).

Results

All patients had 123I-mIBG positive disease at initial staging. After four courses of induction chemotherapy, 63% of patients were still 123I-mIBG positive for the primary tumour and 58% for metastases. After six courses, 34% of patients had 123I-mIBG uptake by the primary tumour and 41% residual 123I-mIBG positive metastatic disease.

Conclusion

Functional imaging with 123I-mIBG scintigraphy can identify poor responders with any persistent metastatic 123I-mIBG uptake who are at a high risk of disease relapse.

IAEA-CN-326/376

The Evolving Role of Positron Emission Tomography/Computed Tomography in Noncancerous Renal Diseases: A Comprehensive Review

S. Moghrabi, A. Al-Ibraheem

King Hussein Cancer Center, Jordan

Noncancerous kidney diseases include a variety of conditions affecting both the structure and function of the kidneys, thereby causing a range of health-related problems. Positron Emission Tomography/Computed Tomography (PET/CT) has emerged as a potential diagnostic tool, offering a multifaceted approach to evaluating noncancerous renal illnesses. Its clinical significance extends beyond its conventional role in cancer imaging, enabling a comprehensive assessment of renal structure and function. This review explores the role of PET/CT in identifying renal inflammation, detecting early complications in transplant recipients, uncovering autoimmune processes, and evaluating renal fibrosis. The current review aims to promote further research and technological advancements in order to popularize PET/CT's clinical utility in diagnosing and treating nonmalignant kidney diseases.

IAEA-CN-326/378

PET tracing of [⁶⁴Cu]-labeled micro-or nano-polystyrene and the assessment of toxicity**J. Shanmugiah^{1,2}, J. Zaheer¹, C. Im^{1,2}, C. M. Kang^{1,2}, J. S. Kim^{1,2}**¹Division of Applied RI, Korea Institute Radiological and Medical Sciences (KIRAMS), Seoul 01812, Republic of Korea²Radiological and Medico-Oncological Sciences, University of Science and Technology (UST), Seoul 01812, Republic of Korea**Background**

Recent studies showed the presence of microplastic in human lungs. There remains an unmet need to identify the biodistribution of microplastic after inhalation. In this study, we traced the biodistribution of inhaled micro-sized polystyrene (mPS) and/or nano-sized PS (nPS) using copper-64 with PET in mice. In addition, we revealed the toxicity of mPS or nPS.

Methodology

We used 0.2-0.3- μ m sized mPS and 20-nm sized nPS throughout. [⁶⁴Cu]Cu-DOTA-mPS, [⁶⁴Cu]Cu-DOTA-nPS or [⁶⁴Cu]CuCl₂ were used to trace the distribution in the murine inhalation model. PET images were acquired using an INVEON PET scanner at 1, 12, 24, 48, and 72 h after intratracheal instillation, and the SUV_{max} for interesting organs were determined, biodistribution was then determined in terms of percentage injected dose/gram of tissue (%ID/g). Ex vivo tissue-radio thin-layer chromatography (Ex vivo-radioTLC) was used to demonstrate the existence of [⁶⁴Cu]Cu-DOTA-PS in tissue. To assess the cytotoxicity, *in vitro* cytotoxicity test was performed using 2D Bronchial Epithelial Organoid.

Results

PET image demonstrated that the amount of [⁶⁴Cu]Cu-DOTA-mPS retained within the lung was significantly higher than [⁶⁴Cu]Cu-DOTA-nPS until 72 h; SUV_{max} values of [⁶⁴Cu]Cu-DOTA-mPS in lungs was 11.7 ± 5.0 , 48.3 ± 6.2 , 65.5 ± 2.3 , 42.2 ± 13.1 , and 13.2 ± 2.3 at 1, 12, 24, 48, and 72 h respectively whereas it was 31.2 ± 3.1 , 17.3 ± 5.9 , 10.0 ± 3.4 , 8.1 ± 2.4 and 8.9 ± 3.6 for [⁶⁴Cu]Cu-DOTA-nPS at the corresponding timepoints. The biodistribution data supported the PET data with a similar pattern of clearance of the radioactivity from the lung. nPS cleared rapidly post instillation in comparison to mPS within the lungs. Higher accumulation of %ID/g for nPS (roughly 2 times) were observed compared to mPS in spleen, liver, intestine, thymus, kidney, brain, salivary gland, ovary, and urinary bladder. Ex vivo-radioTLC was used to demonstrate that the detected gamma rays originated from [⁶⁴Cu]Cu-DOTA-mPS or nPS. The viability of the organoids was determined using the ATP assay post treatment with mPS and nPS. Overall, there was decrease in viability in both the groups.

Conclusion

PET image demonstrated the difference in accumulations of mPS and/or nPS between lungs and other interesting organs. The information provided may be used as the basis for future studies on the toxicity of mPS and/or nPS.

IAEA-CN-326/379

Association of cardiovascular risk factors and coronary calcium burden with epicardial adipose tissue volume obtained from PET/CT imaging in oncological patients

C. Nappi¹, A. Ponsiglione¹, C. Vallone¹, R. Lepre¹, L. Basile¹, R. Green¹, V. Cantoni¹, C. G. Mainolfi¹, M. Imbriaco¹, M. Petretta², A. Cuocolo¹

¹ Department of Advanced Biomedical Sciences, Federico II University of Naples, Italy

² IRCCS Synlab SDN, Italy

Background

Whole-body positron emission tomography (PET)-computed tomography (CT) imaging performed for oncological purposes provide additional parameters such as coronary artery calcium (CAC) and epicardial adipose tissue (EAT) volume with cost-effective prognostic information in asymptomatic people beyond traditional cardiovascular risk factors.

Methodology

We investigated the relationships between cardiovascular risk factors, coronary calcium content and EAT volume in 109 consecutive oncological patients without overt coronary artery disease undergoing whole-body PET/CT imaging with 18F-fluorodeoxyglucose (FDG). Unenhanced CT images were retrospectively viewed for CAC and EAT measurements on a dedicated platform.

Results

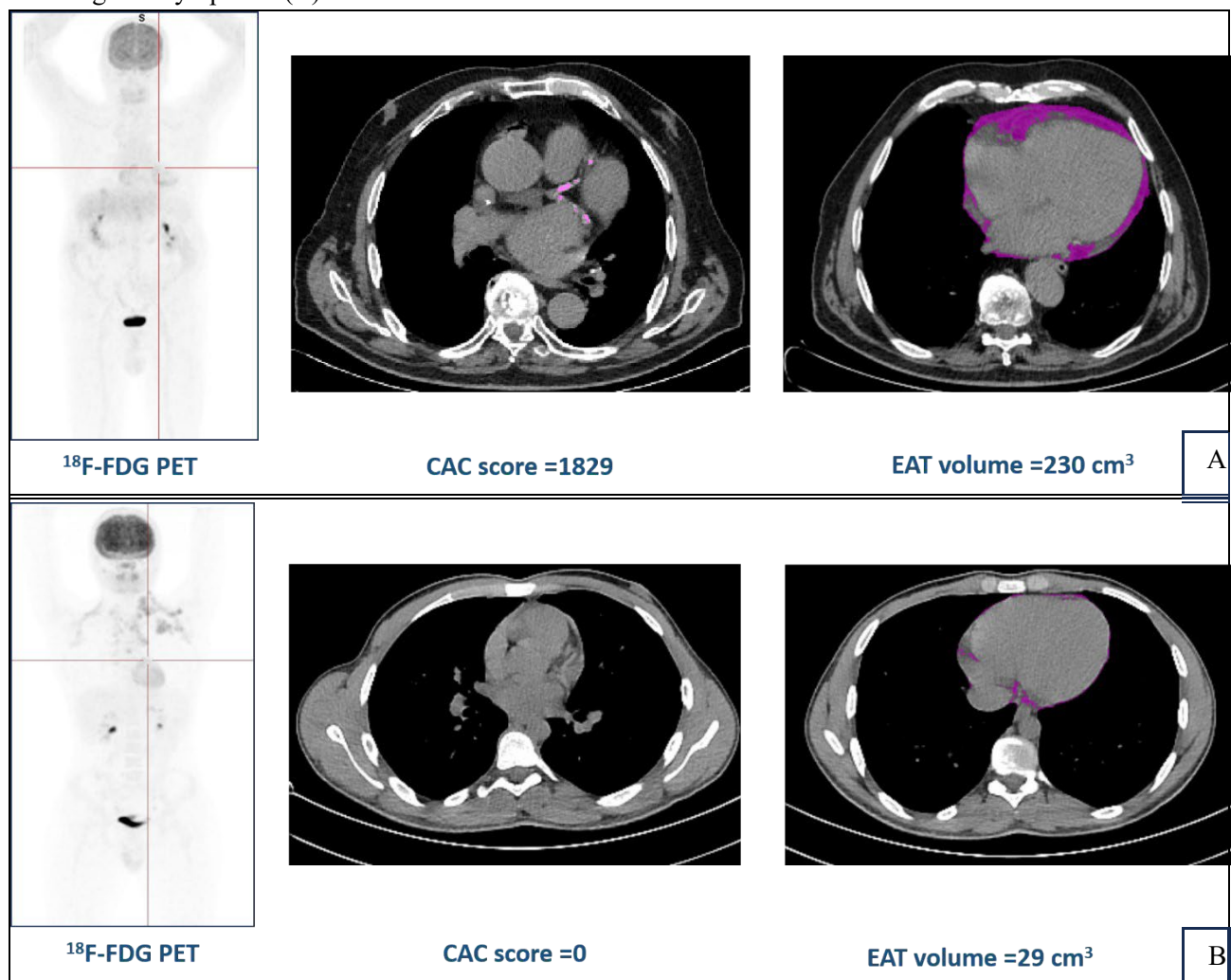
The study population comprised 109 subjects (53 men, 49%), with age ranging from 18 to 74 years. Overall, mean EAT volume was 99 ± 49 cm³. Patients with CAC score ≥ 1 were older than those with CAC = 0 ($p < 0.001$) and the prevalence of hypertension was higher in patients with detectable CAC as compared to those without ($p < 0.005$). EAT volume was higher in patients with CAC than in those without ($p < 0.001$). At univariable analysis age, body mass index (BMI), hypertension and CAC were associated with increasing EAT values (all $p < 0.005$), while at multivariable analysis, only age and BMI were independently associated with increasing EAT (both $p < 0.001$).

Table1. Linear regression analysis for prediction of increasing EAT volume in overall population.

	Univariable analysis			Multivariable analysis		
	SE	β coefficient	P value	SE	β coefficient	P value
Age	0.27	0.47	<0.001	0.32	0.45	<0.001
Male gender	9.3	-0.12	0.21			
Body mass index	0.99	0.31	<0.001	0.9	0.06	<0.001
Diabetes	16.1	0.13	0.18			
Hypertension	9.1	0.28	0.003	8.7	0.30	0.61
Hypercholesterolemia	12.4	0.17	0.70			
Smoking	10	0.14	0.14			
Family history of CAD	11.8	0.11	0.24			
$\ln(\text{CAC}+1)$	1.67	0.35	<0.001	1.83	0.12	0.25

EAT, epicardial adipose tissue, CAD, coronary artery disease.

Figure 1. Case examples of an 80 years old man with colorectal cancer (A) and a 20-year-old man with Hodgkin’s lymphoma(B).



Conclusion

This study suggests the importance of assessing EAT volume alongside CAC score in all oncological patients referred for whole-body PET/CT imaging, regardless the primary clinical inquiry. This approach allows to evaluate at the same time cancer disease and atherosclerotic burden in a single test already included in the clinical work-up.

IAEA-CN-326/380

Role of baseline [18F]FDG PET/CT in patients with primary extranodal lymphoma-experience in Bangladesh

R. Afrin, A. Akhter, S. M. F. Begum, S. Sharmin

Bangladesh Atomic Energy Commission, Bangladesh

Background

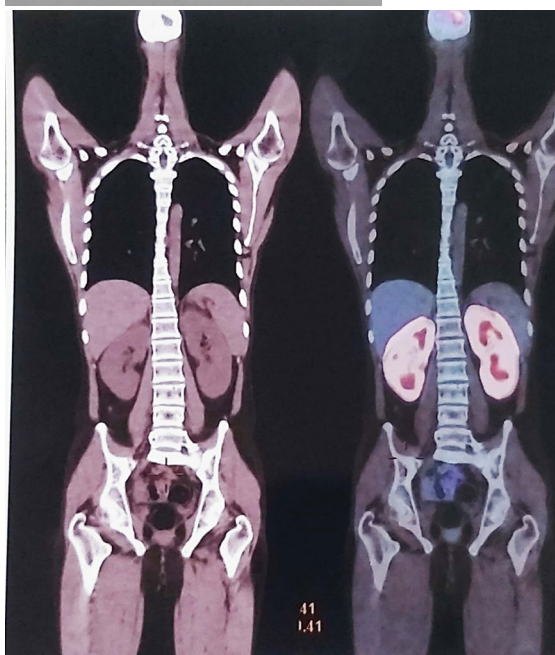
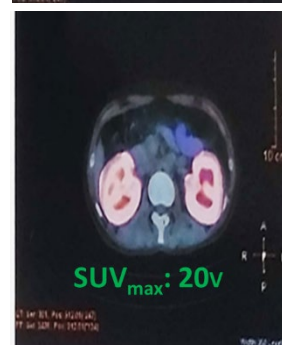
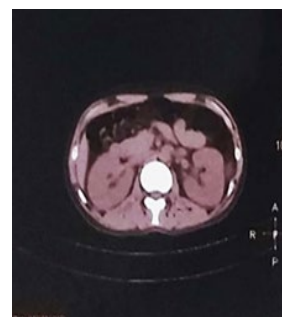
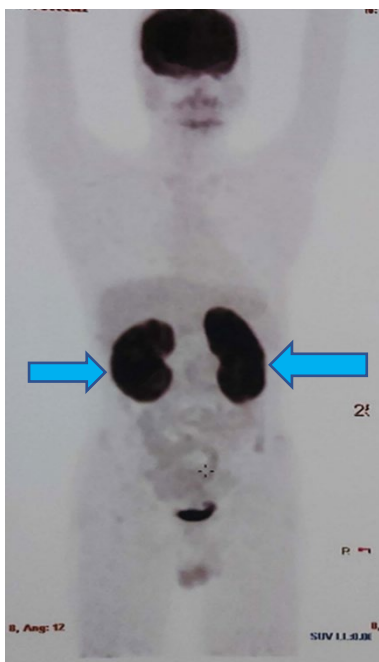
Lymphoma is a hematological malignancy that originates from the lymphatic system and can occur at extranodal sites. Extranodal disease is common as part of the lymphomatous involvement but rarely, this could be the primary anatomical site where lymphoma arises. Primary extranodal lymphoma can involve any organs or systems, sometimes at unexpected sites with non-specific presentations, mimicking carcinoma or infection. (Fluorine-18) fluoro-2-deoxy-d-glucose positron emission tomography with computer tomography (FDG-PET/CT) has become the standard imaging modality for staging and surveillance of the disease. This study was conducted to determine the value of 18 F-FDG PET/CT in newly diagnosed primary extranodal lymphoma patients.

Methodology

This cross sectional study was conducted from January 2021 to December 2023 in a PET/CT center of the capital Dhaka city, Bangladesh. A total 110 patients (aged between 10 and 81 years, mean age 51 years) were included by purposive sampling. Patients presenting with histopathology and immunohistochemistry proven primary extranodal lymphoma were included. Whole body FDG PET CT scan was acquired from vertex to mid-thigh in a whole-body PET/CT scanner after administration of 5 to 10 mCi of 18-F FDG.

Results

54% patients were male and 44% were female. Patients age was in between 10 to 81 years. Maximum 96% patients had Non-Hodgkin's lymphoma and 4% had Hodgkin's lymphoma. Diffuse large B cell lymphoma was the most common subtype. Maximum 28 patients were in between 50-59 years. SUVmax value was in between 5 to 37. 68% patients showed hepatosplenomegaly. Maximum 29% patients had the primary extranodal site of involvement in gastrointestinal tract, 10% in bone, 8% in orbit, 8% in tonsil followed by bone marrow, thyroid, nasopharynx, spleen, ovary and others sites. 24% patients had associated FDG avid lymph nodes. Maximum 52% patients with primary extranodal lymphoma showed SUVmax value in between 11 to 20.



Case 2: 18 years male,

intermediate grade NHL

Conclusion

Primary extranodal lymphoma can affect any organ or system, although challenging to diagnose at presentation, [18F]FDG PET/CT can be a valuable imaging technique. [18F]FDG-PET enables accurate detection of more unusual organs with extranodal lymphomatous infiltration that help in up or down staging the disease.

Keywords: Primary extranodal lymphoma, F-18 FDG, PET/CT

IAEA-CN-326/382

Aortitis secondary to COVID-19 infection showed by 18F-FDG PET-CT imaging

C. Stasiak, S. Almeida, P. Castro, R. Rodrigues, D. Bianchi, R. Barata

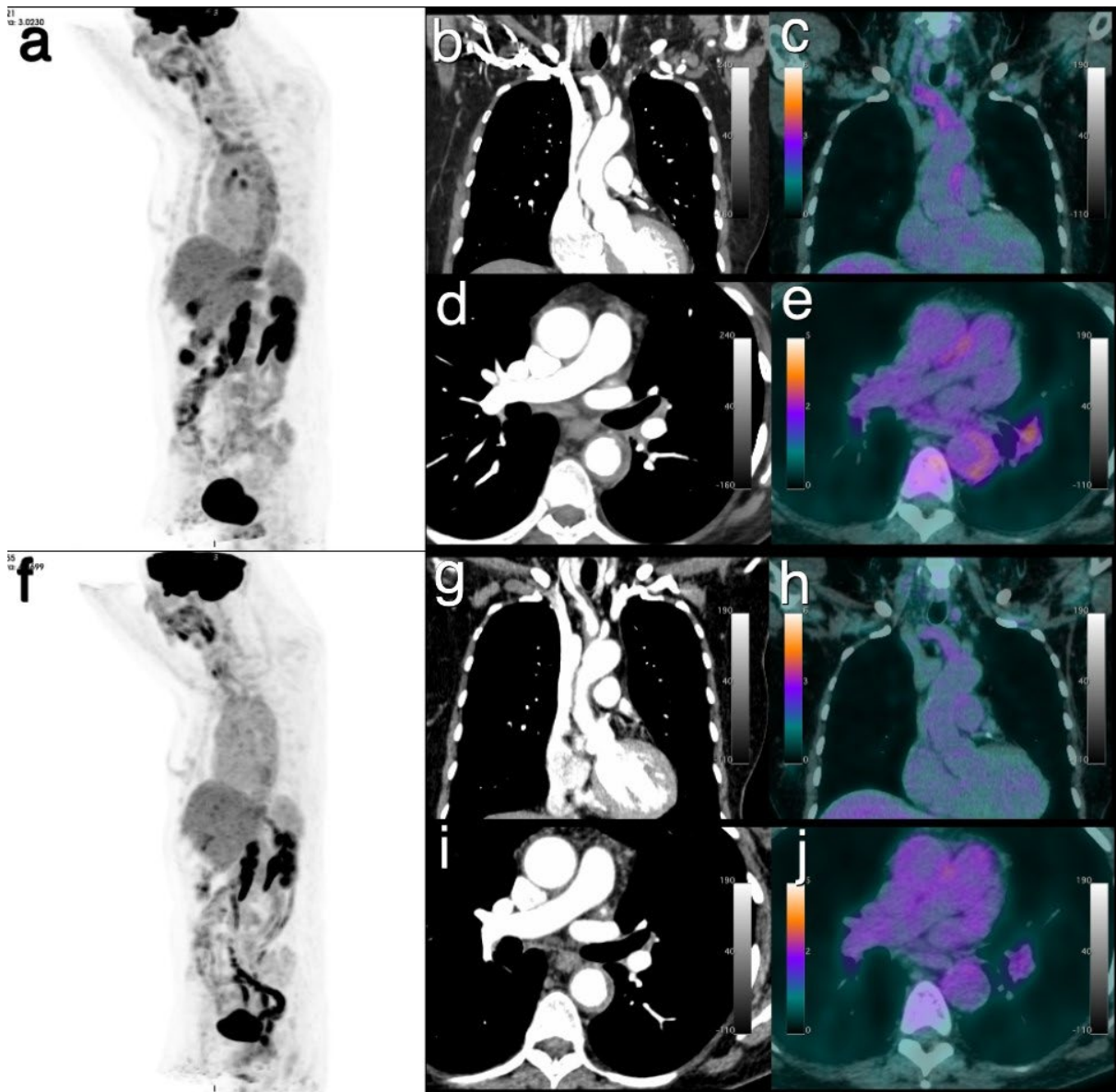
D'Or Institute for Research and Education, Brazil

Background

There are a few case reports in the literature discussing aortitis secondary to SARS-CoV-2 infection. Aortitis is an inflammatory disease that affects the aortic and its main branches wall, and could be classified as infectious and noninfectious. 18F-FDG PET-CT can be used in the diagnosis of large vessel vasculitis and is able to monitor vascular inflammation. The mechanisms involving COVID-19 infection and aortitis is not fully understood but it is hypothesized that it is related to the infiltration of the endothelium by neutrophils and mononuclear cells, provided by angiotensin-converting enzyme-2 receptors, which causes lymphocytic endotheliitis. Furthermore, there is deposition of inflammatory factors such as antibodies and complement proteins which predisposes to thrombosis.

Case Report

A 70-year-old woman presented with SARS-CoV-2 infection confirmed by RT-PCR on January 6th, 2021. She had a dry cough, fever, fatigue and diarrhea. She received supportive treatment but presented worsened symptoms. On January 17th she was admitted to a hospital due to persistent fever and high serum inflammatory markers. On January 22th, she performed a 18F-FDG PET-CT (a, MIP image). Imaging showed radiotracer uptake in a pulmonary consolidation in the anterolateral basal segment of the left inferior lobe, right pleural thickening and in lymph nodes in the inferior paratracheal and subcarinal chains and left pulmonary hilum. Furthermore, diffuse thickening in the wall of several arteries was identified on contrast enhanced CT (b, coronal CT; d, axial CT), which was FDG-avid: left proximal brachiocephalic trunk, left carotid artery, left subclavian artery, pulmonary artery, descending aorta and abdominal aorta with SUV_{max} 3.4 (c, coronal PET-CT; e, axial PET-CT). Aortitis was diagnosed as being secondary to COVID-19 infection. She did not receive any specific medication such as corticosteroids. The patient performed a second 18F-FDG PET-CT imaging on March 26th, 2021 for disease reassessment (f, MIP image). Pulmonary consolidation in the left inferior lobe and pleural reaction which were FDG-avid were no longer observed. Radiopharmaceutical uptake decreased in mediastinal lymph nodes. A reduction in arterial radiotracer uptake was also observed (h, coronal PET-CT; j, axial PET-CT), as well as a reduction in the diffuse thickening of the arterial walls (g, coronal CT; i, axial CT).



Conclusion

^{18}F -FDG PET-CT is an excellent tool that can be used in the diagnosis of large vessel vasculitis and is able to monitor vascular inflammation.

IAEA-CN-326/383

PSMA-68Ga PET-CT showing thyroiditis after initiation of immunotherapy treatment in clear cell renal cell carcinoma

C. Stasiak, D. A. Carvalho, S. Almeida, H. Botelho, P. Castro, C. Magalhães

D'Or Institute for Research and Education, Brazil

Background

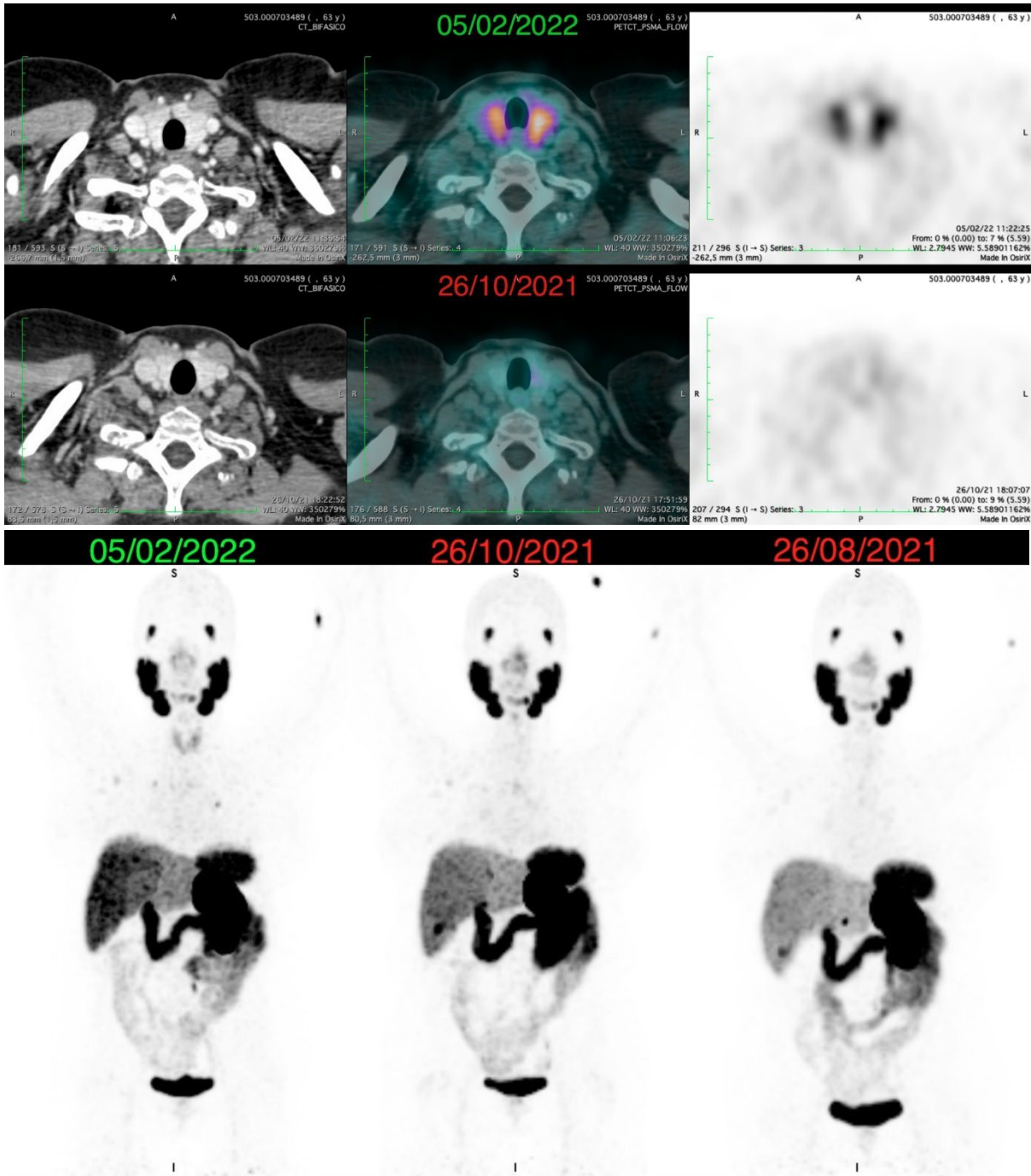
Immunotherapeutic treatment can cause adverse effects, such as thyroiditis, which can be demonstrated by PET-CT with FDG. Increased PSMA expression in thyroiditis secondary to immunotherapy is not a commonly reported finding.

Case report

Female 63 years old patient with a history of clear cell carcinoma. She underwent right nephrectomy on 06/2021 (pT2 - G3 - free margins, without rhabdoid or sarcomatoid component). 68Ga-PSMA PET-CT on 08/2021 showed uptake in a lesion on the right diaphragmatic pillar, which underwent radioablation. PET-CT on 10/2021 showed resolution of uptake in this topography, but increased uptake appeared in multiple pulmonary nodules. She started immunotherapy with nivolumab and ipilimumab on 11/2021. The 02/2022 PET-CT study to evaluate response to therapy showed an increased uptake and increase in the dimensions of pulmonary nodules. Furthermore, diffuse increased uptake appeared in the thyroid gland, with SUVmax of 6.4, without morphological changes in the corresponding tomographic sections. The patient was not using levothyroxine in the study on 10/2021, and when she returned on 02/2022 she had started using it, showing a clinical association with the imaging findings.

Discussion

The appearance of diffuse PSMA uptake in the thyroid after starting treatment with nivolumab and ipilimumab was attributed to probable thyroiditis secondary to immunotherapy. Focal uptake of PSMA has previously been described as subacute granulomatous thyroiditis mimicking renal carcinoma metastasis. Another study found a focus of PSMA uptake consistent with renal cell carcinoma metastasis. Radiopharmaceutical uptake on PSMA PET-CT in Hashimoto's thyroiditis was attributed to PSMA expression in dendritic cells, and not to neovasculature, as in thyroid carcinoma. Cases such as the one reported of increased PSMA expression resulting from thyroiditis secondary to immunotherapy, are not commonly reported.



Conclusion

PSMA PET-CT can help diagnose not only lesions related to the neoplastic tissue itself, but also adverse effects related to the treatment implemented, including immunotherapy.

IAEA-CN-326/384

Case presentation: metastatic calcifications of colorectal cancer**R. Abushawareb**

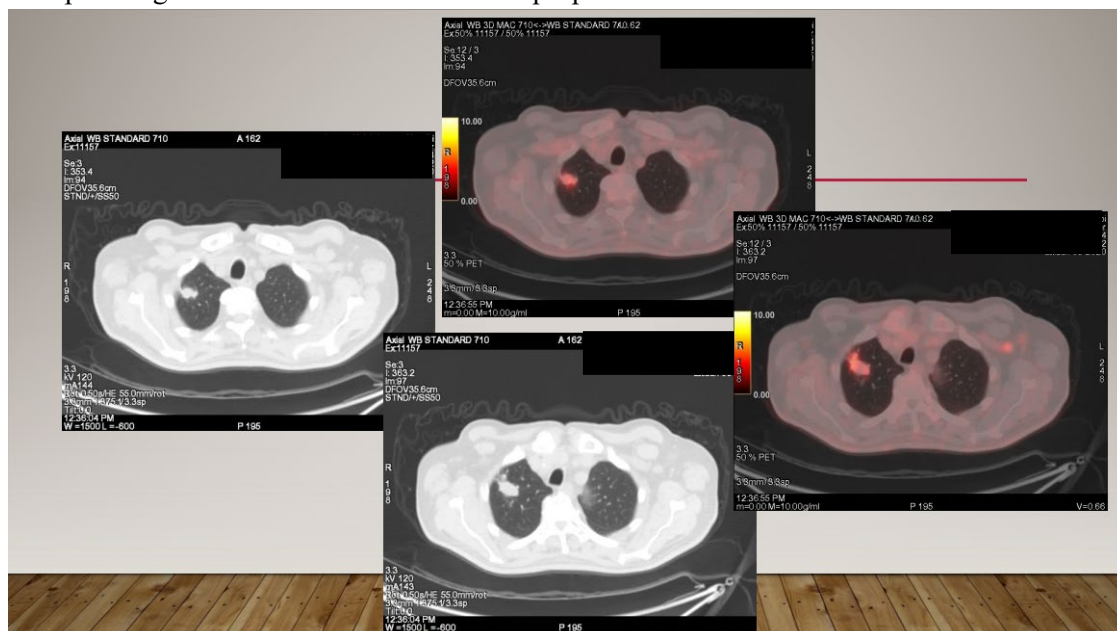
Ministry of Health, Al Amiri Hospital, Kuwait

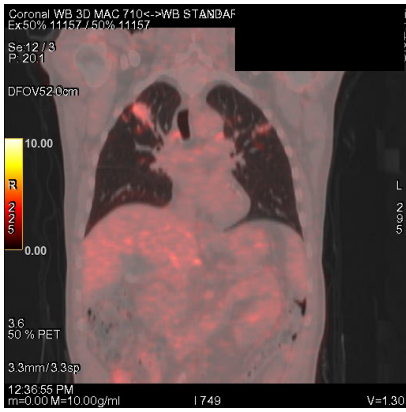
Background

Anorectal adenocarcinomas compromise the vast majority of colon and rectal cancers (98%). Bleeding is the most common symptom of rectal cancer, occurring in 60% of patients. However, many rectal cancers can be asymptomatic and discovered accidentally. Changes in bowel habits (43%), occult bleeding (20%), abdominal and back pain (5%), malaise (9%), as well as rare emergencies like peritonitis (3%) can also be seen. Diagnosis is made by proctoscopy, sigmoidoscopy/colonoscopy, and if metastatic disease (local or systemic) is suspected, a CT scan of the chest, abdomen, and pelvis, while an MRI pelvis is preferred if available. A PET scan is not routinely indicated. Calcified metastatic lesions in rectal cancers usually display scattered punctate patterns to varying degrees on CT scans. Skeletal muscle metastases from colorectal cancers are very rare.

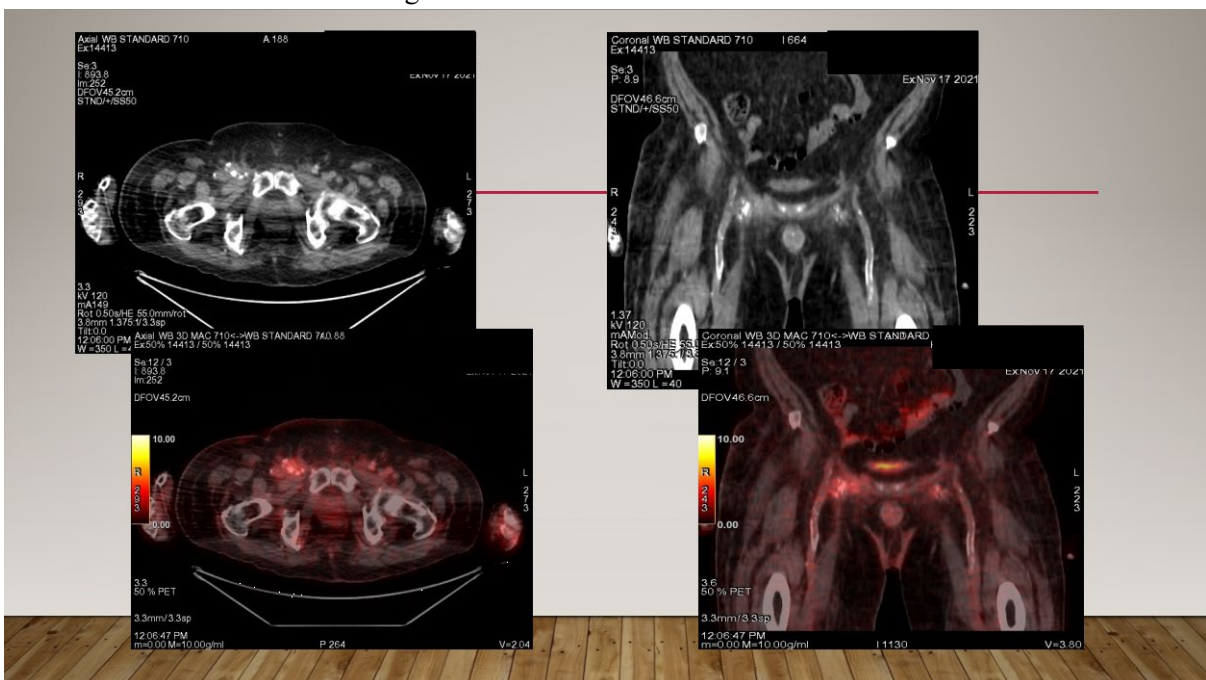
Case Series

This report is a case of a 67-year-old male with anorectal adenocarcinoma who was resected with colostomy in Nov 2018/9 and received chemoradiation therapy. A follow-up CT scan showed suspected lung lesions, so a PET scan was done in Jan 2020 and showed multiple lymphadenopathies (SUV max 7.0) and right upper lobe avid mass (SUV max 4.7) that turned to be TB after histopathological confirmation and received proper treatment course.

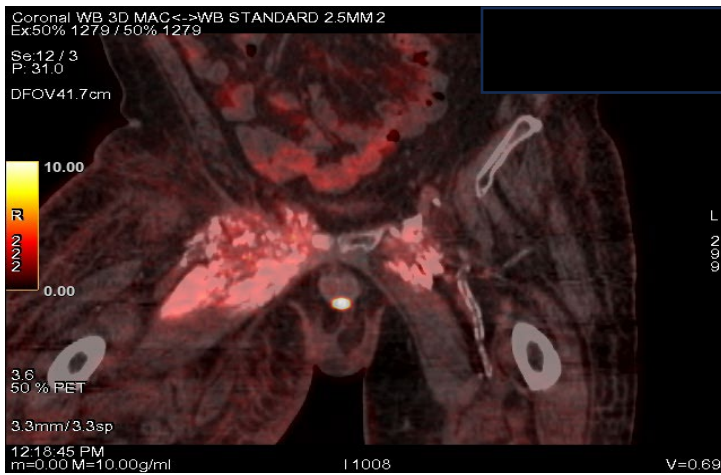
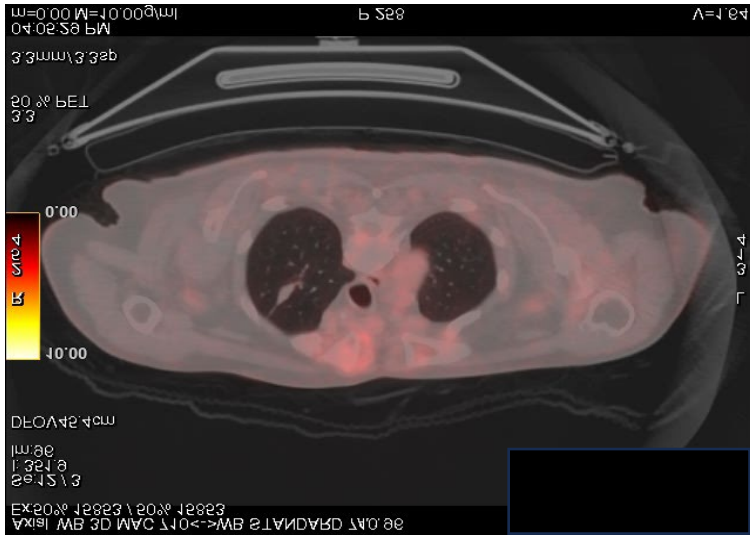




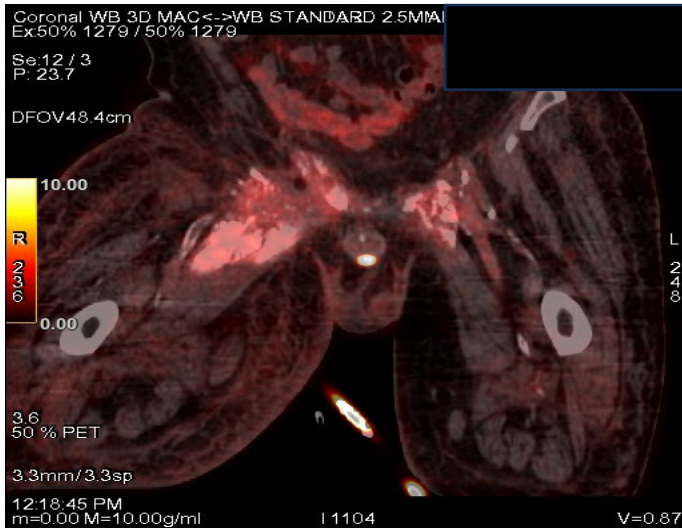
In November 2021, a follow-up PET/CT scan showed resolved lymphadenopathies and a persistent avid right upper pulmonary nodule. A right pectineus muscle avid lesion (SUV max 4.4) with scattered calcifications on CT images was also noted.



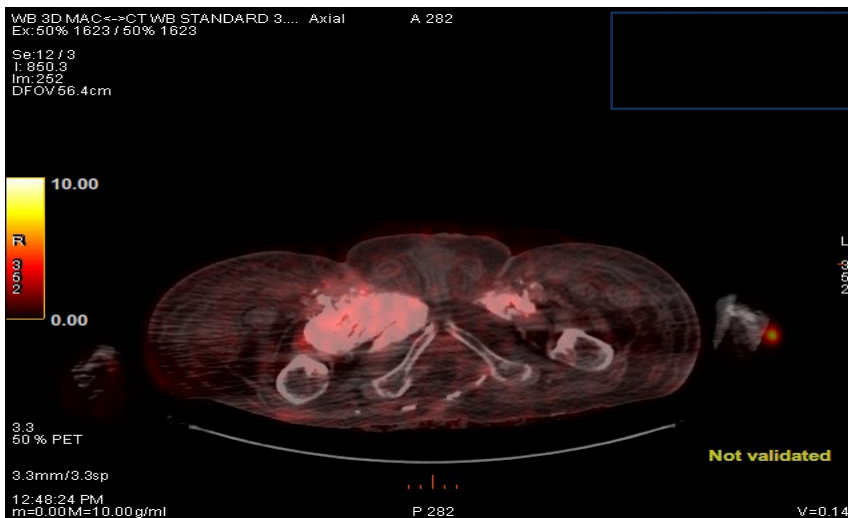
In the December 2022 follow-up PET/CT scan, a time interval decline in the right pulmonary avid nodule was seen (SUV max 1.4), with a marked increase in the morphologic and metabolic appearance of the right pectineus muscle lesion (SUV max 6.4).



Histopathology was done from the right pectineus lesion on June 18th, 2023, and showed infiltrative moderately differentiated adenocarcinoma, likely metastatic from GI or Pancreatic origin. In July 2023, a PET/CT scan showed a time interval increase in morphological appearance, and mild decline in metabolic activity of the right pectineal lesion (SUV max 5.3) and an increase in left side intramuscular lesion (SUV max was 3.2, now 4.0).



He was started on chemotherapy; his last session was in Sep 2023, with a follow-up scan in Nov 2023 that showed a time interval increase in metabolic and morphologic appearance of bilateral inguinal lesions: Right side (SUV max 4.9 was 5.3), Left side (SUV max 4.1 was 4.0).



Conclusion

Intra-muscular metastatic colorectal cancer is rare, with only a few cases being reported in published literature. The prevalence ranges from 0.03 – 16% with different imaging patterns and is associated with poor prognosis. Therefore, early identification is essential to improve patient outcome.

IAEA-CN-326/386

Assessment of occupational exposure working with automatic injection systems and a high sensitivity PET/CT system

K. Skovorodko¹, I. Andriulevičiūtė¹, M. Martinkus¹, R. Komiagienė^{1,2}, B. Gricienė^{1,2}, Christian Bernhardsson³

¹Vilnius University Hospital Santaros Klinikos, Vilnius, Lithuania

²Vilnius University, Faculty of Medicine, Institute of Biomedical Sciences, Vilnius, Lithuania

³Medical Radiation Physics, Department of Translational Medicine, Lund University, Carl Bertil Laurells gata 9, Malmö, Sweden

Background

Monitoring of extremity and whole-body occupational doses of nuclear medicine personnel is essential to ensure that legal limits are not exceeded, and if possible, to optimize workflow. New technologies allow to reduce the radiation exposure to the personnel and patients, however, due to shorter examination times, the workflow may significantly increase resulting in higher doses for staff working with radiopharmaceuticals.

The aim of this study was to assess the extremity and whole-body radiation doses of nuclear medicine personnel working with automatic infusion systems dedicated for [¹⁸F]FDG radiopharmaceutical administration with high sensitivity PET/CT system.

Methodology

To evaluate extremity doses, household NaCl pellets (made at Lund Luminescence Laboratory for Dosimetry (LLLDo Lab), Sweden) readout by optically stimulated luminescence (OSL) were used. For the readout of the pellets, the Risø TL/OSL DA-15 reader (DTU Nutech, Denmark) was used. The calibration of the NaCl pellets was performed directly after readout using a single calibration dose with ⁹⁰Sr/⁹⁰Y beta of the reader and fluorine-18 sources. NaCl pellets were used for point absorbed dose assessments, attached to both hands of the radiology technologist in 15 positions (on fingertips, palm and wrist) of each hand and at a typical monitoring position (base of the middle finger of the dominant hand). Personal dose equivalent, Hp(10), was assessed using the Mirion DMC 3000 (Finland) active personal dosimeter. [¹⁸F]FDG administration was performed with the automatic injection systems IRIDE (Comecer, Italy) and Posijet (Lemer Pax, France). The patients were scanned using Omni Legend PET/CT system (GE Healthcare, United States) equipped with silicon photomultiplier (SiPM)-based detectors with BGO crystals, large axial field of view, and featured with AI-based auto positioning camera. The patients were scanned using a dosage of 2 MBq [¹⁸F]FDG per kg.

Results

The comparison of the doses between the NaCl pellets worn at various positions on the radiology technologists right hand palm showed inhomogeneous dose distribution. It was found that the doses at the fingertips are higher compared to the doses with a typical ring dosimeter position in Lithuania (base of the middle finger of the dominant hand). The measured mean whole body in terms of Hp(10) received by the personnel from one PET examination operating automatic systems was within one μ Sv per patient.

Conclusion

Occupational radiation exposure can be effectively optimized by different means including staff monitoring with active and passive dosimetry in combination with education. Working with the automatic injection systems ensures safe handling and minimization of radiation exposure to the patient and healthcare workers. The results show dose distribution on the personnel extremities, further analysis and optimization is needed for more precise absorbed dose determinations.

IAEA-CN-326/387

The Prognostic Utility of FDG PET/CT In Lymphoma Patients Under CAR-T-Cell Therapy: A Systematic Review and Meta-Analysis

A. Abdlkadir¹, A. Al-Ibraheem²

¹ Department of Nuclear Medicine, Radiotherapy and Nuclear Medicine Hospital, Iraq

² King Hussein Cancer Center, Jordan

Background

Chimeric antigen receptor-engineered (CAR) T-cell therapy has attracted considerable attention since its recent endorsement by the Federal Drug Administration, as it has emerged as a promising immunotherapeutic modality within the landscape of oncology. This study explores the prognostic utility of [18F]Fluorodeoxyglucose positron emission tomography/computed tomography ([18F]FDG PET/CT) in lymphoma patients undergoing CAR-T-cell therapy.

Methodology

PubMed, Scopus, and Cochrane databases were explored to search for relevant topics. English dataset retrieval from inception until December 22, 2023, was carried out. The primary measures of assessment included overall survival (OS) and progression-free survival (PFS). Comprehensive details from each study were collected and subjected to survival analysis using STATA 17.0 software.

Results

A total of 11 studies were found eligible for systematic review and meta-analysis. The majority of retrieved study results showcased promising capabilities for PET-derived parameters. To further acknowledge and ascertain these findings, the pooled hazard ratios of maximum and mean standardized uptake values, metabolic tumour volume, and total lesion glycolysis for OS and PFS will be calculated at a later stage.

Conclusion

[18F]FDG PET/CT offers valuable insights in lymphoma patients undergoing CAR-T-cell therapy.

IAEA-CN-326/388

Effectiveness of fasting alone in suppressing physiological myocardial FDG uptake for evaluation of myocardial inflammation

F. Abdullahi¹, K. Makhdomi¹, J. Shah^{2,3}, S. Gitau¹

¹Department of Radiology, Aga Khan University, Nairobi, Kenya

²Department of Internal Medicine, Aga Khan University, Nairobi, Kenya

³Brain and Mind Institute, Aga Khan University, Nairobi, Kenya

Background

Positron emission tomography (PET) with ¹⁸F-Fluorodeoxyglucose ([¹⁸F]FDG) is used in evaluation of inflammatory disorders of the heart such as cardiac sarcoidosis and myocarditis. However, the normal physiologic uptake of the myocardium needs to be suppressed as it can obscure pathological uptake in these conditions. The primary objective of this study is to determine the effectiveness of fasting duration in suppressing physiological myocardial uptake and thereafter establish an imaging protocol.

Methodology

Retrospective review was conducted on patients who underwent whole-body FDG PET/CT for oncological evaluation at our institution between January 2019 and December 2020. Patients were categorized into three groups based on fasting duration: Group A (<12 hours), Group B (12-17 hours), and Group C (18 hours or more). Two independent readers qualitatively graded myocardial FDG uptake, defining adequate suppression as no uptake (grade 0) or uptake similar to or below liver background (grade 1). Uptake above the liver background (grade 2) was considered inadequate.

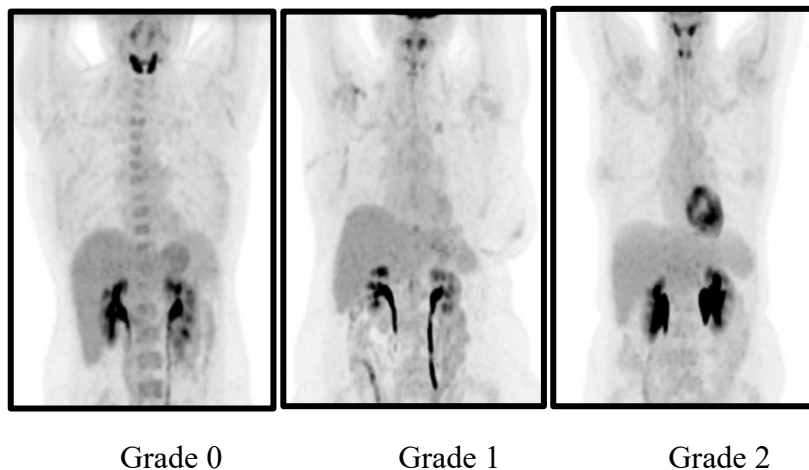


Figure 1. Variable grades of myocardial FDG uptake on maximum intensity projection reconstruction.

Results

A total of 450 patients were included in the study with each fasting duration group containing 150 patients. There was association between duration of fasting and myocardial FDG uptake suppression with 77.3%, 66% and 60% of patients achieving adequate myocardial FDG suppression in Group C, Group B and Group A respectively (P=0.005). There was no significant association between the myocardial uptake pattern and blood glucose level, age and diabetes. However, there was statistically

significant association between the myocardial uptake suppression with gender ($P=0.024$) and body mass index (BMI) ($P=0.006$). There was almost perfect inter-reader agreement (Cohen's Kappa of 0.909 (95% CI= 0.868-0.950)) on visual grading of myocardial FDG uptake.

Conclusion

Fasting for 18 hours or more is effective in suppressing physiologic myocardial FDG uptake to allow for evaluation of myocardial inflammation on FDG PET and provides a practical and easy to implement protocol. Visual grading of myocardial FDG uptake has almost perfect inter-observer agreement which supports the reproducibility of qualitative analysis method.

IAEA-CN-326/389

Stress drives bad outcome in lung cancer - Chronic mental stress as determined by FDG-PET-based biomarker drives T cell exhaustion and adverse outcome in retrospective lung cancer cohort

B. Geist¹, S. Gruenert¹, M. Hacker², C. Vraka¹, L. Herbsthofer¹, L. Kenner¹, K. Kluge¹, O. Kulterer¹, T. Nakuz¹, F. Oberndorfer¹, H. Prosch¹, T. Schweiger¹, C. Spielvogel¹, M. Tomberger¹, K. Trachtova³, J. Yu¹

¹ Medical University Vienna, Austria

² Division of Nuclear Medicine, Department of Biomedical Imaging and Image-Guided Therapy, Medical University of Vienna, Austria

³ Central European Institute of Technology, Czech Republic

Background

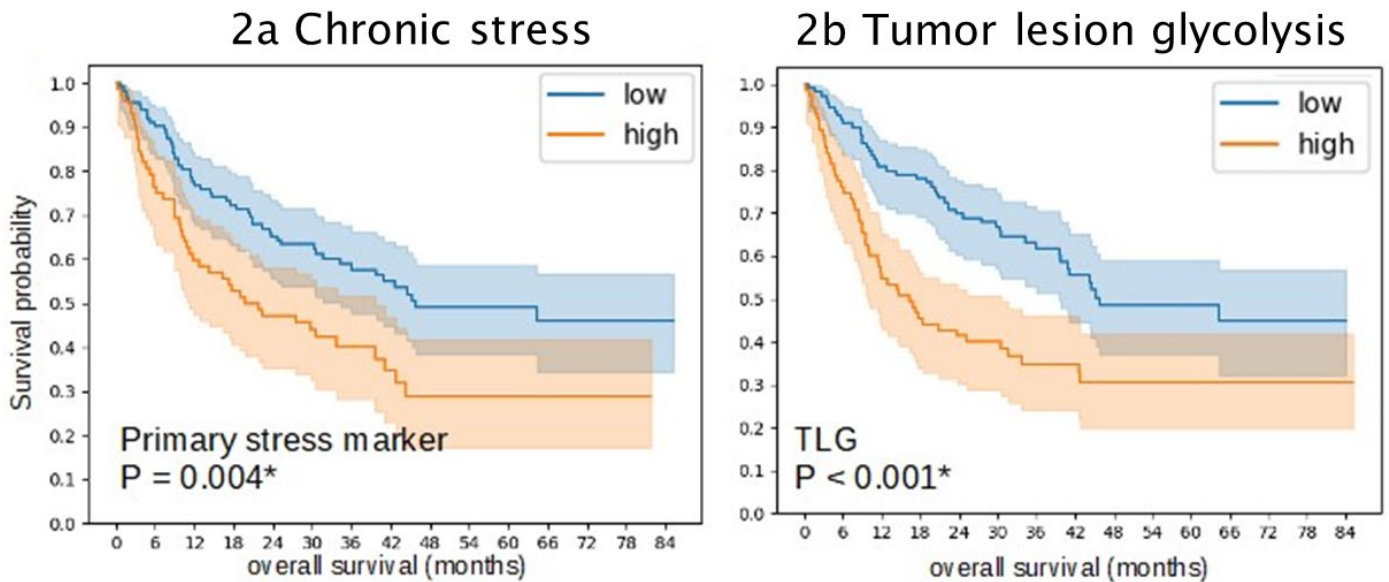
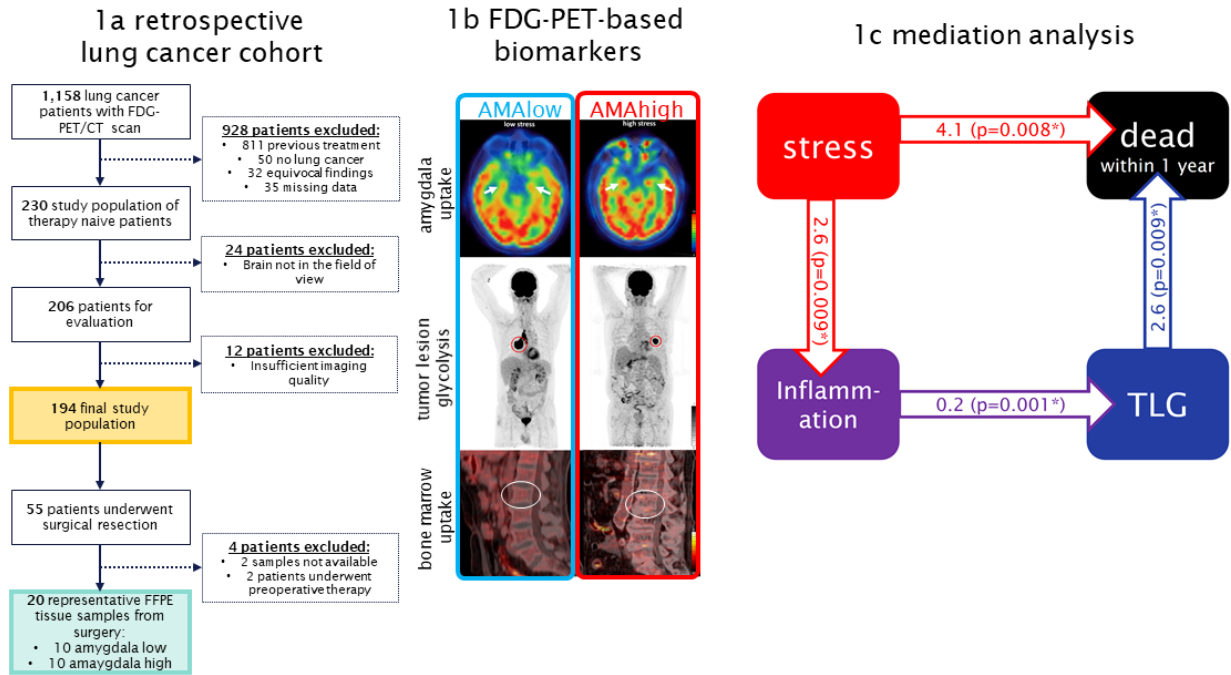
Lung cancer staging relies on [18F]FDG-PET, which provides the predictive imaging biomarker total lesion glycolysis (TLG). However, whole-body PET contains additional information about patient status based on metabolic organ activities, usually not used for clinical decision making. Indeed, elevated amygdala FDG-uptake is an established biomarker for chronic stress, while FDG-uptake in bone marrow correlates with inflammatory status. Our aim was to determine how activation of the amygdala and downstream effectors influence the prognosis of lung cancer patients. We thus explore the predictive potential of novel PET-based imaging biomarkers and advance their use in clinical decision making.

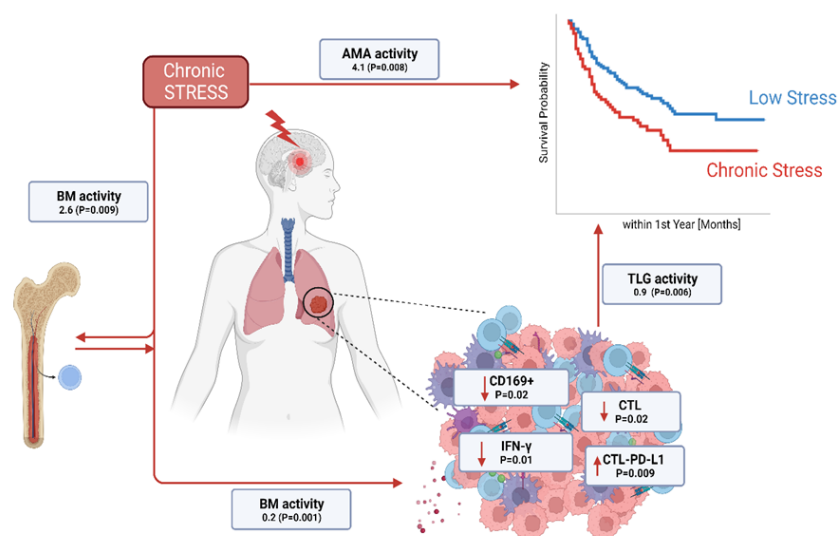
Methodology

This retrospective study assessed amygdala status, tumour parameters and bone marrow activation by whole body [18F]FDG-PET in 194 lung cancer patients at initial diagnosis and followed patients for 85.5 months (Fig. 1a). Subjects were dichotomized into chronic and low stress, based on primary stress marker from left amygdalar activity. Tumour volumes were delineated semi-automatically and TLG served as marker of tumour metabolic activity and FDG uptake in the bone marrow was normalized to blood pool activity. Blood parameters and other patient data were collected manually. For molecular analysis twenty bio-banked tissue samples were used for full genomic sequencing, spatial analysis of tumour tissue was performed using multiplexed immunohistochemistry and spatial transcriptomics.

Results

Univariate regression analysis identified the primary stress marker and TLG ($P < 0.001$) predict a death event within 1 year, while only chronic stress remained significant after multivariate adjustments (Fig. 2). Moreover, chronic stress correlated significantly with bone marrow ($r = 0.24$, $P = 0.001$) and CRP ($r = 0.21$, $P = 0.006$), but not with TLG ($r = 0.1$). Multi-omics analysis of 20 therapy naïve tumour samples identifies chronic stress attenuates in the tumour tissue IFN- γ signaling ($P = 0.01$, NES = -1.58) and CD169 expression ($P = 0.022$, NES = -0.59). In addition, in the tumour microenvironment of chronically stressed patients we detect a reduced number of cytotoxic T cells, which are however more frequently in the vicinity of PD-L1 expressing cells ($P = 0.009$). A mediation analysis confirmed the direct effect (4.1, $P = 0.008$) between the primary stress measure and one-year survival, and also a statistically significant indirect effect (0.5, $P < 0.05$), showing that the relation was serially mediated via (i) inflammation and (ii) TLG (Fig 1c).





Conclusion

We show therapy naïve lung cancer patients can be stratified by [18F]FDG amygdalar activity into chronically stressed individuals with lower life expectancy and chronic stress contributes directly via effects on the TME to lung cancer progression (Fig 3). In particular we find patients with chronic stress bad prognosis coincides with reduced IFN-g signaling and CD169 macrophages, while engagement of cytotoxic T cells with PD-L1 is significantly increased. We identify stress as the upstream event, which elicits bad outcome through chronic inflammation and attenuated tumour surveillance. Therefore, [18F]FDG-uptake in amygdala and bone marrow are robust markers with predictive potential for lung cancer outcome and their use in clinical decision making should be explored in a prospective setting.

IAEA-CN-326/391

Incremental Detection Rate of Distant Metastasis and Impact of FLUORINE-18 FDG PET/CT scan in Imaging Staging and Initial Treatment Planning Change of Pre-treatment NSCLC Patients

K. Heamaturin, A. Kositwattanarerk, C. Nitiwarangkul

Faculty of Medicine Ramathibodi Hospital, Mahidol University, Thailand

Background

In non-small cell lung cancer (NSCLC), precise initial staging is vital for treatment planning and prognosis. FLUORINE-18 FDG PET/CT scans are commonly used for comprehensive staging, providing both morphological and metabolic information to assess thoracic and extra-thoracic metastases simultaneously. However, in countries like Thailand with high tuberculosis rates, the utility of PET/CT scans may warrant careful consideration.

Methodology

This study included 205 newly diagnosed NSCLC patients at Ramathibodi Hospital, staging them with FLUORINE-18 FDG PET/CT scan between January 2011 and March 2023. Findings from conventional imaging and PET/CT scan were meticulously recorded according to the AJCC/UICC 8th edition TNM staging. McNemar's test assessed differences in TNM staging by both imaging modalities. Primary tumour SUVmax was determined, and patients categorized into low and high SUVmax groups. Regression and Spearman's correlation assessed SUVmax's relationships with TNM, clinical stage, and distant metastasis. Logistic regression explored associations with advanced TNM and clinical staging, treatment changes, and distant metastasis, providing insights into NSCLC progression and treatment planning.

Results

The study revealed that 12.7% of patients (26 individuals) showed previously undetected distant metastasis. However, there was no significant difference in metastatic detection between conventional imaging and PET/CT scan ($p=0.058$). Changes in TNM and clinical staging were observed, particularly affecting nodal staging in 88 patients (42.92%, $p<0.001^*$) and metastatic staging in 53 patients (25.85%, $p=0.048^*$). These alterations influenced treatment planning for 50 patients (24.40%, $p=0.048^*$), primarily favoring non-surgical approaches for 32 patients (15.62%). The SUVmax value of the primary tumour correlated positively with TNM stage, clinical stage, and distant metastasis. Tumour staging of T2 and T3 correlated significantly with advances in T, N, or M staging. Advanced age was associated with higher nodal staging and treatment plan changes, while nodal staging of N2 and N3 correlated with advancements in metastatic staging detected by PET/CT scan. Furthermore, patient age and nodal staging of N1 and N2 were significantly associated with changes in clinical stage. The presence of metastasis in conventional imaging and high SUVmax value of the primary tumour correlated significantly with distant metastasis identified by PET/CT scan.

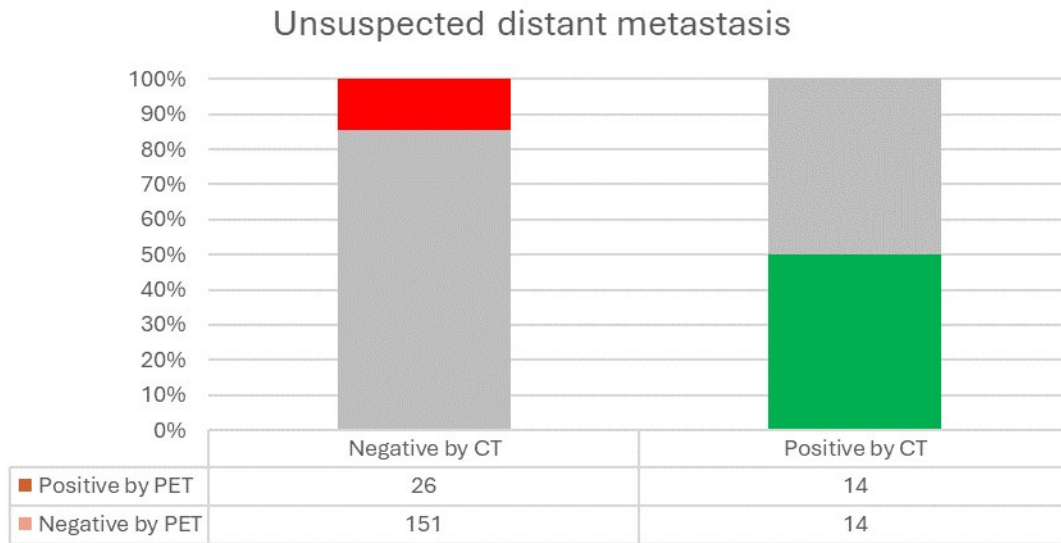


Figure 1. Detection of distant metastasis by PET/CT scan

Conclusion

PET/CT scans revealed a 12.7% increase in detecting previously unnoticed distant metastasis. Significant disparities were noted in TNM and clinical staging, as well as in initial treatment planning when assessed by PET/CT scans compared to conventional imaging workup. The SUVmax value of the primary tumour demonstrated a positive correlation with TNM stage, clinical stage, and distant metastasis. Notably, patient age, TNM staging from conventional imaging, and a high SUVmax value of the primary tumour were significantly associated with more advanced TNM staging, changes in clinical staging and treatment planning, and the presence of distant metastasis as identified by additional PET/CT scan.

IAEA-CN-326/392

Medical Physicists in Radiology and Nuclear Medicine: An urgent need in Tunisia

L. Ounalli

Research Laboratory on Energy and Matter for Nuclear Science Development (LR16CNSTN02), Tunisian Center of Nuclear Sciences and Technology, Technopark Sidi Thabet, Tunisia

Background

Medical physicists have long played an integral role in medical imaging, radiation therapy, and radiation protection. In Tunisia, the status of the profession is flawed, the most important of which is the system of obtaining certificates and the legislative framework that regulates the sector. Most importantly, this situation can negatively impact treatment quality, patient, and worker safety, whether through reluctance or relocation of staff.

Methodology

Statistical studies were conducted on the number and location of medical physicists and a national report on the status of medical physicists was prepared. Gaps have been identified and solutions presented to relevant decision-makers in the form of recommendations to advance the health care system.

Medical physicists exist only in the field of radiation therapy, absent in the fields of medical imaging and metabolic treatment (radiology and nuclear medicine) and radiation protection.

Despite the considerable number of radiology and nuclear medicine departments in the country, there are no medical physicists taking care of the quality assurance of equipment's (CT, SPECT, PET ...) and no implemented internal dosimetry.

About 40 physicists (in radiotherapy departments only) with hospital technician status and no residency program. Not all studied medical physics, some have a physics background.

Results

- Education: Since 2012, the Higher Institute of Medical Technologies of Tunis is running a master's degree in medical physics to meet the demand. About 6-7 medical physics degrees (radiation therapy) graduate each year. Despite the efforts, there are still quantitative and qualitative deficiencies: some modules are missing compared to international medical physics courses such as anatomy, biostatistics, and diagnostic radiology.

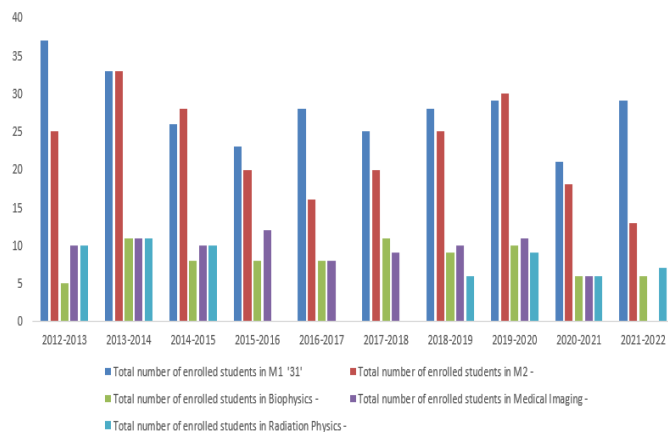


Figure 1. Basic education statistics in "Biophysics-Medical Physics-Medical Imaging" Master degree from 2012 to 2022.

- Residency program:

There is no accredited society that offers a clinical medical physicist's certificate. Here, through this paper, we appeal to the Organizations of Medical Physics (EFOMP, IOMP ...) in the capacity building, empowerment, and experience acquisition of medical physicists in Tunisia. A new Tunisian Medical Physics Society was recently created (Oct. 2022) to fill these gaps.

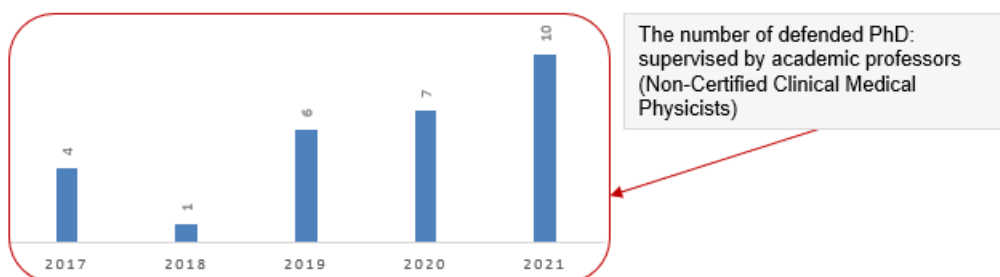


Figure 2. Defended PhD thesis in Biophysics-Medical Physics-Medical Imaging.

- Regional and international collaboration: Masters and Ph.D. students seeking guidance often have difficulties in finding specific expertise needed for their research in Tunisia. The IAEA contributes to providing technical support in the field of medical physics "Radiology and Nuclear Medicine". We cite the regional project RAF6058 "Strengthening the capacities for Radiopharmacy and Medical Physics and Radiology for expansion and sustainability of Medical Imaging Services", the ongoing regional project RAF6060 "Enhancing Member State Capacities for Improved Cancer Diagnosis and Treatment (AFRA)", the Master's Program in Medical Physics from the Abdus Salam International Centre for Theoretical Physics in Italy and the ICTP-IAEA Sandwich Training Educational Programme (STEP).

Conclusion

Medical physics in Tunisia must fulfil the need of hospitals and the current legislative framework must be updated.

IAEA-CN-326/393

[131]I-MIBG metabolic therapy: challenges and performance in Argentina

B. Konowalik, M. Bastianello, G. Pitarch, M. Cimin, R. Chirico, A. L. Lopera

Centro de Educación Médica e Investigaciones Clínicas "Norberto Quirno", Argentina

Background

High dose therapy with [131]I-MIBG is a challenging indication in paediatrics due to structural complications in low resources countries.

The acquisition of radioactive material (RM) in both quality and right dosage, radiological protection and shielding are some of the obstacles that have to be dealt with.

Our aim is to share our successful experience beyond those obstacles.

Methodology

Our nuclear medicine (NM) staff assessed 3 patients, ages 11 to 14, who were candidates to [131]I-MIBG high dose therapy. After their acceptance, planification included not only acquisition and administration of the RM, but also radioprotection of anyone involved, clinical assistance and monitoring of the patient.

The first obstacle to overcome is the obtaining of high specificity [131]I-MIBG that can be bought easily but has to be imported and not every airline transports RM if there is a living creature on cargo.

Once you get the RM, it is important to immerse the staff, patients and their families in radioprotection culture. Patients' age was a challenge, as they couldn't stay with their families for security reasons.

Our University Hospital has a special room that is planned for this use, but does not have any structural lead shielding. We have to empathize that in our country lead is extremely expensive so building with it it's almost impossible.

We placed 3mm lead panel shieldings strategically distributed following the recommendations of our medical physicists.

We manufactured a lead container for the saline that contained the RM.

Patients are monitored by telemetry and have a webcam installed in front of them that also has a mic and speakers so that no one should enter the room to check on them. They are told to stay inside the room, on the bed or next to it.

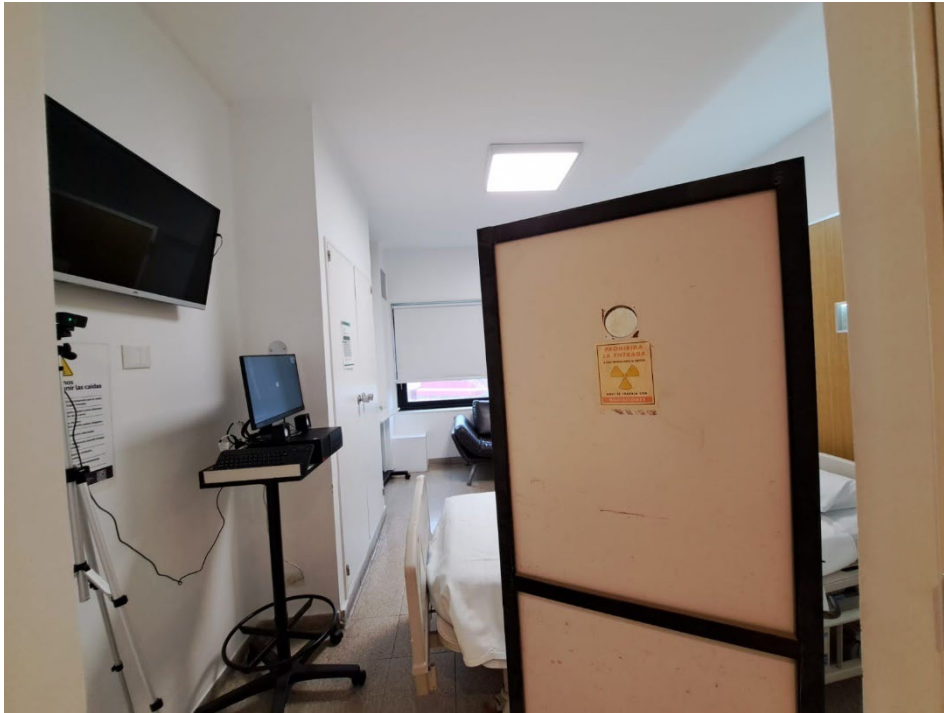
According to local regulations the room is well signalized and protected with safety belts.

Those who must enter know they have to stay behind the shieldings and they can go inside only a little time for specific purposes.

All health personnel that could be involved have a personal dosimeter previously assigned in case they have to go inside.

The NM staff performs environmental monitoring and dose rates measured in key places of the hospital floor.

Once the planification is done, the metabolic therapy can be performed, with the previous clearance of the governmental authority. We count on this and when procedure ends, we send a thorough report including all aspects and measurements performed.



Results

Administrations are performed without any inconvenience due to multidisciplinary teamwork, training and communication, and from each procedure we have learned and incorporated new and better techniques.

Conclusion

Planification and resources optimization are fundamental aspects for developing a successful procedure, regarding all complications that NM teams have to endure in low resources countries. It is necessary to exhaust every opportunity for the patient to receive this therapy in their own country. It is important for every NM team to learn and adapt the resources they count on so that patients can be taken care of efficiently.

IAEA-CN-326/394

Diagnostic performance of [⁶⁸Ga]DOTA PET/CT in tumour-induced osteomalacia experience in Argentina

M. Bastianello, N. Abreu, R. Chirico, M. Cimin, C. Ferrarotti, B. Konowalik, A. L. Lopera, G. Pitarch, D. S. Fernández

Centro de Educación Médica e Investigaciones Clínicas “Norberto Quirno”, Argentina

Background

Tumour induced osteomalacia (TIO) is a low frequency rare disease, characterized by bone pain, myalgia and multiple bone fractures. It is caused by small tumours that secrete fibroblast growth factor 23 (FGF23), which impairs renal tubular reabsorption of phosphate, leading to hypophosphatemia and low levels of 1,25-dihydroxy vitamin D with an important impact in the life quality of the patient.

Complete tumour resection is the current standard of care and is the only definitive therapy for TIO. Early diagnosis and detection of the tumour could be the cure to the disease, for this reason our objective is to characterize the morpho metabolic lesion(s) and their therapeutic implication.

Methodology

We analysed all patients who were referred to our section and [⁶⁸Ga]DOTA PET/CT for tumour localization for suspected TIO.

Whole-body PET/CT scan (Philips Gemini 64 TF) was performed at approximately 60 min after intravenous injection of [⁶⁸Ga]DOTA included hands and feet.

Also low dose CT without intravenous contrast was performed for attenuation correction purposes. Patients in good clinical conditions were administered IV contrast to enhance primary lesion.

Results

[⁶⁸Ga]DOTA PET/CT scans were performed on 18 patients (13 female and 5 male) mean age 47.2 years; age range 34–67 years, referred from the Argentine Working Group on TIO to find the primary lesion(s) with clinical symptoms and signs compatible with the disease, from March 2021 to February 2024. Of the total sample, 4 patients presented more than one scan as a follow up control after implemented treatment and persistence of symptoms.

[⁶⁸Ga]DOTA PET/CT detected at least one area of focal uptake suggestive of TIO in 14 of the 18 patients.

The lesions were confirmed by histopathology (10 lesions were phosphaturic mesenchymal tumour, 2 hemangiopericytoma; 1 glomus tumour). Only two patients were false positive (normal bone and thyroid nodule). The median SUV max of the tumours was 17.22 (range 1.7–42.9).

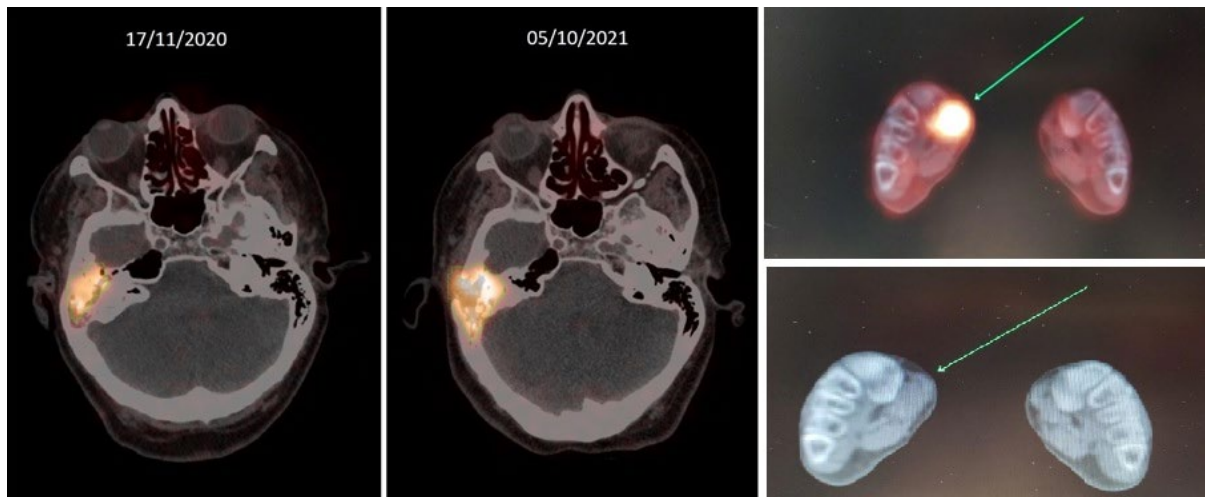
All lesions were characterized by tomography assessment. The use of the intravenous contrast (60%) allowed us to better demonstrate the tumour limits in each case.

The major localization was seven in upper and lower limbs, 6 in craniofacial region and 2 on trunk.

Soft tissue lesions appeared in 10 patients and 5 patients presented extensive compromise on both soft tissue and bone. One of the patients had pulmonary metastasis at the moment of the diagnosis.

On patients with expansive compromise, tumour volume quantification was calculated (median tumour value 29 cm³) to evaluate the tumour in the post treatment follow up.

There were 4 patients that had more than one scan due to failed surgery or radiotherapy treatment, relapse with clinical symptoms or persistent hypophosphatemia.



Conclusion

^{68}Ga -DOTA PET/CT might be the first choice for the diagnosis of TIO because the morpho metabolic characterization is relevant to define therapeutic strategy in this pathology.

IAEA-CN-326/395

Pitfalls and Common Findings in [¹⁸F]FDG PET for Staging Breast Cancer: A Pictorial Assay

G. Estrada

Imagen Tomográfica y Molecular, Mexico

Background

Breast cancer is the most common cancer in women worldwide. Precise clinical staging is a key point for treatment and prognosis. [¹⁸F]FDG PET/CT is very important for breast cancer management, aids in initial staging, restaging, treatment response evaluation and recurrence detection. Many studies comparing [¹⁸F]FDG PET and conventional diagnostic techniques have reported that PET is more sensitive in detecting metastatic lesions. Using conventional imaging methods may under stage the patients with the subsequent undertreating which implicates a higher mortality risk. The NCCN guidelines

Methodology

In this retrospective analysis, women diagnosed with primary breast cancer that underwent [¹⁸F]FDG PET/CT were review. Lesions were categorized visually, and tracer activity was analysed using SUVmax.

They were grouped for their T, N, M status, then N status was split between N1 (level I,II axillary lymph nodes), N2 (Internal mammary nodes), N3 (infra or supraclavicular nodes). Those patients with metastases, were grouped according to the specific site (bone, lung, liver, skin).

Results

The study included 75 female patients (mean age, 50.7 y). Some of the patients returned up to 6 times for their PET scan. 13 patients had level I axillary lymph nodes, 5 patients had level II axillary lymph nodes, 2 patients had Internal mammary nodes, 3 patients infraclavicular nodes, 3 patients had supraclavicular nodes, 7 patients mediastinal lymph nodes, 1 patient contralateral axillary lymph nodes, 10 with lung metastases, 6 with liver metastases, 16 bone metastases, 2 with skin metastases and 3 with pleural metastases. Some of these lesions were not apparent in the CT. 3 patients with brain metastases that didn't show [¹⁸F]FDG uptake.

Conclusion

The CT alone underscores breast cancer patients. [¹⁸F]FDG PET/CT is superior in detecting lymph nodes, especially in the mammary internal chain and distant metastases, especially in the liver and bone. It is well known that the best study to evaluate brain metastases is the MRI, due to the high background uptake in the brain. [¹⁸F]FDG PET should continue to be performed for staging patients with breast cancer.

IAEA-CN-326/396

Retrospective analysis of outcomes and Predictive Biomarkers for 177Lu- PSMA RLT in Metastatic Castration Resistant Prostate Cancer

S. Gandhi

Department of Nuclear Medicine, Zydus Cancer Hospital, India

Objective

To assess the performance of 177Lu PSMA RLT in our real-world practice and to evaluate clinical biomarkers for evaluating treatment responses.

Methodology

We conducted a retrospective observational study including 36 patients with mCRPC treated with 177Lu PSMA RLT at our hospital. Baseline characteristics and clinical parameters were documented. Correlations to treatment response were analysed with differences between groups with responders and non-responders. Patient was considered responder if 2 out of 3 parameters of clinical, biochemical (PSA) or imaging (68Ga PSMA PET/CT) showed response.

Results

Total 26/36 (72%) patients show response to PSMA therapy while 10/36 (28%) patients progressed on PSMA therapy. Out of 26 responding patients, 18 patients (69%) showed continued response while 8 patients (31%) show early response followed by early failure to PSMA therapy. Overall, 50% patients - sustained response, 22% - early response-early failure and 28% - non-responders.

Median age at diagnosis was 63 years and 70 years and Median Gleason Score was 8 and 9 in responders' group and non-responders' group respectively.

There was significant lower absolute PSA value at the diagnosis, at baseline before PSMA therapy and after 1st & 2nd cycles of PSMA therapy in responders' group compared to non-responders' group.

24/26 (92%) patients show >20% reduction in PSA after 1st & 2nd cycles of PSMA therapy in responders' group, while 10/10 (100%) patients show increase in PSA after 1st and 2nd cycles of PSMA therapy in non-responders' group.

20/26 (77%) patients show >6m PSA DT in responders' group, while 10/10 (100%) patients show <6m PSA DT in non-responders' group.

6/26 (17%) of patients had visceral metastasis and 6/26 (17%) of patients had multiple metastasis on 68Ga PSMA PET/CT in responders' group compared to 6/10 (60%) and 4/10 (40%) patients in non-responders' group respectively.

There was significant lower ALP value in responders' group compared to non-responders' group.

Non-responders' group had higher number of patients with symptoms and poorer ECOG score compared to responders' group.

There was no significant difference in Hb and platelet values in both groups.

	Parameter	TOTAL	RESPONSE/SD			PD
			Prolonged response	Early Failure	All Response	
	Age at diagnosis	65.5 (67.0 ± 7.0)	63 (64.78 ± 4.7)	63.5 (64 ± 3.4)	63 (64.54 ± 4.4)	70 (73.4 ± 8.6)
	PSA (Baseline)	74 (109.43 ± 74.5)	11.7 (91.54 ± 151.98)	75.25 (65.77 ± 32.32)	55.53 (82.17 ± 123.4)	158.65 (184.4 ± 126.61)
	GS	8 (8.30 ± 0.79)	8 (8.14 ± 0.63)	8 (8.5 ± 0.86)	8 (8.25 ± 0.75)	9 (8.5 ± 0.95)
	Hb	10.55 (10.38 ± 1.59)	10.2 (10.12 ± 1.57)	10.9 (10.92 ± 0.69)	10.4 (10.41 ± 1.37)	10.7 (10.32 ± 1.98)
	Platelets	270000 (291438 ± 127565)	237700 (282340 ± 181177)	308000 (343500 ± 79134)	281000 (309522 ± 148131)	270000 (291438 ± 127565)
	ALP	141 (168 ± 100.45)	107 (124.22 ± 58.55)	83 (118.7 ± 61.35)	107 (129.15 ± 61.05)	228 (269 ± 111.83)
Local Rx	RP	4	2	0	2 (7.7%)	2 (20%)
	RT	2	2	0	2 (7.7%)	0
	RP+RT	2	0	2	2 (7.7%)	0
	N	28	14	6	20 (77%)	8 (80%)
Systemic Rx	AA/ADT	32	16	8	24	8
	ADT+ARSI	4	2	0	2	2
	ADT+CT	0	0	0	0	0
PSMA PET	LN	26	14	6	20 (55%)	6 (60%)
	B	32	14	8	22 (61%)	10 (100%)
	V	12	2	4	6 (17%)	6 (60%)
	M	10	2	4	6 (17%)	4 (40%)
	SYMPTOMS					
	Y	32	16	6	22 (85%)	10 (100%)
	N	4	2	2	4 (15%)	0 (0%)
	ECOG					
	0	10	6	4	10 (38%)	0 (0%)
	1	14	6	2	8 (31%)	6 (60%)
	2 OR 3	12	6	2	8 (31%)	4 (40%)
	PSA at start of treatment	57.37 (184.83 ± 255.57)	30.76 (139.58 ± 252.60)	45.55 (106.37 ± 128.07)	30.76 (128.51 ± 219.66)	279 (320.02 ± 283.51)
	PSA after 1 cycle	33.6 (194.42 ± 255.57)	15.52 (77.045 ± 166.41)	26.935 (72.2 ± 93.87)	21.2275 (75.55 ± 147.94)	675.5 (580.75 ± 351.02)
	PSA reduction after 1 cycle					
	>20%	24	16	8	24	0
	<20%	12	2	0	2	10
	PSA after 2 cycles	35.19 (224.18 ± 344.71)	12 (70.54 ± 159.81)	21.86 (110.63 ± 164.80)	12 (82.88 ± 162.42)	811 (591.60 ± 415.07)
	PSA reduction after 2 cycles					
	>20%	24	18	6	24	0
	<20%	12	0	2	2	10
	PSA DT					
	>6M	20	16	4	20	0
	<6M	16	2	4	6	10

Conclusion

177Lu PSMA is an effective treatment option in mCRPC in the real-world setting. A PSA decrease >20% after the first cycle is an early marker of response that can be easily implemented in clinical practice. Age, GS & PSA at diagnosis, PSA at start of treatment, visceral & multiple metastasis on PSMA PET/CT, ALP and performance status are relevant important prognostic indicators for PSMA RLT response.

IAEA-CN-326/397

The role of 68 Ga-PSMA - PET/CT and -PET/MRI in the diagnosis of primary prostate cancer and TNM- staging -a systematic literature review

O. Akinmuleya^{1,2}, K. Kairemo^{3,4}, P. Cohen⁵

¹ Shenyang Medical College, Liaoning, China

² Greater Accra Regional Hospital, Ghana

³ Department of Theranostics, Docrates Cancer Center, Helsinki, Finland

⁴ Department of Nuclear Medicine, University of Texas MD Anderson Cancer Center, USA

⁵ Department of Nuclear Medicine, Lions Gate Hospital, Canada

Background

Prostate-specific membrane antigen (PSMA) PET shows potential in addressing diagnostic challenges in prostate cancer.

Methodology

We summarized the literature including existing reviews: 1) 68 GaPSMA imaging in the diagnosis of prostate cancer, 2) its role in TNM staging, 3) its correlation to PSA levels, targeted biopsies and 4) ISUP scores both with simultaneous CT or MRI. Our final analysis was based on more than 70 articles.

Results

PSMA-PET with MRI-targeted biopsy improves the initial diagnosis of clinically significant prostate cancer (csPCa), especially in ambiguous lesion like PI-RADS 3, offering added value beyond MRI alone. 68 Ga-PSMA PET/CT shows promise in cases where MRI findings are inconclusive for csPCa, but standardized protocols could enhance its applicability. PSMA-PET correlates closely with ISUP score and PSA levels, aiding in risk assessment and treatment planning. Its accuracy in detecting primary PCa lesions support its incorporation into initial workups for high-risk patients.

PSMA-PET findings are closely associated with ISUP score, with higher SUV max values which can indicate more aggressive disease and increased tumour aggressiveness. This can provide valuable insights into disease prognosis and managements. The uptake of 68 Ga-PSMA on PET/CT is notably higher in individuals with PCa having a Gleason score of ≥ 8 or a PSA level of ≥ 10 ng/mL, reflecting the aggressiveness and severity of prostate cancer.

PSMA PET imaging, particularly PSMA PET/CT, has emerged as a superior method for N and M staging in high-risk patients. PSMA PET can boost sensitivity and accuracy in detecting lymph node and distant metastases. It offers superior sensitivity and specificity compared to conventional imaging in primary staging. However, PSMA PET/CT is less accurate than multiparametric (mp)MRI in T-staging, particularly in identifying extra prostatic extension and seminal vesicle invasion. However it does help in detecting smaller lesions and provides prognostic information.

Comparatively, PSMA PET/MRI demonstrates superior accuracy in detecting primary prostate cancer compared to mpMRI alone, offering improved sensitivity and specificity, especially in cases classified as PI-RADS 3. Established SUVmax cutoff values aid in discriminating clinically significant prostate cancer, reducing the need for unnecessary biopsies. However, challenges such as the lack of

standardized SUVmax cutoff values for PSMA PET analysis present hurdles in clinical practice, emphasizing the need for further research to optimize PCa detection strategies.

Conclusion

PSMA-PET plays a crucial role in the initial diagnosis and staging of prostate cancer, complementing existing modalities like MRI. Its close correlation with ISUP score and PSA levels, along with its superior sensitivity in detecting primary lesions and metastases, makes it a valuable tool in risk assessment and treatment planning. However, challenges remain in standardizing protocols and interpreting PET findings, warranting further research and validation in clinical practice.

IAEA-CN-326/398

Logistical Complexity in the Production and Commercial Distribution of Magistral Formulas with Gallium-68 Generators: Experience of a 2 Centers in Bogotá D.C., Colombia, the City with the Worst Traffic in the World

C. A. de L. R. Victoria¹, J. Diaz², J. Rada¹

¹Instituto Nacional de Cancerología, Colombia

²Nucleofarma, Colombia

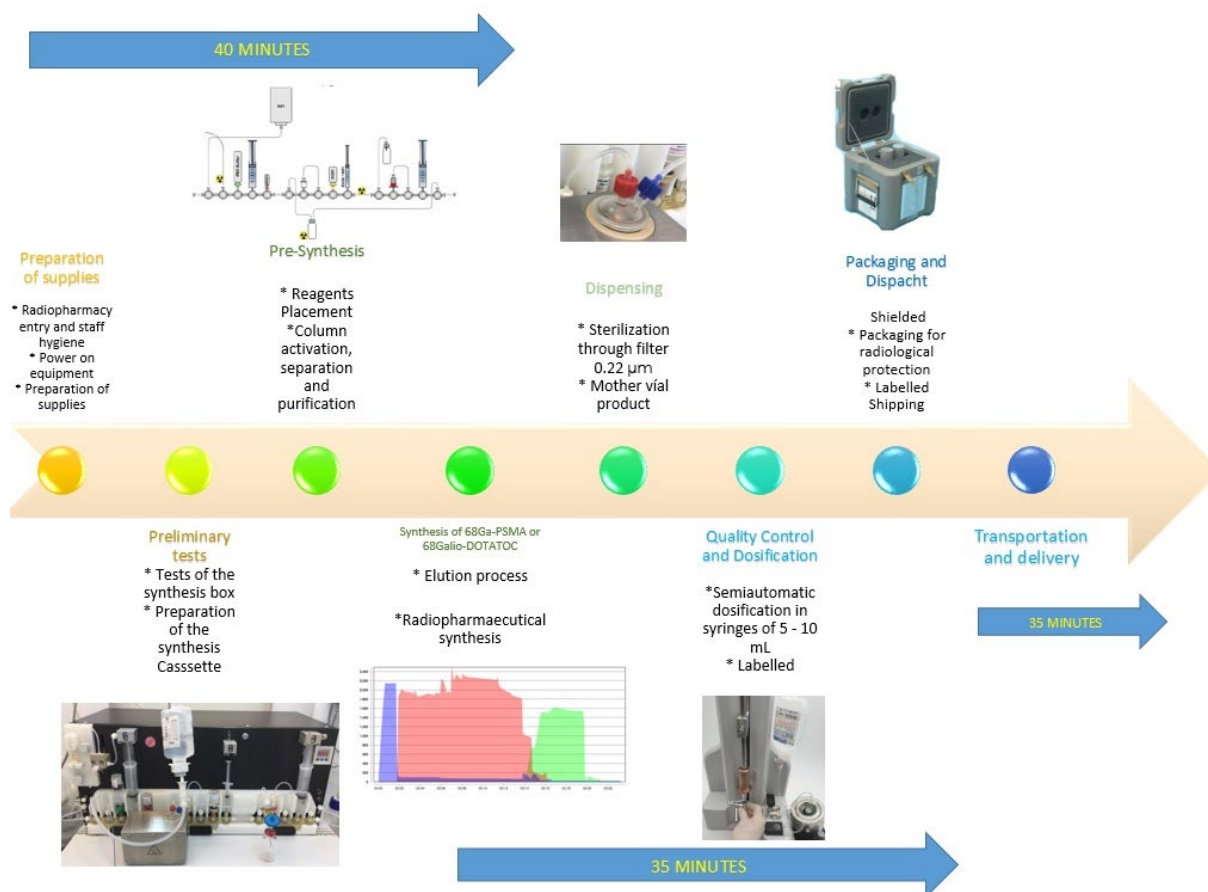
Background

This article will cover all logistical aspects of producing, marketing, and distributing radiopharmaceutical doses radiomarked with 68 gallium generator elution, including raw material procurement, radiopharmacy's intrinsic processes, master formula production, transportation, marketing strategies, distribution to hospitals, and waste reverse logistics.

Methodology

Distribution Chain:

1. Producing radiopharmaceuticals requires the importation of a Gallium 68 generator from a reactor in South Africa. A production order was placed well in advance, a purchase order was prepared, payment was made in advance in dollars, prior permits from INVIMA and the SGS, and the process of air transport and customs clearance was carried out with the respective payment.
2. Importation of peptides and raw materials for quality control was carried out. This chain involved placing a production order well in advance, required preparation of a purchase order, payment was made in advance in dollars, prior permits from INVIMA for raw material importation were obtained.
3. A clinical order was generated: Nucleofarma designed its own radio pharmacy software so that hospitals performing PET nuclear medicine studies can place orders efficiently. The order was placed on a production order list prepared 12-24 hours in advance.
4. Production was carried out by synthesizing the dose in a Neptis synthesis box, for the production of Gallium 68-DOTATOC and Gallium 68-PSMA. This box allowed for the production of 4 doses in a production run with the generator in its first months of useful life. The product was sterilized and packaged to ensure aseptic and antiseptic measures as it is a medication. The duration of the synthesis and dosing process was 1 hour and 5 minutes.
5. Packaging of radiological protection materials was carried out according to Figure 1. The process duration is 5 to 10 minutes.



Results

A Gallium 68 generator allows us a lifespan of 9 months. With production of 4 to 6 doses per day, distributed to 4 Nuclear Medicine services in Bogotá daily. Distribution began at 6 am, and within 35 minutes, the patient received their dose in the nuclear medicine services. In total, a Gallium 68 generator allows for dosing a total of 4 doses, per day, for 5 days a week. This appropriate distribution chain allowed us to provide 180 doses on time for cancer patients.

Discussion

We have developed a distribution scheme that overcomes all predictions for ground transportation in the city of Bogotá, classified as one of the most congested cities in the world, of great logistical importance, and setting an example to follow in the supply chain in the radiopharmaceutical sector.

Conclusion

This article will facilitate sharing and exchanging knowledge in the field of radiopharmacy regarding successful logistical procedures in the distribution of PET radiopharmaceuticals. All of this is leading to the logistical effervescence of restructuring the entire supply chain of radiopharmaceutical companies under a prism of effectiveness and efficiency management: reducing costs and capital invested in inventories. This development allows more resources to be allocated to research and development. Optimizing the supply chain creates value.

IAEA-CN-326/399

Rare Case of Papillary Thyroid Cancer with Liver, Kidney, and Urinary Bladder Metastases

F. M. Resma, R. Ogbac, B. F. Jr. Rodriguez, J. R. Solito

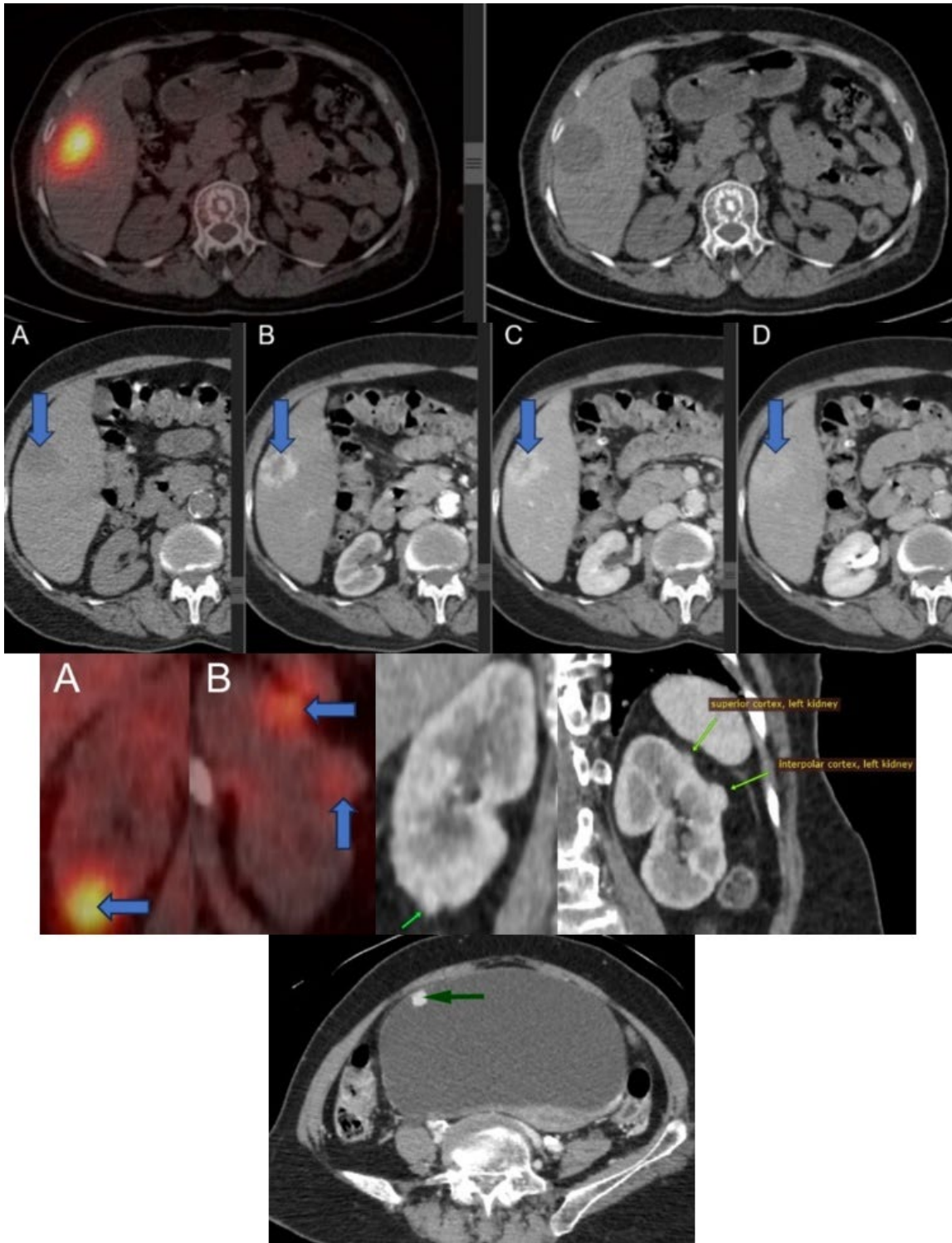
Philippine General Hospital, University of the Philippines, Philippines

Background

Papillary thyroid carcinoma is the most common type of thyroid cancer, constituting 80% of cases. Regional lymph node metastasis is seen in 30-40% of patients with papillary thyroid cancer, while metastases to distant sites occur in 1-4% of cases. The most common sites of distant metastasis are the lungs and bones. Metastasis to the liver, kidney, or urinary bladder from differentiated thyroid cancer is rare.

Case Report

A 65-year-old female with a 30-year history of an enlarging anterior neck mass consulted in our institution due to left hip pain, which began when she fell on her left hip 6 months prior. Radiograph of the pelvis showed a left hip fracture. Neck ultrasound revealed a TI-RADS 5 right thyroid lobe mass, and fine needle aspiration biopsy of the mass had findings suspicious for papillary thyroid carcinoma (Bethesda Category V). Neck, chest, and abdominal CT scan with contrast demonstrated a large right thyroid lobe mass, cervical and mediastinal lymphadenopathies, subcentimeter pulmonary nodules, multiple lytic osseous foci, a nodule in the right liver lobe, and a nodule in the urinary bladder. She underwent left hip surgery, followed by total thyroidectomy with central neck dissection. Histopathology showed papillary thyroid carcinoma with cervical lymph node and bone metastases. Two months after, she had hematuria. Whole abdomen ultrasound revealed a pedunculated solid mass within the urinary bladder. Cystoscopy and transurethral resection of the urinary bladder tumour was performed. Histopathology and immunohistochemistry study with TTF-1 of the urinary bladder tumour were supportive of a metastatic carcinoma from a primary thyroid malignancy. She then received radioactive iodine therapy with 5.55 GBq (150 mCi) of I-131. Post-therapy whole-body I-131 scintigraphy with SPECT/CT demonstrated functioning thyroid tissue remnants, multiple functioning bone metastases, non-RAI-avid nodules in both lungs, and RAI-avid foci in the right liver lobe and both kidneys. Triphasic contrast-enhanced abdominal CT scan showed a hypervascular mass in the right liver lobe and heterogeneously enhancing, mixed solid and cystic nodules (Bosniak IV) in both kidneys, compatible with metastases from the known primary thyroid malignancy. Metastasis to the liver, kidney, or urinary bladder from differentiated thyroid cancer is rare. Combined liver, kidney, and urinary bladder metastases are even rarer. To our knowledge, this is the first reported case.



Conclusion

This is a rare case of liver, kidney, and urinary bladder metastases from papillary thyroid cancer (on top of lymph node, lung, and bone metastases). These lesions can be treated with RAI therapy if they demonstrate I-131 uptake. However, such metastases may be missed on I-131 whole-body scans since their uptake can be masked by physiological uptake in the body. Therefore, the liver, kidneys, and urinary bladder must be carefully reviewed. In these cases, SPECT/CT and other imaging modalities are essential in the detection and evaluation of such lesions.

IAEA-CN-326/400

A high-grade salivary duct carcinoma in its oncocytic variant presenting as diffuse lymph node involvement and hypermetabolic omental cake in [¹⁸F]FDG PET/CT

K. B. Ahmed, H. Noomen, T. B. Mohamed, S. Charfeddine, K. Chtourou

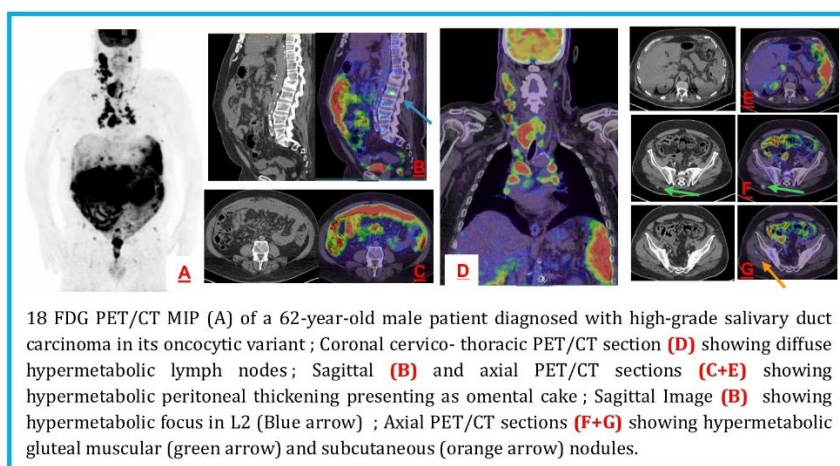
Nuclear Medicine Department, Habib Bourguiba Hospital, SFAX, Tunisia

Background

Salivary gland carcinoma is a relatively rare disease entity arising in the parotid, submandibular, sublingual and minor salivary glands of the head and neck. Salivary duct carcinomas (SDC) represent 5-10% of salivary gland malignancies and can arise de novo or out of a pleomorphic adenoma. The Oncocytic variant is a rare proliferation of malignant oncocytes mainly found in glandular tissue, accounting for 0.5% of all epithelial salivary gland malignancies. Owing to its rarity, identifying distant metastatic sites can be challenging.

Case Report

We report the case of a 62-year-old male patient with newly developed cervical nodes. Cervical and facial MRI revealed suspicious bilateral cervical lymph nodes, with no signal abnormalities in the submandibular, sublingual or parotid glands. Biopsies from these cervical nodes were performed, returning in favour of a high-grade salivary duct carcinoma in its oncocytic variant. In order to better identify the tumour source, and to better explore locoregional and distant extension, a [¹⁸F]FDG PET/CT was requested. The exam was performed on a PET/CT siemens biograph-64 after 6 hours of fasting and 60 minutes after injection of 8.5 mci of [¹⁸F]FDG. The examination showed intensely hypermetabolic cervical, thoracic, peritoneal, retroperitoneal and pelvic nodes (SUVLbm-max=8,6 in the paraaortic chain). Furthermore, the examination revealed the presence of a diffuse hypermetabolic peritoneal thickening, giving the typic presentation of an omental cake (SUVLbm-max=12,8). In addition, hypermetabolic focus in L2 (SUVLbm-Max= 8) gluteal muscular nodules (SUVLbm-Max= 6,24) and cervico-thoracic subcutaneous nodes were discovered. Due to the extraordinary presentation of peritoneal metastases for cervical cancer, omental biopsy was performed and confirmed the same histopathological features of oncocytic variant of a high grade salivary duct carcinoma.



18 FDG PET/CT MIP (A) of a 62-year-old male patient diagnosed with high-grade salivary duct carcinoma in its oncocytic variant; Coronal cervico- thoracic PET/CT section (D) showing diffuse hypermetabolic lymph nodes; Sagittal (B) and axial PET/CT sections (C+E) showing hypermetabolic peritoneal thickening presenting as omental cake; Sagittal Image (B) showing hypermetabolic focus in L2 (Blue arrow) ; Axial PET/CT sections (F+G) showing hypermetabolic gluteal muscular (green arrow) and subcutaneous (orange arrow) nodules.

Conclusion

Cervical lymph nodes metastases are known to be independent prognostic factor in salivary duct carcinomas. Therefore, nodal staging is important for treatment planning and predicting the prognosis of malignant SDC. Previous studies showed higher accuracy of [¹⁸F]FDG PET/CT compared with conventional imaging study in the detection the number of positive lymph nodes since SDC are highly [¹⁸F]FDG avid. Secondly, CT studies are limited to lymph node size, which is not a reliable criteria for nodal involvement. Furthermore, [¹⁸F]FDG PET/CT provides potential impact on treatment planning by detecting distant metastasis, which are seen more frequently in high-grade SDC. Peritoneal carcinomatosis is an exceptional form of distant metastasis for high-grade salivary duct carcinoma. To our knowledge, no such case has ever been described before.

IAEA-CN-326/401

18F-FDG PET-CT in Infective endocarditis: a case report

S. Dumont^{1,2}, G. Freitas¹, R. Gomes¹, V. Marino^{1,2}

¹ Faculty of Medicine, Hospital Felício Rocho, Brazil

² Federal University of Minas Gerais, Belo Horizonte, Brazil

Background

Infective endocarditis (IE) is a serious and challenging condition with substantial morbimortality. Diagnosis is based on modified Duke criteria (MDC) that was updated in 2023. Abnormal metabolic activity involving the native or prosthetic valve on 18F-FDG PET-CT is now a imaging major criteria, focus on its high positive predictive value (PPV).

Case Report

This is a report of a biological prosthetic aortic valve endocarditis (labcor 25) in a 46-year-old man. The patient has a previous history of infectious endocarditis in the native mitral and aortic valve, requiring valve replacement in 2017. In 2024, he experienced malaise, night sweat and weight loss, without fever, for six months. Blood cultures and trans-oesophageal echocardiography (TEE) were carried out. 18F-FDG PET-CT was performed under a prolonged fasting period of 12 hours, high fat and low carbohydrate diet for 48 hours and 50 IU/kg heparin. 18F-FDG PET-CT showed heterogenous glycolytic hypermetabolism in prosthetic aortic valve, paravalvular and in a 4L lymph node that points to infection. Focal hypermetabolism at the left first metatarsophalagenal joint was further confirmed to be post-traumatic osteomyelitis and probable microorganism entry point. Imaging specialist should be concerned about causes of false positive (scatter artefacts and BioGlue). 18F-FDG uptake patterns detected at least three (3) months after prosthetic valve surgical implantation are included as a Major Criterion in 2023 update in MDC. In native valves, 18F-FDG PET-CT is insufficiently sensitive to exclude IE but has a very high PPV and was also included as a Major Criterion.

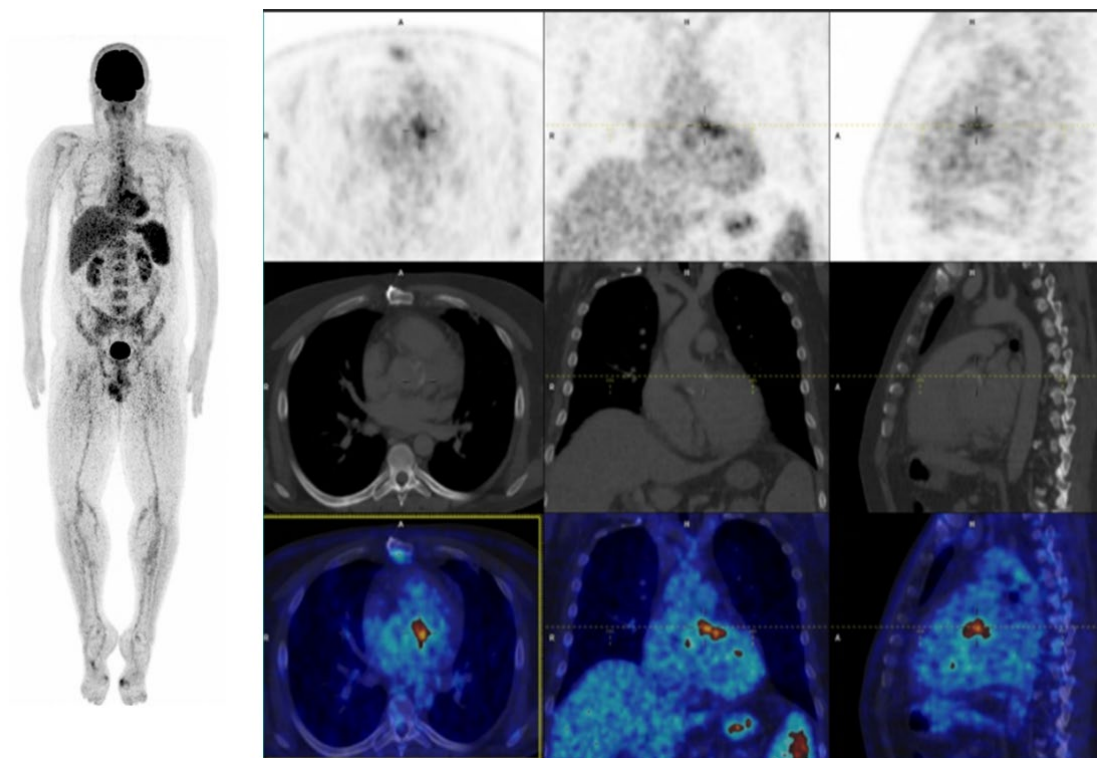


Figure 1. 18F-FDG PET-CT scan of a 46 years old man biological prosthetic aortic valve endocarditis (labcor 25) showing glycolytic hypermetabolism in prosthetic aortic valve that points to infection.

Conclusion

18F-FDG PET-CT significantly improves the identification of definite prosthetic valve endocarditis (PVE) and can be useful in detecting extracardiac foci of infection, with high sensitivity and specificity. Actions to expand 18F-FDG PET-CT access to public health system dependent population, in countries like Brazil, needs to be taken.

IAEA-CN-326/402

Performance Clinical Deep Learning Reconstructions applying Half dose FDG PET/CT protocols

E. A. Marino^{1,2}, G. A. Peña¹

¹ Fundación Escuela Medicina Nuclear (FUESMEN), Argentina

² Comisión Nacional de Energía Atómica (CNEA), Argentina

Background

In November 2022, FUESMEN (Fundación Escuela de Medicina Nuclear) incorporated a new digital PET/CT UMI 550 enables high-speed scanning by combining the advanced AI iterative reconstruction engine. This technology duplicated the number of scan patients and reduced the injected doses to half compared with the prior analogic BGO PET/CT system.

Purposed: Evaluate the image quality of Deep Progressive Reconstruction (DPR) compared with standard OSEM in FDG scan patients with half doses injected.

Methodology

Image quality was evaluated in one hundred oncology patients injected with 2.035 MBq/kg to reduce the radiation dose by optimizing FDG PET/CT protocols. Two PET reconstructions were applied: standard OSEM (2 iter, 20 subsets) and AI recon (DPR ST1). Volume of interest (VOI) in the liver, blood pool and muscle were located. For the VOIs measurement were obtained SUV max, SUV mean and standard deviation (SD). Image quantitative analysis applying coefficient of variation percentual (COV) in the liver (COV_{liver}) were compared between OSEM and DPR reconstructions. Normal physiological biodistribution in liver, muscle and blood pool were compared, a T-student test was performed to establish the relationship. For each overall image quality was subjectively rated by the referring physician on a 4-point scale (IQ score: 1 excellent, 2 good, 3 poor but interpretable, 4 poor not interpretable). SUVmax measurements and anatomic axial size were obtained from 92 malignant lesions.

Results

Normal physiological distribution values were SUV_{mean-liver-OSEM}= 2.414 and SUV_{mean-liver-DPR}= 2.438, T-student test found a statistically significant relationship between SUV_{mean OSEM} and SUV_{mean DPR} [p = 0.006 (95% CI) values and pearson coefficient of 0.98(Figure 1). In the image quantitative analysis values in the liver were COV-DPR_{mean} = 6.98 and COV-OSEM_{mean} = 11.39, obtaining 40.29 % of high reduction noise(Figure 3). The size range of the metastatic lesions was from 4 mm to 82 mm. The SUV max values presented a linear correlation with a determination coefficient of 0.871 (Figure 3). For half dose image quality score evaluation 92 % for PET OSEM were IQ good and for DPR were IQ Excellent.

DPR reconstructions present a promising tool in PETCT protocols, offering excellent image quality with half the activity injected per patient.

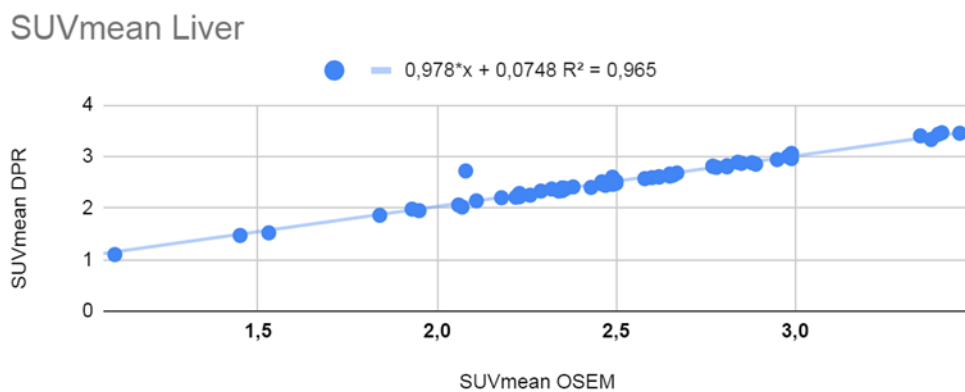


Figure 1. SUVmean liver OSEM vs SUVmean liver DPR

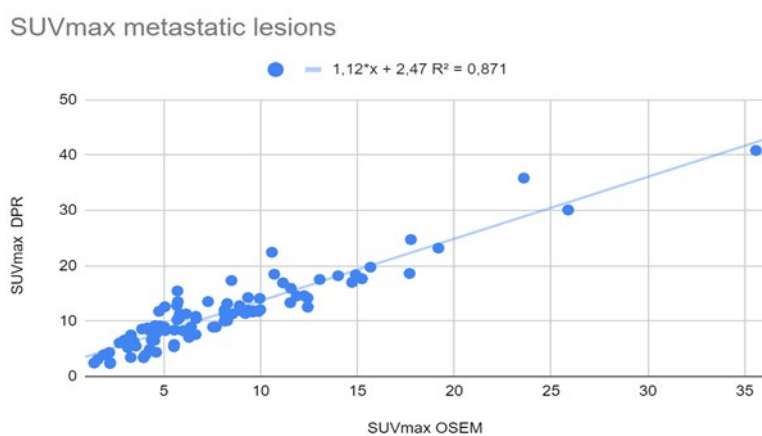


Figure 2. SUVmax lesions OSEM vs SUVmax lesions DPR

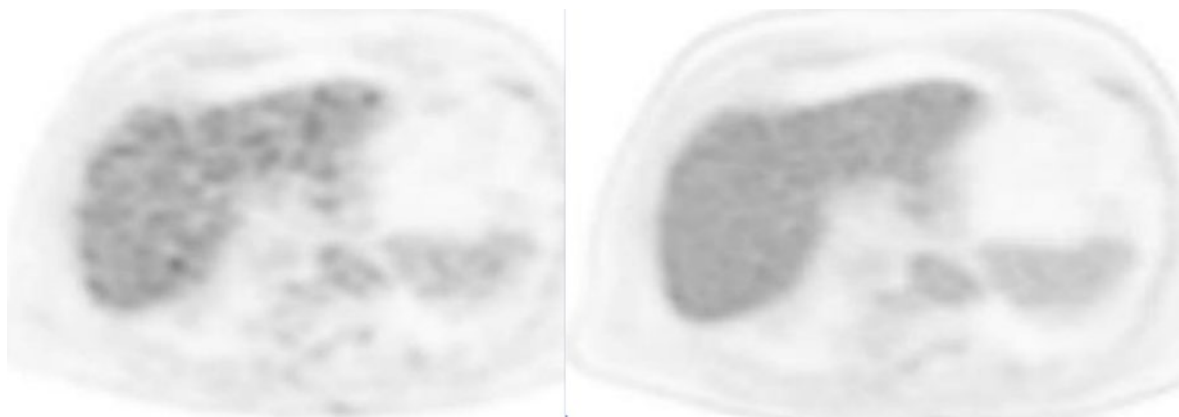


Figure 3. Patient 79 kg, 4,4 mCi FDG dose injected. Reconstruction OSEM and DPR respectively. OSEM recon represent COV liver of 9,8 % vs COV liver DPR of 4,37 %.

IAEA-CN-326/405

Composite serum PSA factor in the PI-RADS category improves the detection accuracy in patient with suspected prostate cancer

F. F. A. Saad, Y. Balakrishnan, M. H. Zakaria

Universiti Putra Malaysia, Malaysia

Background

Prostate Imaging Reporting and Data System (PI-RADS) has been made to standardize the evaluation and reporting system for multiparametric MRI prostate (mpMRI) which has been incorporated into part of diagnostic work up for prostate carcinoma. There remains equivocal PIRADS 3.0 lesion with the malignant changes which pose uncertainty to the true positive findings. This study was undertaken to determine diagnostic accuracy of a composite PI-RADS (V2.1) and the serum Prostate specific antigen (PSA) in evaluating the suspicious prostate cancer patients.

Methodology

Cross-sectional retrospective study was done which included 36 patients who underwent 3.0T multi parametric -MRI (Mpr -MRI), Siemens PRISMA (Figure 1-2). The images were evaluated by an experienced radiologist based on the PIRADS (V2.1) categories who were blinded to the histology findings. PI-RADS scoring was combined with the serum PSA (ng/ml/cc). The patients were dichotomized into the PIRADS-only (PIRADS >3 versus PIRADS >4) and the composite PIRADS-serum PSA for the category of (PIRADS >3 versus PIRADS >4) for the high susceptibility of malignancy.

Results

The median patient age, PSA level and PSA density were 67, 10.5 ng/ml and 0.31ng/ml. Thirty-four patients (94.0%) had lesions with PIRADS 3 and above in the mp-MRI. The biopsy results were positive for prostate carcinoma in 14 patients (39.0%). The PIRADS-only category, the sensitivity and specificity of PIRADS >3 and PIRADS > 4 were 78.6% and 81.8% and 100% and 91.0% respectively.

The PIRADS -only category, utilizing the PSA of 10 ng/ml and 0.3 ng/ml, the PIRADS >3 versus >4 subcategory revealed the sensitivity and specificity of 85.7% and 61.5%. versus 85.7% and 63.6% respectively. The composite PIRADS-serum PSA category, utilizing the PSA at the cut-off value of 10 ng/ml and 0.3 ng/ml/cc, the PIRADS >3 versus >4 subcategory revealed the sensitivity and specificity of 86.0% and 68.0% versus 92.0% and 73.0% respectively.

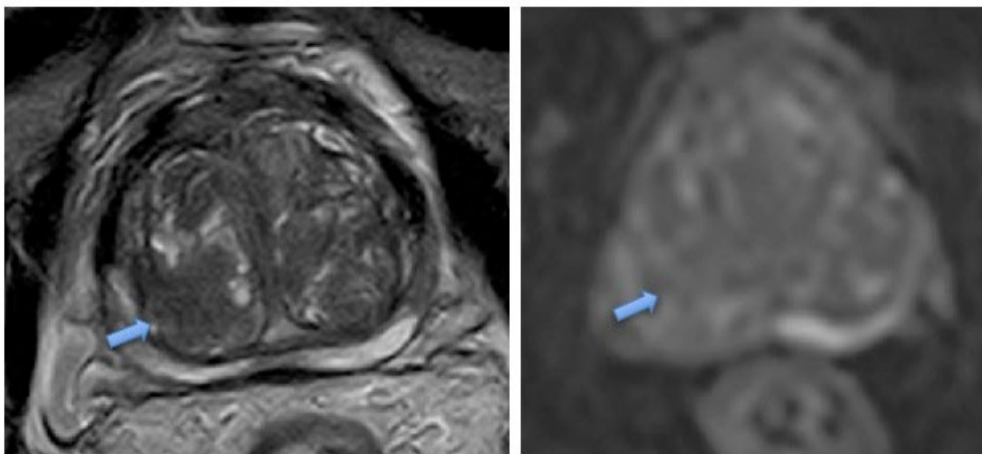


Figure 1: PI-RADS III (prostate cancer). (Left) Axial T2-WI shows TZ heterogeneous signal intensity with obscured margins. (right) Axial ADC map shows focal mild hypointensity.

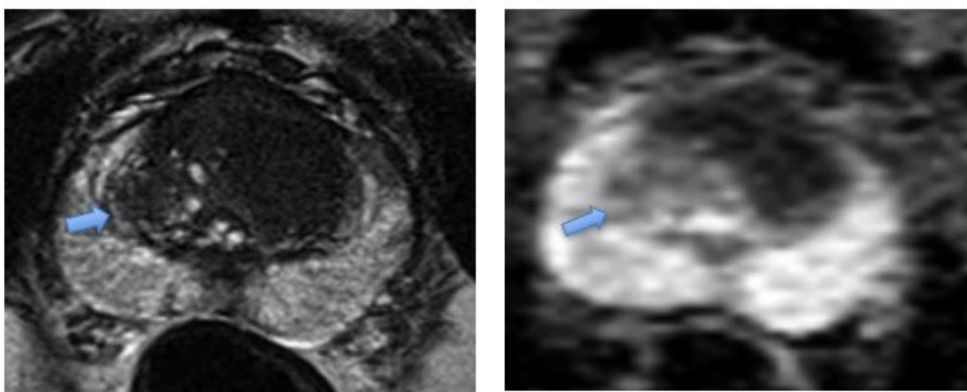


Figure 2: PI-RADS V lesion in the transition zone. (Left) Axial T2-weighted sequence (dominant sequence for the transition zone) showing a circumscribed lenticular 20 mm hypointense mass in the anterior transition zone. (right) ADC map correspondingly shows focal markedly hypointense signal intensity of the mass.

Conclusion

The PIRADS V2.1 category 4-5 is highly accurate in detecting prostate carcinoma with improved sensitivity of the category 3-5 when the serum PSA level is used as an integral factor for the composite PIRADS category.

IAEA-CN-326/406

Navigating The Prostate Cancer Frontier: A Bibliometric and Altmetric Analysis of [225Ac]Ac-PSMA Therapy

A. Al-Ibraheem¹, H. Al-Abdallat²; R. Al-Rashdan¹, A. S. Abdulkadir¹, D. A. Sweedat¹, S. F. Alyasjeen¹; M. Ghesani³, K. Kairemo^{4,5}, M. M. Sathekge⁶⁻⁸

¹ Department of Nuclear Medicine, King Hussein Cancer Center (KHCC), Amman, 11941, Jordan

² School of Medicine, The University of Jordan, Amman 11942, Jordan

³ Department of Diagnostic, Molecular and Interventional Radiology, Icahn School of Medicine at Mount Sinai, New York, United States

⁴ Department of Molecular Radiotherapy and Nuclear Medicine, International Comprehensive Cancer Center Docrates, Saukonpaadenranta 2, FI-00180 Helsinki, Finland

⁵ Department of Nuclear Medicine, University of Texas, MD Anderson Cancer Center, Holcombe Blvd, 77030 Houston, Texas, United States.

⁶ Department of Nuclear Medicine, University of Pretoria & Steve Biko Academic Hospital, Pretoria 0001, South Africa

⁷ Nuclear Medicine Research Infrastructure (NuMeRI), Steve Biko Academic Hospital, Pretoria 0002, South Africa.

⁸ Department of Nuclear Medicine, Steve Biko Academic Hospital, Pretoria 0001, South Africa

Rationale

The main aim of this study was to evaluate the current state of bibliometric and altmetric research output of [225Ac]Ac-Prostate specific membrane antigen (PSMA) and its implications for prostate cancer (PC).

Methodology

Both PubMed and Scopus digital libraries were systematically explored to retrieve relevant data on the topic of interest. The study of various bibliometric and altmetric indices was facilitated through the use of Microsoft Excel, Stata (Version 17.0), and VOSviewer (Version 1.6) Software. The parameters included in this study comprised the examination of published articles, annual trends, countries, institutions, authors, journals, and co-occurring keywords.

Results

From 2014 to 2024, our study examined a total of 100 publications within the given domain. The studies that received the highest citations primarily centered on the crucial topic of metastatic castration-resistant prostate cancer, with a particular emphasis on evaluating the safety and effectiveness of [225Ac]Ac-PSMA therapy. Moreover, much scholarly inquiry has been devoted to examining the [225Ac]Ac-PSMA adverse effects. Three high prolific countries (namely, Germany, United States, and South Africa) dominated the research render in terms of publications and citations. Finally, A strong correlation was observed between altmetric score and citation number ($p < 0.001$).

Conclusion

The observed surge in scholarly research output and altmetric indicators associated with [225Ac]Ac-PSMA signifies a shift in emphasis towards embracing alpha targeted therapy in PC.

Keywords: [225Ac]Ac-PSMA, PSMA, Theranostics, Bibliometric Analysis, Altmetric Analysis

IAEA-CN-326/407

Individualized calibration of estimated glomerular filtration rate for serial renal function monitoring

B. Mekonnen, J. L. Holness, B. D. Berndorfler, J. M. Warwick

Nuclear Medicine Division, Department of Medical Imaging and Clinical Oncology, Stellenbosch University, Cape Town, South Africa

Aim

Serum creatinine based estimates of glomerular filtration rate (eGFR) are known to be imprecise compared to GFR measurement (mGFR). In addition eGFR is frequently also inaccurate in many patient populations. While inaccuracy can be reduced by applying a population specific calibration, the problem of imprecision remains. We aim to investigate the performance of a novel individually calibrated estimated GFR (iceGFR) formula for estimation of GFR by comparison with measured GFR (mGFR).

Methodology

Retrospective data from patients who had undergone two radionuclide based GFR measurements within 3 months of serum creatinine measurement at the nuclear medicine division, Tygerberg Hospital, between January 2009 and December 2022 were included. A patient specific calibration factor (K_{pt}) was derived from the ratio of mGFR and estimated GFR (eGFR) at an initial GFR measurement.

For subsequent GFR measurements iceGFR was calculated using the formula:

$$\text{iceGFR} = K_{pt} * \text{eGFR}_i$$

A population calibrated GFR (pceGFR) was also determined. Bland-Altman analyses were used to compare the performance of eGFR, pceGFR and iceGFR relative to mGFR.

Results

Fifty-three patients (24 women and 29 men; median age, 60.5 y; age range, 25-75 y) were included. Using Bland-Altman analyses, the bias for eGFR, pceGFR and iceGFR was -16, -5 and -3 ml/min/1.73m² respectively. The limits of agreement for eGFR, pceGFR and iceGFR were -51 to 20, -40 to 30 and -27 to 21 ml/min/1.73m² respectively.

Conclusion

Compared to eGFR, pceGFR had an improved accuracy but similar imprecision. A novel iceGFR formula outperformed eGFR and pceGFR with improvements in both bias and precision. iceGFR shows promise for serial renal function monitoring in environments with limited access to GFR measurement.

IAEA-CN-326/408

The next wave of innovation: Exploring the new possibilities of automation in radiopharmacy practices

A. Vukadinović¹, M. Ravlić², M. Matović³, D. Janković¹, M. Perić¹, S. Vranješ-Đurić¹

¹“Vinča” Institute of Nuclear Sciences-National Institute of the Republic of Serbia, Belgrade, Serbia

²Prizma company, Kragujevac, Serbia

³Clinical Center Kragujevac, Center of Nuclear Medicine, Kragujevac, Serbia

Background

The adoption of automated modules for the preparation of PET and therapeutic radiopharmaceuticals, and also the systems for preparing iodine-131 capsules has started a new chapter in radiopharmacy, highlighting the beginning of significant changes. The progress in artificial intelligence (AI) and humanoid robotics is now opening up even more opportunities for automation within the field of radiopharmaceuticals. This move towards more automated processes is in line with the ALARA principle, aiming to minimize personnel exposure to ionizing radiation as much as reasonably possible. Moreover, the push for automation is not just about keeping staff safe; it's also about making treatments safer for patients. One of the main benefits is reducing the risk of microbiological contamination, which means the medications that patients receive are safer. This work looks into the new possibilities that recent advances in automation are bringing to radiopharmacy. It discusses how these technological developments could improve the way radiopharmacies operate, making them more efficient and safer for both the people who work there and the patients they serve.

Methodology

We designed and constructed a new robotic system for the preparation of small batches of radioiodine capsules in clinical radiopharmacies. The central component of the device is a robotic arm controlled by software that includes AI-based spatial image recognition. The system autonomously performs the entire preparation procedure, including checking the activity on the dose-calibrator and packing the capsules into a lead container. Human presence is required only to monitor the operation via a workstation. The next step, currently in the development phase, is training a humanoid robot for various tasks in radiopharmacy.

Results

The system has been trained and validated in an operational environment. It can dispense volumes from 0.1 to 50 μL without changing accessories and achieves an accuracy of $\pm 2\%$ of the declared activity for volumes above 1 μL . For smaller volumes (up to 1 μL), the system achieves an accuracy of $\pm 5\%$.

Conclusion

We have demonstrated the significant potential for improving automated systems in radiopharmacy through the use of AI. In addition to modules and robotic arms, new possibilities are emerging, such as the use of humanoid robots capable of almost completely replacing humans in the manipulation of radioactive sources in radiopharmacy.

IAEA-CN-326/409

Stability Test for Radiochemical Purity of ^{177}Lu -EDTMP in the Presence of Human Serum Albumin

L. D. Pertiwi¹, A. Amanda², P. Widayati¹, S. Sulaiman¹, Y. Sugiharto¹, W. Lestari¹, V. Y. Susilo¹, S. Setiyowati¹, T. Triningsih¹

¹ Research Center for Radioisotope, Radiopharmaceutical, and Biodosimetry, Organization for Nuclear Energy, National Research and Innovation Agency, Indonesia

² Indonesian Nuclear Technology Polytechnic, Indonesia

In drug development, stability tests should be conducted to identify the characteristics of the drug which demonstrates the strength and the quality of the drug. Stability tests can be used for evaluating drug degradation in change of physical, chemical, and biology so that the drug meets the standardized for efficacy and complies with the specifications. In radiopharmaceutical, stability is a time when radioisotope can be used as it is expected and safe for the patient, and it should be carried out to indicate the effectiveness of the product. In this study, the stability of radiochemical purity from three variation of ethylenediamine tetramethylene phosphonic acid (EDTMP) freeze-dried kit produced by Research Centre for Radioisotope, Radiopharmaceutical, and Biodosimetry labeled with $^{177}\text{LuCl}_3$ in presence of human serum albumin to simulate in vivo condition was carried out to ensure the radiochemical purity (RCP) complies with the specification. RCP test was conducted using a thin layer chromatography method with W31 ET as stationary phase and buffer phosphate 0,01 M pH 7,4 as its mobile phase. ^{177}Lu -EDTMP complex in presence of human serum albumin was incubated in 37°C, the stability of RCP was performed in several time intervals up to 168 hours. To assure the results, the experiment was carried out two times, afterwards a t-test was executed to evaluate the results. The results shows that the RCP from three variations of EDTMP labeled with $^{177}\text{LuCl}_3$ for 168 hours still met the specification which is >95%, it can be said that ^{177}Lu -EDTMP was stable in the presence of human serum albumin. The t-test result demonstrates $t\text{-stat} < t\text{-value}$ which means no significance difference in two repetition experiments; hence it can support the statement that the product is stable.

IAEA-CN-326/410

Novelty of ^{18}F -Fluorocholine Positron Emission Tomography-Computed Tomography (^{18}F -FCH PET/CT) in Predicting Quality of Life in Malignant Breast Cancer Patients

M. H. Zakaria¹, S. Shaharuddin², F. F. Ahmad Saad¹

¹Centre for Nuclear Diagnostic Imaging, University of Putra Malaysia

²National Defence University of Malaysia

Background

To determine novelty of [^{18}F]FCH PET/CT as predictor breast cancer aggressiveness and its association with quality of life (QOL) in breast cancer patients.

Methodology

This is a retrospective study. 21 patients with known case primary/recurrent breast carcinoma (BI-RADS 4/5 breast lesions) underwent [^{18}F]FCH PET/CT prior to biopsy. Histopathological examination (HPE) is obtained and dichotomized into malignant and benign groups and HER2-ve and HER2+ve groups. Maximum standardized uptake value (SUV_{max} (g/dl)) was used to predict two groups of variables for cellular breast cancer aggressiveness. QOL assessed SF-36[®], SF36v2[®], SF-1,2[®] and SF-12v2[®] Health Surveys. Questionnaires used under Medical Outcome Trust and QOL domains: Global Health Status (GHS), Physical Function (PF), Role Function (RF) and Social Function (SF).

Results

21 patients-mean age of 52.82 ± 10.71 years. 18 patients-malignant (18/21; 85.8%) on histology with 11 (52.4%) are HER2-ve. There is significant difference between [^{18}F]FCH SUV_{max} (g/dl) of HER2-ve and HER2+ve (1.99 g/dl vs 0.2 g/dl; $p < 0.05$). The malignant group has a higher SUV_{max} (g/dl) value compared to the benign group (1.36 ± 0.13 ; $p < 0.05$). High SUV_{max} (g/dl)-FCH predicted malignant breast lesions and the HER2-ve at cut-off value of 0.75 ($p < 0.05$). 15 patients being followed up for prediction of categorized FCH (High/Low) with QOL domains: GHS, PF, RF and SF at 6 and 24 months.

Symmetric Measures (N = 21)			
	Method	SUV value	Approximate Significance
Nominal by Nominal	Contingency Coefficient	0.599	0.001
Interval by Interval	Pearson's R	0.748	.000
Ordinal by Ordinal	Spearman Correlation	0.748	.000
Measure of Agreement	Kappa	0.734	0.001

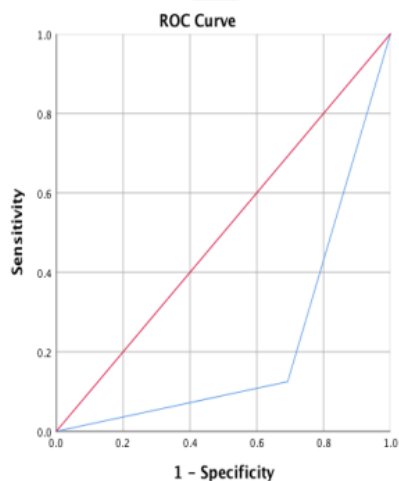


Table 1: Table and Regression Curve (ROC) for high SUV_{max} (g/dl) [¹⁸F]FCT PET/CT predict the aggressive breast cancer

QOL Scores	GHS	PF	RF	SF
FCH (High Vs Low)	1.667	8.067	3.267	5.4
Asymp. Sig.	0.197	0.005	0.071	0.02

Significant when p<0.05

GHS: Global Health Status

PF: Physical Function

RF: Role Function

SF: Social Function

The score 1- 5: Poor – Good)

Based on questionnaires

Table 2: Association of cut off categorized SUV [¹⁸F]FCH PET/CT with QOL at 6 months

Conclusion

The SUV_{max}(g/dl) [¹⁸F]FCH PET/CT of > 0.75 was a good predictor to signal aggressive breast carcinoma, hence predict QOL (Physical & Social Function satisfaction) at 6 months.

Comments

This research is to determine novelty of [¹⁸F]FCH PET/CT as predictor breast cancer aggressiveness and its' association with quality of life (QOL) in breast cancer patients. This is a pilot study in which the [¹⁸F]FCH PET/CT had been done for breast cancer patients to determine the tumour aggressiveness as well as its significant association with quality of life.

IAEA-CN-326/413

A case of recurrent carotid body paraganglioma : when [¹⁸F]FDG PET/CT reveals occult lymph nodes and bone metastases

K. B. Ahmed, H. Noomen, W. Amouri, S. Charfeddine, K. Chtourou

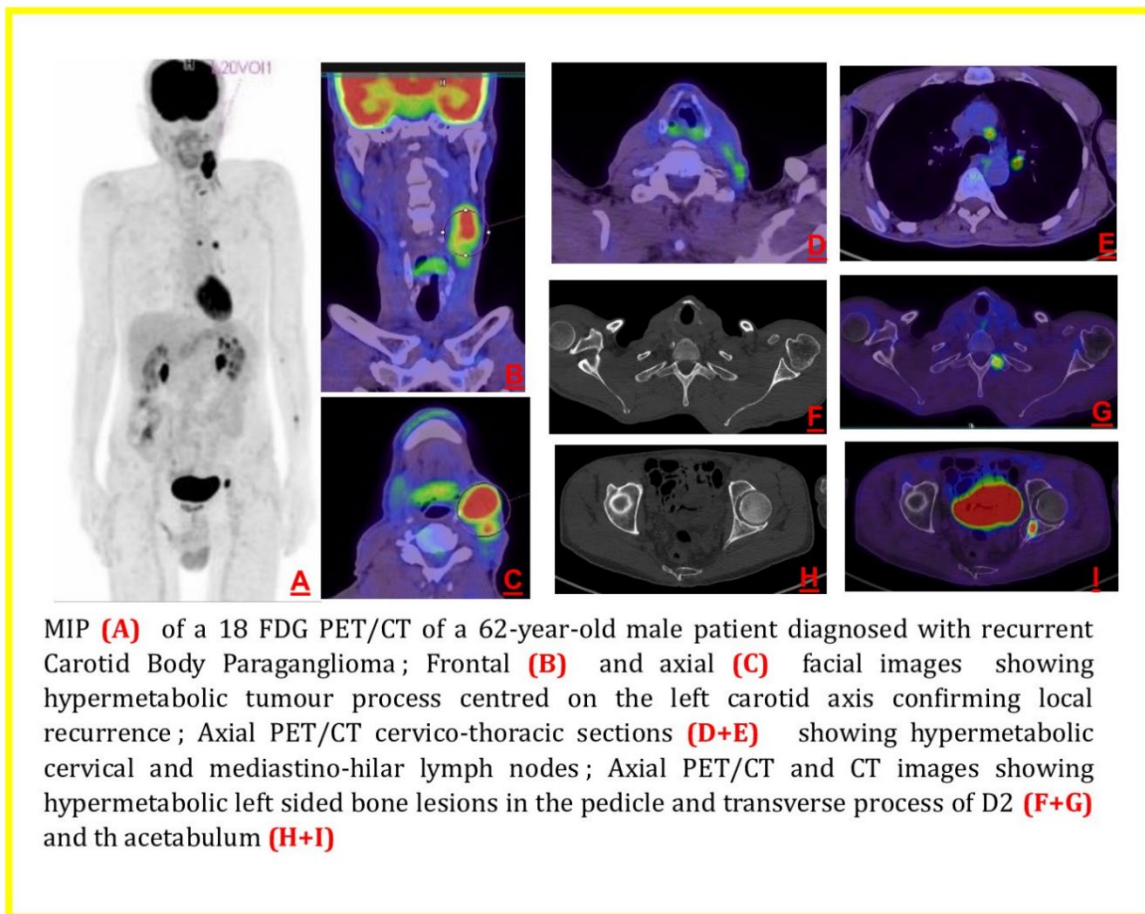
Nuclear Medicine Department, Habib Bourguiba Hospital, SFAX, Tunisia

Background

Head and neck paragangliomas are neuroendocrine tumours derived from the parasympathetic nervous system representing approximately 0.6% of all head and neck tumours. These tumours mainly occur in the carotid body. Carotid body tumours develop in glomus cells generated from the embryonic neural crest close to the carotid bifurcation. Although they are mostly benign, painless, slow-growing tumours, 10% to 20% show malignant behaviour. To date, there are no histopathological criteria for the diagnosis of malignant paraganglioma, and the sole reliable manifestation of malignancy is the presence of distant metastasis.

Case Report

We report the case of a 62-year-old male patient with a history of bilateral carotid body paraganglioma diagnosed 25 years ago. The paraganglioma had been treated by surgery and radiotherapy, and yearly scans had not shown any progression since treatment. Recently, he presented with a left cervical swelling. Clinical examination revealed a pulsatile mass and a head and neck ultrasound examination found a soft tissue mass on the left carotid artery. A recurrence of his carotid body paraganglioma was suspected. A 18 FDG PET/CT examination was requested to evaluate the locoregional tumour extension and occult metastases. The exam was performed on a PET/CT siemens biograph-64 after 6 hours of fasting and 60 minutes after injection of 7 mci of [¹⁸F]FDG. The examination revealed intense hypermetabolism in a tumour process centred on the left carotid axis (SUVLbm-max= 13,45) confirming local recurrence. Furthermore, the examination showed the presence of hypermetabolic cervical and mediastino-hilar lymph nodes (SUVLbm-max= 5,88 in the left hilar nodes) and suspicious pulmonary nodules of low metabolism due to their small size. In addition, there was hypermetabolic left sided lesions in pedicle and transverse process of D2 (SUVLbm-max= 3,67) and the acetabulum (SUVLbm-max=7,87) . A biopsy from the left acetabulum was performed and the histopathological results came back in favour of paraganglioma metastasis.



Conclusion

Paragangliomas are rare neuroendocrine tumours arising from neural crest progenitors located outside the adrenal gland. These tumours are homologous to adrenal pheochromocytomas and derive from sympathetic ganglia in abdomen and thorax (sympathetic paragangliomas) or from parasympathetic tissues in the head and neck (parasympathetic paragangliomas) regions. Carotid body tumours are uncommon paragangliomas, and malignant behaviour with metastasis is extremely rare. The current case demonstrates the importance of the additional information provided by the FDG PET/CT about unknown cervico-thoracic lymph node and bone metastases, thereby leading to an optimal therapeutic approach.

IAEA-CN-326/414

PET/CT-Guided Biopsy of Suspected Lung Lesions Leads to More Conclusive Results Than CT-Guided Biopsy

J. J. Cerci, C. C. P. Neto, C. Krauzer, D. G. Sakamoto, J. V. Vitola, R. J. Cerci, M. Masukawa

Quanta - Diagnóstico e Terapia, Brazil

Background

Tumour sampling is indispensable to diagnostic and therapeutic decision making. [¹⁸F]FDG PET/CT has the potential to discriminate between viable and non-viable tissues. The purpose of this study was to compare [¹⁸F]FDG PET/CT and CT performance in guiding percutaneous biopsies with histologic confirmation of lung lesions.

Methodology

We prospectively evaluated 626 patients, 316 underwent [¹⁸F]FDG PET/CT-guided biopsy and 310 underwent CT-guided biopsy. The pathology results, lesion size, complications, and re-biopsy rate in the 2 groups were evaluated.

Results

Of the 316 biopsies with PET/CT guidance, histology demonstrated 270 lesions (85.4%) to be malignant. In the CT-guided group, of 310 lesions, 218 (70.3%) were malignant and 92 (29.7%) were benign ($p < 0.001$). Inconclusive results prompted the need for a second biopsy in 40 patients: 27 of 310 (8.7%) in the CT group and 13 of 316 (4.1%) in PET group ($p = 0.001$). Complications were pneumothorax (12.6%), haemothorax (1.4%), and haemoptysis in 4 patients (0.6%). No life-threatening adverse events or fatalities were reported. The difference in complication rates between the 2 groups was not significant ($p = 0.6$). Malignant lesions showed a greater mean size than benign lesions regardless of the group ($p = 0.015$).

Conclusion

PET/CT-guided biopsy of lung lesions led to more conclusive results, fewer inconclusive biopsies than CT-guided biopsy, with similar complication rates. PET/CT, being an essential component of cancer staging, may serve as a one-stop shop for the management of these patients' conditions.

IAEA-CN-326/415

Incidental Adrenocortical Lesions and Hybrid Imaging: A Single-Center Experience

A. Kilicaslan, B. Cagdas, N. C. M. Gülaldi

Ankara Bilkent City Hospital, Department of Nuclear Medicine, Ankara, Turkiye

Background

Adrenal incidentalomas are adrenal lesions of uncertain significance detected on F-18 FDG PET/CT imaging performed for some other reason. They are diagnosed more frequently today due to increasing imaging examinations. This study aimed to examine the F-18 FDG PET/CT findings of operated adrenocortical incidentalomas according to their histopathological types.

Methodology

59 adrenal incidentaloma patients operated on between 2019 and 2024 were evaluated. 13 patients without F-18 FDG PET/CT imaging, 16 patients with a histopathological diagnosis of adrenomedullary lesion, and 3 patients reported as metastasis were excluded from the study. Metabolic parameters (SUVmax, SUVmean, SUVpeak), CT parameters (Hounsfield units, size), histopathological features, and secretory features (function status) of 23 patients who met the inclusion criteria were retrospectively examined. The lesions were measured anteriorly and posteriorly in the widest section, and the surface area was measured as cm². Two patients diagnosed with neoplasia were not included in the statistical comparison due to small number.

Results

13 (56.5%) of the patients were female and 10 (43.4%) were male. The mean age was 48±9 years. Histopathologically, 6 patients (26%) were compatible with adrenocortical carcinoma, 2 patients (8.6%) with adrenocortical neoplasm of uncertain malignant potential, and 15 patients (65.3%) with adrenocortical adenoma. Groups that did not show normal distribution were evaluated with paired sampled t-test and Wilcoxon signed rank test. There was a significant difference in SUVmax, SUVpeak and SUVmean values between both groups ($p < 0.05$). The mean SUVmax for adrenocortical carcinoma was 10.32, the mean SUVmean was 6.17, and the mean SUVpeak was 9.36, while for adenoma, the mean SUVmax was 3.78, the mean SUVmean was 2.56, and the mean SUVpeak was 3.17, respectively. Additionally, the median value for the lesion sizes were 8,702 cm² in adrenocortical carcinoma and 9,24 cm² in adenoma, showing a significant difference ($p < 0.05$). Of the patients diagnosed with adrenal cortical adenoma, 5 (21%) were nonfunctional and 10 (46%) were functional. The SUVmax value of 13 patients was < 3.5 . Two patients with SUVmax values above 3.5 (SUVmax: 10.96 and 8.73, respectively) had non-functional cortical adenoma. The average Hounsfield unit value of these patients was 15.12.

IAEA-CN-326/417

The Relationship Between Histopathological, Immunohistochemical, and PET Parameters in Invasive Carcinoma, NST Cases

B. Cagdas, N. C. M. Gülaldi, A. Kilicaslan

Ankara Bilkent City Hospital, Department of Nuclear Medicine, Ankara, Türkiye

Background

We aimed to investigate the relationship between histopathological parameters characterising tumour differentiation and mitotic activity, immunohistochemical parameters showing hormone profiles that could determine treatment options, and the proliferation index, along with metabolic parameters obtained from [¹⁸F]FDG PET/CT imaging for disease staging.

Methodology

A total of 368 female patients who underwent [¹⁸F]FDG PET/CT imaging for breast cancer staging between 2019 and 2024 were screened. A total of 147 patients diagnosed with invasive carcinoma, NST (no special type), with known Nottingham scoring, histological grade, Ki-67 proliferation index, hormone receptors, and HER2 expression status at the time of diagnosis without treatment before [¹⁸F]FDG PET/CT imaging, met the inclusion criteria and were retrospectively analysed. Metabolic parameters including SUV_{max}, SUV_{mean}, SUV_{peak}, MTV (Metabolic Tumour Volume), and TLG (Total Lesion Glycolysis) were calculated, considering SUV_{max} at 42% of the threshold value in the primary lesion for the [¹⁸F]FDG PET/CT imaging. None of the parameters fit into the normal distribution. Therefore, Mann-Whitney-U, Kruskal-Wallis, and Spearman correlation tests were applied.

Results

The mean age was 56 (34–94) years. 5 cases had a Nottingham score of 4, 19 cases had a score of 5, 52 cases had a score of 6, 40 cases had a score of 7, 24 cases had a score of 8, and 7 cases had a score of 9. ER positivity was detected in 130 cases, PR positivity in 129 cases, and HER2 positivity in 35 cases. In the Kruskal-Wallis analysis among Nottingham Score groups, significant differences were found in SUV_{max}, SUV_{mean}, SUV_{peak}, and TLG values ($p < 0.05$). Significant differences were found in SUV_{max} (11.21 vs 8.25 g/ml), SUV_{mean} (6.92 vs. 5 g/ml), SUV_{peak} (8.33 vs 6.17 g/ml), and TLG (103 vs. 57 g/ml) values between cases with HER2 amplification and those without, with higher values observed in cases with HER2 amplification ($p < 0.05$). Cases showing ER receptor expression had lower SUV_{max} (8.16 vs 14.89 g/ml), SUV_{mean} (4.99 vs 8.87 g/ml), and SUV_{peak} (6.1 vs. 10.96 g/ml) values compared to cases not showing expression ($p < 0.05$). Similarly, cases showing PR receptor expression had lower SUV_{max} (8.1 vs. 14.97 g/ml), SUV_{mean} (4.95 vs. 8.96 g/ml), and SUV_{peak} (6.05 vs. 11.09 g/ml) values compared to cases not showing expression ($p < 0.05$). A moderately positive correlation was found between the Ki-67 proliferation index of the cases and the TLG ($\rho: 0.38$), SUV_{max} ($\rho: 0.45$), SUV_{mean} ($\rho: 0.44$), and SUV_{peak} ($\rho: 0.46$) parameters.

Conclusion

A positive correlation between the Ki-67 proliferation index and SUV_{max}, SUV_{mean}, SUV_{peak}, and TLG metabolic parameters of the [¹⁸F]FDG PET/CT scan gives clues to the clinicians for more aggressive disease as in HER2 amplification. However, tumours with ER and PR

receptor expression tends to have lower glucose utilisation suggesting having less aggressive behaviour than those who do not.

IAEA-CN-326/418

Detector Block-Pairwise Dead Time Correction for the Siemens 3T MR-BrainPET Insert**A. S. M. Issa, C. R. Brambilla, H. Herzog, J. Mauler, J. Scheins, L. Tellmann, N. J. Shah, P. Lohmann, C. Lerche****Institute of Neuroscience and Medicine 4, INM-4, Forschungszentrum Jülich, Jülich, Germany****Background**

The implementation of dead time correction (DTC) is crucial for achieving highly accurate quantification in positron emission tomography (PET). Many PET systems use global DTC, i.e., an average DTC factor (Fdt) is computed for all scintillation detector blocks. However, the count rates of the individual scintillation detector blocks are potentially very different due to the individually varying irradiation of each detector block, especially for systems where the allocation of radiation shields is not possible, as in the case of the Siemens 3T MR-BrainPET insert. In this case, global DTC will not completely compensate dead time (DT) losses, leading to a distortion of measured time-activity curves (TAC) and erroneous tissue uptake values. For a dedicated head PET scanner, the uncorrected count rate varies significantly depending on the position of the detector block relative to the imaged object, resulting in different DTs for each block. To address this issue, we have developed a blockpairwise DTC method.

Methodology

We extended upon a previously published method that uses the delayed random coincidence count rate to estimate DT within individual planes. Our new method was evaluated using decay experiments using phantoms with homogenous and inhomogeneous activity concentrations, with and without out-of-field of view (FOV) activity. We compared the accuracy and the noise behaviour with measurements using a three-compartment phantom. The Fdt for all 10,944 block pairs (32 detector modules with six blocks each) was computed and used to correct the prompt counts in every block pair, incorporating triples correction. We also cross-calibrated both methods against each other. Furthermore, we assessed differences in quantified images resulting from the administration of various radioactive tracers in volunteers and patients, i.e., [11C]-ABP688, O-(2-[18F] fluoroethyl)-L-tyrosine (18F-FET) for the brain tumours.

Results

The new method successfully corrected DT losses of the true coincidence counts when applied to the 3T MR-BrainPET insert, surpassing the performance of the currently employed global DTC. In the case of the average prompt count rate from the homogenous phantom, the maximum deviation between DT-corrected measured trues and the ideally expected trues was 1.5% at most. Including a correction for detected triple coincidences further enhanced accuracy. The statistical noise in the Fdt of the new method was about 10 times less than the expected count rate variations of prompt coincidences when estimating the correction factor per second. Consequently, no relevant noise propagation was observed in the PET image. The phantom measurements showed that the global DTC led to significant quantification biases in regions with high activity concentrations, while the blockpairwise DTC led to substantially less bias. Evaluation of typical human studies revealed differences between the two DTC methods which are particularly important for research applications in

neuroscience. For example, PET imaging with [11C]ABP688 demonstrated considerably reduced bias in the neuroreceptor volume of distribution (VT) across all examined brain regions when employing the new block-wise DTC. In [18F]-FET-PET, differences in tumour to background ratios (TBRmax) of up to 10% were observed when comparing both DTC methods.

IAEA-CN-326/419

Diffuse lesions of the skull bones in a patient with treated nasopharyngeal carcinoma: is it always that easy to make a difference on FDG PET

L. Zaabar^{1,2}, H. Rokbani¹, S. Cherif¹, D. Ben Sellem^{1,2}, A. Mhiri^{1,2}

¹ Nuclear Medicine Department, Salah Azaeiz Institute, Tunisia.

² Faculty of Medicine of Tunis, Tunis El-Manar University. Tunisia

Background

Nasopharyngeal carcinoma (NPC) has a limited prognosis. In addition to its often late initial diagnosis, its locoregional and distant aggressiveness, we report the significant rate of recurrences, which requires close monitoring. While follow-up, several diagnoses will be considered when faced with the discovery of bone lesions on CT imaging. [18F]FDG-PET/CT has showed high diagnostic accuracy in the differential diagnosis of unclassified lesions, especially at the bone.

The aim of this case presentation was to report an aspect of osteonecrosis (ORN) doubtful of bone recurrence in NPC patient, to highlight the contribution of [18F]FDG-PET/CT in differential diagnosis.

Case Presentation

We discussed the case of a 32 years old woman referred to us for [18F]FDG PET/CT in the context of a clinical and radiological suspected recurrence of her nasopharyngeal cancer, initially classified T4N1M0, treated 16 years ago with radiochemotherapy. PET/CT (06/03/2024) was performed 60 minutes after intravenous injection of 4,1mCi of 18FDG. It showed an hypermetabolic thickening of the posterior and posterolateral wall of the nasopharynx with bilateral secondary laterocervical lymph nodes, consistent with loco-regional tumour recurrence. Elsewhere, we objectified the mixed and diffuse lacunar appearance of the bones of the base of the skull and the facial relief, remaining however without cortical rupture or extension to neighbouring structures or pathological hypermetabolism. The absence of any hypermetabolism was reassuring to conclude on the diagnosis of radioosteonecrosis.

ORN is indeed a rare and debilitating complication that can arise following definitive chemoradiotherapy for head and neck cancers. The earliest radiological sign is an increase in bone density, associated with periosteal thickening, sometimes in conjunction with areas of hypodensity of bone. Later, hypodensity extends with a “flaky” appearance, with blurred edges, containing some hyperdense areas. These first-radiological signs appear when osteolysis reaches 30 to 50%. The progression is towards the appearance of sequestra and pathological fractures [1]. It is difficult to distinguish between ORN and recurrent or progressive disease, as clinical and radiologic features may be similar. To distinguish between them a comprehensive evaluation is necessary involving clinical examination, imaging studies, biopsy, and [18F]FDG-PET/CT. In [18F]FDG PET/CT, it is normally challenging to distinguish between ORN and recurrent disease since both can be hypermetabolic, but different aspects can be seen. Likewise, It is also important to keep in mind that ORN can be hypermetabolic due to infection (osteomyelitis). finally, and given the prolonged delay compared to radiotherapy we could consider in this patient a radiation-induced osteosarcoma.

Conclusion

In summary, while ORN is a rare complication of radiation therapy for head and neck cancers, it poses significant challenges in diagnosis due to similarities with disease recurrence. [18F]FDG

PET/CT is part of a multidisciplinary approach to accurately differentiate between these conditions and in some cases it can easily distinguish between them, limiting the use of biopsies, especially when the ORN is non hypermetabolic.

Keywords: Osteoradionecrosis, Tumour recurrence, 18-Fluro-deoxy-glucose, Positron emission tomography/computerized tomography, Nasopharyngeal carcinoma, bone metastasis

IAEA-CN-326/421

FDG PET as Predictor of Neo-Adjuvant Chemotherapy Benefit in Stage 3 Colon Cancer

V. Agarwal

Bharat Cancer Hospital, India

Background

Neo-adjuvant chemotherapy in stage III colon improves cancer outcome but all patients do not benefit from it. Our main hypothesis is that the absence of metabolic response of the primary tumour after 1 pre-operative chemotherapy course predicts the absence of benefit from adjuvant chemotherapy. This strategy's aim is to spare the patient's from useless toxicities and better management of scarce resources.

Methodology

Patient's aged more than 18 years of age and diagnosed with curative resectable colon cancer were eligible for study. Baseline FDG PET CT was repeated after 1 cycle of chemotherapy, followed by surgery.

Results

52 patients were enrolled in this study with 35 patients being male. Pre-operative FDG PET CT was done in all of them, stage IV cancer being diagnosed in 10 of them therefore they were excluded from the study. In the remaining 42 patients, SUVmax was calculated in the base-line scan. The baseline SUVmax ranged from 7.89 – 12.31, with a mean of 10.17. The SUVmax baseline was compared with the FDG scan done after 1 cycle of chemotherapy. Metabolic regression was observed in almost 58% of these patients. Twenty-four patients showed metabolic regression of which 18 patients had complete response and 06 patients showed partial response (SUVmax ranging from 2.36 – 5.67, with a mean of 4.05).

Conclusion

One course of neo-adjuvant chemotherapy is beneficial before curative resection for stage III colon cancer without inducing excessive toxicity or surgical morbidity. Metabolic response assessment indicated chemo-resistance in almost 42% of the primary tumours.

IAEA-CN-326/422

Radiolabeling of Metal Complex of α -Mangostin Using Iodine-131 for Radiopharmaceutical of Theranostics Breast Cancer

R. Mardianingrum¹, I. Daruwati², V. Y. Susilo², W. Lestari², A. M. Forentin², M. Muchtaridi³, R. Ruswanto⁴

¹ Department of Pharmacy, Faculty of Health Sciences, Universitas Perjuangan, Indonesia

² Research Center for Radioisotope, Radiopharmaceutical, and Biodosimetry Technology, Research Organization for Nuclear Energy, National Research and Innovation Agency (BRIN), BJ Habibie Science and Technology Area, Indonesia

³ Department of Pharmaceutical Analysis and Medicinal Chemistry, Faculty of Pharmacy, Universitas Padjadjaran, Indonesia

⁴ Pharmacy Program, Universitas Bakti Tunas Husada, Indonesia

Background

According to data from the International Agency for Research on Cancer, in 2024 there will be 19.9 million cases of cancer worldwide. In 2020, breast cancer cases worldwide have grown and reached 2.26 million new cases and rank first in incidence (24.5%) and mortality (15.5%) in women. One of the most dangerous cancers is breast cancer. This study aims to optimize of radiolabeling from α -mangostin metal complex derivatives and the cellular uptake of MCF-7.

Methodology

AM-Co, AM-Pt, and AM-Fe (α -mangostin derivative complexes) were labeled by direct reaction with Na¹³¹I using the chloramine T (CAT) method. In a 0.2 mL microtube, 1 mg of α -mangostin derivative complexes was dissolved in 0.5 mL of absolute ethanol, then 10–100 μ L CAT (1 mg/mL) was added. The microtube was placed into a Pb container, and then 5–10 μ L of Na¹³¹I solution with radioactivity between 1.85–3.7 MBq (50–100 μ Ci) was added. It was then shaken until homogeneous. The solution was shaken with a vortex stirrer for some time from 1–15 min at room temperature. Immediately, 10–100 μ L of sodium metabisulfite solution with a concentration of 2.5 mg/mL was added to stop the reaction. Then, The optimization of CAT, ligand and it's stability were conducted. Culture cells were incubated in RPMI/DMEM media for 24 hours in 24 well plates. Cells were removed one by one with a micropipette, then rinsed with 1 mL HBSS 10 μ L sample solution consisting of ¹³¹IAM-Co, ¹³¹IAM-Pt, ¹³¹IAM-Fe, and ¹³¹I standard added to the triple well. Incubate at room temperature for 10, 30, and 60 minutes. Then the cells were lysed by adding 60 μ L 0.2N NaOH. Then, the radioactivity of each cell lysate was measured with an automatic gamma counter. The cellular uptake of the samples was analysed by comparing it with standards (% cellular uptake).

Results

The process radiochemical purity of ¹³¹IAM-Co (99.21%), ¹³¹IAM-Pt (98.40%), and ¹³¹IAM-Fe (99.49%). The labeling optimization results show that the best conditions for labeling ¹³¹IAM-Co, ¹³¹IAM-Pt, and ¹³¹IAM-Fe are at a temperature of 4°C and 30 minutes of incubation time with a ligand amount of 250 μ g. while the amount of chloramine t in the three optimal ligands varies for ¹³¹IAM-Co (25 μ g), ¹³¹IAM-Pt (100 μ g), and ¹³¹IAM-Fe (50 μ g). Based on the results of the stability analysis of radiochemical preparations, it was found that the best level of stability was on average at -20°C (freezer) compared to 4°C (refrigerator).

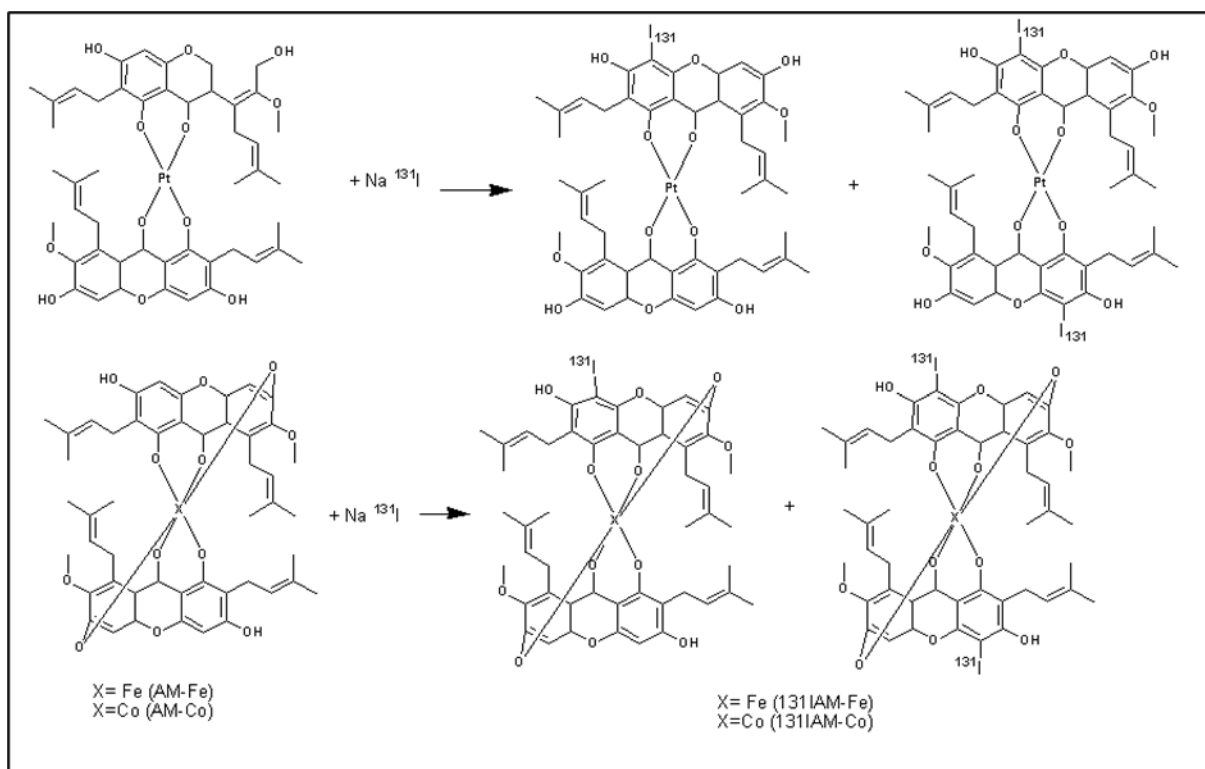
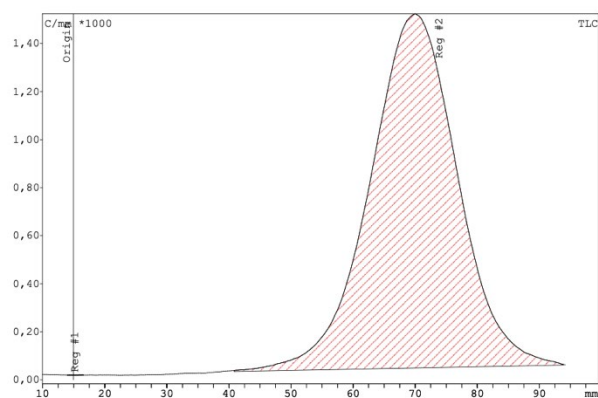
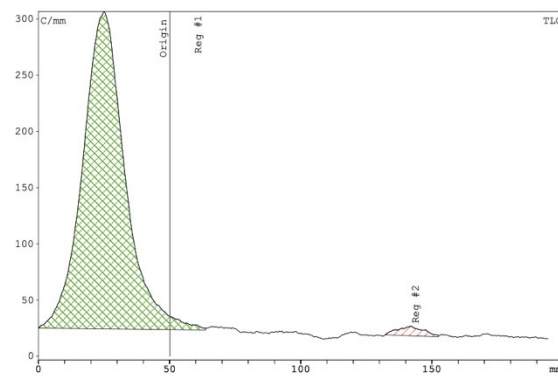


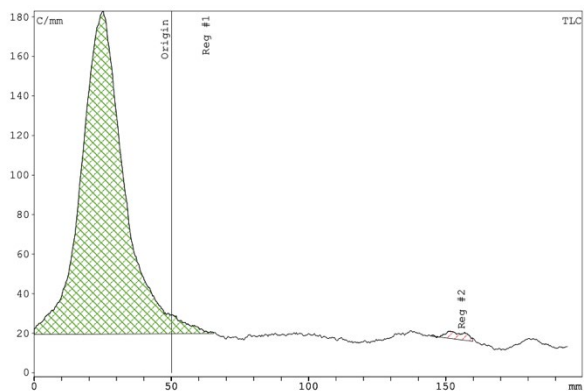
Figure 1. Prediction Radioiodination Reaction $^{131}\text{IAM-Co}$, $^{131}\text{IAM-Pt}$, and $^{131}\text{IAM-Fe}$



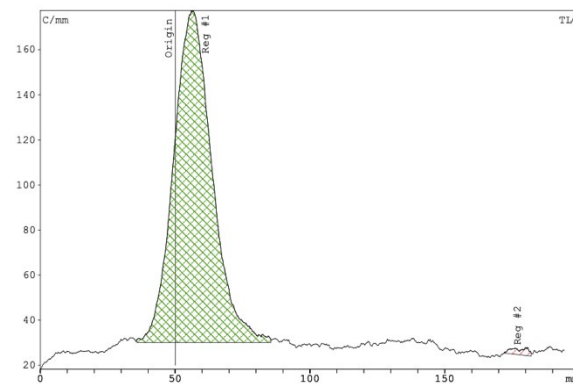
(a) Iodine-131



(b) $^{131}\text{IAM-Co}$



(c) $^{131}\text{IAM-Fe}$



(d) $^{131}\text{IAM-Pt}$

Figure 2. Radiochromatogram Profile of Iodine-131 (a), ¹³¹IAM-Co (b), ¹³¹IAM-Fe (c), and

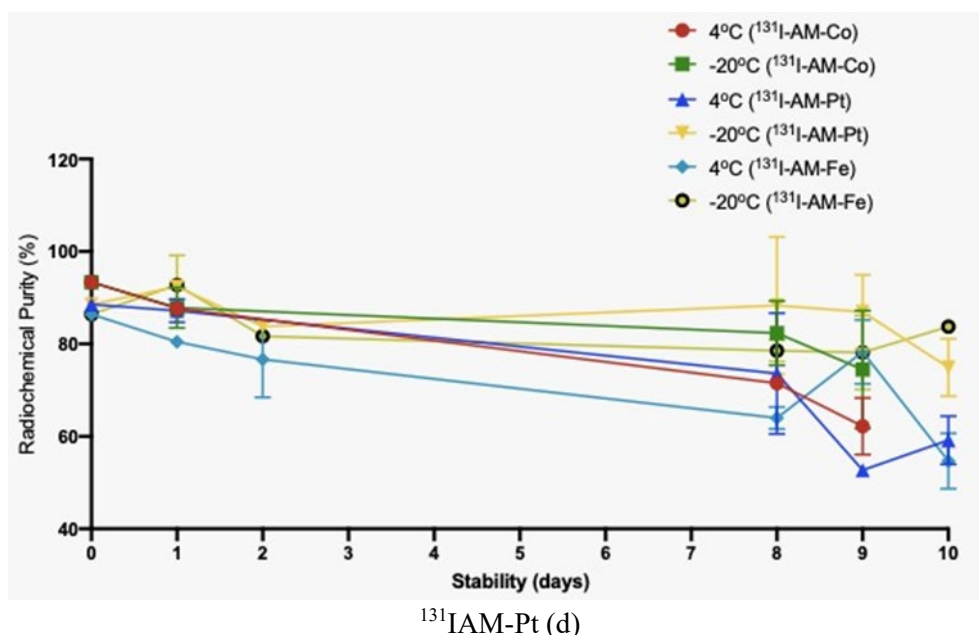


Figure 3. Stability test of ¹³¹IAM-Co, ¹³¹IAM-Pt, and ¹³¹IAM-Fe in several temperatures and storage periods

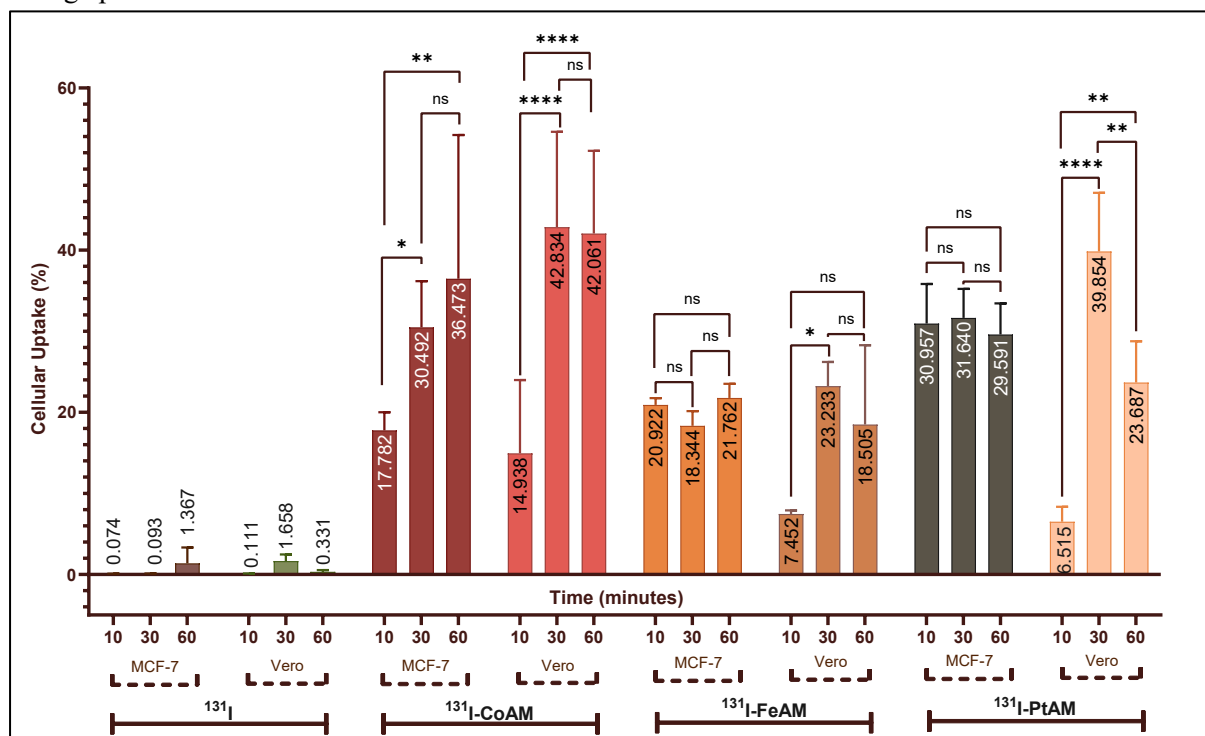


Figure 4. Uptake of compounds labeled ¹³¹I-CoAM, ¹³¹I-FeAM, and ¹³¹I-PtAM in MCF-7 and Vero cells with incubation for 10, 30, and 60 minutes

Conclusion

The radiochemical purity of ¹³¹IAM-Co (99.21%), ¹³¹IAM-Pt (98.40%), and ¹³¹IAM-Fe (99.49%) at a temperature of 4°C and 30 minutes of incubation time with a ligand amount of 250 µg, while the amount of chloramine t in the three optimal ligands varies for ¹³¹IAM-Co (25 µg), ¹³¹IAM-Pt (100 µg), and ¹³¹IAM-Fe (50 µg). Based on the results of the stability analysis of radiochemical

preparations, it was found that the best level of stability was on average at -20°C (freezer) compared to 4°C (refrigerator). The cellular uptake rate of all the test compounds in the MCF-7 cells was ^{131}I IAM-Co (17.782%), ^{131}I IAM-Fe (20.22%), and ^{131}I IAM-Pt (30.957%) respectively.

IAEA-CN-326/423

Master of Masquerade: Disseminated Tuberculosis with Unexpected Gynaecological Involvement Depicted on FDG PET/CT**S. Z. A. Hassan, M. F. M. Rohani, A. Z. Zaniat**

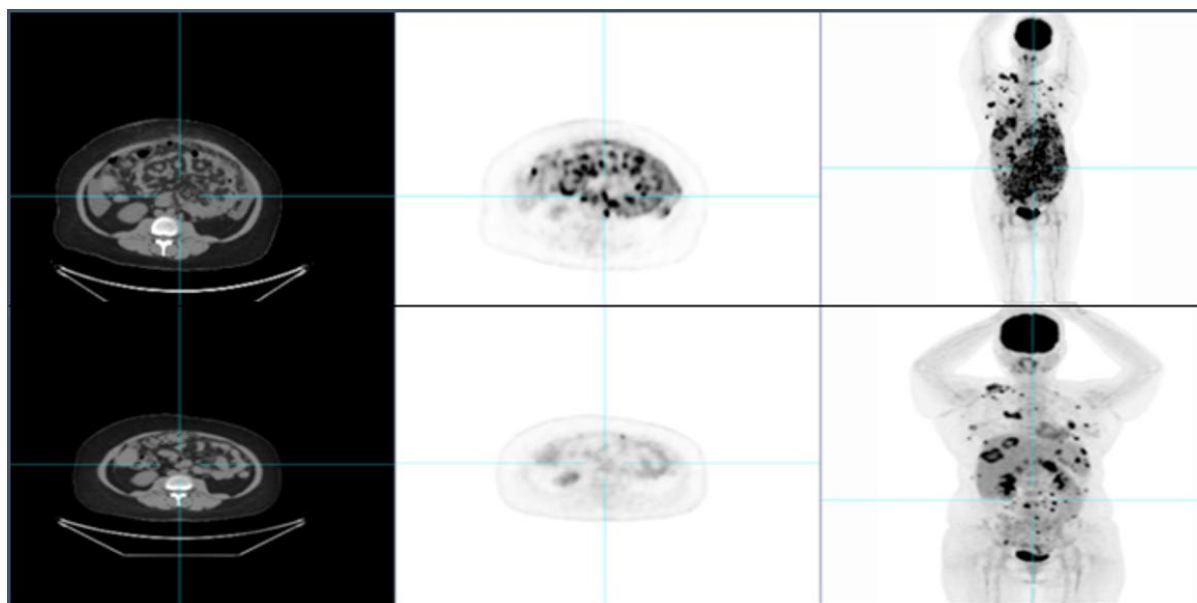
Nuclear Medicine Department, General Hospital Kuala Lumpur, Malaysia

Background

Fluorodeoxyglucose positron emission tomography-computed tomography (FDG PET/CT) is well established in management of primary gynaecological malignancies. However, there are uncommon pathologies involving gynaecological system that may cause dilemma in patient management. In selected cases particularly suspected unknown primary malignancy or fever of unknown origin, FDG PET/CT may facilitate the assessment of patients. We report a case of disseminated tuberculosis involving gynaecological tract depicted on FDG PET/CT and discuss the promising role of this hybrid imaging modality in patient management.

Case Report

39-year-old lady presented with pronounced abdominal distention and markedly raised serum Ca125. However, no obvious constitutional symptoms reported. CT scan demonstrated features of metastatic pleural disease and overall abdominal findings suggestive of pseudomyxoma peritonei with possible primary of ovaries or appendix. Further assessment with FDG PET/CT (16.12.2020) revealed extensive FDG-avid disease mainly in both lungs, liver, bilateral adnexa, abdominopelvic lymphadenopathies, peritoneal and mesenteric nodules. As it appeared to be a primary abdominopelvic disease, diagnostic laparoscopy with biopsy of peritoneal nodules was performed. It showed chronic granulomatous inflammation secondary to tuberculosis. She was then started on intensive anti-tuberculosis therapy. Repeat FDG PET/CT (27.5.2021) to monitor treatment response showed reduction in numbers and intensities of the known extensive FDG-avid lesions.



Conclusion

Extrapulmonary tuberculosis with gynaecological involvement is uncommon and may even mimic advanced ovarian cancer with disseminated FDG-avid disease. This case report highlighted the promising role of FDG PET/CT that may facilitate biopsy decision and treatment response evaluation in such patient.

IAEA-CN-326/424

Role of SPECT/CT and PET/CT in the Early Identification of Radioiodine Refractory Differentiated Thyroid Cancer: A case report

A. Khelifa, D. Meziane, A. Talbi, L. I. Chelghoum, S. E. Bouyoucef

Nuclear Medicine Department, University Hospital of Bab El Oued, Algiers, Algeria

Background

Radioiodine therapy (RAI) plays a crucial role in the management of high-risk differentiated thyroid cancer (DTC) after surgery. Nuclear medicine functional imaging SPECT/CT (Single Photon Emission Computed Tomography computed tomography) enables the identification of lesions that concentrate or do not concentrate radioiodine both within and outside the thyroid bed during the initial therapeutic whole-body scan (WBS). Fluorodeoxyglucose positron emission tomography/computed tomography ($[^{18}\text{F}]$ FDG PET/CT) is crucial for early confirmation of aggressive lesions and identifying patients with RAI-refractory disease for optimal management strategy.

Case Presentation

We report the case of a 42-year-old woman who was referred to our department for radioiodine therapy after surgical resection of a papillary thyroid carcinoma (PTC) classified T3bN1bMx. The pathology showed 15 metastatic cervical lymph nodes, vascular emboli, and involvement of the resection margins.

The patient received RAI using 3700 MBq of iodine-131, followed by post-RAI WBS with anterior and posterior views, complemented by SPECT/CT imaging in the cervicothoracic region. Two months later, $[^{18}\text{F}]$ FDG PET/CT imaging was performed. The post-RAI WBS and SPECT/CT showed no uptake in the cervical region or on the rest of explored body. Stimulated serum thyroglobulin levels were elevated at 52 ng/mL with negative anti-thyroglobulin antibodies at 21 $\mu\text{UI/mL}$. On the CT, we observed a cluster of cervicomedial lymph nodes and pulmonary micronodules that did not exhibit radioiodine uptake.

The maximum intensity projection (MIP) PET/CT showed multiple hypermetabolic foci with an SUV_{max} at 9 within the cervical and mediastinal lymph nodes, as well as the pulmonary nodules and micronodules. This confirmed progressive metastatic disease, leading to reclassification of the PTC to stage T3bN1bM1. Since the patient presented a cervical formation at clinical examination, she was referred for surgery again.

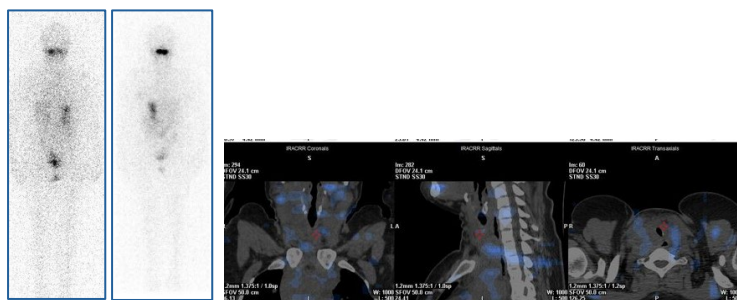


Figure A. Negative WBS, no uptake in cervical and pulmonary SPECT/CT lesions

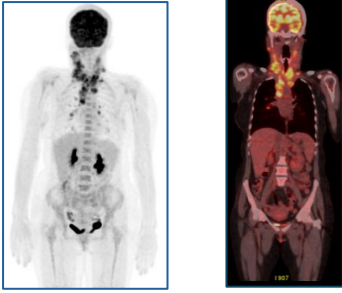


Figure B. Positive PET/CT with multiple cervicomedial lesions that concentrate $[^{18}\text{F}]$ FDG

Conclusion

Our case suggests that DTC can be effectively classified as RAI refractory when there is no uptake observed on the initial WBS SPECT/CT coupled with morphological CT findings that reveal lesions concentrating $[^{18}\text{F}]$ FDG on PET/CT imaging. This advocates for the potential interest of SPECT/CT and PET/CT in the early detection of RAI-refractory DTC, allowing for timely adjustments in management strategies and the implementation of more effective treatments.

IAEA-CN-326/425

Establishing the First GMP Facility Certification for Radiopharmaceuticals in Indonesia Hospital

R. R. Ismuha

Dharmais Cancer Hospital, Indonesia National Cancer Center, Indonesia

Background

Radiopharmaceuticals are a crucial aspect of healthcare, playing a pivotal role in diagnosing and treating a range of medical conditions. However, to ensure their safety, efficacy, and quality, strict regulations and quality control measures must be in place throughout their manufacturing and use. In Indonesia, establishing the first Good Manufacturing Practices facility certification for radiopharmaceuticals in hospital-based facilities is a significant milestone in advancing healthcare standards and promoting public health. The certification process required collaborative efforts from various stakeholders, including regulatory bodies, the Ministry of Health, and hospital management. The process of obtaining the certification started in 2022, and the facility has already produced PET radiopharmaceuticals and has served patients since 2013. However, significant gaps and adjustments were required to fulfil the criteria set by the Indonesian Food and Drug Authority guidelines that became effective in 2020. After two years of battle, the facility finally received the GMP facility certification. The significant corrections included the facility, procedures, qualifications, and validations, while continuous improvement should apply to all the processes. The certification is a significant achievement and a testament to the facility's commitment to maintaining the highest standards in manufacturing radiopharmaceuticals.

Methodology

Establishing the first Good Manufacturing Practice (GMP) facility certification for radiopharmaceuticals in Indonesia involved a comprehensive methodology. This methodology integrates regulatory development, infrastructure enhancement, training, quality management system (QMS) implementation, and regulatory inspection. The report was analysed to identify all findings, and a follow-up plan was made based on specific guidelines and regulations tailored to radiopharmaceutical manufacturing provided in 2020. Additionally, the report benchmarked against international standards such as the International Conference on Harmonisation (ICH) guidelines, and stakeholders were engaged to identify regulatory gaps and requirements.

Results

The process of obtaining GMP facility certification for radiopharmaceuticals requires several essential steps.

1. These include the development of a regulatory framework in collaboration with regulatory authorities to ensure that guidelines and regulations tailored to radiopharmaceuticals' manufacturing, handling, and quality control are well understood by all parties involved.
2. We did specialized training programs for personnel involved in radiopharmaceutical manufacturing to ensure compliance with GMP standards. These programs emphasize GMP compliance, radiation safety, and quality assurance.
3. To align with GMP requirements, robust quality management systems encompassing documentation, validation, calibration, and quality control procedures must also be addressed.

4. Finally, regulatory authorities rigorously inspect the facility to assess compliance with GMP standards, and certification is granted upon successful adherence to regulatory guidelines.

No	Aspect	Number Of Finding
1	Qualification	27
2	Validation Method	16
3	Facility	11
4	Quality System	9
5	Production	9
6	Process Validation	7
7	Documentation	5
8	Self-Inspection	3
9	Calibration &	2
10	Personnel	2
11	Raw Material Process	2
12	Quality Control	2
Total		95

Conclusion

Establishing the first GMP facility certification for radiopharmaceuticals in Indonesia is a significant achievement toward ensuring these specialized pharmaceuticals' quality, safety, and effectiveness. This milestone highlights Indonesia's dedication to improving healthcare standards, encouraging innovation, and protecting public health. Continued collaboration, adherence to GMP principles, and ongoing regulatory oversight are necessary to maintain and expand the benefits of this accomplishment in nuclear medicine and radiopharmaceuticals.

IAEA-CN-326/428

Unknown orbital location in Erdheim Chester disease revealed by [18F]FDG PET/CT: A case report analysis

S. Cherif¹, L. Zaabar^{1,2}, H. Rokbani¹, D. Ben Sellem^{1,2}, A. Mhiri^{1,2}

¹ Nuclear Medicine Department, Salah Azaeiz Institute, Tunisia.

² Faculty of Medicine of Tunis, Tunis El-Manar University. Tunisia

Background

Erdheim-Chester disease (ECD) is a multisystem disease, with highly variable clinical manifestations. It is a rare non-Langerhans cell histiocytosis of unknown origin with a slight male preponderance. Approximately 1000 cases of ECD reported to date presenting a significant diagnostic challenge. The diagnosis and treatment require the integration of clinical data, imaging examinations, and pathology assessments. The most common manifestation is diaphyseal and metaphyseal osteosclerosis of long bones.

Fluorodeoxyglucose-positron emission tomography (FDG-PET/CT) offers the advantage of concurrently assessing both skeletal and extra-skeletal disease extent and stands out as a valuable imaging modality for differentiating ECD from other histiocytosis.

The aim of this case presentation was to highlight the value of [18F]FDG-PET/CT in the complete lesion assessment of the ECD, revealing unknown locations, which makes it possible to adapt the most appropriate treatment.

Case Presentation

It is about a 23-year-old male with a 1-year history of bone pain underwent radiological investigations following a car accident. The discovery of bone abnormalities on standard X-rays triggered further imaging investigation with CT scan suggesting the presence of mesenteric panniculitis and bilateral symmetric cortical osteosclerosis of the diaphyseal and metaphyseal regions in femurs and humerus. Axial and pelvic skeletal involvement was also described. MRI showed a diffuse infiltration of the bone marrow involving diametaphyseal regions and sparing the epiphyses. Bone biopsies showed mild fibrotic background associated with classical foamy histiocytes. Histiocytes were positive for CD68 immunostains and negative for CD1a. [18F]FDG PET/CT scan revealed symmetrical areas of increased [F-18]2-fluoro-2-deoxyglucose (FDG) uptake in the known long bones locations. Furthermore, the [18F]FDG PET/CT showed a left retro-orbital infiltration unrecognized on CT scan, considered diagnostic of Erdheim-Chester disease.

ECD can be localized in the orbit, creating an intra-orbital infiltration, often bilateral, but without bone erosion. This damage causes uni/bilateral exophthalmos in 20% of cases, increasing to 36.6% if associated with central nervous system damage. This orbital involvement is rarely a main or initial symptom, discovered rather through imaging. It will be confirmed by orbital excisional biopsy.

The treatment to be carried out differs depending on the location. In the literature, «pegylated interferon-alpha» was without notable effectiveness for retro-orbital tumours, such as case of our patient. On the other hand, «vemurafenib» had shown better effectiveness specifically for orbital tumours [1].

The questioning of our patient did not note any ocular symptoms. The clinical examination did not show exophthalmos. A specific ophthalmological examination was scheduled as well as an orbital MRI.

Conclusion

[18F]FDG PET/CT results can help establish a diagnosis, guide biopsies and changes the treatment. It can detect occult visceral involvement and depict severity and extent of the disease.

Keywords: Erdheim-Chester disease, Orbit, Tumour, 18-Fluro-deoxy-glucose, Positron emission tomography/computerized tomography, bone metastasis.

IAEA-CN-326/430

Comparative Study between Absorbed and Effective Radiation Doses of some Oral Tissue after Panoramic and Cone Beam CT Radiograph

A. K. Talha¹, A. M. H. Abaza², O. S. A. El-Shall³, G. El- Shanshoury⁴

¹ Nuclear and Radiological Safety Research Center, Egypt

² Radiation Protection Department, Nuclear and Radiological Safety Research Center, Egypt

³ Diagnosis and Radiology Faculty of Dental Medicine for Girls, Al-Azhar University, Egypt

⁴ Radiation Safety Department, Nuclear and Radiological Safety Research Center, Egypt

Background

Radiation exposure must be accompanied by a related benefit that overwhelming the associated risks for the use of that radiation especially in diagnostic imaging. Additionally, the absorbed dose is the basic physical dose quantity, and is the mean energy imparted to matter of mass by ionizing radiation. Moreover, dental diagnostic imaging was dominated by radiographs during the last century.

Panoramic radiography is a radiologic technique that provides an overview of the jaws and surrounding structures. However, with the introduction of cone beam computed tomography (CBCT), there was much interest in the technology due to its advantages. Although exposure dose from CBCT is relatively low, it is 10 times higher than that of intraoral and extraoral radiography used in dentistry. Thus, the increase in patient dose during examination is a matter of concern. This study aimed to compare the absorbed and effective radiation doses of some oral tissues after exposure to ionizing radiation through panoramic radiograph and CBCT.

Methodology

Forty-seven patients (34 females and 13 males) were selected from who referred to the oral medicine department, Periodontology, Oral Diagnosis & Radiology, Faculties of Dental Medicine, Al-Azhar university for Panoramic and CBCT examination for various dental purposes. Patients divided into two groups, one was subjected to Panoramic examination (22 patients) and the other was subjected to CBCT examination (25 patients). Six positions /sites for radiological measurements were used for each patient using thermo-luminescent dosimeter (TLD) and the dose was separately measured.

Results

The parotid gland followed by the submandibular gland was the most examination sites affected by radiation as regard the absorbed radiation skin dose in the Panoramic radiography (The P-value was < 0.001, < 0.001, and < 0.05 in the two positions of parotid and submandibular glands, respectively), and the oral mucosa followed by parotid gland regarding the effective radiation skin dose (The P-value was <0.001, 0.05, and < 0.01 in the oral mucosa and two positions of parotid, respectively). The most examination site affected by radiation was the oral mucosa regarding the absorbed and the effective radiation skin doses in the CBCT radiography (P-value was <0.01 and <0.001 respectively). The effective radiation skin doses of CBCT are greater than that for Panorama technique at all the examined areas. The oral mucosa and parotid gland absorbed a higher radiation dose than the other oral structures, after both techniques. However, the effective radiation doses were importunately higher in case of the CBCT compared to the Panorama by 3.33 times in the present study. The upper central tooth was the most site to be affected in CBCT followed oral mucosa by 7.39 & 4.34 times more than in Panorama, respectively.

Conclusion

The dentist must weigh the benefits of taking dental radiographs against the risk of exposing a patient to x-rays hazards and to the accumulating radiation from multiple sources over time. The potential benefits of CBCT in maxillofacial disciplinary are undisputed; however, it is imperative that their use be fully justified over conventional technique before they are carried out.

Keywords: absorbed radiation skin dose, effective radiation dose, Panoramic radiograph, Cone beam CT.

IAEA-CN-326/432

Staging with 68Ga-PSMA PET in patients with intermediate and high-risk prostate cancer suitable for radical prostatectomy correlates with histology

J. J. Cerci, R. J. Cerci, M. Masuka, F. R. A. Oliveira, C. C. P. Neto, M. M. F. da Silva, J. V. Vitola

Quanta Diagnóstico e Terapia, Brazil

Background

Accurate staging of localized and metastatic prostate cancer is crucial for the guidance of treatment. Gallium-68 prostate-specific membrane antigen positron emission tomography/computed tomography (68Ga-PSMA PET/CT) has increasingly been utilized globally to assess the local and metastatic burden of prostate cancer.

We aimed to characterize the metastatic spread of PCa in relation to 68Ga-PSMA, compare 68Ga-PSMA PET/CT findings with radical prostatectomy histopathology findings and treatment change based on 68Ga-PSMA information.

Methodology

The study included 56 consecutives newly diagnosed, biopsy-proven, treatment-naive, unfavourable/high-risk PCa patients primary-staged by 68Ga-PSMA PET/CT. 68Ga-PSMA PET/CT findings were compared with histology findings in radical prostatectomy. Pre and post 68Ga-PSMA treatment information was collected.

Results

68Ga-PSMA PET/CT detected metastatic disease (M1) in 19.6% of patients (11/56) and was associated with higher prostate-specific antigen level and ISUP grade. Seminal vesicles commitment were detected in 46.4% (26/56), lymph nodes (N1/M1a) were detected in 32.1% (18/56) and bone metastases (M1b) in 17.9% (10/56). The PSMA PET/CT sensitivity and specificity value for seminal vesicle detection were 84.6%, 81.8%, respectively and for lymph nodes detection were 81.8% and 94.6% respectively. Undetected LNMs either were micrometastases located in the lymph node. 68Ga-PSMA PET/CT information changed treatment in 51.8% (29/56)

Conclusion

In this unfavourable/high-risk cohort, about one third is metastatic at diagnosis. PSMA PET has good sensitivity and specificity value for seminal vesicle and lymph nodes detection, changing treatment in more than half of patients.

IAEA-CN-326/433

Case Report: Bertolotti's Syndrome Diagnosed on Bone Scintigraphy in a Patient Initially Suspected of Septic Arthritis of the Hip-Joint

M. Megawatti

Indonesian Society of Nuclear Medicine and Molecular Theranostic, Indonesia

Background

Septic arthritis, marked by joint invasion and inflammation, commonly affects the knee and hip joints. Diagnosis is challenging, particularly in neonates and young children, where symptoms like feeding refusal, crying, discomfort during diaper changes (if the hip is involved), or joint immobility may be the only observable signs. Standard radiographs are limited in detecting early-stage infections. However, a three-phase bone scan can identify skeletal infections within 2-3 days of onset. Integrating Single-Photon Emission Computed Tomography (SPECT) with Computed Tomography (CT) allows precise anatomical localization of scintigraphic findings. Fusion imaging with SPECT/CT enhances sensitivity and specificity, reducing equivocal interpretations compared to planar scintigraphy or SPECT alone.

Methodology

This case study employed a comprehensive approach to data collection, including interviews, observations, and document reviews.

Case Presentation

A 4-year-old boy with a history of pulmonary tuberculosis presented with intermittent hip pain and fluctuating fever, despite no trauma history. The patient, unable to clearly express his pain, had normal vital signs and no visible swelling or redness upon physical examination. Suspecting septic arthritis of the left hip joint, an orthopaedic surgeon referred him for a bone scan evaluation. The patient underwent a three-phase bone scan with Technetium-99m MDP, along with SPECT/CT imaging.

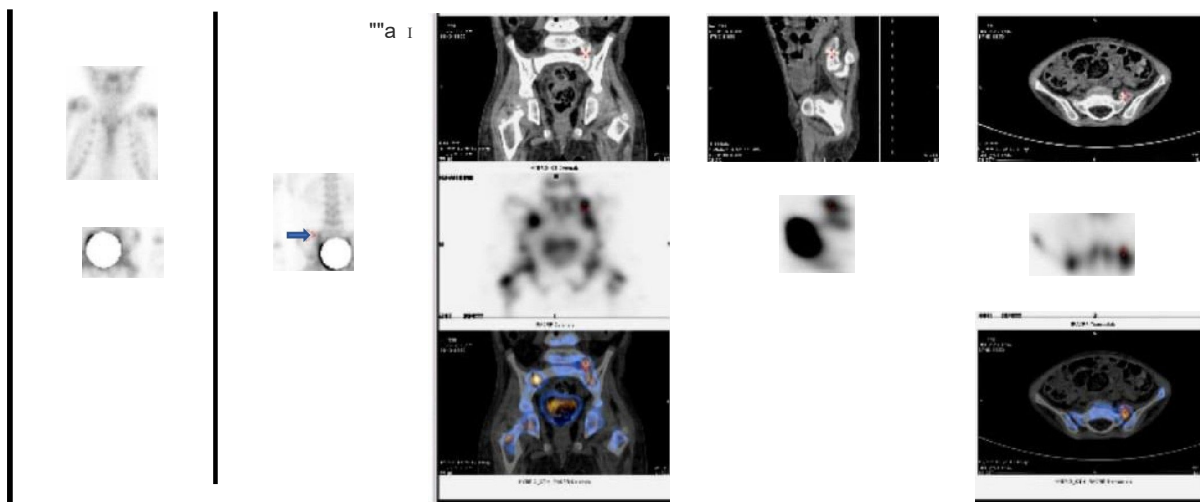
Results

The vascular and blood pool phases of the bone scan were normal, but the delayed phase revealed Technetium-99m MDP activity in the superior projection of the left sacroiliac joint. An asymmetry was noted, with the left side of the sacroiliac joint appearing longer than the right. SPECT/CT imaging showed an enlarged left transverse process of the fifth lumbar vertebra, along with Technetium-99m MDP uptake between the left transverse process and the sacrum. No abnormal uptake of Technetium-99m MDP was detected in the left hip-joint.

Discussion

A radiograph often misses changes in septic arthritis cases, but bone scans are highly sensitive in detection. The typical indication is heightened activity across all three phases. In this case, asymmetrical sacroiliac-joint appearance and left transverse process enlargement with Technetium-99m MDP uptake were observed during the delayed phase and SPECT/CT. The patient's pain could be due to Bertolotti's syndrome, characterized by abnormal enlargement of the lumbar vertebra transverse process(es), potentially causing fusion with the sacrum or ilium. This case falls under Type II incomplete lumbarization, creating a pseudoarticulation between the final lumbar vertebra and the

first sacral segment. Surgical resection is an option for patients not responding to conservative treatment linked to this anomaly.



Conclusion

Bone scintigraphy, particularly when combined with SPECT and CT imaging, offers crucial diagnostic insights for paediatric patients experiencing skeletal pain. Integration of SPECT and CT not only enhances diagnostic accuracy but also facilitates better therapeutic decisions. In a specific case, the diagnosis of Bertolotti's syndrome, characterized by abnormal lumbar vertebra transverse process enlargement, was achieved through bone scintigraphy, highlighting its diagnostic efficacy in complex clinical scenarios.

IAEA-CN-326/434

Role of Ischemia-guided angioplasty with IQ-SPECT MPI in a STEMI patient with two-vessel disease**A. Jimenez-Heffernan, P. Romero-Fernandez, L. Brero-Sanchez, S. Camacho-Freire, A. Moreno-Ballesteros, A. Rodriguez-Pajuelo**

Hospital Juan Ramon Jimenez, Spain

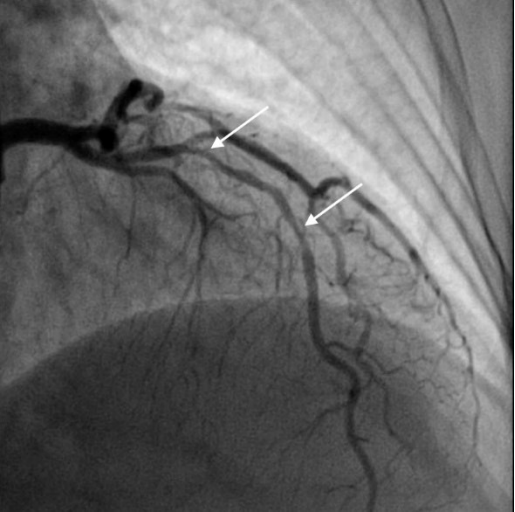
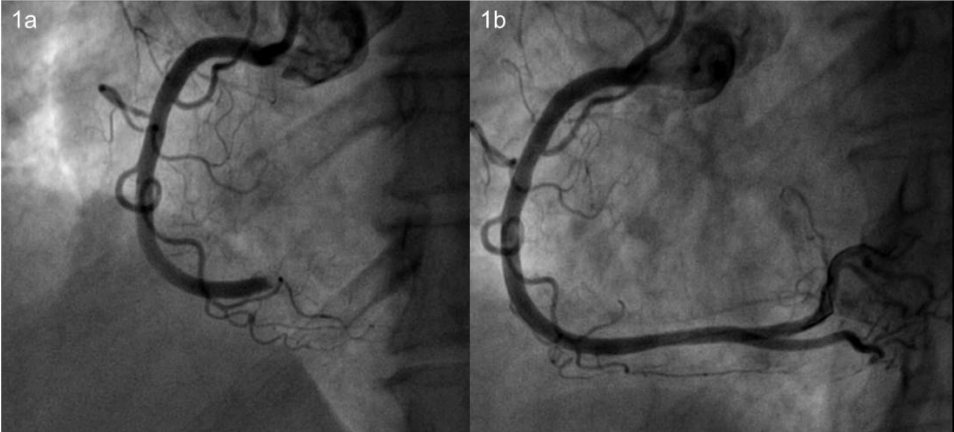
As part of the IAEA SPECT STEMI trial a 59-year-old female, smoker and dyslipidemic with BMI 23 presented with ST segment elevation myocardial infarction localized to the inferior wall. Ticagrelor, aspirin, morphine and nitrates were administered, and she underwent coronary angiography showing a dominant right coronary artery (RC) with a thrombotic occlusion in the distal segment and TIMI flow 0 (fig 1A); a left anterior descending (LAD) artery with a large and severe stenosis in the middle segment and a good distal bed (fig 2); and a circumflex (Cx) artery with no lesions. Smartzoom multifocal cardio-focused collimation allows half and quarter acquisition times with high quality images using conventional NaI camera SPECT.

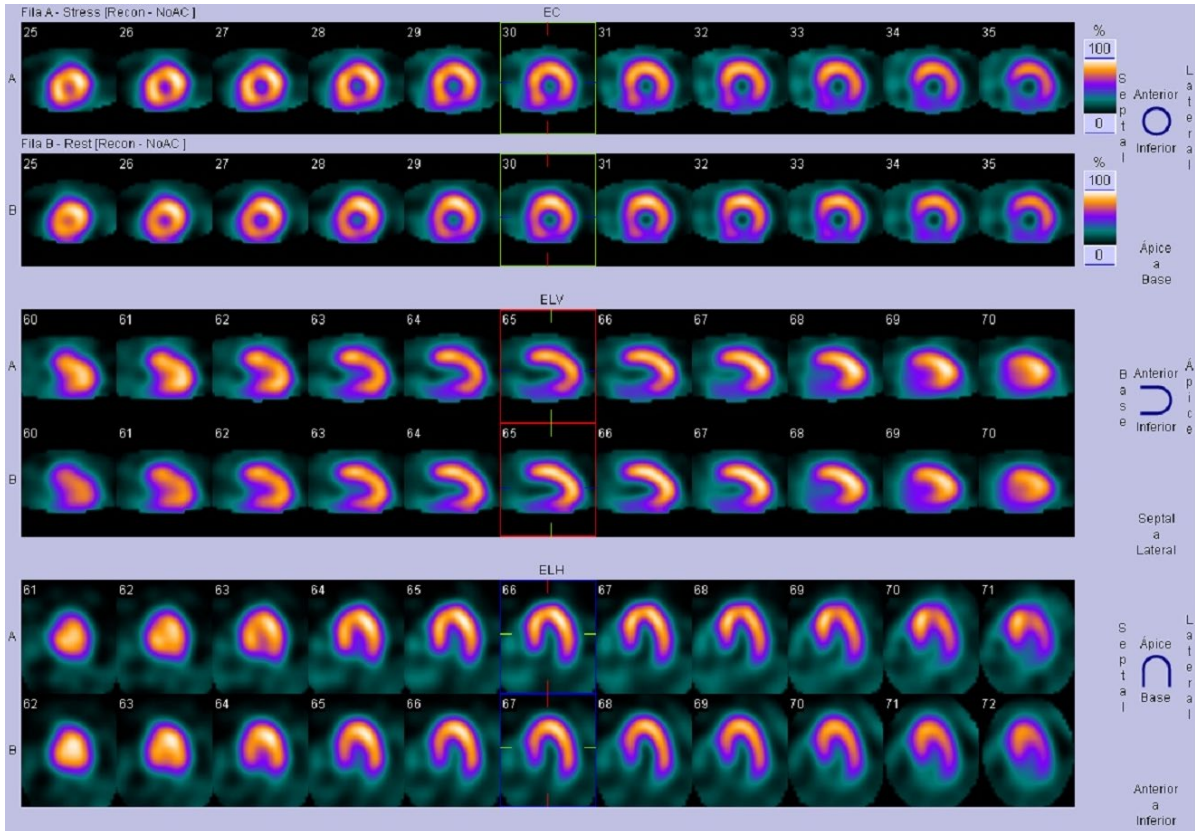
Culprit-vessel percutaneous coronary intervention (PCI) was performed on the RC and a sirolimus-eluting stent was placed obtaining TIMI flow 3 (fig 1B). LAD revascularization was to be performed as a staged procedure in the following days. The patient was admitted to the coronary intensive care unit and released to the cardiology hospitalization ward 24 hours later. 48 hours after STEMI IQ-SPECT MPI was performed to ascertain the functional significance of the LAD lesion using a 1-day stress/rest protocol with 9 mCi and 25 mCi of tetrofosmin for the stress and rest studies respectively delivering an estimated effective dose of 8.9 mSv. Acquisition parameters were 208° scan arc, 6 angular steps, 17 views/detector, 9 seconds/view, angle between detectors set at 76° and matrix 1282 with a total acquisition time of 5 minutes. Reconstruction included resolution recovery, CT-based attenuation correction (AC) and energy window-based scatter correction. Stress was pharmacologic combined with low-level exercise walking on the treadmill at 3.5 km/h, inclination 0° for 4 minutes with regadenoson administered between minutes 1 and 2. Heart rate and blood pressure rose from 76 to 105 bpm and from 108/66 to 134/67 mmHg respectively. ECG showed no changes and the patient reported a dry mouth and tiredness. Post-stress images showed a moderate inferobasal defect with slight improvement on rest images and good intensity homogeneous myocardial uptake in all other territories (fig 3). ECG-gated study showed inferobasal hypokinesis and rest LVEF 56% that increased to >60% post-stress. These results suggest necrosis and residual ischemia in the RC territory and no ischemia in the LAD and Cx territories. Non-culprit PCI was cancelled as the IQ-SPECT showed no ischemia in the LAD region.

The patient remained stable and asymptomatic and was discharged from hospital 96 hours after admission. Medical therapy with aspirin, ticagrelor, bisoprolol, atorvastatin, rampril and omeprazole was prescribed and healthy dietary and life-style recommendations were given especially regarding smoking cessation.

This case outlines 3 important facts: 1. the important role of ischemia guided revascularization of non-culprit vessels that avoids unnecessary PCI procedures when lesions are not functionally significant; 2. the easy performance of MPI with the short duration SPECT using IQ-SPECT smartzoom; and 3.

the safety of performing stress MPI 48 hours after STEMI in patients with successful culprit-vessel PCI.





IAEA-CN-326/437

Uveal Melanoma: Value of [18F]FDG PET/CT in detecting hepatic and extra-hepatic metastases

H. Rokbani¹, T. B. Ghachem^{1,2}, S. Cherif¹, L. Zaabar^{1,2}, A. Mhiri^{1,2}

¹ Nuclear Medicine Department, Salah Azaeiz Institute, Tunisia

² Faculty of Medicine of Tunis, Tunis El-Manar University, Tunisia

Background

Uveal melanoma (UM) is the most common primary ocular malignancy in adults, with an incidence of 2 to 8 cases per million inhabitants in European countries. Up to 50% of patients develop metastases, mainly to the liver, usually within 3 years of diagnosis of the ocular tumour. The prognosis is poor, with a median progression-free survival and overall survival of 3 and 12 months respectively, that's why accurate and reliable staging methods are crucial for optimal care for these patients. [18F]FDG PET/CT has recently emerged as a staging tool by detecting distant metastatic lesions that conventional imaging studies may miss.

The aim of this case presentation was to demonstrate the superiority of [18F]FDG PET/CT over conventional imaging in the early detection of distant UM metastasis.

Case Presentation

This is the case of a 70 years old woman referred to us for [18F]FDG PET/CT in the context of screening for distant metastases of a melanoma of the anterior uvea of the left eye, with facial cutaneous metastases, classified as pT3b, and treated by primary enucleation and facial metastasectomy. Morphological imaging (CT Scan and abdominal ultrasound) showed only a solid pulmonary nodule with a non specific aspect. A whole body [18F]FDG PET/CT was performed 60 minutes after intravenous injection of 5,1mCi of 18FDG. It showed hypermetabolic bilateral cervical lymph nodes, a moderately hypermetabolic solid lung nodule in the right middle lobe, a focal hypermetabolism in segment VI of the liver and an hypermetabolic osteocondensing lesion of the vertebra L4. These [18F]FDG PET/CT findings are secondary metabolically active nodal and extra-nodal sites (lungs, liver and bones).

The detection of metastatic UM upon diagnosis of the primary tumour is uncommon, yet it carries significant prognostic consequences. It was concluded that abdominal ultrasound, liver function tests and chest X-ray exhibit high specificity but lack high sensitivity in the early detection of metastatic disease. To enhance diagnostic accuracy, staging UM patients using full-body [18F]FDG PET/CT has been proposed. The combination of metabolic and structural data offered by [18F]FDG PET/CT has enhanced tumour staging accuracy, recurrence detection, and significantly influenced patient care. It is commonly known that whole-body [18F]FDG PET/CT allows detection of extra-hepatic disease but this case and some previous reports have highlighted the high sensitivity rates and the effectiveness of [18F]FDG PET/CT in detecting hepatic metastases from UM.

Conclusion

Whole body [18F]FDG PET/CT has been shown to play a significant role in detecting regional and distant metastases from UM, even in the liver. [18F]FDG PET/CT and abdominal ultrasound are complementary in the staging of UM and early detection of metastases to ensure the optimal care for these patients.

Keywords: Uveal melanoma, Orbital tumours, metastases, hepatic metastases, 18-Fluro-deoxy-glucose, Positron emission tomography/computerized tomography, cancer staging.

IAEA-CN-326/438

Observer-based detectability of lung lesions on images obtained from decimated and CNN-based denoised [18F]FDG PET/CT scan (simulating lung cancer screening with FDG PET)

D. Faist¹, S. Gnesin², S. Medici², A. Khan², M. N. Lalonde¹, N. Schaefer¹, A. Depeursinge¹, M. Conti³, J. Schaefferkoetter³, J. O. Prior¹, M. Jreige¹

¹ Department of Nuclear Medicine and Molecular Imaging, Lausanne University Hospital and University of Lausanne, Switzerland

² Institute of Radiation Physics, Lausanne University Hospital and University of Lausanne, Switzerland

³ Siemens Medical Solutions USA, Tennessee, USA

Background

[18F]FDG PET/CT is a key step for lung cancer staging, follow-up and lung lesion (LL) characterization. The simultaneous development of digital PET enhancing image sensitivity and the increased access to AI for medical imaging, re-address the question of required injected activity for LL detectability. In this retrospective study, we investigated the impact of PET decimation and AI image denoising on LL detectability simulating different levels of injected activity, representing an optimization for clinical routine (decreasing radiation dose and thus FDG activity and cost) as well as very low-dose conditions for cancer screening.

Methodology

In this retrospective study, we analysed full statistics and decimated (30%, 10%, 5%, 2%, 1% of the full injected activity) [18F]FDG PET/CT simulating reduced levels of injected activity in 30 patients presenting at least one LL. Full statistics [18F]FDG PET were acquired on a Biograph Vision 600 (Siemens Medical Solutions, Knoxville TN, USA) and retrospectively decimated to the different percentages. Full and reduced statistics datasets were denoised using a convolutional neural network (CNN) algorithm trained to reproduce the original full statistics PET image from the low-dose reconstruction. Three readers assessed in consensus a LL detectability Likert scale varying from score 0 (non-visible) to 3 (clearly visible) on a total of 12 randomized images per subject (6 with denoising, 6 without). SUVmax as a function of the decimation level was reported. LL detectability by two human observers in consensus and quantitative measurements were compared between full statistics and the different decimation levels with and without denoising.

Results

In total, we analysed 77 lung lesions with mean diameter 19.1 - 20.6 mm across 360 [18F]FDG PET/CT reconstructions. Without denoising, we could not reject the null hypothesis stating the scores belonged to different distributions down to 5% decimation compared to full statistics ($p=0.91$ for 30%, $p=0.19$ for 10%, $p=0.27$ for 5%) and found significant differences in LL scores in 2 and 1% decimation ($p=0.001$ for 2% and $p=0.000$ for 1%). With denoising, significant differences were observed for 5, 2 and 1% decimation levels in comparison to full statistics ($p=0.036$ for 5%, $p=0.002$ for 2%, $p=0.000$ for 1%). There was no significant differences in normalized SUVmax according to decimation level across the different decimations compared to full statistics, except for 2 and 1% decimation ($p<0.001$) with and without denoising.

Conclusion

Simulating reduced levels of injected activity, we found similar LL detectability up to 5% of the full injected activity and 10% for the denoised PET decimation. This result shows promising perspectives for clinical routine in drastically reducing injected activity without compromising lung lesion detectability and sets the scene for low-dose [18F]FDG PET/CT in lung cancer screening.

IAEA-CN-326/439

Patient Journey for Cancer Patients in Accessing Hybrid PET in Kenya: A Case Study at KUTRRH

L. Muikamba

Kenyatta University Teaching Referral & Research Hospital, Kenya

Background

Cancer remains a significant health challenge globally and it's the third leading cause of death in Kenya, with the country witnessing 42,116 new cancer cases and 27,092 deaths annually as of 2020. Up to 30% of cancer cases are curable if detected early, but many are diagnosed at advanced stages, limiting treatment options. Access to advanced diagnostic imaging like PET/CT is crucial for comprehensive cancer management.

Kenyatta University Teaching Referral and Research University (KUTRRH) is the only operational public hospital that offers PET/CT services in Kenya since January 2022. The hospital has two G.E Discovery MI PET/CT cameras and a commercial cyclotron. Despite serving patients nationwide, especially from remote areas, several challenges hinder efficient patient journeys, including issues with referral processes, documentation accuracy, preliminary reporting, facility awareness, modality distinctions, data security, insurance preauthorization, appointment coordination, network reliability, and travel logistics.

The abstract aims to provide insights into improving the patient journey for oncology patients at KUTRRH and enhancing the role of nuclear medicine and diagnostic radiology in cancer management.

Methodology

The patient journey for accessing PET/CT in Kenya has been established through several key methods. Firstly, raising awareness and education for oncology patients, support groups, healthcare administrative staff, and healthcare providers. This awareness covers booking, documentation, eligibility criteria, and patient preparation. Secondly, optimizing referral systems and coordination between primary care providers, oncology specialists, imaging centers, and the National Health Insurance Fund (NHIF). This involves streamlining communication and processes to expedite referrals and ensure timely access to imaging services.

Results

Kenya has five qualified nuclear physicians/ radiologist consultants. Currently, there are three doctors undergoing training for nuclear medicine physician in Kenya. KUTRRH has outsourced four from other countries to meet the demand. The department operates with seven technicians who handle the equipment and assist in the scanning process, utilizing tracers from production sourced from the KUTRRH commercial cyclotron. The main indications for PET/CT scans at KUTRRH include diagnostic purposes, post-treatment assessment, and staging.

The patient journey for cancer patients accessing the Hybrid PET at KUTRRH started in January 2022 with a total of 3,164 patients scanned by 2022 and 6,841 patients scanned by 2023 demonstrating a significant utilization increase over time (Fig. 1).

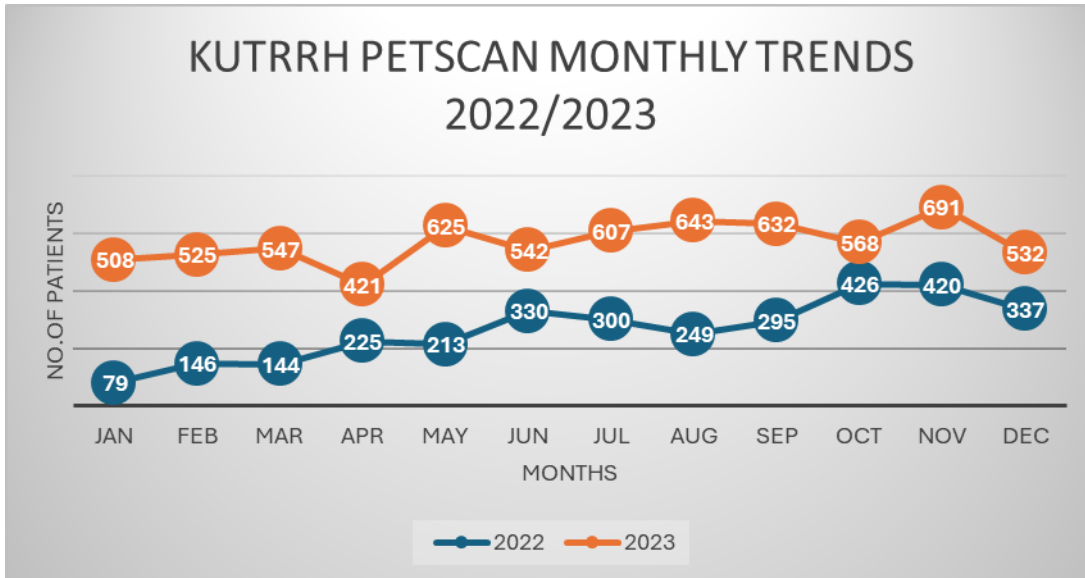


Figure 1. KUTRRH PET Scan Monthly Trends 2022/2023

Conclusion

Strengthening the patient journey requires enhanced referral systems, multidisciplinary collaboration, and leveraging technology for improved communication and data management, KUTRRH, through its IMIC department, has optimized the patient journey experience, providing PET/CT to over 10,000 patients in the last two years fully funded by the government of Kenya through NHIF. This milestone has not only improved patient outcomes but also reduced the number of Kenyans seeking cancer treatment abroad. Therefore, continued investment in these areas is crucial for sustaining and ensuring timely and equitable access to advanced diagnostic imaging for all cancer patients in Kenya.

IAEA-CN-326/440

A Retrospective Multicenter Analysis of the Relationship between SUV_{max} values and Overall Survival at FDG PET scans in Patients with Leiomyosarcomas

B. Ronchi¹, G. Peña²

¹ Department of Nuclear Medicine, Fundación Escuela Medicina Nuclear (FUESMEN), Mendoza, Argentina

² Department of PET, Fundación Escuela Medicina Nuclear (FUESMEN), Mendoza, Argentina

Background

Our retrospective study aimed to assess the potential benefit of SUV_{max} in FDG-PET/CT and FDG-PET/MR scans for the characterization of leiomyosarcomas and its impact on overall survival. The researchers looked at FDG-PET/CT and FDG-PET/MR scans from a heterogeneous population of 12 patients. They found that patients with an SUV_{max} value in the primary lesion under 11, were correlated with a 5-year overall survival and did not have metastatic disease at the moment of the diagnosis. These findings suggest that SUV_{max} values could be a clinically significant dependent prognostic marker for progression-free survival. The study highlights the importance of pre-surgery PET scans as a prognostic factor and helping doctors choose the best treatment option.

Methodology

This retrospective, observational cohort study included 12 patients with leiomyosarcoma tumours confirmed by anatomopathology findings between 2018 and 2023 at FUESMEN and COIR. We excluded patients with other sarcoma subtypes and patients without FDG-PET scans before surgery. We retrospectively reviewed their medical records.

We utilized 2 different diagnosis modalities that differ due to their disponibility and the medical request from the oncologist: a PET/TC GE-STE-16 and a 3.0T PET/MRI SIGNA GE with 3D TOF. Univariate analysis with Fisher analysis was performed between SUV_{max} values and the presence of metastasis at the first visit, tumour greatest dimension, and mainly with a 5-year overall survival.

Results

After anatomopathological confirmation, 12 patients were considered including 4 men (33%) and 8 women (66%). The primary localization of the leiomyosarcoma differed: 4 raised from the inferior vena cava (33.3%), 4 from the uterus (33.3%), 2 originated in the muscle of the inferior extremity (16.6%), 1 from the scrotum (8.3%) and the last one from the retroperitoneal as unknown origin. The median SUV_{max} of the primary tumour lesion was 13.09 (range, 5-17.4). Distant metastasis was observed in 58.3% of the total.

Treatment options differed among patients, nevertheless, chemotherapy was performed up to 75%. A summary of these clinicopathological and treatment characteristics is shown in Table 1.

By our primary aim of the study, we noticed that the patients with an SUV_{max} value in the primary tumour equally or higher than 11 had distant metastasis at the moment of the diagnosis and particularly, they died in less than 5 years. This association was seen independently of the location of the primary lesion, age, gender, or tumour's greatest dimension. Thus, an SUV_{max} value higher than 11 could be related to a 5-year OS rate in leiomyosarcomas malignancies ($p < 0.01$).

We also compared in a per-patient analysis, the characteristics of the SUVmax about the different locations of the LMS. We did not find a statistical association between the diverse origins, SUVmax 11 taken as objective, disease relapse nor a medium of tumour greatest dimension. The p-values retrieved by the Fisher exact test are summarized in Table 2.

Table 1. Clinicopathologic and treatment characteristics.

Characteristic	Median	IQR
Age at diagnosis (y)	61.4	47-79
Gender	F >M	-
SUVmax of the primary tumour	13.09	5-17.45
Tumour greatest dimension(mm)	89.4	7-220
Metastatic disease at the diagnosis	58.33%	-
Surgery	66.6%	-
Chemotherapy and/or radioteraphy	75%	-

Table 2. Univariate analysis of the variables taken into consideration.

Characteristic	Fisher's Exact Test p Value
5-years OS	0.01
Disease relapse	0.52
Medium tumour greatest dimension(mm)	0.22

Conclusion

SUVmax values could be a clinically significant dependent prognostic marker for progression-free survival. The study highlights the importance of pre-surgery PET scans as a prognostic factor and to choose the best treatment option.

IAEA-CN-326/441

Diagnostic performance of positron emission tomography for cardiac amyloidosis imaging: a systematic review and meta-analysis**D. Yahiro, L. F. L. da Silva, L. D. da Conceição, L. E. Machado, C. Mesquita**

Hospital Universitário Antônio Pedro, Brazil

Background

Cardiac amyloidosis (CA) is a complex and underdiagnosed condition characterized by the abnormal accumulation of misfolded proteins in cardiac tissues. Approximately 95% is caused by two proteins: transthyretin (ATTR) or light chain (AL). Although [^{99m}Tc]Pyrophosphate can replace the biopsy for ATTR diagnosis, AL subtype requires a complex pathway, requiring gammopathy and the use of multimodality imaging to diagnose. Positron emission tomography (PET) imaging with tracers such as [¹¹C]PiB and [¹⁸F]NaF has emerged as a promising modality for the detection of CA, leveraging the ability to visualize amyloid protein deposits within the myocardium. However, the diagnostic accuracy of PET imaging for CA remains to be precisely defined.

Methodology

PubMed, Embase and Web of Science database were searched for studies evaluating the diagnostic performance of PET for patients with cardiac amyloidosis. A bivariate diagnostic random-effects model was employed to estimate pooled sensitivity, specificity and area under the receptor operator curve (AUC) using the Restricted Maximum Likelihood estimation method. Heterogeneity was examined with I² statistics and statistical analysis was conducted with R studio, utilizing the Zhou and Dendukuri approach.

Results

Following the retrieval of 956 studies, a total of 331 patients from ten studies met the eligibility criteria for inclusion in the meta-analysis. Among these, six studies assessed [¹¹C]PiB, while four studies assessed [¹⁸F]NaF. The pooled results from these studies indicate a specificity of 99% (95%CI [0.67-1], I²=0%), a sensitivity of 89.5% (95%CI [0.74-0.96], I²=0%) for diagnostic performance, and the pooled area under the curve (AUC) was 0.91. Moreover, subgroup analysis of PET with [¹¹C]PiB for cardiac amyloidosis with AL subtype revealed a specificity of 92.4% (95%CI [0.53;0.99], I²=0%), a sensitivity of 96.7% (95%CI [0.87;0.99], I²= 0%), and a AUC of 0.94 (95%CI [0.82;0.94]). The [¹⁸F]NaF obtained a sensitivity of 86.0% (95%CI [0.63;0.96], I²= 0%), specificity of 86.0% (95%CI [;], I²= 0%) and AUC 0.80.

Conclusion

Positron Emission Tomography demonstrates high sensitivity and specificity in detecting CA. Notably, [¹¹C]PiB exhibits relatively lower specificity despite its high sensitivity. [¹⁸F]NaF revealed a low sensitivity and low specificity for cardiac amyloidosis.

IAEA-CN-326/442

Can Artificial Intelligence provide information on PET/CT in clinical practice?

D. Yahiro, L. Freitas, L. Ávila, C. Mesquita

Hospital Universitário Antônio Pedro, Brazil

Background

Artificial intelligence platforms are becoming increasingly popular due to their diverse applicabilities. Recently, Chatbots, powered by Large Language Models, have gained prominence due to their ability to simulate conversations. Some examples of their applications include: (1) answering questions; (2) translating texts; (3) aids in education; (4) content production. In this context, some studies have researched the reliability of such technologies regarding medical subjects. Providing accessible information through AI would be of great benefit for the use of Positron Emission Tomography combined with computed tomography (PET/CT) in clinical practice for professionals, patients, and as support for health education. Therefore, our work aimed to evaluate the responses of 3 chatbot platforms about PET/CT.

Methodology

We selected 3 free of charge chatbots for evaluation, ChatGPT 3.5, Copilot, and Gemini, and formulated ten questions on various PET/CT topics. Questions addressed: (1) common indications for requesting a PET/CT; (2) contraindications; (3) use during pregnancy and breastfeeding; (4) monitoring patients with prostate cancer; (5) assessing the risk of developing cancer; (6) applicability in infections; (7) neurological diseases; (8) early detection of cancer; (9) utility in heart diseases; (10) evaluation of metastases. All three chatbots were evaluated on the same questions. The responses were systematically recorded in a database, and a nuclear medicine physician assessed the accuracy and relevance of the responses.

Results

Gemini did not contraindicate breastfeeding, considering it a serious error. Copilot and ChatGPT 3.5 had only one error each, while Gemini had 2. However, qualitatively, Gemini's software responses generally provided more concise and assertive answers, while Copilot and ChatGPT 3.5 tended to be more generic. Copilot was considered more comprehensive as it provided references for consultation, enabling the verification of information.

	ChatGPT 3.5	Gemini	Copilot
Q1	+++	+++	+++
Q2	+++	+	+++
Q3	+++	+++	+++
Q4	+++	++	+++
Q5	+	+++	+
Q6	+++	+++	+++
Q7	+++	+	+++
Q8	++	+++	++
Q9	+++	+++	+++
Q10	+++	+++	+++

+ : Unsatisfactory

++: Satisfactory

+++: Excellent

Table 1 - Evaluations of responses generated for each Large Language Model.

Conclusion

Despite some discrepancies and limitations, all three chatbots proved useful in providing information about PET/CT in medical practice. However, caution is warranted, and information should be cross-checked with other sources. Further research could explore ways to enhance the accuracy and reliability of chatbot responses in clinical contexts.

IAEA-CN-326/443

The role of radioactive iodine therapy as adjunctive treatment in papillary thyroid microcarcinoma: A meta-analysis

J. E. A. Kuizon, M. A. G. E. Dumatol, I. S. Bandong

Philippine Heart Center, Philippines

Background

Papillary thyroid microcarcinomas (PTMC), defined WHO as carcinomas measuring < 1 cm in the greatest dimension, is the most common subset of thyroid carcinomas. It usually has an excellent prognosis; hence, most guidelines recommend surgery alone as sufficient management. However, a previous study, reported nodal involvement after I-131 whole body scan in a significant part of low risk DTC patients. Other studies also reported recurrence in 4-16% of patients, with many even developing distant metastasis. With its incidence increasing globally, controversy continues as to its optimal management. Whether or not radioactive iodine ablation should play a role in the primary treatment remains to be a topic of debate among clinicians. This is of particular importance in populations who typically present with more aggressive thyroid carcinomas such as in the local setting, as well as in low resource settings where active surveillance is not always an option. This study therefore aims to assess the effect of RAI ablation on the recurrence of PTMC.

Methodology

Two reviewers performed independent comprehensive literature search of PubMed, Cochrane library, Medline, Embase, and Google Scholar for studies comparing the recurrence rate of PTMC between patients treated with surgery followed by RAI vs. surgery alone, according to the PRISMA guidelines. Each reviewer also assessed the included studies for risk of bias and quality using the modified Newcastle-Ottawa scale (NOS). The meta-analysis was performed using review manager (Revman) version 5.4. Subgroup analyses were also done.

Results

A total of 11 studies which met all the inclusion criteria, with a corresponding total of 5167 eligible patients, were assessed. All patients were considered either low or intermediate risk based on their tumour, node, and metastasis staging. All included studies were retrospective cohorts. Any site recurrence rate (median follow-up of < 6 years) for patients treated with surgery followed by RAI was significantly lower than those treated with surgery alone (3.0% vs. 12.7%, RR = 0.19, $p < 0.00001$). Recurrence with structural evidence was also significantly lower in patients treated with RAI compared to those treated with surgery alone (1.9% vs 4.7%, RR = 0.36, $p = 0.0007$).

Conclusion

Radioactive iodine remnant ablation significantly decreases the recurrence of PTMC in low to intermediate risk patients after surgery.

Any site recurrence in Low-Intermediate Risk PTMC Patients

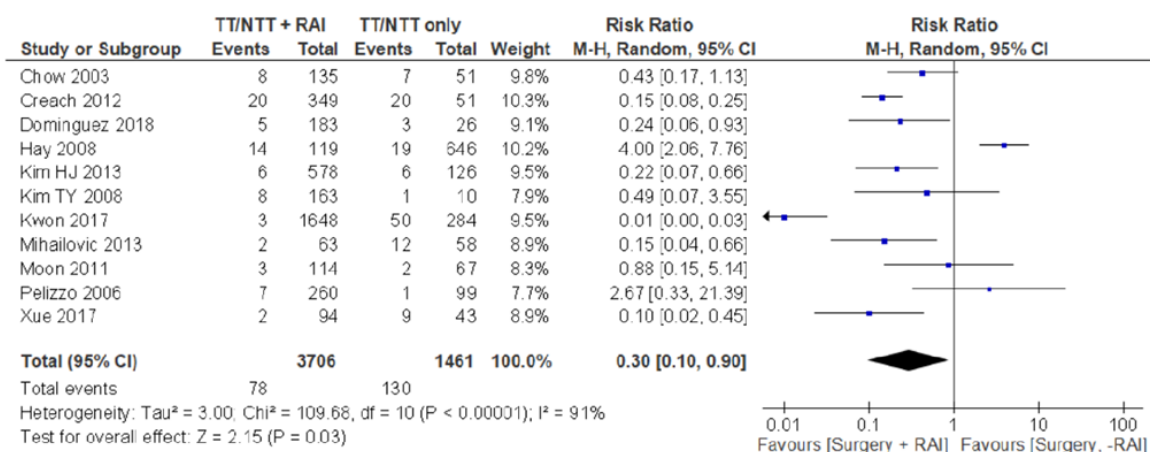


Figure 1. Any site disease-recurrence in LR-IR PTMC patients. *Heterogeneity was found in this comparison group.*

Structural recurrence in LR-IR PTMC patients

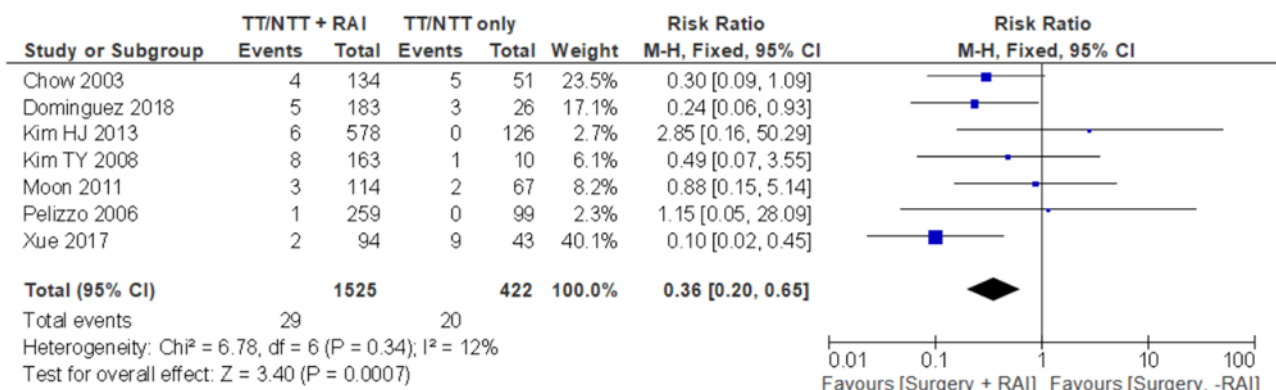


Figure 2. Any site disease-recurrence in LR-IR PTMC patients, with median follow-up of < 6 years. *No heterogeneity was found in this comparison group.*

Recurrence rate in LR-IR patients (Median follow up <6 yrs)

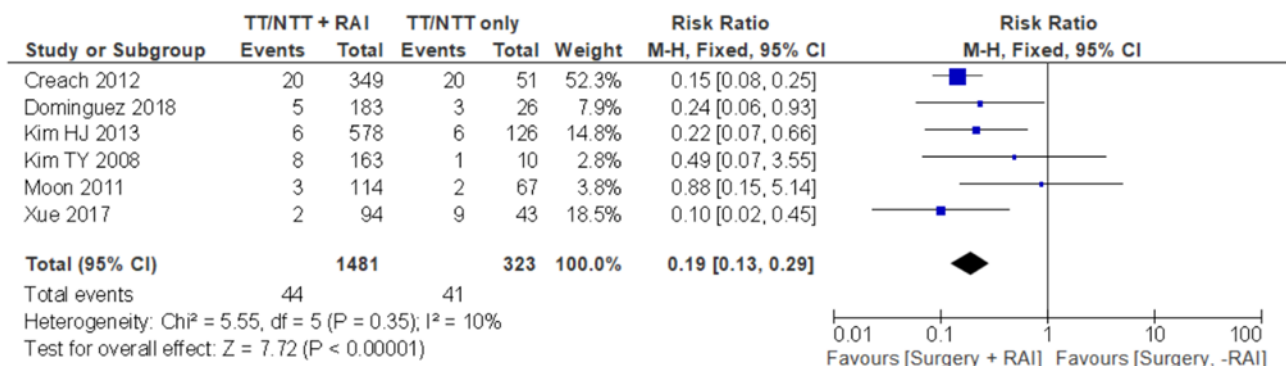


Figure 3. Structural disease-recurrence in LR-IR PTMC patients. *No heterogeneity was found in this group.*

IAEA-CN-326/444

An interesting case of a Left-sided adrenocortical carcinoma invading a duplicate inferior vena cava: contribution of [¹⁸F]FDG PET/CT in initial staging and post-operative recurrence

K. B. Ahmed, H. Noomen, W. Amouri, S. Charfeddine, K. Chtourou

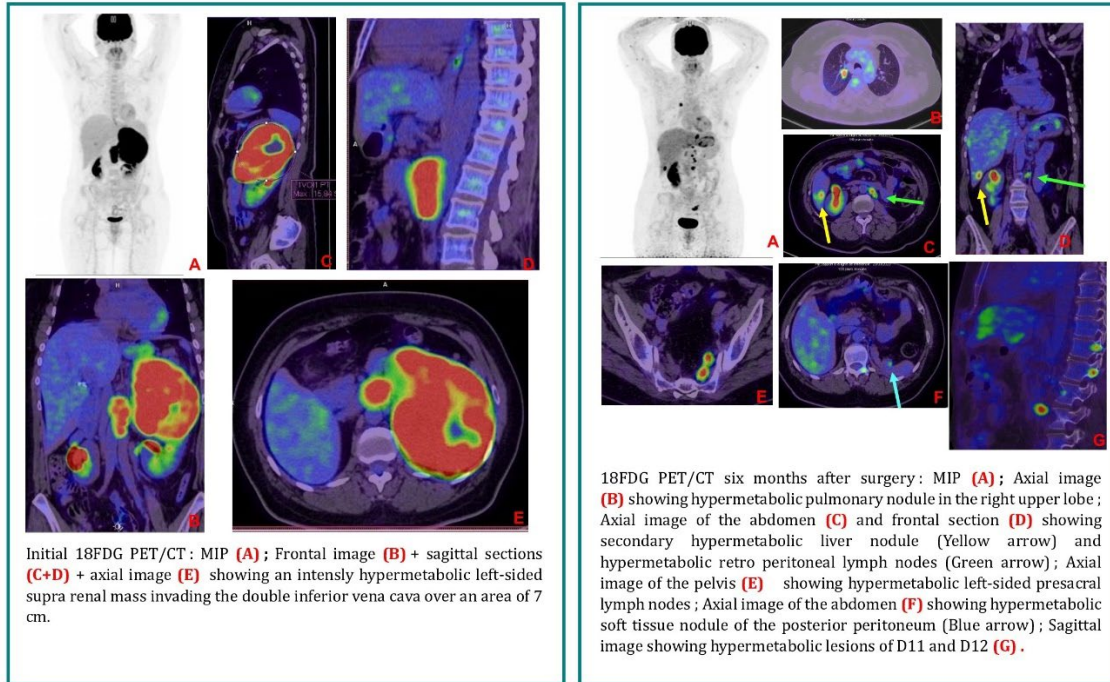
Nuclear Medicine Department, Habib Bourguiba Hospital, SFAX, Tunisia

Background

Adrenocortical carcinoma is a rare, aggressive malignant tumour accounting for less than 1% of adrenal masses and 0.02% of all cancers reported annually . Inferior vena cava (IVC) invasion, which has reported incidence of 10% in patients with ACC, occurs most commonly with larger, right-sided tumour. Abnormal inferior vena cava (IVC) anatomy may present unique challenges for urologists when performing retroperitoneal surgery. In an oncological context, case reports have been described of double left inferior vena cava invasion from colic and gynaecological tumours, but in no case of adrenocortical carcinoma. Thus, in the rare case of association of a left-sided ACC with left anatomical variant of IVC, it is mandatory for the correct diagnosis to be preoperatively detected.

Case Report

Here we report the case of 48-year-old female patient, with a history of surgically treated breast tuberculosis, who presented in march 2023 with abdominal pain. An abdominal ultrasound examination revealed a left sided supra renal mass exceeding 10 cm . The diagnosis of adrenocortical carcinoma was suspected. Therefore, a [¹⁸F]FDG PET/CT was requested to evaluate the metabolic pattern of this mass, locoregional tumour extension and occult metastases. The exam was performed on a PET/CT siemens biograph-64 after 6 hours of fasting and 60 minutes after injection of 9 mci of [¹⁸F]FDG. The examination found a large, intensely hypermetabolic left adrenal mass (SUVLbm-max= 15,8) invading surprisingly a double inferior vena cava over 7 cm, and the rest of the whole body study was without abnormality. She was then treated by surgery removing the left suprarenal mass, kidney and accessory inferior vena cava . Two months later, on a follow-up CT scan, suspicious peritoneal nodules were identified. A relapse of her tumour was then advanced. A [¹⁸F]FDG PET/CT was therefore requested. The examination found hypermetabolic nodular thickening of the posterior peritoneum extending into the left renal space. Unfortunately, multiple hypermetabolic lesions were also discovered indicating tumour progression. These lesions were identified in the upper lobe of the right lung (SUVLbm-max= 5.39) , in the liver (SUVLbm-max= 6 in the VI segment) , retroperitoneal lymph nodes (SUVLbm-max= 6) and bone (left pedicles of D11 SUVLbm-max= 4 and D12 SUVLbm-max=5).



Conclusion

Duplication of the inferior vena cava (IVC) is a congenital anomaly with an incidence of 0.1% to 3.5%. Although intracaval extension from ACC is a rare complication, the imaging diagnosis is of great significance in identification of tumour duplicate IVC involvement, to ensure correct surgical access and avoid the neoplastic embolization risk. The accurate re-staging of ACC and, particularly, the detection of metastatic regions are substantially important in patient management. These data can result in a change in treatment strategies and be used as a basis for the selection of surgical or systemic therapy options. [¹⁸F]FDG-PET/CT detects local recurrence and distant metastases with high accuracy in the re-staging of operated adrenocortical carcinoma.

IAEA-CN-326/446

Identification of Coronary Calcium in Planning Tomography for Radiotherapy for Patients with Left Breast Cancer

V. V. G. Leiva¹, J. A. C. Gonzalez², C. M. Figueroa³

¹Department of Nuclear Cardiology, ISSS Hospital Oncología, El Salvador

²Department of Radiotherapy, ISSS Hospital Oncología, El Salvador

³Department of Nuclear Medicine, ISSS Hospital Oncología, El Salvador

Background

Breast cancer (BC) management requires a multidisciplinary approach in which surgery, systemic treatments (chemotherapy, hormonal therapy and/or targeted therapies), and radiotherapy (RT). However, long-term follow-up in some trials has shown that RT can also increase the risk of ischemic heart disease, presumably through incidental infrared radiation (IR) of the heart.

It remains to be considered that despite low mean heart doses, relevant areas of the heart can be exposed to doses between 40 and 50 Gy. Pirot et al, conclude that heart toxicities due to RT of the breast—particularly left sided breast RT—are rare but clearly recognizable, but modern techniques permit sufficient protection of the heart and lungs in most cases. In addition to mean heart dose, breast cancer RT treatment planning should also include constraints for cardiac subvolumes such as LV and LAD.

Methodology

The 194 thoracic tomography scans for RT planning of patients with left BC, who attended the Radiotherapy service of the Oncological Hospital of the Salvadoran Institute of Social Security (ISSS) during the year 2023 were reviewed; looking for the presence of coronary calcium.

Results

Women with an average age of 54 years (maximum age 94 years and minimum age 26 years), of which 43% are contributors and 30 (15.5%) had coronary calcium. Of the 30 patients with coronary calcium, the mean age was 68 years (maximum age 94 years and minimum age 38 years), 7 with involvement of the left coronary trunk, 22 (73.3%) Anterior Descending, 10 Circumflex and 9 Right Coronary. In a second phase, functional studies will be applied to these patients in search of ischemia.

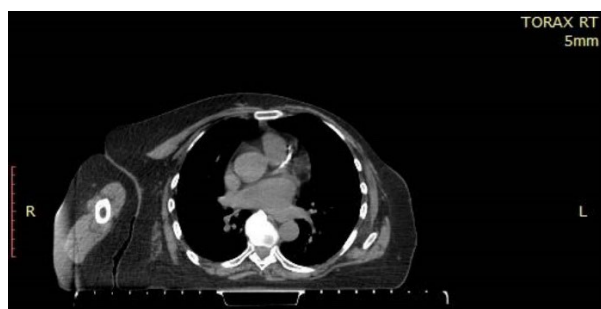


IMAGE 1. Non-contrast, non-cardio-dedicated, non-gated chest tomography of a 63-year-old female. Presence of coronary calcium in the Anterior Descending Coronary territory.

Conclusion

Presence of coronary calcium was evident in patients with left BC who started RT in the ISSS during the year 2023, with Anterior Descending Coronary Artery being the most common involved. These have a higher risk of ischemic complications related to RT. The use of multimodal imaging techniques applied to the patient reveals information that allows the reclassification of the risk of cardiotoxicity with chemotherapy, special considerations in the administration of RT and early access to follow-up by Cardiology for the indication of functional stratification studies that allow access to revascularization when necessary.

IAEA-CN-326/447

Artificial Intelligence-based quantitative SPECT with synthetic CT in the whole-body bone studiesS. Barna¹, A. Kovacs², B. Husztik², A. Budai¹, I. Garai¹, M. Szolikova²¹ ScanoMed Ltd, Hungary² Mediso Ltd, Hungary**Background**

Computed tomography (CT) is currently used for attenuation correction (AC) and anatomical localization in quantitative bone SPECT (single-photon emission computed tomography) imaging. However, bone SPECT/CT shows potential in assisting with quantitative patient follow-up and inter-patient comparisons. Additionally, it can help image interpretation by enabling global scaling through SUV (standard uptake value), thereby eliminating scaling challenges (for example caused by a hot bladder). In order to ensure accurate quantification and improve the visual interpretation and more precise localisation in SPECT imaging, AC is essential. Furthermore, several studies demonstrated that AC helps to reduce diagnostic uncertainty as well. Non-uniform AC technique, which utilizes attenuation-maps generated from CT imaging, is the standard solution of the current clinical routine. Nevertheless, this approach is associated with several pitfalls, including increased radiation exposure, greater expenses, and potential for misalignment between SPECT and CT scans.

Hence, an artificial intelligence (AI) based approach that produces synthetic CT images and localization features from SPECT data was developed. This innovative method allows for quantitative SPECT imaging comparable to conventional CT-based correction, all without the need for an actual CT scan.

Methodology

A convolutional neural network (CNN) solution, combining supervised and unsupervised techniques, was developed. Task of the neural network was to produce a synthetic CT-like image from SPECT data and corresponding attenuation map. Retrospective study involved clinical bone subjects injected with [^{99m}Tc]Tc-MDP, images were acquired using Triple-Detector SPECT/CT system in nuclear medicine department of ScanoMed Ltd. SPECT data was reconstructed both using the original CT volume (CT-AC) and using the synthetic CT (SyCT-AC) for attenuation correction. After the technical performance evaluation, our group consisting of three nuclear medicine specialists performed the clinical evaluation of the novel method. We compared the reconstructed SPECT images using the original CT-based method as the reference. Blinded retrospective study comparing 20 clinical samples, including visual assessment of the reconstructed SPECT volumes (appearance of bones and image quality), as well as marking and counting detectable lesions was executed. Furthermore, lesion-based quantitative analysis was also performed.

Results

According to the evaluation performed by three nuclear medicine specialists, we did not observe significant differences either in visual interpretation, in intensity appearance of the images or in the detectability of lesions between the original and synthetic CT-based reconstructed SPECT volumes. Lesion-based analysis of radiopharmaceutical distributions (kBq/ml) measured in CT-AC and SyCT-AC SPECT volumes also showed promising results. Based on regression analysis, we observed a

strong correlation between reference and AI-generated volumes in terms of both Maximum and Mean activity-concentration values. Bland-Altman analysis was also employed, and did not show significant differences between measurements. Furthermore, statistical t-test also did not indicate significant differences ($p>0.05$) between the activity concentration values.

Conclusion

Our evaluation indicated that novel SyCT-AC method was consistent with the standard CT-AC. This new method enables accurate quantification and patient follow-up even in the case of SPECT equipment that does not have an integrated CT. In addition to providing accurate quantification and CT-like anatomical localization, it eliminates additional patient radiation exposure, registration mismatch and motion artefacts.

IAEA-CN-326/448

The role of IAEA Technical Cooperation Department in Enhancing Nuclear Medicine in Sudan

A. Hassan

Sudan Atomic Energy Commission, Sudan

Sudan joined the IAEA in 1958 and the first radiotherapy and nuclear center was established in 1967 with IAEA support. Since then the support of the IAEA continued through provision of equipment and capacity building.

In Sudan, cancer is ranked high as one of the top ten killing diseases. The number of people developing cancer is growing and is predicted to continue to increase steadily. According to the National Cancer Registry Report from 2009–2013, a total of 43 102 cases of malignant cancer were registered in Sudan. 23 148 cases were females, and 19 954 cases were males. Cancer of the breast, leukaemia, prostate, lymphoma, colorectal and oesophagous were the top six cancers and they made up over half of all registered cancer cases. According to the World Health Organization (WHO), the annual childhood cancer cases are 3421.

This increase in numbers of patients is not matched by an increase in cancer control services. In many areas of Sudan, the reality of cancer management services fails to cover the lower accepted level of required services. The poor are still far less likely to get medical service and even lack awareness. This has exacerbated the country's disease burden.

For nuclear medicine, the services are provided in seven centers; three are governmental and four in the private sector. The governmental centers are: Khartoum Oncology Hospital in Khartoum State, the National Cancer Institute in Gezira State – Central region, and Tumour Therapy and Cancer Research Center; Shendi University in River Nile State-Northern region. The total number of gamma cameras in the governmental facilities are five, the ages of three is more than 15 years and two were recently installed; 2022. The private hospitals are: Royal Care, Fadhil Hospital, Alneelain Medical Centre, and Universal Hospital. It is important to note that all these private hospitals are located in the capital city Khartoum.

Currently, the radiopharmaceuticals are imported from Turkey and Poland; 360 generators annually. There is a restriction on exporting most of products to Sudan due to the sanctions. The average number of patients over the last five years were 48000, the most frequent studies were bone, cardiac, thyroid, renal, pulmonary studies. There is no cyclotron in the country but it is needed due to the high demand.

Regarding human resources in nuclear medicine, currently there are 4 nuclear medicine physicians, 16 nuclear medicine technologist and radiographers, 3 radiopharmacists, 19 medical physicists (oncology/nuclear medicine), and 6 nurses. With one nuclear physician is currently in training. The capacity building in nuclear medicine mostly depends on external programmes. The only available training (Bachelor and Master degrees). in Sudan is for the technologists and radiographers. The main obstacles that hinder the enhancement of the services in this area are: sanctions which led to limitation of sources for equipment and radiopharmaceuticals, limited of capacity building programmes and the lack of cyclotron in the country that makes the cost of PET unaffordable.

 IAEA-CN-326/451

A case report of different SPECT-based PSMA ligands to follow-up the treatment of castrate-resistant metastatic prostate cancer

A. Ankrah¹, E. Hammond², S. Teye², C. Korsah, M. Yartey¹, A. A. Sarkodie

¹ National Radiotherapy Oncology and Nuclear Medicine Centre, Korle Bu Teaching Hospital, Ghana

² Ghana Atomic Energy Commission Hospital, Ghana

Background

PET-based PSMA radioligands have significantly improved prostate cancer imaging. SPECT-based radioligands are available but less widespread than PET-based tracers. Different types of SPECT-based tracers are being validated and upgraded. The different SPECT tracers may not always be available. One type of SPECT-based tracer may be available at the start of treatment, and a different SPECT-based tracer may be used.

Aim

We present a case report where different PSMA ligands were used in the baseline and follow-up of a patient with castrate-resistant metastatic prostate cancer who underwent treatment with [¹⁷⁷Lu]Lu-PSMA.

Methodology

An 82-year-old male patient with castrate-resistant metastatic prostate cancer was treated with [¹⁷⁷Lu]Lu-PSMA at the Korle Bu Teaching Hospital in Accra, Ghana. He received three cycles. The baseline [^{99m}Tc]Tc-PSMA was done with [^{99m}Tc]Tc-PSMA-GCK01, while the follow-up study after the three cycles was done with [^{99m}Tc]Tc-EDDA/HYNIC-PSMA as these were the only ligands available at the respective times. Both [^{99m}Tc]Tc-PSMA ligands were prepared according to the manufacturer's instructions. The patient was injected with 536.5MBq (14.5mCi) of [^{99m}Tc]Tc-PSMA-GCK01 for the baseline study and 555MBq (15mCi) of [^{99m}Tc]EDDA/HYNIC-PSMA for the follow-up study. Whole-body planar and SPECT/CT imaging were performed after 2 hours and 2 hours 15 minutes on a GE 670 Discovery SPECT/CT camera for the baseline and follow-up study, respectively.

Results

The diagnostic scans correlated well with the post-therapeutic study, which also corresponded to the PSA levels of 9600ng/ml at baseline and had decreased to 2100ng/ml after the third cycle. There was a significant improvement from baseline to the post-third therapy cycle in the sternum, thoracic and lumbar vertebrae, pelvis, humeri and femora. The skull lesion has slightly progressed on both the diagnostic and the post-therapeutic scan. The image shows the anterior projection (images on the left) and posterior projection (images on the right) from baseline to follow-up.

Discussion

SPECT-based tracers are well suited for countries and centers where only SPECT imaging is available, but no PET/CT imaging is available, such as in most resource-constrained countries. SPECT-based PSMA tracers are still being optimized, and a particular ligand may be available but

may be unavailable during a patient's treatment, as we experienced during our patient's treatment. It may be necessary to interchange the PSMA ligand used for diagnostic imaging.

Conclusion

Our case demonstrates that it is possible to use different PSMA-SPECT ligands if necessary for metastatic prostate cancer.

IAEA-CN-326/452

Contribution of Nuclear Medicine Department; Shendi University in enhancing diagnostic and therapeutic services in Sudan

S. Abuelkasim

Tumour Therapy and Cancer Research Centre of Shendi University River Nile State, North Sudan, Sudan

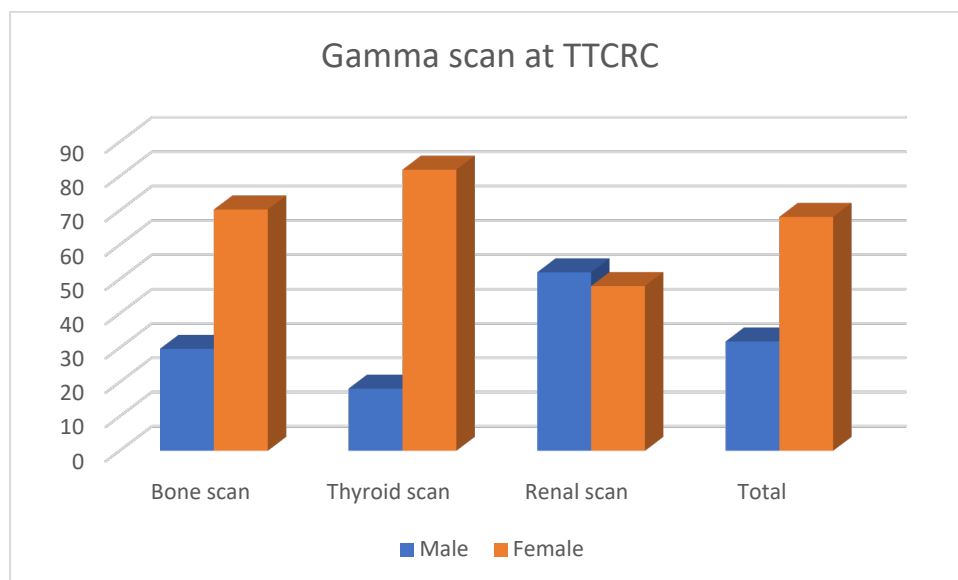
Background

The Tumour Therapy and Cancer Research Centre (TTCRC) of Shendi University River Nile state, North Sudan in mid 1990s to provide diagnostic and therapeutic services for Cancer patients. The department has two core units: the imaging unit and the radioactive iodine therapy unit.

The Imaging Unit

Since its establishment in 2010, the department provided routine imaging by single head gamma camera with SPECT (MEDISO, Hungary). The Camera is 14 years old and there is a plan to upgrade or replace it with a new one through an IAEA national technical cooperation programme which be implemented in this year or early in 2025. There is one nuclear medicine physician, one radiopharmacist, four nuclear medicine technologists and two medical physicists.

The bone scan is conducted for cancer patients to determine the extent of the disease and, in cases of severe pain in the skeleton to find out the causes (total 431 patients; 303 females); Renal scan is conducted to study the renal function (125; 60 females) and thyroid scan to determine thyroid physiology and also if to diagnose and malignancy (116; 95 females); more details in the figure below.

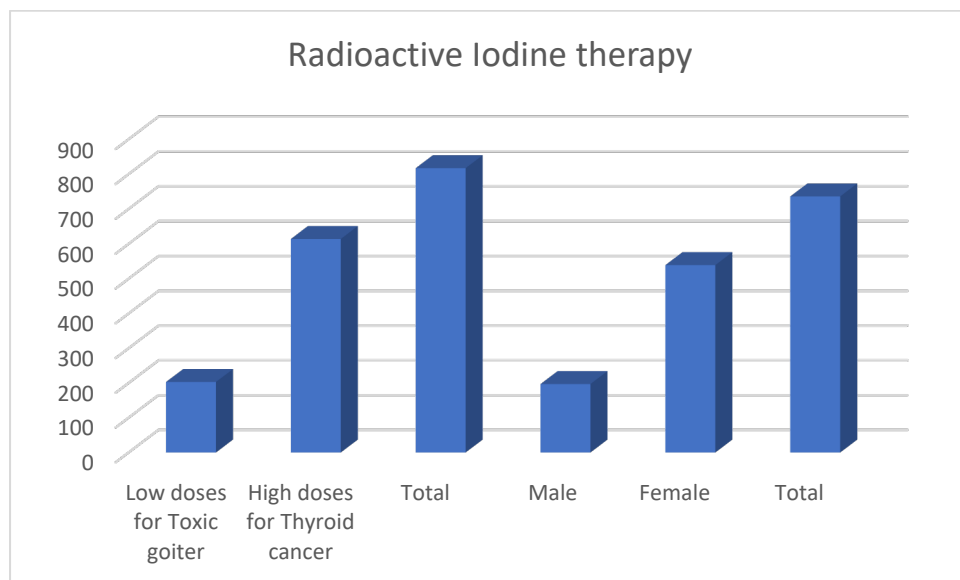


Radioactive Iodine Therapy Unit

The department provided radioactive Iodine therapy; 817 doses (203 low doses for toxic goiter and 614 high doses for well differentiated thyroid cancer). A total of 539 females received radioactive iodine therapy compared to 197 males (total to 736); there were 81 patients with repeated doses, the below figure shows more details.

The treatment dose for the Benign thyroid disease ranged from 5 to 30 mCi while for well differentiated thyroid cancer treatment ranged from 50 to 200 mCi.

The patients are admitted for two weeks while the IAEA recommendations and the regulations of the Sudanese Nuclear and Radiological Regulatory Authority are implemented during the treatment and after the discharge of the patients.



Challenges Facing the Department

1. Limited supply of the Tc generators; the generators are imported from Turkey with only one shipment a month.
2. Lack of equipment and tools, the current equipment will need to be replaced soon. The following equipment are needed: a new gamma camera, a new dose calibrator and QC tools (TLC, HPLC).
3. Shortage in the capacity building of the workforce.

National Plan to Overcome the Challenges

The Federal Ministry of Health through bilateral collaboration with international donors is seeking financial support while the IAEA is expected to provide the technical support as well as equipment and tools to enhance the cancer management in Sudan via Technical Cooperation Projects (national, regional and interregional) and also via the Rays of Hope Initiative.

IAEA-CN-326/454

A case report of detection of recurrent prostate cancer by [^{99m}Tc]Tc-PSMA in a patient with biochemical recurrence

A. Ankrah¹, E. Hammond², S. Teye²

¹ National Centre for Radiotherapy and Nuclear Medicine, Korle Bu Teaching Hospital, Ghana

² Ghana Atomic Energy Commission Hospital, Ghana

Background

After brachytherapy or radical prostatectomy for the treatment of early prostate cancer, serum PSA is monitored and will start rising if there is disease recurrence. When a patient has a rising PSA after brachytherapy or radiotherapy, the patient is referred for imaging to detect disease. If the imaging modalities available do not reveal underlying disease, the patient is said to have biochemical recurrence. The ability to detect recurrent prostate cancer will depend on the imaging modalities used.

Aim

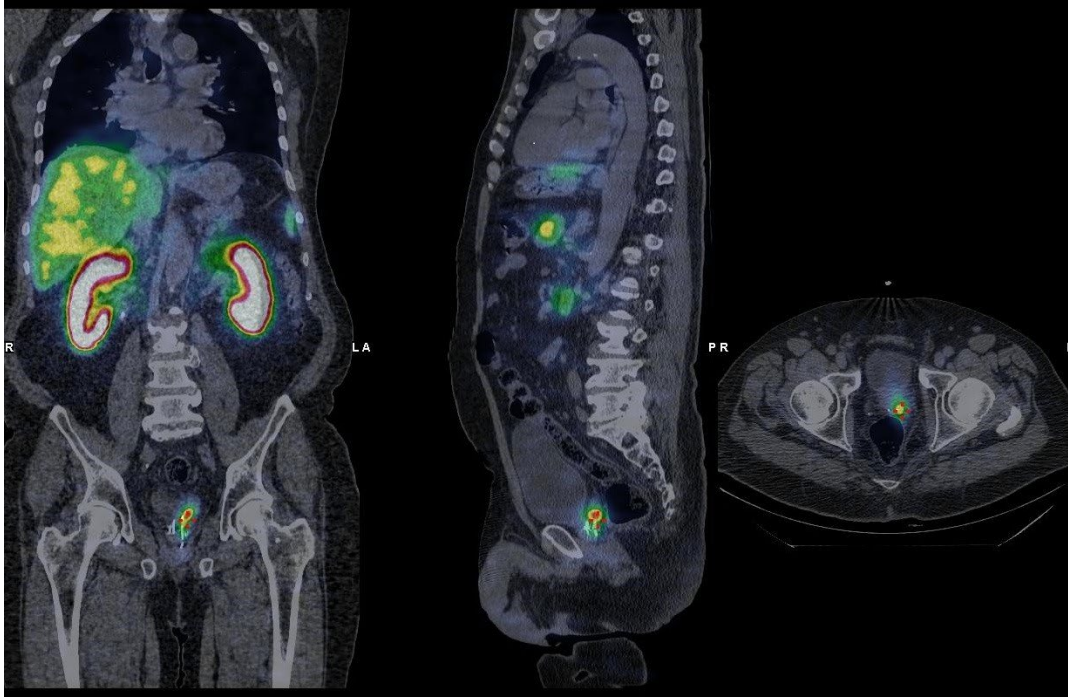
We present a case report of a biochemical recurrence of prostate cancer in a patient for more than two years. Recurrent disease was detected by [^{99m}Tc]Tc-PSMA when other imaging modalities were negative.

Methodology

A 70-year-old male patient had brachytherapy for prostate cancer for eight years. He presented for a [^{99m}Tc] Tc-PSMA scan in Ghana. Two years ago, his PSA started rising, and the patient underwent multiple imaging methods such as pelvic MRI, diffusion-weighted whole-body MRI, CT scan of the abdomen and pelvis, and [^{99m}Tc]Tc-MDP at different time points over the last 2 years, but they all came back with no evidence of recurrent diseases. At the time of presentation for the scan, his latest PSA was 13ng/ml. No PET/CT was available in Ghana at the time of his presentation, so he was preparing to travel out of his country to undergo a PSMA PET/CT when [^{99m}Tc] Tc-PSMA became available in Ghana. The [^{99m}Tc]Tc-EDDA/HYNIC-iPSMA. The [^{99m}Tc]Tc-PSMA was prepared according to the manufacturer's instructions for reconstitution of the kit. The patient was injected with 828.8MBq (22.4mCi) of [^{99m}Tc]Tc-PSMA and a whole-body planer, and SPECT/CT imaging was performed after 3 hours on a GE 670 Discovery SPECT/CT camera.

Results

The whole body showed a faint PSMA uptake in the region of the prostate gland. The whole SPECT/CT showed a PSMA avid lesion in the prostate bed extending into the left seminal vesicle. The figure attached shows the axial, coronal, and sagittal fused SPECT/CT images showing the PSMA avid lesion in the prostate bed extending the left seminal vesicle. There was intense physiologic uptake in the salivary glands, liver, spleen, kidneys, and bowels.



Discussion

Nuclear medicine images physiology and can detect disease early when anatomical changes may not have occurred. In our patient, the PSMA expression by the tumour was detected on the SPECT/CT when sensitive anatomical modalities could not pick up a lesion. The diagnosis and treatment of prostate cancer have advanced dramatically with the introduction of PSMA ligands. The benefits of PSMA ligands have been limited to countries and nuclear medicine clinics with PET/CT. Our finding shows that SPECT/CT with $[^{99m}\text{Tc}]\text{Tc-PSMA}$ can bring the benefits that PET/CT imaging with PET-PSMA ligands has brought and improve prostate cancer imaging in countries and centres without SPECT/CT.

Conclusion

$[^{99m}\text{Tc}]\text{Tc-PSMA}$ is helpful in the detection of recurrent prostate cancer in patients following brachytherapy when other imaging modalities are not able to detect the disease.

IAEA-CN-326/456

Accuracy of [¹⁸F]F-PSMA-1007 PET/MRI for Prostatic Cancer Tumour Staging

A. E. Hussein

King Hamad University Hospital, Bahrain

Aim

To test the accuracy of [¹⁸F]F-PSMA-1007 PET/multiparametric prostate MRI for prostate tumour staging (T-staging) versus multiparametric prostate MRI alone.

Methodology

80 patients with prostate cancer were examined by random non-targeted 12-core transrectal ultrasound (TRUS) guided biopsy and whole-body [¹⁸F]F-PSMA-1007 PET/CT used mainly for nodal staging (N-staging) and metastasis staging (M-staging) followed by a same day simultaneous regional prostate [¹⁸F]F-PSMA PET/multiparametric MRI (mpMRI). Both studies were used for primary tumour staging (T-staging). Regional PET/MRI versus mpMRI alone was tested to predict the likelihood of cancer in the posterior part of the prostate which was divided into 12 regions according to TRUS results where each region was given a binary visual score in PET (positive or negative) and PIRAD score in multiparametric MRI using Prostate Imaging–Reporting and Data System (PI-RADS) version 2 where only PI-RADS 4 & 5 were considered as positive results.

Results

39/80 patients were diagnosed as microacinar, 35/80 as acinar, and 6/80 as mixed acinar & ductal adenocarcinoma after TRUS biopsy; meanwhile, 1 patient needed targeted transperineal biopsy to diagnose prostate cancer based on PSMA PET results and 2/80 patients underwent radical prostatectomy.

A significant correlation was observed between the Gleason score and maximal PSMA uptake value ($p < 0.01$ and < 0.01 , respectively). Sensitivity, specificity, PPV, and NPV of PSMA PET/MRI were 90.1%, 100%, 100%, and 87.7%. For mpMRI, they were 85.9%, 100%, 100%, and 81.9% respectively. PSMA PET/MRI confirmed Extra-Capsular Extension (ECE) in 6 patients, was equivocal for ECE in 6 patients, excluded ECE in 30 patients, confirmed Seminal Vesicle Invasion (SVI) in 7 patients, Bladder Invasion (BI) in 3 patients, and Rectal Invasion (RI) in 4 patients, and confirmed metastatic bone lesions in 2 patients.

Conclusion

Simultaneous [¹⁸F]F-PSMA-1007 PET/multiparametric prostate MRI is more accurate than PSMA PET/CT or multiparametric MRI alone in T-staging especially for ECE, SVI, bladder and rectal invasion. PSMA PET/MRI also precisely localizes sites of the most hypermetabolic tumour foci compared with either PSMA PET/CT or mpMRI alone which will lead to targeted biopsy and may change Gleason Score and hence patient management.

IAEA-CN-326/458

Using Hybrid Computed Tomography/Ultrasound Approach in Gynecologic Intracavitary High Dose Rate Brachytherapy

F. Gning

Dalal Jamm Hospital, Sénégal

Purpose: To evaluate if the combination of Ultrasound (US) and Computed Tomography (CT) allows to evaluate the dose-volume Histograms (DVHs) of sigmoid, bladder, rectum and tumour (HR CTV and IR CTV)

Methodology

All ten patients with advanced cervix cancer received a total dose prescription of 45 Gy in 25 fractions due to 1.8 Gy / fr in external beam radiation therapy (EBRT) to the whole pelvis undergoing both US and CT after application insertion with ring/tandem applicator. The brachytherapy dose was 7Gy times 4 fractions the total dose of high and internal risk target clinical target volume (HR CTV) and (IR CTV), the bladder, rectum and sigmoid from EBRT and HDR brachytherapy were summated and normalised to the biologically equivalent dose of 2 Gy per fraction EQD2.

Results

The goal of this study was to assess and the use of hybrid system in HDR brachytherapy. the prescribed mean dose (D90) for HRCTV: 88 (Gy) and for IRCTV: 61.8 (Gy); D2cc sigmoid: 60.2 (Gy), D2cc bladder: 75.9 (Gy), D2cc rectum: 71.1 (Gy). These results are in the same range than the guidelines recommendation.

Conclusion

During our study we observe that the use of US/CT achieve similar mean dose to the target volume and the organs at risk than another hybrid system the OARs are clearly visualized and help to decrease dose to critical organs without compromising coverage to CTV.

In future we plan to do additional studies to assess the feasibility of using US alone in HDR brachytherapy.

Keywords: DVHs; High Dose Rate; Brachytherapy; EBRT; Ultrasound; Computer tomography

IAEA-CN-326/463

The role of ¹⁸F Sodium fluoride PET/CT in localising the pain generator in patients with musculoskeletal pain in the lower limb

A. Subrhamanian, A. Bhattacharya, R. Kumar, B. R. Mittal, S. Aggarwal

Postgraduate Institute of Medical Education and Research (PGIMER), Chandigarh, India

Background

Pain in the lower limb (hip, knee, ankle, and foot joints) might be due to a variety of conditions with pathology involving the bones, tendons, and ligaments. As there is no gold standard for accurate localization of pain generators, precise localization and diagnosis would help surgeons and physicians in planning appropriate management early, thus preventing permanent damage and improving the patient's quality of life. ¹⁸F Sodium fluoride (NaF) is a commonly available PET tracer with high sensitivity, better image resolution, high target-to-background ratio and the possibility to image the whole body in a shorter time. In this study, we evaluated the role of ¹⁸F Sodium fluoride PET/CT in localising the pain generator in patients with musculoskeletal pain in the lower limb.

Methodology

A prospective study done in patients with complaints of lower limb musculoskeletal pain (hip, knee, ankle, foot, heel pain) in whom a clear diagnosis could not be made with conventional radiographic imaging methods. PET/CT scan was performed after injection of 0.04-0.1 mci/kg of ¹⁸F NaF intravenously. The findings in the ¹⁸F NaF PET/CT images were assessed. The final probable diagnosis was made after correlating the findings of ¹⁸F NaF PET/CT with clinical data and prior radiological investigations if available and by clinical follow up of the patient after appropriate management.

Results

35 patients were included with complaints of hip (n = 4), knee (n = 3), ankle (n = 4), foot (n = 20) and heel (n = 4) pain. The lesions were divided according to the probable structures involved (based on clinical suspicion) into bone lesions (n = 5), soft tissue lesions (n = 9) involving tendons, ligaments, fascia and joint (articular) lesions (n = 21). ¹⁸F NaF PET/CT showed lesions in 28 patients out of total 35 patients (5 bone, 5 soft tissue and 18 joint pathologies) with 80% lesion detectability. It revealed bone lesions of stress fracture, osteoid osteoma, benign cysts, osteomyelitis and oostigonum. The soft tissue lesions detected were plantar fasciitis, Achilles tendonitis and joint lesions were hip, foot and patellofemoral joints arthritis, coalition of foot bones and osteonecrosis.

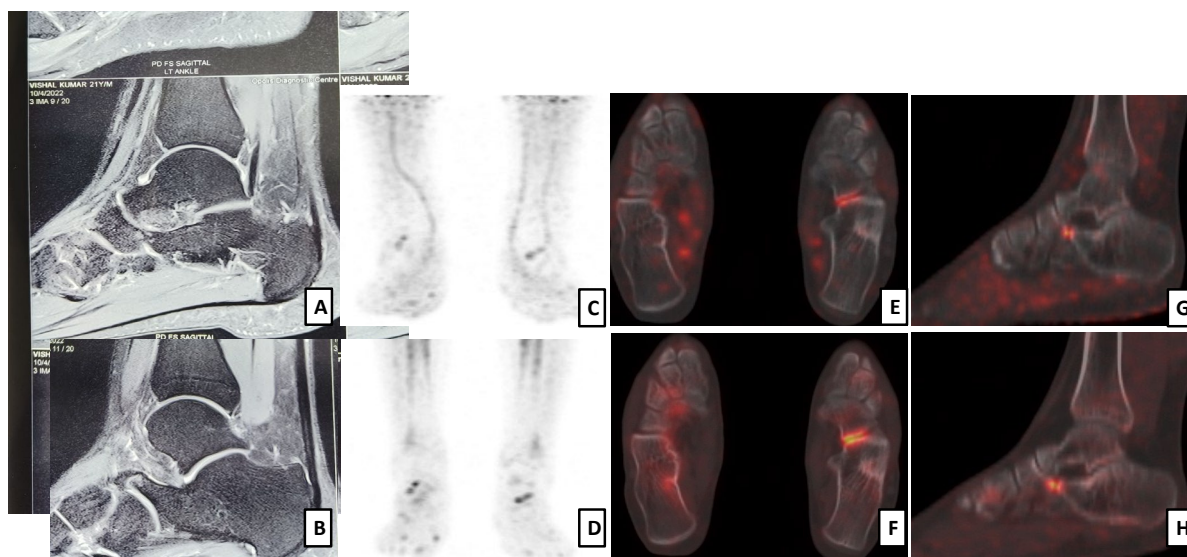


Figure 1. A 21 year old male patient had left foot pain for 5 months. MRI of the left foot (A, B) showed calcaneonavicular coalition and oedema in the calcaneonavicular joint and talus (arrows). Images at 5 minutes (C, E, G) and 45 minutes of ^{18}F NaF PET/CT (D, F, H) images showed increased tracer uptake (SUVmax, early – 2.3, delayed – 7.2) in the left calcaneonavicular joint region (arrows).

Conclusion

^{18}F NaF tracer helps in identifying the disease at an early stage. ^{18}F NaF PET/CT is also useful in detecting bone and joint pathologies in the lower limb but limited role in soft tissue lesions. ^{18}F NaF PET/CT aids the clinician in accurately diagnosing the site of origin of musculoskeletal pain and planning specific targeted treatment.

IAEA-CN-326/464

Utility of MIBI SPECT and SPECT/CT imaging in the localization of abnormal parathyroid glands: A retrospective analysis

M. Kapitán, J. Lemos, C. Ferreira, C. Gonzato, V. Gómez, M. Ramos, F. Mut

Nuclear Medicine Service, Italian Hospital, Montevideo, Uruguay

Background

MIBI SPECT imaging is valuable for localizing parathyroid (PT) adenomas or hyperplastic glands in patients (pts) with hyperparathyroidism (HPT). It is especially useful in cases where traditional imaging techniques like ultrasound or CT may not clearly identify the PT glands. The method is useful to localize pathologic glands when surgical removal is planned, which is particularly challenging in cases of ectopic tissue. Hybrid SPECT/CT imaging adds crucial anatomic information for successful treatment and is commonly used where available, either through simultaneous or separate acquisitions.

Methodology

We retrospectively reviewed pts referred for PT imaging from (January 2017 to December 2023). In all pts, 10-15 mCi (370-555 MBq) of [^{99m}Tc]MIBI were injected intravenously, and imaging was performed using a dual-head SPECT gamma camera. Acquisition started 15 min after injection, taking a planar image of the neck and upper thorax, which was repeated at 2.5 h. In most cases, 5 mCi (185 MBq) of [^{99m}Tc]-O4- were then injected and an additional planar image was obtained in the same position, to delineate the thyroid gland. SPECT was performed at 2 h, between early and late planar acquisitions, When a CT study was available, co-registration and fusion with SPECT was accomplished using appropriate software tools (figure).

Results

A total of 347 pts was analysed (72.3% women, ages 60.1 ± 13 years). 68% had primary HPT, 8.4% secondary HPT and 23.6% other reasons for testing (increased PT glands in ultrasound, renal lithiasis, etc.). PT glands were identified in 162 pts (46.7%), 148 cases (42.6%) were negative and 37 (10.7%) equivocal. In positive cases, planar imaging showed PT glands in 108 (66.6%), with additional 54 (33.3%) detected with SPECT, which also helped in topographic location. Regarding number of glands, 1 was identified in 80% of positive cases, 2 in 18%, and 3 or more in 2%. Single glands location was right inferior in 38.8%, left inferior in 34.1%, left superior in 6.2% and right superior in 3.9%, while 17% (n=26) were ectopic. Of these, 12 (46.2%) were pre-vertebral between C6 and T2, 8 (30.8%) retro-sternal and 6 (23%) mediastinal. In 9/26 (34.6%) pts with ectopic glands, fusion with external CT was performed, of which 7 were successfully operated using radioguided surgery, and 2 are still in pre-operative workup. Two additional ectopic glands were removed through radioguided surgery with SPECT information only and 6 using conventional surgery, while other pts are under medical treatment or were lost for follow-up.

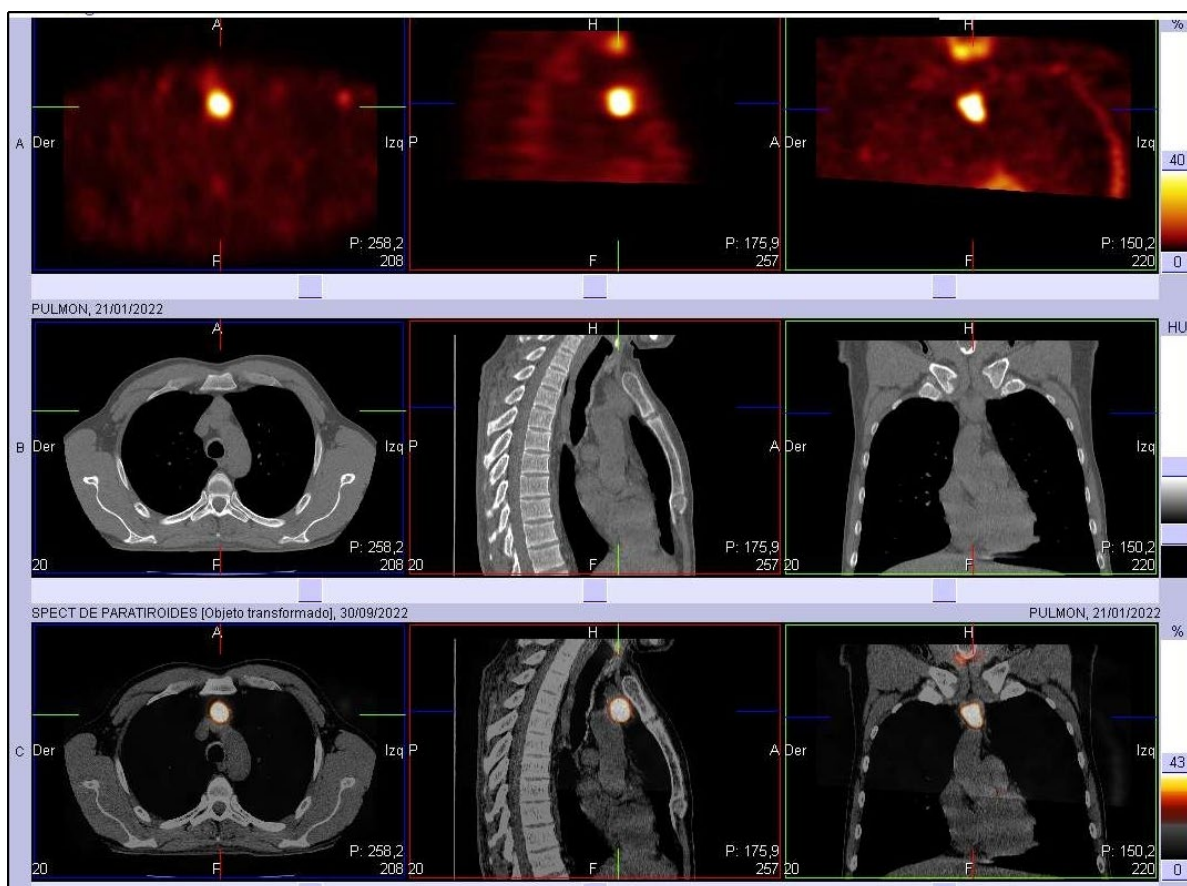


Figure 1. 45-year-old male with primary HPT. SPECT/CT showing ectopic gland in upper mediastinum.

Conclusion

In our series, HPT was more common in women (3:1). SPECT was able to detect 30% additional positive cases compared to double-phase planar imaging only. Where hybrid SPECT/CT equipment is not available, co-registration and fusion with remotely performed CT is a valuable and cost-effective alternative to aid in surgical planification, especially in the case of ectopic glands. This strategy together with radio-guided surgery, is being more frequently used in our environment, allowing shorter, more precise and effective procedures.

IAEA-CN-326/466

The added value of [^{99m}Tc]Tc-PSMA over [^{99m}Tc]Tc-MDP scintigraphy in a patient with prostate cancer- a case report

A. Ankrah¹, M. Yartey¹, C. Korsah, A. A. Sarkodie, S. Teye², E. Hammond²

¹ National Radiotherapy Oncology and Nuclear Medicine Centre, Korle Bu Teaching Hospital, Ghana

² Ghana Atomic Energy Commission Hospital, Ghana

Background

[^{99m}Tc]Tc-MDP scintigraphy has been used for decades in prostate cancer imaging. The sensitivity but lack of specificity of [^{99m}Tc]Tc-MDP has led to the search for more specific tracers. PSMA-based ligands have improved diagnostic imaging of prostate cancer.

Aim

We present a case of a prostate cancer patient who had both [^{99m}Tc]Tc-MDP and [^{99m}Tc]Tc-PSMA studies. We evaluate the added value of the [^{99m}Tc]Tc-PSMA to the [^{99m}Tc]Tc-MDP, which is still the main scintigraphic imaging available in resource-poor countries for prostate cancer.

Methodology

A 55-year-old man with histologically confirmed prostate with a Gleason score of 4 +3 = 7/10 and a PSA- 25,6ng/ml. He was involved in a motor vehicle accident six months before he had his [^{99m}Tc]Tc-MDP study, and he developed progressive pain in the left hip. A [^{99m}Tc]Tc-PSMA study was performed three weeks after the bone scan. We injected the patient with 666 MBq (18mCi) of [^{99m}Tc]Tc-MDP for the bone scan, and we imaged the patient after 3 hours on a GE discovery 670 SPECT/CT. For the PSMA study, we administered 555MBq (15mCi) of [^{99m}Tc]Tc-PSMA and we imaged the patient on the same camera after 2 hours. We used PSMA-GCK01 as the ligand for the PSMA imaging, and we labelled the [^{99m}Tc]Tc-PSMA as per the manufacturer's instructions. In both studies, we acquired whole-body images and SPECT/CT, including the pelvis.

Results

The bone MDP scan showed an intense irregular osteoblastic lesion with no other abnormal uptake. The PSMA study showed a PSMA-avid lesion in the area, and the MDP bone scan showed an osteoblastic lesion. In addition to the hip lesion, the PSMA study noted lesions in the sacrum and a focal irregular lesion in the prostate bed.

Discussion

PSMA is distributed to tissues that express the PSMA receptor, which includes prostate cancer and some benign lesions. PSMA uptake has been reported in healing fractures but is generally low-grade. Again, the lesion in the sacrum, in correlation with the accompanying CT, was localized to the bone and not the ganglion, which could also give a false negative result for prostate cancer. PSMA SPECT/CT, in contrast to conventional scintigraphy, allows one to evaluate the soft tissue in addition to bone lesions. We carefully reviewed the bone scan for the sacral lesion but could not find it, suggesting that PSMA scintigraphy may detect lesions earlier than conventional bone imaging.

Conclusion

Our case suggests that $[^{99m}\text{Tc}]\text{Tc-PSMA}$ may detect lesions earlier than conventional bone scintigraphy, which could impact management. The SPECT/CT PSMA study also allows the evaluation of the soft tissue in addition to the skeletal lesions.

IAEA-CN-326/467

PET/CT Experience in Brazil: A Review**L. Machado, J. Cunha de Azevedo, J. P. Marins Assunção, P. H. Rodrigues Pontes**

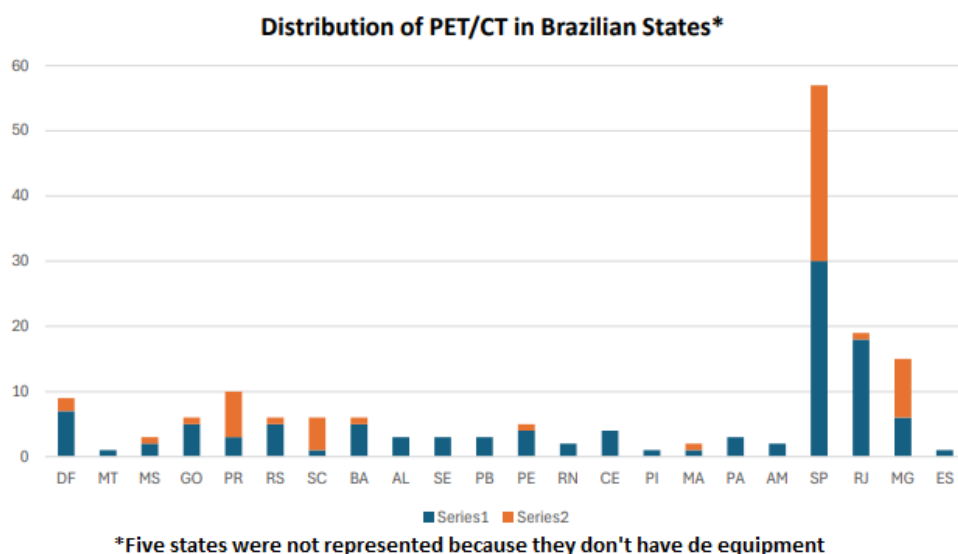
Hospital Universitário Antônio Pedro/Universidade Federal Fluminense - Niterói, Brazil

Eight years ago, a study was presented at IPET 2016 regarding the implementation and progress of Positron Emission Tomography (PET) in Brazil. This data illustrated the technology's evolution since the first device was installed, noting a total of 101 operational PET/CT scanners at that time. This equated to approximately one device for every 2 million Brazilians and 600 registered nuclear medicine specialists. Building upon our colleague's research, we extended the study to analyze the current state of PET/CT in Brazil.

Information from the National Commission for Nuclear Energy (CNEN) website was used to gather the total number of services authorized for PET scans in 2024. Additionally, a search of the Brazilian public health system (DATASUS) database revealed the number of scans performed by the system in the past 8 years.

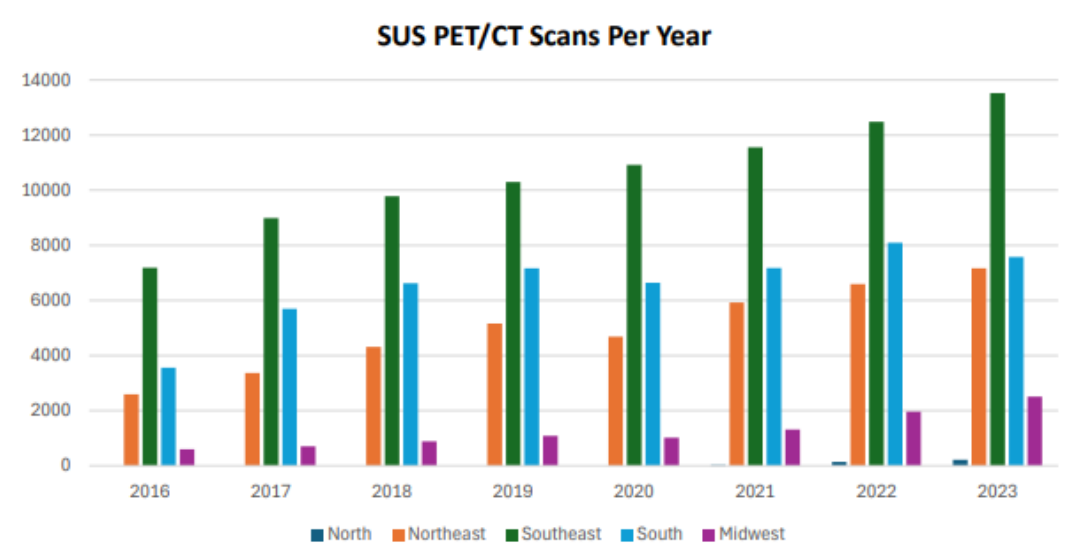
From 2016 to 2023, the number of facilities authorized to perform PET/CT scans in Brazil increased by about 65%, going from 101 to 167 services. This translates to approximately 1 PET/CT scanner for every 1.215 million people. Currently, there are 11 cyclotrons in Brazil, none of which are located in the northern region. The southeast region, particularly São Paulo state (SP), has a high concentration of services, accounting for over 32% of the total PET/CT scanners, consistent with findings from previous studies.

In Brazil, 70% of the population depends solely on the national public health system (SUS). Since 2014, SUS has added 5 indications for PET/CT scans to the list of covered exams: non-small cell lung cancer, colorectal cancer with exclusively hepatic metastasis eligible for resection, Hodgkin's and non-Hodgkin's lymphomas, and more recently, small cell lung cancer.



Annually, there is a 22% growth in the number of scans performed, resulting in a 122% increase over the 8 years observed. We anticipate that as the number of indications expands and access to the service increases, there will be a significant increase in the number of procedures in the coming years.

Although there has been growth in the number of PET/CT facilities and the annual number of scans, access to the exam remains uneven. Five states, all in the northern Amazon rainforest region, lack installed PET/CT scanners, leaving a significant portion of the population without access to this technology.



Furthermore, there are about 1,100 medical specialists in nuclear medicine, representing an increase of about 83%, however most of them are concentrated in the southeast region.

Despite the IAEA's efforts to promote nuclear medicine in Latin America, access for the population is restricted. This is due to high operational costs, the need for imported raw materials, logistical challenges, a limited number of cyclotrons, and the concentration of specialists in major centers, all of which hinder universal access to PET/CT scans.

IAEA-CN-326/469

The long-term results of treatment with autologous bone marrow-derived mesenchymal stem cells (AMSCCM) of patients with pharmaco-resistant epilepsy by data of neuroimaging by cEEG, PET/CT

E. Slobina¹, T. Dokukina², F. Khlebokazov³, N. Misuik³

¹ National Research Nuclear University MEPhI (Moscow Engineering Physics Institute) (JSC Medicina/DITI NIYAU MEPhI), Russia

² State Medical University

³ Belarus National Center for Mental Health, Belarus

Aim

The long-term results of treatment with autologous bone marrow-derived mesenchymal stem cells (AMSCCM) of patients with pharmaco-resistant epilepsy were evaluated.

Methodology

The study included: the main group: 34 patients with pharmaco-resistant epilepsy and generalized convulsive seizures and 34 patients of the comparison group. Patients in the main group received stem cell treatment, whereas in the comparison group the treatment was performed only according to the current protocol. In patients of both groups the indices of brain bioelectrical activity (computerized EEG - cEEG), PET/CT, MRI, immune status, BDNF content were determined. A total of 104 AMSCCM transplants were performed on patients of the main group from 2011 to 2023: 52 intravenous and 52 intrathecal (14 men and 20 women). The safety of AMSCCM transplantation was evaluated in the first 18 patients undergoing a single course of cell therapy during the follow-up period from 10 to 12 years (Me - 11 years). No side effects and complications were registered. 14 patients received 2 courses of cell therapy and 2 patients - 3 courses.

Results

Retrospective analysis of treatment results (in 24 and more months) of 16 patients who received 2 and more courses of cell therapy showed absence of generalized convulsive seizures in 5 (35,71%) patients with follow-up period from 4 to 7 years. Of these, two patients had remissions for 14 and 40 months, after which the attacks resumed. After 3 courses of cell therapy in these patients, the seizures stopped. Significant reduction of generalized seizures (more than 50%) or their transformation into milder forms was observed in 6 (37.5%) patients. Unsatisfactory treatment results were obtained in 5 (31.25%) patients, including 2 patients with hippocampal sclerosis and 2 patients with simple and complex partial seizures only.

All of results correlate with data of neuroimaging by cEEG, PET/CT. The diagnostic accuracy of the method using this technology for temporal lobe epilepsy was 89.0%.

Conclusion

It has been established that PET/CT with 18-FDG is a highly informative method of radiodiagnostics, allowing high accuracy to identify epileptic foci in patients with locally caused epilepsy. The level of metabolic disorders detected using 18-FDG PET in the affected area in patients with locally caused epilepsy is in a significant correlation with the clinical severity of the disease.

In individuals with a single course of cell therapy, PET data with 18-FDG are crucial for assessing the prognosis of the development of epilepsy, as well as quickly (before regression of clinical symptoms of the disease) assess the effectiveness of treatment.

IAEA-CN-326/470

Monte Carlo Simulation of the Preclinical High Field 9.4T PET/MR System

M. Almuttairi¹, C. Kuntner-Hannes², Z. Chalampalakis¹, N. Jurjew³, I. Rausch¹

¹QIMP Team, Center for Medical Physics and Biomedical Engineering, Medical University of Vienna, Vienna, Austria

²Department of Biomedical Imaging and Image-Guided Therapy, Medical University of Vienna, Vienna, Austria

³Institute of Nuclear Medicine, University College London, London, United Kingdom

Background

GATE is a dedicated medical imaging Monte Carlo simulation tool designed for modelling realistic PET imaging systems. The present abstract summarizes the validation of the GATE model developed to simulate the performance of the Preclinical PET/MR system at high magnetic field against the experimental data.

Methodology

GATE v8.2 was used to simulate the Bruker Preclinical PET/MR system. The model implemented all the design parameters provided by the vendor. The simulations and the measurements were done with RF coils inside the scanner bore and a 9.4T magnetic field on. The outcomes of the simulation were validated with experimental data, adhering to the NEMA NU 4-2008 standards for evaluating the sensitivity, scatter fraction (SF) and noise equivalent count rate (NECR), of the preclinical PET/MR system. The spatial resolution test is currently being validated.

Results

The maximum absolute sensitivity reached 10.5, with a discrepancy of 7.3% from measurements. Simulation and measurements for both SF and NECR showed good agreement in mouse phantom validation. SF was approximately 22% across all simulated activities and in alignment with experimental data. The NECR peak for simulation and measurement were 400 kcps at 26 MBq and 429 kcps at 29 MBq, respectively, with an average difference of 9.2%. The simulated count rates did not align with the experimental data for the rat phantom. Experimentally, SF rapidly declined at very low activities, then linearly increased with activity, peaking at 64% at 157 MBq. Aberrantly, the simulated SF remained consistent at around 41% across all activity levels, aligning with theoretical expectations.

Figure 1: Measured and simulated absolute sensitivity of the PET scanner.

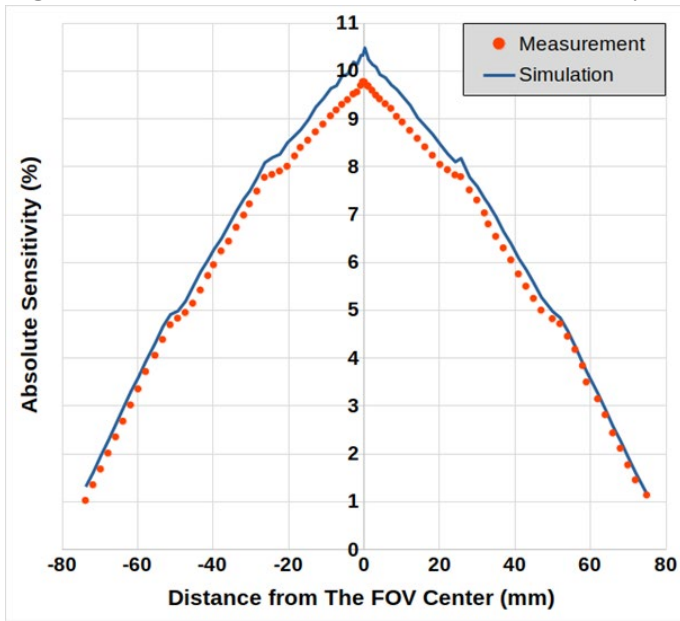
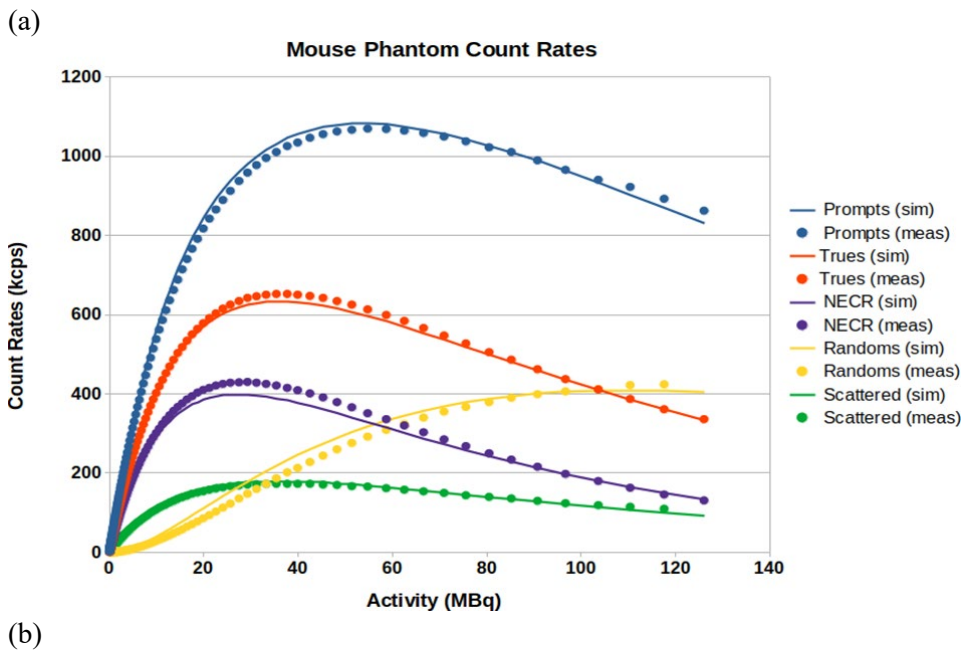


Figure 2: Measured and simulated count rates for (a) the mouse and (b) the rat phantoms.



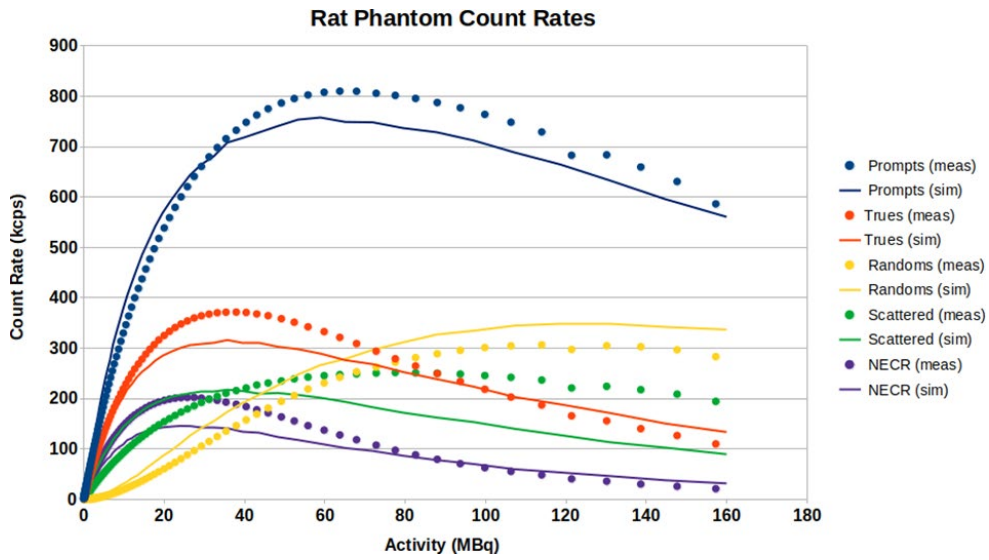
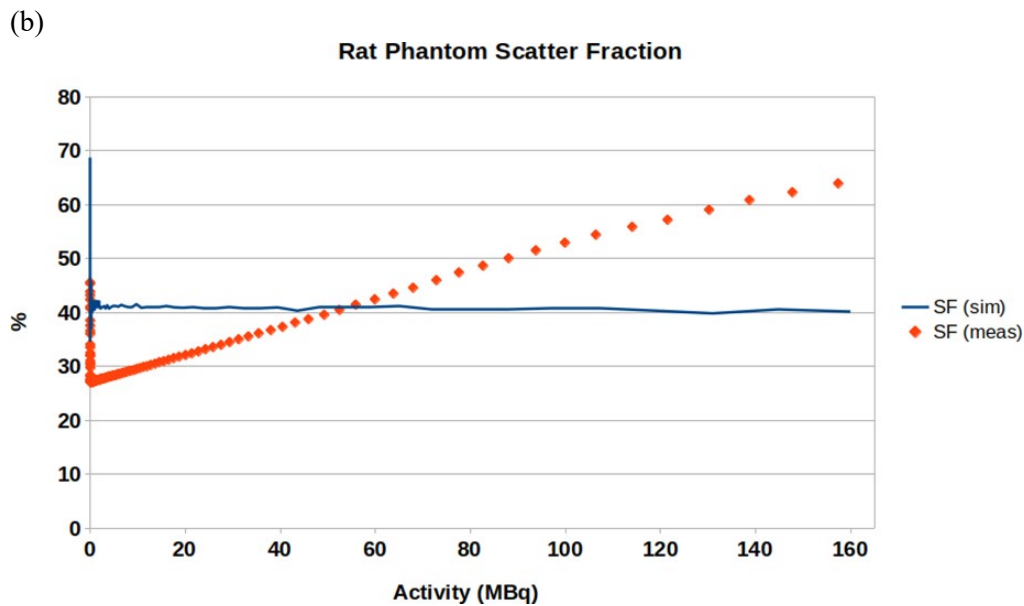
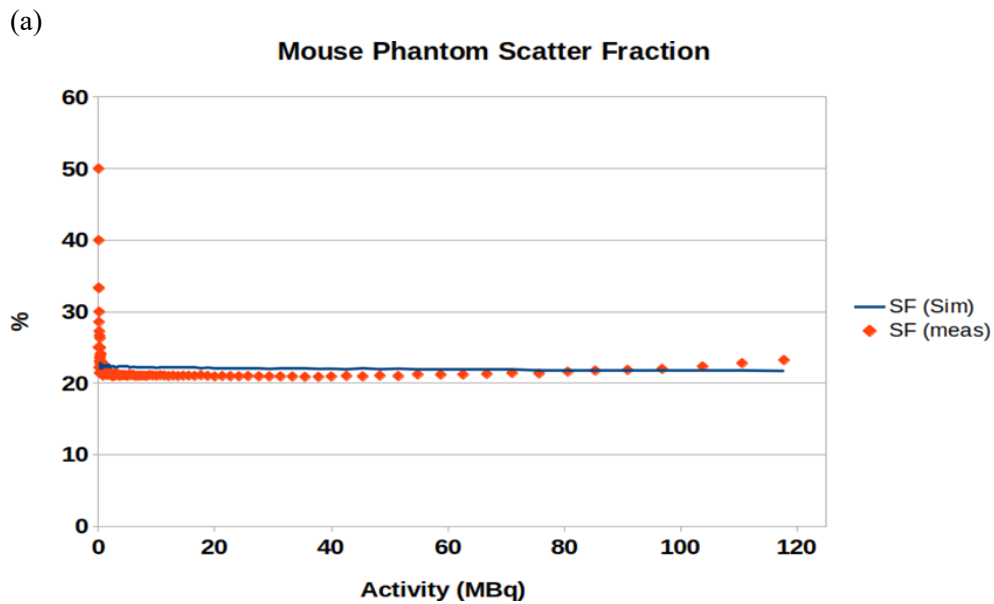


Figure 3: Measured and simulated scatter fraction for (a) the mouse and (b) the rat phantoms.



Conclusion

The findings demonstrated the ability of the model in precisely simulating the standard performance characteristics of the Bruker Preclinical PET/MR system with experimental validation for the sensitivity and the mouse phantom measurements. Experimental data behaviour of the rat phantom requires further investigation.

Keywords: Preclinical PET/MR, NEMA Performance, GATE

IAEA-CN-326/471

Deep Learning-based Dosimetry Model for Patient-Specific ⁹⁰Y Radioembolization Therapy

I. Scarinci, M. Valente, P. Pérez

CONICET – IFEG – FaMAF, Argentina

Background

Selective internal radiotherapy (SIRT) with yttrium-90 microspheres has become a cornerstone in the treatment of metastatic liver cancer and hepatocellular carcinoma. Accurate dosimetry is essential to ensure the efficacy and safety of such interventions. Recent years have seen significant advances in imaging capabilities, both pre- and post-treatment, with techniques such as [^{99m}Tc]Tc-MAA microspheres, [⁹⁰Y]Y-bSPECT and [⁹⁰Y]Y-PET offering promising avenues for refining dosimetry calculations. There is also growing interest in harnessing the power of deep learning algorithms to streamline dosimetry calculations while maintaining accuracy and reducing computational time compared to traditional Monte Carlo methods. This study presents a novel deep learning model, 3D-DosiNet, designed for tailoring patient-specific dosimetry in yttrium-90 radioembolization therapy, considering tissue density heterogeneities and inhomogeneities in the source distribution.

Methodology

For the 3D-DosiNET training, a dataset of 5500 patches of voxels of, taken from ten CT scans, was used. The dose voxel kernel (DVK) for each patch was calculated using Fluka MC, considering the yttrium-90 source is homogeneously distributed in the central voxel. The proposed model has a ResUNet type architecture and was trained using 4500 patches for training, 500 for evaluation, and 500 for testing. Finally, the model was evaluated using a dataset of six patients treated with yttrium-90 microspheres. For each patient, three images were considered: the pre-treatment [^{99m}Tc]Tc-MAA SPECT/CT, the post-treatment [⁹⁰Y]Y-PET, and [⁹⁰Y]Y-bSPECT/CT. The absorption map for each patient and image was calculated using GATE MC. Each image is compared with the absorbed dose map calculated by 3D-DosiNET. In particular, the absorbed doses in the liver, right lung, and lesions are compared.

Results

The proposed model has shown great performance in obtaining the DVK for distributions of inhomogeneous densities. They achieved a mean MAE of 3.73×10^{-4} . The performance of 3D-DosiNet when is applied in patient-specific dosimetry in healthy liver the mean difference were $1.11 \pm 1.54\%$, $-0.17 \pm 2.31\%$, and $-3.23 \pm 2.80\%$ for [^{99m}Tc]Tc-MAA, [⁹⁰Y]Y-PET and [⁹⁰Y]Y-bSPECT respectively. In lesions the mean differences were $1.1 \pm 1.90\%$, $-0.85 \pm 3.27\%$, and $-1.78 \pm 3.10\%$ for [^{99m}Tc]Tc-MAA, [⁹⁰Y]Y-PET and [⁹⁰Y]Y-bSPECT respectively. Finally, in lung right, the mean differences were $23.85 \pm 4.56\%$, $30.52 \pm 7.90\%$ and $32.49 \pm 25.00\%$ for [^{99m}Tc]Tc-MAA, [⁹⁰Y]Y-PET and [⁹⁰Y]Y-bSPECT respectively.

Conclusion

The 3D-DosiNet is a deep learning model that accurately generates dose maps for patient-specific dosimetry in radioembolization treatments with yttrium-90. The model's precision is close to Monte Carlo (MC) simulations but demands shorter calculation times.

IAEA-CN-326/475

Usefulness of 18-F PSMA PET/CT in Prostate Adenocarcinoma Staging and Biochemical Recurrence Assessment in Moroccan patients. Cases report

H. Bennani, N. Abaouz, H. Batani, A. Guensi

Hassan II University, FMPC, Laboratory of Cellular and Molecular Inflammatory, Degenerative and Oncologic Pathophysiology, Morocco

Background

Prostate cancer (PCa) is the second most prevalent cancer among males globally, posing a significant burden on healthcare systems worldwide. Accurate staging of PCa is crucial for optimal treatment planning and patient management. Positron emission tomography (PET) using prostate-specific membrane antigen (PSMA) ligands has emerged as a superior imaging modality for biochemical recurrence in unfavorable Intermediate Risk Prostate Cancer. In this study, we present the outcomes of utilizing 18-F PSMA PET/CT in two patients with prostatic adenocarcinoma, focusing on staging and biochemical recurrence assessment.

Patients

- Patient 1: 85-year-old male with untreated prostatic adenocarcinoma, Gleason score 7 (4+3), and PSA level of 14 pg/mL.
- Patient 2: 59-year-old male with untreated prostatic adenocarcinoma, Gleason score 7 (4+3), bone metastasis, and PSA level of 23.28 ng/mL.

Method

PET scans of the craniocaudal region were performed 100 and 120 minutes after intravenous injection of 210 MBq and 215 MBq respectively of 18F-PSMA, coupled with CT scans for attenuation correction and anatomical localization.

Results

- Patient 1 showed high uptake in prostatic foci without suspicious uptake outside prostate.
- Patient 2 exhibited uptake in the prostate and diffuse metastatic bone involvement involving the axial and proximal peripheral skeleton, with no suspicious uptake elsewhere.

Discussion

Accurate staging of PCa is essential for determining the appropriate treatment approach. Recent guidelines recommend PSMA-PET/CT as the primary imaging modality for initial staging due to its superior sensitivity and specificity compared to conventional imaging techniques. In men with newly diagnosed unfavorable intermediate-risk PCa. Early detection of biochemical recurrence is critical for timely intervention with targeted therapies. PSMA PET imaging has shown promise in detecting biochemical recurrence, influencing treatment strategies, and predicting disease progression. PSMA-PET/CT offers several advantages over conventional imaging methods, including its ability to simultaneously stage primary tumors, visceral, bone, and lymph node metastases without relying on size criteria. This comprehensive assessment within a single examination can significantly impact treatment decisions and patient outcomes. In our study, 18-F PSMA PET/CT effectively identified

primary tumor sites and metastases in patients with prostatic adenocarcinoma, aiding in accurate staging and guiding treatment planning. Furthermore, the technique demonstrated potential in assessing biochemical recurrence, which is crucial for implementing timely interventions and improving patient survival rates.

IAEA-CN-326/477

A rare case of ectopic ACTH syndrome due to chemodectoma**A. Llamas**

Los Cobos Medical Center, Colombia

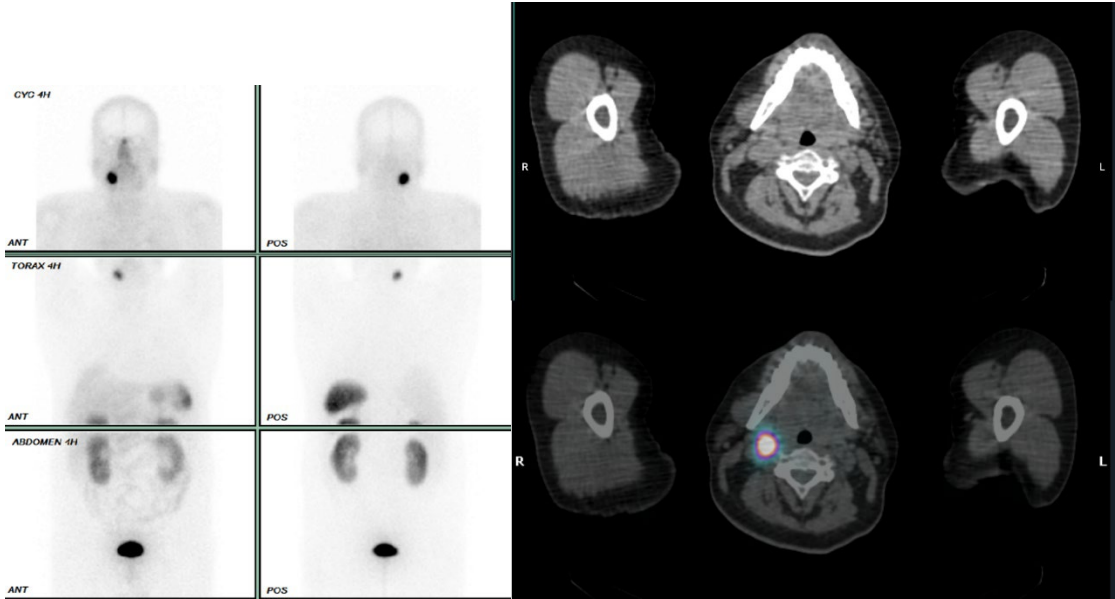
Background

Ten to 20% of cases of ACTH-dependent Cushing syndrome (CS) are due to ectopic ACTH production (EAS). Neuroendocrine tumours may cause EAS, the most frequent being small cell lung carcinoma (SCLC); carcinoid tumours (especially of the lungs, thymus and gastrointestinal tract); islet-cell tumours, pheochromocytoma, and medullary thyroid carcinomas. Early diagnosis and localization of the source of ACTH is crucial to avoid adrenalectomy and reduce the risk of metastases. Aside from SCLC (readily diagnosed), the primary lesion may go unidentified for years in 9-27% of cases (occult ECS). After diagnosis confirmation, the most powerful first examination is CT body scan, followed by MRI. In the case of occult ECS or non-conclusive conventional imaging, [⁶⁸Ga]SSTR PET/CT can detect up to 100% of the lesions. Somatostatin receptor scintigraphy using In-111- or [^{99m}Tc]labeled somatostatin analogs have been reported to be 64% sensitive in cases of occult ECS.

Head and neck paragangliomas (HNPGs) originating from parasympathetic cells in the carotid glomus, also known as chemodectomas, are usually benign and slow-growing tumours with an incidence of 1:30,000 – 1:100,000. Risk factors for HNPGs include conditions associated with chronic hypoxia, such as living at a high altitude, respiratory or heart diseases with chronic arterial hypoxemia. EAS by chemodectomas is a rare event as less than a handful of cases have been reported in medical literature.

Case Report

A 45-year-old male was diagnosed with Cushing syndrome due to ectopic ACTH secretion and consequent severe hypercortisolism. The most relevant lab test results showed hyperglycemia (570 mg/dl), hypokalemia, leukocytosis with neutrophilia and monocytosis. An abdominal CT scan described bilateral adrenal-gland hyperplasia (fig. 1). Additional tests ordered accordingly demonstrated increased 24-h urinary free-cortisol levels (3.045 ug/24 h. Reference values: 1.5 – 6.3 ug/24 h), increased AM cortisol, 29.4 (ref. 4.82 – 19.5) and PM cortisol 61.8 (ref. 2.47 – 11.9) and mildly elevated ACTH levels, i.e. 67.6 pg/ml (ref. 7.2 – 63.3). A normal sella turcica was described on MRI ruling against a central etiology. A solid solitary pulmonary nodule localized in the left lower lobe was found on his Chest CT scan (fig. 2), whereas the head and neck CT scan showed a glomus tumour occupying the right carotid bifurcation (fig. 3). A somatostatin-receptor (SSTR) SPECT/CT using [^{99m}Tc]Tc-HYNIC-Tyr3-octreotide was then obtained to identify a peripheral source of ectopic ACTH production. Intense uptake (Krenning score +4) was noted in the right carotid bifurcation (fig. 4-7).



Conclusion

HNPGLs are an exceedingly rare cause of ectopic ACTH-dependent Cushing syndrome (EAS). Somatostatin receptor SPECT/CT can be particularly useful in cases of occult EAS.

IAEA-CN-326/478

Diagnostic performance of ^{99m}Tc -iFAP SPECT/CT in the initial staging of patients with lung cancer: A comparative analysis with ^{18}F FDG-PET/CT

F. Garcia Perez¹, D. Gutierrez¹, G. Ferro-Flores², F. A. Sinisterra Solis¹

¹ Instituto Nacional de Cancerologia, Mexico

² Instituto Nacional de Investigaciones Nucleares, Mexico

Background

Lung cancer is a major problem worldwide, with the highest morbidity and mortality of all cancers. Fluorodeoxyglucose remains the most widely used PET marker for the diagnosis of malignant diseases. However, there are limitations in the availability of PET equipment in many countries. Therefore, a more accessible diagnostic modality at an early stage is crucial and inspired us to evaluate the performance of ^{99m}Tc EDDA HYNIC-iFAP SPECT/CT for lung cancer patients with that of ^{18}F FDG PET/CT as the reference standard.

Methodology

A prospective controlled analysis from September 2023 to February 2024, of 16 individuals with suspected lung cancer who underwent ^{99m}Tc -iFAP SPECT and ^{18}F FDG PET/CT was conducted. Histopathological findings were used for final diagnostic determinations for all primary tumours. The performance of the two imaging modalities was compared based on visual assessment, rates of cancer detection, and semi-quantitative parameters (target-to-background ratio [TBR] for both primary tumours and metastases.

Results

In total, this study enrolled 16 participants (8 female; median age: 57.5 years, range: 35 –79 years. A total of 253 lesions were analysed. For the 16 primary tumours ^{99m}Tc -iFAP and ^{18}F FDG had identical detection performance (16/16). ^{99m}Tc -iFAP detected 36 of 78 locoregional lymph nodes (46%), and 44 of 159 metastatic lesions on the central nervous system (2/4), pulmonary contralateral lymph nodes (2/5), non locoregional lymph nodes (11/45), adrenal glands (2/3), bone lesions (18/93). Furthermore, ^{99m}Tc -iFAP SPECT/CT demonstrates good performance on metastases in pleura (6/6), liver (2/2), and omental lesions (1/1). There were no statistically significant differences between TBR values in relation to that of ^{18}F FDG and ^{99m}Tc -iFAP SPECT/CT. There was no significant difference in detection of primary tumours, lymph nodes, and metastases based on pathological type: adenocarcinoma (13), squamous cell carcinoma (2), and small cell carcinoma (1), between the two examination modalities. We also found the lowest sensitivity of the iFAP in the detection of lymph nodes smaller than 14 mm, and visceral metastases smaller than 20 mm.

Conclusion

^{99m}Tc iFAP SPECT imaging of lung cancer is feasible and provides diagnostic image quality in the assessment of pulmonary masses. In response to the limited availability of infrastructure and resources in developing countries to offer PET/CT studies to their population. Our results demonstrate non-inferiority in primary diagnosis with ^{99m}Tc iFAP SPECT in comparison with PET in lung cancer. This could encourage its use and promote the benefit of its clinical utility.

IAEA-CN-326/481

18FDG PET/CT scan scanning in non-Hodgkin lymphoma management in Moroccan patients

H. Batani, Z. Ouzafar, H.Bannani, A. Guensi

Hassan II University, FMPC, Ibn Rochd university Hospital, Morocco

Background

18FDG PET/CT scan has become an indispensable tool for the management of patients with non-Hodgkin's lymphoma. It provides a more accurate assessment at the decision-making stages of treatment: at the initial workup, by uncovering infra-morphological localizations; during the early response to therapy, by identifying refractory disease; and at the end of the procedure, by detecting residual disease.

Methodology

Our work is a retrospective descriptive study of 100 patients who underwent 18 FDG PET-CT in the nuclear medicine department of the CHU ibn rochd in Casablanca, with the aim of assessing the contribution of 18FDG PET in the evaluation of non-Hodgkin's lymphoma in 2023 in Moroccan patients.

Results

The mean age of our patients was 51 years, with extremes of 07 and 76 years, we found that our patients were predominantly male (61%). The main histologic type was large B-cell lymphoma in 49 % of patients and follicular lymphoma (11%), mantle cell lymphoma (9%) and Burkitt Lymphoma (9%). In our study, 18FDG PET scans were performed in 70 % of patients as part of the initial work out only, 20 % of patients have had an initial and interim 18FDG PET scan. 10 % of patients have had an interim and end of treatment 18FDG PET scans. The 18FDG PET scans has staged 10 % of patients in Ann Arbor stage II, 30 % stage III and 70 % stage IV. The Deauville score was 1 in 25 %, 2 in 17 %, 3 in 19 %, 4 in 31 % and 5 in 8 % of patients. Because of the limited availability of 18FDG PET CT scan, the Moroccan patient with non-Hodgkin lymphoma don't get 18FDG PET/CT in initial staging, interim assessment, and end of treatment assessment.

IAEA-CN-326/482

The novel Targeted Alpha Radiopharmaceutical Therapy: Opportunities and Challenges

B. Ochieng¹

¹ Technical University of Kenya, Kenya

Introduction

Alpha(α) -particle emitters administered systemically or locoregionally are highly potent therapeutic agents, novel in their mechanism and impervious to radiation resistance. Their short range of 50–100 μ m and high linear energy transfer (LET) results in high radiobiological effectiveness (RBE) and cytotoxicity compared to the β -emitters, leading to induction of numerous DNA double-strand breaks along their respective tracks.

Methodology

In ²²³Ra dichloride therapy, ²²³Ra leaves the blood and is taken up in bone and bone metastases. Imaging ²²³Ra and its progeny is done using a gamma camera while dosimetry is achieved through quantitative measurements. Compounds labelled with ²²⁵Ac (T_{1/2}= 9.9 days) and ²¹³Bi (T_{1/2} =49 mins) are under development, production and use. ²²⁵Ac and ²¹³Bi are produced from the radiochemical extraction from ²²⁹Th (T_{1/2} =7917 years) accelerator-based methods.

Results

The implementation of ²¹³Bi-TAT with DOTATOC results in a high number of long-lasting antitumour responses including a complete remission. For ²²⁵Ac-PSMA617 for therapy of prostate cancer, the pharmacokinetics of PSMA617 characterized by rapid tumour uptake within a few hours, its extended tumour retention as well as its rapid renal clearance of unbound compound provide an excellent match to the ²²⁵Ac decay characteristics of long-lived internalization. Several challenges have however, manifested in such techniques. The inability to perform 3D imaging and surrogate imaging agents being unable to provide information on the distribution of free α -particle emitting daughters. Potential solutions to these are the advancements in the image reconstruction techniques for SPECT and developments in SPECT instrumentation; and pharmacokinetic modelling combined with direct imaging based validation respectively.

Conclusion

The therapeutic efficacy of alpha emitters has elicited a lot of demand that must be satisfied by employing a variety of production routes hence a common quality criterion should be established. Clinical use of alpha- particle therapy poses no major radiation safety risks in terms of external irradiation, contamination and incorporation compared to their beta counterparts.

IAEA-CN-326/483

PET imaging as an effective tool for Cancer Care

S. Issahaku

Ghana Atomic Energy Commission, Ghana

These PET scans use a substance, called a radiotracer, to highlight areas of activity within the body that are suggestive of cancer. The most common type of PET radiotracer used in cancer care is FDG, which is a radioactive substance similar to glucose. The objective of this study was to assess the current state of cancer care in Ghana and provide an overview of the potential positive impact PET imaging in cancer care in Ghana for policy makers. Currently, two PET imaging facilities are being put up to support cancer care in Ghana. Over 20000 patients are diagnosed of various cancers cases in Ghana. 90% of this number are diagnosed in an advance state, which results in very little therapeutic benefit to patients. An overview of the current situation in diagnostic procedure with our current SPECT/CT and MRI require the introduction of PET to complement and improve the diagnostic outcome. A review of 1567 cancer patients treatment folders reveal that 62% even though made an attempt to seek medical attention only 10% were properly diagnosed. In conclusion, the introduction of PET imaging will significantly improve clinical diagnoses in Ghana.

IAEA-CN-326/484

Radiomics-Based Texture Analysis of ^{177}Lu -DOTATATE Post-Therapeutic Images of Neuroendocrine Tumours for the Estimation of Therapeutic Outcome

Z. Besenyi, L. Pávics, G. Sipka

University of Szeged, Faculty of Health Sciences, Department of Nuclear Medicine, Hungary

Background

Neuroendocrine tumours are a very diverse group of malignancies, but they share several common characteristics, including the overexpression of somatostatin receptors. These receptors can be targeted with therapeutic radionuclide agents. The aim of our study was to compare the texture-based information and somatostatin receptor expression of these pathological lesions on ^{177}Lu -DOTATATE post-therapeutic SPECT/CT images with other specific histological, immunohistochemical, clinical and laboratory results to find any relevant correlations between these parameters.

Methodology

In our retrospective analysis, 19 post-PRRT quantitative SPECT/CT images (acquired with AnyScan® TRIO SPECT/CT system of Mediso Ltd.) of 7 patients (4 female, 3 male, with mean age of 67 years) were evaluated. On baseline scans 89 lesions were determined, and total of 209 tumour contours were defined during follow-up examinations. Lesion contour definition, quantitative evaluation and texture analysis (49 features) were performed in InterView™ FUSION software. Baseline lesions were contoured using a threshold-based standard method and the resulting lesion textures were evaluated. Disease status (progression vs. response in terms of stability/decline/response) was determined for each lesion on ^{177}Lu -DOTATATE SPECT/CT performed during the next PRRT cycle. All features (SPECT and clinical) were also correlated with follow-up data and features significantly associated with response in a site-specific analysis (liver, lymph nodes and bone).

Results

In total, 112 unique features were extracted from the images and clinical data. We found that the liver metastases showed significantly higher somatostatin receptor expression (Mann-Whitney, $p < 0.001$). All tumour tissues of patients indicated for PRRT were chromogranin and synaptophysin positive, but also shared CK7 and CK20 negativity. In terms of therapeutic efficacy, liver metastases were prominent, but bone metastases had a greater reduction in activity (Mann-Whitney; $p < 0.001$). Our patients, those with primary pancreatic neuroendocrine tumours, had a better therapeutic response (Mann-Whitney; $p < 0.001$). Radiomic correlations revealed that the Krenning score showed a high correlation with several texture parameters (entropy, short zone emphasis etc.), while the success of therapeutic response showed correlation with cumulative dose, perineural spread, tumour size.

Conclusion

Radiomic processing data suggests that post-therapy ^{177}Lu -DOTATATE SPECT/CT may be able to find specific features for early estimation of therapeutic success. Our results demonstrate that the therapeutic response of pancreatic neuroendocrine tumours to PRRT is excellent. With further refinement of the dataset, a more optimal selection process of patients for PRRT may be achieved in the future.

IAEA-CN-326/485

Optimization and Validation of Radiochemical Purity Test Method of Ethylene Diamin Tetra Methylene Phosphate Radiopharmaceutical Kit Labelled by Samarium 153 Using Thin Layer Paper Chromatography Method

P. Widayati¹, A. Amanda², D. Ariyanti², M. C. Prihatiningsih², A. K. Dewi²

¹ Research Center for Radioisotope Technology, Radiopharmaceuticals, and Biodosimetry, Puspitek Serpong Area, Indonesia

² Indonesian Polytechnic of Nuclear Technology, Indonesia

Background

In 2021, WHO says it will be 20 million people are diagnosed with cancer and 10 million people die from cancer. Types of cancer The highest causes of death each year are lung, prostate, liver, stomach, colorectal, and breast cancer. Cancer cells are growing in the human body can metastasize to the bone tissue which causes pain in the patients. This pain can be reduced by therapeutic methods using radiopharmaceutical form Ethylen Diamine Tetra Methylene Phosphonate (EDTMP) characterized by radionuclide Samarium-153. However, the standard system to test the radiochemical purity of ¹⁵³Sm-EDTMP uses materials that are volatile and dangerous for workers. Therefore, an optimal system is needed to replace the system. In this research, the ¹⁵³Sm-EDTMP purity test method was optimized using a variety of stationary phase types Whatman-1 (W-1), W-3MM, W31. ET, W-4, DC-Alufolien Cellulose, TLC Cellulose Aluminum, TLC Aluminum Oxide 60 F254 neutral, TLC Silica gel 60 F254 and ITLC-SG and variations of phosphate buffer mobile phase with concentrations of 0.01, 0.05, and 0.1 M at pH 7, 7.5, and 8. The TLC results were characterized using a Radio TLC-Scanner which can determine the level of purity of ¹⁵³Sm-EDTMP radiochemistry.

Methodology

Labeling EDTMP (freeze-dried kit) with ¹⁵³SmCl₂. Three batches of kit EDTMP were dissolved in 1 mL ¹⁵³SmCl₂, then the activity was measured using a dose calibrator. Incubate the solution for 10 minutes and check the pH afterwards.

The radiochemical purity of ¹⁵³SmCl₂ and ¹⁵³Sm-EDTMP was tested using thin layer chromatography with various stationary phases (Whatman-1 (W-1), W-3MM, W31. ET, W-4, DC-Alufolien Cellulose, TLC Cellulose Aluminum, TLC Aluminum Oxide 60 F254 neutral, TLC Silica gel 60 F254 and ITLC-SG) and phosphate buffer concentrations (0.01, 0.05, and 0.1 M) pH (7, 7.5 and 8) as the mobile phase. The samples obtained were scanned using a TLC- Scanner (Comecer) and the chromatograms were analysed using Gina software.

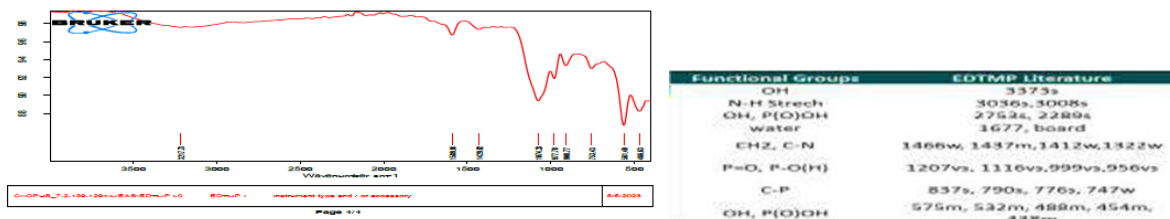


Quality test of radionuclides using dose callibrator and gamma spectrophotometer, radiochemical purity test using TLC Scanner, and quality test of EDTMP ligand using FTIR.

Results

In developing new radiopharmaceuticals, usually the guidelines will recommend TLC method for analyzing radiochemical purity (RCP) which provides simple technique and faster result 6 The peak

of $^{153}\text{SmCl}_2$ and EDTMP labeled with $^{153}\text{SmCl}_2$ from FTIR that has been done appeared as in the picture below:



The analysis results indicate that the EDTMP used in the study has functional groups that are almost the same as those found in the literature analysis. Therefore, the EDTMP used in the study is deemed suitable for further analysis.

The labeling process results in a clear visual appearance of the used preparation, indicating that the ^{153}Sm -EDTMP specimen being tested does not contain colloid impurities that could interfere with the radiochemical purity results. The examination of the acidity level shows that the used preparation has a pH of 7, which is considered very good because it falls within the suitable range for the human body, between the values of 6.5 and 8.5

The identification results indicate the presence of gamma energy emitted by Sm-153 at 69.81 keV, 97.36 keV, 103.16 keV, and 172.84 keV, which is consistent with the literature which affects the measurement background. This indicates that the identified $^{153}\text{SmCl}_3$ solution can be used for further analysis.

There are papers that cannot separate the ^{153}Sm -EDTMP component with Sm^{3+} not binding, resulting in R_f values and radiochemical purity of 0. This is because it has very small pore sizes, making it impossible for the solution to move upward.

In this variation, 3 papers with short elution times and high radiochemical purity values were taken, namely W31 ET, W-3MM, and ITLC-SG

Higher pH will affect the purity value to be higher because of better stability. The optimal chromatographic system was W31-ET with a mobile phase of 0.01 M concentrated phosphate buffer at pH 7.5.

Conclusion

This research resulted an optimal system using the type of stationary phase W-31ET and mobile phase phosphate buffer solution with a concentration of 0.01 M and pH 7.5 which gave a radiochemical purity of 99.64% with an R_f value of 0.82, this result is not much different from the standard chromatographic system (standard) in the analysis of radiochemical purity of ^{153}Sm - EDTMP with a shorter time and lower cost which is compared by the results of the T test not significantly different at the 95% confidence level and the Pearson correlation coefficient (r) is 1.

IAEA-CN-326/486

[¹⁸F]FDG PET/CT in distinguishing benign from malignant lytic lesions in the skeleton: A radiomics study**M. Asadi¹, B. Fallahi¹, S. A. Mirshahvalad¹, H. Vosoughi¹, Z. Vosoughi²**¹ Department of Nuclear Medicine, Shariati Hospital, Tehran University of Medical Sciences, Iran² Department of Medical Physics, School of Medicine, Shahid Sadoughi University of Medical Sciences, Iran**Background**

Whole-body low-dose CT is recommended as the initial imaging to evaluate the skeleton in some clinical scenarios, i.e., the evaluation of multiple myeloma patients. Additionally, it is a component of [¹⁸F]FDG PET/CT imaging. Accurate interpretation of whole-body CT can be cumbersome and time-intensive in skeletal lesions, mainly small-sized ones. Determination of the nature of the lytic lesions can be another challenge in the routine clinical setting. Thus, a robust algorithm to classify lytic lesions may improve the value of this imaging modality, as well as help in the interpretation of hybrid techniques such as [¹⁸F]FDG PET/CT. Hence, we aimed to develop radiomics-based machine learning models and determine their diagnostic performance in distinguishing benign from malignant lytic lesions.

Methodology

In this retrospective study, we reviewed all [¹⁸F]FDG PET/CT studies performed in our referral center. We searched through the molecular imaging expert-written reports and extracted those that contained “lytic” lesions. The CT-only images of the studies were blindly re-read and interpreted to diagnose the detected lytic lesions. A consensus session was held to assign the final diagnosis to each lesion. For this purpose, along with the [¹⁸F]FDG PET/CT images and original report, any available follow-up data in patients’ hospital information systems to help with the diagnosis was also included. Final indeterminate findings were excluded. Next, the eligible lytic bone lesions were annotated. These lesions were contoured using 3D Slicer (version 5.2.1). Then, from each volume of interest, a total of 1288 radiomics features were extracted by the Python-based open-source Pyradiomics package (version 3.0.1). These features included shape, first-order, GLCM, GLRLM, GLSZM and GLDM features. Ten optimal features that had the most correlation with lesions were found by Recursive Feature Elimination with cross-validation (RFEcv). Finally, the most robust features were considered eligible for model building. Models were built based on five different machine learning classifiers, support vector machine (SVM), logistic regression (LR), random forest (RF), decision tree (DT), and K-nearest neighbours (KNN). Their performance was evaluated using receiver-operating characteristic (ROC) curve analysis and the derived area under the curve (AUC) after 3-fold cross-validation. The average performance of each model through cross-validations was reported.

Results

A total of 90 lesions in 40 patients were included. Among them, 50(56%) were malignant, while 40(44%) were benign. The built models had AUCs of 0.83±0.07, 0.83±0.06, 0.86±0.03, 0.78±0.04 and 0.83±0.02 for SVM, LR, RF, DT and KNN, respectively. The best-performing model was RF, with AUCs of 0.83, 0.86 and 0.90 in different folds.

Conclusion

Our findings showed that radiomics features may reliably help diagnose the nature of the detected lytic lesions in patients referred for oncology assessment. Our best-performing proposed model could reach an AUC of 0.86. This model can be further incorporated into the automatic lesion detection algorithms to enhance them regarding lesion characterization. Having said that, implementing these models in a large external population still needs to be done to have a robust evaluation in the routine clinical setting.

Glossary of Terms

μm	micrometer
$[^{11}\text{C}]\text{PiB}$	C-labeled Pittsburgh Compound-B
^{177}Lu	Lutetium-177; Lu-177
^{18}F	Fluorine-18
3-D	three-dimensional
^{64}Cu	Copper-64; Cu-64
^{68}Ga	Gallium-68; Ga-68
$[^{68}\text{Ga}]\text{CBP8}$	Gallium-68 labelled Collagen Binding Probe #8
^{89}Zr	Zirconium-89; Zirconium-89
^{99}Tc	Technetium-99; Tc-99
$^{99\text{m}}\text{Tc}$	Technetium-99m; Technetium-99m
$\tilde{\text{A}}$	cumulative activities
AD	absorbed dose
AE	adverse event
AI	artificial intelligence
AJCC	American Joint Committee on Cancer
ALARA	as low as reasonably achievable
ALK	anaplastic lymphoma kinase
ARPi	androgen receptor pathway inhibitor
ASCO	American Society of Clinical Oncology
BC	breast cancer
BI	bladder invasion
BI-RADS	Breast Imaging-Reporting and Data System
BMI	body mass index
Bq	becquerel
CADMG	congenital abnormalities in the development of the mammary glands
cc	cubic centimeter
CECT	contrast-enhanced computed tomography
CI	confidence interval
cm	centimeter
CR	complete response
CRP	IAEA Coordinated Research Projects
CS	cavernous sinus
CSS	cavernous sinus syndrome
CT	computed tomography
CTCAE	Common Terminology Criteria for AEs
CuCl_2	copper (II) chloride
CUP	cancer of the unknown primary
CXCR4	chemokine receptor 4
DCR	disease control rate
DFO	desferoxamine
dl, dL	deciliter
DLR	deep learning reconstruction
DOTA	tetraxetan
EANM	European Association of Nuclear Medicine
ECE	extra-capsular extension
EGFR	epidermal growth factor receptor

ePLND	extended pelvic lymph node dissection
ER	oestrogen receptor; estrogen receptor
ESMO	European Society of Medical Oncology
FCH	fluorocholine
FDA	Food and Drug Administration, USA
FDG	fluorodeoxyglucose
FES	fluoroestradiol
FWHM	full width at half-maximum
g	gram
GBq	gigabecquerel; 10^9 Bq
GBM	glioblastoma multiforme
GEP-NET	gastroenteropancreatic-neuroendocrine tumour
GHS	global health status
GI	gastrointestinal
h	hour
h-R3	antibody h-R3 (Nimotuzumab)
HER2	human epidermal growth factor receptor 2
HER2+ve	human epidermal growth factor receptor 2 positive
HER2-ve	human epidermal growth factor receptor 2 negative
HIV	human immunodeficiency virus
HR	hazard ratio
HRCT	high-resolution chest CT
HRUS	high resolution ultrasound
IAEA	International Atomic Energy Agency
ICHD	International Classification of Headache Disorders
ID	intensity dose
IHC	immunohistochemistry
IL-6	interleukin 6
iPD-L1	cyclic peptide inhibitor programmed death-ligand 1
IQR	interquartile range
IR	infrared radiation
IRB	institutional review board
ISSS	Salvadorian Institute of Social Security
IV	intravenous
kcps	kilocounts (of photons) per second
kg	kilogram
LAD	left anterior descending
LD-RT	low-dose radiation therapy
LNI	lymph node involvement
LV	left ventricular
MBq	megabecquerel; 10^6 Bq
mCi	millicurie
mCRPC	metastatic castration-resistant prostate cancer
MeV	Mega electron Volt
MG	mammography
mHSPC	metastatic hormone-sensitive prostate cancer
MI	molecular imaging
MIP	maximum intensity projection

MIM	Medical Image Merge
ml, mL	milliliter
MLV	metabolic lesion volume
mm	millimeter
mo	month
mpMRI	multiparametric MRI
mPS	micro-sized polystyrene
MRI	magnetic resonance imaging
MSKCC	Memorial Sloan Kettering Cancer Center
MTV	metabolic tumour volume
NaF	sodium fluoride
NECR	noise equivalent count rate
Necsa	South African Nuclear Energy Corporation
NEMA	National Electrical Manufacturers Association
NET	neuroendocrine tumour
ng	nanogram
NK	natural killer
nPS	nano-sized polystyrene
NPV	negative predictive value
NST	no special type
ORR	objective response rate
OS	overall survival
OSEM	ordered subset expectation maximization
PCa	prostate cancer
PD	progressive disease
PD-1	programmed cell death protein 1
PD-L1	programmed death-ligand 1
PERCIST	PET Response Criteria in Solid Tumours
PET	positron emission tomography
PET/CT	positron emission tomography computed tomography
PF	physical function
PFS	progression-free survival
PI-RADS	Prostate Imaging–Reporting and Data System
PPV	positive predictive value
PR	progesterone receptor, partial response
PRRT	peptide receptor radionuclide therapy
PSA	prostate specific antigen
PSMA	prostate specific membrane antigen
PSMA _{total}	total prostate specific membrane antigen
PSMA _{vol}	total volume prostate specific membrane antigen
QOL	quality of life
RCD	revised comprehensive diagnostic
RCY	radiochemical yield
RD	related disease
RECIST	Response Evaluation Criteria in Solid Tumours
RF	role function
rho	thermal resistivity
RI	rectal invasion

ROC	receiver operating characteristic
RT	radiotherapy
SD	standard deviation, stable disease
SF	social function, scatter fraction
SLNB	sentinel lymph node biopsy
SNR	signal-to-noise ratio
SPECT	single photon emission CT
SUL	standard uptake lean body mass
SUL _{peak}	peak SUL in a spherical 1 cm ³ volume of interest
SUV	standardized uptake value
SUV _{max}	maximum standardized uptake value
SUV _{mean}	mean standardized uptake value
SUV _{peak}	average standardized uptake value within a small fixed-size region of interest
SVI	seminal vesicle invasion
TAC	time activity curve
TB	tuberculosis
TBR	tumour-to-background ratio
TLA	total lesion activity
TLC	thin layer chromatography
TLG	total lesion glycolysis
TLU	total lesion uptake
TNBC	triple-negative breast cancer
TNF- α	tumour necrosis factor alpha
TRUS	transrectal ultrasound
TTB	total tumour burden
TV	tumour volume
US	ultrasound
USG	ultrasonography
VOI	volumes of interest
VMT	vitreomacular traction
y/o	year old